Effects of Oncostatin-M Receptor overexpression on cervical squamous cell carcinoma cells and their extracellular vesicles

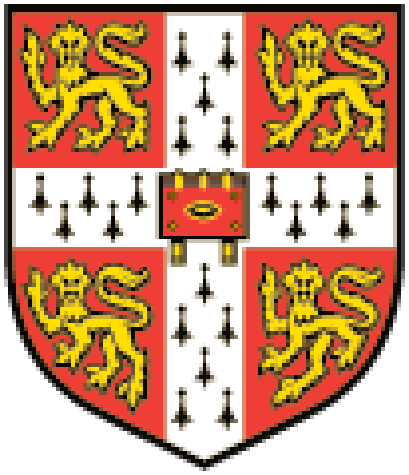

Jennifer Elaine Trendell

Corpus Christi College

Department of Pathology

The University of Cambridge

This dissertation is submitted for the degree of

Doctor of Philosophy

September 2019

DECLARATION

This dissertation is the result of my own work and includes nothing which is the outcome of work done in collaboration except as declared in the Preface and specified in the text.

It is not substantially the same as any that I have submitted, or, is being concurrently submitted for a degree or diploma or other qualification at the University of Cambridge or any other University or similar institution except as declared in the Preface and specified in the text. I further state that no substantial part of my dissertation has already been submitted, or, is being concurrently submitted for any such degree, diploma or other qualification at the University of Cambridge or any other University or similar institution except as declared in the Preface and specified in the text.

It does not exceed the prescribed word limit for the relevant Degree Committee.

Jennifer Trendell

September 2019

THESIS SUMMARY

Name: Jennifer Elaine Trendell

Thesis Title: Effects of Oncostatin-M Receptor overexpression on cervical squamous cell carcinoma cells and their extracellular vesicles

Cervical carcinoma remains the fourth most common cause of cancer in women worldwide. Cytological screening and introduction of prophylactic HPV vaccines have drastically decreased incidence rates in high income countries. However, it is still one of the leading causes of cancer morbidity in middle and low income countries and the prognosis for advanced or recurrent cervical carcinoma remains poor. Further research to enhance the current understanding of molecular aberrations driving cervical carcinoma is, therefore, vital in order to develop effective novel therapies.

The oncostatin-M receptor (OSMR) frequently undergoes copy-number gain and overexpression in squamous cell carcinomas (SCC) at multiple sites, consistently associated with an adverse overall survival independent of tumour stage. OSM-OSMR signalling activates STAT3 and MAP-kinase pathways and induces a pro-malignant phenotype including increased cell migration, invasion and angiogenesis. Bidirectional communication between cancer cells and cells of the tumour microenvironment (TME) is essential for tumour progression. There is mounting evidence to suggest that extracellular vesicles (EVs) are key mediators of intercellular communication and can promote tumour progression through various mechanisms.

The work presented in this PhD thesis aims to determine the effect of OSM-OSMR signalling on mRNA and miRNA expression in cervical SCC cells and their extracellular vesicles. Next generation sequencing (NGS) was used to investigate global changes in mRNA and miRNA expression. These experiments were performed using SW756 cells, a cervical SCC cell line with OSMR copy number gain and overexpression, and an OSMR knock down (KD) SW756 cell line generated by CRISPR-Cas9. OSM-OSMR signalling was found to be capable of modulating both cellular and EV mRNA expression. Treatment of SW756 cells with OSM resulted in significant ($p \leq 0.01$) upregulation of 225 (cell) and 88 (EV) mRNAs and downregulation of 98 (cell) and 202 (EV) mRNAs. Treatment of SW756 OSMR KD cells with OSM resulted in no significant changes in cellular or EV mRNA expression. Pathway analysis revealed that genes primarily involved in cytokine mediated signalling, hypoxia response, interferon response and negative regulation of viral lifecycle, myeloid leukocyte activation and angiogenesis were all upregulated in response to OSM, whereas, genes

involved in cell cycle regulation, cellular organisation and cell differentiation were downregulated. Effects of OSM-OSMR signalling on cellular and EV miRNA expression was found to be less pronounced.

The effect of OSM-OSMR signalling on tumour growth *in vivo* was also investigated. OSMR KD cells had a reduced growth rate following sub-cutaneous transplantation in NOD-SCID mice, compared with SW756 cells. Similarly, SW756 cells with constitutive-overexpression of OSM grew more quickly than SW756 *in vivo*. Together, this work indicates that OSM-OSMR signalling is an important driver of cervical SCC tumour progression both *in vitro* and *in vivo*, and demonstrates, for the first time, that OSM-OSMR signalling alters EV composition in cervical SCC cells. Subsequent work will focus on elucidating the functional importance of these EVs and their effects on cells of the TME.

ACKNOWLEDGEMENTS

I would firstly like to thank my supervisor, Professor Nicholas Coleman, for offering me the opportunity to undertake this PhD project and for all his support.

I am also very grateful for the support and friendship of all members of the Coleman laboratory, both past and present. In particular, I would like to acknowledge Dr Cinzia Scarpini, to whom I am indebted, for all her support over the duration of my PhD. I would like to thank her for her advice regarding interpretation of results and constructive input, both of which greatly assisted me in writing this PhD thesis. I would also like to say a big thank you to Dr Danita Pearson and Dawn Ward for sharing with me their technical expertise, assisting in experiments and being happy to help with any problem or question that I might have. Thank you also to Dr Stephen Smith for all his help with bioinformatics analysis. I would also like to acknowledge Dr Marta Paez Ribes for her help and guidance with animal experiments and scientific input during the first year of my PhD. I would also like to thank Dr Lorena Verduci and Dr Matthew Murray for being great colleagues and a pleasure to work alongside. I would like to extend a special thank you to the other PhD students in the lab who have shared this experience with me: Luz, Marta, Shivani and Valtteri. I have really appreciated all your support, help with experiments and most importantly, your friendship! Thanks also to Taylor for keeping me company (and most importantly keeping me sane!) during this challenging period as we wrote up our theses together.

I'm very grateful to Anton Enright and Stephanie Wenlock for their help with NGS and bioinformatics support. Thank you also to Carlos Passos Bastos for all his help and patience with Nanosight experiments.

I would like to say a huge thank you to all my Corpus friends, particularly Josca, Mikey, Patrick, Emma, Edward, Michael, Seba and Sarah for making my time in Cambridge such an enjoyable and memorable experience. I am immensely grateful for your support and encouragement; I definitely wouldn't have gotten through the last four years without you! Thank you also to all my friends from home, particularly Kat, for always being there whenever I needed you. Finally, I would like to say the biggest thank you of all to my family, in particular, Pauline, Duncan, my brother Connor, and my loving parents, Lynne and Jeff - for all their support and encouragement over the years. To my parents in particular: thank you for always being there for me, for believing in me and for helping me to have confidence in myself. I definitely would not have gotten to this point without you.

Table of Contents

Figure Summary

Table Summary

Supplementary Information Summary

1. INTRODUCTION

1.1 Cervical cancer incidence and subtypes

Cervical carcinoma is the fourth most commonly diagnosed cancer and the fourth leading cause of cancer mortality in women worldwide with an estimated 570,000 new cases and 311,000 deaths in 2018[1]. The distribution of cervical cancer is not uniform; incidence rates are highest in middle and low-income countries and almost 90% of the world's cervical cancer deaths occur in these regions[2]. The highest incidence and mortality rates are reported in Sub-Saharan Africa, Central and South America, and South-Eastern Asia[1] (Figure 1.1).

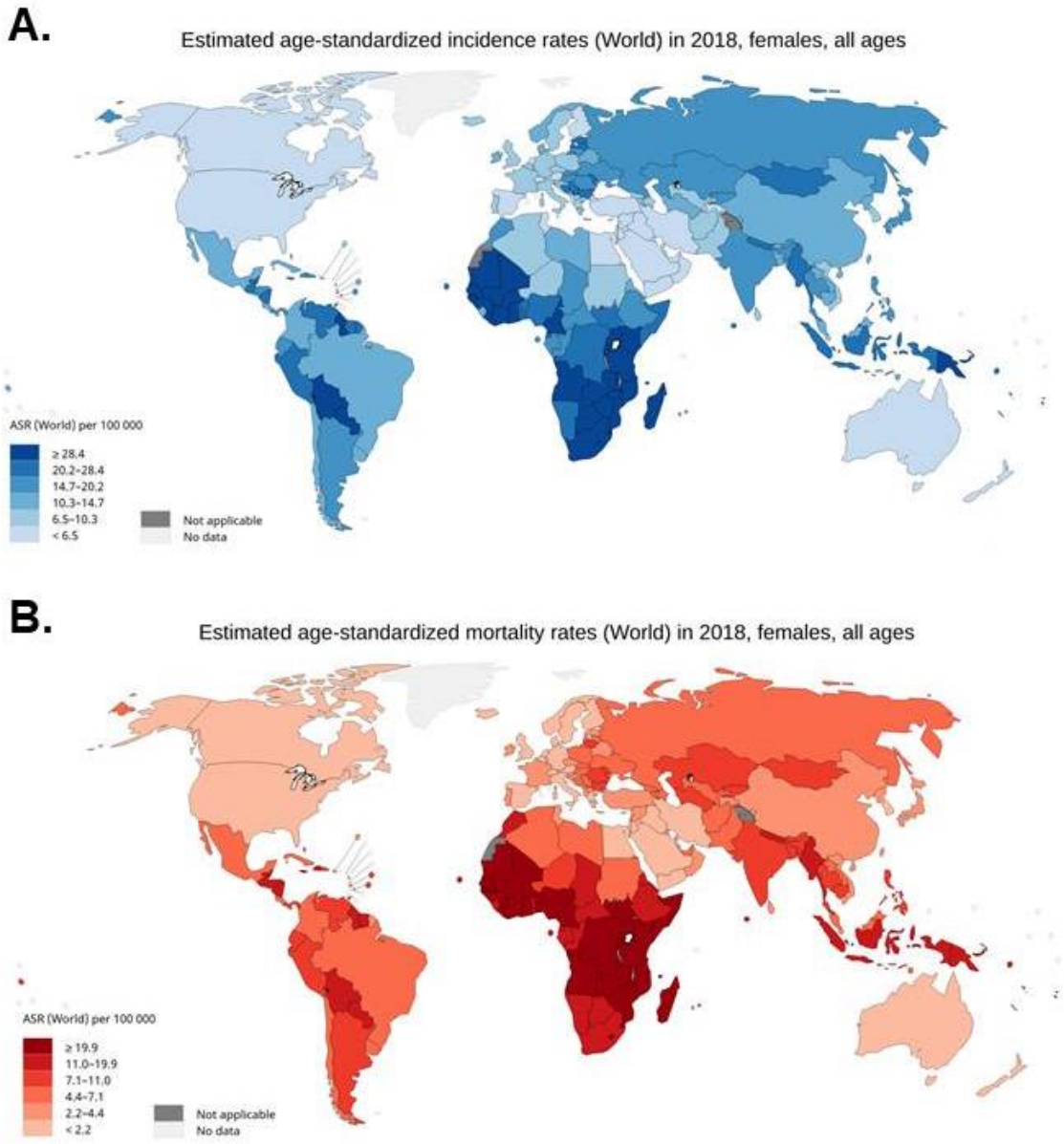

Figure 1.1: Cervical cancer incidence and mortality
Cervical cancer: estimated age-standardised A) incidence and B) mortality rates in women worldwide in 2018. **Data generated from https://gco.iarc.fr/today/online-analysis-map**

Cervical carcinomas are predominantly epithelial in origin and can be divided into three histological subtypes: squamous, adenocarcinoma or other (which include adenosquamous carcinoma, neuroendocrine tumours and undifferentiated carcinoma)[3]. Squamous cell carcinomas (SCCs) are the most predominant subtype, accounting for approximately 70-80% of all cervical carcinomas[3]. They most commonly arise in squamous epithelial cells located within the squamo-columnar junction where squamous cells of the ectocervix meet columnar epithelial cells of the endocervix[4]. Adenocarcinomas (AC) account for 20-25% of cervical carcinomas and arise in glandular cells of the endocervical canal[3,5]. Due to their location, adenocarcinomas are often diagnosed at a later stage than squamous cell carcinomas[5]. These two subtypes have been reported to differ in their risk factors[6], prognosis[7], incidence of metastasis[8] and sensitivity to radiotherapy treatment[9,10]. However, despite a drive for the development of new subtype-specific treatments, treatment recommendations remain predominantly the same for both cervical squamous cell carcinoma and adenocarcinoma[11].

1.2 Cervical SCC: from pre-cancerous lesions to malignancy

Persistent infection with human papillomavirus (HPV) has been established as a necessary initiating event in cervical carcinogenesis[12]. Less than 10% of invasive cervical carcinoma cases are defined as HPV negative; most of which are non SCCs[13,14]. It is believed that the majority of HPV-negative cervical carcinomas are attributable to false diagnosis, cancers associated with non high risk HPV subtypes or false negative results following HPV testing due to technical difficulties[13,14]. However, a small proportion of truly HPV negative cervical carcinomas have been reported[14,15]. It is estimated that 10.4% of women worldwide are carriers of cervical HPV DNA, this equates to 291 million women[16]. There are over 200 HPV subtypes[17], of which around 40 can infect the genital tract. These are denoted as low risk (LR) or high risk (HR) based on their oncogenic capacity[18]. Of the 15 HR-HPV subtypes (HPV 16, 18, 31, 33, 35, 39, 45, 51, 52, 56, 58, 59, 68, 73, and 82), HPV 16 and HPV18 are most frequently detected in cervical carcinomas[18]. HPV16 is the most common subtype detected in cervical squamous cell carcinomas whereas HPV18 is most frequently detected in cervical adenocarcinomas[18,19]. This thesis will focus on cervical squamous cell carcinomas.

Human papillomaviruses are small non-enveloped double-stranded DNA viruses[20]. The HPV genome can be divided into three domains: an early region, a late region and a long control region (LCR). The early region has seven open reading frames (ORFs) which encode eight proteins involved in viral gene expression and replication (E1-8) by alternate splicing[21]. The

late region contains two ORFs, L1 and L2, which encode capsid proteins. Finally, the LCR contains promoter sequences that direct transcription of both early and late genes and cis elements which regulate viral replication, gene expression and viral packaging[20,21].

Cervical SCCs develop from non-invasive precancerous lesions following persistent infection with oncogenic HR-HPV subtypes which infect undifferentiated basal epithelial cells; these are the only cells in the stratified cervical epithelium able to undergo active cell division[22]. Following entry into a cell, HPV genomes are established as extrachromosomal episomes in the host nucleus and replicate in synchrony with the host DNA, undergoing low-level amplification to approximately 100 copies per cell[23,24]. In these productive infections, expression of oncogenic viral E6 and E7 genes are tightly regulated by the viral E2 gene and high-level expression is only observed in post-mitotic suprabasal cells[25] where viral genomes are amplified prior to virion synthesis[26].

Cervical SCCs develop through a series of well-defined histological changes involving progression from low to high grade squamous intra-epithelial lesions (HSIL and LSIL, respectively ; Figure 1.2)[27–29]. HSILs confer a greater risk of progression to invasive disease and often demonstrate integration of the HPV genome into the host chromosomes[30]. Integration is not a normal part of the HR-HPV life cycle and represents an abortive infection in which viral gene expression becomes deregulated, and the normal life cycle of the virus cannot be completed[31]. Integration usually results in disruption or deletion of the E1 and/or E2 ORF, releasing E6 and E7 from transcriptional repression[30,32]. Not all cervical cancers arise from HPV integration. However, when integration does not occur, there are often genetic or epigenetic changes within the regulatory regions of E6 and E7[33], indicating that dysregulation of E6 and E7 is crucial for tumorigenesis[17].

A key feature of cervical SCC is genomic instability, caused by dysregulated expression of HR-HPV E6 and E7 in proliferating epithelial cells[34]. The E7 protein binds to and degrades the retinoblastoma (RB) tumour suppressor protein, releasing the transcription factor E2F from transcriptional repression. HPV viruses are replicated in differentiated epithelial cells that are growth arrested and thereby unable to support DNA synthesis[20]. E2F transactivates genes required for DNA replication, such as cyclins A and E, thereby reactivating cellular DNA synthesis by host cells, creating an environment that is permissive for viral DNA replication[35]. E2F also activates the tumour suppressor p53, inducing p53-mediated apoptosis[36]. The most well-documented function of the E6 protein is its role in degradation of p53, thus preventing the induction of growth arrest and apoptosis in response to E7 mediated activation of the cell cycle[17,37]. In addition, E7 has been shown to induce

centrosome abnormalities[38] and may function as a mitotic mutagen, increasing the chance of errors during each round of cell division[39].

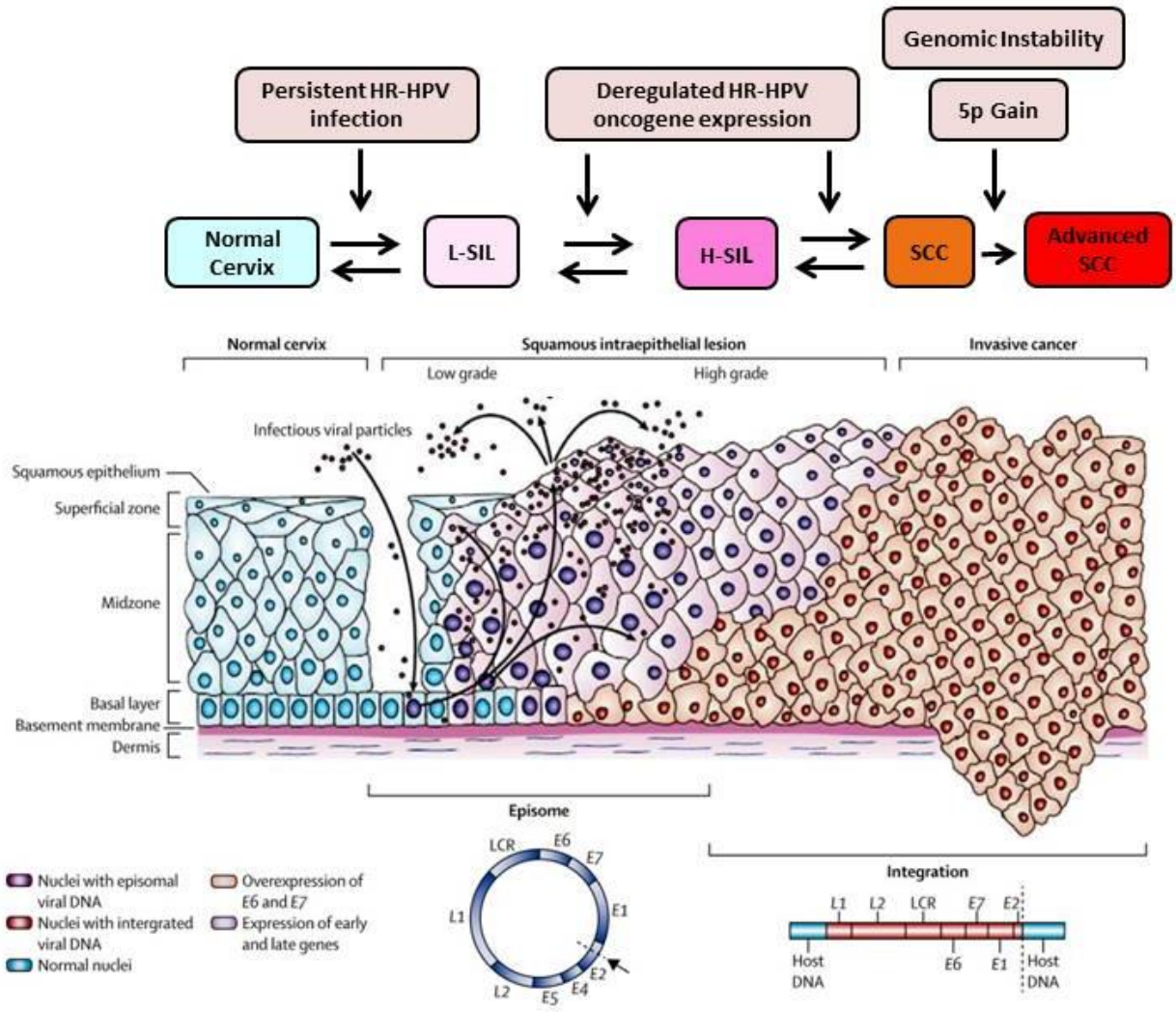

Figure 1.2: HPV mediated progression of cervical cancer
Illustration of the histological changes involved in transformation of normal cervix to invasive cancer. **Adapted from Woodman et al (2007)**[27]

While infection with HR-HPV is a necessary step in cervical carcinogenesis, infection alone is not sufficient for progression to malignancy. The majority of HR-HPV infections spontaneously resolve and both LSILs and HSILs can regress[40,41]. While the mechanism for this is poorly understood, it has been attributed to the development of HPV antigen specific immune response[42]. Only a small minority of women infected with HR-HPV will ultimately develop cervical carcinoma, usually many years after initial infection[43]. The continuous stimulation of cell proliferation and loss of the p53-mediated DNA damage response (as a result of deregulated E7 and E6 expression, respectively) promotes the accumulation of secondary mutations in the host chromosomes that eventually lead to cancer[31].

1.3 Cervical cancer screening

Population-based screening programmes have reduced cervical cancer incidence and mortality in high income countries by up to 80% over the last 5 decades[44]. This was initially performed by conventional cytology, also known as the Papanicolaou (Pap) smear test. This involves collection of exfoliated epithelial cells from the outer opening of the cervix which are then directly smeared onto a glass slide. Slides are then fixed, stained and examined by a pathologist for presence of abnormal cells[45]. This was later replaced by liquid based cytology which was shown to produce fewer false negatives than conventional cytology and to reduce the number of unsatisfactory tests[46,47]. Collected cells are directly placed into fixative and processed to remove blood, mucus and inflammatory cells. The processing and distribution of cells onto slides is automated and results in a homogenous monolayer of cells[45].

Recently, several countries have moved to HPV testing as the primary method of population-based screening for cervical cancer[48]. HPV testing has been shown to have superior sensitivity for the detection of both pre-cancerous disease and cervical cancer compared to cytology, providing a 60-70% increase in protection against the development of invasive cervical carcinoma. Increased sensitivity also allows for increased screening intervals[49–51]. Following screening, women with positive cytology or HPV tests are investigated by colposcopy and directed biopsies. HSIL are treated by loop electrosurgical excision procedure (LEEP) or laser excision[52].

While screening has led to a dramatic reduction in cervical cancer incidence and mortality in high income countries, implementation of screening programmes has not been successful in low and middle income countries. This is due to logistical obstacles in health systems and lack of infrastructure and funding to support national screening programmes[2]. As such, there has in fact been a rapid increase in cervical cancer incidence and mortality in these regions in recent generations. This is most likely due to increased risk factors such as changing sexual practices, increased smoking and increased HIV incidence[1,2,44].

1.4 Prophylactic HPV vaccine

The introduction of the prophylactic vaccination for HR-HPV subtypes is expected to further decrease cervical cancer incidence and mortality. Three prophylactic HPV vaccines are currently available: Cervarix, Gardasil and Gardasil 9. All three vaccines protect against HPV 16 and 18. Both Gardasil and Gardasil 9 also protect against HPV 6 and 11; LR-HPVs which cause genital warts. Moreover, Gardasil 9 protects against 5 additional HR-HPV subtypes: HPV 31, 33, 45, 52 and 58[53,54]. HPV vaccines that are currently available are preventive in

nature and are based on the discovery that the HPV L1 capsid protein has the capacity to assemble into virus-like particles (VLP) that are indistinguishable from the outer shell of authentic virions, but lack the encapsulated HPV viral genome[55]. Like authentic virions, they induce high titres of serum antibodies capable of neutralising HPV, without being infectious or oncogenic[55]. Denatured L1 does not induce neutralising antibodies[3] and, therefore, the HPV vaccines are comprised of highly purified HPV L1 derived VLPs for different HPV subtypes together with an adjuvant designed to further stimulate the immune response[56,57].

Gardasil was the first HPV vaccine to be licensed in 2006, followed by Cervarix in 2007 and Gardasil 9 in 2014. Since then, multiple high income countries have implemented vaccination programmes for girls generally aged from 9 to 12 years old and, more recently, for boys as well, leading to dramatic reductions in pre-cancerous disease[54,58,59]. In 2014, the World Health Organization (WHO) endorsed the use of a two-dose schedule instead of the previously used three-dose schedule. This reduced delivery costs while maintaining high immunogenic protection[57]. However, similar to cervical screening programmes, vast disparities exist in the global implementation of HPV vaccination programmes. In 2016, 71% of high income countries had introduced the vaccine compared to 35% of upper middle income, 8% of lower middle income and 6% of low income countries[60]. The average price of HPV vaccines has dropped substantially since they were first introduced. In Europe, the price of the first-generation Gardasil vaccine has decreased from an average of €101.80 per dose in 2007 to €28.40 in 2017, while, the average price of Gardasil 9 in 2016–2017 was €49.10 per dose[61].

While there was indication of a tiered-pricing strategy, whereby vaccine manufacturers charge more per dose from wealthier countries than poorer countries, vaccine prices still prohibit the implementation of vaccination programmes in many low to middle income countries[61]. The importance of affordability is demonstrated by the fact that nearly 50% of middle income countries that have introduced HPV vaccination programmes over the last 5 years are located within the Americas region. This is the result of the Pan American Health Organisation (PAHO) Revolving Fund, which recently secured a reduced price for HPV vaccines, thus facilitating bulk purchases at discounted prices for participating countries[57]. However, in the coming years, it is likely that considerably more low income countries will introduce national vaccination programmes as the HPV vaccine has recently been added to the Global Alliance for Vaccines and Immunisations (GAVI) portfolio[57]. This allows low income countries to apply for support to implement pilot or national vaccination programmes. To date, 23 countries have been approved for this pathway, 19 of which are in Africa[57,62].

1.5 Current treatments for cervical cancer

Despite promising steps towards increased global uptake of HPV vaccination programmes, HPV vaccines are prophylactic and do not treat existing HPV infections[53]. In the UK, only women born after 1991 will have been eligible for vaccination[58]. Therefore, availability of effective treatment regimes for cervical carcinoma remains essential. Like most cancers, the stage at diagnosis is one of the most significant prognostic factors. The International Federation of Gynecology and Obstetrics (FIGO) staging for cervical cancer[63] is summarised in Table 1.1.

Table 1.1: FIGO staging for cervical carcinoma.
Adapted from Bhatla *et al* (2019)[63]

STAGE	DESCRIPTION
Stage I	**Carcinoma is strictly confined to the cervix uteri**
IA	Invasive carcinoma that can be diagnosed only by microscopy, with maximum depth of invasion <5mm
IB	Invasive carcinoma with measured deepest invasion ≥5 mm (greater than stage IA), lesion limited to the cervix uteri
Stage II	**Carcinoma invades beyond the uterus, but has not extended onto the lower third of the vagina or to the pelvic wall**
IIA	Involvement limited to the upper two-thirds of the vagina without para-metrial involvement
IIB	With para-metrial involvement but not up to the pelvic wall
Stage III	**Carcinoma involves the lower third of the vagina and/or extends to the pelvic wall and/or causes hydronephrosis or non-functioning kidney and/or involves pelvic and/or para-aortic lymph nodes**
IIIA	Carcinoma involves the lower third of the vagina, with no extension to the pelvic wall
IIIB	Extension to the pelvic wall and/or hydronephrosis or non-functioning kidney (unless known to be due to another cause)
IIIC	Involvement of pelvic and/or para-aortic lymph nodes, irrespective of tumour size and extent
Stage IV:	**Carcinoma has extended beyond the true pelvis or has involved the mucosa of the bladder or rectum**
IVA	Spread of the growth to adjacent organs
IVB	Spread to distant organs

Patients diagnosed with localised early invasive disease (stage IA- IIA) have a 91.8% five-year relative survival rate[64]. The primary treatment of early-stage cervical cancer is either surgery or radiotherapy[11]. The type of surgery is determined by stage and whether fertility preservation is required. Patients with stage IA disease are treated by conisation or trachelectomy with or without pelvic lymph node dissection. A hysterectomy may also be performed if fertility preservation is not required[11]. For patients with IB and IIA disease, standard treatment involves radical hysterectomy with bilateral lymph node dissection[3]. These patients may also receive concurrent chemoradiation[11,65]. Women presenting with

locally advanced disease (stage IIB – IVA)[11] have a 56.3% five year relative survival rate[64]. Standard of care for locally advanced disease involves radiotherapy with concurrent adjuvant platinum based chemotherapy, preferably using cisplatin[65,66]. For patients without nodal disease, or with disease limited to the pelvis, radiotherapy will consist of external beam radiation therapy (EBRT) and brachytherapy[11]. Patients with positive para-aortic and pelvic lymph nodes will also receive extended field EBRT to also target the lymph nodes[11,65]. However, 25% to 40% of patients with locally advanced disease will relapse[66,67]. The outcome for women diagnosed with metastatic or recurrent cervical cancer is poor, with little improvement in survival outcomes over the last three decades[67]. Women presenting with distant metastasis (stage IVB) have a 16.9% five year relative survival rate[64]. The current standard of care for these patients involves chemotherapy with cisplatin and paclitaxel[68]. The recent addition of bevacizumab, a monoclonal antibody that inhibits angiogenesis by binding to vascular endothelial growth factor A (VEGFA), has increased overall survival from 13.3 to 16.8 months[69]. While modest, this increase represents the most promising improvement in advanced and metastatic cervical cancer outcomes in recent years. There is, therefore, an urgent need for the development of new targeted therapies for the treatment of cervical carcinoma.

Currently, a number of targeted agents have entered clinical trials for the treatment of cervical carcinoma. These include: vascular endothelial growth factor receptor (VEGFR) inhibitors, immune checkpoint inhibitors using antibodies targeting programmed cell death (PD-1) or cytotoxic T-lymphocyte-associated antigen 4 (CTLA4), poly ADP-ribose polymerase (PARP) inhibitors which prevent DNA repair and therapeutic vaccines targeting HPV E7[67]. Further research to enhance the current understanding of molecular aberrations driving cervical carcinoma is vital in order to develop effective new therapies.

1.6 OSMR

A key feature of advanced cervical SCC is genomic instability, driven by dysregulated expression of HR-HPV E6 and E7[34]. The most frequent genomic imbalance in cervical carcinoma involves copy number gain and amplification of the short arm of chromosome 5 (5p)[70,71]. Previous work in our[70] own and other laboratories[71,72] has identified candidate genes located within this region that show a significant association between gene copy number and mRNA expression levels. Initial work by Ng *et al* (2007)[70] first identified the potential oncogenic role for Oncostatin M receptor (OSMR) in cervical SCC. Both cervical SCC cell lines and tissue samples derived from patients with LSILs, HSILs or advanced SCC were screened by array comparative genomic hybridisation (CGH). The most commonly

occurring regions that displayed both copy number and amplification in both cell lines and SCC samples were 5p15.2–14.3, 5p13.3, and 5p13.2–13.1[70].

Three candidate oncogenes at these loci: OSMR (5p13.1), PDZ domain containing protein 3 (PDZK3; 5p13.3) and triple functional domain (TRIO; 5p15.2–5p14.3), were identified as having expression levels that significantly correlated with gene copy number. Gain of OSMR, PDZK3, and TRIO were detected in 60.9%, 57.3%, and 54.5% of cervical SCC tumours, respectively. While copy number gain of both OSMR and PDZK3 were each associated with adverse overall patient survival, only gain of OSMR was found to adversely influence overall patient survival independent of tumour stage[70]. Relative risk of death was 3.6 times greater for patients with OSMR copy number gain than those without. Moreover, OSMR overexpression was also found to be associated with adverse overall survival in analysis of cervical SCC samples using The Cancer Genome Atlas (TCGA) data[73] (Figure 1.3). OSMR was not found to undergo copy number gain or overexpression in either LSILs or HSILs indicating that acquisition of OSMR gain and overexpression occurs relatively late in the progression of cervical SCC[70].

OSMR is a cell surface cytokine receptor which associates with gp130 to form the high affinity receptor for its principal ligand, oncostatin M (OSM). OSM is a glycoprotein belonging to the interleukin-6 (IL-6) family of inflammatory cytokines which include: IL-6, IL-11, IL-27, IL-35, IL-39, leukaemia inhibitory factor (LIF), cardiotrophin-1 (CT-1), cardiotrophin-like cytokine factor 1 (CLCF1), and ciliary neurotrophic factor (CNTF)[74]. Of these family members, OSM shares many structural and biological properties with LIF. Moreover, the genes encoding these two cytokines are located less than 20kb apart on chromosome 22q12, suggesting that these two genes may have evolved by gene duplication[75].

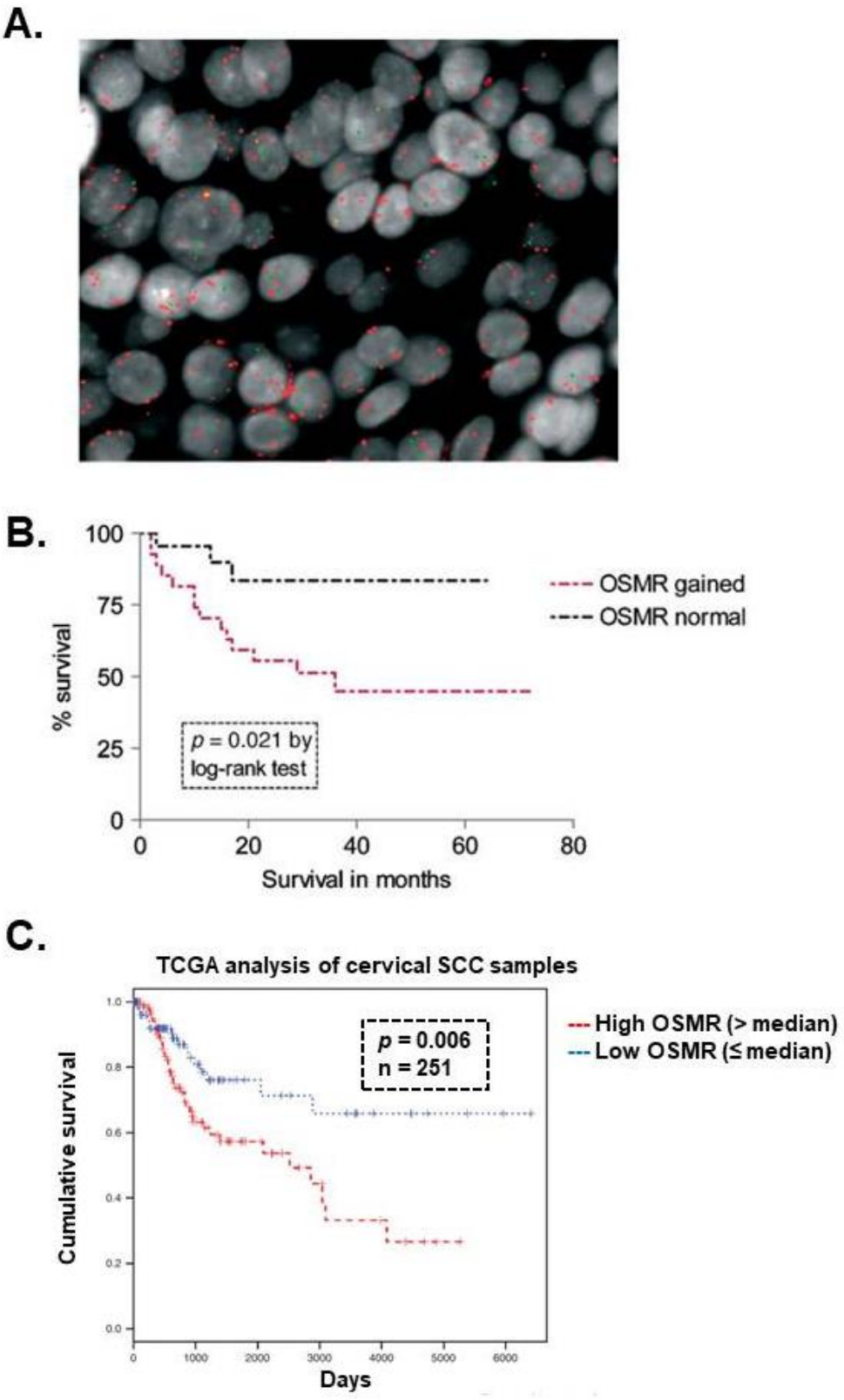

Figure 1.3: Effect of OSMR copy number gain and overexpression on patient survival
A) Tissue microarray fluorescence in situ hybridization of a representative primary cervical SCC sample displaying gain of OSMR in interphase nuclei. Red = multiple copies of overlapping BAC clones located within OSMR. Green = chromosome 5 centromeric BAC control clones (B) Correlations between copy number gain of OSMR and clinical outcome in cases of cervical SCC. C) Kaplan–Meier curves showing overall survival for cervical SCCs with high vs low expression of OSMR, as determined from TCGA analysis.
Figures adapted from Ng *et al* (2007; A+B)[70] and Kucia-Tran *et al* (2016; C)[73].

1.7 OSMR and IL6 cytokine family receptor signalling

While each of the IL-6 family cytokines signals through a distinct receptor, they all utilise a common glycoprotein 130 (gp130) subunit in their receptor complexes, which is critical for signal transduction[76]. Common signalling through gp130, in concert with their individual cytokine receptor subunits, means that IL-6 family members have both overlapping and unique functions[77]. IL-6 cytokines bind to their respective receptors with low affinity and subsequently associate with gp130 to form a high affinity signal transducing hetero dimeric or trimeric receptor complex[74,78]. IL6 cytokine-receptor complexes are depicted in Figure 1.4.

OSM and IL-35 are the only members of this group capable of binding directly to gp130[78–81]. OSM binds with low affinity to gp130 and subsequently recruits either LIFR or OSMR to form either type I or type II OSM receptor complexes, respectively[78,80,81] (Figure 1.4). OSM-gp130 complexes bind to OSMR with higher affinity than LIFR[80]. The ability of OSM to bind gp130 has been attributed to the presence of a unique α-helical loop between its B and C helixes, a structure which is absent in other IL-6 cytokines[80]. Whilst not a member of the IL-6 family, IL-31 is also able to bind OSMR and signals through a heterodimeric receptor composed of OSMR and IL-31 receptor alpha (IL-31RA), in the absence of gp130[82].

IL-6 cytokine-receptor complexes transduce intracellular signals via activation of the JAK/STAT (janus kinase/ signal transducer and activator of transcription) pathway. Receptor associated JAKs phosphorylate tyrosine residues in the cytoplasmic domains of receptor subunits (both gp130 and its co-receptors)[76,83,84]. This leads to the activation of several downstream signalling pathways including: STAT proteins, MAPK (mitogen-activated protein kinase), PI3K/AKT (phosphoinositide 3-kinase/ AKT) and SRC/YAP/NOTCH signalling cascades[76,83,84]. Whilst all IL-6 family members share common signal transduction pathways[84], the degree to which specific pathways are activated can differ depending on the cytokine, cell type and physiological setting[83].

OSMR has been shown to be a stronger activator of the MAPK pathway than IL-6 or LIF. This is due to exclusive recruitment of the adaptor protein SHC by OSMR, as opposed to gp130 mediated recruitment of SHP-2 by other IL6 family receptor complexes, which subsequently drives MAPK pathway activation[85]. OSMR has also been demonstrated to be one of the strongest inducers of the JAK/STAT pathway[86]. OSM-OSMR receptor binding leads to phosphorylation of STAT1, STAT3, STAT5B and STAT6[87]. Potent phosphorylation of STAT5B is unique to OSM, which is attributable to the presence of a STAT5B recruiting tyrosine motif on the OSM receptor[88,89]. Similarly, activation of STAT6 has not been observed for any of the other IL6 cytokines; the mechanisms driving OSM induced STAT6

activation remain to be fully elucidated[87]. Following phosphorylation, STATs dimerise and translocate to the nucleus where they bind to STAT specific DNA response elements of target genes, modulating gene expression[90].

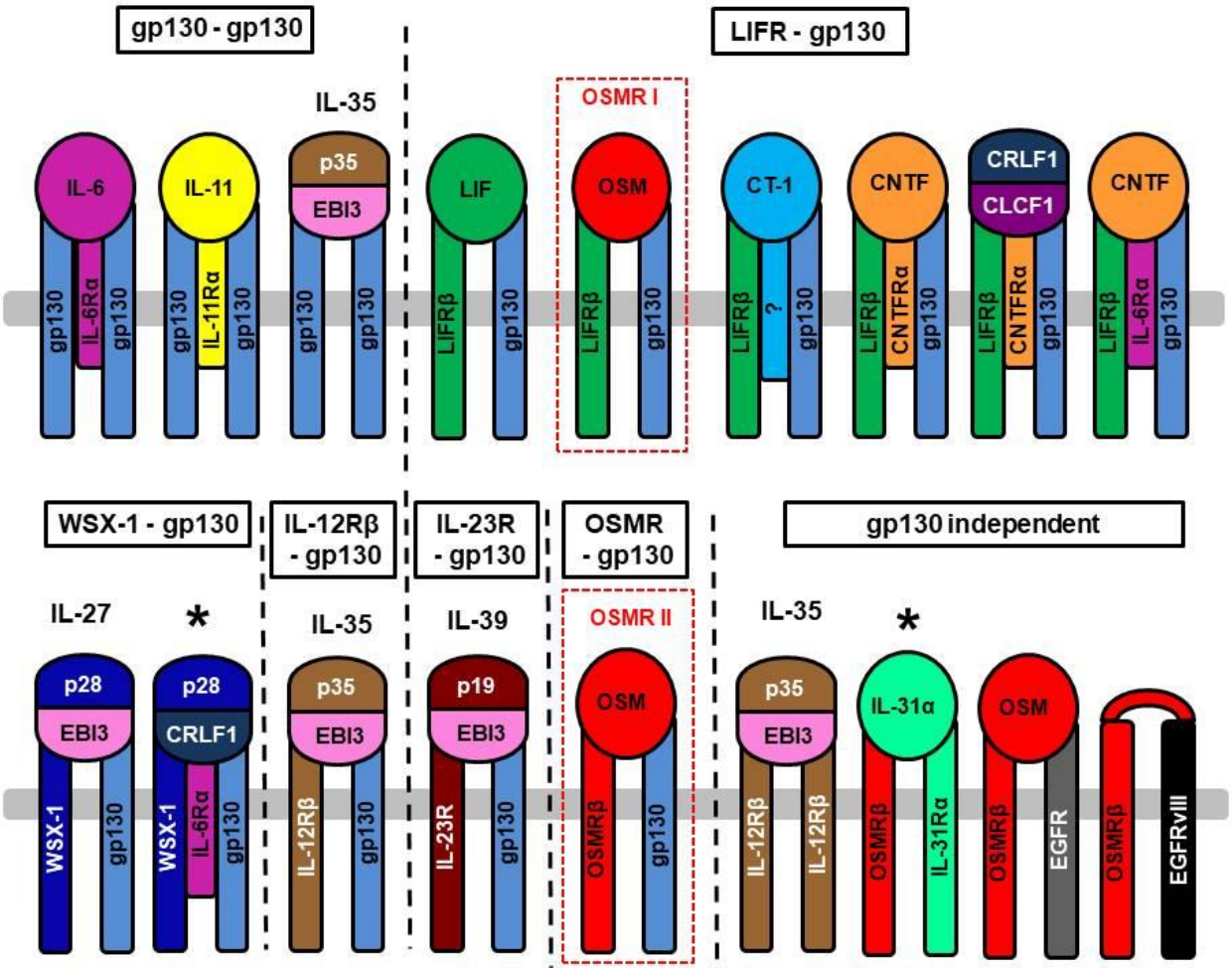

Figure 1.4: IL-6 family cytokine-receptor complexes

The gp130 signal transducing subunit is shared by all ten IL-6 family members: IL-6, IL-11, IL-27, IL-35, IL-39, LIF, CT-1, CLCF1 and CNTF. These cytokines signal through gp-130 homodimers (with or without an additional receptor) or receptor complexes comprised of gp130 and either LIFR, WSX-1, IL-12Rβ, IL-23R or OSMR (either as heterodimeric complexes or as heterotrimeric complexes with addition of a third receptor). IL-27, IL-35 and IL-39 are heterodimeric glycoproteins composed of disulfide-linked α (p28, p35 or p19, respectively) and β (EBI3) chains. CLCF1 forms a complex with the CRLF1 chaperone protein prior to receptor binding. The IL-27 α chain (p28) is also able to bind to CRLF1 and signal through a WSX-1, IL-6Rα and gp130 receptor complex. LIFR-gp130 = type I OSM receptor; OSMR-gp130 = type II OSM receptor. Additionally, IL-35 is able to signal in a gp130 independent manner through the IL-12Rβ homodimer receptor complex. IL-31α is also able to signal through OSMR using an OSMR-IL-31Rα receptor complex. OSMR has also been shown to form heterodimeric receptor complexes with EGFR in the presence of OSM (gp130 independent) and with the mutated EGF receptor, EGFRvIII, in glioblastoma. OSMR-EGFRvIII complexes do not require a ligand for receptor activation. * = not a member of IL-6 cytokine family.

In addition to the receptor complexes previously described, OSMR was recently shown to form a co-receptor with epidermal growth factor receptor (EGFR) in glioblastoma leading to enhanced STAT3 activation (Figure 1.4); this interaction was stimulated by OSM but not EGF[91]. Moreover, OSMR was found to act as an essential co-receptor for the constitutively active EGFR mutant receptor, EGFRvIII. EGFRvIII-OSMR complexes activated STAT3 in the absence of ligand binding. OSMR was shown to be a direct transcriptional target of STAT3 in glioblastoma; OSMR-EGFRvIII signalling therefore upregulated expression of OSMR in a feed-forward loop, driving glioblastoma tumour growth[91]. Recent work in our laboratory has confirmed that OSMR is also a direct target of STAT3 in cervical SCC. OSM-OSMR signalling led to STAT3 activation and subsequent upregulation of both OSM and OSMR signalling, in a feed-forward loop[92]. Whether this pathway is also mediated by EGFRvIII in cervical SCC cells is still to be investigated.

1.8 Investigation of OSM-OSMR signalling *in vivo*

Investigation of OSM-OSMR signalling *in vivo* using mouse models has been complicated by the finding that OSM-OSMR binding is species-specific. As previously discussed, human OSM (hOSM) has been shown to bind both human LIFR (hLIFR)-gp130 and human OSMR (hOSMR)-gp130 heterodimers with high affinity, forming OSMR I and OSMR II complexes, respectively[78,80,81]. However, in the murine system, mouse OSM (mOSM) has been shown to predominantly signal via the OSMR II receptor complex; mOSM only binds the murine OSMR (mOSMR)-gp130 heterodimer with high affinity, whereas mOSM binds to mouse LIFR (mLIFR)-gp130 heterodimers with very low affinity[93] (Figure 1.5). Moreover, when mOSM binds to mLIFR-gp130, different signal transduction cascades occur compared to binding of mouse LIF (mLIF). mLIF-mLIFR binding leads to phosphorylation of STAT1 and STAT3 and activation of their respective target genes, whereas mOSM-mLIFR binding only leads to phosphorylation of STAT1[94].

Human OSM is able to signal via mLIFR, activating STAT1 and STAT3 akin to mLIF[94]. However, it is unable to signal via mOSMR[93,95] (Figure 1.5). Human LIF is also capable of signalling through the mLIFR[96]. Conversely, neither mOSM or mLIF display cross-species reactivity; neither is able to activate signalling via either hOSMR or hLIFR[96,97] (Figure 1.5). Individual amino acids within the AB loop of mOSM and hOSM have been demonstrated to be responsible for species-specific receptor activation[97]. The presence of Lys-44 within the hOSM AB loop appeared to prevent mOSMR activation[97]. Similarly, the presence of residues Asn-37, Thr-40 and Asp-42 within the AB loop in mOSM were shown to be responsible for the lack of affinity of mOSM toward mLIFR, hLIFR and hOSMR[97]. In particular, the Asn37

residue replaces a Gly residue that was found to be conserved in both hOSM and hLIFR. This Gly residue has been shown to be essential for hOSMR activity, therefore, substitution may result in alteration of the secondary structure of the mOSM AB loop preventing receptor binding[97].

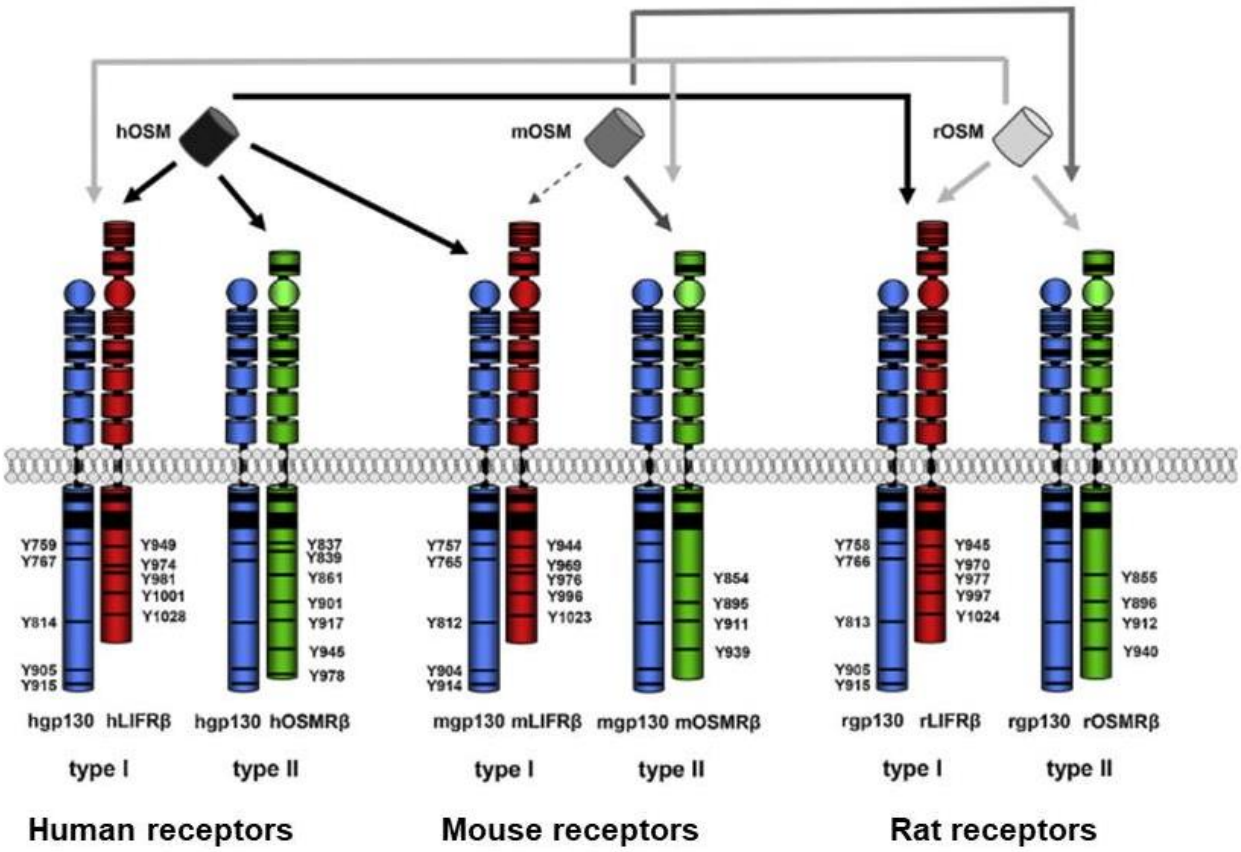

Figure 1.5: Receptor usage and cross-species reactivity for human, murine and rat OSM

Receptor usage and cross-species reactivity of human, murine and rat OSM (hOSM, mOSM and rOSM, respectively) is shown. Receptors are colour coded as follow: blue=gp130, red= LIFRβ, green=OSMRβ. Dotted arrow represents low affinity binding, Cylinders depict fibronectin-type III domains, circles the Ig-like domain. The location of tyrosine motifs in the intracellular regions are shown. **Adapted from Hermanns (2015)**[87]

Interestingly, rat OSM (rOSM) has been shown to bind to both rat LIFR (rLIFR) and rat OSMR (rOSMR) with high affinity, forming both type I and type II receptor complexes comparable to the human system[98]. Thus, rOSM appears to be more homologous to hOSM than to mOSM. This was an unexpected finding as rOSM and mOSM share 60% sequence identity while rOSM and hOSM only share 49% sequence identity[98]. Furthermore, rOSM was found to be able to signal through hLIFR but not hOSMR and, conversely, through mOSMR but not mLIFR[98]. Similar to the cross reactivity of hOSM with murine receptors, hOSM was

shown to activate rLIFR but not rOSMR. Murine OSM was able to activate rOSMR but not rLIFR[87, 98] (Figure 1.5).

1.9 Roles of OSM and OSMR in cancer

OSM is a pleiotropic cytokine which has been shown to have different roles in multiple cell types, both in tissue homeostasis and disease. It is known to contribute to liver regeneration, bone metabolism, haematopoiesis, metabolism, homeostasis of the central nervous system and modulation of the innate immune system in response to infection[77,84,87,99]. Moreover, it has also been shown to play a role in cardiovascular disease, conditions involving chronic inflammation (such as rheumatoid arthritis, atherosclerosis, and inflammatory lung and skin conditions), tissue fibrosis and cancer[77,84,87,100].

OSM is mainly secreted by leucocytes including activated T lymphocytes, neutrophils, dendritic cells, monocytes, macrophages, eosinophils and mast cells[83,101–103]. Whereas, OSMR is expressed by a wide array of non-haematopoietic cells types including endothelial cells, hepatic cells, leucocytes, epithelial cells, fibroblasts, glial cells, neurons, smooth muscle cells, mesothelial cells, osteoblasts, adipocytes and many tumour cell types[83,100,101,104]. In the context of cervical SCC, OSMR was found to be almost exclusively expressed by tumour cells, while OSM is expressed by infiltrating immune cells[73], indicating that OSM-OSMR signalling involves interaction of tumour cells with cells of the tumour microenvironment (TME).

In the cancer setting, the role of OSM-OSMR signalling appears to be context and cell type dependent. OSM has been shown to function as a tumour-suppressor, exerting an anti-proliferative effect on melanoma[105], lung adenocarcinoma[106], neuroblastoma[107], glioblastoma[108] and select breast cancer cell lines[109,110]. Conversely, OSM has also been implicated in cancer progression. OSM is elevated in a range of tumours, and has been shown to act as tumour promotor in cervical SCC[73], skin SCC[111], breast cancer[112–114], prostate cancer[115], ovarian cancer[116], endometrial cancer[117] and Ewing sarcoma[118] by promoting tumour cell growth, migration, invasion, epithelial-mesenchymal transition (EMT), angiogenesis and/or metastasis. Moreover, OSM has been shown to be elevated in the serum of colon cancer patients, and has been implicated as a possible biomarker for diagnosis of this disease due to correlation of OSM levels with clinical stage[119]. In addition, it has been demonstrated that OSMR overexpression in breast cancer is associated with a pro-malignant phenotype, increased risk of tumour recurrence and reduced overall

survival[120]. OSMR has also been shown to play a role in glioblastoma progression acting as a co-receptor for EGFRvIII driving tumour growth independent of OSM[91].

1.10 OSM-OSMR signalling in cervical SCC

Overexpression of OSMR was found to enhance the sensitivity of cervical SCCs to OSM, *in vitro*[121]. OSM treatment was demonstrated to induce transcription of the pro-angiogenic factors VEGFA and inhibitor of DNA binding protein 1 (ID-1) in OSMR over expressing cervical SCC cell lines[70,121]. Conditioned media from OSM stimulated cervical SCC cells was shown to induce angiogenesis in an endothelial-fibroblast co-culture system[121]. Depletion of OSMR by small interfering RNA (siRNA) or treatment with neutralising antibodies against either OSM or VEGFA were found to abrogate induction of angiogenesis[92,121]. This demonstrates that induction of VEGFA by cervical SCC cells is the principal mechanism by which OSM-OSMR signalling promotes angiogenesis in this system (Figure 1.6).

Moreover, OSM-OSMR signalling was found to result in increased cervical SCC cell migration and invasion *in vitro*[121]. Tissue transglutaminase (TGM2) was identified as an essential mediator of this process, and was found to be upregulated in response to OSM treatment in OSMR over expressing cervical SCC cell lines[122]. OSM induced TGM2 localised to the cell surface where it interacted with integrin-α5β1 and fibronectin to promote cell migration and invasion through an extracellular matrix (ECM) *in vitro*[122] (Figure 1.6). All members of the TGM2–integrin-α5β1–fibronectin pathway are upregulated in cervical SCC cells, moreover, their expression correlates with disease progression and OSMR levels in samples from patients with cervical SCC[122].

Additionally, Kucia-Tran *et al* (2016) demonstrated that OSM stimulation of OSMR over-expressing cervical SCC cells leads to increased metastatic ability *in vivo* involving induction of EMT like changes[73]. EMT is characterised by down-regulation of epithelial genes (particularly the cell-cell adhesion protein, E-cadherin) and up-regulation of mesenchymal markers (including N-cadherin, vimentin, fibronectin and EMT associated transcription factors)[123]. This leads to loss of epithelial characteristics (such as cell-cell adhesion, cell-ECM adhesion and apical-basal polarity) and increased mesenchymal traits (such as increased motility, and increased migratory and invasive capacity)[124,125]. EMT plays a central role in development and has also been shown to be critical for tumour progression. EMT enables cancer cells to acquire abilities required for the following metastatic processes: dissociation from the primary tumour, degradation and invasion of the local ECM, intravasation (invasion of endothelial cell lining of blood vessels enabling entry into the

circulation) and extravasation from blood vessels into target organs[126,127]. A complex network of multiple signalling cascades induce and regulate EMT, including signalling induced by: tumour growth factor β (TGF β), EGFR, fibroblast growth factor (FGF), bone morphogenic proteins (BMPs), hepatocyte growth factor (HGF), Wnt/β-catenin, and Notch pathways[123,126]. These signalling cascades induce common EMT-associated transcription factors including SNAI1, SNAI2 (also known as SLUG), TWIST, ZEB1 and ZEB2[128–130].

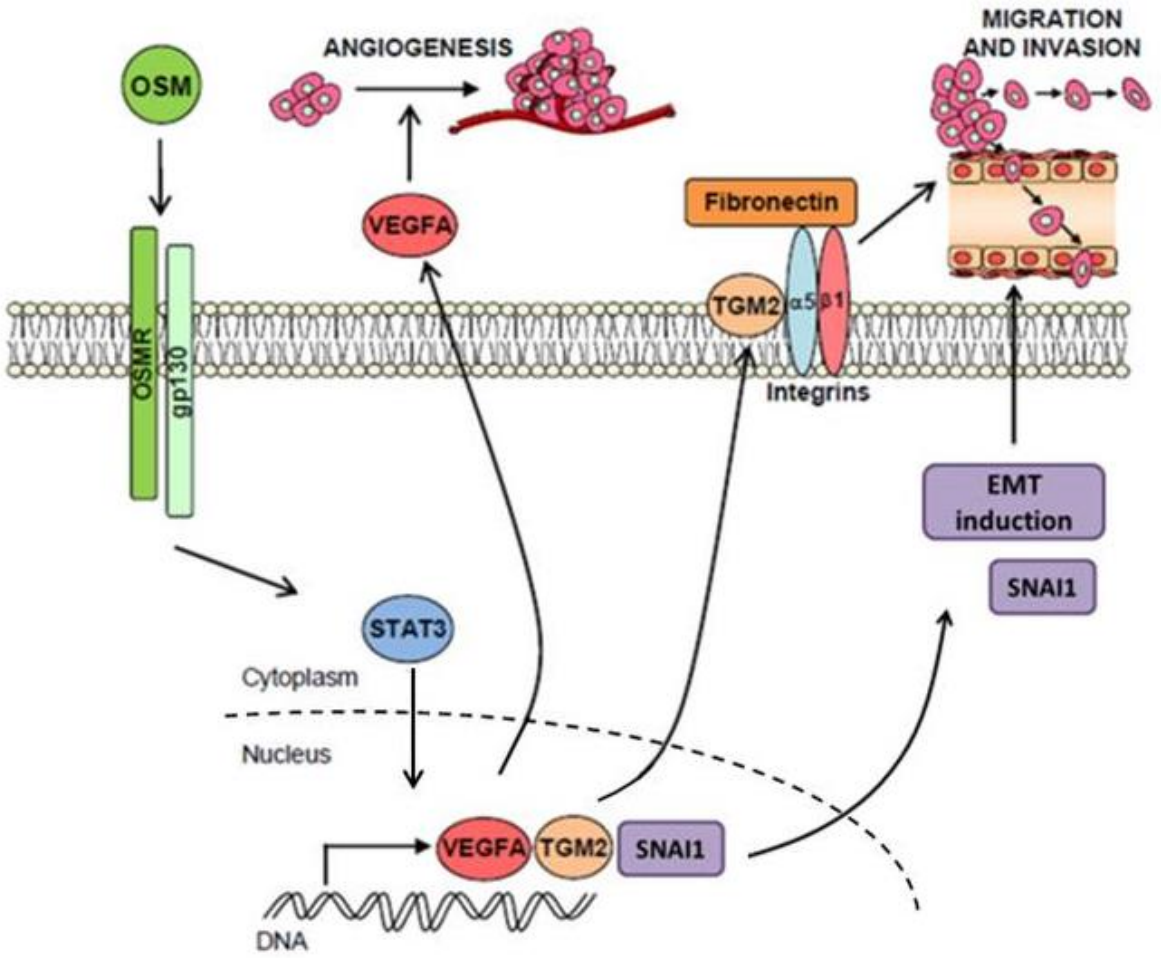

Figure 1.6: Pro-malignant effects of OSM-OSMR signalling in cervical SCC cells
OSM-OSMR binding results in activation of STAT3 and MAPK pathways leading to increased transcription of target genes including VEGFA, TGM2 and SNAI1 which contribute to increased angiogenesis, cell migration and invasion, and EMT, respectively. **Adapted from Caffarel and Coleman (2014)[131].**

TCGA analysis of cervical SCC patient samples revealed a significant positive correlation between OSMR expression and expression of a number of EMT markers including: fibronectin (FN1), FOXC2, HMGA2, integrin-a5 (ITGA5), MMP10, SNAI1, SNAI2 and ZEB[73]. Similar correlations were also observed in head and neck SCCs and lung SCCs. Treatment

of OSMR overexpressing cervical SCCs with OSM led to downregulation of the epithelial marker, E-cadherin, and upregulation of several mesenchymal markers including Fibronectin, SNAI1 and ZEB2. Treatment also resulted in increased expression of the matrix metalloproteinases (MMP) MMP9 and MMP10[73] which are key mediators of ECM degradation[132]. Phosphorylation of STAT3 was demonstrated to be essential for OSM-OSMR induced expression of mesenchymal markers (Figure 1.6). In line with the finding that OSM-OSMR induced characteristic EMT gene expression *in vitro*, OSM-OSMR signalling was found to enhance the metastatic capacity of cervical SCC cell *in vivo*. Mice injected intravenously with SW756 cells, an OSMR over expressing human cervical SCC cell line, showed significantly increased lung colonisation following intraperitoneal administration of hOSM compared to mice treated with PBS control[73]. Pre-treatment of cells with siRNA against STAT3 or with an anti-OSM antibody led to reduced lung colonisation, both in the presence and absence of exogenous hOSM[92].

Subsequent investigation has demonstrated that OSM-OSMR induced activation of pro-malignant signalling in cervical SCC cells is predominantly mediated by JAK-STAT signalling. OSM treatment of OSMR overexpressing cervical SCC cell lines was shown to result in phosphorylation of STAT3, STAT5, AKT and the following MAPKs: MAPK 44/42 and extracellular signal-regulated kinase 1/2 (ERK 1/2)[70,92]. Phosphorylation of these targets was abrogated by depletion of OSMR but not LIFR, demonstrating that OSM predominantly signals via Type II OSMR complexes in cervical SCC cells[92]. In SW756 cells, OSM induction of VEGFA, SNAI1 and TGM2 expression was found to be significantly reduced by both JAK inhibitors and STAT3 depletion using siRNA[92]. Treatment with a PI3K inhibitor partially reduced VEGFA expression but had no effect on SNAI1 or TGM2 expression, whereas, inhibitors targeting MEK or mTOR (members of the MAPK pathway) had no effect on target gene expression[92].

Together, these findings suggest that blockade of OSM-OSMR signalling may prove to be a promising therapeutic target for the treatment of cervical SCC. Treatment of OSMR overexpressing SCC cells with an anti-OSM antibody was found to cause dose-dependent inhibition of OSMR target genes, VEGFA, TGM2 and SNAI1[92]. Moreover, the use of an anti-OSM antibody inhibited OSM-OSMR mediated induction of angiogenesis by cervical SCC cells[92,121], reduced cervical SCC invasion *in vitro* and abrogated lung colonisation *in vivo*[92].

Paradoxically, Stroeder *et al* (2018) have recently shown that OSM treatment sensitises cervical SCC cell lines to chemo-radiotherapy induced cell death *in vitro*[133]. Moreover, this

effect was also observed in radio-resistant cervical SCC cell lines. Blockade of STAT3 signalling abolished OSM mediated sensitisation to chemo-radiotherapy[133]. This group has previously reported that the pro-apoptotic factor, interferon regulatory factor 1 (IRF1), was significantly upregulated in cervical SCC cell lines in response to OSM treatment in a STAT3 dependent manner[134]. Ectopic expression of IRF1 was shown to sensitise cervical SCC cells to cisplatin (a platinum-based compound that induces DNA damage), and etoposide (a topoisomerase II inhibitor) mediated cell death in a dose-dependent manner. Moreover knock down of endogenous IRF1 expression with short interfering RNA (siRNA) abrogated OSM induced sensitivity of cervical SCC cells to the aforementioned chemotherapeutic agents[134]. However, the authors did not demonstrate whether induction of IRF1 expression by OSM led to induced apoptosis in these cell lines in response to chemotherapy. Additionally, IRF1 was implicated as a predictive marker for chemo-radiotherapy response: patients with complete response to chemo-radiotherapy displayed higher levels of IRF1 expression in pre-therapeutic biopsies than patients who partially responded to therapy[134]. These studies suggest that OSM-OSMR signalling may have a dual role in cervical cancer. Therapeutic blockade of OSM-OSMR signalling to inhibit the pro-malignant effects previously described may, therefore, concurrently block OSM induced sensitivity to chemo-radiation. While further investigation is required to determine whether similar effects are observed *in vivo,* these preliminary findings indicate that therapeutic blockade of OSM-OSMR signalling may only be effective when administered subsequent to first line treatment with chemo-radiation.

1.11 Extracellular Vesicles: background

OSM-OSMR signalling requires interactions between cancer cells and OSM producing cells within the TME and subsequently activates genes involved in remodelling of the TME. One of the main aims of this thesis is to investigate whether OSM-OSMR signalling affects the cargo of extracellular vesicles (EVs) released from cervical SCC cells. EVs are a heterogeneous group of small, membrane-bound, nanoparticles which play key roles in bidirectional cell-cell communication, and have been demonstrated to facilitate interaction of cancer cell with cells of the TME[135,136]. EVs are released by almost all mammalian cell types and have been detected in all biological fluids, including: blood, urine, saliva, bile, breast milk, semen, ascites and cerebrospinal fluid[137]. Moreover, EVs are also secreted by plant cells, bacteria, archaea, fungi and parasites, suggesting that they are an important evolutionarily conserved mechanism of intercellular signalling[138,139]. EVs have been shown to contribute to multiple physiological and pathological processes and, in recent years, have

incited particular interest in the cancer field due to their potential for use as diagnostic or prognostic markers, as novel therapeutic targets or as therapeutic delivery vehicles[140].

1.12 EV subtypes

Three main classes of EVs have been identified – exosomes, microvesicles and apoptotic bodies - which are classified based on their different mechanisms of biogenesis. Exosomes are formed as part of the endocytosis pathway[140]. The principal role of endocytosis is to regulate the composition of the cell surface; this is achieved by internalisation of macromolecules and cell surface proteins by invagination of the plasma membrane[141]. Once molecules are internalised they are trafficked through a series of vesicular compartments, collectively known as endosomes, which are responsible for either recycling molecules back to the plasma membrane or delivering them to the lysosome for degradation[141]. Endosomal compartments undergo maturation from early endosomes to late endosomes, otherwise known as multivesicular bodies (MVBs). This process involves invagination of the endosomal membrane to form intraluminal vesicles (ILVs) within the lumen of the MVB. MVBs are either directed to the lysosome where their contents are degraded or transported to the plasma membrane[142]. Fusion of MVBs with the plasma membrane results in ILV release; ILVs are subsequently known as exosomes following their release into the extracellular space[143] (Figure 1.7A).

In contrast, microvesicles are formed by direct outward budding and fission of the plasma membrane[144,145] (Figure 1.7B). Both exosomes and microvesicles are composed of a lipid bilayer and contain a small cytosol devoid of any cellular organelles[146]. Whilst exosomes and microvesicles are released from viable cells, apoptotic bodies are exclusively released by cells undergoing apoptotic cell death. Apoptotic bodies are produced during the process of apoptotic cell disassembly. This involves the formation of plasma membrane blebs on the cell surface, generation of membrane protrusions and subsequent fragmentation, resulting in the release of apoptotic bodies containing nuclear and cytoplasmic components[147,148] (Figure 1.7C).

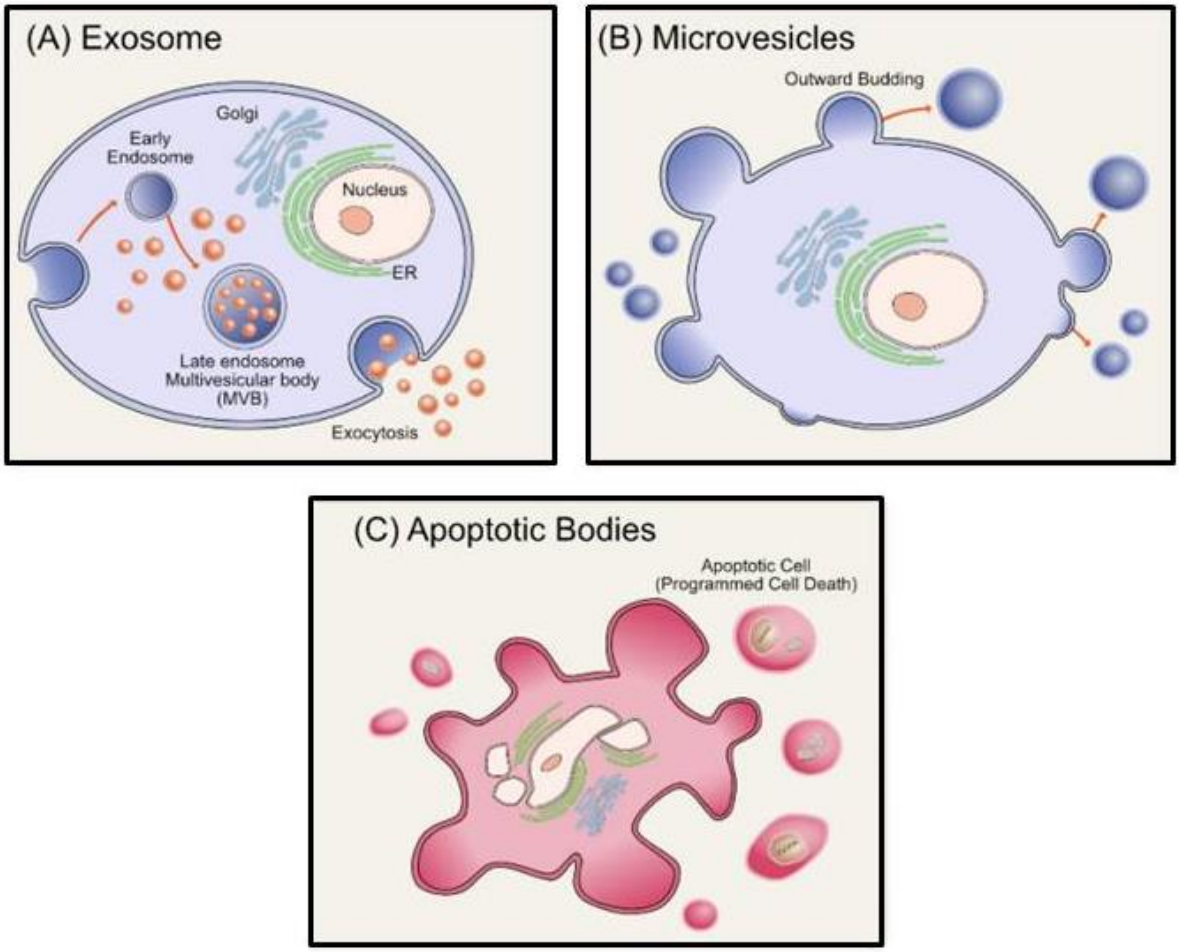

Figure 1.7: Schematic of EV biogenesis and release
A) Exosomes are of endocytotic origin and are released via fusion of the multivesicular body (MVB) with the plasma membrane. B) Microvesicles are released by outward budding of the plasma membrane. C) Apoptotic bodies are released from apoptotic cells via the process of apoptotic cell disassembly. **Adapted from Gurunathan *et al* (2019)[146].**

1.13 Regulation of EV Biogenesis

1.13.1 Exosomes

Exosome biogenesis commences with the formation of ILVs within the MVB. This process is driven by recruitment of endosomal sorting complexes required for transport (ESCRTs) which are also involved in protein sorting into the ILVs. These are composed of around thirty proteins that assemble into four different ESCRTs complexes - ESCRT 0, I, II and III, which function in a stepwise manner[149]. ESCRT 0 recognises and sequesters ubiquitinated transmembrane proteins in the endosomal membrane and recruits TSG101, involved in the ESCRT I complex. ESCRT I and ESCRT II are the initiators and drivers of ILV membrane budding whereas ESCRT III is responsible for vesicle scission[150]. ESCRT proteins function in concert with additional non ESCRT proteins including VPS4, VTA1, ALIX and heat shock protein 70 (HSP70)[151].

Exosomes can also be formed in an ESCRT independent manner, via the ceramide dependent pathway which relies on the ability of neutral sphingomyelinase enzymes (nSMases) to convert sphingomyelin into ceramide[152]. Accumulation of ceramide promotes membrane invagination of ILVs. Knock down (KD) of nSMase expression, or blockade using the GW4869 inhibitor has been demonstrated to reduce exosome release[152]. Additionally, the tetraspanins CD9, CD63, CD81, and CD82 are specially enriched in exosomes, and have been demonstrated to participate in ESCRT independent ILV biogenesis and protein loading[153].

EV release is mediated by fusion of the MVB with the plasma membrane. This has been shown to be regulated via several RAB GTPases which promote trafficking and docking of MVBs to the cell membrane, facilitating fusion and exosome release. In particular, RAB27A and RAB27B have been shown to play key roles in this process[154]. *N*-ethylmaleimide-sensitive factor attachment protein receptors (SNAREs) are also known mediators of MVB fusion with the plasma membrane. Two SNARE proteins in particular, vesicle-associated membrane protein 7 (VAMP7) and YKT6, have been demonstrated to be necessary for exosome release[143]. Mechanisms of exosome biogenesis are summarised in Figure 1.2A panel i.

1.13.2 Microvesicles

Compared to exosomes, the biogenesis of microvesicles is less well defined. A combination of factors has been implicated in microvesicle formation and release. These include aggregation of phospholipids within plasma membrane microdomains, facilitating membrane bending, and contraction of the actin-myosin machinery[144,155]. ADP-ribosylation factor 6 (ARF6), a GTP-binding protein, has been shown to play a regulatory role in microvesicle release[156]. ARF6 acts through phospholipase D and extracellular signal-regulated kinases (ERKs) to phosphorylate the myosin light chain kinase (MLCK). MLCK is a contractile protein which subsequently activates the myosin light chain promoting contraction of the actin cytoskeleton and subsequent microvesicle release[156].

A variety of proteins have been shown to be selectively incorporated into microvesicles, including proteins that are transported by the ARF-6 regulated endosomal recycling pathway, such as major histocompatibility complex class I protein (MHC class I), vesicle associated membrane protein 3 (VAMP3), MMP membrane type 1 (MT1-MMP) and β1 integrin receptors[156]. Moreover, the ESCRT I subunit, TSG101, has been shown to bind a tetrapeptide PSAP motif on arrestin domain-containing protein 1 (ARRDC1), resulting in recruitment of TSG101 to the plasma membrane, promoting in turn the release of

microvesicles containing TSG101 and ARRDC1[157]. VPS4 ATPase and the E3 ligand WWP2 are required for microvesicle formation via this pathway[157]. Moreover, calcium-dependent processes, RAB proteins (particularly RAB22A) and RHO GTPases, are also believed to play a role in microvesicle formation and release[145,155]. Similar to exosomes, generation of ceramide at the plasma membrane has been demonstrated to contribute to microvesicle release. In the microvesicle context, ceramide is generated by acidic sphingomyelinase rather than neutral sphingomyelinase[158]. Mechanisms of microvesicle biogenesis are summarised in Figure 1.8B panel i.

1.13.3 Apoptotic Bodies

Formation and release of apoptotic bodies via the process of apoptotic cell disassembly is distinct from microvesicle release. The plasma membrane channel pannexin 1 (PANX1)[159] and Rho-associated protein kinase (ROCK I)[160] have been shown to be key regulators of this process. ROCK I is cleaved during apoptosis by activated caspases, and subsequently drives contraction of actin-myosin filaments leading to membrane blebbing[160]. Inhibition of either PANX1 or ROCK I prevents the release of apoptotic bodies[159,160]. Apoptotic bodies are not homogenous; nuclear materials and mitochondria were found to be distributed to subsets of apoptotic bodies[147].

1.14 Challenges in EV classification

EVs have classically been isolated from culture media or biological fluids by sequential ultracentrifugation (with or without the inclusion of a density gradient step) which separates particles based on their buoyant density[161]. Whilst ultracentrifugation is still one of the most commonly used methods for EV isolation, a number of alternative methods have also been developed. These include: precipitation based methods, immunoaffinity isolation using EV markers, flow cytometry, ultrafiltration, size-exclusion chromatography and microfluidic devices[137,162].

Following isolation, EV subtypes are typically distinguished based on their size and expression of different membrane proteins. However, this has been complicated by the fact that there is no definitive consensus within the literature regarding specific size ranges and that different EV subtypes have been shown to have overlapping size ranges. Exosomes are typically reported to be 30 -150nm in diameter, whereas microvesicles have a much broader size range, and encompass particles from 50nm -1µm[153,155,163]. Apoptotic bodies are generally considered to be much larger, ranging from 1µm - 5µm in diameter; however, isolation of much smaller apoptotic bodies, <1µm in size, has also been reported[148].

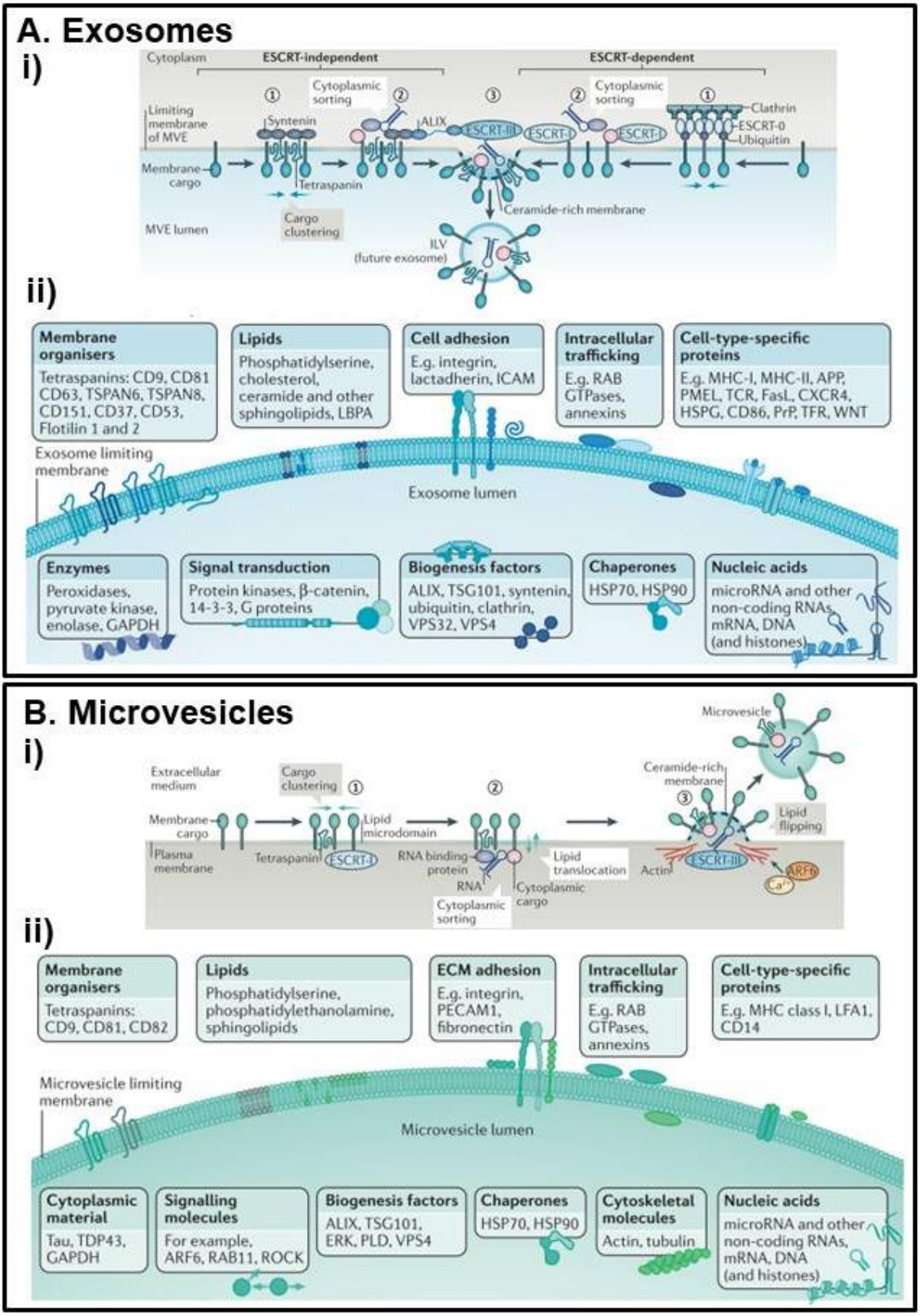

Figure 1.8: Biogenesis and marker expression of exosomes and microvesicles
Schematic of A) Exosome i) biogenesis and ii) marker expression.
B) Microvesicle i) biogenesis and ii) marker expression.
Adapted from Van Neil *et al* (2018)[153]

Moreover, despite different modes of biogenesis, exosomes and microvesicles display a similar composition that makes it difficult to ascertain their origin following isolation from culture media or biological fluids. Proteins involved in MVB function, trafficking and ILV biogenesis such as ALIX, TSG101, CD9, CD63, CD81, MHC class II or class I molecules, HSP 70 and flotillins were traditionally considered to be exosome specific and used as markers of successful exosome isolation. However, many of these markers (such as CD9, CD63 and CD81) have subsequently been shown to also be present in microvesicles and apoptotic bodies[164,165]. Similarly, MHC class I and class II molecules, HSP70 and flotillins have been found in all EV types[166]. Some of the markers known to be expressed by exosomes and microvesicles are summarised in Figure 1.8. Moreover, isolation of distinct EV populations based on characteristic marker expression has been further complicated by recent identification of subpopulations of exosomes with differential marker expression to other exosome populations[167]. Therefore, there has been a general consensus in the field to move towards classification of particles isolated following differential ultracentrifugation at 100,00 *xg* (or equivalent isolation protocols) as small EVs (sEVs) rather than exosomes[168].

1.15 EV cargo

EVs play a key role in cell-cell communication by transfer of proteins, lipids, DNA and RNA between cells[169]. EV cargo has been demonstrated to include multiple RNA species including (but not limited to): messenger RNA (mRNA), microRNA (miRNA), and long non-coding RNA (lncRNA)[170–172]. Importantly, EV cargo can be substantially different to the composition of the originating cell, indicating an active and highly controlled sorting process[173]. The content of EVs varies in respect to cell type of origin and physiological conditions. Multiple groups have demonstrated that both the number of EVs released, and the composition of EVs, can be altered in response to environmental changes. For example, exposure to hypoxic conditions, radiation or chemotherapeutic agents have all been shown to result in elevated secretion of EVs with altered protein, mRNA and/or miRNA content compared to untreated cells[174–177].

1.16 Targeting of EVs to recipient cells

There is a growing body of evidence to suggest that EVs from different sources preferentially interact with specific recipient cell types. For example, EVs isolated from oligodendroglial cells were shown to be efficiently internalised by microglia cells but not by neurons, astrocytes or oligodendrocytes[178]. Similarly, EVs derived from rat epithelial cells expressing oncogenic human HRAS were taken up by fibroblasts and endothelial cells, but not by untransformed epithelial cells or astrocytes. Interestingly, when epithelial cells were

transformed via ectopic expression of HRAS, they acquired the ability to internalise these EVs[179]. This demonstrates that uptake of EVs by recipient cells may be dependent on the specific properties of the recipient cell itself.

Targeting of EVs to specific recipient cells is mediated by the presence of ligands on the EV surface binding to corresponding receptors on the cell surface, and vice versa. Several ligand/receptor pairs have been identified to be involved in cell-EV interactions; these are likely to have specificity related to the cell type of EV origin and of EV uptake. Receptor-ligand combinations reported to date include binding of integrins to adhesion proteins such as vascular cell adhesion molecule (VCAM-1) or intercellular adhesion molecule 1 (ICAM1) or integrin binding to ECM proteins such as laminins or fibronectins in a process often mediated by tetraspanins[150,180]. Binding of lectin to proteoglycans or glycolipids and phosphotidylserine (PS) to PS receptors such as T cell immunoglobulin and mucin domain containing (TIM4) have also been implicated to mediate cell-EV interactions[150,180]. Receptor-ligand combinations are summarised in Figure 1.9.

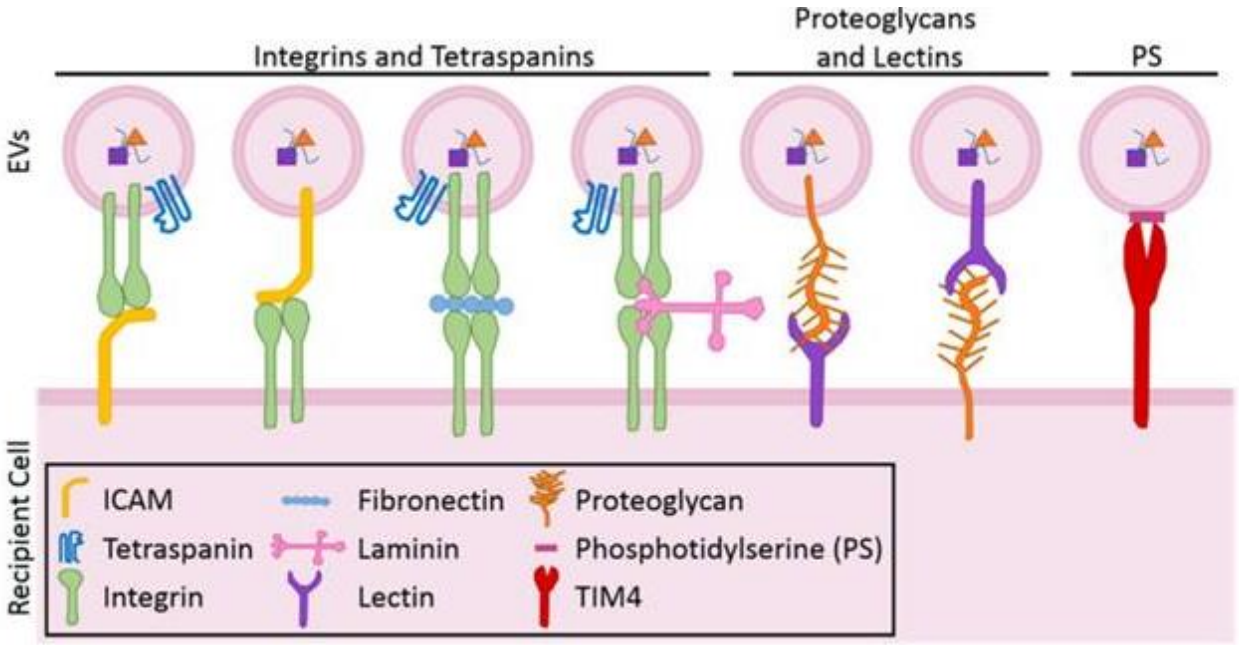

Figure 1.9: Cell-EV receptor complexes mediating EV uptake
Schematic of currently known receptor-ligand complexes known to facilitate EV uptake by recipient cells. **Taken from French *et al* (2017)[180].**

In some instances, receptor-ligand binding is sufficient to induce signalling cascades within the recipient cell, inducing physiological changes without requiring release of EV contents. For example, EVs released from mature dendritic cells have been shown to express functional MHC II-peptide complexes and ICAM1 on their surface. These EVs can be captured by CD8 positive dendritic cells by LFA1-ICAM1 binding (in which LFA1 is

expressed by the cell and ICAM1 by the EV). EVs were also demonstrated to act as antibody presenting microdomains at the surface of dendritic cells, and were able to activate T cells via their MHC II-peptide complex without being internalised by either cell type[181]. Similarly, EVs derived from neural stem/precursor cells have been shown to transfer interferon gamma (IFN-γ) from interferon gamma receptors (IFNGR1) on the surface of EVs to IFNGR1 on the surface of recipient somatic fibroblast cells. This was demonstrated to result in activation of STAT1 signalling in recipient cells[182].

However, in most cases, in order to elicit functional effects, it is necessary for EV contents to be internalised by the recipient cell, either by direct fusion with the plasma membrane or by endocytosis. Endocytotic uptake of EVs by recipient cells can occur by several different mechanisms including: clathrin-dependent endocytosis, caveolin-dependent endocytosis, phagocytosis, macropinocytosis or involvement of lipid rafts[180,183]. Multiple studies have used fluorescent lipophilic dyes which stain EV membranes or bioluminescent donor cell lines producing bioluminescent EVs to directly visualise EV uptake by recipient cells, either by confocal microscopy or flow cytometry[183]. Moreover, EV uptake by recipient cells has also been indirectly demonstrated by multiple studies showing functional transfer of EV cargo to recipient cells. This indicates that EV cytosol had merged with the cytoplasm of the host cell, facilitating the release of EV cargo. An instrumental study of this nature was performed by Valadi *et al* (2007) who demonstrated that EVs isolated from mouse mast cells could transfer functional murine mRNA to human mast cells. Murine proteins, not present in the EVs, were subsequently identified in the human recipient cells demonstrating that EV delivered mRNAs were translated into protein by the recipient cell[169]. However, while multiple studies to date have similarly demonstrated functional delivery of EV cargo to recipient cells, the mechanisms regulating escape or active transport of EV cargo out of the endosome into the cytosol remains unknown[184].

1.17 EVs in cancer

EVs have been demonstrated to play a key role in cell-cell communication, conferring numerous physiological and pathological functions to recipient cells. They are of particular interest in the oncology field where bidirectional communication between cancer cells and TME is essential for tumour growth and metastasis. The TME comprises the ECM and stromal cells including: cancer-associated fibroblasts (CAFs); immune and inflammatory cells; blood vessels; and lymphatic vessels[185].

Currently, eight major 'hallmarks of cancer' have been universally acknowledged, which describe biological capabilities acquired by cancer cells during neoplastic progression. These include: sustained proliferation, evasion of growth suppression, inhibition of apoptosis, enabling replicative immortality, induction of angiogenesis, activation of invasion and metastasis, reprogramming of energy metabolism and evading immune destruction[186]. EVs released by cancer cells have been demonstrated to contribute to virtually every aspect of tumorigenesis described above[187,188].

1.17.1 Horizontal transfer of EVs between tumour cells

EV production is elevated in cancer cells compared to normal cells, leading to the detection of high levels of cancer derived EVs in the plasma, ascites and pleural effusions of cancer patients[189]. Tumour derived EVs can facilitate horizontal transfer of oncogenic cargo to other cancer cells, enabling aggressive cancer cells to transform less malignant cells within the tumour. For example, aggressive glioma cells expressing oncogenic EGFRvIII have been shown to transfer EGFRvIII via their EVs to less aggressive glioma cells lacking this isoform. This results in transformation of recipients cells, including activation of MAPK and AKT signalling pathways, expression of EGFRvIII mediated genes and increased capacity for anchorage-independent growth[190]. Moreover, Zomer *et al* (2015) used a cre-lox system to demonstrate *in vivo* that EVs released from tumours established from highly malignant MDA-MB-231 breast cancer cells were taken up by less malignant T47D tumour cells located in either proximal or distant sites to the MDA-MB-231 tumour. Uptake of MDA-MB-231 EVs resulted in increased migratory behaviour and metastatic capacity of the less malignant T47D cells[191]

1.17.2 EV mediated communication between cancer cells and the TME

A vast number of studies have demonstrated that tumour-derived EVs interact with multiple cell types within the TME to promote tumour growth, angiogenesis, ECM remodelling, metastasis and immune evasion[135,136]. For example, cancer cell derived EVs have been shown to drive differentiation of fibroblasts into a myofibroblast-like phenotype typical of CAFs, via transfer of specific proteins or miRNAs[192,193]. Transformed fibroblasts subsequently secrete growth factors and cytokines that promote tumour growth and angiogenesis[192,140]. Moreover, EVs secreted by stromal cells are able to reciprocally modulate oncogenic capacity of tumour cells[187,188,194,195]. For instance, EVs secreted by CAFs are able to drive proliferation, migration and invasion of cancer cells and increase their metastatic capacity *in vivo* [195,196].

Furthermore, tumour derived EVs have been demonstrated to play a role in promoting the formation of a pre-metastatic niche. *In vivo* experiments have revealed that EVs released from cancer cells enter the bloodstream and accumulate at future metastatic sites[197,198]. Hoshino *et al* (2016) demonstrated that EVs from different cancer cell types were found to accumulate within different organs. Targeting of EVs to specific organs was shown to be regulated by differential integrin expression of the surface of EVs derived from different cancer cell types. Integrin-blocking decoy peptides reduced EV uptake by target organs which, in turn, reduced metastasis[198]. Thus EVs appear to induce changes at secondary sites that make them more permissive to colonisation by circulating tumour cells[197,198].

1.17.3 EVs mediate resistance to therapy

Additionally, cancer derived EVs have been shown to contribute to resistance of tumours to therapeutic agents. Cisplatin resistant ovarian cancer cell lines display increased secretion of cisplatin via their EVs compared to non-resistant cell lines, indicating a potential role for EVs in the export of drugs from tumour cells[199]. Moreover, chemo-resistant cancer cells have been shown to transmit resistance capacity to chemotherapy sensitive cells by transfer of specific miRNAs and proteins via their EVs[177,200–202]. Similarly, tumour derived EVs are able to modulate resistance to radiotherapy. EVs isolated from irradiated head and neck SCC cells induced proliferation of non-irradiated recipient SCC cells. Moreover, EV treatment resulted in increased survival of recipient cells in response to irradiation following EV transfer, demonstrating EV mediated transfer of radiation resistant properties[203]. Furthermore, in some instances EVs have been shown to act as drug decoys, shielding tumour cells from targeted therapies[187]. For example, in B cell lymphoma, EVs expressing CD20 on their surface were able to sequester anti-CD20 antibodies, thus enabling lymphoma cells to escape from immunotherapy by limiting the amount of antibody available to bind to cancer cells[204].

1.18 EVs as biomarkers, therapeutic targets and drug delivery vehicles

As tumour derived EVs contain specific oncogenic cargos and are released into the blood stream, ascites and pleural effusions of cancer patients, they have gained attention for potential use as biomarkers for diagnosis of cancer and prediction of therapeutic response[205]. For instance, circulating EVs are a promising predictor of therapeutic response in Non-Hodgkins Lymphoma. Presence of BCL-6 and c-MYC mRNA in EVs derived from the plasma of patients prior to treatment was predictive of reduced response to first line therapy and worse progression free survival[206].

Due to their diverse range of oncogenic properties, blockade of EV mediated intercellular signalling could represent a promising novel therapeutic target. This could be achieved by inhibiting EV formation or release, targeting of circulating EVs or preventing EV uptake by recipient cells[207]. A number of studies have demonstrated that blockade of EV release, via knock down of nSMase2, results in decreased metastatic and pro-angiogenic capacity of tumour cells *in vivo*[208,209]. Other groups have achieved similar results via therapeutic blockade of RAB27A using siRNA[210]. An alternative strategy would be to target circulating EVs. Nishida-Aoki *et al* (2017) recently used a breast cancer mouse model to demonstrate that treatment with anti-CD63 and anti-CD9 antibodies resulted in increased uptake of tumour derived EVs by macrophages, resulting in reduction of circulating EVs. Moreover, this led to reduced metastasis of breast cancer cells *in vivo*[211]. Inhibiting EV uptake by recipient cells is another potential mechanism to therapeutically prevent EV mediated delivery of oncogenic cargo. However, the pathways involved in EV uptake are less well understood and, currently, there are no *in vivo* studies demonstrating inhibition of EV signalling via this mechanism. The strategies discussed above outline some promising implications for the development of targeted therapies against EV mediated signalling. However, EVs are implicated in a wide range of physiological processes; therefore, it remains to be elucidated whether such strategies would prove to be viable therapeutic options[207].

Interestingly, it has also been suggested that EVs have promising clinical potential as drug delivery vehicles. Their stability in circulation and ability to target specific cell types make EVs ideal vehicles for delivery of siRNA, chemotherapeutic agents, protein, mRNA or miRNAs to target cells while reducing off target toxicity[136,207]. Loading of EVs can be achieved either passively or actively. Passive loading is achieved by exposing cells in culture to high levels of the molecule of interest prior to EV isolation. Active incorporation is performed following EV collection via co-incubation or electroporation of EVs with molecules of interest[136]. Moreover, EVs can be engineered to express plasmid fusion constructs with specific ligands fused to extracellular membrane proteins, thus enabling them to target specific cell types[136]. This was demonstrated by Tian *et al* (2014)[212] who engineered immature mouse dendritic cells to express a known EV surface protein, LAMP2B, fused to an αv-integrin-specific iRGD peptide. iRGD binds to αv integrins that are highly expressed on tumour cells and tumour-associated vascular. EVs isolated from these cells were loaded with the chemotherapeutic agent, doxorubicin. When injected *in vivo* these EVs specifically targeted αv integrin expressing breast cancer cells; targeted delivery of doxorubicin resulted in inhibition of tumour growth[212]. To date, multiple studies have demonstrated effective EV mediated delivery of many different types of cargo in a range of cancer models[207, 213].

2. AIMS

The overall aim of this thesis was to investigate the effects of OSM-OSMR signalling on cervical SCC cells and their extracellular vesicles. The work is divided into three sections:

1) Effect of OSM signalling on EV cargo in cervical SCC cells

In this section, preliminary hypothesis generating experiments were performed in order to determine whether OSM-OSMR signalling was capable of modulating cellular and EV miRNA expression in cervical SCC cells. These experiments utilised two representative cervical SCC cells lines: SW756 cells which have OSMR copy number gain and baseline OSMR overexpression and ME180 cells which do not overexpress OSMR. The experiments conducted in this section aimed to:

- Confirm that EVs could be successfully isolated by sequential ultracentrifugation from these two cell lines.
- Confirm that OSM treatment led to greater activation of downstream targets of OSM-OSMR signalling in OSMR overexpressing SW756 cells compared to ME180 cells, in line with previous experiments utilising these cell lines[121,122].
- Determine whether OSM-OSMR signalling was capable of modulating cellular and EV miRNA expression. qPCR was used to investigate the expression of a panel of nine miRNAs in SW756 and ME180 cells and their EVs in response to OSM.
- Perform functional assays in order to determine whether EVs from PBS and OSM treated cells differed in their ability to induce proliferation and migration of cancer cells and angiogenesis in endothelial-fibroblast co-cultures.
- Establish an OSMR Knock down (KD) SW756 cell line by CRISPR-Cas9 which could later be used to investigate global changes in miRNA and mRNA expression in cervical SCC cells and their EVs in response to OSM-OSMR signalling.

The experiments performed in this section demonstrated that EVs could be successfully isolated from cervical SCC cell lines. Moreover, OSM-OSMR signalling was found to differentially modulate cellular and EV miRNA expression in cervical SCC cell lines with different levels of OSMR expression. Finally, an OSMR KD SW756 cell line and a control SW756 cell line transfected with an empty CRISPR plasmid (empty plasmid SW756 cells) were generated by CRISPR-Cas9. These cell lines were used in subsequent sections.

2) NGS of cells and EVs following OSM Treatment

In this section next generation sequencing (NGS) was performed in order to investigate the global effects of OSM-OSMR signalling on cellular and EV miRNA and mRNA expression. This was performed using empty plasmid SW756 cells (EP cells) which overexpress OSMR and OSMR KD SW756 cells (KD cells) generated in section 1. The experiments conducted in this section aimed to:

- Determine the optimum kit to use for small RNA sequencing experiments. This was achieved by comparing sequencing results for a single sample sequenced using both Nextflex and Somagenics small RNA library preparation kits.
- Determine whether OSM-OSMR signalling altered mRNA and miRNA expression by cervical SCC cells and their EVs. To achieve this, EP cells and KD cells were treated with either PBS or OSM and RNA collected from both cells and EVs. NGS was performed to investigate effects of both OSM treatment and OSMR KD on mRNA and miRNA expression.
- Perform pathway analysis in order to elucidate functional effects of differential mRNA expression between cell-cell and EV-EV comparisons.
- Use qPCR to verify a subset of mRNAs and miRNAs found to be differentially expressed in NGS datasets.

3) Establishing a model to investigate OSM-OSMR signalling *in vivo*

In addition to investigating effects of OSM-OSMR signalling on EV mRNA and miRNA expression, parallel experiments were performed in order to elucidate the effects of OSM-OSMR signalling on growth of cervical SCC cells *in vivo*. The main aim of this section was to establish an *in vivo* model that could be utilised to study the effects of OSM-OSMR signalling on primary tumour growth and metastasis. The experiments conducted in this section aimed to:

- Investigate the effect of OSMR KD on cervical SCC growth *in vivo,* using subcutanous xenografts of empty plasmid and OSMR KD SW756 cell lines.
- Investigate the effect of intraperitoneal administration of exogenous hOSM on growth of empty plasmid and OSMR KD SW756 subcutaneous xenografts.
- Establish a model in which hOSM was continually delivered to OSMR overexpressing SCC cells *in vivo*. SW756 cells were stably transfected with a

plasmid driving hOSM expression; cell lines with varying levels of endogenous hOSM production were generated. Whether varying levels of endogenous OSM expression affected growth of SW756 subcutaneous xenografts was subsequently investigated.

3. MATERIALS AND METHODS

3.1 Cell Culture

Table 3.1: Reagents and equipment for cell culture	
Reagent	**Company**
• Glasgow Minimum Essential Medium (GMEM), no Glutamine • Penicillin-Streptomycin : 10,000 units penicillin + 10mg streptomycin/ ml in 0.9% NaCl (100x stock) • 200mM L-Glutamine (100x stock) • Dulbecco's Phosphate Buffered Saline modified without calcium chloride and magnesium chloride (PBS) • Dimethyl sulphoxide (DMSO)	Sigma-Aldrich, St. Louis, MO, USA
• 10X Trypsin-EDTA: porcine trypsin (5g/ml) and EDTA (2g/ml) • Heat Inactivated Fetal Bovine Serum (FBS)	Gibco, Thermo Fisher Scientific, Waltham, MA, USA
• 100 µg/mL Recombinant Human Oncostatin M Protein (Rh-OSM)	R&D Systems, Minneapolis, MN, USA
• Trypan blue stain (2X) 0.4% solution • Countess cell counting chamber slides • Countess Automated cell counter • Mr Frosty TM container	Invitrogen, Thermo Fisher Scientific, Waltham, MA, USA
• Tissue culture flasks - 25 cm^2 , 75cm^2 and 175cm^2 • 2ml Cryo.s™ Freezing Tubes 'cryovials'	Griener Bio-one, Kremsmünster, Austria
• 15ml and 50ml Falcon Tubes • 6 well plates	Corning, NY, USA
• Cell Lines	American Type Culture Collection (ATCC-LGC, Middlesex, UK).

3.1.1 Cell Lines

OSMR copy number and expression in a panel of keratinocyte cell lines derived from cervical SCCs has been previously established in our laboratory[121]. As it was not feasible to carry out work with all cell lines previously studied, we selected two representative cervical SCC cell lines (Table 3.2). SW756 was selected as a representative cervical SCC cell line with baseline OSMR copy number gain and overexpression and ME180 was chosen as a representative cell line with normal levels of OSMR (no baseline OSMR overexpression).

Table 3.2: Summary of Cervical SCC Cell Lines Used				
Cell Line	**ATCC Number**	**Site of Isolation**	**HPV Type**	**OSMR status**
SW756	CRL-10302	Primary Site	18	OSMR overexpressing
ME180	HTB-35	Metastatic Site: Omentum	39	Non-OSMR over-expressing

OSMR Knock down SW756 cell lines and OSMR overexpressing SW756 cell lines (pOSM) generated in sections 3.3 and 3.4, respectively, were also cultured. In addition, VF2

fibroblasts, a primary cell line established from normal diploid human fibroblasts originating from juvenile foreskin material after routine circumcision were also cultured[214]. These cells were kindly provided by Professor Gillian Murphy, The University of Cambridge.

3.1.2 General Cell Culture

Cells were maintained in 175cm^2 tissue culture flasks in their respective media (Table 3.3) at 37°C in 5% CO_2.

Table 3.3: Culture Media for cell lines used

Cell Line	Media Used	FBS	Other
SW756 (WT, empty plasmid and OSMR KD)	GMEM	10%	100 units/ml penicillin, 100 µg/ml streptomycin and 2mM L-glutamine
SW756 pUNO/pOSM	GMEM	10%	100 units/ml penicillin, 100 µg/ml streptomycin and 2mM L-glutamine, 5 µg/ml of Blasticidin
ME180	GMEM	10%	100 units/ml penicillin, 100 µg/ml streptomycin and 2mM L-glutamine
VF2	DMEM	10%	100 units/ml penicillin, 100 µg/ml streptomycin and 2mM L-glutamine

Enzymatic passaging using 1X Trypsin-EDTA (0.5% trypsin, 0.2% EDTA) was performed twice weekly when cells reached 80-90% confluence. In brief, culture media was removed by aspiration, adherent cells were washed with 20ml of sterile PBS and 5ml of pre-warmed Trypsin-EDTA was added to cells. Cells were subsequently incubated at 37°C until they had fully detached from the flask surface, as determined by visual inspection under a microscope. Cells were then resuspended in 11ml of pre-warmed media to neutralise the trypsin and 2ml of this suspension transferred to a new 175cm^2 flask along with 20ml pre-warmed media (1:8 ratio).

3.1.3 Cell Counting and Seeding for Experiments

Cells were trypsinised and resuspended in media as previously described. 20µl of cell suspension was mixed in a 1:1 ratio with 0.4% Trypan blue stain solution and 10µl of the mixture added to each chamber of a Countess slide. Trypan blue stains dead cells blue, thereby enabling distinction between live and dead cells. The number of live cells present in each chamber was determined using a Countess automated cell counter; counts from the two chambers were averaged and used to determine the concentration of cells in the original sample. Unless otherwise specified, 5x10^5 cells/well were seeded in 6 well plates and 1x10^7 cells were seeded in 175cm^2 flasks.

3.1.4 Cell Freezing and Thawing

To freeze cell stocks, cells were trypsinised, neutralised in pre-warmed media and counted by Countess cell counter. Cells were frozen at a density of 4 x10^6 cells/cryovial. Cells were centrifuged for 4.5mins at 400x*g*, media was removed by aspiration and cell pellets resuspended in freezing media consisting of 90% volume FBS and 10% volume of DMSO, at a concentration of 4x10^6 cells/ml. 1ml of cell suspension was aliquoted per cryovial, and vials placed into a Mr Frosty™ container and stored overnight at -80°C to achieve a gradual freezing process. After 24hours at -80°C, cryovials were removed from the container and transferred to a liquid nitrogen tank.

To thaw cells, cryovials were removed from liquid nitrogen and gently agitated in a water bath at 37°C. The cell suspension was then transferred to a 15ml falcon tube and centrifuged 4.5mins at 400x*g*. Supernant was subsequently removed by aspiration and the cell pellet resuspended in 5ml of pre-warmed media. This cell suspension was then transferred to a 25cm^2 flask and incubated at 37°C in 5% CO2.

3.2 Extracellular Vesicle Isolation and Characterisation

Table 3.4: Reagents and equipment for EV isolation and characterisation

Reagent	Company
• Heat Inactivated FBS	Gibco, Thermo Fisher Scientific, Waltham, MA, USA
• Rh-OSM	R&D Systems, Minneapolis, MN, USA
• 15ml and 50ml Falcon Tubes • 100mm tissue culture dishes	Falcon, Corning, NY, USA
• 50ml polycarbonate tubes • 38.5ml polycarbonate tubes • Ultra-Clear ½ x 2 inch centrifuge tubes • Avanti J-20 centrifuge • JA-20 rotor • Optima L-100 XP Centrifuge • SW-28 rotor • SW-55Ti rotor	Beckman Coulter Life Sciences, Indianapolis, IN, USA
• 0.2µm Minisart syringe filter	Sartorius AG, Göttingen, Germany
• Hexagonal 400 mesh copper grids • 1% Uranyl acetate	Agar Scientific Ltd, Stansted, UK
• Paraformaldehyde	Insight Biotechnology Ltd, Wembley, UK
• Glutaraldehyde	Sigma-Aldrich, St. Louis, MO, USA
• Eppendorf 5810 R centrifuge	Eppendorf, Hamburg, Germany
• FEI Tecnai™ G2 Transmission Electron Microscope	FEI, Oregon, USA
• Nanosight NS500 • Nanoparticle Tracking Analysis (NTA software)	Malvern Instruments, Malvern, UK

3.2.1 Preparation of EV depleted media

FBS was centrifuged at 100,000*xg* overnight (for approximately 16hours) at 4°C in 38.5ml polycarbonate tubes using an Optima L-100 XP Centrifuge with SW-28 rotor. Supernatant constituting EV depleted serum was collected, passed through a 0.2µm Minisart syringe and used to supplement GMEM media. 'EV depleted media', therefore, contained GMEM supplemented with 10% EV depleted FBS, instead of normal FBS.

3.2.2 Cell culture for EV collection – comparison of SW756 and ME180 cells

Experiments were performed using SW756 and ME180 cells. For each experiment three 100mm tissue culture dishes were plated for each cell line per condition: PBS or OSM were treated at 12, 24, 48 and 72 hour timepoints. Cells were seeded at a density of $2x10^4$ cells/cm^2 in 5ml normal media and incubated at 37°C in 5% CO_2. Cells were cultured for 48hours in normal media. Media was then removed by aspiration and cells washed with PBS, and media either replaced with fresh normal media (12 and 24 hour timepoints) or with EV depleted media supplemented with 10ng/ml Rh-OSM - consistent with the concentration used in previous studies to stimulate sustained (>24 hour) effects of OSM-OSMR signalling[121,215] - or an equal volume of PBS control (48 and 72 hour timepoints). Media for 12 and 24 hour timepoints was replaced with EV depleted media supplemented with 10ng/ml Rh-OSM or an equal volume of PBS control at 84 and 72 hours post seeding, respectively. After a total period of 96hours (12, 24, and 48 hour timepoints) or 120 hours in culture (72 hour timepoint) conditioned media was removed from all dishes; supernatant from each set of three replicates was pooled (to give a total volume of 15ml) and EVs isolated by ultracentrifugation (see section 3.2.3). This protocol is summarised in Table 3.5 and Figure 3.1. This experiment was repeated three times for both cell lines to provide three biological replicates for each condition (each biological replicate contained pooled media from three dishes). Following removal and pooling of supernatants, one dish from each condition was used to perform a representative cell count, the second was used for cellular RNA extraction (section 3.6.2) and the third was used for protein extraction (section 3.8.1).

Table 3.5: Summary of Treatment Timepoints			
Treatment Group	**Time in culture prior to treatment with OSM/PBS in EV depleted media (hours since seeding)**	**Duration of Treatment (hours)**	**Total Culture Time (hours)**
12hours PBS/OSM	84	12	96
24hours PBS/OSM	72	24	96
48hours PBS/OSM	48	48	96
72hours PBS/OSM	48	72	120

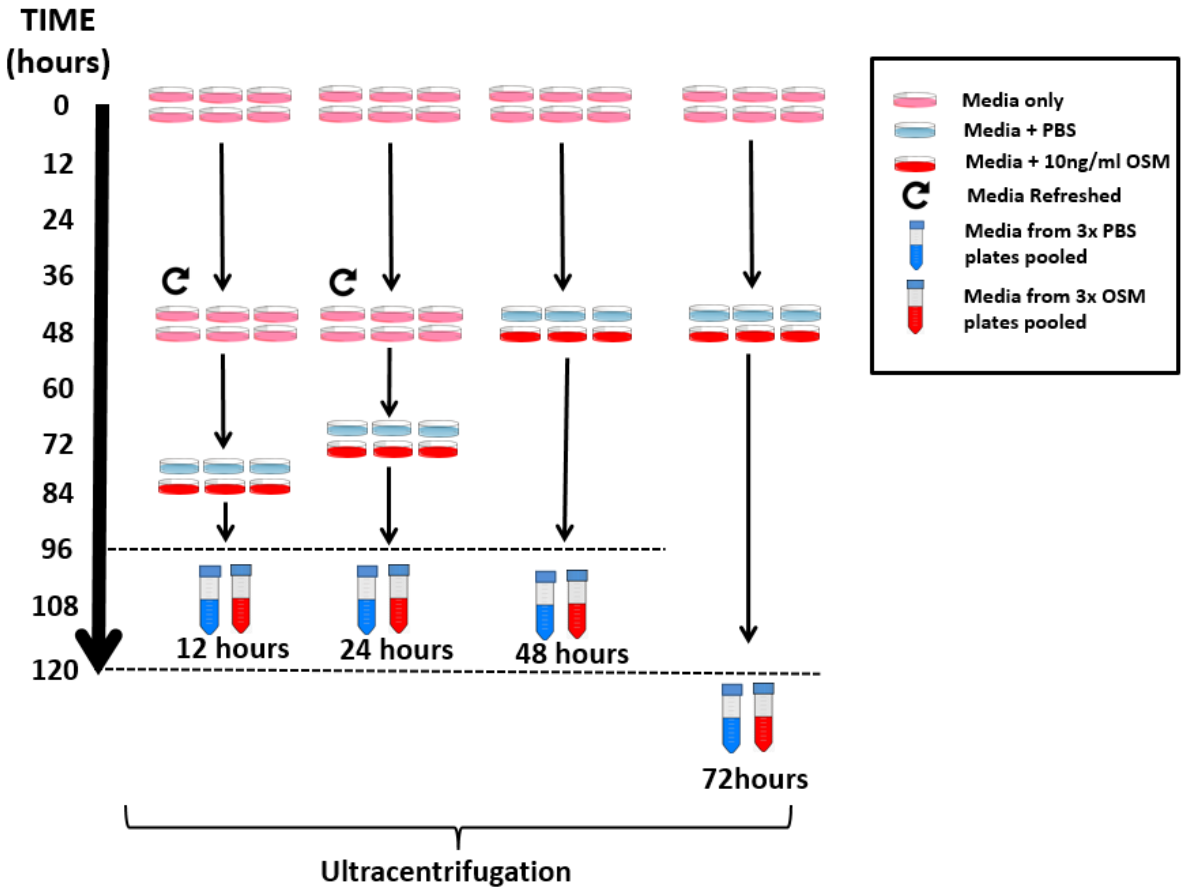

Figure 3.1: Illustration of OSM Treatment Protocol

3.2.3 Cell culture for EV collection – all other experiments

For all other EV experiments, cells were seeded in normal media in 175cm^2 flasks at a density of 5.71x10^4 cells/cm^2 (1x10^7 cells/flask) and incubated at 37°C in 5% CO_2, unless otherwise stated. After 48hours media was removed, cells were washed with PBS and 15ml of EV depleted media, either supplemented with 10ng/ml Rh-OSM or an equal volume of PBS control was added to cells. After a further 48hours in culture, conditioned media was collected into 15ml falcon tubes and EVs isolated as described in section 3.2.4.

3.2.4 EV Isolation

This protocol has been adapted from Thery *et al* (2006)[161] and is summarised in Figure 3.2. Conditioned media was transferred to a 15ml or 50ml falcon tube and spun at 1000*xg* for 15mins at 4°C using an Eppendorf 5810R centrifuge to remove live cells from the sample. The supernatant was then transferred into a new 15ml or 50ml falcon tube and centrifuged again, this time at 2000*xg* for 15mins, in order to remove dead cells and large cell debris. Supernatant was transferred to 50ml polycarbonate tubes, topped up to 20ml with sterile PBS, and samples centrifuged at 17,000*xg* for 20mins at 4°C using an Avanti J-20 centrifuge and JA-20 rotor in order to remove apoptotic bodies and cell debris. Supernatant was subsequently transferred to 38.5ml polycarbonate tubes and samples spun at 100,000*xg* for 80mins at 4°C using an Optima L-100XP Centrifuge with SW-28 rotor. The supernatant was discarded and the EV containing pellet re-suspended in 3ml PBS and transferred to an Ultra-Clear ½ x 2 inch centrifuge tube ('5ml centrifuge tubes'). Samples were centrifuged at 100,000*xg* for 40mins at 4°C using a SW-55Ti rotor. This step was performed to remove contaminating protein. Supernatant was discarded and EV pellets either frozen at -80°C for future mRNA or miRNA extraction or resuspended in the desired volume of PBS (TEM, Nanosight, protein extraction) or media (functional assays) for downstream applications.

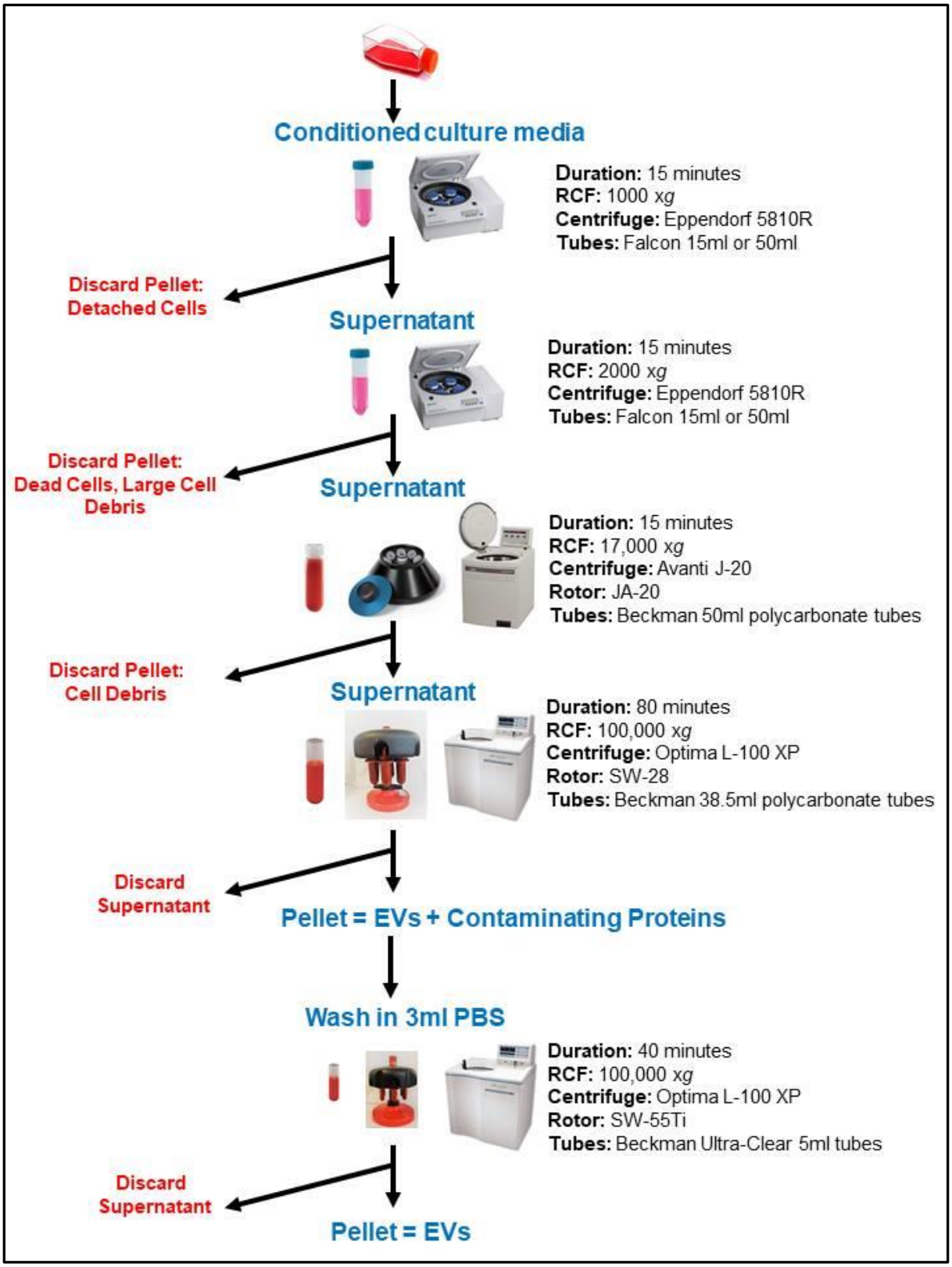

Figure 3.2: Summary of EV Isolation Protocol

3.2.5 EV Characterisation – Transmission Electron Microscopy (TEM)

EVs were visualised using transmission electron microscopy. Following ultracentrifugation, the volume of remaining PBS in which EV pellets were suspended was measured by pipette. EVs were then fixed by mixing EV pellets in a 1:1 ratio with 4% PFA, (final concentration 2%); samples were incubated for 10mins on ice. A 20µl drop of EV suspension was placed on a sheet of parafilm and a formvar carbon-coated copper electron microscopy grid placed coated-side down on top of the droplet for 2mins. This was repeated using a second droplet of EV suspension. Grids were subsequently washed by transfer through three sequential 50µl droplets of sterile PBS, for a period of 30secs each. Grids were then transferred to a 50µl droplet of 1% glutaraldehyde for 5mins. Grids were then washed by transfer through eight sequential 50µl droplets of nuclease-free water, for a period of 1min per droplet. To contrast the sample, grids were transferred to 20µl droplets of 1% uranyl acetate solution for 2mins and incubated in the dark. Grids were removed from the droplets and then left coated-side up to air dry. EVs were visualised using a FEI Tecnai™ G2 Transmission Electron Microscope operated at 80kV.

3.2.6 EV Characterisation – Nanosight

Following ultracentrifugation, volume of EV pellets was measured and samples were diluted to a total volume of 200µl using PBS. Particle size was quantified using a Nanosight NS500 with Nanoparticle Tracking Analysis (NTA) Software following manufacturer's instructions. This was performed in collaboration with Carlos Passos Bastos in Dr Nuno Faria's research group at The Department of Veterinary Medicine, Cambridge University. For optimum performance, samples were run using a range of 1:250–1:1000 dilutions (prepared in PBS) of the original 200µl sample; dilution used for each sample was dependent on the concentration of particles present.

The Nanosight NS500 visualises nanoparticles in liquid suspension and provides analysis of particle size distribution and concentration based on their rate of Brownian motion. Particles are passed through a flow chamber and are illuminated using a laser source. The light scatter produced is recorded using a video camera attached to a x20 magnification microscope. The camera captures a video of the particles moving under Brownian motion; small particles will move further than large particles (Figure 3.3). NTA software tracks multiple particles individually but simultaneously and uses the Stokes Einstein equation to calculate their hydrodynamic diameters on an individual particle basis[216].

Between three and five videos were recorded for each sample replicate. High vibrations during recording can result in an overestimation of the particles counted, therefore this was

used as a quality control and videos with high levels of vibrations were excluded from analysis. Based on the total number of particles counted, the NTA software generates data displaying the concentration of particles present in 1nm size bins. These concentrations were subsequently corrected by multiplying by the dilution factor in order to determine both the total concentration of particles present in each sample replicate and the true concentration of particles within each size bin. Mean and mode (i.e. the most frequently found) particle size, as well as D10, D50 and D90 values, which refer to the particle size which 10%, 50% and 90% of particles in the sample are smaller than, respectively, were then calculated. In order to compare samples, the percentage particle concentration for each size bin was calculated by dividing the particle concentration for each size bin by the total particle concentration for that sample. The total number of EVs present in the sample was calculated by multiplying the corrected concentration by the original 200µl sample volume. The number of particles released per cell was calculated by dividing this value by the number of cells present in the flask at time of EV collection (determined by Countess cell counter). For each sample values obtained for two biological replicates were averaged.

Overall true sample concentration = overall concentration x dilution factor

True sample concentration for each size bin = bin concentration x dilution factor

Percentage particle concentration = bin concentration / total concentration

Total EVs present in sample = Overall true sample concentration x sample volume (0.2ml)

EVs released per cell = total EVs present in sample/ number of cells

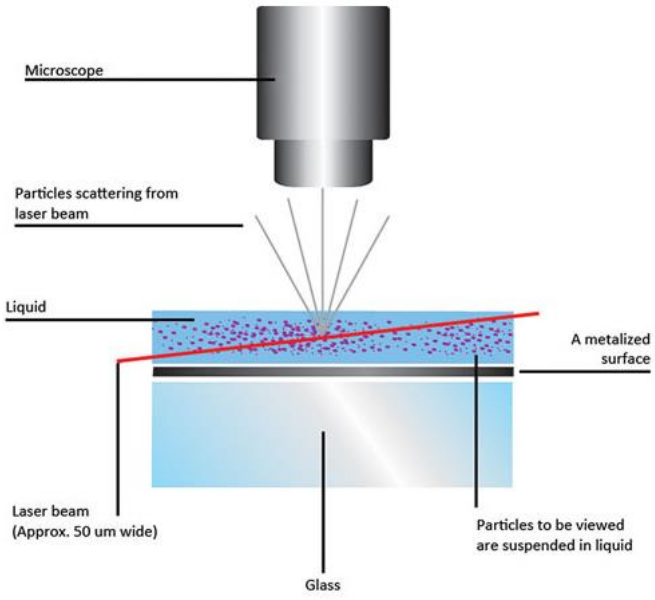

Figure 3.3: Schematic representation of the Nanosight NTA system
http://www.malvern.com/en/products/technology/nanoparticle-tracking-analysis[217]

3.3 Generation of an OSMR Knock down (KD) Cervical SCC Cell Line

Table 3.6: Reagents and equipment for OSMR KD	
Reagent	**Company**
• *BsaI* enzyme • *EcoRI* enzyme • BbSI enzyme • BamHI enzyme • T4 Polynucleotide Kinase • T4 DNA Ligase • 10X CutSmart® Buffer • 10X T4 DNA Ligase Reaction Buffer • EcoRI Buffer • NEB Buffer 2.1 • BamHI Buffer	New England Biolabs, Ipswich, MA, USA
• Nuclease-free water • DH5α competent cells • 1Kb DNA ladder (0.5 µg/ µl)	Invitrogen, Thermo Fisher Scientific, Waltham, MA, USA
• Agarose	Roche, Basel, Switzerland
• TAE Buffer • LB Broth • Agar Plates (100 µg/ml Ampicillin) • super optimal broth (SOC) media	Hutchison/MRC Media Kitchen, Cambridge, UK
• Ampicillin	Melford Laboratories, Ipswich, UK
• QIAquick™ gel extraction kit • QIAquick PCR purification kit	Qiagen, Hilden, Germany
• Ethidium Bromide 10mg/ml in water • 10X Orange G loading buffer • GenElute™ Plasmid Miniprep Kit • Nanodrop 2000 spectrophotometer	Sigma-Aldrich, St. Louis, MO, United States
• Lipofectamine® LTX with PLUS™ Reagent • Lipofectamine LTX DNA Transfection Reagent • Opti-MEM® Medium • PLUS™ Reagent	Thermo Fisher Scientific, Waltham, MA, USA
• Inoculating loop	Copan Diagnostics, Murietta, CA, USA
• Bio-Rad Gel dock	Bio-Rad Laboratories, Hercules, CA, USA
• MJ Research Tetrad PTC-225 Peltier Thermal Cycler	Bio-rad Laboratories, Hercules, CA, USA

OSMR expression was knocked down in the OSMR overexpressing SW756 cervical SCC cell line using a CRISPR-Cas9^{D10A} Nickase Based System. The Ensemble Genome Browser (www.ensemble.org, build GRCh37.p13) was used to determine the transcripts of the human OSMR gene. This gene has five transcripts, three of which are protein coding; this is depicted in Figure 3.4.

A.

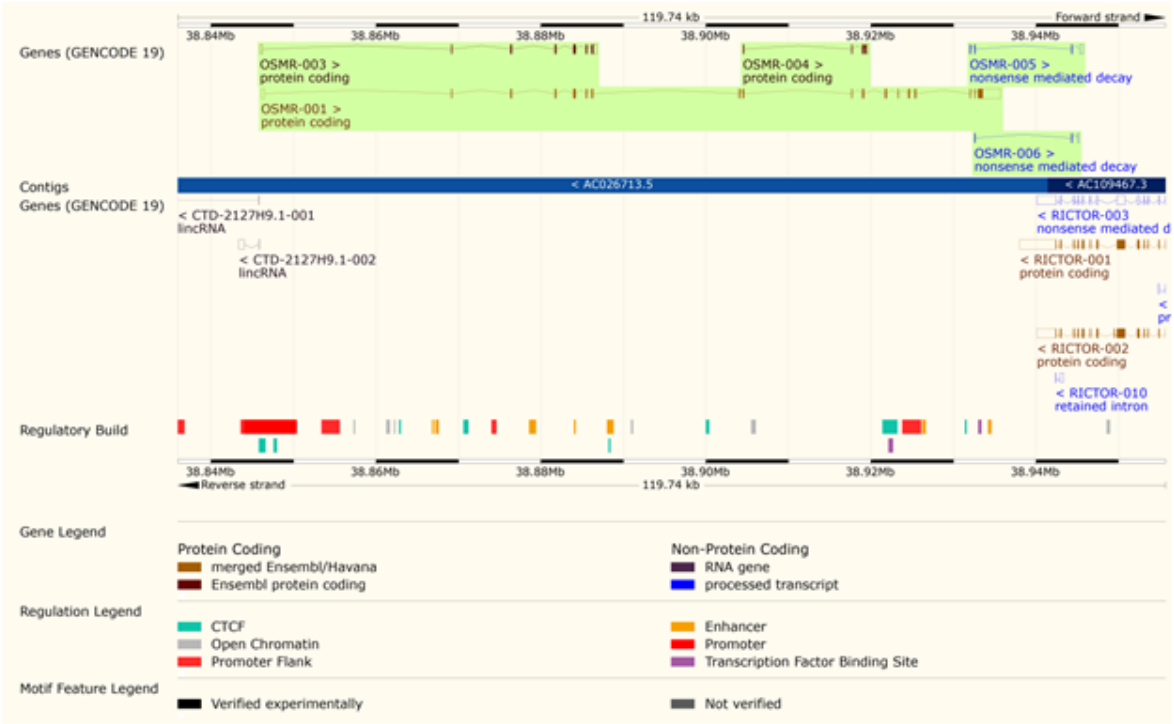

B.

OSMR Gene Transcripts						
Name	**Transcript ID**	**Transcript Length (bp)**	**Protein Length (aa)**	**Biotype**	**Number of exons**	**Number of coding exons**
OSMR-001	ENST00000274276.3	5539	979	Protein coding	18	17
OSMR-003	ENST00000502536.1	1740	342	Protein coding	7	6
OSMR-004	ENST00000513831.1	766	188	Protein coding	4	4
OSMR-005	ENST00000509237.1	653	62	Nonsense mediated decay	4	3
OSMR-006	ENST00000508882.1	361	35	Nonsense mediated decay	3	2

Figure 3.4: Annotation of the human OSMR gene
A) OSMR gene B) Details of OSMR transcripts

3.3.1 sgRNA Design

A pair of sense (gRNA1) and antisense (gRNA2) single guide RNAs (sgRNAs) were designed using http://crispr.mit.edu to target an exon within transcripts OSMR-001 and OSMR-003, as depicted in Figure 3.4. Protospacer adjacent motifs (PAMs) were removed from the 3' end and the following motifs added to the 5' end of each sequence to created overhangs enabling cloning into *BsaI* and *BbsI* sites respectively: forward gRNA – ACCG and reverse gRNA – AAAC. sgRNAs were reconstituted in nuclease-free water at a concentration of 100µM; sequences are shown in Table 3.7.

Table 3.7: CRISPR sgRNA Sequences	
sgRNA Name	**Sequence**
OSMR gRNA1 forward	ACCGCAAACTCTGACGCGTAGAAT
OSMR gRNA1 reverse	AAACATTCTACGCGTCAGAGTTTG
OSMR gRNA2 forward	ACCGCCACAACCTTCCTTATCATC
OSMR gRNA2 reverse	AAACGATGATAAGGAAGGTTGTGG

3.3.2 Oligo annealing and cloning into backbone vector

An all-in-one Cas9D10A nickase vector was kindly provided by Professor Stephen Jackson, the University of Cambridge[218]; the structure of this plasmid is detailed in Figure 3.5 below.

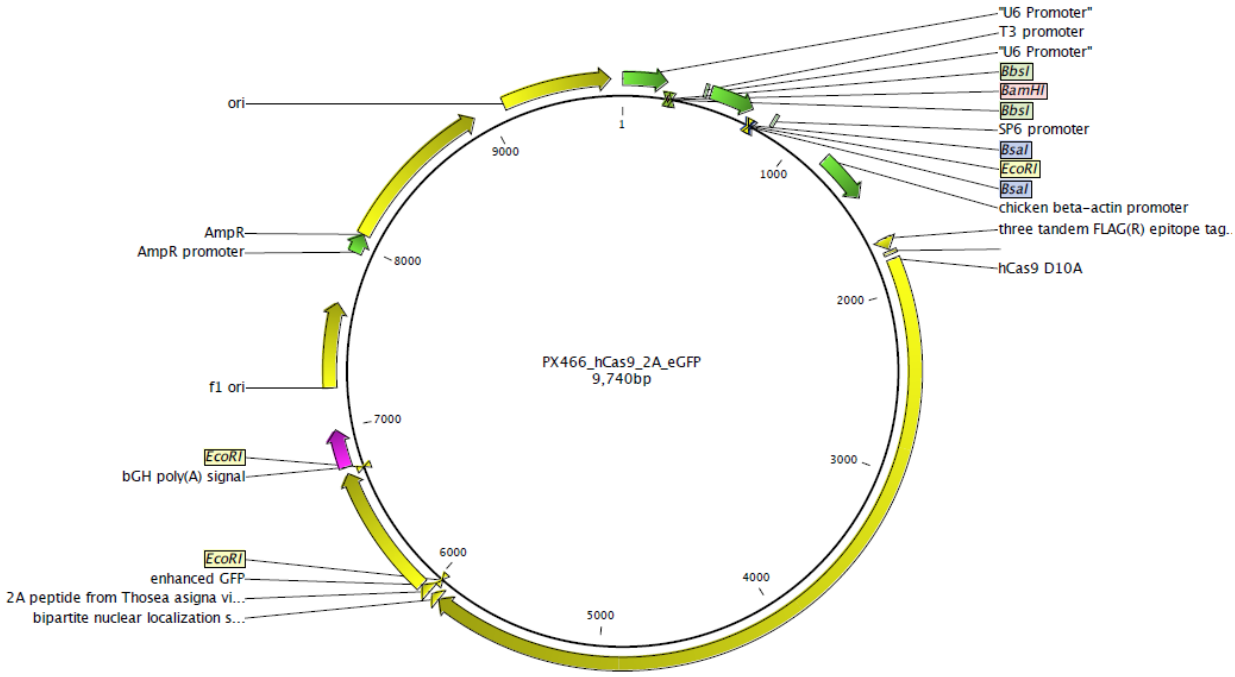

Figure 3.5: Structure of the PX466 Cas9-D10A-GFP Plasmid

The PX466 Cas9-D10A-GFP vector has two BsaI sites located in close proximity to one another, with an EcoRI site in between (Figure 3.5). 2µg of vector was linearised using *BsaI* enzyme (Table 3.8). The reaction was incubated at 37°C for 1hour and the enzyme subsequently deactivated by incubation at 65°C for 20mins.

Table 3.8: BsaI digest	
Reagent	**Volume per Reaction**
PX466 Cas9-D10A-GFP vector (2µg/µl)	1µl
BsaI enzyme	2µl
10X CutSmart® Buffer	2µl
Nuclease-free water	15µl
TOTAL	20µl

An agarose gel was prepared by dissolving 0.5g agarose in 50ml 1xTAE buffer (1%) by heating in a microwave. Once cooled, 2µl (10µg) of ethidium bromide was added to the solution which was then poured into a gel mould. Once set, the gel was placed in a gel tank and covered with 1xTAE buffer. 1.5µl of Orange G 10X loading buffer was added to 10µl of linearised or uncut vector and samples were loaded onto the gel along with 6µl (3µg) of 1Kb ladder. Samples were run at 110V for 30mins and the gel visualised using a Bio-Rad Gel dock. The band corresponding to plasmid linearised with *BsaI* was cut from the gel and subsequently purified using a QIAquick™ gel extraction kit following manufacturer's instructions. Linearised vector at a final concentration of 24ng/µl was obtained.

3.3.3 Oligonucleotide Annealing and Phosphorylation

The following reactions, using reagents shown in Table 3.9, were performed for each set of sgRNA primer pairs:

1) OSMR gRNA 1 (Forward + Reverse)
2) OSMR gRNA 2 (Forward + Reverse)

Table 3.9: Oligonucleotide annealing and phosphorylation

Reagent	Volume per Reaction
Forward sgRNA (100µM)	1µl
Reverse sgRNA (100µM)	1µl
T4 Polynucleotide Kinase	1µl
10X T4 DNA Ligase Reaction Buffer	1µl
Nuclease-free water	6µl
TOTAL	10µl

SgRNAs were annealed in a thermocycler using the following programme: 37°C for 30mins; 95°C for 5mins; then cool down ramp for 1hour to 4°C. Samples were subsequently incubated on ice for 15mins and then diluted 1:100 in nuclease-free water.

3.3.4 Ligation of sgRNA1 into vector backbone

The ligation reaction was set up as shown in Table 3.10. The reaction was incubated overnight at 16°C.

Table 3.10: Ligation of sgRNA1 into vector backbone

Reagent	Volume per Reaction
100ng digested vector (24ng/µl)	4µl
gRNA1 primer (oligo duplex 1:100 dilution)	2µl
T4 DNA Ligase	1µl
10X T4 DNA Ligase Reaction Buffer	5µl
Nuclease-free water	38µl
TOTAL	50µl

3.3.5 Transformation of Competent DH5α cells

Ligated plasmid was used to transform DH5α competent cells; 10µl of the ligated plasmid was added to 50µl of DH5α cells and incubated on ice for 5mins. The cells were then heat shocked at 42°C for 90secs, and returned to ice for a further 90secs. 400µl of super optimal broth (SOC) media was added to the cells, which were then shaken at 200rpm for 1hour at 37°C. Cells were subsequently transferred onto, and spread evenly across, the surface of a pre-prepared LB agar plate containing 100µg/ml Ampicillin. The plate was incubated for 3hours at room temperature and was then turned upside down and incubated overnight at 37°C. The next day 16 colonies were selected and streaked onto a new agar plate using an inoculating loop. Colonies were incubated for 3hours at room temperature; the plate was then turned upside down and incubated overnight at 37°C. The loops used to streak the first four colonies were subsequently used to inoculate tubes containing 5ml of LB broth with 100µg/ml Ampicillin. Tubes were incubated for 3hours at room temperature and were subsequently shaken at 250rpm at 37°C overnight. In total, one plate with 16 colonies and 4 individual LB broth inoculated colonies were grown up.

3.3.6 DNA Extraction

DNA was extracted from each of the four colonies grown up in LB broth. This was performed using a GenElute™ Plasmid Miniprep Kit following manufacturer's instructions. DNA was eluted in a final volume of 70µl nuclease-free water. DNA concentrations were subsequently measured using a Nanodrop 2000 spectrophotometer.

3.3.7 Confirmation of gRNA1 insertion

The PX466 Cas9-D10A-GFP vector contains three EcoRI sites, one of which is located within the two Bsa1 sites (Figure 3.5) which were targeted for linearisation of the plasmid prior to gRNA1 insertion. An EcoRI digest was, therefore, performed to determine if gRNA1 was inserted successfully. EcoRI digests were performed as shown in Table 3.10, using 150-200ng DNA. Samples were incubated at 37°C for 1hour.

Table 3.11: EcoRI digest

Reagent	Volume per Reaction
EcoRI Buffer	1.0µl
EcoRI enzyme	0.3µl
150 – 200 ng DNA	0.5µl
Nuclease-free water	8.2µl
TOTAL	10µl

10µl of each sample was subsequently run on a 1% agarose gel, as previously described, at 110V for 30mins and the gel visualised using a Bio-Rad Gel dock. Samples with the

appropriate number of bands corresponding to gRNA1 insertion were diluted to 100ng/µl, and 10µl sent for sequencing at the Department of Biochemistry, University of Cambridge (three samples per each insert) using 10µM of primer with the following sequence: CTTGATGTACTGCCAAGTGGGC.

3.3.8 Linearisation of Vector by BbSI Digest

The PX466 Cas9-D10A-GFP vector has two BbSI sites located in close proximity to one another, with a BAMHI site in between (Figure 3.5). 2µg of vector DNA was linearised using *BbSI* enzyme (Table 3.12). The reaction was incubated at 37°C for 1hour and the enzyme subsequently deactivated by incubation at 65°C for 20mins. Samples were run on a 1% Agarose gel. 2µl of each sample (corresponding to 0.2µg DNA) was diluted with 8µl of nuclease-free water, and added to 1.5µl of 10X Orange G loading buffer. 0.2µg of uncut sample (diluted to 10µl in nuclease-free water) was also loaded onto the gel along with 6µl (3µg) of 1Kb ladder. Samples were run at 110V for 30mins and the gel visualised using a Bio-Rad Gel dock.

Table 3.12: Reagents for BbSI digest

Reagent	Volume per Reaction DNA conc = 559.7ng/µl
Vector DNA (2µg)	3.57µl
BbSI enzyme	0.5µl
NEB Buffer 2.1	2µl
Nuclease-free water	13.93µl
TOTAL	20µl

3.3.9 Purification of Vector Backbone

Following *BbSI* digestion, samples were purified using a QIAquick PCR purification kit following manufacturer's instructions; samples were eluted in 20µl nuclease-free water. This kit purifies fragments from 100bp to 10kb in size; therefore, only the vector backbone was purified and the small DNA fragment between the two BbSI sites was removed. DNA concentration was measured with Nanodrop 2000.

3.3.10 Ligation of sgRNA2 into vector backbone

Ligation reactions were set up in duplicate according to Table 3.13 for insertion of gRNA2 into the vector backbone already containing gRNA1. The reaction was incubated overnight at 16°C.

Table 3.13: Ligation of sgRNA2 into vector backbone	
Reagent	**Vector DNA conc = 31.2ng/µl**
	Volume per Reaction
Vector DNA (100ng)	3.21µl
10X T4 DNA Ligase Reaction Buffer	1µl
T4 DNA Ligase	2µl
gRNA2 primer (oligo duplex 1:100 dilution)	2µl
Nuclease-free water	1.79µl
TOTAL	10µl

The following day, 10µl ligated plasmid was used to transform 50µl of DH5α competent cells as previously described in section 3.3.5. As in the previous transformation, transformed cells were spread across surface of an LB agar plate (containing100µg/ml Ampicillin) and incubated overnight at 37°C. The next day, 16 colonies were selected and streaked on a new agar plate which was incubated overnight at 37°C. The loops used to streak the first four colonies were subsequently used to inoculate tubes containing 5ml of LB broth with 100µg/ml Ampicillin, which were shaken at 250rpm at 37°C overnight. Therefore, one plate with 16 colonies and 4 individual LB broth inoculated colonies were grown.

3.3.11 DNA Extraction

DNA was extracted from each of the four colonies grown up in LB broth. This was performed using a GenElute™ Plasmid Miniprep Kit following manufacturer's instructions; DNA was eluted in a final volume of 70µl nuclease-free water. DNA concentration was subsequently measured using Nanodrop 2000.

3.3.12 Confirmation of gRNA2 insertion

The PX466 Cas9-D10A-GFP vector contains a BamHI site located between the two BbsI sites, which were targeted for linearisation of the plasmid prior to gRNA2 insertion (Figure 3.5). Plasmids with successful insertion of gRNA2 no longer contain a BamHI site and DNA remains uncut, whereas plasmids without gRNA2 insert will be linearised following BamHI digestion. BamHI digests were performed (Table 3.14) using 200ng DNA. Samples were incubated at 37°C for 1hour.

Table 3.14: BamHI digest	
Reagent	**Volume per Reaction**
BamHI Buffer	1.0µl
BamHI enzyme	0.3µl
200 ng DNA	0.4µl
Nuclease-free water	8.3µl
TOTAL	10µl

10µl of digested samples and paired undigested controls were subsequently run on a 1% agarose gel, as previously described, and the gel visualised using a Bio-Rad Gel dock. Samples positive for gRNA2 insertion were diluted to 100ng/µl, and 10µl sent for sequencing at the Department of Biochemistry using primer (10µM) with the following sequence: CTTGATGTACTGCCAAGTGGGC.

3.3.13 Transfection of SW756 cells with OSMR CRISPR Plasmid

SW756 cells were seeded in 6well plates in antibiotic-free GMEM supplemented with 10% FBS and 2mM L-glutamine at a density of 2.6 $x10^6$ cells/well. After 48hours, wells had reached approximately 70% confluence and were transfected using Lipofectamine®LTX with PLUS™ Reagent with either empty PX466 Cas9-D10A-GFP plasmid, subsequently referred to as empty plasmid, or plasmids containing sgRNAs against OSMR. Transfections were performed in triplicate for each condition as follows: Lipofectamine LTX DNA Transfection Reagent (6µl) was diluted in 150µl Opti-MEM® Medium. In a separate tube, 2.5µg plasmid DNA was diluted in 175µl Opti-MEM® Medium with the addition of 3.5µl PLUS™ Reagent. Diluted DNA was then added to diluted lipofectamine LTX DNA Transfection Reagent and incubated at room temperature for 15mins. Media was removed from cells; wells were washed in PBS and 2ml fresh antibiotic-free GMEM was added to each well in addition to 300µl of the plasmid DNA/ Lipofectamine® LTX/ PLUS™ Reagent mixture. Cells were incubated at 37°C in 5% CO2. After 8hours transfection media was removed, wells were washed with PBS and 2ml fresh antibiotic-free GMEM added.

As the PX466 Cas9-D10A-GFP plasmid encodes enhanced green fluorescent protein (EGFP), cellular EGFP expression was used to confer successful cell transfection. A DM LB light microscope with 488nm laser and filter (Leica) was used to evaluate EGFP levels at 0, 24 and 48 hours post transfection. At 48hours post transfection cells were trypsinised, and the number of cells/well determined by Countess cell counter. The three wells transfected per condition were combined and centrifuged for 4mins at 400*xg*. Supernatant was removed and cells were washed in PBS, centrifuged for a further 4mins at 400*x*g and resuspended in 1ml PBS. EGFP positive cells then underwent single cell sorting using an Astrios EQ flow cytometry cell sorter and 488nm excitation laser. Untransfected control sample was used to set gating parameters. One EGFP positive cell was plated in each well of a 96 well plate containing 50µl antibiotic-free GMEM. Remaining EGFP positive cells for each sample were seeded in 6well plates in 1ml of antibiotic-free GMEM – these are subsequently referred to as pooled samples. Cell sorting was performed with the assistance of Nigel Miller and Joana Cerveira.

3.3.14 Confirmation of OSMR KD

Once cells derived from single cell FACs sorting reached confluence, six colonies for each treatment group (empty plasmid and plasmid with gRNAs), as well as the pooled sample originating from multiple EGFP positive cells, were selected and bulked up until there were enough cells to perform DNA, RNA and protein extractions for investigation of OSMR KD as detailed in sections 3.5, 3.6 and 3.8, respectively.

3.3.15 Generation of additional OSMR KD cells lines

The CRISPR protocol was repeated in order to generate additional OSMR KD cell lines. WT SW756 cells were transfected as previously described (section 3.3.13) with empty PX466 Cas9-D10A-GFP plasmid (empty plasmid) or plasmid containing sgRNAs against OSMR. A mock transfection control in which cells were treated with lipofectamine but no plasmid was also included. Following single cell sorting of EGFP positive cells by FACS, six clonal cell lines transfected with empty plasmid and 36 clonal cell lines transfected with plasmid containing sgRNAs against OSMR were expanded for investigation of OSMR KD.

3.4 Generation of SW756 cell lines with endogenous OSM Production

Table 3.15: Reagents for generation of cell line with endogenous OSM production

Reagent	Company
• pGL4.51 plasmid	Promega, Madison, USA
• pUNO1-hOSM plasmid • pUNO1-mcs plasmid	InvivoGen, Toulouse, France
• Amaxa Nucelofector System Kit V • pmaxGFP vector	Lonza, Basel, Switzerland
• Lipofectamine LTX DNA Transfection Reagent • Lipofectamine LTX PLUS reagent • Opti-MEM® Medium • G418 sulfate	Thermo Fisher Scientific, Waltham, MA, USA

SW756 cells were stably transfected by Justyna Kucia-Tran with both a plasmid conferring firefly luciferase (luc2) expression and either a plasmid expressing hOSM under a hEF1/HTVT promoter (pUNO1-hOSM plasmid) or an empty control plasmid (pUNO1-mcs plasmid) in order to generate a bioluminescent OSMR overexpressing cervical SCC cell line with hOSM over-expression.

3.4.1 Transfection of SW756 cells with pGL4.51 plasmid

In brief, WT SW756 cells were transfected with pGL4.51 plasmid by nucleofection using the Amaxa Nucleofector System Kit V following manufacturer's instructions. 1 x10^6 cells were

placed in 100µl electroporation solution along with 0.5µg pGL4.51. Cells were nucleofected using programme U-20 and plated in 100mm tissue culture dishes; pmaxGFP vector containing green fluorescent protein (GFP) was used as positive control for the transfection process. The pGL4.51 plasmid contains the NeoR gene which confers resistance to the G418 antibiotic. The day after transfection media was changed and cells selected with 1.2 mg/ml G418 sulfate for 2 weeks. Stably transfected clonal pools were expanded in media containing 0.6mg/ml G418 sulfate. Cells stably transfected with pGL4.51 are referred to as SW756-pGL4.

3.4.2 Transfection of SW756 cells with pUNO1-hOSM plasmid

SW756-pGL4 cells were transfected with pUNO1-mcs or pUNO1-hOSM plasmids (Figure 3.6) using Lipofectamine LTS with PLUS reagent. 1.9 x10^6 SW756-pGL4 cells were seeded in 6well plates in antibiotic-free GMEM supplemented with 10% FBS and 2mM L-glutamine. After 24hours, wells were transfected using Lipofectamine®LTX with PLUS™ Reagent with either pUNO1-hOSM or pUNO1-mcs plasmids. Transfections were performed for each condition as follows: 3µl of Lipofectamine LTX DNA Transfection Reagent was diluted in 100µl Opti-MEM® Medium and incubated for 5mins at room temperature. In a separate tube, 1µg plasmid DNA was diluted in 100µl Opti-MEM® Medium with addition of 1µl PLUS™ Reagent. Diluted DNA was then added to diluted Lipofectamine LTX DNA Transfection Reagent and incubated at room temperature for 20mins. Media was removed from cells; wells were washed in PBS and 800µl fresh antibiotic-free GMEM was added to each well in addition to 200µl of the plasmid DNA/Lipofectamine® LTX/PLUS™ Reagent mixture. Cells were incubated at 37°C in 5% CO_2. Cells transfected with a pmaxGFP vector were used as a positive control. After 8hours transfection media was removed, wells were washed with PBS and 2ml fresh antibiotic-free GMEM added. The pUNO1-mcs and pUNO1-hOSM plasmids both contain the BsrS2R gene which confers resistance to Blasticidin antibiotic. The following day, media was changed and cells selected with 5µg/ml Blasticidin for 2 weeks. Stably transfected clonal pools were harvested and expanded in Blasticidin-free media. Cells transfected with pUNO-mcs plasmid are here onwards referred to as pUNO cells, whereas cells transfected with pUNO1-hOSM plasmid will be referred to as pOSM cells.

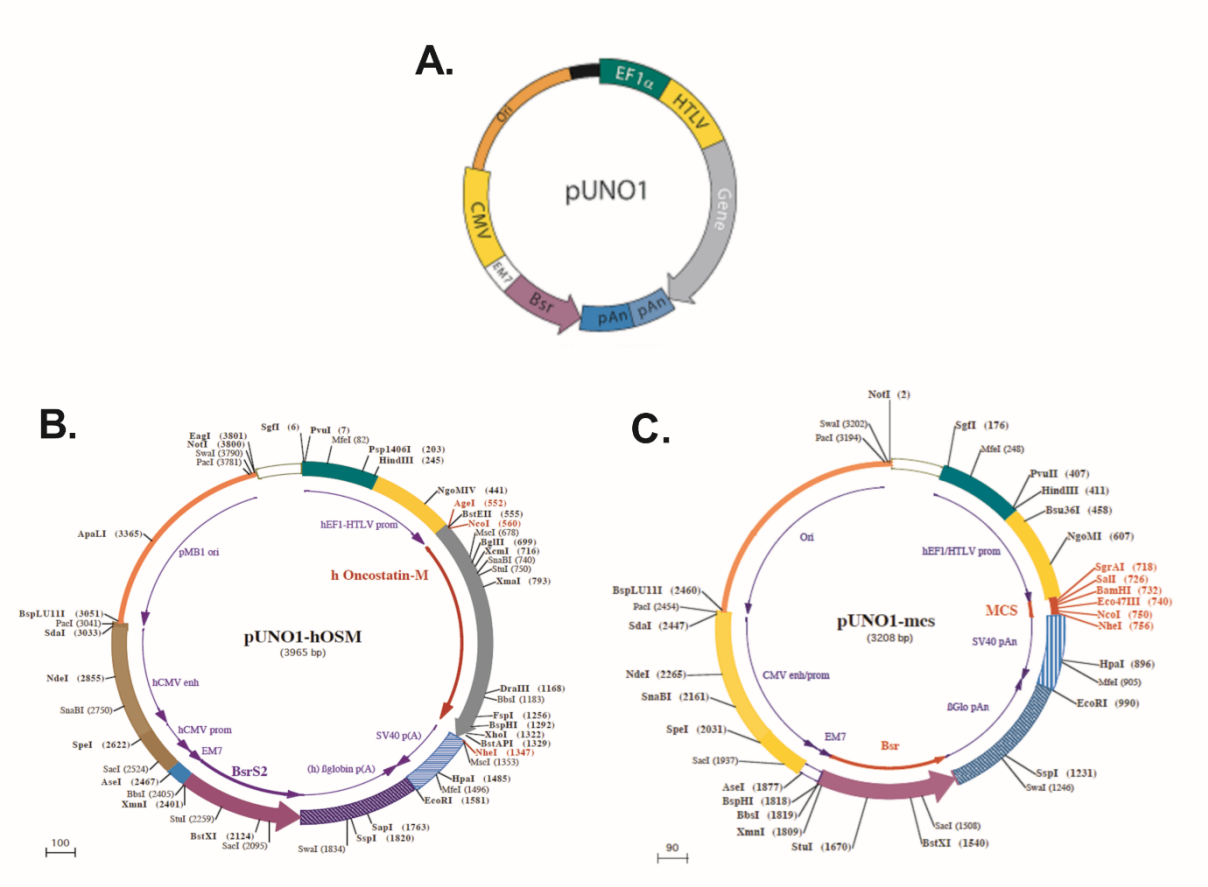

Figure 3.6: Structure of pUNO1-hOSM and pUNO1-mcs plasmids
A) Schematic of main features of pUNO1 plasmid structure
B) Structure of pUNO1-hOSM plasmid (OSM overexpressing plasmid)
C) Structure of pUNO1-mcs plasmid (empty plasmid)

3.4.3 Re-transfection of SW756 cells with pUNO1-hOSM plasmid

Transfection of SW756-pGL4 cells pUNO1-mcs or pUNO1-hOSM plasmids (Figure 3.6) was repeated as described in section 3.4.2 in order to generate SW756 cells with lower levels of hOSM overexpression than the original pOSM cell line. This was performed by Dr Danita Pearson. Following Blasticidin selection cells were harvested, counted by Countess cell counter and diluted in order to seed 30 cells per 96 well plate, enabling single cell cloning. These cells were expanded and levels of OSM determined by ELISA and qPCR. Levels of downstream targets were determined by qPCR and western blot. Results are shown for four of these clonal cell lines, denoted pOSM clone 1 (pOSMc1), clone 2 (pOSMc2), clone 3 (pOSMc3) and clone 4 (pOSMc4). Cells transfected with pUNO1-mcs plasmid in this repeat experiment are referred to as pUNO2.

3.5 DNA Experiments

Table 3.16: Reagents and buffers for DNA experiments	
Reagent	**Company**
• 1MM Tris-Cl (pH 8) • EDTA, 1mM, pH8 • 10% SDS • Sodium acetate	Hutchison/MRC Media Kitchen, Cambridge, UK
• 20mg/ml proteinase K	Melford Laboratories, Ipswich, UK
• Phenol • Chloroform • Ethanol • JumpStart™ Taq DNA polymerase	Sigma-Aldrich, St. Louis, MO, United States
• 0.2ml non-flex PCR tubes	Starlab, Milton-Keyes, UK
• QIAquick PCR purification kit	Qiagen, Hilden, Germany
Buffer	**Components**
• TE Buffer (per Litre)	98.8ml H_20 + 1ml 1MM Tris + 200µl 0.5MM EDTA
• Lysis Buffer (per ml)	960µl TE Buffer + 40µl 10% SDS + 2.5µl 20mg/ml proteinase K

3.5.1 DNA Extraction

Adherent cells from a 75cm^2 culture flask were trypsinised as previously described (though 3ml trypsin and 7ml media were used for this size of flask). 2.5ml of cell suspension was transferred to a 5ml falcon tube and centrifuged at 400*xg* for 4.5mins. Supernatant was removed and cell pellets were washed in PBS and centrifuged as above. Pellets were resuspended in 2ml lysis buffer, mixed and incubated overnight at 37°C to allow digestion. Samples were then mixed and 1x volume of phenol added. Samples were shaken by hand and centrifuged at 3200*xg* for 10mins at room temperature. The top aqueous layer was transferred to a new 5ml falcon tube; this step was repeated once more. 1x volume of saturated chloroform was then added, samples centrifuged at 3200*xg* for 10mins at room temperature and the top aqueous layer transferred to a new 5ml falcon tube. This step was repeated once more (i.e. two chloroform extractions). Subsequently, 1/10th volume sodium acetate and 3x volumes cold 100% ethanol (EtOH) were added to samples which were mixed by gentle inversion and left overnight at -20°C. Samples were then centrifuged at 3200*xg* for 30mins at 4°C. Pellets were then washed in 1ml 70% EtOH, mixed by pipetting, transferred to a 1.5ml Eppendorf tube and centrifuged at 16,000*xg* for 5mins at 4°C. Ethanol was removed and pellets allowed to air dry. Pellets were resuspended in TE buffer and left overnight at 4°C. The following day DNA concentration was determined using Nanodrop 2000.

3.5.2 Polymerase Chain Reaction (PCR)

Primers to assess for genomic loss were designed using the website 'Primer3' (http://bioinfo.ut.ee/primer3-0.4.0/). Forward and reverse primers were designed to amplify a small fragment of the OSMR gene that was targeted by sgRNAs during CRISPR (200-250 bps) or to amplify a larger fragment (~1kb) for subsequent sequencing, within the region targeted. They were designed to be between 18 and 23 nucleotides (nt) in length (optimal size = 20 nucleotides). Primer pairs were screened using PRIMER BLAST (https://www.ncbi.nlm.nih.gov/tools/primer-blast/) in order to identify primers that were specific to the intended PCR target. This method uses the Basic Local Alignment Search Tool (BLAST) and a global alignment algorithm to screen primers against a user-selected database to avoid primer pairs that could result in non-specific amplification. Primers were purchased from Sigma Aldrich and reconstituted at 100µM in nuclease-free water. Primer sequences are shown in Table 3.17**.** Primers were subsequently diluted to 2µM for PCR.

Table 3.17: PCR Primers for genomic DNA

Primer	Sequence
OSMR KD gRNA Forward	TGACTCTTCAATCATGCTCCTAT
OSMR KD gRNA Reverse	TTACTTACCACCCAGATGACATT
OSMR Sequencing Primer Forward	GGTATGTTGCTGGTCTCATCG
OSMR Sequencing Primer Reverse	TCTTCGTGGCTCTCTGGAAT

DNA samples were diluted to 12.5ng/µl in nuclease-free water. PCR reactions were performed using a JumpStart^{TM} Taq DNA polymerase kit (reaction components are listed in Table 3.18 below) in 0.2ml non-flex PCR tubes.

Table 3.18: PCR Reagents

Reagent	Volume Per Reaction
10x PCR Buffer	2.5µl
dNTP mix (2mMol of each base)	2.5µl
Forward Primer (2µM)	2.5µl
Reverse Primer (2µM)	2.5µl
JumpStart^{TM} Taq DNA polymerase	0.5µl
DNA (12.5ng/ µl)	2.0µl
Nuclease-free water	12.5µl
TOTAL	**25µl**

PCR reactions were performed using a MJ Research Tetrad PTC-225 Peltier Thermal Cycler using the reaction conditions listed in Table 3.19

Table 3.19: PCR Reaction Conditions			
PCR Step	**Time**	**Temperature**	**Number of Cycles**
Taq Activation	5mins	94°C	1
Denaturation	30secs	94°C	40
Annealing	30secs	55°C	
Extension	30secs	72°C	
Elimination of Enzyme Activity	7mins	72°C	1
Hold	unlimited	4°C	

1.5µl of Orange G 10X loading buffer was subsequently added to 10µl of each sample, and run on a 1% agarose gel as previously described, and the gel visualised using a Bio-Rad Gel dock.

3.5.3 Sequencing for detection of OSMR KD cell lines

For PCR performed with OSMR sequencing primers, PCR products were purified from the PCR reaction using a QIAquick PCR purification kit, following manufacturer's instructions; samples were eluted in 30µl nuclease-free water. DNA concentration was determined using a nanodrop 2000 spectrophotometer. OSMR Sequencing primers (both forward and reverse, as listed in Table 3.17) were diluted to 10µM in nuclease-free water. DNA sequencing was performed by the Department of Biochemistry, University of Cambridge. Sequencing data was analysed with SnapGene and Synthego ICE software in order to compare sequences from each sample (generated using either forward or reverse prime) with those of wild-type SW756 cells in order to determine if any changes had occurred to the section of the OSMR gene targeted by CRISPR.

3.6 RNA Experiments

Table 3.20: Reagents for RNA Experiments	
Reagent	**Company**
• Qiazol • miRNeasy Mini Kit • miRNeasy Serum/Plasma Kit • miRNeasy Serum/Plasma Cel-miR-39 Spike-In Control	Qiagen, Hilden, Germany
• MS2 bacteriophage RNA	Roche Diagnostics, Risch-Rotkreuz, Switzerland
• Chloroform • Ethanol • TriReagent • Isopropyl alcohol • Glycogen • mRNA qPCR primers	Sigma Aldrich, St Louis, MO, USA
• Distilled water (DNase/RNase Free) • Universal Template cDNA made from Universal Human Reference RNA (Ambion)	Thermo Fisher Scientific, Waltham, MA, USA
• Quantitect Reverse Transcription Kit	Qiagen, Hilden, Germany
• Taqman MicroRNA Reverse Transcription Kit • Taqman MicroRNA Primers • Taqman MicroRNA Probes	Applied Biosystems, Foster City, CA, USA
• 2X qPCR Bio Sygreen Lo-Rox Mix	PCR Biosystems Ltd, London, UK
• Flat top full skirt 96 well qPCR plate	SSI bio, Lodi, CA, USA

3.6.1 mRNA Extraction: Cells

Adherents cells grown in 6 well plates were washed in PBS, homogenised in 1ml TriReagent and cell suspensions transferred to 1.5ml Eppendorf tubes. Samples were incubated at room temperature for 5mins to permit complete dissociation of the nucleoprotein complex. 200µl saturated chloroform was added and samples vigorously shaken by hand for 15secs. Samples were then incubated at room temperature for a further 2mins before undergoing centrifugation at 12,000*xg* for 30mins at 4°C. Following centrifugation the mixture separated into three layers: a lower red phenol-chloroform organic phase, a white protein containing interphase and an upper colourless aqueous phase containing RNA. The RNA containing aqueous phase was removed to a new Eppendorf tube and 1µl glycogen and 500µl isopropyl alcohol added. Samples were mixed thoroughly and incubated overnight at -20°C to precipitate RNA. Samples were centrifuged at 12,000*xg* for 30mins at 4°C. Supernatant was removed and discarded and the RNA pellet subsequently washed with 1ml 75% ethanol. Samples were briefly vortexed then centrifuged at 7,500*xg* for 10mins at 4°C. Supernatant was discarded and pellets allowed to air-dry for 10mins at room temperature. RNA was resuspended in an appropriate volume of nuclease-free water and heated to 60°C

for 10mins to promote resuspension. RNA concentration was quantified using a Nanodrop 2000.

3.6.2 Total RNA Extraction (mRNA + miRNA): Cells

Adherent cells were trypsinised and counted as previously described. 3.5 x10^6 cells per sample were centrifuged for 4.5mins at 400x*g,* cell pellets resuspended in 700µl Qiazol lysis reagent and vortexed for 30secs. Samples were then incubated at room temperature for 5mins. 140µl saturated chloroform was added and samples vigorously shaken by hand for 15secs. Samples were then incubated at room temperature for a further 2mins before undergoing centrifugation at 12,000*xg* for 15mins at 4°C. The upper aqueous RNA containing phase was removed to a new Eppendorf tube and 1.5x volumes 100% ethanol added and mixed thoroughly. Total RNA was extracted using a miRNeasy Mini Kit with RNeasy Mini spin columns according to manufacturer's instructions. Samples were subsequently eluted through two sequential centrifugations at 8,000*xg* for 1min using 30µl of nuclease-free water to obtain a total elution volume of 60µl.

3.6.3 Total RNA Extraction (mRNA + miRNA): EVs and plasma

Following ultracentrifugation, EV pellets were resuspended in 200µl PBS; for plasma samples 200µl was used. Reagents (Table 3.21) were added to each sample. For samples used for qPCR analysis MS2 was used as a RNA carrier and cel-miR-39-3p spike in control added. 10µg/sample glycogen was used as a RNA carrier for samples to be used for next generation sequencing (NGS); cel-miR-39-3p spike-in control was not added.

Table 3.21: Reagent volumes for EV total RNA Extraction

Solution	Volume per sample Downstream application: qPCR	Volume per sample Downstream application: NGS
Qiazol	1000µl	1000µl
MS2 Stock Solution (0.8 µg/µl)	1.56µl	-
Cel-miR-39-3p spike-in control (1.6 x 10^8 copies/µl)	3.5µl	-
Glycogen (6.41µg/µl)	-	1.56µl
TOTAL	**1005.06µl**	**1001.56µl**

Samples were mixed by vortexing and incubated at room temperature for 5mins. 200µl chloroform was added to each sample. Samples were mixed again, incubated at room temperature for 2mins then centrifuged for 15mins at 12000xg at 4°C. The RNA containing aqueous phase was collected into a new Eppendorf tube and 1.5 x Vol of 100% EtOH added to each sample; samples were mixed thoroughly. Total RNA was extracted using a

miRNeasy Serum/Plasma Kit and RNeasy MinElute spin columns following manufacturer's instructions. Samples were subsequently eluted through two sequential centrifugations at 16,000*xg* for 1min using 14µl (elution 1) and 10µl (elution 2) of nuclease-free water to obtain a total volume of 24µl.

3.6.4 Total RNA Extraction (mRNA + miRNA): Tumour Tissue

Frozen tissue samples were weighed and homogenised in Qiazol lysis reagent (700ul/30mg of tissue). This was performed in 50ml falcon tubes using an Omni µH handheld micro tissue homogenizer (Omni International, Kennesaw, GA, USA). Samples were then allowed to dissociate for 5mins at room temperature, saturated chloroform added (140µl/30mg starting material) and samples shaken vigorously by hand for 15secs. Samples were incubated at room temperature for 2mins then centrifuged at 12,000*xg* for 15mins at 4°C. The upper aqueous RNA containing phase was removed to a new tube, 1.5x volumes 100% ethanol was added and mixed thoroughly. Total RNA was extracted using a miRNeasy Mini Kit with RNeasy Mini spin columns according to manufacturer's instructions. Samples were split over multiple spin columns if more that 30mg start material was used. Samples were pooled following elution so that one final sample was obtained for each tumour sample. RNA concentration was quantified using a Nanodrop 2000.

3.6.5 Reverse Transcription: mRNA

Table 3.22: Reagents used for Reverse Transcription (mRNA)

Reagent	Volume per Sample
Quantiscript RT Buffer (5X)	4µl
RT Primer Mix	1µl
Quantiscript Reverse Transcriptase	1µl
TOTAL	6µl

The Quantitect Reverse Transcription Kit was used to reverse transcribe mRNA into complementary DNA (cDNA) following manufacturer's instructions. RNA samples were diluted to 1µg in a total volume of 12µl nuclease-free water and 2µl gDNA Wipeout Buffer (7X) added. Samples were incubated at 42°C for 2mins to eliminate genomic DNA and reagents listed in Table 3.22 were subsequently added (final sample volume = 20µl). Samples were mixed and run on a MJ Research Tetrad PTC-225 Peltier Thermal Cycler under the following conditions: 42°C for 30mins and 95°C for 5mins. Samples prepared without the addition of reverse transcriptase or RNA template were used as negative controls. cDNA was subsequently diluted 1:80 in nuclease-free water before being used as template for PCR.

3.6.6 Primer Efficiency

Quantitative Real-Time PCR was performed using qPCR Bio Sygreen Lo-Rox Mix and a RealPlex2 MasterCycler (Eppendorf, Hamburg, Germany). This system uses a fluorescent dye that binds to double stranded DNA molecules by intercalating between the DNA bases. When the dye is free in the reaction mix it emits only a small amount of fluorescence; when bound to DNA the structure of the dye is altered and a much greater fluorescent signal is emitted. As primers are extended by Taq polymerase and template replication occurs, the dye is intercalated into the replicated strand, and thus total amount of fluorescence increases with the number of cycles performed. Increase in fluorescent intensity is directly proportional to increase in double stranded DNA, and therefore levels of fluorescence is measured at the end of each amplification cycle to determine how much cDNA has been amplified.

PCR is an exponential process until one of the reagents becomes limited (plateau phase). The cycle threshold (Ct) value is defined as the cycle in which there is a significant increase in fluorescence above the threshold level (i.e. amount of background fluorescence) and amplification is in its exponential phase. The more abundant the template sample, the quicker this point is reached, thus giving earlier Ct values.

Table 3.23: qPCR conditions for primer efficiency

Step	Temperature	Time	
Initial denaturation	95°C	2mins	
Denaturation	95°C	5secs	45 cycles
Annealing	65°C	25secs	
Extension	76°C	8secs	
Melt curve	78°C	8mins	3 cycles
	95°C	15secs	
	65°C	15secs	
	95°C	15secs	

'Primer efficiency' reflects how well target cDNA is amplified per cycle using a specific set of primers: ideally target cDNA will double per cycle and this would correspond to a primer efficiency of 2.0. Universal template cDNA was used to test primer efficiency of each pair of primers used. cDNA (5ng/µl) was diluted 1:2, 1:4, 1:10, 1:50 and 1:100 in nuclease-free water. A 12µl/well mastermix, comprising 10µl 2x qPCR Bio Sygreen Lo-Rox Mix and 2µl of relevant primer pair (4µM; Table 3.24), was added to a 96 well PCR plate along with 8µl of diluted template cDNA. Each cDNA sample dilution was run in triplicate. Quantitative-PCR was performed on a RealPlex2 MasterCycler (Table 3.23); melt curve analysis was also performed to confirm amplification of a single PCR product by each primer pair.

Table 3.24: mRNA primers used for qPCR analysis				
Gene	**Primer Efficiency**	**Primer Efficiency %**	**Forward Primer Sequence (5' → 3')**	**Reverse Primer Sequence (5' →3')**
HMBS	2.01	102.3	GGCAATGCGGCTGCAA	GGGTACCCACGCGAATAC
RPL13A	1.97	93.3	CCTGGAGGAGAAGAGGAAAGAGA	TTGAGGACCTCTGTGTATTTGTCAA
YWHAZ	2.00	100.0	ACTTTTGGTACATTGTGGCTTCAA	CCGCCAGGACAAACCAGTAT
H1_KIAA1199 (CEMIP)	2.06	114.8	ATTTCTTGGAGGTGAAGATG	ACTTCAATGTAAGCGAAGTC
H1_CHI3L1	2.09	123.0	TGTACCCACATCATCTACAG	ACAGACAAGAGAGTCTTCAG
H1_CPA4	1.89	77.6	AGAAATGGAGACGAGATCAG	GGGAGATTTCCAGAAATTGAG
H1_EGFR	1.98	95.5	AGTGCCTGAATACATAAACC	GTAGTGTGGGTCTCTGC
H1_FMOD	1.95	89.1	AACAGTCTAACCAACAATGG	CTCATTGATCCTATTGCCTTG
H1_LIFR	1.98	95.5	AAGTTTATCCCCATACTCCTAC	CCTGGTAAATGCCAAGAAAG
H1_OSM	2.08	120.2	TCCTTGCACTCCTGTTTC	GATACGTATATAGGGGTCCAG
H1_OSMR	2.01	102.3	GTGTACAAGATTCTACTGG	GTTTCCCTTCCAAATAACA
H1_PCSK1N	1.88	75.9	ACGTCCAGAGCAACTTAC	TTGCTTCAGATCATGTTTATTG
H1__PLAUR	1.99	97.7	AATCCTGGAGCTTGAAAATC	CAGTCAATGAGGAAAGTCTC
H1_PLCB4	1.91	81.3	AGAATGATGAAATTGAGCCC	AGATCTTCTATATCTGTCCGAG
H1_PTPRR	2.05	112.2	CTTCGTATGGATAGAGGTGG	GAGATTGATGGTCTGACAAG
H1_RAB38	2.07	117.5	GATATCGCAGGTCAAGAAAG	TCGAAGACAATAAATGCACC
H1_SERPINA1	FAILED	FAILED	TAAGGATTCTCGAGTGAGAG	TGTCCTCGTCCGTATTTAAG
H1_SNAI1	1.91	81.3	TCGGAAGCCTAACTACAGCGA	AGATGAGCATTGGCAGCGAG
H1_STAT3	2.01	102.3	GGTACATCATGGGCTTTATC	TTTGCTGCTTTCACTGAATC
H1_TGM2	1.94	87.1	CTTCATTTTGCTCTTCAAC	AGGATCCCATCTTCAAACTG
H1_VEGFA	2.04	109.6	AATGTGAATGCAGACCAAAG	GACTTATACCGGGATTTCTT

Primer efficiency was calculated using an Excel Primer Efficiency Calculator programme designed by Dr Ian Roberts. Percentage copy number of target cDNA in each dilution compared to the original undiluted sample was calculated (neat = 100%, 1:2 = 50%, 1:4 = 25%, 1:10 = 10%, 1:50 = 2% and 1:100 = 1%). The log of these values was calculated and plotted versus Ct value for each cDNA dilution. Linear regression was performed to determine a line of best fit, and the slope of the line calculated. Primer efficiency values were then calculated using the following equation:

Primer efficiency value = $10^{(-1/\text{slope})} - 1$

Primer efficiency percentage = $10^{(\text{primer efficiency value})}$

3.6.7 Quantitative Real-Time PCR (qPCR): mRNA

cDNA samples diluted 1:80 in nuclease-free water were used as template for qPCR. A 12µl/well mastermix comprising 10µl 2X qPCRBio Sybergreen Mix Lo-Rox and 2µl of relevant primer pair (4µM; Table 3.24) were added to a 96 well PCR plate along with 8µl of template cDNA. Each gene/sample under investigation was run in triplicate. Quantitative-PCR was performed on a RealPlex2 MasterCycler (Table 3.25).

Table 3.25: qPCR conditions for mRNA qPCR

PCR Step	Temperature	Time	
Initial denaturation	95°C	2mins	
Denaturation	95°C	5secs	40 cycles
Annealing	65°C	25sec	
Extension	76°C	8sec	

The comparative Ct method described by Pfaffl *et al* (2001)[219] was used to calculate the relative expression levels of target genes in each sample. This method compares the Ct value of a target gene to Ct levels of an endogenous control gene within each sample. Relative expression levels (fold change) are calculated by comparing gene expression levels in each sample to those of a comparator sample (i.e. OSM treated compared to PBS control) while taking into account primer efficiency of each gene:

$$\text{Abundance} = 2^{-\text{CT gene} - \text{CT endogenous control}}$$

$$\text{Fold Change} = \frac{\text{Primer Efficiency Target Gene}^{(\text{CT control sample} - \text{CT treated sample})}}{\text{Primer Efficiency Endogenous Control}^{(\text{CT control sample} - \text{CT treated sample})}}$$

Three endogenous control genes, HMBS, RPL13A and YWHAZ, were used for analysis[220]. Abundance and fold change were plotted using Graph Pad Prism software and analysed for statistical significance using a one way ANOVA with Tukey's multiple comparison post-hoc test (when comparing multiple sample groups) or unpaired T-tests (when comparing two groups of samples). P values of ≤0.05 were regarded as significant.

3.6.8 Reverse Transcription: miRNA

Table 3.26: Reverse Transcription (miRNA)	
Reagent	**Volume per Sample**
Nuclease-free water	0.7µl
RT Buffer (10X)	1.0µl
0.1x dNTPs (10mM)	1.0µl
0.1x RNase Inhibitor (2units/µL)	1.3µl
MultiScribe™ Reverse Transcriptase (50units/µL)	0.67µl
Specific TaqMan miRNA Primer (5X)	2.0µl
Relevant RNA (15ng/µl)	3.33µl
TOTAL	10µl

Following RNA extraction samples were diluted to 15ng/µl in nuclease-free water. Taqman MicroRNA Reverse Transcription Reagents (Table 3.26) were used to reverse transcribe miRNA into cDNA using stem-looped primers, as depicted in Figure 3.7. Separate mastermixes were prepared for each miRNA under investigation using miRNA specific TaqMan miRNA primers; details of miRNA primers are listed in Table 3.27.

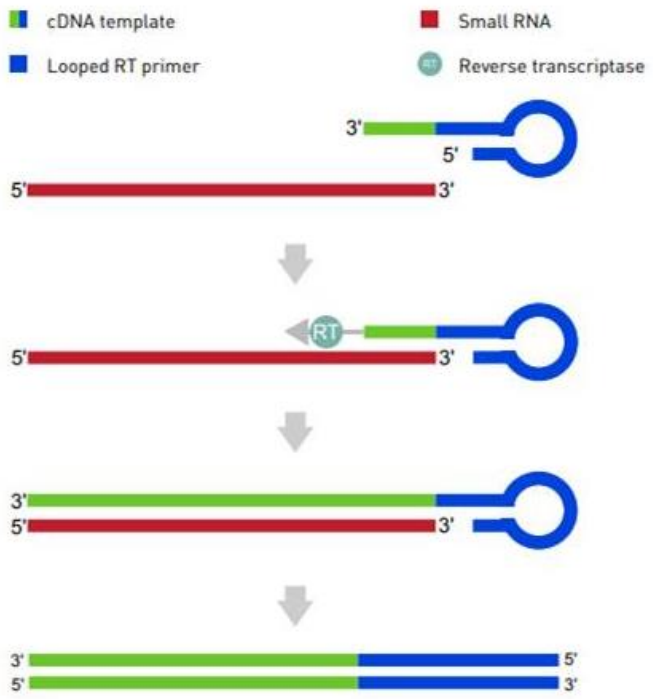

Figure 3.7: miRNA reverse transcription using Taqman stem-loop primers
https://assets.thermofisher.com/TFS-Assets/LSG/manuals/4364031_TaqSmallRNA_UG.pdf

Samples were incubated on ice for 5mins then run on a MJ Research Tetrad PTC-225 Peltier Thermal Cycler under the following conditions: 16°C for 30mins (pre-incubation), 42°C for 30mins (annealing/extension), and 85°C for 5mins (enzyme inactivation). Samples

prepared without the addition of reverse transcriptase or RNA were used as negative controls.

Table 3.27: miRNA Assay Primers and Probes			
Assay Name	**NCBI Accession Number**	**miRBase Accession Number**	**Control Sequence/ Mature miRNA Sequence**
RNU 24	NR_002447		ATTTGCTATCTGAGAGATGGTGATGACA TTTTAAACCACCAAGATCGCTGATGCA
Cel-miR-39-3p		MIMAT0000010	UCACCGGGUGUAAAUCAGCUUG
hsa-miR-9-3p		MIMAT0000442	AUAAAGCUAGAUAACCGAAAGU
hsa-miR-10b-5p		MIMAT0000254	UACCCUGUAGAACCGAAUUUGUG
hsa-miR-23b-3p		MIMAT0000418	AUCACAUUGCCAGGGAUUACC
hsa-miR-29b-3p		MIMAT0000100	UAGCACCAUUUGAAAUCAGUGUU
hsa-miR-30b-5p		MIMAT0000420	UGUAAACAUCCUACACUCAGCU
hsa-miR-31-5p		MIMAT0000089	AGGCAAGAUGCUGGCAUAGCU
hsa-miR-34c-5p		MIMAT0000686	AGGCAGUGUAGUUAGCUGAUUGC
hsa-miR-101-3p		MIMAT0000099	UACAGUACUGUGAUAACUGAA
hsa-miR-126-5p		MIMAT0000444	CAUUAUUACUUUUGGUACGCG
hsa-miR-194-3p		MIMAT0004671	CCAGUGGGGCUGCUGUUAUCUG

3.6.9 Quantitative Real-Time PCR (qPCR): miRNA

Cellular and EV miRNA expression was quantified by q-PCR. For each sample, the reagents shown in Table 3.28 were added to a 96 well PCR plate; separate mastermixes were prepared for each miRNA under investigation using miRNA specific TaqMan miRNA probes. Probe details are shown in Table 3.27.

Table 3.28: q-PCR (miRNA) mix per sample	
Reagent	**Volume per Sample**
2X qPCR Bio Sygreen Lo-Rox Mix	7.5µl
Nuclease-free water	5.42µl
Specific TaqMan miRNA Probe (20X)	0.75µl
Specific RT Product	1.33µl
TOTAL	15µl

For each gene under investigation, cDNA samples were run in triplicate. Quantitative-PCR was performed on a RealPlex2 MasterCycler under the following settings: 95°C for 10mins (Taqman enzyme activation) and then 40 cycles of 95°C for 15secs (denaturation) and 60°C for 1min (annealing/extension).

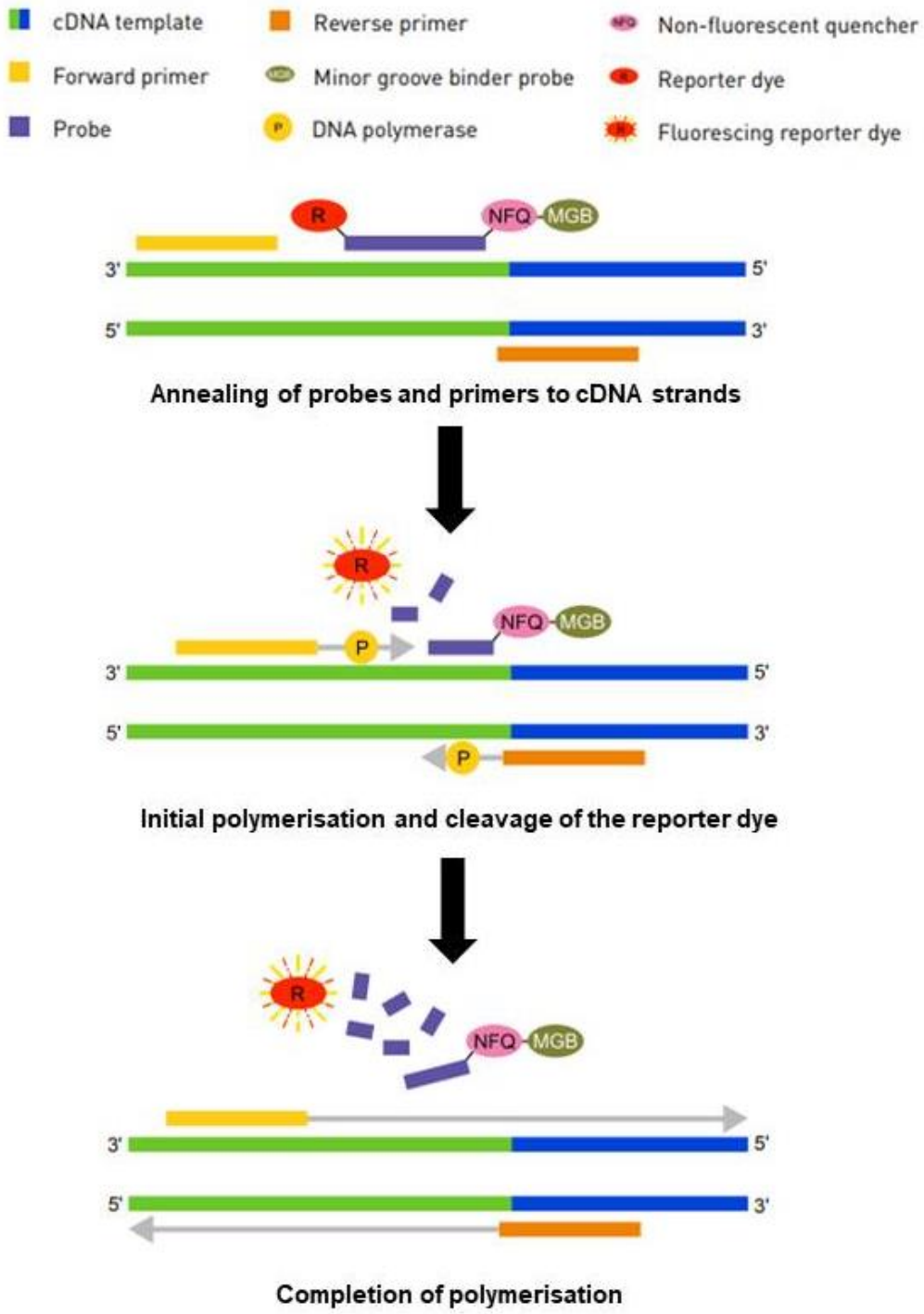

Figure 3.8: Schematic of miRNA qPCR using Taqman probes
https://assets.thermofisher.com/TFS-Assets/LSG/manuals/4364031_TaqSmallRNA_UG.pdf

Each Taqman probe mix for qPCR contains miRNA-specific forward and reverse primers and a miRNA-specific probe. Probes have a reporter dye on their 5' end and a non-fluorescent quencher (NFQ) dye and a minor groove binder (MGB) at their 3' end. The MGB increases the probe's melting temperature without increasing its length. During PCR the

forward and reverse primers anneal to complementary sequences along the denatured cDNA template strands. The probe anneals to a complementary sequence located between the forwards and reverse primer sites. Proximity of the probe's reporter dye to the NFQ suppresses the reporter fluorescence. During polymerisation, DNA polymerase cleaves probes that are hybridised to the target sequence, releasing the reported dye which results in an increase in fluorescence which can be detected by the RealPlex machine. Cleavage only occurs if the target sequence is amplified during PCR. Extension of the probe does not occur during polymerisation as its 3' end is blocked by the NFQ dye and MGB. This is summarised in Figure 3.8.

Due to their specificity, primer efficiency is not expected to vary between different Taqman miRNA primers and probes. They are expected to have a primer efficiency of 2.0. Therefore, primer efficiency analysis was not performed and relative expression was calculated via the double delta Ct method (ΔΔCT), summarised in Figure 3.9. Within each experiment the sample with the lowest cel-miR-39 spike-in Ct was identified; this is the sample with the greatest number of copies of cel-miR-39 and therefore had the greatest RNA extraction efficiency. RNA extraction efficiency was corrected between samples from the same experiment by subtracting this value from the cel-miR-39 Ct values of all other samples; producing an RNA extraction correction factor for each sample. The levels of an endogenous control miRNA ('housekeeper miRNA'; RNU24 or miR-30b) within each sample were subsequently corrected for RNA extraction efficiency by subtracting the RNA extraction correction factor from the HK Ct value. RNU24 and miR-30b were selected as HK miRNAs as they were previously shown to be abundant and stably expressed across several cervical and non-cervical cell lines commonly used within our laboratory (Shivani Bailey, unpublished) and have previously been demonstrated to be reliable housekeepers for qPCR analysis of miRNA expression in cervical tissue samples[221]. The relative expression level of each target miRNA (ΔCT) was calculated by normalising target miRNA Ct values to Ct values for the HK miRNA. These values were transformed using the logarithmic equation $Y=2^{(-\Delta CT)}$ to give gene abundance relative to HK expression. ΔCT values for each sample were then normalised (ΔΔCT) to ΔCT values from calibrator samples (i.e. cells treated with PBS control) and transformed using the logarithmic equation $Y=2^{(-\Delta\Delta CT)}$ to give fold change. Abundance and fold change were plotted using Graph Pad Prism software and analysed for statistical significance using a one way ANOVA with Tukey's multiple comparison post-hoc test or Unpaired T-tests. *P* values of ≤0.05 were regarded as significant.

RNA Extraction Correction Factor
= CT cel-miR-39 (sample) –CT cel-miR-39 (lowest per experiment)

RNA Extraction Efficiency Correction
= CT HK miRNA (sample) – RNA Extraction Correction Factor (sample)

ΔCT = CT target miRNA – CT HK miRNA (corrected for RNA extraction efficiency)

Abundance = $2^{-\Delta CT}$

ΔΔCT = ΔCT sample - ΔCT calibrator sample (i.e. PBS control)

Fold difference = $2^{-\Delta\Delta CT}$

Figure 3.9: Summary of miRNA fold change calculation

3.7 Next Generation Sequencing

Table 3.29: Reagents used for Next Generation Sequencing	
Reagent	**Company**
• Somagenics Real-Seq®-AC miRNA Library Kit for Illumina sequencing	Somagenics, Santa Cruz, CA, USA
• NEXTFLEX® Small RNA-Seq Kit v3	Bioo Scientific Corporation, Austin, TX, USA
• SMART-Seq® v4 Ultra® Low Input RNA kit	Takara Bio USA Inc, Mountain View, CA, USA
• Nextera® XT DNA kit	Illumina, San Diego, CA, USA

SW756 empty plasmid and SW756 OSMR KD cell lines (generated in section 3.3) and their resultant EVs were used for these experiments. Cells were treated with OSM or PBS control for 48hours prior to EV collection.

3.7.1 Optimisation of library preparation for small RNA sequencing

An initial optimisation experiment was performed to determine the best library preparation kit to use for small RNA sequencing of EVs, which have low input quantities of RNA. Following RNA extraction (section 3.6.3), RNA concentration and quality of individual EV preparations were determined by a 4200 TapeStation using a high sensitivity RNA Screen Tape assay and TapeStation Analysis Software (Agilent Technologies, Santa Clara, CA, USA). This was performed by Cambridge Genomic Services, Department of Pathology, Cambridge. Concentrations for each of the four EV samples are shown in Table 3.30.

Table 3.30: Concentration of RNA obtained from single EV preparations			
Sample	**Concentration**	**Volume**	**Total amount of RNA per EV prep**
SW756 Empty Plasmid + PBS - EVs	1140 pg/µl	20µl	22.8ng
SW756 Empty Plasmid + OSM - EVs	777 pg/µl	20µl	15.5ng
SW756 OSMR KD + PBS - EVs	745 pg/µl	20µl	14.9ng
SW756 OSMR KD + OSM - EVs	1160 pg/µl	20µl	23.2ng
AVERAGE	**955.5 pg/µl**	**20µl**	**19.1ng**

As collection of EVs is a labour-intensive process, cellular RNA from SW756 empty plasmid cell, diluted to a similar concentration as would be obtained from EVs, was used to select which small RNA sequencing kit to use. For each library prep kit, three aliquots of 30ng 'low input' and three aliquots of 250ng 'high input' RNA were used. Three aliquots of 100ng 'medium input' RNA were also included for the Somagenics library preparation kit. Experimental design is depicted in Figure 3.10.

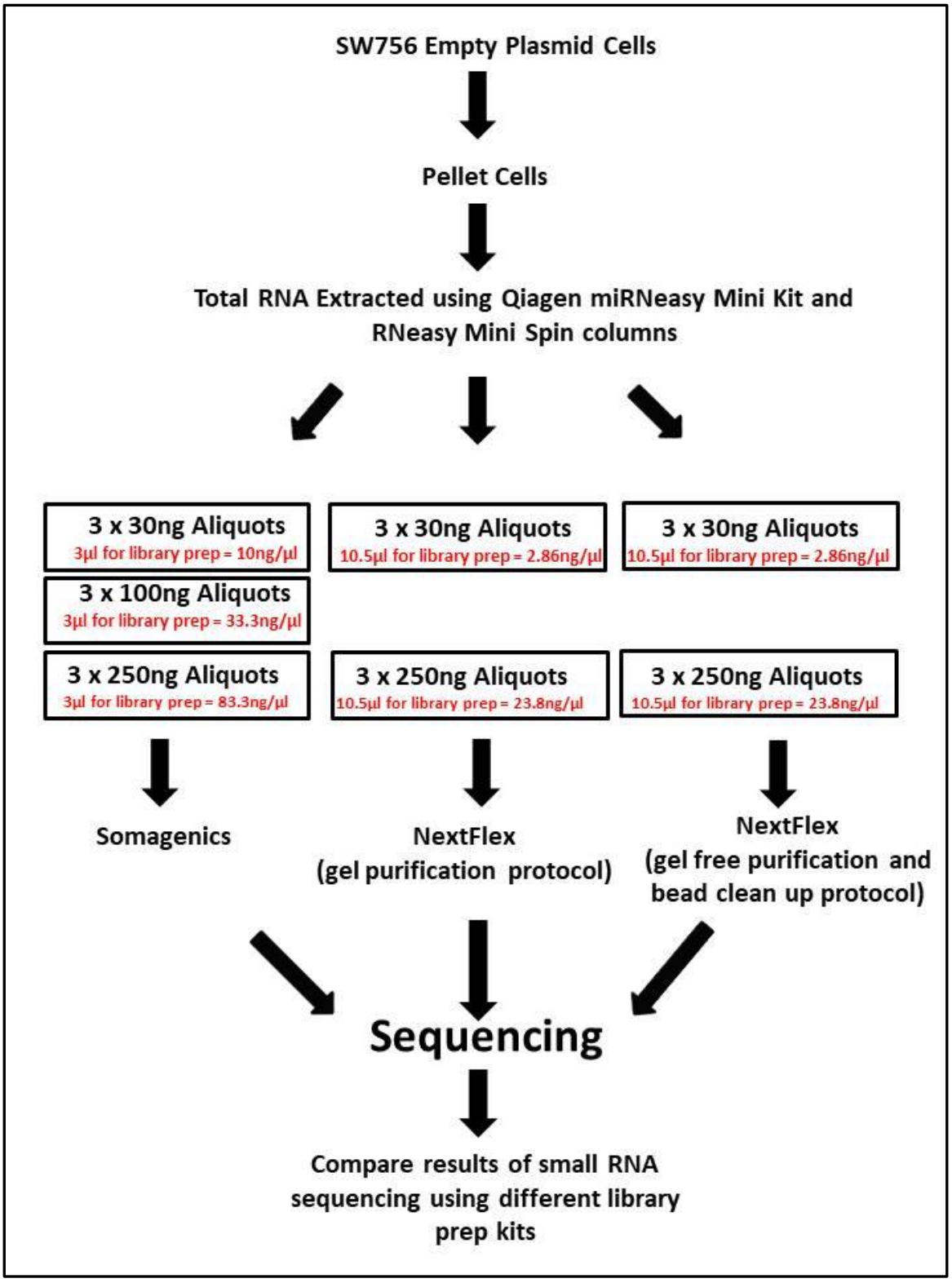

Figure 3.10: Experimental design for comparison of small RNA library preparation kits

Libraries were prepared according to manufacturer's instructions by Cambridge Genomic Services. Samples were then run on a NextSeq500, with a 75 cycles High Output kit, at a final concentration of 1.8pM with 20% PhiX spike-in control. Bioinformatic analysis was

performed by Dr Anton Enright and Stephanie Wenlock (section 3.7.4). NEXTFLEX® Small RNA-Seq Kit v3; using gel free size selection and bead clean up protocol was selected as the optimum small RNA library preparation method. An input of 30ng RNA was selected for subsequent experiments.

3.7.2 Sequencing - Sample Collection

An average of ~19ng RNA was found to be obtained from a single EV isolation experiment (Table 3.30). In order to obtain enough material to split samples for mRNA and miRNA library preparation and sequencing, five EV preps were pooled per 'biological replicate' so that each replicate would contain ~100ng RNA. Therefore, treatments of cells with PBS/OSM and subsequent isolation of EVs were performed 25 times so that so that five EV preps could be combined for each experimental condition, producing five pooled replicates per treatment group (five replicates per condition x five pooled samples = 25 individual EV isolations per experimental condition). Treatment of SW756 empty plasmid cells typically results in reduction of cell number; two different batches of OSM were used for these experiments – potency of OSM has previously been found to vary between batches. To ensure that 'biological replicates' comprised evenly distributed samples, the following factors were taken into consideration when deciding which five samples/ replicate to pool: cell stock (as multiple vials of cells were defrosted for this experiment), cell passage number, batch of OSM used and fold change in cell number of empty plasmid cells following OSM treatment.

Total RNA extraction from cell samples was performed as described in section 3.6.2; phenol-chloroform extraction was performed for each individual sample. Following the addition of 1.5x volume 100% ethanol per sample, five samples per condition were pooled, mixed in a 15ml falcon tube and split between two spin columns. The remainder of the protocol was conducted as previously described. Following elution the eluates from the two spin columns were combined to give a total volume of 120µl for each biological replicate.

A similar protocol was employed for pooling of EV samples. Total RNA extraction from EVs was performed as described in section 3.6.3. Phenol-chloroform extraction was performed for each individual sample. Following the addition of 1.5x volume 100% ethanol per sample, five samples per condition were pooled, mixed in a 15ml falcon tube and the remainder of the protocol was conducted as previously described using a single spin column. Final elution volume was 24µl for each biological replicate.

3.7.3 Library Preparation

Libraries preparation was performed by Cambridge Genomic Services. Quality and RNA concentration for each EV sample were determined using an Agilent 2100 Bioanalyser

G2938B (Agilent Technologies). Cellular RNA concentration and quality were determined using a 4200 TapeStation using a RNA Screen Tape assay and TapeStation Analysis Software (Agilent Technologies). Samples were split for miRNA and mRNA library preparation.

mRNA cDNA libraries were prepared using a SMART-Seq® v4 Ultra® Low Input RNA kit using 5ng input RNA, according to manufacturer's instructions. cDNA was subsequently input into the Nextera® XT DNA kit for library preparation according to manufacturer's instructions. miRNA libraries used 30ng input RNA in a total volume of 10.5µl and were prepared with a NEXTFLEX® Small RNA-Seq Kit v3, using the gel-free size selection and bead clean up protocol according to manufacturer's instructions. Samples were run on a NextSeq 500, using a 75 cycles High Output kit, at a final concentration of 1.8pM with 10% or 20% PhiX (mRNA and small RNA, respectively).

3.7.4 Bioinformatic Analysis – mRNA

The bioinformatics analysis detailed in this section was performed by Dr Anton Enright, Stephanie Wenlock and Dr Stephen Smith. Quality control was performed on raw data using FastQC v0.11.4. Reads were trimmed using TrimGalore v0.4.1 and mapped to Ensembl Homo_sapiens.GRCh38 (release 92) reference genome using STAR v2.5.2a. The number of reads that mapped to genomic features was calculated using HTSeq v0.6.0[222]. Either a DESeq2[223] or EdgeR[224] normalisation procedure was applied to raw counts generated by HTSeq. Statistical analysis was performed in order to investigate differential gene expression between samples. This was executed using three different analysis packages – DeSeq2, EdgeR and EdgeR Voom. The negative binomial Wald's test was used to determine significant differences between groups. A log fold change (LFC) threshold of +/- 0.5 and a False Discovery Rate (FDR) significance threshold of ≤0.05 were applied.

3.7.5 Bioinformatic Analysis – miRNA

The bioinformatics analysis detailed in this section was performed by Dr Anton Enright, Stephanie Wenlock and Dr Stephen Smith. Adapter stripping, filtering of low quality basecalls and removal of the Nextflex 4 nucleotide add-ons, were completed using a custom Perl script and Reaper tool[225]. Cleaned and filtered reads were mapped against all known mature miRNA sequences in miRBase using Chimira[226]. Raw counts generated by Chimira for each sample, were plotted in R. A DESEq2 normalisation procedure was subsequently applied to the raw counts[223]. Statistical analysis was performed to investigate differential miRNA expression between samples. The negative binomial Wald's test was used to

determine significant differences between groups. A LFC of +/-0.5 and a FDR significance threshold of 0.05 were applied.

3.8 Protein Experiments

Table 3.31: Reagents for protein work

Reagent	Company
• RIPA buffer (1X) • RIPA buffer (10X) • Protease and phosphatase inhibitor mini tablets • Pierce BCA Protein Assay Kit • Bovine serum albumin for BCA (vials)	Pierce, Thermo Fischer Scientific, Waltham, MA, USA
• 96 well flat bottom microtitre plate • 20x Transfer Buffer • Restore western blot stripping buffer • BSA for western blot • Expedeon Two-Color SDS marker • SeeBlue™ Plus2 Pre-stained Protein Standard	Thermo Fisher Scientific, Waltham, MA, USA
• NuPAGE LDS sample buffer (4x) • NuPAGE sample reducing agent (10x) • NuPAGE antioxidant • NuPAGE MOPS SDS running buffer(20x) • 4-12% NuPAGE Bis-Tris Mini Gels	Invitrogen, Life Technologies, Thermo Fisher Scientific, Waltham, MA, USA,
• Ponceau-S Staining Solution • Methanol	Sigma Aldrich, St Louis, MO, USA
• Immobilon-P microporous polyvinylidene fluoride (PVDF) Membrane	Millipore Sigma, Billerica, MA, USA
• Blotting Paper	Sartorius Stedim Biotech, Aubagne, France
• Dulbecco's Phosphate Buffered Saline (PBS) • ELISA grade BSA • Glycerol • Tween-20	Sigma Life Sciences, Sigma Aldrich, St Louis, MO, USA
• TBS	Hutchison/MRC Media Kitchen, Cambridge, UK
• Milk powder	Marvel, Premier Foods, St. Albans, UK
• human OSM DuoSet ELISA containing (ELISA substrate solution, anti-OSMR detection antibody, ELISA stop solution) • High-binding 96-well microtiter plates	R&D Systems, Minneapolis, MN, USA
• ECL western blotting detection reagents • ECL prime western blotting detection reagents	Amersham, GE Healthcare, Little Chalfont, UK

Table 3.32: Buffers for protein experiments	
Buffer	**Component**
• 1x Transfer Buffer	850ml dH20 + 100ml methanol + 50ml 20x Transfer Buffer + 1ml antioxidant
• BSA buffer	1x TBS + 5% BSA + 0.1% Tween-20
• Blocking buffer	1x TBS + 5% milk powder + 1% Tween-20
• Antisera Buffer	1x TBS + 5% milk powder + 0.1% Tween-20
• WB Wash Buffer	1x TBS + 0.1% Tween-20
• ELISA Wash Buffer	1x PBS + 0.05% Tween
• ELISA Dilutant	PBS + 1% ELISA grade BSA
• ELISA substrate solution	1:1 mixture of colour reagent A (H_2O_2) and colour reagent B (tetramethylbenzidine)

3.8.1 Protein Extraction – Cells

Following cell culture in 6 well plates, media was removed and cells were washed with PBS. 100µl/well 1xRIPA buffer supplemented with protease and phosphatase inhibitors (1 tablet/10ml) was added and plates incubated on ice for 5mins. Cells were detached using a cell scraper and lysate transferred to a 1.5ml eppendorf tube. Samples were incubated on ice for 30mins, with occasional agitation by gentle pipetting, and 1/10th volume 80% glycerol subsequently added. Cell debris was removed by centrifugation of samples at 16,000 x*g* for 15mins at 4°C. Supernatant was transferred to a new tube and protein concentration measured by Bicinchoninic Acid (BCA) assay.

3.8.2 Protein Extraction – EVs

Following ultracentrifugation the volume of EV suspension was measured by pipette. Either the entire sample, or a small proportion of the sample, was resuspended in 10x RIPA buffer supplemented with protease and phosphatase inhibitors (1tablet/ml). This depended on whether samples would be used for western blot or if protein quantification was performed on a small aliquot prior to resuspension of a required quantity of EVs in media for functional assays, respectively. 1/10th volume of 10x RIPA buffer was added to samples to achieve a final 1x RIPA concentration. Samples were mixed by pipette and incubated on ice for 20mins. Samples were then centrifuged at 16,000x*g* for 15mins at 4°C and supernatant removed to a new Eppendorf tube.

3.8.3 Protein Quantification

Protein concentration of each sample was determined using a Pierce BCA protein assay kit. First, a standard curve was prepared by dilution of 2µg/µl BSA in 1x RIPA buffer (cell standard curve) or 10x RIPA diluted 1:10 in PBS (EV standard curve) to the following concentrations: 2, 1.8, 1.6, 1.4, 1.2, 1, 0.833, 0.667, 0.5, 0.333, 0.167, 0.08 and 0 µg/µl.

Protein collected from cell samples was diluted at a 1:4 or 1:7 dilution in RIPA buffer, whereas EV samples were not diluted. 3µl of each standard and sample were loaded in triplicate onto a 96 well flat bottom microtitre plate. Pierce BSA assay reagents A and B were mixed in a 50:1 ratio and 100µl/well added. The plate was then incubated for 30mins at 37°C in the dark. Presence of protein in the alkaline medium results in reduction of Cu^{2+} to Cu^{+} (biuret reaction); subsequent chelation of Cu^{+} with two BCA molecules produces a purple-coloured reaction product which enables protein concentration to be determined colourmetrically with high sensitivity. The absorbance of each sample was measured after the 30min incubation at a wavelength of 570nm using a Dynex Technologies plate reader and Revelation software. The BSA standards were used to form a standard curve of known protein concentration by plotting known protein concentration (x axis) against absorbance at 570nm (y axis). This was then used to extrapolate the protein concentration of each sample.

3.8.4 SDS Page

According to the results of protein quantification by BCA assay, 20µg of protein for each sample was diluted in PBS to a total volume of 13µl or 15µl, depending on whether SDS Page would be performed under reducing or non-reducing conditions, respectively. 5µl NuPAGE LDS sample buffer (4x) and 2µl NuPAGE sample reducing agent (10x; if using reducing conditions) were added to each sample to obtain a final protein concentration of 1 µg/µl (in a total volume of 20µl). Samples were mixed by vortexing, briefly centrifuged, and then denatured by heating to 95°C for 10mins.

Precast 4-12% Nu-PAGE Bis-Tris mini gels were placed in an XCell SureLock Mini-Cell (Thermo Fisher Scientific), in front of the buffer core. The gel tension wedge was locked in place behind the buffer core and the central buffer core chamber filled to capacity with 200ml 1x NuPAGE MOPS SDS running buffer (diluted in ddH_20) containing 500µl NuPAGE antioxidant. The outer chamber was filled to the level of the mini gel well base with 500ml 1x MOPS SDS running buffer without antioxidant. 7µl of Expedeon Two-Color SDS marker or SeeBlue™ Plus2 Pre-stained Protein Standard was loaded in the first well of the mini gel and, depending on the size of the gel, the following volumes of protein sample were loaded: 15µl (for 15 well gels) or 20µl (12 well gels). Proteins were separated by electrophoresis at 150V for 2hours.

3.8.5 Western Blot

A PVDF membrane and two pieces of 3MM blotting paper were cut to the size of a SDS-PAGE gel. The PVDF membrane was activated by incubation in 100% methanol for 15 sec followed by a 2min rinse in distilled water (dH_2O). The PVDF membrane was then

transferred to ice-cold 1x transfer buffer for at least 5min to equilibrate. Blotting paper and four blotting sponges were also pre-soaked in 1x transfer buffer.

Following electrophoresis, protein samples separated by SDS-PAGE were transferred to the PVDF transfer membrane using the XCell SureLock Mini-Cell and XCell IITM blot module (Thermo Fisher Scientific). The gel cassette was removed from the mini-cell and the two plates of the cassette separated using a gel knife. Wells of the gel were subsequently removed with a gel knife and a piece of pre-soaked filter paper was placed on top of the gel. The gel and filter paper were carefully peeled away from the cassette and the equilibrated PVDF membrane placed on top of the gel, ensuring no air bubbles were present. An additional piece of pre-soaked filter paper was placed on top of the membrane.

Two pre-soaked blotting sponges were placed on top of the cathode core of the XCell IITM blot module. The filter paper – gel – membrane – filter paper 'sandwich' was placed on top of the sponges and an additional two pre-soaked sponges placed on top of the 'sandwich'. The lid of the blot module was placed on top and the whole assembly inserted into the XCell SureLock™ Mini-Cell (Figure 3.11). The blot module was filled with 1x transfer buffer; ice-cold dH20 was added to the outer reservoir. The protein transfer was performed for 2hours at 30 V at 4°C.

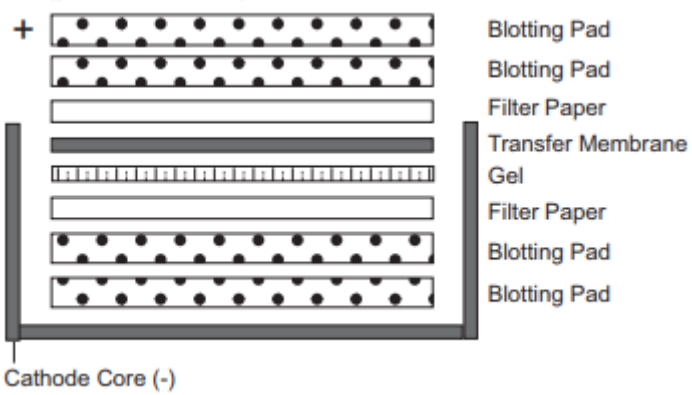

Figure 3.11: Depiction of protein transfer
https://assets.thermofisher.com/TFS-Assets/LSG/manuals/blotmod_pro.pdf

After completion of the transfer, the blot module was dismantled and, if necessary, the PVDF membrane stained with Ponceau-S Staining Solution to assess the quality of the protein transfer. Following ponceau-S staining, membranes were washed first with dH2O, then three times for 5mins in WB wash buffer. Membranes were then incubated in either BSA buffer or

blocking buffer for 1hour at room temperature with constant shaking, depending on whether primary antibodies were phosphorylated or unphosphorylated, respectively.

Membranes were incubated at 4°C overnight with constant shaking with primary antibody diluted in BSA buffer or antisera buffer, depending on whether primary antibodies were phosphorylated or unphosphorylated, respectively (Table 3.33). The following day, the membranes were washed three times for 5mins with WB wash buffer and incubated for 1hour at room temperature with constant shaking in species-specific HRP-conjugated secondary antibodies diluted in BSA buffer or antisera buffer (again depending on whether primary antibody is phosphorylated or not, respectively).

Following three further washes with WB wash buffer, the membrane was developed using enhanced standard chemiluminescence (ECL) or ECL prime western blotting detection reagents according to the manufacturer's instructions and exposed onto autoradiography films at various time-points in a dark room. If required, primary antibodies were stripped from the membrane with Restore western blot stripping buffer for 10mins at room temperature in the dark. Blots were then washed with WB wash buffer, blocked in either BSA buffer or blocking buffer and re-probed with different primary antibodies.

Table 3.33: Antibodies for Western Blot

	Antibody Name	Host Species	Dilution	Conditions	Company and Catalogue Number
PRIMARY ANTIBODIES	OSMR	rabbit	1:500	Reducing Non-phosphorylated	Santa Cruz, SC-30010
	STAT3	mouse	1:1000	Reducing Non-phosphorylated	Cell Signalling Technology, 9139
	Phospho-STAT3	rabbit	1:1000	Reducing Phosphorylated	Cell Signalling Technology, 9145
	SNAI1	rabbit	1:1000	Reducing Non-phosphorylated	Cell Signalling Technology, 3879
	Alix	mouse	1:200	Reducing Non-phosphorylated	Santa Cruz, sc53540
	CD63	mouse	1:200	Non-reducing non- phosphorylated	Invitrogen, 10628D
	CD9	mouse	1:500	Non-reducing non- phosphorylated	Invitrogen,10626d
	Cytochrome C1	mouse	1:100	Reducing Non-phosphorylated	Santa Cruz, sc-514435
	β-Actin	mouse	1:100,000	Reducing Non-phosphorylated	Abcam, ab6276
SECONDARY ANTIBODIES	anti mouse HRP conjugated antibody	goat	1:2000	N/A	Dako, P044701
	anti rabbit HRP conjugated antibody	goat	1:2000	N/A	Dako, P044801

3.8.6 ELISA for hOSM expression

Secretion of hOSM by OSMR overexpressing cell lines was measured by hOSM DuoSet ELISA according to manufacturer's instructions by Dr Danita Pearson. OSM capture antibody was diluted to 2µg/ml in PBS and 100µl/well used to coat high-binding 96-well microtiter plates, which were incubated overnight at room temperature. The following day conditioned media was harvested and cell number determined by Countess cell counter in order to normalise OSM concentration. Conditioned media was centrifuged at 12,000*xg* for 1min to remove cell debris. Plates were washed three times with ELISA wash buffer and incubated for 1hour with 300µl/well of ELISA dilutant. 100µl of OSM standards of varying known OSM concentration or conditioned media from cell culture were then added to each well in duplicate and incubated for 2hours at room temperature. Plates were then washed in ELISA wash buffer and subsequently incubated for 2hours with 100µl of anti-OSM detection antibody (30ng/ml in ELISA dilutant) at room temperature. Plates were subsequently washed in ELISA wash buffer and incubated for 20mins in the dark at room temperature in 100µl/well of streptavidin-horse radish peroxidase (HRP; diluted 1:200 in ELISA dilutant). Plates were washed again and 100µl of substrate solution added to each well. Samples were incubated at room temperature for 20mins in the dark at room temperature before 50µl of ELISA stop solution was added to each well and absorbance measured at a wavelength of 450nm with background subtraction of 570nm using a Dynex Technologies plate reader with Revelation software. Absorbance for OSM standards of different known concentrations were used to generate a standard curve which was then used to extrapolate OSM concentration in test samples based on their absorbance.

3.9 Functional Assays

Table 3.34: Reagents and equipment for functional assays

Reagent	Company
• V2A kit	Cellworks, Buckingham, UK
• MTT cell growth Assay kit	Merck Millipore, Burlington, MA, USA
• Isopropyl alcohol • HCL	Sigma Aldrich, St Louis, MO, USA
• DM LB light microscope • DC500 digital camera	Leica, Wetzlar, Germany

For cell growth and migration assays, EVs were collected by ultracentrifugation from SW756 or ME180 cells treated with PBS/OSM in EV depleted media for 48hours. Quantity of EV protein was determined by performing a BCA assay on a small aliquot of sample.

3.9.1 Cell growth

SW756 cells were seeded at a concentration of 2 x10^4 cells/well in 6 well tissue culture plates in normal media. After 24hours in culture, media was removed and wells were washed with sterile PBS. 1.5ml of fresh EV depleted media supplemented with 1µg of EVs from PBS or OSM treated SW756 cells or PBS control of an equal volume was added to the 6 well plates. Cells were trypsinised and counted by Countess cell counter at the following timepoints: 3, 5 and 7 days post treatment. Three wells were counted for each experimental condition at each timepoint.

Alternatively, cell numbers were inferred from MTT (3-(4,5-dimethythiazol2-yl)-2,5-diphenyl tetrazolium bromide) assays. Cells were seeded and treated with PBS/OSM as described above and measured at 3, 5, 7 and 10 days post treatment with MTT. MTT is a colorimetric assay which measures mitochondrial metabolic rate, and is therefore used to indirectly reflect viable cell number. MTT is a yellow substrate that is reduced by mitochondrial succinate dehydrogenase in living cells to an insoluble, dark purple coloured formazan precipitate. When solubilised with isopropanol, its absorbance at 570nm compared to that of media only control can be used to infer changes in cell number[227]. At each timepoint, media was removed, wells washed with PBS and 0.5ml fresh media added. 0.5ml 12mM MTT was added per well and incubated at 37°C in 5% CO_2 for 2hours. 0.5ml solubilisation solution (0.04N HCL in isopropyl alcohol) was added per well and gently mixed. 100µl/sample was loaded in triplicate on a 96 well flat bottom microtitre plate. The absorbance of each sample was measured at a wavelength of 570nm using a Dynex Technologies plate reader and Revelation software. For each timepoint, cell viability was calculated by normalisation of sample absorbance to that of a control media only sample.

3.9.2 Migration Assay

In order to determine whether EVs derived from OSMR overexpressing cells had an effect on cell migration the following experiments were performed:

- Addition of EVs derived from PBS/OSM treated SW756 cells to SW756 recipient cells
- Addition of EVs derived from PBS/OSM treated SW756 cells to VF1 recipient cells
- Addition of EVs derived from PBS/OSM treated ME180 cells to ME180 recipient cells

SW756 and ME180 cells were seeded at a concentration of 5 x10^5 cells/well in 6 plates; whereas VF2 cells were seeded at a concentration of 4 x10^5 cells/well. After either 48hours (SW756 and ME180 cells) or 7 days (VF2 cells) in culture cells reached confluency and a line was scored down the centre of each well using a 1ml pipette tip. Media was removed

and cells were washed in sterile PBS. 2ml of fresh EV depleted media supplemented with one of the following experimental conditions was added to each well in triplicate:

1) 0.1µg EVs (ME180 and SW756 recipient cells only)
2) 1µg EVS (ME180 and SW756 recipient cells only)
3) 10µg EVS (all 3 recipient cell lines)
4) 2ml EV depleted conditioned media (supernatant from EV ultracentrifugation following first 100,000 *xg* spin to pellet EVs; ME180 and SW756 recipient cells only)
5) OSM Treated (10ng/ml; VF2 recipient cells only)
6) PBS control (equal volume to EVs; all 3 recipient cell lines)

Closure of scratches was visually assessed at regular intervals for the next 20hours and photographed using a using a DM LB light microscope with DC500 digital camera (both Leica, Wetzlar, Germany). Marks were drawn on the base of the well to ensure that photographs for each timepoint were taken at the same position. Data analysis was performed using Image J software. Scratch diameter was measured at two separate fields of view for each well at each timepoint. Percentage wound closure at each timepoint was calculated as follows:

$$\% \text{ wound closure} = 100 - \left(\frac{\text{Diameter at } x \text{ hours}}{\text{Diameter at 0 hours}} \times 100 \right)$$

Percentage wound closure was averaged for both fields of view to obtain a single value for each well at each timepoint. The three biological replicates for each treatment group were subsequently averaged at each timepoint.

3.9.3 Angiogenesis Assay

Angiogenesis assays were performed using a V2A kit (Cellworks, Buckingham, UK) according to manufacturer's instructions. This kit utilises co-cultures of human umbilical vein endothelial cells (HUVECs) and primary human fibroblasts. Cells were thawed in V2a seeding media and evenly seeded into 24 well plates. Cells were cultured for 24hours at 37°C in 5% CO_2, media was then aspirated and 0.5ml of the following treatment added to each well:

1) Untreated control (V2a growth medium only)
2) VEGFA positive control (at a final concentration of 2pg/µl V2a growth medium)
3) Suramin negative control (0.02mM in V2a growth medium)
4) Conditioned media from SW756 cells treated with PBS control
5) Conditioned media from SW756 cells treated for 48hours with 10ng/ml Rh-OSM

6) EVs isolated from SW756 cells treated with PBS control
7) EVs isolated from SW756 cells treated with 10ng/ml Rh-OSM

Cells were treated with the conditions described above every 48hours for a total period of 14 days (treatment added on days 2, 4, 6, 8, 10, 12). Media was removed by aspiration at each timepoint and fresh V2a media supplemented with the respective treatment added to cells. Each treatment condition was performed in duplicate.

For wells treated with conditioned media from SW756 cells, donor SW756 cells were cultured in 6 well plates. After 48hours in culture, media was removed, wells were washed with PBS and cells were treated with media supplemented with 10ng/ml Rh-OSM or an equal volume of PBS control. After a further 48hours, conditioned media was collected from these cells and centrifuged for 5mins at 6000*xg* to remove detached cells. Media was then diluted 1:1 in V2a growth media and 0.5ml added to relevant wells of the angiogenesis assay.

For wells treated with EVs from SW756 cells: donor SW756 cells were cultured in 175cm^2 flasks. After 48hours in culture, media was removed, wells were washed with PBS and cells were treated with EV depleted media supplemented with 10ng/ml Rh-OSM or an equal volume of PBS control. After 2hours treatment media was removed and cells were washed with PBS. Fresh EV depleted media was added to cells, and they were cultured for a further 48hours. Media was subsequently collected and EVs isolated by ultracentrifugation. EV pellets were resuspended in 1ml V2A media and 0.5ml added to relevant wells of the angiogenesis assay.

After 14 days culture wells were washed in PBS and fixed with 0.5ml of ice-cold 70% ethanol for 30mins at room temperature. Ethanol was removed and wells washed 3 times with 0.5ml blocking buffer (PBS supplemented with 1% BSA). Wells were probed for CD31 in order to visualise tubules. Mouse anti-human CD31 (provided in V2a kit) was diluted 1:400 in blocking buffer and 0.5ml added to each well. The plate was incubated for 1 hour at 37°C; primary antibody was then removed and wells washed three times with 0.5ml PBS for 5mins at room temperature. 0.5ml goat-anti-mouse IgG Alkaline Phosphatase (AP) linked secondary antibody (provided in V2a kit) was added to wells at a 1:500 dilution in blocking buffer. Wells were incubated with secondary antibody for 1hour at 37°C. Secondary antibody was then removed and wells washed three times with 0.5ml dH_20 for 5mins at room temperature. Staining was then performed using 5-bromo-4-chloro-3-indolyl-phosphate/nitro blue tetrazolium (BCIP/NBT). Two BCIP/NBT tablets (provided in V2a kit) were dissolved in

20ml dH_20. This solution was then filtered using a 0.2µM filter. 0.5ml was added to each well and incubated at room temperature for 5mins until tubules developed a dark purple colour. Wells were then washed three times with dH_20 and left to air dry. Five images were subsequently taken at five different fields of view for each well using a DM LB light microscope with x4 objective and a DC500 digital camera. Images were subsequently analysed using AngioSys 2.0 Image Analysis Software (Cell works); this calculated the tubule length, total number of branches, total number of junctions and mean branch length for each image. These were then averaged to provide a single value/well. Measurements from two independent wells were used per condition.

3.10 *In vivo* Experiments

All procedures were performed under the project licence number PPL 80/2610 and personal licence number IC038BAB6. All mice were maintained in conventional cages within a specific pathogen-free animal facility and were treated in strict accordance with the local ethical committee (University of Cambridge Licence Review Committee) and the UK Home Office guidelines.

3.10.1 Subcutaneous xenograft of human OSMR KD cervical SCC cells

Subcutaneous tumours were induced in 6 week old female NOD-SCID mice (NOD.CB17-*Prkdc*^{scid}/NCrCrl; Charles River Ltd.). Injection sites (right hand side flanks) were shaved and sterilised with HiBiSCRUB antimicrobial skin cleanser (Mölnlycke Health Care, Gothenburg, Sweden) prior to injection. 5 x10^6 SW756 empty plasmid or SW756 OSMR KD cells (as detailed in section 3.3) were injected subcutaneously (SC) in a total volume of 200µl sterile PBS; 6 mice were injected for each cell line. Mice were injected intraperitoneally (IP) daily with 1200ng Rh-OSM (approximately 60ng/g bodyweight) in 100µl PBS, or an equal volume of PBS control, for 13 days beginning on the day of subcutaneous cell injection. Thus treatment groups were as follows:

- SC injection SW756 empty plasmid cells + IP injection OSM (n=3)
- SC injection SW756 empty plasmid cells + IP injection PBS control (n=3)
- SC injection SW756 OSMR KD cells + IP injection OSM (n=3)
- SC injection SW756 OSMR KD cells + IP injection PBS control (n=3)

Mice were weighed and their tumours measured with digital calipers (VWR, Radnor, PA, USA) daily during the 13 day period of IP OSM/PBS injection. After completion of IP injections, mice were weighed and SC tumours measured three times per week. Length and

width of tumours were measured and tumour volume calculated according to the following formula[228]:

$$\text{Tumour volume } (mm^3) = \frac{width^2 \times length}{2}$$

Experimental endpoint was reached when tumour volume reached 1500mm^3, if the weight of the mouse decreased by 20%, if the surface of the tumour appeared inflamed or ulcerated, if the mouse developed ascites or dyspnoea, or if notable changes in posture and/or behaviour were observed. Once endpoint was reached, mice were anesthetised with isoflurane and their blood collected by cardiac puncture as described in section 3.10.3. Mice were then culled by cervical dislocation (while still anesthetised) and dissected to determine whether metastasis had occurred. For each mouse the tumour, lungs, diaphragm, liver, spleen, mesentery, cervix, femurs and brain were all collected, photographed, weighed and fixed in formalin. Prior to fixation, tumour samples were divided into 3 pieces by scalpel and either:

1) fixed in formalin
2) flash frozen in an Eppendorf tube on dry ice and transferred at -80°C freezer for subsequent RNA extraction
3) placed in an Eppendorf tube containing DMEM media and placed on ice for subsequent *ex vivo* growth and EV isolation

3.10.2 Subcutaneous xenograft of human cervical SCC cells with endogenous OSM production

Subcutaneous tumours were induced in 6 week old female NOD-SCID mice as described above by injection of either 5 x10^6 SW756 pOSM cells (n=6) or 5 x10^6 SW756 pUNO cells (n=6; cell lines detailed in section 3.4.2) in a total volume of 200µl sterile PBS. This experiment was performed together with Dr Marta Paez-Ribes and Valtteri Tulkki. Mice were weighed and their tumours measured with digital callipers three times per week; tumour volume was calculated as described in section 3.10.1. Mice injected with pOSM cells displayed rapid weight loss and the experiment was, therefore, terminated after three weeks. Mice were culled by cervical dislocation and their tumours, lungs, livers, spleens, femurs and brains were all collected, photographed, weighed and fixed in formalin.

This experiment was subsequently repeated using human cervical SCC cell lines with lower levels of endogenous human OSM production than pOSM cells, as described in section 3.4.3. 6 week old female NOD-SCID mice were subcutaneously injected with pUNO2, pOSM_c2 or pOSM_c3 cells; n=3 for each group; 5 x10^6 cells in a total volume of 200 µl

sterile PBS were injected. Mice were weighed and their tumours measured with digital callipers three times per week; tumour volume was calculated as described in section 3.10.1.

Experimental endpoint was reached when tumour volume reached 1500mm^3, if the weight of the mouse decreased by 20%, if the surface of the tumour appeared inflamed or ulcerated, if the mouse developed ascites or dyspnoea, or if notable changes in posture and/or behaviour were observed. Once endpoint was reached, mice were anesthetised with isoflurane and their blood collected by cardiac puncture described in section 3.10.3. Mice were then culled by cervical dislocation (while still anesthetised) and dissected to determine whether metastasis had occurred. For each mouse the tumour, lungs, diaphragm, liver, spleen, mesentery, cervix, femurs and brain were all collected, photographed, weighed and fixed in formalin. Prior to fixation, tumour samples were divided into 3 pieces by scalpel and either:

1) fixed in formalin
2) flash frozen in an Eppendorf tube on dry ice and transferred at -80°C freezer for subsequent RNA extraction
3) placed in an Eppendorf tube containing DMEM media and placed on ice for subsequent *ex vivo* growth and EV isolation

3.10.3 Supplementary methods

See supplementary methods for details of the following protocols:

- Plasma collection by cardiac puncture
- *Ex vivo* tumour culture and EV isolation
- H&E staining of tissue sections

4. RESULTS: Effect of OSM signalling on EV cargo in cervical SCC cells

4.1 Introduction

4.1.1 MicroRNA Biogenesis

MicroRNAs (miRNAs) are small non-coding RNA molecules, approximately 20-23 nucleotides long, which can regulate gene expression at the post-transcriptional level by inducing RNA degradation or translational suppression of a target mRNA[229]. Mature miRNAs are either processed from introns of transcripts of protein coding genes[230], if the DNA sequences encoding for them are intragenic, or from transcripts originating from their own specific promoters if their genes are located within intergenic non-coding regions[231]. Moreover, miRNAs can be encoded as individual genes or in clusters that are transcribed together as polycistronic transcripts[232].

The transcription of most mammalian miRNAs is driven by RNA Polymerase II and produces primary miRNA transcripts (pri-miRNA) which are long, polyadenylated molecules that fold into double-stranded stem-loop structures[233]. Pri-miRNAs are cleaved in the nucleus by the microprocessor complex which is composed of DROSHA, a RNAse III endonuclease, and DiGeorge syndrome critical region gene 8 (DGCR8), a double-stranded RNA binding protein[234]. Cleavage produces a 60-70 nucleotide stem loop intermediate known as precursor miRNA (pre-miRNA)[234]. Pre-miRNAs are subsequently exported to the cytoplasm by EXPORTIN 5 (EXP5) where they are cleaved by a second RNAse III endonuclease, DICER, in concert with the transactivation response element RNA-binding protein (TRBP)[235]. This step removes the terminal loop, resulting in a 20-25 nucleotide long mature double stranded miRNA[236,237].

Finally, in a process known as RNA-induced silencing complex (RISC) loading, the double-stranded miRNAs are loaded onto ARGONAUTE (AGO) proteins which select one strand to become the mature miRNA (guide strand) and discards the other strand (known as the passenger strand)[237]. Mature miRNAs are approximately 19–25 nucleotides long and are denoted as miRNA-5p or miRNA-3p depending on whether the guide strand was generated from the 5’ or 3’ arm of the precursor double stranded miRNA. This process, summarised in Figure 4.1, is the primary ‘canonical’ pathway of miRNA biogenesis. In addition to the pathway described, there also exist alternative pathways for miRNA biogenesis in which mature miRNAs are produced independent of some of the factors mentioned above[238].

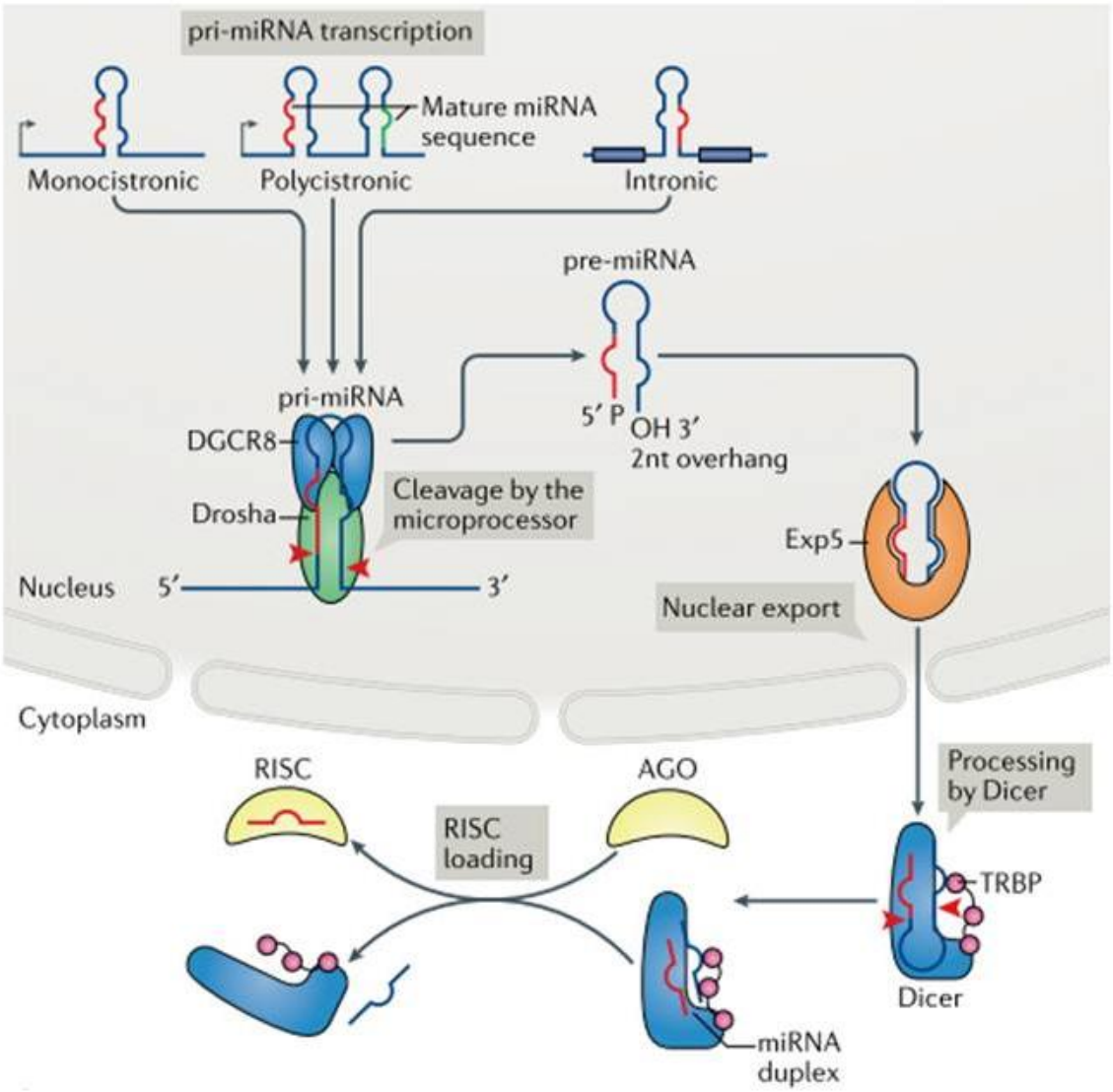

Figure 4.1: Canonical pathway of microRNA biogenesis
Taken from Treiber et al (2019)[232]

4.1.2 miRNA regulation of mRNA levels

Mature miRNA-RISC complexes interact with complementary sequences on mRNA targets called miRNA response elements (MRE). These are generally located in the mRNA's 3'-untranslated region (UTR); however, miRNAs have also been shown to target regions in 5′ UTRs and ORFs[239,240]. miRNAs can regulate gene expression at the post-transcriptional level either by mRNA cleavage or translational repression. The degree of miRNA-mRNA complementarity is a key factor in determining which regulatory mechanism is employed. Perfect complementarity between miRNAs and their target mRNAs results in AGO2-mediated cleavage of the RNA[241]. However, complete sequence complementarity between mammalian miRNA and their mRNA targets is rare[242]. Most mammalian miRNAs bind to mRNA with mismatches and bulges with the first 8 nucleotides at the 5' end of the miRNA, known as the seed region, providing most of the pairing specificity[243]. Binding can occur in

seed regions with 6, 7 or 8 nucleotides of complementarity; termed 6-mers, 7-mers and 8-mers, respectively[244,245]. In this instance, mRNA cleavage by AGO2 is inhibited, and AGO proteins instead recruit additional protein partners to mediate mRNA silencing through a combination of translational repression and mRNA destabilisation. This is achieved via multiple mechanisms including: deadenylation and degradation, 5' capping and ribosome detachment[238,246].

4.1.3 Dysregulation of miRNAs in cervical cancer

Individual miRNAs are capable of binding to hundreds of target mRNAs. Likewise, individual mRNAs can be bound by multiple miRNAs[247,248]. Moreover, computational analysis has predicted that >60% of human protein coding genes are regulated by miRNAs[249,250]. Thus miRNAs regulate many physiological processes and dysregulated miRNA expression has been demonstrated to play a key role in the development and progression of cancers. Altered miRNA expression profiles in cancer have been shown to be driven by multiple mechanisms including (but not limited to): genetic alterations, epigenetic changes (such as histone modifications and aberrant DNA methylation)[251], defects in miRNA biogenesis machinery and altered transcription factor activity[252].

miRNA loci are frequently located at fragile sites and cancer associated genomic regions[253]. Previous work in our laboratory has shown that, in addition to OSMR, chromosome 5p copy number gain and amplification in cervical cancer are associated with copy number gain and overexpression of *DROSHA*, the miRNA processing enzyme involved in cleavage of pri-miRNAs to pre-miRNAs[254]. Elevated DROSHA overexpression in cervical SCC resulted in global changes in miRNA profiles, which were shown to contribute to increased motility and invasiveness of these cells[254,255]. Dysregulated miRNA expression has also been shown to result from other common chromosomal alterations in cervical cancer including gain of chromosomes 1q and 3q and loss of chromosome 11q[256].

Moreover, miRNA expression profiles have been demonstrated to undergo progressive changes between normal cervical tissue, cervical intraepithelial neoplasia and cervical SCC[256–259]. Some studies have attributed such changes to expression of the HR-HPV oncogenes E6 and E7[259–261]. miRNA loci have also been shown to occur at a higher incidence near HPV integration sites than in the rest of the genome; genomic deletions, amplifications or rearrangements in these regions may drive aberrant miRNA expression[253]. Additionally, various research groups have identified miRNA profiles which were found to be promising biomarkers for diagnosis of cervical cancer[262–264] and prediction of patient survival[264–266]. Comprehensive reviews of miRNAs implicated in cervical cancer have been

published, for example, Granados-Lopez *et al*. (2014)[267], He *et al*. (2016)[268] and Pardini *et al*. (2018)[269].

4.1.4 Role of EVs in miRNA transport

miRNAs are actively exported from cells[270] and can stably exist extracellularly in body fluids despite high extracellular RNase activity. Mechanisms by which extracellular miRNAs are shielded from degradation include association with other molecules, such as the RNA-binding proteins AGO2 or nucleophosmin 1 (NPM1)[270] or packaging into EVs[169,271,272]. Packaging of miRNAs into EVs has been shown to be a specific and selective process; however, the mechanisms mediating this process are still poorly understood. Various factors have so far been implicated to facilitate this process including: RNA-binding protein Y-box protein I (YBX1)[273], sumoylated heterogeneous nuclear ribonucleoprotein A2/B1 (hnRNPA2B1)[274] and endosomal sorting complexes required for transport (ESCRT)[173].

EVs play a key role in cell-cell communication by transfer of miRNAs as well as DNA, proteins, lipids and mRNAs between cells[169]. Bidirectional communication between cancer cells and the TME is essential for tumour progression and metastasis. There is mounting evidence to suggest that tumour-derived EVs interact with cells of the TME to promote tumour growth, angiogenesis, extracellular matrix (ECM) remodelling, metastasis and immune evasion[135,136].

4.1.5 Role of EVs in miRNA transport

Experiments detailed in this chapter were performed using two representative cervical SCC cell lines with differing levels of OSMR expression. SW756 cells were selected as a representative cell line with OSMR copy number gain and overexpression and ME180 cells were selected as a cell line with average OSMR expression. These two cells lines have been extensively characterised in previous publications by our research group[70,121]. In preliminary experiments, cellular and EV expression of a panel of miRNAs was investigated in response to OSM treatment. These miRNAs were selected from the literature for having a known role as a tumour promoter or suppressor in cervical SCC or displaying an expression profile that significantly correlated with OSMR or STAT3 expression in TCGA analysis of patients samples with cervical SCC (OSMR: Figure S4. 1, STAT3: Figure S4. 2). A brief summary of each miRNA investigated, and its suspected role in cervical cancer, is provided in Table 4.1.

Table 4.1: miRNA selected for investigation	
Suspected Role in Cervical Cancer: Tumour Promoters	
miR-9	miR9 is significantly upregulated in cervical SCC compared to normal cervix and is associated with reduced overall survival[275,276]. Elevated levels of miR-9 in cervical SCC is associated with both gain of chromosome 1q[256] and activation by HPV E6[277]. Its upregulation has been shown to result in increased proliferation and migration of cervical SCC cells *in vitro*[256] and increased tumour growth *in vivo*, associated with dysregulation of apoptosis due to downregulation of *FOXO3*[276]. Moreover, miR-9 has been implicated as a possible prognostic marker for cervical carcinoma[276]. miR-9 expression was found to correlate negatively with *STAT3* expression in TCGA analysis of cervical SCC samples.
miR-31	miR-31 was found to be significantly upregulated in cervical carcinoma compared to normal cervix, and in cervical cancer cell lines[278,279,280]. Moreover, increased expression of miR-31 was found to significantly correlate with increased FIGO stage, increased lymph node metastasis and vascular invasion and reduced overall survival[278,279,280]. Overexpression of miR-31 has been shown to promote cervical cancer cell proliferation, migration, invasion and EMT *in vitro* and tumour growth *in vivo*[278,279,280]. Overexpression of miR-31 in cervical carcinoma is believed to be driven by both *DROSHA* copy number gain and overexpression[255] and HPV16 E6/E7 expression[279]. miR-31 overexpression results in downregulation of *BAP1*[280] and *ARID1A*[278] expression in cervical cancer cells. miR-31 expression was found to correlate positively with OSMR expression in TCGA analysis of cervical SCC samples.
Suspected Role in Cervical Cancer: Tumour Suppressors	
miR-10b	miR-10b has been shown to be significantly downregulated in cervical carcinoma compared to normal cervix, and in cell lines from cervical cancer cells[281,282]. Overexpression of miR-10b *in vitro* has been shown to result in inhibition of cervical cancer cell proliferation, migration and invasion and increased apoptosis[281,282]. Downregulation of miR-10b in cervical cancer may possibly be a result of HPV mediated methylation of TFAP2 binding element located within the miR-10b promoter[282]. Potential targets of miR-10b include *IGF-1R*[281] and *TIAM1*[281].
miR-23b	miR-23b expression has been shown to be downregulated in HR-HPV positive cervical cancer tissues and cell lines[262]. Moreover, miR-23b downregulation is associated with cancer progression with significantly lower levels detected in cervical cancer biopsies compared to LSIL and HSILs[283]. Downregulation of miR-23b in cervical carcinoma has been shown to be a result of both inactivation of p53 by HPV 16 E6[284] and methylation of the miR-23b promoter[283], and results in increased cell migration and invasiveness[284]. Overexpression of miR-23b resulted in downregulation of its suggested targets: *UPA*[283,284], *C-MET* and *ZEB1*[283]. miR-23b expression was found to correlate negatively with OSMR expression in TCGA analysis of cervical SCC samples.
miR-29b	miR-29b was found to be significantly downregulated in cervical cancer and HSIL tissues compared to normal cervix[285,286]. miR-29b was shown to suppress invasion, EMT and angiogenesis of cervical cancer cells *in vitro* and inhibit tumour growth *in vivo* by supressing STAT3 signalling[285]. miR-29b has been identified as a therapeutic target: it is upregulated in cervical cancer cell lines and cervical cancer tissues in response to treatment with cisplatin[285] and has also been shown to enhance radio-sensitivity of radio-resistant cervical cancer cells both *in vitro* and *in vivo*[286].
miR-101	miR-101 has been shown to be significantly downregulated in cervical cancer tissues compared to normal cervix[287,288,289,290] and is also downregulated in

	cervical cancer cell lines[289,291]. Downregulation of miR-101 was associated with poor overall survival[289,290]. Overexpression of miR-101 in cervical cancer cells has been shown to result in inhibition of proliferation, invasion and cell cycle progression, and increased apoptosis *in vitro*[291,292] and decreased tumour growth in vivo[289]. This has been reported to occur via downregulation of a number of miR-101 targets including COX-2[287,291], CXCL6[289], JAK2[288] and FOS[292]. miR-101 expression was found to correlate negatively with OSMR expression in TCGA analysis of cervical SCC samples.
miR-126	miR-126 is significantly downregulated in cervical cancer tissues and cell lines, compared to normal cervix and normal cervical epithelial cell lines, respectively[293,294,295]. This downregulation has been reported to be temporarily and spatially specific, occurring in the stromal endothelium in the early invasive stage of cervical cancer[296]. Downregulation of miR-126 was shown to be associated with cancer progression, metastasis and decreased overall survival[295]. Restoration of miR-126 expression in cervical cancer cells *in vitro* results in increased apoptosis via downregulation of *BCL212*[294] and decreased cell proliferation, migration and invasion via inhibition of ZEB1 which in turn resulted in suppression of MMP2, MMP9, p-JAK2 and p-STAT3 expression[293]. Furthermore, miR-126 was shown to suppress angiogenesis and tumour growth *in vivo*[296].
Suspected Role in Cervical Cancer: Unclear	
miR-34c	The role of miR-34c in cervical carcinoma remains to be fully elucidated. miR-34c has been shown to be upregulated in CIN I-III compared to normal cervical epithelium[256,257]. Moreover, the miR-34c promoter is significantly hypomethylated in CIN I-III and SCC tissues compared to normal cervical epithelium[297]. While upregulation in cervical carcinoma suggests miR-34c may play an oncogenic role, Córdova-Rivas *et al* (2019) recently demonstrated that miR-34c inhibited cervical cancer cell proliferation and migration *in vitro*[298]. miR-34 has been selected for investigation as its expression has been shown to correlate positively with OSMR expression in analysis of TGCA data of patients with cervical SCC.
miR-194	The known role of miR-194 in cervical cancer is limited. Liu *et al* (2019) reported miR-194 to be significantly upregulated in patients with cervical cancer and found that high levels of miR-194 were associated with both recurrence and conversely also prolonged overall survival[299]. Whereas, Park *et al* (2014) found that miR-194 was specifically upregulated in cervical adenocarcinoma but not cervical SCC[300]. miR-194 has been selected for investigation as its expression has been shown to negatively correlate with OSMR expression in analysis of TGCA data of patients with cervical SCC.

4.1.6 CRISPR-Cas9

Subsequent experiments in this chapter detail how OSMR expression was knocked down in the OSMR overexpressing SW756 cell line using a CRISPR-all-in-one Cas9^{D10A} nickase vector system[218]. Type II Clustered, regularly interspaced, short palindromic repeats (CRISPR)-Cas systems function in the adaptive immune response of prokaryotes, enabling them to attack invading genetic elements such as bacteriophages and plasmids. The CRISPR-Cas9 system has been adapted to perform genome editing in mammalian cells[301]. To create gene disruptions, small 20 nucleotide non-coding guide RNAs (sgRNAs) are designed to be complementary to target regions of DNA, neighbouring protospacer adjacent

motifs (PAM). sgRNAs guide Cas9 nuclease to induce site-specific DNA cleavage resulting in double strand breaks (DSBs) in the DNA. The Cas9-gRNA complex will bind any genomic sequence with a PAM; however, cleavage will only occur if sufficient homology exists between the sgRNA and the target sequence. DSBs are subsequently repaired by the non-homologous end joining DNA repair pathway (NHEJ) or the homology directed repair (HDR) pathway. NHEJ is error prone and frequently results in small nucleotide insertions or deletions at the repair site which can result in frameshift mutations leading to premature stop codons within the open reading frame (ORF) of the targeted gene. Alternatively, knockins can be created by HDR.

However, in addition to the target gene, gRNAs are likely to have partial homology to other sites throughout the genome and creation of DSBs in these regions can have 'off-target' effects. One method to reduce off-target effects is the use of mutant Cas9 nickases, such as $Cas9^{D10A}$, which, unlike wild-type Cas9, contain only one active catalytic domain and are therefore only able to induce single strand breaks (SSBs) which can be repaired using the intact DNA strand as template[218]. In order to create DSBs, a double-nicking strategy is used which employs two paired sgRNAs that direct Cas9 nickases to target opposite strands of a target DNA sequence, thus minimising off-target effects[218]. For the CRISPR experiments performed in this body of work, an all-in-one plasmid designed by Chiang *et al* (2016) was used which contains dual sgRNAs under the control of a U6 promoter and $Cas9^{D10A}$ nickase coupled to EGFP[218].

4.1.7 Chapter Aims

The aim of this chapter was to investigate whether OSM-OSMR signalling was capable of modulating cellular and EV miRNA expression in cervical SCC cells. Experiments were performed using two representative cervical SCC cell lines with differing levels of OSMR expression: SW756 cells and ME180 cells. In preliminary experiments, cellular and EV expression of a panel of miRNAs was investigated in response to OSM treatment. Functional assays were subsequently employed in order to determine whether EVs from PBS and OSM treated cells differed in their ability to induce proliferation and migration of cancer cells and angiogenesis in endothelial-fibroblast co-cultures. Subsequent experiments detailed in this chapter aimed to establish an OSMR KD SW756 cell line by CRISPR-Cas9 which could later be used to investigate global changes in miRNA and mRNA expression in cervical SCC cells and their EVs in response to OSM-OSMR signalling.

4.2 Confirmation of EV isolation from SW756 and ME180 cells

Initial experiments were carried out to establish that EVs could be successfully isolated from the conditioned media of SW765 and ME180 cell lines. For all EV experiments in this chapter, cells were treated as follows unless otherwise stated. SW756 or ME180 cells were treated for 48 hours in EV depleted media supplemented with either 10ng/ml OSM or PBS control. EVs were subsequently isolated by sequential ultracentrifugation, as described in Figure 3.2. This protocol is based on the ultracentrifugation protocol described by Théry *et al* (2006)[161] and separates particles according to their buoyant density. For experiments that used EV depleted conditioned media, supernatant was collected following the first 100,000 *xg* spin in the EV isolation protocol. The terminology summarised in Table 4.2 will be used herein to describe treatment conditions.

Table 4.2: Summary of abbreviations used to describe treatment conditions

Abbreviation	Description
SW756-PBS-cells	SW756 cells treated with PBS
SW756-OSM-cells	SW756 cells treated with OSM
ME180- PBS-cells	ME180 cells treated with PBS
ME180-OSM-cells	ME180 cells treated with OSM
SW756-PBS-EVs	EVs isolated from SW756 cells following PBS treatment
SW756-OSM-EVs	EVs isolated from SW756 cells following OSM treatment
ME180- PBS-EVs	EVs isolated from ME180 cells following PBS treatment
ME180-OSM-EVs	EVs isolated from ME180 cells following OSM treatment
SW756-PBS-CM	Total conditioned media from SW756 cells following PBS treatment
SW756-OSM-CM	Total conditioned media from SW756 cells following OSM treatment
SW756- PBS-DM	EV depleted conditioned media from SW756 cells following PBS treatment
SW756-OSM-DM	EV depleted conditioned media from SW756 cells following OSM treatment
ME180-PBS- DM	EV depleted conditioned media from ME180 cells following PBS treatment
ME180-OSM-DM	EV depleted conditioned media from ME180 cells following OSM treatment

Following ultracentrifugation, EV pellets were visualised by transmission electron microscopy (TEM; Figure 4.2). Spherical structures with cup-shape morphology stereotypical of EVs were identified in samples from both cell lines. EV populations were heterogeneous and ranged in size from approximately 50-200nm. As expected, EVs were not detected in a control sample of EV depleted culture media that was subjected to the same ultracentrifugation protocol as the experimental samples (results not shown).

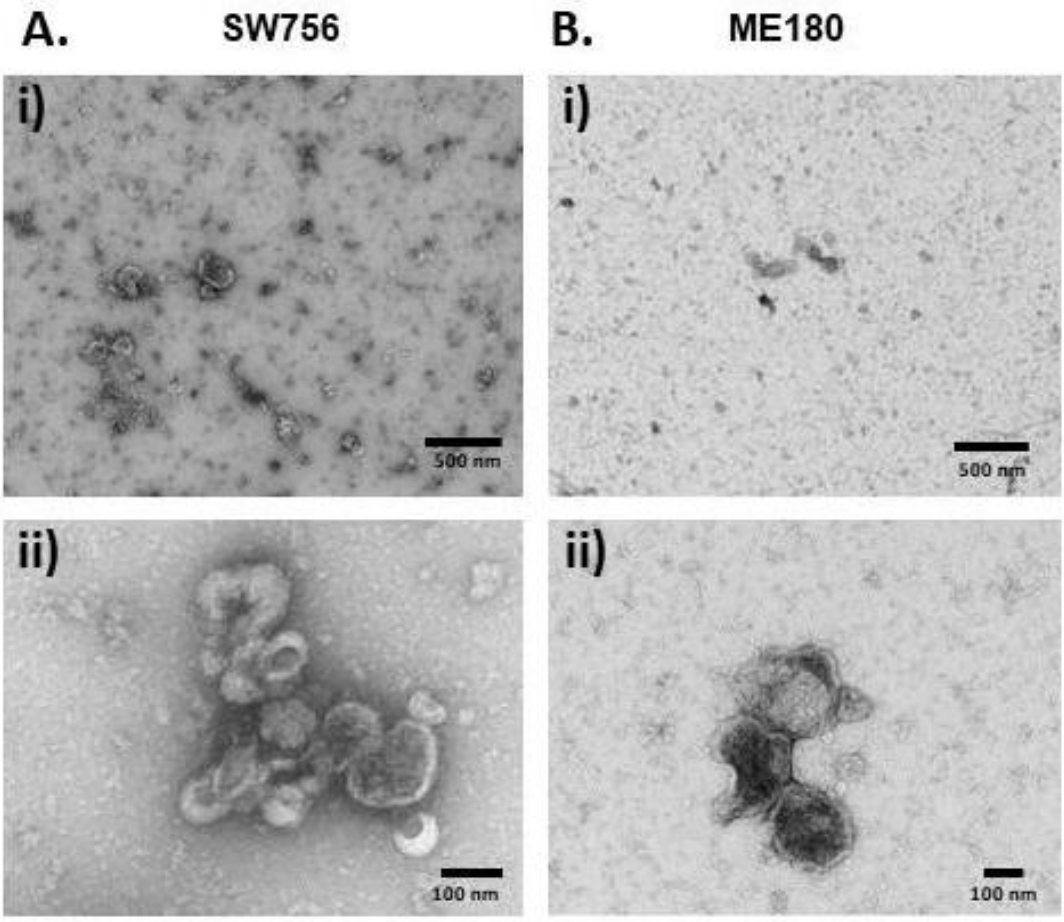

Figure 4.2: Visualisation of EVs by Transmission Electron Microscopy (TEM)
EV preparations isolated by ultracentrifugation were mounted onto carbon coated copper microscopy grids and visualised using a FEI Tecnai™ G2 Transmission Electron Microscope. Samples were fixed with 2% PFA and 1% glutaraldehyde and negatively contrasted with 1% uranyl acetate. Images depict EVs isolated from (A) SW756 cells or (B) ME180 cells at i) low (scale bar = 500nm) or ii) high (scale bar = 100nm) magnification.

To further characterise the isolated EVs, particle size was investigated by NanoSight in collaboration with Carlos Passos Bastos in Dr Nuno Faria's research group at The Department of Veterinary Medicine, Cambridge University. Following ultracentrifugation EVs were resuspended in an equivalent volume of PBS and particle size was measured using a NanoSight and NTA software (Figure 4.3). This method establishes the concentration of particles present in 1nm size bins. An accurate representation of particle size within a sample can be determined using the mean and mode (the value that appears most often) particle sizes in addition to D10, D50 and D90 values, which refer to the size which 10%, 50% and 90% of particles in the sample are smaller than, respectively (depicted in Figure 4.3A).

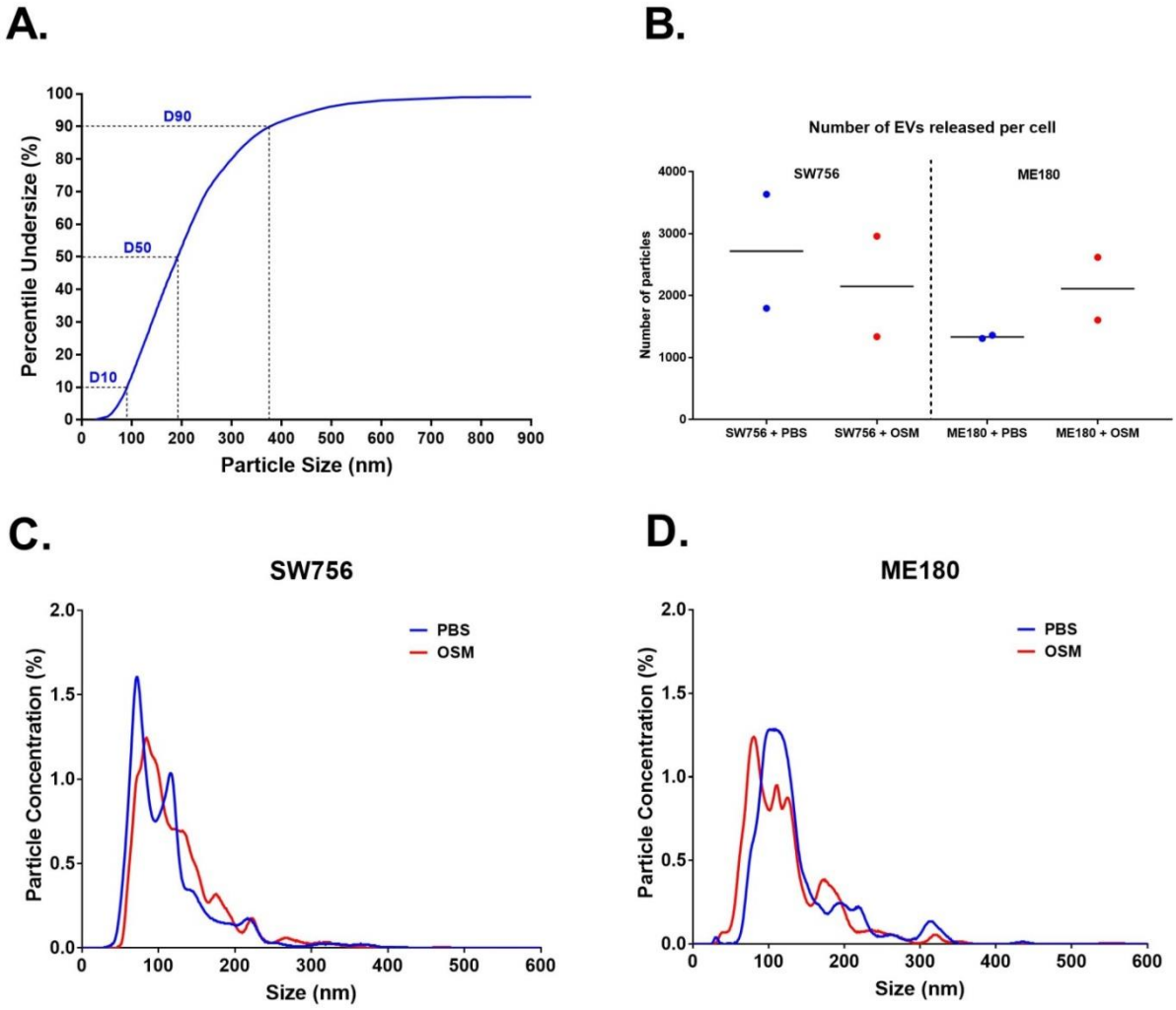

	PBS	OSM
Mean	125 ± 12 nm	124 ± 1 nm
Mode	99 ± 13 nm	88 ± 8 nm
D10	69 ± 5 nm	72 ± 3 nm
D50	111 ± 15nm	109 ± 3 nm
D90	209 + 23nm	198 ± 12 nm
Concentration (particles/ml)	3.91×10^{11}	2.88×10^{11}

	PBS	OSM
Mean	138 ± 8 nm	124 ± 1nm
Mode	108 ± 4 nm	94 ± 8 nm
D10	84 ± 2 nm	69 ± 6 nm
D50	119 ± 3 nm	108 ± 6nm
D90	216±22nm	191 ± 1 nm
Concentration (particles/ml)	2.23×10^{11}	3.53×10^{11}

Figure 4.3: NanoSight analysis of EVs isolated from SW756 and ME180 cells

NanoSight analysis showing size distribution of EVs extracted from culture medium of SW756 and ME180 cervical SCC cell lines treated with OSM or PBS control. (A) Schematic of how D10, D50 and D90 values are calculated from percentage undersize graphs. D10, D50 and D90 refer to the particle size which 10%, 50% and 90% of particles are smaller than, respectively. (B) Number of EV particles released per cell for each condition (C) size of particles produced by SW756 cell line (D) size of particles produced by ME180 cell line. N=2 for each condition.

Both SW756 and ME180 EVs were found to have similar size distributions and to be composed of heterogeneous populations of multiple sized particles. SW756 EVs had an average particle size of 125nm (Figure 4.3C), whereas ME180 EVs were slightly larger with average particle size of 138nm (Figure 4.3D). For both cell lines the average particle size was larger than the mode, reflecting the presence of a small population of larger particles in the 200-400nm size range. Treatment with OSM did not appear to affect size of EVs released by either cell line. As expected, particles were not detected in a PBS control sample (results not shown). One of the main limitations of this technique is that it detects all particles present in the sample, not just EVs. However, particles detected were within the expected EV size range and were consistent with the size range of particles with stereotypical EV morphology observed by TEM.

The total number of EVs present in each sample was calculated by multiplying the particle concentration by the input volume. The number of particles released per cell was subsequently calculated by dividing this value by the number of cells present in the flask at the time of EV collection. There were no obvious differences between either the mean number of EVs released per cell for SW756 or ME180 cell lines or in the mean number of EVs released by either cell line in response to OSM treatment; however there was a high degree of variability between replicates (Figure 4.3B). This may reflect limitations of this technique; NTA analysis has previously been shown to have high inter-experimental variability when used to determine particle concentration. This has been attributed to variations in the number of particles detected between video replicates of the same sample and limitations in detecting particles <50nm in diameter[302,303].

In conclusion these experiments demonstrated that EVs could be successfully isolated by sequential ultracentrifugation from both SW756 and ME180 cells. EVs derived from both cell lines were of similar size and displayed stereotypical EV morphology. Treatment with OSM had no effect on EV size or the number of EVs released per cell.

4.3 SW756 and ME180 cell line validation

The effects of OSM-OSMR signalling on cellular and EV miRNA expression was subsequently investigated. SW756 and ME180 cells were treated for 12, 24, 48 or 72 hours with EV depleted media supplemented with 10ng/ml OSM or PBS control. Total RNA was extracted from both cells and EVs for each treatment group.

SW756-PBS-cells and ME180-PBS-cells at the 48 hour timepoint were used for validating cervical SCC cell lines in order to confirm that they were behaving as previously described and represented cervical SCC cell lines with differing levels of OSMR expression. As expected, SW756 cells were found to have significantly higher baseline expression of OSMR than ME180 cells at both the mRNA (5.8 fold, Figure 4.4B) and protein (Figure 4.4A) levels, as determined by qPCR and western blot, respectively (western blot was performed by Valtteri Tulkki). Western blots performed for OSMR throughout this thesis display multiple bands. The predicted molecular weight for full length OSMR is 180 kDa (according to the datasheet sheet supplied by Santa Cruz for the anti-OSMR antibody used).

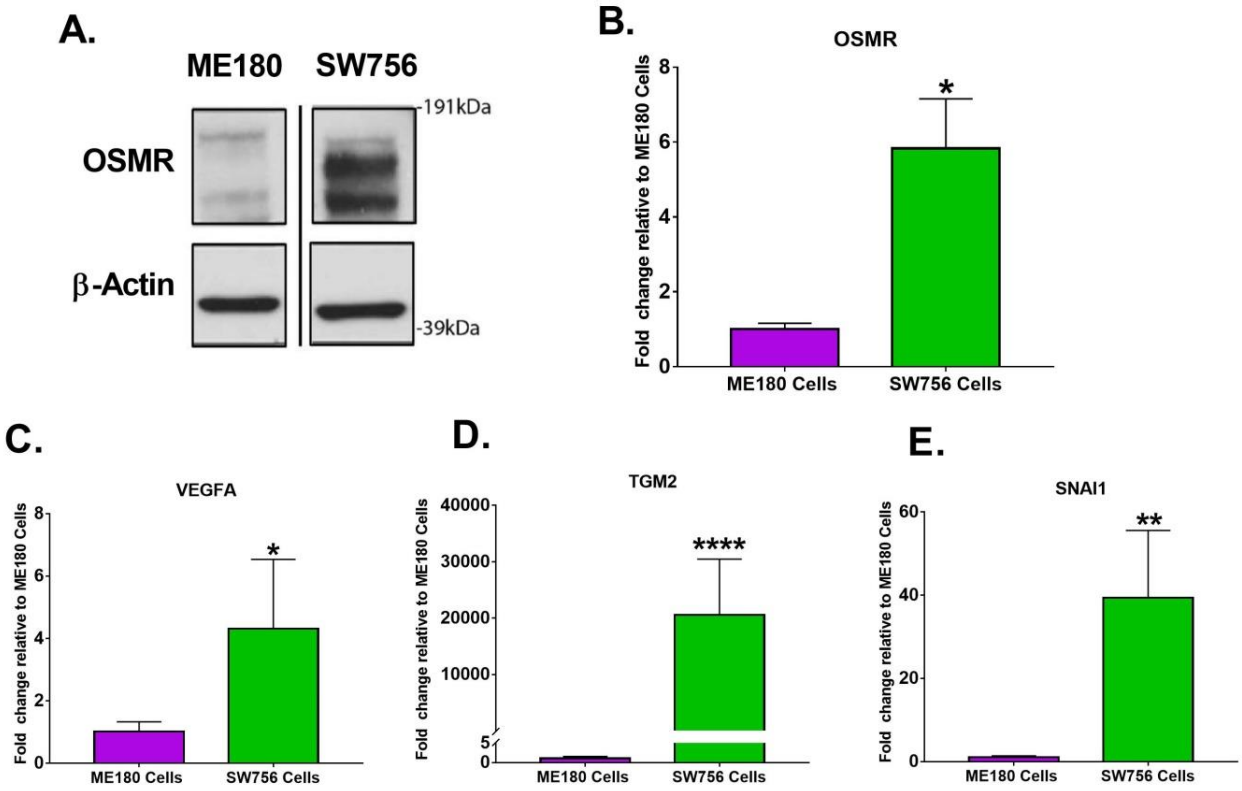

Figure 4.4: Expression of OSMR and known targets in SW756 and ME180 cell lines
SW756 and ME180 cells following 48 hours culture in media supplemented with PBS control. A) Western blot displaying OSMR protein expression. B-E) Quantitative RT-PCR for B) OSMR, C) VEGFA, D) TGM2 and E) SNAI1 mRNA expression. Fold change in gene expression in SW756 cells compared to ME180 cells is shown. Error bars represent SEM, n=3 independent experiments for each condition. Values were analysed for statistical significance using a using Unpaired T-test with Welch's correction. * = $P \leq 0.05$, ** = $P \leq 0.01$, *** = $P \leq 0.001$, **** = $P \leq 0.0001$.

OSM-OSMR signalling is known to activate STAT3 signalling in cervical SCC cells. Therefore, baseline mRNA levels of known downstream targets of STAT3 signalling were also investigated by qPCR. Expression of VEGFA was 4.3 fold greater in SW756-PBS-cells compared to ME180-PBS-cells (Figure 4.4C). ME180-PBS-cells were found to express very low levels of TGM2 and SNAI1; expression of these mRNAs was 20,500 and 39 fold greater in SW756-PBS-cells, respectively (Figure 4.4D-E).

Treatment with OSM appeared to result in upregulation of OSMR in SW756-OSM-cells (Figure 4.5A) at all timepoints, however due to variability between replicates, difference in treated and untreated cells did not reach statistical significance. OSMR expression was also upregulated in ME180-OSM-cells at all timepoints; upregulation was statistically significant at 12, 24 and 72 hours (Figure 4.5E). Greater upregulation of OSMR was observed in ME180-OSM-cells at 12 and 72 hour timepoints, compared to SW756-OSM-cells. However, even following treatment with OSM, OSMR levels in ME180-OSM-cells remained less than that of SW756-PBS-cells.

Treatment with OSM appeared to induce VEGFA expression in SW756-OSM-cells at all 4 timepoints compared to SW756-PBS-cells. However, due to variability between replicates, differences in VEGFA expression between treatment groups was only found to be statistically significant at 72 hours post treatment (Figure 4.5B), where a 4.8 fold increase in VEGFA levels was observed in SW756-OSM-cells. VEGFA was also significantly upregulated in ME180-OSM-cells at 72 hours post treatment with OSM compared to ME180-PBS-cells; however upregulation was to a lesser extent than that observed in SW756 cells (1.4 fold; Figure 4.5F). TGM2 expression was significantly upregulated in SW756-OSM-cells at 12 hours post OSM treatment i (Figure 4.5C); mRNA levels remained elevated up to 48 hours post treatment, however, differences at these timepoints were not statistically significant. TGM2 levels in ME180-OSM-cells did not change at any of the timepoints investigated (Figure 4.5G). In SW756-OSM-cells SNAI1 was upregulated at all timepoints; however, this was not found to be statistically significant (Figure 4.5D). No significant difference in SNAI1 expression was observed between ME180-PBS-cells and ME180-OSM-cells at any timepoint (Figure 4.5H). Together, these findings indicate that OSMR overexpressing SW756 cells are overall more responsive to OSM treatment than non-OSMR overexpressing ME180 cells, as demonstrated by their greater upregulation of the downstream STAT3 targets VEGFA, TGM2 and SNAI1 in response to treatment.

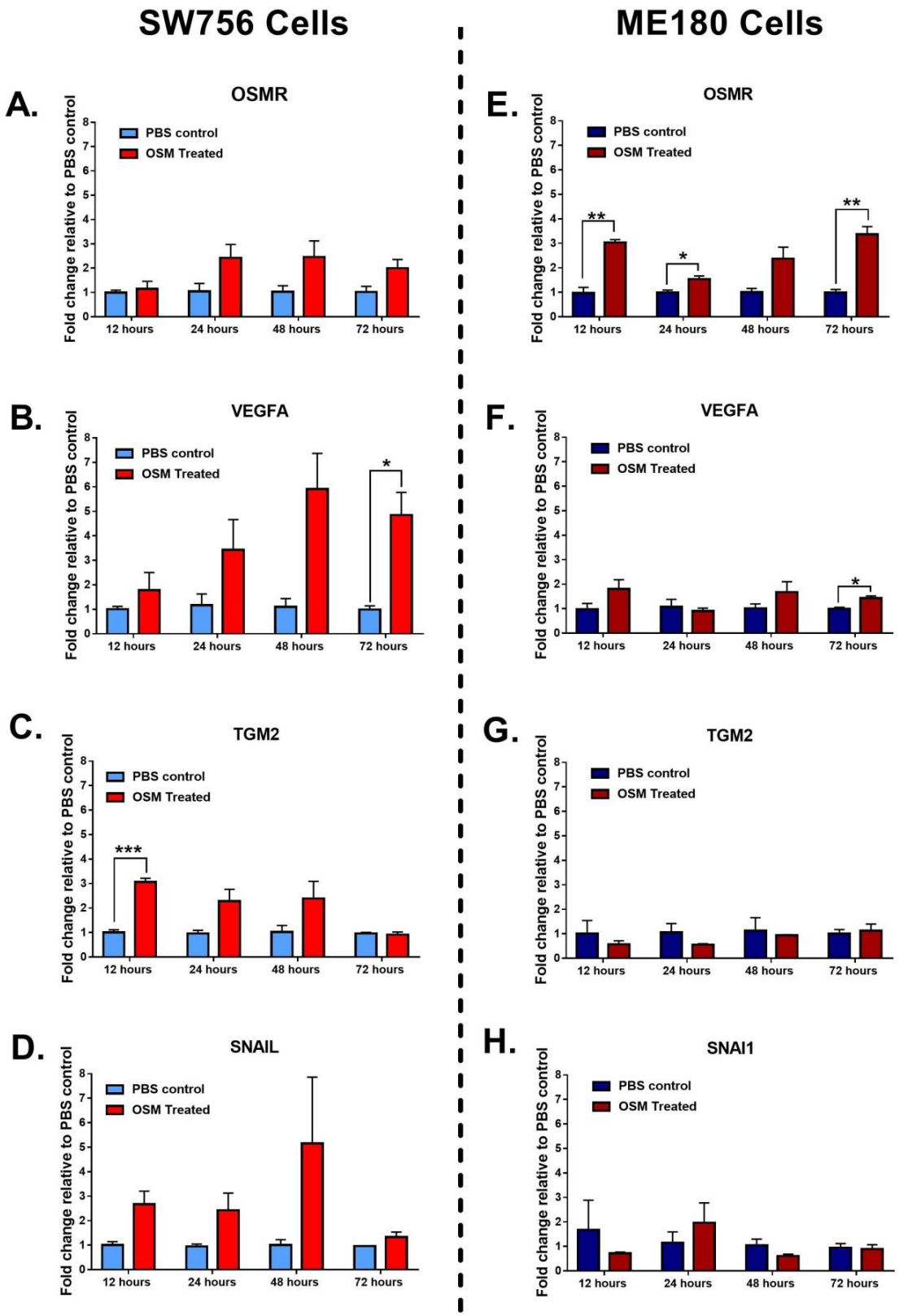

Figure 4.5: Response of SW756 and ME180 cell lines to OSM Treatment (mRNA)

Quantitative RT-PCR for SW756 and ME180 cells treated for 12, 24, 48 or 72 hours with 10ng/ml OSM or PBS control. Fold change in gene expression in OSM treated cells was normalised to PBS control at corresponding timepoints. A-D) SW756 cells E-H) ME180 cells. A+E) OSMR, B+F) VEGFA, C+G) TGM2, D+H) SNAI1. Error bars represent SEM, n=3 independent experiments for each condition. Values were analysed for statistical significance using a using Unpaired T-test with Welch's correction * =.$P \leq 0.05$, ** = $P \leq 0.01$.

4.4 QPCR analysis of cellular and EV miRNA levels in response to OSM

The experiments discussed above confirmed that SW756 and ME180 cells represented two cervical SCC cell lines with differing levels of OSMR expression and response to OSM. OSM-OSMR signalling was shown to affect transcription of downstream mRNA target genes, consistent with previous findings from our research. Whether OSM-OSMR signalling was also capable of modulating cellular and EV miRNA expression was subsequently investigated. As previously described, a panel of nine miRNAs was selected for investigation (Table 4.1).

Baseline levels of these 9 miRNAs were investigated by qPCR in SW756 and ME180 cells and EVs, collected at 12, 24, 48 and 72 hour timepoints from PBS control samples (Figure S4. 3A,B,D,E); miRNA expression was normalised to the endogenous control RNU24. In both cell lines, all 9 miRNAs were enriched in EVs compared to cells. miR-31, which is believed to act as a tumour promoter in SCC, was the most abundant miRNA in both SW756-PBS and ME180-PBS cells and EVs. With the exception of miR-23b, which was significantly more abundant in ME180-PBS-EVs at 72 hours compared to 48 hours (Figure S4. 3D), there was no difference in miRNA expression levels between timepoints for either PBS treated cells or EVs.

As miRNA abundance in PBS treated cells and EVs did not vary at different timepoints, the potential differences in baseline miRNA expression in SW756 and ME180 cells lines was compared at a single representative timepoint (48 hours). The majority of miRNAs appeared to be expressed at higher levels in SW756-PBS compared to ME180-PBS cells and EVs; however, this difference was not statistically significant. miR-9 and miR-31 were expressed at significantly lower levels in SW756-PBS-cells compared to ME180-PBS-cells (Figure S4. 3C). miR-31 was also shown to be expressed at significantly lower levels in SW756-PBS-EVs compared to ME180-PBS-EVs (Figure S4. 3F).

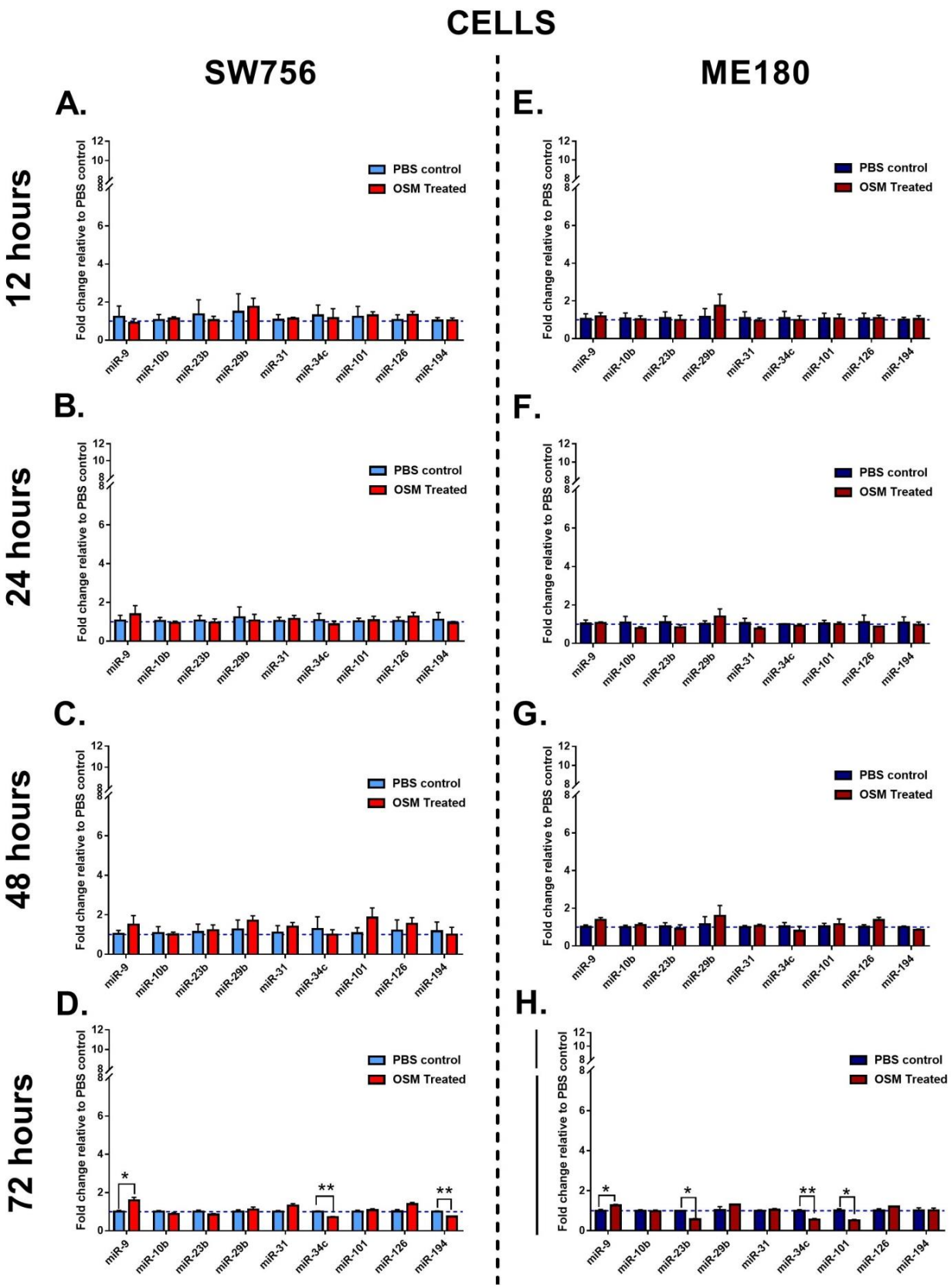

Figure 4.6: Effect of OSM treatment on cellular miRNA expression

Quantitative RT-PCR for SW756 (A-D) and ME180 (E-H) cells treated for 12 (A, E), 24 (B, F), 48 (C, G) or 72 (D, H) hours with 10ng/ml OSM or PBS control. Fold change in miRNA expression in OSM treated cells was normalised to PBS control at corresponding timepoints. Error bars represent SEM, n=3 independent experiments for each condition. Values were analysed for statistical significance using unpaired T-tests with Welch's correction. * =.P≤0.05, ** = P≤0.01, *** = P≤0.001.

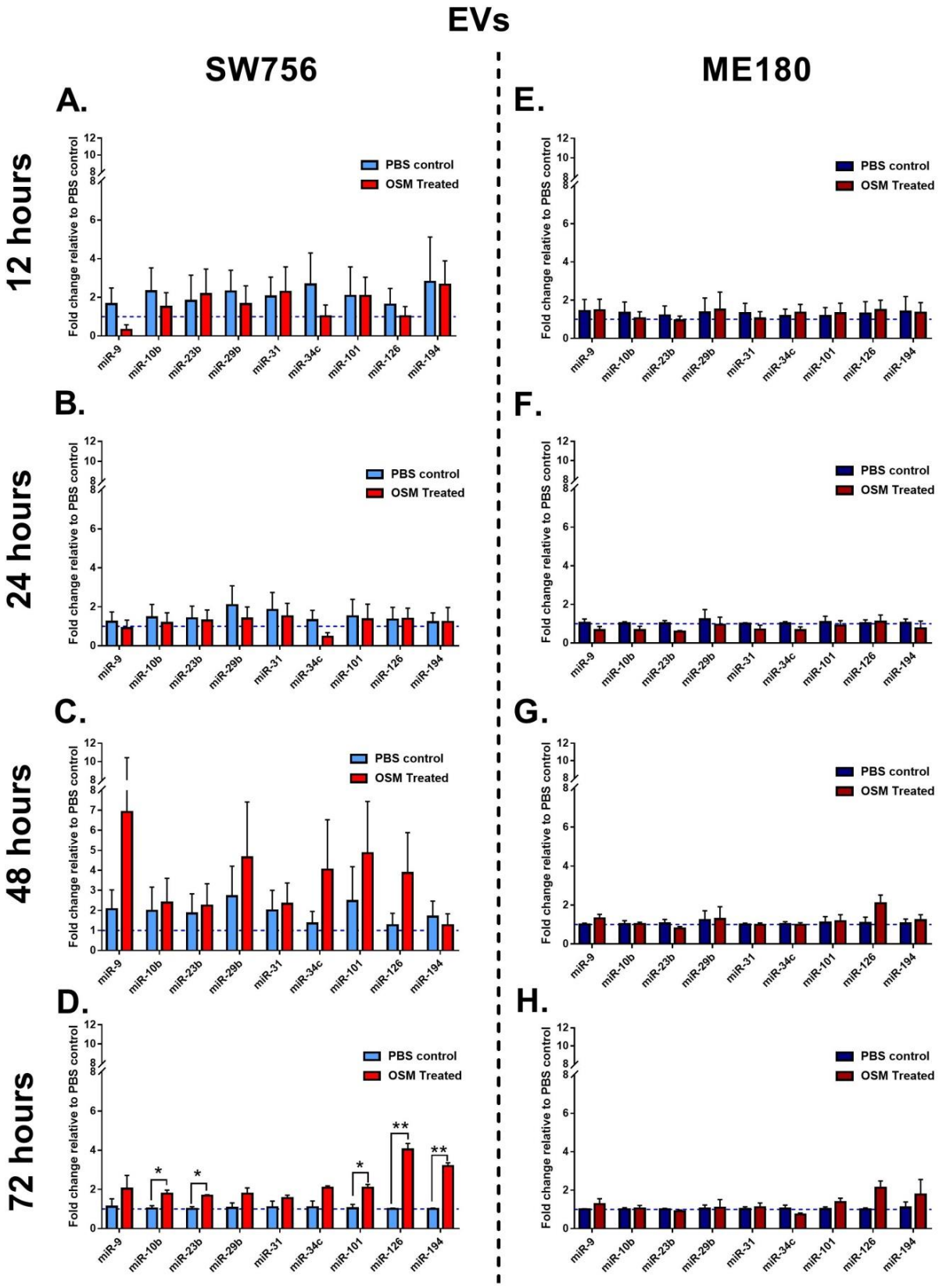

Figure 4.7: Effect of OSM treatment on EV miRNA expression

Quantitative RT-PCR for SW756 (A-D) and ME180 (E-H) EVs treated for 12 (A, E), 24 (B, F), 48 (C, G) or 72 (D, H) hours with 10ng/ml OSM or PBS control. Fold change in miRNA expression in EVs from OSM treated cells was normalised to EVs from PBS treated controls at corresponding timepoints. Error bars represent SEM, n=3 independent experiments for each condition. Values were analysed for statistical significance using unpaired T-tests with Welch's correction. * =.P≤0.05, ** = P≤0.01, *** = P≤0.001.

Treatment with OSM had varied effects on cellular (Figure 4.6) and EV (Figure 4.7) miRNA expression in each cell line. OSM had little effect on cellular miRNA expression at the 12, 24 or 48 hour timepoints for either cell line (Figure 4.6. A, B, E, F). While not statistically significant, there was an interesting trend in modest upregulation of multiple miRNAs in SW756-OSM-cells at the 48 hour time point (Figure 4.6C). At the 72 hour timepoint, miRNA response to OSM was more varied: in SW756 cells, miR-9 was significantly upregulated, whereas, miR-34c and miR-194 were significantly downregulated (Figure 4.6D). Similarly, in ME180-OSM-cells miR-9 was significantly upregulated, whereas, expression of miR-23b, miR-34c and miR-101 were significantly downregulated (Figure 4.6H).

The effect of OSM treatment on SW756 and ME180 EV miRNA expression was also less pronounced at 12 and 24 hour timepoints than later timepoints (Figure 4.7). At the 48 hour timepoint all miRNAs under investigation, except for miR-194, appeared upregulated in SW756-OSM-EVs; however, due to high levels of variability between replicates differences did not reach statistical significance (Figure 4.7C). This is similar to the expression pattern observed for SW756-OSM-cells at the same time point, however much greater upregulation was observed in the EVs. At 72 hours all miRNAs were upregulated in SW756-OSM-EVs and upregulation of five of the nine miRNAs were found to be statistically significant (Figure 4.7D). Upregulation was greater than that observed in cells at this timepoint (fold change ranged from 1.6-4.0). OSM appeared to have a less substantial impact on ME180-OSM-EV miRNA expression at 48 and 72 hour timepoints. miRNA levels remained predominantly unchanged in response to OSM at both the 48 hour (Figure 4.7G) and 72 hour timepoints (Figure 4.7H).

This data suggests that OSM treatment had a greater impact on EV miRNA expression in the SW756 OSMR-overexpressing cell line compared to ME180 EVs, a non-OSMR overexpressing cell line. Greatest changes in both cellular and EV miRNA expression were observed at later timepoints, following 48 and 72 hour treatment with OSM. Levels of the STAT3 targets *TGM2* and *SNAI1* appeared to begin to decline in SW756 cells at 72 hour timepoint. Therefore, 48 hours was selected for all subsequent experiments as both mRNAs and miRNAs were upregulated in SW756 cells in response to OSM at this timepoint (Figure 4.5).

4.5 EV Functional Assays

As OSM-OSMR signalling was found to alter EV miRNA cargo, subsequent experiments were performed to determine whether changes in EVs following OSM treatment of cervical SCC cells had any functional effects. To achieve this, following ultracentrifugation, the amount of EV protein was determined by BCA assay and a specified amount of EVs was diluted in fresh EV depleted media and added to either naive tumour cells or other cells of the TME.

4.5.1 Effect of EVs on cancer cell growth

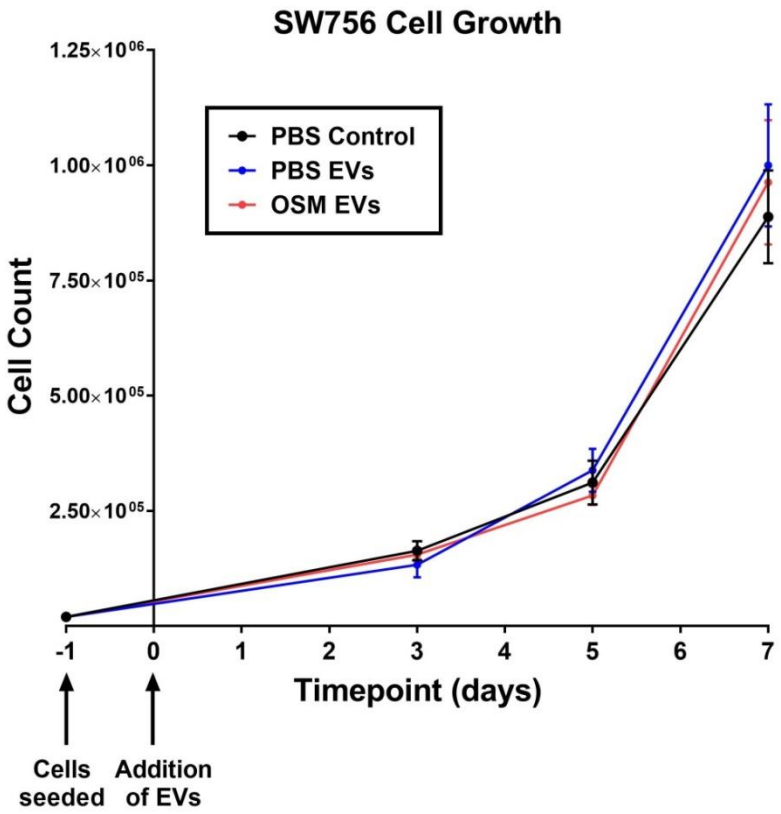

Figure 4.8: Effect of SW756 EVs on SW756 cell growth
SW756 cells were seeded at a concentration of $2x10^4$ cells/well. After 24 hours in culture, media was removed and 1.5ml of fresh EV depleted media added, supplemented with 1µg of EVs from PBS or OSM treated SW756 cells or PBS control of an equal volume. Cells were counted by countess at 3, 5 and 7 days post treatment. N=3 for each experimental condition at each timepoint. Values were analysed for statistical significance at individual timepoints using one way analysis of variance (ANOVA) with Tukey's multiple comparison post-hoc tests.

Seven of the nine miRNAs investigated (miR-9, miR-31, miR-10b, miR-29b, miR-101, miR-126 and miR-34c) have previously been linked to either positively or negatively regulating cervical SCC proliferation. As these miRNA were found to be altered in SW756 EVs in response to OSM-OSMR signalling, it was subsequently investigated whether SW756-PBS-EVs and SW756-OSM-EVs had differing functional effects on cervical SCC growth. The addition of 1µg of SW756-PBS-EVs or SW756-OSM-EVs to naive SW756 cells had no effect on cell growth at any of the three times points investigated (3, 5 and 7 days) compared to cells treated with PBS control (Figure 4.8).

4.5.2 Effect of EVs on Cell Migration

It has previously been shown in our laboratory that treatment of SW756 cells with OSM leads to increased cell migration[121]. Six of the nine miRNAs investigated (miR-9, miR-31, miR-10b, miR-23b, miR-126 and miR-34c) have previously been linked to regulation of cervical SCC cell migration. It was therefore investigated whether SW756-OSM-cells could confer their migratory advantage to naïve SW756 cells via their EVs.

Either SW756 or ME180 cells were used as recipient cells for the migration assays. A scratch was made in the centre of confluent wells and media containing 0.1µg, 1µg or 10µg of EVs from PBS or OSM treated donor cells added. SW756 and ME180 recipient cells were treated with EVs isolated from their corresponding cell lines. Closure of scratches was visually assessed at regular intervals and percentage wound closure calculated

SW756 cells treated with PBS were found to have significantly increased migration compared to PBS treated ME180 cells (Figure 4.9A). Moreover, SW756 and ME180 responded in opposing ways to treatment with EV depleted media or EVs. SW756 cells treated with SW756-PBS-DM displayed significantly reduced migration at the 13 hour timepoint compared to cells treated with PBS control; migration also appeared reduced at 16 and 20 hours post treatment in SW756-PBS-DM treated SW756 cells compared to cells treated with PBS control; however differences were not statistically significant. Treatment with SW756-OSM-DM also appeared to reduce migration at all three timepoints; however, results did not reach statistical significance (Figure 4.9B panel i). Similarly, treatment of SW756 cells with SW756-PBS-EVs and SW756-OSM-EVs appeared to result in reduced cell migration at all timepoints for all three concentrations of EVs investigated (Figure 4.9B panels ii–iv). Treatment of SW756 cells with the highest EV concentration, 10µg, led to significantly reduced migration at the 13 hour timepoint regardless of whether EVs originated from SW756-OSM-cells or SW756-PBS-cells (Figure 4.9 panel iv).

Interestingly, the opposite effect was observed in ME180 cells. Treatment with both ME180-PBS-DM and ME180-OSM-DM appeared to increase cell migration at all three timepoints (Figure 4.9C panel i). Similarly, treatment of ME180 cells with either ME180-PBS-EVs or ME180-OSM-EVs resulted in increased cell migration at all timepoints for all three concentrations of EVs investigated (Figure 4.9C panels ii–iv). However, these differences were not found to be statistically significant.

This data indicates that SW756 and ME180 cells release differing factors, either directly into the conditioned media, or packaged into their EVs, which have opposing effects on migration of other cancer cells. Untreated SW756 cells were found to migrate more quickly than ME180 cells. It was hypothesised that, as a result of their increased baseline migratory capacity, SW756 cells may release factors that inhibit cell migration in a negative feedback mechanism to regulate migration of cells away from the primary tumour site. Conversely, as ME180 cells had reduced baseline migratory capacity, negative feedback may not be required and factors released from these cells instead promote migration of other cancer cells.

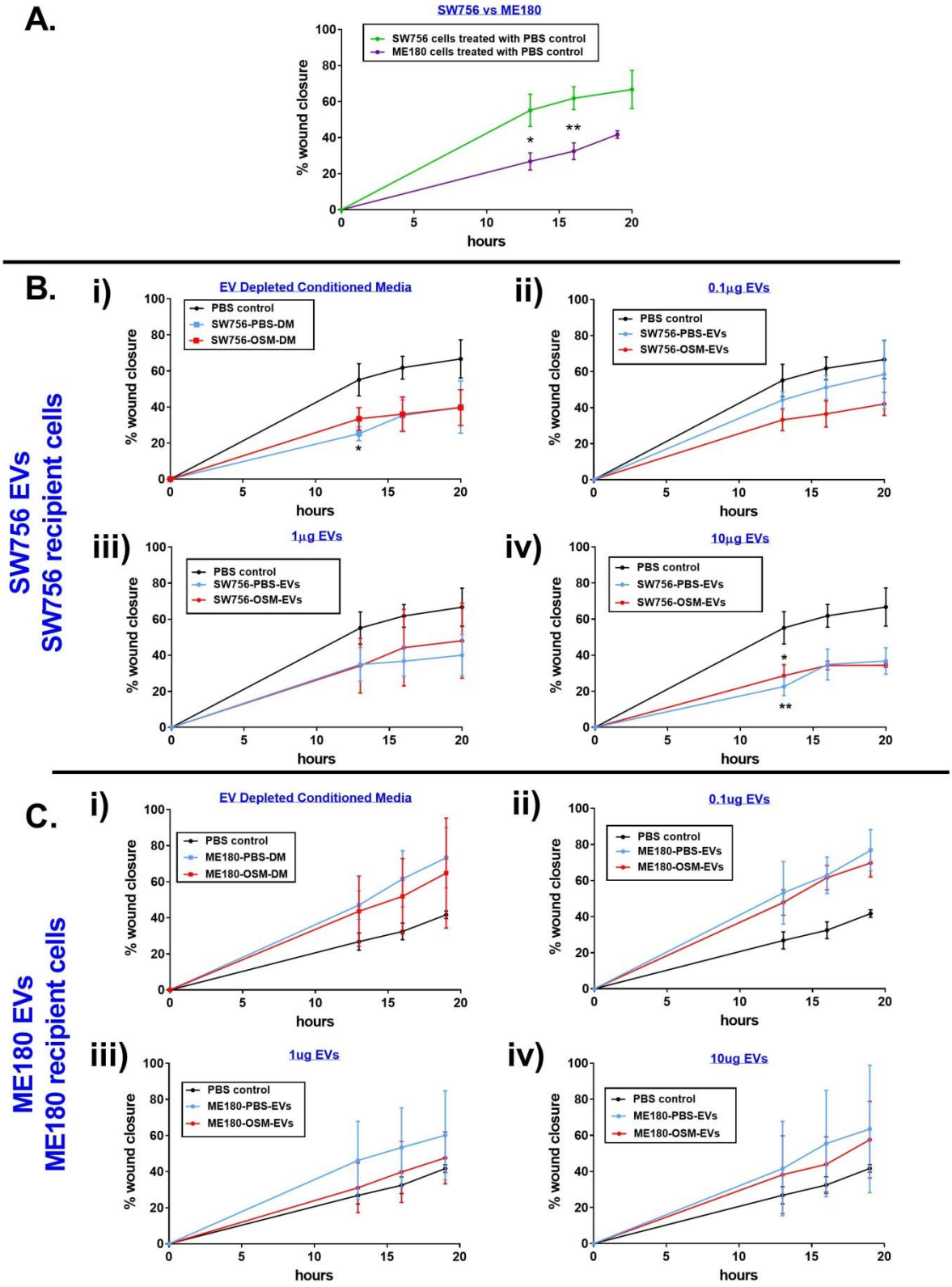

Figure 4.9: Effect of cervical SCC derived EVs on migration of cervical SCC cells

After 48 hours culture SW756 and ME180 cells were scratched with a 1ml pipette. Media containing PBS control, 0.1µg, 1µg or 10µg of EVs or EV depleted conditioned media from PBS or OSM treated cells was added and wound closure assessed over a 20 hour period. A) Comparison of wound closure in SW756 and ME180 cells treated with PBS control. Treatment of B) SW756 cells or C) ME180 with i) EV depleted conditioned media (DM) ii) 0.1µg EVs iii) 1µg EVs or iv) 10ug EVs from PBS or OSM treated SW756 (B) or ME180 cells (C). N=3 for each experimental condition at each timepoint. Error bars represent SD. Values were analysed for statistical significance at each timepoint using unpaired T-tests with Welch's correction (A) or one way ANOVA with Tukey's multiple comparison post-hoc tests (B and C). * =P≤0.05, ** = P≤0.01.

Similar experiments were also performed using SW756 donor cells and VF-2 recipient cells; normal diploid human fibroblasts originating from juvenile foreskin material. Wells were scratched as previously described and VF2 cells treated with media supplemented with either 10ng/ml OSM or an equal volume of PBS control, or with either 10µg of SW756-PBS-EVs or SW756-OSM-EVs.

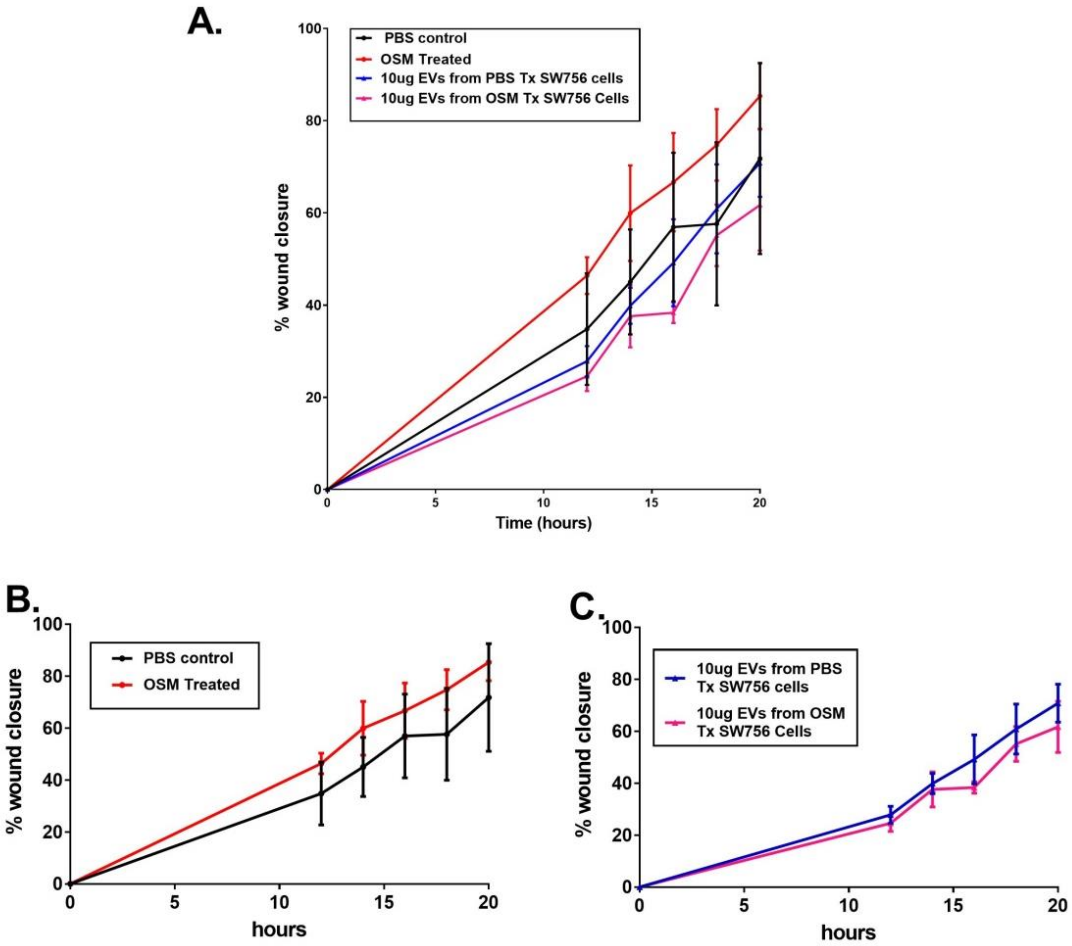

Figure 4.10: Effect of SW756 EVs on migration of VF2 fibroblasts
After 7 days culture VF2 cells were scratched with a 1ml pipette. Media containing PBS control, 10ng/ml Rh-OSM, or 10µg of EVs from PBS or OSM treated cells was added and wound closure assessed over a 20 hour period. Comparison of wound closure in A) all 4 treatment groups, B) PBS and OSM treated VF2 cells and C) VF2 cells treated with EVs from PBS or OSM treated cells are shown. N=3 for each experimental condition at each timepoint. Error bars represent SD. Values were analysed for statistical significance at each timepoint using a one way ANOVA with Tukey's multiple comparison post-hoc tests.

Treatment with OSM had no significant effect on migration of VF2 cells at all timepoints compared to cells treated with PBS control (Figure 4.10). Similarly, treatment with either SW756-PBS-EVs or SW756-OSM-EVs had no significant effect on VF2 migration compared to treatment with PBS control. OSM has previously been shown to promote migration of OSMR overexpressing cervical SCC cells in a dose-dependent manner[121]. However, SW756-OSM-EVs did not confer this migratory advantage when EVs were used to treat

naive cancer cells or VF2 cells. This may possibly be due to the fact that concentrations of downstream factors of OSM-OSMR signalling were at too low a concentration in the EVs to have functional effects compared to SW756-PBS-EVs or PBS control. Additional replicates should be included to reduce variability and to allow for better assessment of statistical differences between treatment groups.

4.5.3 Effect of EVs on Angiogenesis

Subsequent experiments aimed to determine whether SW756-PBS-EVs and SW756-OSM-EVs had an effect on angiogenesis. Angiogenesis assays were performed using HUVECs and primary human fibroblasts co-cultures. Previous experiments using the same assay have shown that treatment of co-cultures with SW756-OSM-CM lead to increased angiogenesis compared to treatment with SW756-PBS-CM[92]. For these experiments SW756 cells were treated with a 2 hour pulse of OSM or PBS control. Media was then replaced and conditioned media collected 48 hours later. Therefore, for this experiment EVs were collected from SW756 cells treated in the same way.

Co-cultures were treated with media supplemented with the following: media control, VEGFA positive control, suramin negative control, SW756-PBS-CM or SW756-OSM-CM (48 hours continuous treatment) and SW756-PBS-EVs or SW756-OSM-EVs (2 hour treatment pulse). Representative images from the angiogenesis assay for each treatment condition are shown in Figure 4.11A. Treatment of co-cultures with both SW756-PBS-CM and SW756-OSM-CM led to significantly increased angiogenesis in a similar manner to co-cultures treated with VEGFA (Figure 4.11B). They displayed increased total tubule length and increased number of junctions and branches compared to media control. Mean branch length was also significantly reduced in co-cultures treated with VEGFA or SW756-OSM-CM (Figure 4.11B panel ii), likely as a result of the increased number of branches and junctions. Thus, factors present in SW756 conditioned media were capable of promoting angiogenesis. Moreover, SW756-OSM-CM appeared to induce angiogenesis at higher levels than SW756-PBS-CM.

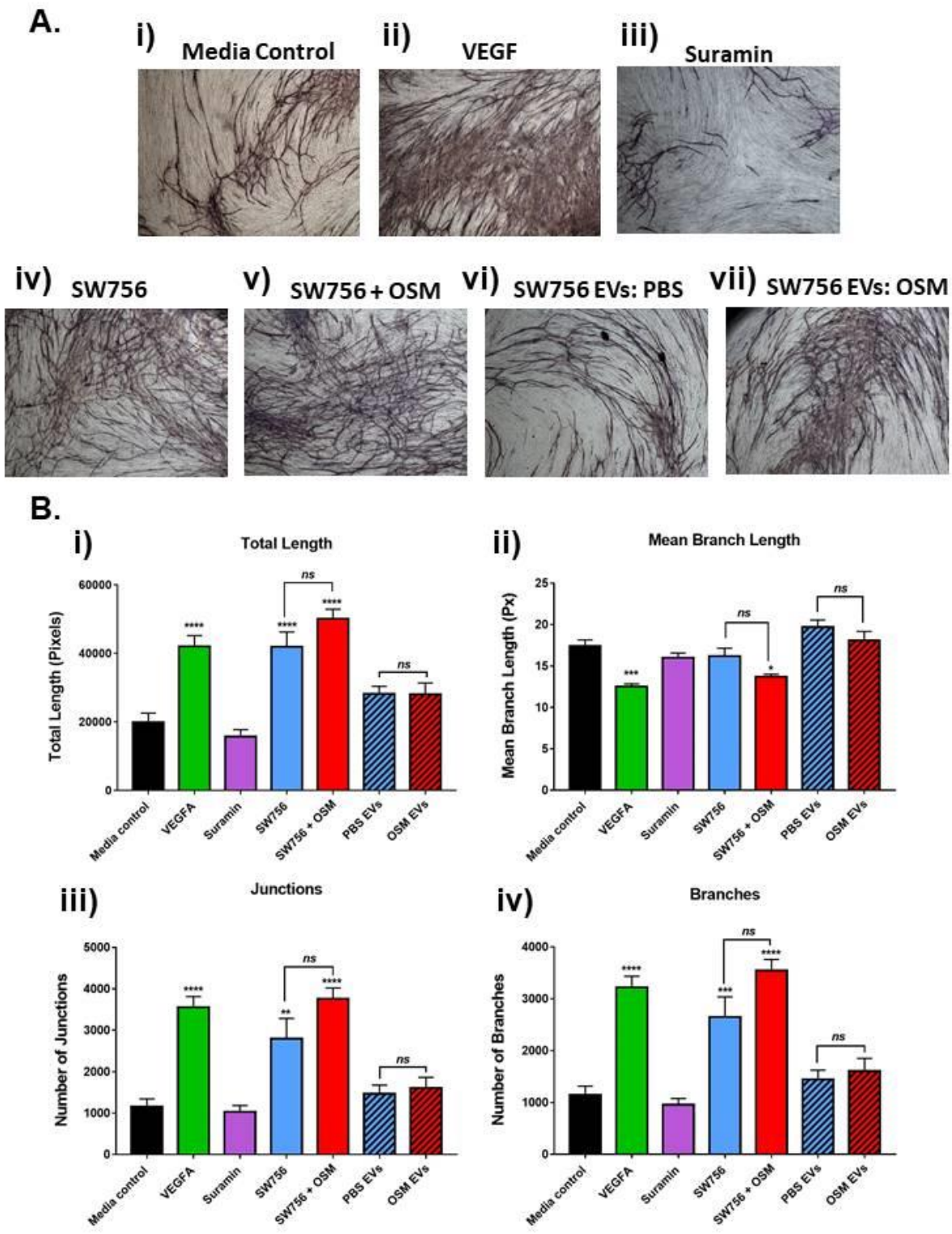

Figure 4.11: Effect of EVs on Angiogenesis Assay

A) Representative images of CD31 stained tubules in HUVEC-primary fibroblast co-cultures treated every 48 hours with i) media control, ii) VEGFA, iii) suramin, iv) conditioned media from SW756 cells treated with PBS, v) conditioned media from SW756 cells treated with OSM, vi) EVs isolated from SW756 cells treated with PBS and vii) EVs from SW756 cells treated with OSM. B) AngioSys 2.0 Image Analysis Software was used to quantify i) total tubule length, ii) mean branch length, iii) number of junctions and iv) number of branches for images collected from 5 different fields of view for each sample. N=2 independent replicates for each condition. Values were analysed for statistical significance using an ANOVA with Tukey's multiple comparison post-hoc tests. * =P≤0.05, ** = P≤0.01, *** = P≤0.001 and **** = P≤0.0001.

Co-cultures treated with SW756-PBS-EVs or SW756-OSM-EVs displayed increased total tubule length, number of junctions and number of branches compared to co-cultures treated with control media. However, differences were not found to be statistically significant (Figure 4.11B). No differences were evident between co-cultures treated with SW756-PBS-EVs or SW756-OSM-EVs. Therefore, while cervical SCC derived EVs appeared to have some effect on angiogenesis, this was to a lesser extent than that observed for EV depleted conditioned media. This indicates that soluble EV-independent factors are responsible for the majority of the angiogenic effects observed. SW756 cells were shown in earlier experiments to secrete VEGFA. Therefore, while VEGFA and other pro-angiogenic factors may be packaged into the EVs, they may not be present at levels high enough to have a substantial impact on angiogenesis.

While the miRNA cargo of EVs isolated from cervical SCC cells was found to be altered in response to OSM treatment, we were unable to identify the functional significance of these changes using the various assays described above. It is difficult to elucidate the functional relevance of these changes when only a small number of miRNAs was investigated. Therefore, we subsequently aimed to determine the overall effects of OSM treatment on cellular and EV mRNA and miRNA expression.

4.6 Generation of an OSMR KD SW756 cell line

Preliminary experiments using cell lines with different baseline levels of OSMR expression – SW756 and ME180 cells – indicated that OSM-OSMR signalling was capable of modulating cellular and EV miRNA expression. These experiments focused on a small panel of miRNAs; therefore, we aimed to implement a global approach using next generation sequencing in order to determine the overall effects of OSM treatment on cervical SCC cellular and EV mRNA and miRNA expression. The aim was to identify pathways that were altered in response to OSM-OSMR signalling in both cells and EVs in order to assist in the design of future experiments to investigate functional effects.

In order to eliminate confounding effects of comparing two cervical SCC cell lines that are likely to vary in more aspects than just their levels of OSMR expression, it was determined that creating an OSMR KD cell line would be a more appropriate control. A CRISPR-Cas9 approach was therefore used to generate an OSMR KD SW756 cell line. This was performed using a CRISPR-all-in-one Cas9^{D10A} nickase vector system[218] which contains dual sgRNAs under the control of a U6 promoter and Cas9^{D10A} nickase coupled to EGFP[218].

4.6.1 Cloning of gRNAs into vector backbone

A pair of sense (gRNA1) and antisense (gRNA2) gRNAs were designed to target an exon within transcripts OSMR-001 and OSMR-003, as depicted in (Figure 3.4). The structure of the PX466 Cas9-D10A-GFP vector is shown in (Figure 3.5). The vector was linearised by BsaI digest and gRNA1 ligated into the vector backbone. Ligated plasmid was used to transform DH5α competent cells. DNA was extracted from four resultant colonies and gRNA1 insertion confirmed by EcoRI digest (Figure 4.12A). The PX466 Cas9-D10A-GFP vector contains three EcoRI sites, one of which is located between the two BsaI sites (Figure 3.5) in which the gRNA1 was inserted. Therefore, EcoRI digestion can be used to diagnose successful cloning, since digestion of the original plasmid (i.e. plasmid without gRNA1 insertion) will produce 3 fragments (4kb, 5kb and 0.8kb in size) whereas, plasmids with insertion of gRNA1 will only be cut twice, producing two fragments 9kb and 0.8kb in size.

DNA from three colonies was identified as having the appropriate number of bands corresponding to successful insertion of gRNA1 (Figure 4.12A) and these were denoted gRNA1 colonies A-C. DNA from these colonies was sent for sequencing and all were confirmed to have successful insertion of gRNA1 (Figure S4. 4). DNA from the colony with the greatest DNA concentration was selected for subsequent experiments.

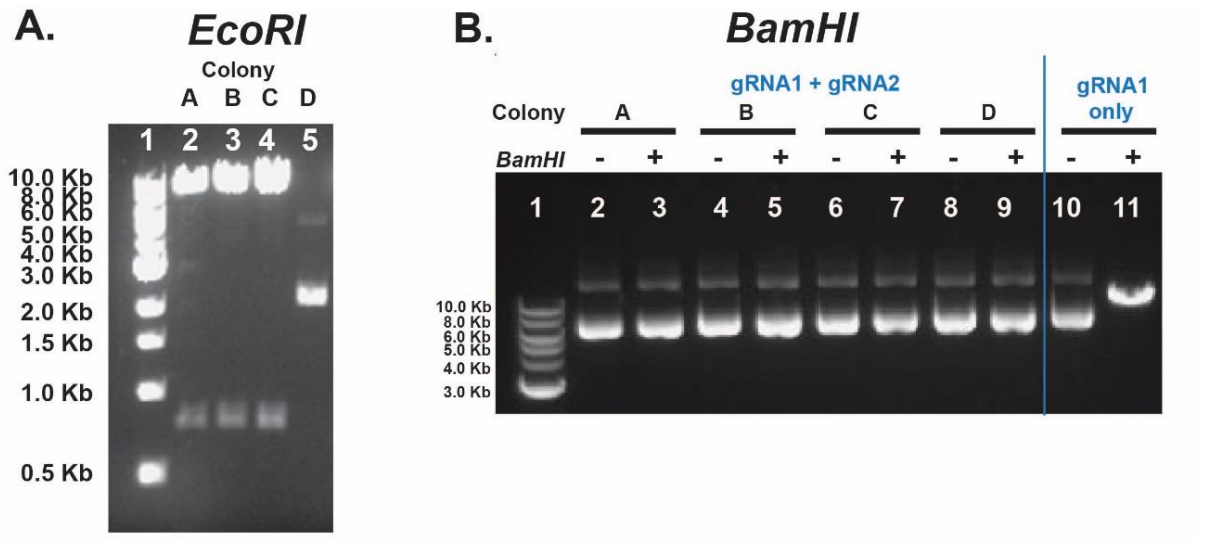

Figure 4.12: CRISPR – Confirmation of gRNA insertion into vector

(A) EcoRI digest to confirm gRNA1 insertion (1 = 1Kb ladder; 2-5 = Plasmid + gRNA1, colonies A-D, respectively). B) BamHI digest to confirm gRNA2 insertion (1= 1Kb ladder, 2 = Colony A undigested, 3= colony A digested with BamHI, 4 = Colony B undigested, 5= colony B digested with BamHI, 6 = Colony C undigested, 7= colony C digested with BamHI, 8 = Colony D undigested, 9= colony D digested with BamHI, 10 = plasmid containing gRNA1 only undigested, 11= plasmid containing RNA1 only digested with BamHI).

Vector containing gRNA1 was subsequently linearised by BbSI digestion and gRNA2 was ligated into the vector backbone. Ligated plasmid was used to transform DH5α competent cells and DNA was extracted from four resultant colonies and gRNA2 insertions confirmed by BamHI digest. The PX466 Cas9-D10A-GFP vector contains a BamHI site located between the two BbsI sites. Colonies with successful insertion of gRNA2 will no longer contain a BamHI site, whereas plasmids without gRNA2 insertion will be linearised following BamHI digestion. DNA from all four colonies was unaffected by BamHI digest corresponding to successful gRNA2 insertion (Figure 4.12B). These were denoted gRNA1+gRNA2 colonies A-D. DNA from these colonies was sent for sequencing and all were confirmed to have successful insertion of both gRNA1 and gRNA2 (Figure S4. 5). The colony with the highest DNA concentration was selected for subsequent experiments.

4.6.2 Transfection of SW756 cells with OSMR CRISPR Plasmid

SW756 cells were transfected with either empty PX466 Cas9-D10A-GFP plasmid (empty plasmid) or plasmid containing sgRNAs against OSMR. Experimental design is depicted in Figure 4.13A. As the PX466 Cas9-D10A-GFP plasmid encodes EGFP, cellular EGFP expression was used to confer successful cell transfection. Only cells transfected with PX466 Cas9-D10A-GFP plasmid were found to express EGFP (Figure 4.13B).

EGFP positive cells then underwent single cell sorting; untransfected control samples were used to set gating parameters. For cells transfected with empty plasmid or plasmids containing sgRNAs against OSMR, a single EGFP positive cell was plated in each well of a 96 well plate. Remaining EGFP positive cells for each sample were seeded in 6 well plates – these are later referred to as “pooled samples”. Cell sorting was performed with the assistance of Nigel Miller and Joana Cerveira.

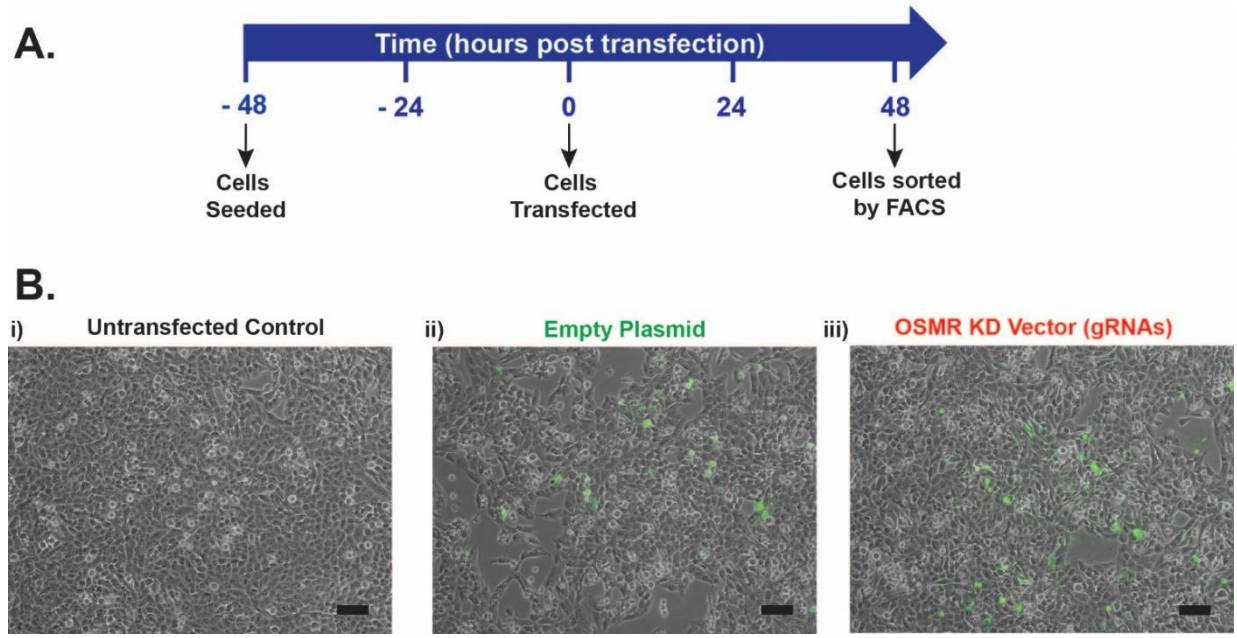

Figure 4.13: Transfection of SW756 cells with PX466 Cas9-D10A-GFP plasmid
A) Schematic of experimental design. B) EGFP expression in SW756 cells transfected with: i) untransfected control, ii) empty plasmid iii) plasmid containing sgRNAs.

4.6.3 Confirmation of OSMR KD – genomic DNA

Once cells derived from single cell FACs sorting reached confluence, 6 colonies for each treatment group (empty plasmid and plasmid with sgRNAs) were selected and bulked up until there were enough cells to perform DNA, RNA and protein extractions. Pooled samples were also expanded. Genomic DNA primers were designed to amplify a small fragment of the OSMR gene (240 base pairs in length) that was targeted by the CRISPR gRNAs. PCR was performed on genomic DNA collected from SW756 cells that had been transfected with either empty plasmid or plasmid containing sgRNAs (Figure 4.14A). All clonal cell populations transfected with empty plasmid displayed a band of the expected size for wild-type OSMR (Figure 4.14A). From the cells transfected with plasmid containing gRNAs targeting OSMR, only clone 5 appeared to have a mutation that altered the size of the fragment amplified (Figure 4.14A).

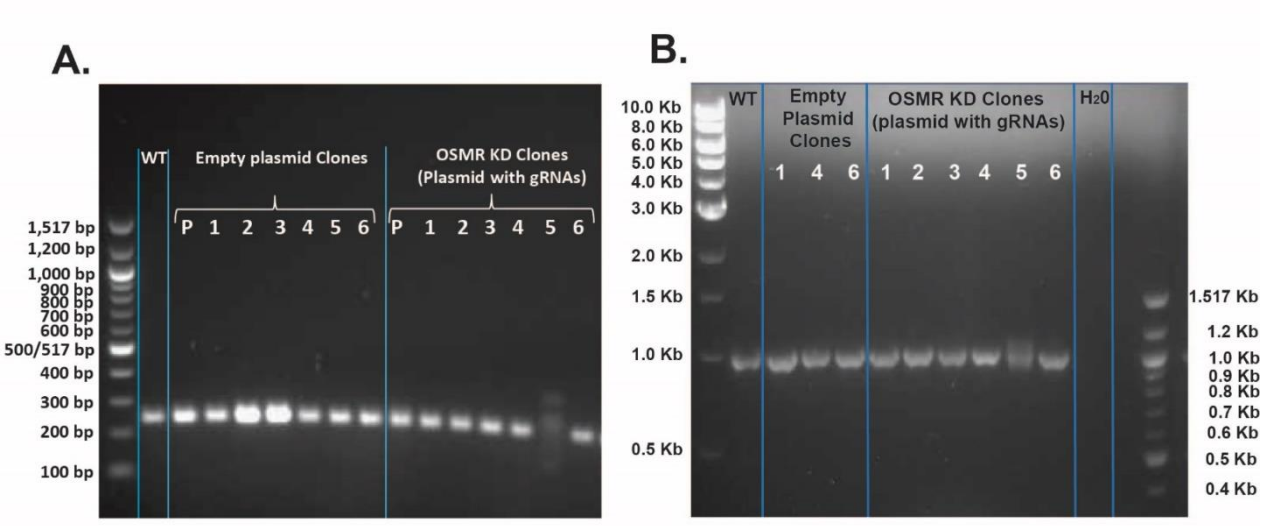

C.

	Forward Sequencing Primer		Reverse Sequencing Primer	
	Indel %	KO Score	Indel %	KO Score
Empty Plasmid Clone 1	0	0	0	0
Empty Plasmid Clone 4	0	0	0	0
Empty Plasmid Clone 6	43	21	0	0
OSMR KD Clone 1	0	0	0	0
OSMR KD Clone 2	0	0	0	0
OSMR KD Clone 3	0	0	0	0
OSMR KD Clone 4	0	0	0	0
OSMR KD Clone 5	57	55	43	37
OSMR KD Clone 6	0	0	0	0

Figure 4.14: Detection of genomic mutations in OSMR following CRISPR
A) PCR using primers designed to amplify a 240bp region with gRNA sites. P = pooled, non clonal samples. B) PCR of genomic DNA using sequencing primers designed to amplify a region of 1006bp spanning the gRNA sites. C) Summary of Synthego ICE analysis of sequencing results, following alignment of each sample to sequences from Wild-Type SW756 cells.

Subsequently, sequencing primers were designed to amplify a larger fragment (1006bp) within the region targeted by CRISPR. PCR was performed on wild type SW756 cells, SW756 cells transfected with empty plasmid (clones 1, 4 and 6 were selected) and SW756 cells transfected with OSMR KD plasmid (clones 1-6). When PCR products were run on an agarose gel, OSMR KD Clone 5 was the only cell line that appeared to have a perturbed band (Figure 4.14B). PCR products were purified and sent for sequencing using both forward and reverse primers. Sequencing data was analysed with SnapGene (results not shown) and Synthego ICE software: sequences from each sample (using either forward or reverse prime) was compared with that of wild-type SW756 cells in order to determine if any changes had occurred to the targeted section of the OSMR gene. Synthego ICE calculates

the percentage of insertions and/or deletions of bases (indels) and generates a knock out (KO) score for each sample. As indicated by PCR, only OSMR KD clone 5 was found to have an altered OSMR sequence. Representative read outs of Synthego ICE analysis displaying sample alignment, discordance and indel plots compared to wild-type are shown for OSMR KD clone 2 (no changes to DNA sequence) and OSMR KD clone 5 (altered DNA sequence) in Figure S4. 6. The results of the analysis for all clones investigated are summarised in Figure 4.14C. OSMR KD Clone 5 was found to have KO scores of 55 and 37 when alignment of sequencing reads was performed using forward and reverse primers, respectively.

4.6.4 Confirmation of OSMR KD – protein

Knock down of OSMR protein expression was subsequently confirmed by western blot in OSMR KD clone 5 (Figure 4.15). While clones 1, 3 and 6 also appeared to have reduced protein levels compared to WT, mutations were not detected in the genomic DNA sequences and therefore only clone 5 was selected for further experiments. All empty plasmid clones displayed protein OSMR levels similar to that of WT SW756; empty plasmid clone 1 was selected for further experiments. From here onwards OSMR KD clone 5 will be referred to as SW756 OSMR KD cells and empty plasmid clone 1 will be referred to as SW756 empty plasmid cells.

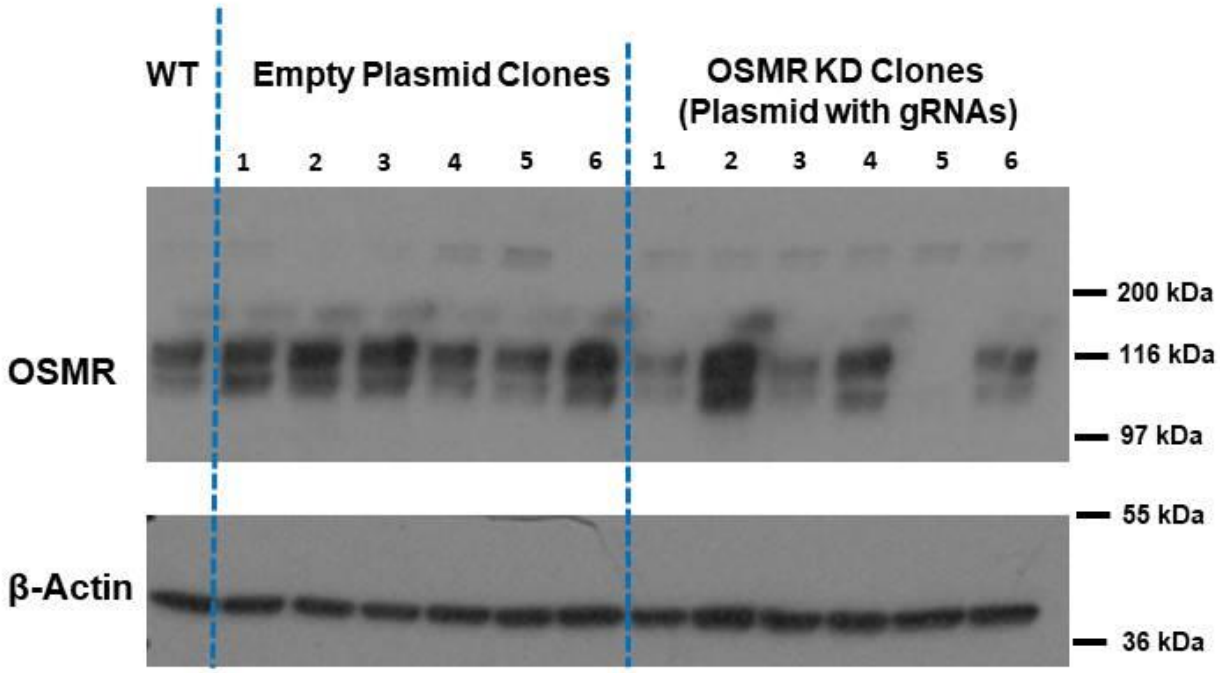

Figure 4.15: Clonal OSMR protein expression following CRISPR

4.7 Characterisation of OSMR KD Cell Line

Empty plasmid and OSMR KD SW756 cell lines generated by CRISPR-Cas9 were further characterised to determine their response to OSM. Abbreviations shown in Table 4.3 will be used from here onwards.

Table 4.3: Summary of abbreviations used for CRISPR cell lines

Abbreviation	Description
WT cells	Wild type SW756 cells
EP cells	Empty plasmid SW756 cells
KD cells	OSMR KD SW756 cells
WT-PBS-cells	SW756 wild-type cells treated with PBS
WT-OSM-cells	SW756 wild-type cells treated with OSM
WT-PBS-EVs	EVs isolated from wild-type SW756 cells following PBS treatment
WT-OSM-EVs	EVs isolated from wild-type SW756 cells following OSM treatment
EP-PBS-cells	SW756 empty plasmid cells treated with PBS
EP-OSM-cells	SW756 empty plasmid cells treated with OSM
EP-PBS-EVs	EVs isolated from empty plasmid SW756 cells following PBS treatment
EP-OSM-EVs	EVs isolated from empty plasmid SW756 cells following OSM treatment
KD-PBS-cells	OSMR KD SW756 cells treated with PBS
KD-OSM-cells	OSMR KD SW756 cells treated with OSM
KD-PBS-EVs	EVs isolated from OSMR KD SW756 cells following PBS treatment
KD-OSM-EVs	EVs isolated from OSMR KD SW756 cells following OSM treatment

Baseline levels of OSMR mRNA were unchanged in EP-PBS-cells compared to WT-PBS-cells (Figure 4.16). OSMR expression was found to be significantly reduced in KD-PBS-cells compared to both WT-PBS-cells and EP-PBS-cells (Figure 4.16A). Baseline levels of downstream STAT3 targets VEGFA, TGM2 and SNAI1 were unchanged in KD-PBS-cells compared to WT-PBS-cells control. In response to 48 hours treatment with 10ng/ml OSM, WT-OSM-cells and EP-OSM-cells displayed similar patterns of expression of downstream STAT3 targets; OSMR, VEGFA, TGM2 and SNAI1 were all found to be significantly upregulated to similar levels in both cell lines (Figure 4.16B-E). Conversely, in KD-OSM-cells, no upregulation in OSMR, VEGFA, TGM2 or SNAIL mRNA levels was detected following treatment with OSM. Levels of EGFR were also investigated (Figure 4.16F). OSM has been shown to signal via an OSMR-EGFR receptor complex in glioblastoma[91]. Moreover, OSM was previously shown to increase levels of EGFR protein but not mRNA in SW756 cells[92]. Therefore, OSMR may increase EGFR protein stability. Baseline levels of *EGFR* were unaltered across all three cell lines. Treatment with OSM led to a small but significant increase in EGFR expression in EP-OSM-cells.

As previously discussed, some previous experiments by our research group used a 2 hour pulse of OSM, followed by RNA collection 48 hours later, rather than continuous treatment for 48 hours[92]. It was hypothesised that this protocol might be preferable for EV experiments, as it would reduce the likelihood of free OSM being co-isolated with EVs during ultracentrifugation. In order to determine whether this was a plausible treatment regime for use, response of these three cell lines to a 2 hour pulse of treatment with OSM was investigated. Treatment with a 2 hour pulse of OSM was not found to be sufficient to activate upregulation of OSMR or its downstream targets at 48 hours after treatment in WT-OSM-cells or EP-OSM-cells (Figure 4.17). As expected, no changes in KD-OSM-cells were detected in response to treatment. All subsequent experiments detailed in this thesis involving treatment of cervical SCC cells with OSM were performed for a continuous 48 hour period, rather than 2 hour pulse.

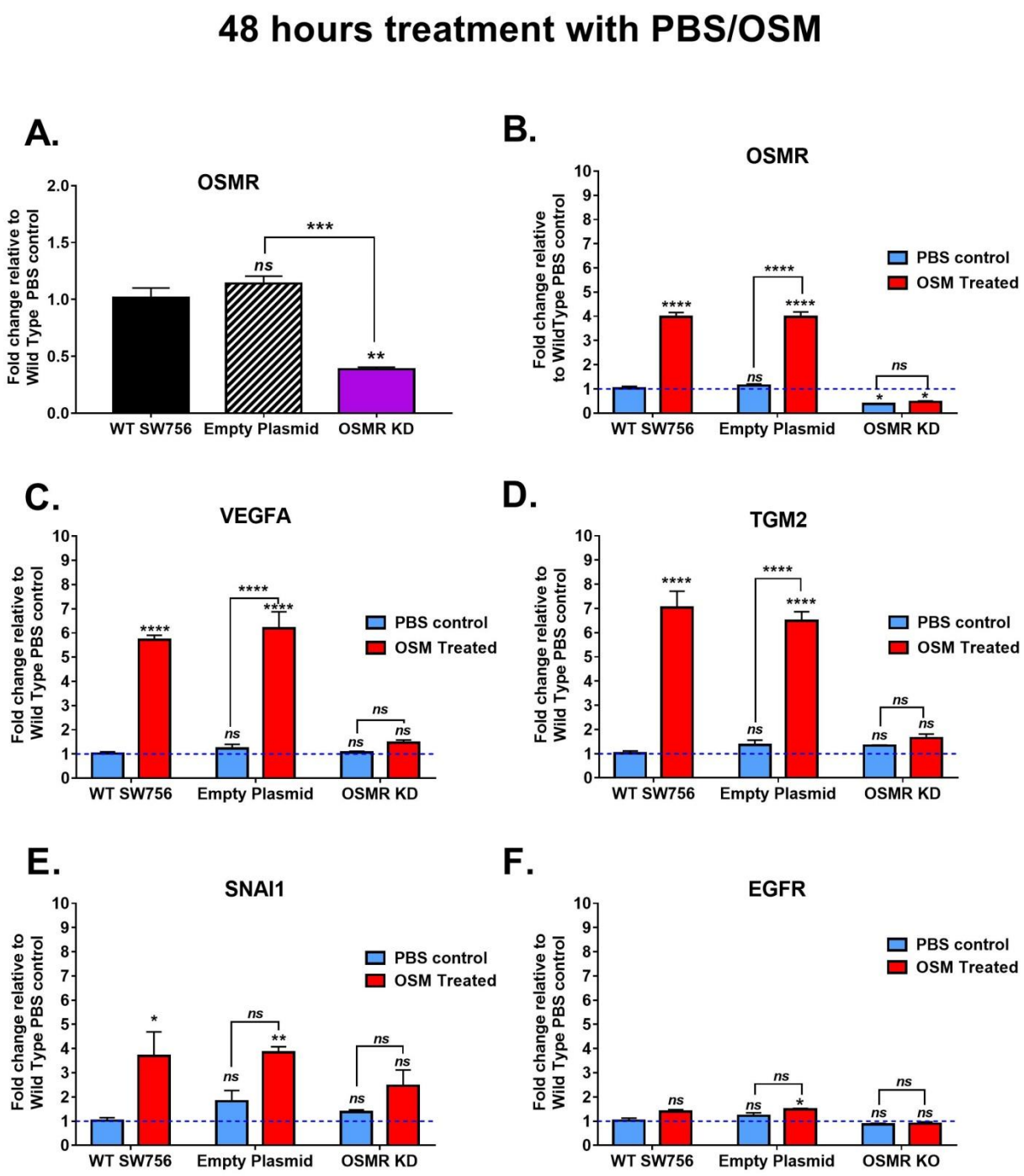

Figure 4.16: mRNA expression – 48 hour treatment with OSM

Quantitative RT-PCR for SW756 Wild-type, empty plasmid and OSMR KD cell lines following 48 hours treatment with 10ng/ml OSM or PBS control. A) Baseline levels of OSMR in PBS treated samples compared to WT control. B-F) Fold change in gene expression in PBS and OSM treated samples relative to WT+PBS control. Changes in mRNA expression of B) OSMR C) VEGFA D) TGM2 E) SNAI1 and F) EGFR were investigated. Error bars represent SEM, n=3 independent experiments for each condition. Values were analysed for statistical significance using a one way ANOVA with Tukey's multiple comparison post-hoc tests. * =.$P \leq 0.05$, ** = $P \leq 0.01$, *** = $P \leq 0.001$, **** = $P \leq 0.00001$.

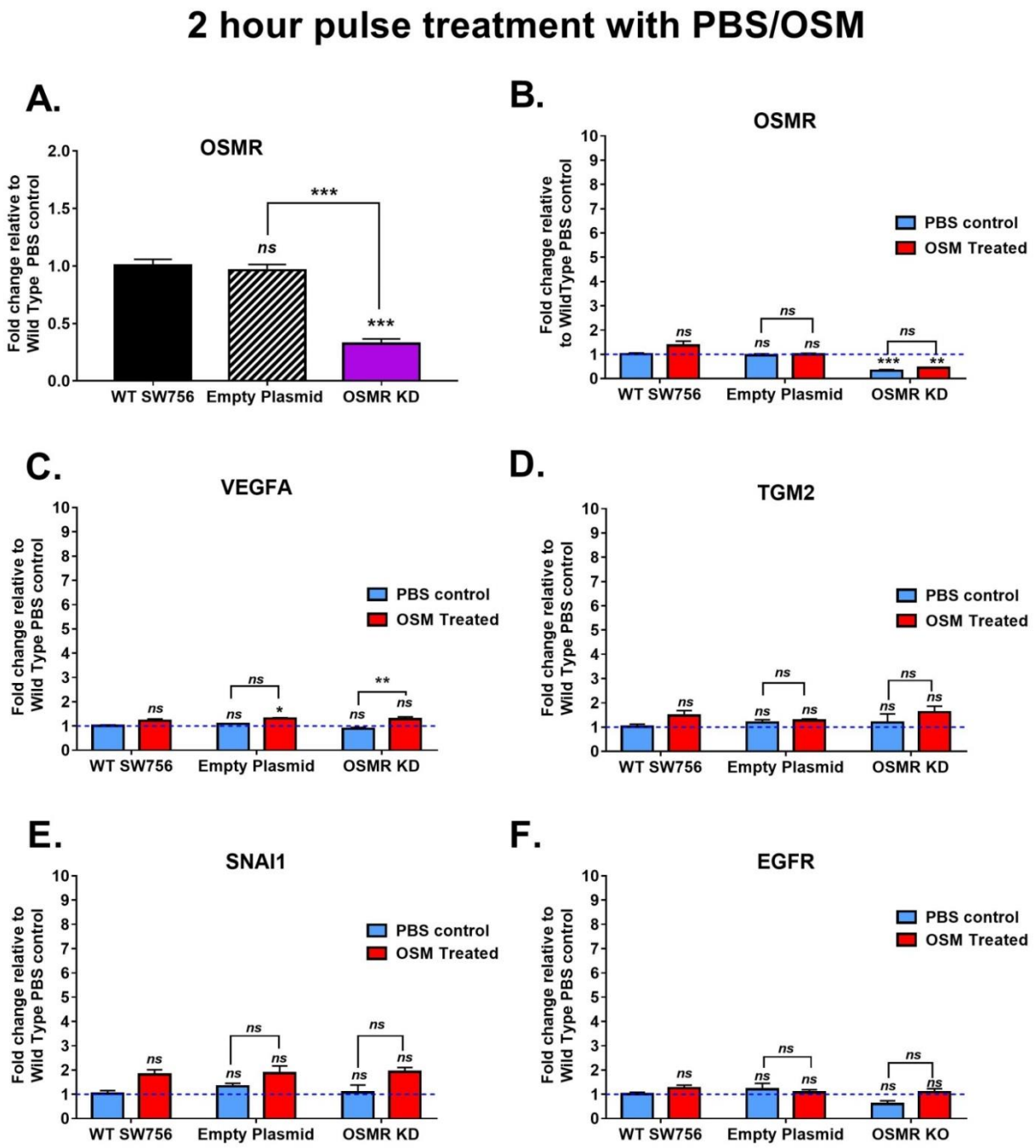

Figure 4.17: mRNA expression – Treatment with OSM using a 2 hour pulse

Quantitative RT-PCR for SW756 Wild-type, empty plasmid and OSMR KD cell lines following a 2 hour pulse of treatment with 10ng/ml OSM or PBS control. RNA was extracted 48 hours after treatment. A) Baseline levels of OSMR in PBS treated samples compared to WT control. B-F) Fold change in gene expression in PBS and OSM treated samples relative to WT+PBS control. Changes in mRNA expression of B) OSMR C) VEGFA D) TGM2 E) SNAI1 and F) EGFR were investigated. Error bars represent SEM, n=3 independent experiments for each condition. Values were analysed for statistical significance using a one way ANOVA with Tukey's multiple comparison post-hoc tests. * =.$P \leq 0.05$, ** = $P \leq 0.01$, *** = $P \leq 0.001$, **** = $P \leq 0.00001$.

Response of these 3 cell lines to OSM treatment was also investigated at the protein level (Figure 4.18). As previously shown in Figure 4.15 baseline levels of OSMR protein expression were reduced in KD-PBS-cells compared to WT-PBS-cells and EP-PBS-cells. KD-PBS-cells also displayed reduced baseline levels of pSTAT3 protein expression compared to WT-PBS-cells and EP-PBS-cells, but did not differ in their levels of Total STAT3. Treatment for 48 hours with OSM did not appear to alter OSMR protein expression in any of the three cell lines. However, WT and EP cells expressed greater levels of pSTAT3 in response to treatment with OSM for 48 hours. KD-OSM-cells did not display increased expression of pSTAT3 compared to KD-PBS-cells (Figure 4.18A).

Previous experiments by Kucia-Tran *et al* (2018)[92] have shown that ME180 cells, a non OSMR overexpressing cell line, display upregulation of OSMR and pSTAT3 protein expression in the first 8 hours following treatment with OSM. However, upregulation is not maintained at 48 hours post-treatment. Therefore, in order to confirm that OSMR was truly knocked down in the newly-generated cell line, protein was collected from WT, EP and KD cells at 30 minutes and 1 hour post treatment with OSM (Figure 4.18B).

In parallel with 48 hours of treatment, pSTAT3 protein expression was increased in WT and EP cells following 30 minutes or 1 hour of treatment with OSM (Figure 4.18B). While slight upregulation of pSTAT3 was also observed in OSMR KD cells at both 30 minutes and 1 hour timepoints in response to OSM, levels were substantially lower than that observed for WT-OSM-cells and EP-OSM-cells. Therefore, these cells are likely to have partial knock-down of OSMR expression rather than being complete knock-outs.

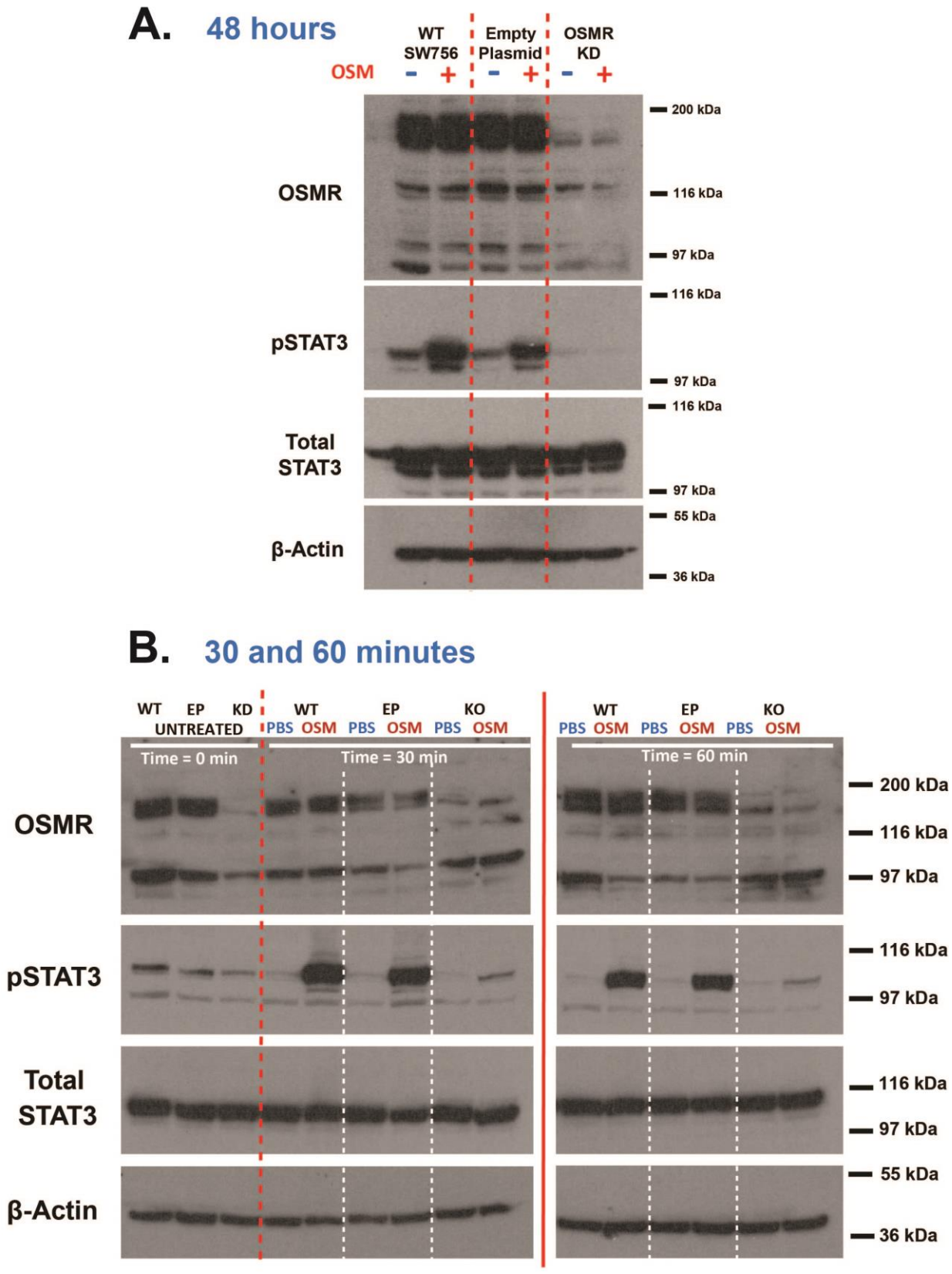

Figure 4.18: Western blot for confirmation of OSMR KD
Levels of OSMR, pSTAT3, Total STAT3 and β-ACTIN protein in wild-type, empty plasmid and OSMR KD SW756 cells treated with OSM or PBS control for A) 48 hours or B) 30 minutes or 1 hour.

The effect of OSMR KD on cell growth was subsequently investigated using both direct cell counts and MTT assay. Both methods showed that there was no difference in growth between WT-PBS-cells and EP-PBS-cells. MTT assay found cell growth of KD-PBS-cells to be significantly reduced compared to WT-PBS-cells (Figure 4.19B panel i), and a similar but non-significant trend was observed using cell counts (Figure 4.19A panel i). Both measurement methods revealed that treatment with OSM led to a significant reduction in cell number of WT-OSM-cells and EP-OSM-cells. No changes in growth were observed in KD-OSM-cells compared to KD-PBS-cells (Figure 4.19). Taken together these results indicated that knock down of OSMR results in the inability of cells to maintain prolonged response to OSM. Moreover, KD cells have reduced proliferation compared to their OSMR expressing counterparts and this finding is in agreement with similar experiments performed in mouse SCC cell lines where OSMR KD also impaired cell growth (Valtteri Tulkki, unpublished)

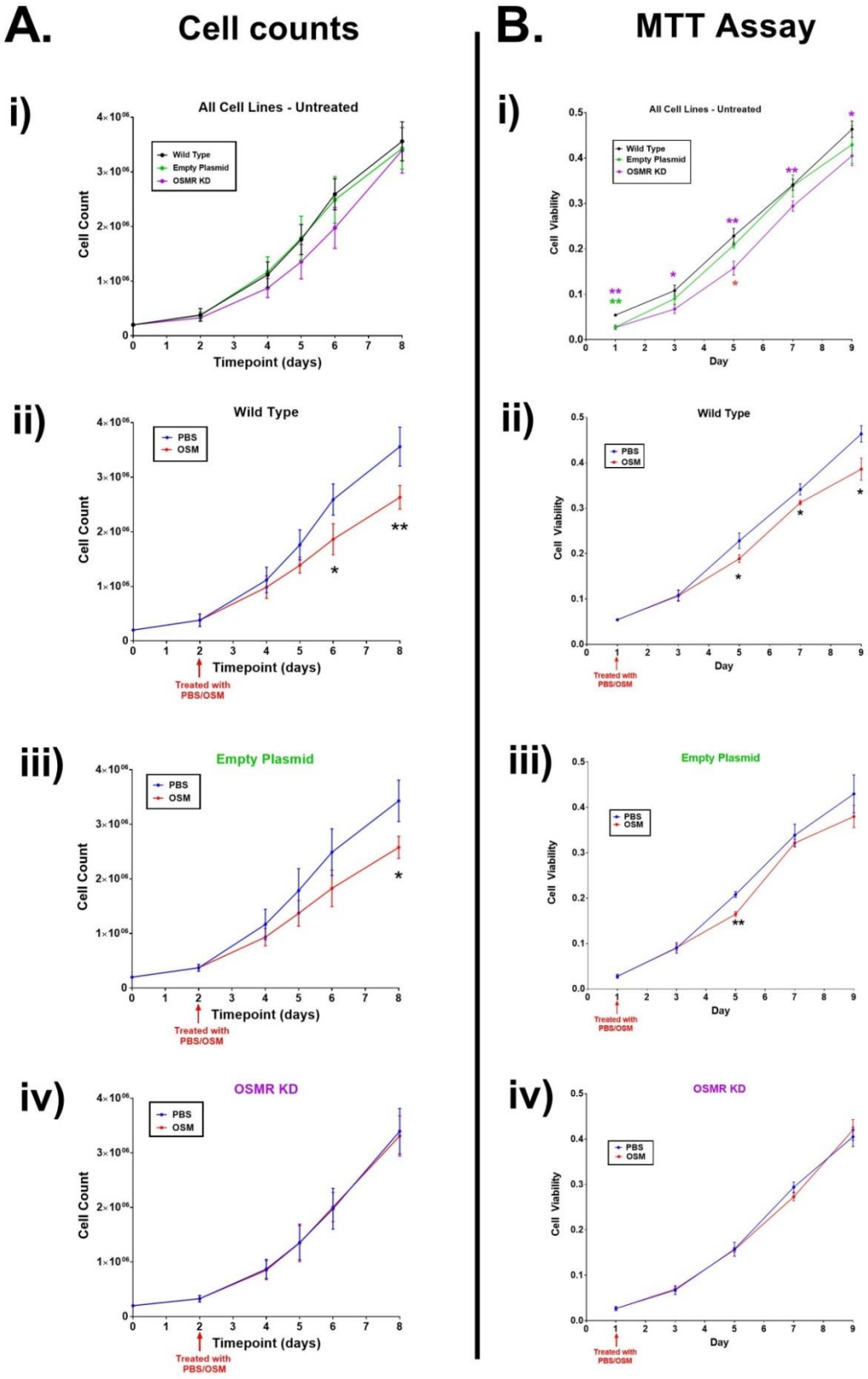

Figure 4.19: Effect of OSMR KD on cell growth

Cell growth was measured by A) automated cell counting using a countess (n=4 for each condition) or B) MTT viability assay (n=3 for each condition). i) Comparison of cell growth in WT, empty plasmid and OSMR KD cell lines. ii) Effect of OSM treatment on growth of WT SW756 cells. iii) Effect of OSM treatment on growth of empty plasmid SW756 cells. iv) Effect of OSM treatment on growth of OSMR KD SW756 cells. Values were analysed for statistical significance using i) one way ANOVA with Tukey's multiple comparison post-hoc tests or ii-iv) unpaired T-tests with Welch's correction * =.$P \leq 0.05$, ** = $P \leq 0.01$.

4.8 EV Isolation from SW756 Empty Plasmid and OSMR KD Cell Lines

The experiments detailed in this chapter have confirmed that an OSMR KD SW756 cell line was successfully generated by CRISPR-Cas9. Prior to use of this cell line for investigation of global effects of OSM-OSMR signalling on cellular and EV miRNA and mRNA expression, it was first necessary to confirm that EVs could be successfully isolated from these cells. EVs were isolated from wild type, empty plasmid and OSMR KD SW756 cell lines by ultracentrifugation and characterised based on their size, morphology and expression of EV markers.

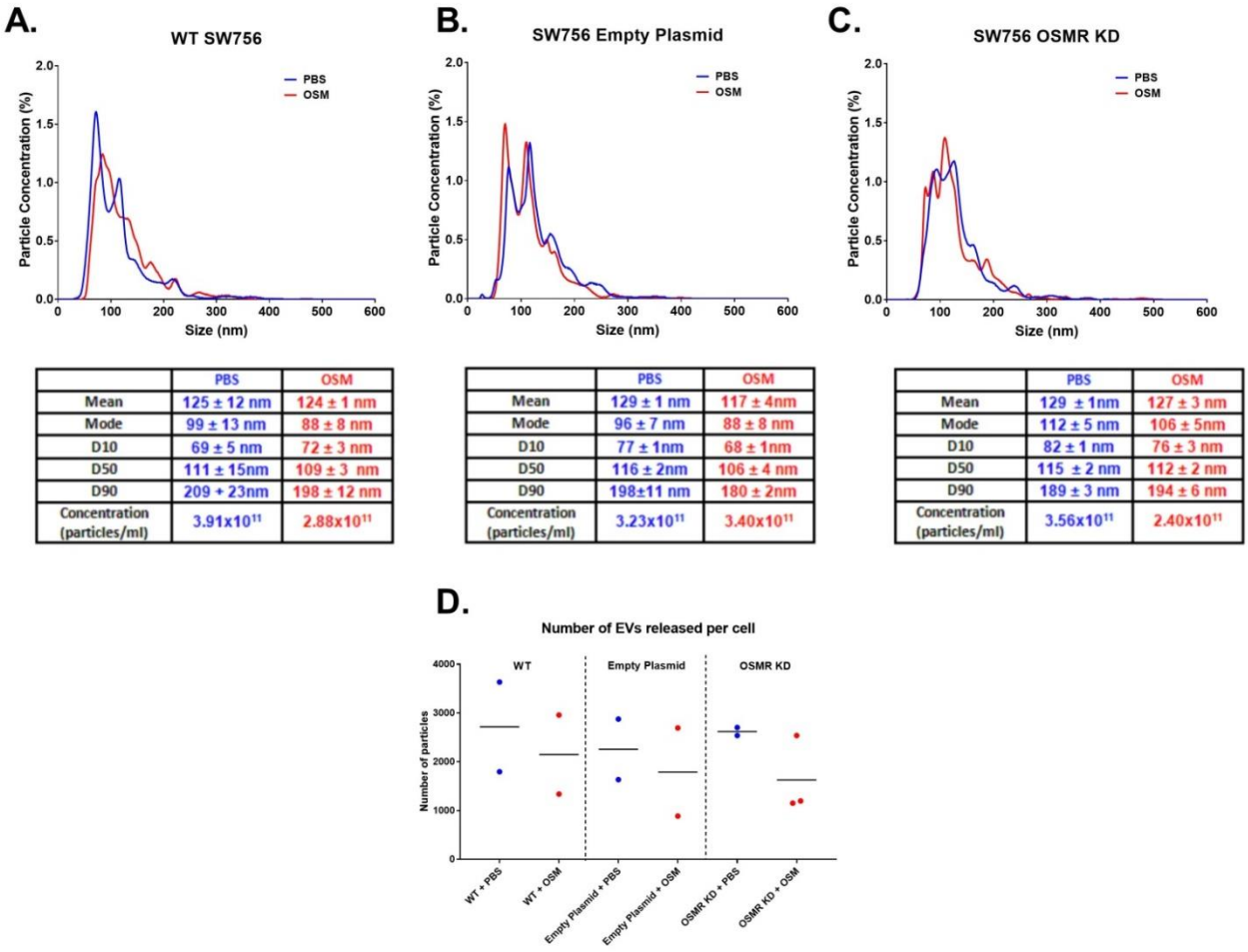

	PBS	OSM
Mean	125 ± 12 nm	124 ± 1 nm
Mode	99 ± 13 nm	88 ± 8 nm
D10	69 ± 5 nm	72 ± 3 nm
D50	111 ± 15nm	109 ± 3 nm
D90	209 + 23nm	198 ± 12 nm
Concentration (particles/ml)	$3.91x10^{11}$	$2.88x10^{11}$

	PBS	OSM
Mean	129 ± 1 nm	117 ± 4nm
Mode	96 ± 7 nm	88 ± 8 nm
D10	77 ± 1nm	68 ± 1nm
D50	116 ± 2nm	106 ± 4 nm
D90	198±11 nm	180 ± 2nm
Concentration (particles/ml)	$3.23x10^{11}$	$3.40x10^{11}$

	PBS	OSM
Mean	129 ± 1nm	127 ± 3 nm
Mode	112 ± 5 nm	106 ± 5nm
D10	82 ± 1 nm	76 ± 3 nm
D50	115 ± 2 nm	112 ± 2 nm
D90	189 ± 3 nm	194 ± 6 nm
Concentration (particles/ml)	$3.56x10^{11}$	$2.40x10^{11}$

Figure 4.20: NanoSight analysis of EVs isolated from cell lines generated by CRISPR
NanoSight analysis showing size distribution of EVs extracted from culture medium of SW756 A) WT B) emty plasmid and C) OSMR KD cell lines lines treated with 10ng/ml OSM or PBS control. (D) Number of EV particles released per cell for each condition. N=2 for each condition (except OSMR KD + OSM where n=3).

As previously described for SW756 and ME180 cell lines, NanoSight was used to determine particle size (Figure 4.20). EVs isolated from all three cell lines were found to have similar size distributions and to be composed of heterogeneous populations of multiple sized particles. EVs isolated from WT-PBS-cells, EP-PBS-cells and KD-PBS-cells had similar average particles sizes: 125nm (Figure 4.20A), 129nm (Figure 4.20B) and 129nm, respectively (Figure 4.20C). For all three cell lines the average particle size was larger than the mode, reflecting the presence of a small population of larger particles in the 200-400nm size range. Treatment with OSM did not affect the size of EVs released by any of the three cell lines. There were also no significant differences between cell lines in the number of EVs released per cell or in the number of EVs released in response to OSM treatment (Figure 4.20D). As such, OSM-OSMR signalling did not appear to alter the size or quantity of EVs released by SW756 cells.

EV morphology from each of the three cell lines was investigated by TEM. The presence of spherical structures with a cup-shape morphology stereotypical of EVs was identified in samples from WT, EP and KD cells (Figure 4.21A). As reflected by NanoSight, EV populations were heterogeneous as expected and ranged in size from approximately 50-300nm. To further confirm that the particles isolated were EVs, western blot was performed for the following proteins which are known to be enriched in EVs: ALIX, a protein involved in MVB biogenesis, CD63 and CD9, tetraspanins known to be enriched in EVs, particularly exosomes[304,305]. Samples were also probed for cytochrome C, a mitochondrial protein expected to be under-represented in EVs[306] (Figure 4.21B). ALIX, CD63 and CD9 were all found to be highly expressed by EVs isolated from all three cell lines. While enriched in EVs, these markers were also detected in the cellular extracts. Cytochrome C was found to be enriched in cell extracts compared to EVs (Figure 4.21B). Taken together this data demonstrates that OSMR does not appear to have any influence on the size, number or structure of EVs released or on the expression of stereotypical EV markers.

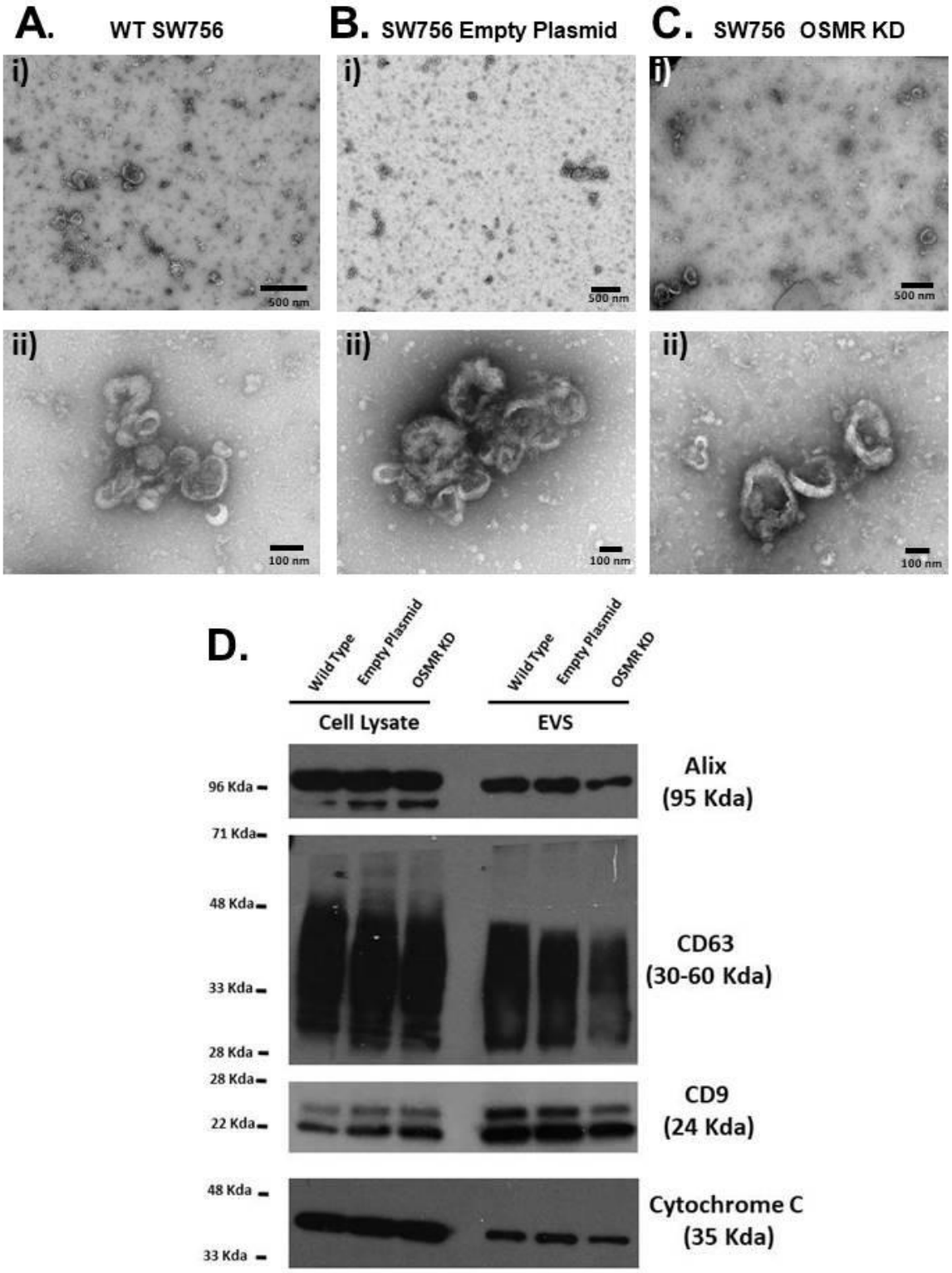

Figure 4.21: Confirmation of EV isolation - TEM and WB for EV markers

A-C) EV preparations isolated by ultracentrifugation were visualised using Transmission Electron Microscopy. Samples were fixed with 2% PFA and 1% glutaraldehyde and negatively contrasted with 1% uranyl acetate. Images depict EVs isolated from (A) WT (B) Empty Plasmid or (C) OSMR KD SW756 cells at i) low (scale bar = 500nm) or ii) high (scale bar = 100nm) magnification. (D) Western blot of protein extracted from SW756 WT, empty plasmid and OSMR KD cells and EVs. Samples were probed for markers known to be enriched in EVs: ALIX, CD63 and CD9. Probing for Cytochrome C was performed as a negative control.

4.9 Repeat CRISPR

Having confirmed that OSMR was successfully knocked down in a clonal SW756 cell line by CRIPSR, and that EVs (characterised by their size, morphology and expression of expected EV markers) could be effectively isolated by ultracentrifugation, the empty plasmid and OSMR KD SW756 cell lines detailed in this chapter (and their respective EVs) were subsequently used for next generation sequencing experiments as detailed in Chapter 5. However, the CRISPR experiments detailed above only generated a single clonal cell line with verified KD of OSMR, at the DNA, mRNA and protein levels. It is possible that clonal cell lines may contain other non-CRISPR associated mutations that influence gene expression. Therefore, the CRISPR protocol was repeated in order to generate additional OSMR KD SW756 cell lines for validation of sequencing results.

WT SW756 cells were transfected with empty plasmid or plasmid containing sgRNAs against OSMR as previously described. In these experiments a mock transfection control, in which cells were treated with lipofectamine alone, was also included. As in the previous CRISPR experiments, only cells transfected with empty vector or vector containing sgRNAs expressed EGFP (Figure S4. 7). Following single cell sorting of EGFP positive cells, six clonal cells derived from SW756 cells transfected with empty plasmid and 36 clonal cell lines derived from SW756 cells transfected with plasmid containing sgRNAs against OSMR were expanded for investigation of OSMR KD. PCR was performed for these clones as previously described using genomic DNA primers designed to amplify a small 240p fragment within the OSMR region targeted by sgRNAs (Figure S4. 8A). All clonal cell populations transfected with empty plasmid displayed a band of the expected size for WT OSMR (Figure S4. 8Ai). Out of the cells transfected with plasmid containing gRNAs targeting OSMR, 23 of the 36 clones displayed bands of a different size to that of WT control (Figure S4. 8A panels i-iii).

Similarly, sequencing primers designed to amplify a 1006bp fragment spanning both gRNA sites confirmed that all 6 clones transfected with empty plasmid produced fragments similar in size to the WT fragment, whereas 20 of the 36 clones treated with sgRNA against OSMR had bands of perturbed size (Figure S4. 8Bi-iii). PCR products for all 6 empty plasmid cells lines and all 36 OSMR KD cell lines were sent for sequencing using both forward and reverse primers. Sequencing data was analysed with SnapGene (results not shown) and Synthego ICE software as previously described. Sequences from each sample (using either forward or reverse prime) were compared with that of WT SW756 cells. The results of the Synthego analysis for all clones investigated is summarised in Table 4.4. Only clones with altered sequences detected by both Synthego ICE and Snapgene alignment methods were selected for further investigation (highlighted in yellow in Table 4.4).

Table 4.4 Summary of CRISPR2 sequencing alignments

Summary of Synthego ICE analysis of sequencing results, samples were aligned with sequences from Wild-Type SW756 cells. Red = samples with mutations detected by Synthego ICE. Yellow = samples selected for further analysis which displayed an altered sequence when using both Synthego ICE and Snapgene analysis

	Forward Sequencing Primer		Reverse Sequencing Primer	
	Indel %	KO Score	Indel %	KO Score
Empty Plasmid Clone 1	0	0	0	0
Empty Plasmid Clone 2	17	13	0	0
Empty Plasmid Clone 3	0	0	0	0
Empty Plasmid Clone 4	0	0	0	0
Empty Plasmid Clone 5	0	0	0	0
Empty Plasmid Clone 6	0	0	0	0
OSMR KD Clone 1	42	35	45	34
OSMR KD Clone 2	0	0	0	0
OSMR KD Clone 3	63	63	56	53
OSMR KD Clone 4	60	57	60	57
OSMR KD Clone 5	80	55	75	52
OSMR KD Clone 6	0	0	0	0
OSMR KD Clone 7	42	32	52	48
OSMR KD Clone 8	2	0	0	0
OSMR KD Clone 9	75	41	54	39
OSMR KD Clone 10	82	58	80	53
OSMR KD Clone 11	0	0	0	0
OSMR KD Clone 12	0	0	0	0
OSMR KD Clone 13	10	10	9	7
OSMR KD Clone 14	28	25	27	24
OSMR KD Clone 15	6	6	28	26
OSMR KD Clone 16	0	0	0	0
OSMR KD Clone 17	66	61	69	65
OSMR KD Clone 18	69	61	72	53
OSMR KD Clone 19	0	0	0	0
OSMR KD Clone 20	0	0	0	0
OSMR KD Clone 21	57	49	64	55
OSMR KD Clone 22	13	13	14	13
OSMR KD Clone 23	45	38	58	55
OSMR KD Clone 24	66	55	67	55
OSMR KD Clone 25	11	0	10	0
OSMR KD Clone 26	1	1	3	3
OSMR KD Clone 27	0	0	0	0
OSMR KD Clone 28	10	10	0	0
OSMR KD Clone 29	55	55	61	60
OSMR KD Clone 30	73	64	80	78
OSMR KD Clone 31	65	58	67	62
OSMR KD Clone 32	0	0	0	0
OSMR KD Clone 33	48	28	45	23
OSMR KD Clone 34	69	65	77	75
OSMR KD Clone 35	52	32	55	50
OSMR KD Clone 36	71	69	75	75

Knock-down of OSMR and pSTAT3 protein expression in these selected clones was subsequently investigated by western blot (Figure 4.22). OSMR KD clones 3, 30, 15, 23 and 35 appeared to have reduced baseline levels of the two proteins compared to wild-type SW56 cells and empty plasmid clones. Response to treatment with OSM was then investigated for this subset of OSMR KD clones and two empty plasmid clones (clone 1 and 4).

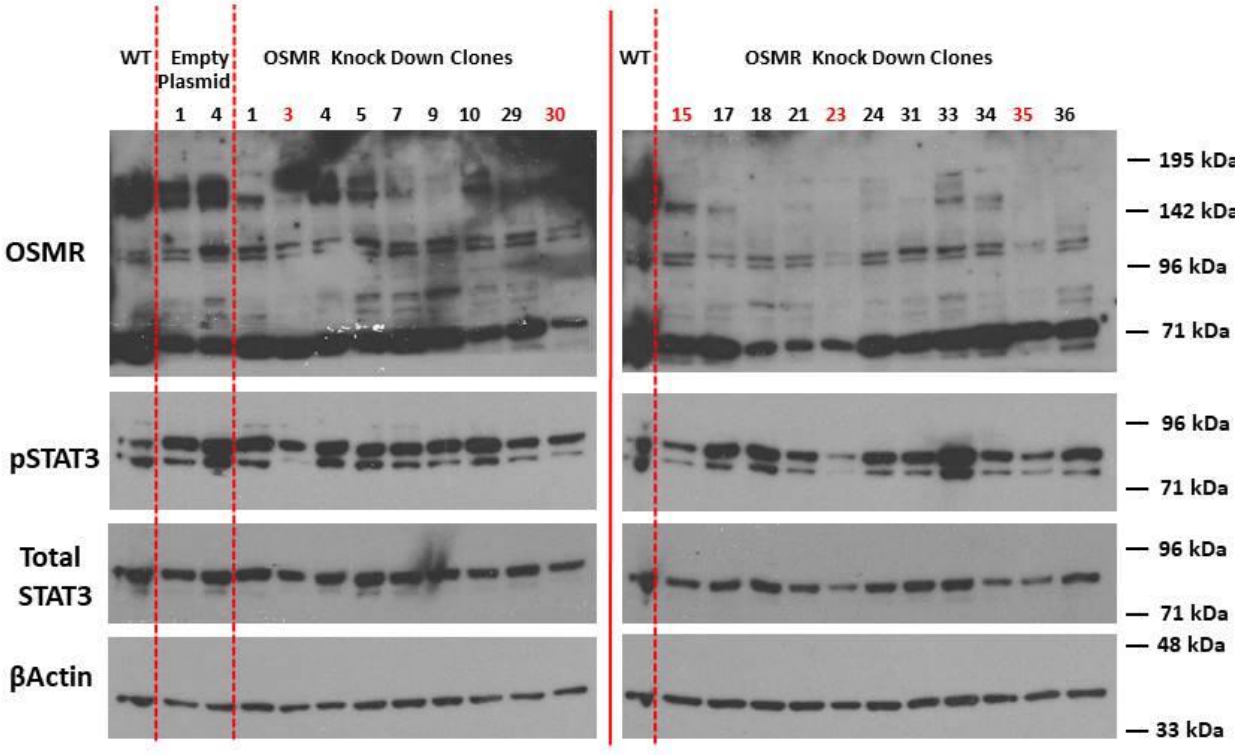

Figure 4.22: OSMR and pSTAT3 protein expression in untreated CRISPR2 clones
Western blot for OSMR, pSTAT3, Total STAT3 and β-Actin in untreated clones from repeated CRISPR experiment

Baseline levels of OSMR mRNA were unchanged in empty plasmid clones 1 and 4 compared to WT SW756 cells (Figure 4.23Ai). Baseline levels of OSMR mRNA expression were found to be significantly reduced in OSMR KD clone 3. While they appeared downregulated in the other 4 clones investigated, differences were not significant. OSMR KD had no effects on baseline levels of VEGFA (Figure 4.23Aii). As expected, treatment for 48 hours with OSM led to significant upregulation in OSMR and VEGFA mRNA expression by both newly-generated empty plasmid SW756 cell lines. Treatment with OSM did not lead to significant upregulation of OSMR expression by any of the 5 OSMR KD clones. However, upregulation of OSMR in response to OSM in clones 15 and 35 appeared greater than that observed for the other OSMR KD clones. Accordingly, clones 15 and 35 displayed significant upregulation in VEGFA levels in response to treatment with OSM (Figure 4.23A panel ii); whereas levels in clone 3, 30 and 23 remained unchanged. VEGFA was upregulated to a

lesser extent in these cell lines than in empty plasmid cell lines (CRISPR 2 OSMR KD clone 15 – 4.6 fold, clone 35 – 3.7 fold; CRISPR 2 Empty Plasmid Clone 1 = 5.7 fold, clone 4 - 9.0 fold increase).

Treatment of these cells for either 30 minutes or 48 hours with OSM led to upregulation of pSTAT3 in both newly-generated SW756 empty plasmid cell lines at both time points, similar to WT SW756 cells and empty plasmid cells generated from the first CRISPR experiment (Figure 4.23B). Baseline levels of pSTAT3 were reduced in all 5 KD cells lines compared to WT or empty plasmid SW756 controls. However, OSMR KD clones 15, 23 and 35 still appeared to be responsive to OSM-OSMR signalling and following treatment with OSM upregulation of pSTAT3 expression was detected in these cell lines at both the 30 minute and, to a lesser extent, 48 hour timepoints (Figure 4.23B). Levels of pSTAT3 in response to OSM in OSMR KD clones 3 and 30 were closer to those observed for OSMR KD cells from the first CRISPR experiment. Accordingly, OSMR KD clones 3 and 30 were selected for validation of sequencing results. They will subsequently be referred to as OSMR KD 2 (KD2) and OSMR KD 3 (KD3), respectively. SW756 empty plasmid clone 1 cells were selected as the control cell line for validation experiments as they displayed OSM-OSMR activation at similar levels to WT SW756 cells and SW756 empty plasmid cells generated from the first set of CRISPR experiments; they will subsequently be referred to as SW756 empty plasmid 2 (EP2).

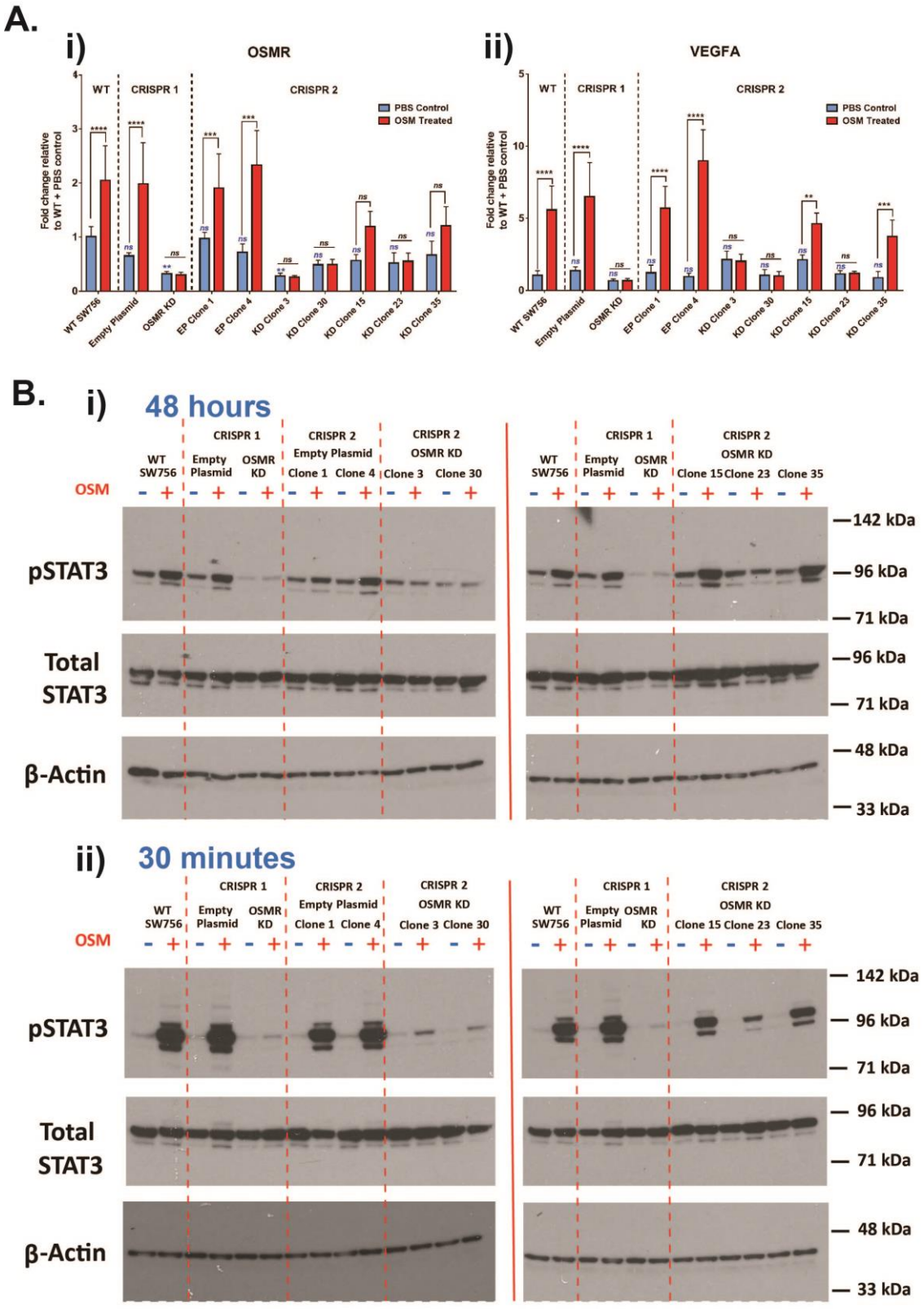

Figure 4.23: Response of CRISPR2 OSMR KD clones to OSM Treatment

A) Response of newly generated CRISPR cell lines to 48 hours treatment with OSM. qPCR for i) OSMR and ii) VEGFA mRNA expression is shown. N = 6 for each condition. Fold change in gene expression compared to WT PBS treated SW756 cells is shown. Values were analysed for statistical significance using a one way ANOVA with Tukey's multiple comparison post-hoc tests. * =.$P \leq 0.05$, ** = $P \leq 0.01$, ** = $P \leq 0.001$ and **** = $P \leq 0.0001$. B) Western blot for protein expression of OSMR, pSTAT3, total STAT3 and beta actin following i) 30 minutes or ii) 48 hours treatment with OSM.

4.10 Chapter Discussion

4.10.1 EV Isolation and characterisation

Two representative cervical SCC cell lines with differing levels of baseline OSMR expression were used to elucidate whether OSM-OSMR signalling altered miRNA expression in cervical SCC cells and their extracellular vesicles. EVs were successfully isolated from conditioned media of both SW756 and ME180 cells and were found to be morphologically similar. TEM revealed heterogeneous populations of cup-shaped spherical structures stereotypical of EVs. This cup-shaped morphology is most likely caused by EV collapse following dehydration during the TEM sample preparation process[161,307]. Moreover, EVs isolated from both SW756 and ME180 cells were found to have similar size distributions and to be composed of heterogeneous populations of multiple sized particles. Treatment with OSM did not affect size or number of EVs released per cell for either cell line. A heterogeneous population was expected as a density gradient step was not included in the isolation protocol. Thus, the population of EVs isolated most likely represents exosomes and small microvesicles. The density gradient step was excluded as recent research has highlighted that, while it aids in the removal of contaminating proteins, it is not necessarily possible to separate exosomes and microvesicles based on their size alone[308]. Moreover, typical markers historically thought to be exosome specific, such as CD9, CD63 and CD81, have been shown to be expressed by both MVs and apoptotic bodies[164,165]. Isolation of distinct EV populations based on characteristic marker expression has been further complicated by recent identification of different subpopulations of exosomes with differential marker expression to other exosome populations[167,309]. Therefore, the experiments detailed in this thesis focused on the effects of OSM-OSMR signalling on a mixed EV population rather than trying to determine effects on exosomes or microvesicles alone.

4.10.2 SW756 and ME180 cell line validation

Having shown that EVs could be successfully isolated from both SW756 and ME180 cells, the effects of OSM-OSMR signalling on cellular and EV miRNA expression were subsequently investigated. In order to validate the system, it was first investigated whether treatment of these cells with OSM produced changes in expression of the pro-tumorigenic markers VEGFA, SNAI1 and TGM2, which have previously been shown to be downstream of OSM-OSMR signalling[70,122]. Findings were in agreement with previously published data[121,122]. As expected, SW756 cells were found to have significantly higher basal expression of OSMR, VEGFA, TGM2 and SNAI1 than ME180 cells. Treatment of these cells with OSM for 12, 24, 48 or 72 hours led to upregulation of OSMR at all timepoints in both cell lines. Levels of OSMR upregulation were greater in ME180 cells compared to SW756 cells;

this is consistent with previous experiments by Winder *et al* (2011) using the same two cell lines[121]. However, it is important to note that even following treatment with OSM, OSMR levels in OSM-treated ME180 cells remained less than that of untreated SW756 cells.

Treatment with OSM led to induction of VEGFA in SW756 cells at all timepoints. Similarly, TGM2 and SNAI1 appeared upregulated in these cells at the 12, 24 and 48 hour timepoints in response to OSM. In ME180 cells VEGFA expression was also upregulated, to a lesser extent, in response to OSM, whereas levels of TGM2 and SNAI1 remained unchanged. The differences in response to OSM between these two cell lines are similar to previous observations[92] and confirm that, as expected, OSMR-overexpressing SW756 cells were more responsive to OSM treatment than non-OSMR overexpressing ME180 cells.

4.10.3 Analysis of cellular and EV miRNA levels in response to OSM

The effect of OSM-OSMR signalling on cellular and EV miRNA expression was subsequently investigated in these two cell lines; 9 miRNAs were selected from the literature for investigation. MiR-31, which is believed to act as a tumour promoter in cervical SCC, was the most abundantly expressed miRNA in cells and EVs from both cell lines. This is in accordance with previous reports that miR-31 is expressed at high levels in cervical SCC cell lines[278,279,280]. Moreover, miR-31 was found to be expressed at significantly higher levels in ME180 cells and EVs than SW756 cells and EVs, respectively. Previous work by our research group has shown that *DROSHA* copy number gain and overexpression in cervical SCC drives miR-31 overexpression. Both SW756 and ME180 cell lines were found to overexpress *DROSHA* compared to normal cervix. Moreover, ME180 cells were shown to have greater levels of miR-31 expression than SW756 cells, consistent with the results of the current study[255].

Treatment with OSM had the greatest effects on cellular and EV miRNA expression at the 48 and 72 hour timepoints. Multiple miRNAs were upregulated in both SW756-OSM-cells and ME180-OSM cells at the 48 hour time point. At the 72 hour timepoint miRNA expression was more varied. In SW756-OSM-cells; miR-9 and miR-31, which have been implicated in cervical SCC tumour progression[256,276,278–280], were significantly elevated, as was miR-126. In contrast, miR-23b, miR-34c and miR-194 were found to be significantly downregulated. A similar pattern of expression was seen in ME180-OSM-cells at this timepoint: miR-9, miR-29b and miR-126 remained significantly upregulated, whereas expression of miR-23b, miR-34c and miR-101 were significantly downregulated. OSM-OSMR signalling is known to activate STAT3 and MAP-kinase pathways and induce a pro-malignant phenotype including increased cell migration, invasion and angiogenesis[92,73]. It was therefore hypothesised that

OSM treatment would lead to upregulation of suspected tumour promoting miRNAs and downregulation of suspected tumour suppressing miRNAs in SW756 cells, but would have little effect on miRNA expression in ME180 cells. However, this was not the case as miRNAs were upregulated in both cell lines irrespective of their suspected role in tumour progression. Interestingly, miR-29b and miR-126 were upregulated in response to OSM in both cell lines at the 48 hour timepoint. Both of these miRNAs have been shown to be significantly downregulated in cervical cancer and are believed to inhibit tumour growth by suppressing STAT3 signalling[285,293]. Therefore, their upregulation in response to treatment with OSM could, potentially, be part of a negative feedback loop explaining changes in miRNA expression between the 48 and 72 hour timepoints.

Similar to cells, the effect of OSM treatment on SW756 and ME180 EV miRNA expression was most pronounced at 48 and 72 hours. All miRNAs under investigation, except for miR-194, appeared upregulated in SW756-OSM-EVs at the 48 hour timepoint; this mirrors the expression pattern observed for cells. MicroRNA levels remained elevated in SW756-OSM-EVs at the 72 hour timepoint; upregulation was greater than that observed in cells. The rise in cellular miRNA at 48 hours, followed by a decline at 72 hours could, therefore, potentially be due to packaging of miRNAs into EVs. OSM appeared to indiscriminately upregulate all 9 miRNAs in SW756 EVs at the 48 hour and 72 hour timepoints, regardless of whether they had suspected roles as tumour promoters or suppressors. OSM had a less substantial impact on ME180 EV miRNA expression; expression remained predominantly unchanged in response to OSM at all timepoints. Thus, OSM appeared to have a greater impact on altering EV miRNA expression in the SW756 OSMR-overexpressing cell line compared to ME180 EVs, a non-OSMR overexpressing cell line. Moreover, duration of treatment with OSM appeared to be important for both cellular and EV miRNA expression, with greatest changes observed following 48 and 72 hours of treatment with OSM.

4.10.4 EV Functional Assays

As OSM-OSMR signalling was found to alter EV miRNA cargo, subsequent experiments were performed in an attempt to elucidate the functional effects of these changes. Various studies have demonstrated that EVs isolated from adenocarcinoma[310], gastric cancer[311] and hepatoma[312] cell lines stimulate proliferation of corresponding recipient cancer cells. This is likely to be due to horizontal transfer of factors promoting cell growth in a positive feedback loop[311]. Seven of the nine miRNA investigated in this chapter have previously been shown to either promote (miR-9, miR-31) or inhibit (miR-10b, miR-29b, miR-101, miR-126 and miR-34c) cervical SCC proliferation (Table 4.1). As these miRNAs were found to be altered in SW756-OSM-EVs, it was investigated whether SW756-PBS-EVs and SW756-OSM-EVs had

differing functional effects on cervical SCC growth. Experiments detailed in this chapter showed that treatment of SW756 cells with OSM led to reduction in cell growth *in vitro*. However, SW756-OSM-EVs did not confer this reduction in cell growth to recipient SW756 cells. SW756-PBS-EVs also had no impact on cell growth. Previous studies that have shown positive effects of cancer derived EVs on proliferation of recipient cancer cells used much higher concentrations of EVs than the current experiment. Concentrations ranged from 10µg/ml to 400µg/ml[310–312], compared to 0.67µg/ml (1µg in a total volume of 1.5ml media) used in the current study. Therefore, if the experiment was repeated with higher doses of EVs functional effects on SW756 cell proliferation may be observed. However, it is debatable whether treatment with such high concentrations of EVs would accurately reflect physiological conditions.

Similarly, whether EVs derived from OSM treated cervical SCC cells affected migration of recipient cervical SCC cells was investigated. Six of the nine miRNAs investigated in this chapter have previously been shown to either promote (miR-9 and miR-31) or inhibit (miR-10b, miR-23b, miR-126 and miR-34c) migration of cervical SCC cells. It has previously been shown in our laboratory that treatment of SW756 cells with OSM leads to increased cell migration[121]. It was therefore investigated whether SW756-OSM-cells could confer their migratory advantage to naïve SW756 cells via their EVs. Cell lines with varying levels of OSMR expression were found to differ in their migratory capacity; untreated SW756 cells were found to migrate significantly faster than ME180 cells. However, differences in migration between these cell lines may not necessarily be a result of varying levels of OSMR expression; migration may be driven by different mechanisms in each cell line. For example, ME180 cells were demonstrated to express much higher levels of miR-205 than SW756 cells. Overexpression of this miRNA has been shown to promote growth and migration of multiple cervical SCC cell lines (including SW 756 cells)[313]. Similarly, ME180 cells have been shown to express higher levels of EGFR than SW756 cells[314]. EGF signalling through EGFR has been shown to induce EMT and promote cell migration in ME180 cells[314].

Interestingly, treatment of SW756 recipient cells with both EV-depleted SW756 conditioned media and SW756 EVs resulted in reduced cell migration. The opposite effect was observed in ME180 cells. Treatment of ME180 cells with ME180 conditioned media or ME180 EVs appeared to increase cell migration. For both cell lines, no significant differences were observed between recipient cells treated with OSM-CM and OSM-EVs compared to PBS-DM and PBS-EVs, respectively. This data indicates that SW756 and ME180 cells release differing factors, either directly into the conditioned media or packaged into their EVs, which have opposing effects on migration of other cancer cells. This effect appeared to be

independent of OSM. Suppression of SW756 migration following treatment with SW756-EVs or SW756-DM was an unexpected finding, as previous studies in multiple cancer cell types have found that cancer derived EVs transfer migratory properties to other cancer cells[315]. It is possible that as they display high baseline migratory behaviour, SW756 cells may release factors that inhibit cell migration, via a negative feedback mechanism to regulate migration of cells away from the primary tumour site. Conversely, as ME180 cells had reduced baseline migratory capacity, negative feedback may not be required, and factors released from these cells may instead promote migration of other cancer cells. It would be interesting to repeat these experiments to determine whether conditioned media and EVs from SW756 and ME180 cells have the same effect on recipient cells of the opposite cell type.

Similar experiments were also performed using SW756 donor cells and VF-2 recipient cells, normal diploid human fibroblasts. Fibroblasts are one of the many cell types found in the tumour microenvironment and play a key role in ECM remodelling[316]. Treatment with OSM promoted migration of VF2 cells. Response of these cells to OSM is unsurprising as stromal cells have been shown to ubiquitously express OSMR and demonstrate OSM-induced signal transduction[100,83]. Moreover, the role of OSM-OSMR signalling in fibroblasts has been investigated in multiple disease contexts[317,318]. Treatment of VF2 cells with SW756-EVs had little effect on VF2 migration, independent on whether EVs were isolated from PBS or OSM treated cells.

One of the main limitations of the migration experiments used in this chapter was the variability of scratch diameters; scratches were manually inflicted on monolayer cells using a 1ml pipette tip. The variability of initial scratch widths contributed to the high level of variability between replicates, thus making statistical analysis challenging. To address this, I attempted to repeat these experiments using IBIDI 2 well wound healing assay culture inserts (IBIDI GmbH, Gräfelfing, Germany). This system is comprised of a two chamber insert which is stuck to the bottom of a tissue culture plate. Cells are plated within the two chambers and, once confluent, the insert is removed leaving an even 500µm cell-free gap between the cells from each chamber. This gap is more consistent than the manual scratch used for the migration assays described above. Unfortunately, SW756, ME180 and VF2 cells would not grow in these chambers; this is most likely due to the glue used to bind the chambers to bottom of the well.

Previous experiments performed in our laboratory demonstrated that treatment of HUVEC-primary fibroblast co-cultures with SW756-OSM-CM leads to increased angiogenesis compared to co-cultures treated SW756-PBS-CM. This pro-angiogenic effect was abrogated

when co-cultures were treated with SW756-OSM-CM that had been pre-treated with an anti-OSM antibody[92]. For these experiments SW756 cells were treated with a 2 hour pulse of OSM or PBS control. Media was then replaced and conditioned media collected 48 hours later. As the conditioned media used for these experiments was not EV depleted, we subsequently investigated whether transfer of angiogenic factors was mediated by the EVs.

In the current experiment, EVs were collected from SW756 cells treated with a 2 hour pulse of PBS or OSM, similar to the previous experiment. EV isolation by ultracentrifugation has been shown to result in co-isolation of non EV proteins, predominantly those of high molecular weight and protein aggregates[319]. While the final PBS wash step aims to limit such contamination, non EV proteins may still be co-isolated during the ultracentrifugation protocol. Therefore, we hypothesised that treatment with a 2 hour pulse of OSM followed by media replacement may be optimal for use in EV experiments. This is due to the fact that it is likely to reduce confounding effects of transfer of OSM that was not taken up by treated cells to recipient cells when co-isolated with EVs.

Treatment of co-cultures with both SW756-PBS-CM and SW756-OSM-CM (48 hour continuous treatment) led to significantly increased angiogenesis in a similar manner to co-cultures treated with VEGFA. Moreover, while not statistically significant, SW756-OSM-CM appeared to induce angiogenesis at higher levels than SW756-PBS-CM. This was consistent with previous findings and is unsurprising as SW756 cells have been shown to secrete VEGFA both in the absence of OSM and at increased levels following OSM treatment. Co-cultures treated with SW756-PBS-EVs or SW756-OSM-EVs (2 hour pulse) displayed subtle increases in angiogenesis compared to control media. However, differences were not found to be statistically significant. No differences were evident between co-cultures treated with SW756-PBS-EVs or SW756-OSM-EVs. This finding indicates that soluble, EV-independent factors were responsible for the majority of the angiogenic effects observed. While VEGFA and other pro-angiogenic factors may be packaged into the EVs, they may not be present at levels high enough to have a substantial impact on angiogenesis.

Subsequent experiments demonstrated that a 2 hour pulse of OSM was not sufficient to generate upregulation of pSTAT3 targets that could be detectable 48 hours after treatment. Further issues with induction of STAT3 targets led us to test different batches of OSM ordered from R&D systems and to discover that batches varied in their potency, as determined by their ability to activate the STAT3 targets OSMR, VEGFA, TGM2 and SNAIL in SW756 cells (results not shown). For subsequent experiments each new batch of OSM was tested following purchase prior to its experimental use (results not shown). Differences

between batches of OSM may explain why the 2 hour pulse of treatment used in Kucia-Tran *et al* (2018)[92] was still sufficient to activate downstream signalling and promote angiogenesis. Thus, it is not clear whether the lack of difference between effects of EVs isolated from PBS or OSM treated SW756 cells on angiogenesis is due to the fact that OSM treatment was insufficient to activate downstream signalling in these cells or whether effects were simply not propagated in the EVs. These experiments will, therefore, be repeated in the future using EVs collected from SW756 cells treated for a continuous 48 hour period with OSM or PBS control.

While the miRNA cargo of EVs isolated from cervical SCC cells was found to be altered in response to OSM treatment, we were unable to identify the functional significance of these changes using the assays described above. This does not necessarily mean that EVs isolated from cervical SCC cells treated with OSM or PBS control do not have differential functional affects when put back on to cancer cells themselves or cells of the TME. The wrong assays may simply have been selected for investigation or suboptimal concentrations of EVs may have been used. One of the main limitations of interpretation of the functional assays discussed above was that experiments were not performed to demonstrate successful uptake of EVs by recipient cells. Therefore, it is difficult to conclude whether lack of functional effects is due to the lack of EV uptake or whether EVs simply do not transfer signals which mediate cancer cell growth, migration or angiogenesis. This could be achieved by visualisation of EV uptake using a fluorescent lipophilic dye such as PKH67 to stain vesicles or by creation of bioluminescent donor cell lines[320].

4.10.5 Generation of an OSMR KD SW756 cell line

The experiments described indicated that OSM-OSMR signalling was capable of influencing cervical SCC EV cargo. Moreover, EVs derived from cervical SCC cell lines appeared to have modest effects on cancer cell migration and angiogenesis. We subsequently aimed to adopt a global approach in order to investigate the overall effects of OSM-OSMR signalling on mRNA and miRNA expression by cervical SCC cells and their EVs. In order to achieve this, OSMR KD SW756 cell lines were successfully generated by CRISPR-Cas9. These cell lines were confirmed to have reduced levels of OSMR mRNA and protein expression compared to WT and EP SW756. OSMR KD cells were not responsive to OSM treatment; no upregulation of pSTAT3, OSMR, VEGFA, TGM2 or SNAIL was detected following 48 hours treatment with OSM. However, slight upregulation in pSTAT3 protein expression was detected in OSMR KD cells at 30 minute or 1 hour timepoints following treatment with OSM. This upregulation was substantially lower than that observed for WT and EP cells. Therefore, these cells are likely to have partial knock-down of OSMR expression rather than being

complete knock-outs. This is not surprising as SW756 cells possess multiple copies of the OSMR gene, therefore gRNAs may not have targeted all copies present. As levels of OSMR in these cells and activation of downstream targets of OSM-OSMR signalling were substantially reduced; they were deemed to have a sufficient degree of OSMR KD for use as an OSMR non-responsive cell line in subsequent sequencing and *in vivo* experiments

Diminished response of OSMR KD cells to OSM was further characterised by the finding that treatment with OSM result in reduced growth of WT and EP SW756 cells, but had no effect on growth on OSMR KD cells. This is not surprising as OSM is a well-known cytostatic cytokine in multiple cell types[87]. Reduced cell growth in response to OSM treatment was used as read out that OSM was functioning as expected in subsequent sequencing experiments.

EVs were successfully isolated from WT, EP and OSMR KD SW756 cell lines; all were found to be of similar size and morphology. Treatment with OSM did not affect size or quantity of EVs released by any of the three cell lines. Proteins which are known to be enriched in EVs - Alix, CD63 and CD9[304,305] - were all found to be highly expressed by WT, EP and KD EVs. While enriched in EVs, these markers were also detected in the cellular extracts. This is as expected because, in addition to being EV markers, tetraspanins are also localised to cell membranes and endosomes while ALIX is known to be present in the cytosol[321].

4.10.6 Summary

The experiments detailed in this chapter constitute a promising pilot study to demonstrate that OSM-OSMR signalling is capable of differentially modulating cellular and EV miRNA expression in cervical SCC cell lines with different levels of OSMR expression. However, the functional impact of these changes remains to be elucidated. In order to investigate global changes in miRNA and mRNA expression in response to OSM treatment, an OSMR KD SW756 cell line was successfully generated by CRISPR-Cas9. It was shown that EVs of expected size, morphology and marker expression could be successfully isolated from SW756 empty plasmid and OSMR KD cell lines. Consequently, SW756 empty plasmid and OSMR KD cells and their respective EVs were used for next generation sequencing experiments detailed in Chapter 5.

5. RESULTS: NGS of cells and EVs following OSM Treatment

5.1 Introduction

5.1.1 RNA cargo of extracellular vesicles

To date, multiple studies have demonstrated the presence of lipids, proteins and nucleic acids within EVs isolated from both biological fluids and cell conditioned media. The use of high throughput sequencing methods has revealed the presence of many different RNA species within EVs including: miRNA, mRNA, lncRNA, tRNA, small nuclear RNA (snRNA), piwi-interacting RNA (piRNA), small nucleolar RNA (snoRNA), small conditional RNA (scRNA), ribosomal RNA (rRNA), circular RNA (circRNA), vault RNA (vRNA), signal recognition particle RNA (SRP-RNA), long Ro-associated Y RNAs (Y RNA), long interspersed elements (LINEs) and long terminal repeats (LTRs)[170–172].

The majority of studies performed to date have focused on the small RNA fraction of EV cargo, with miRNAs being the principal RNA species selected for investigation. However, recent studies have also demonstrated the importance of mRNA cargo, and have shown that functional mRNAs can be transferred via EVs to recipient cells where they are capable of altering cell phenotype following translation by the recipient cells[169,209,322–324].

Studies that have used NGS to investigate EV cargo tend to focus on either long or small RNAs, due to the inclusion of size selection steps during library preparation[325]. This chapter aimed to investigate the effect of OSM-OSMR signalling on both miRNA and mRNA expression by cervical SCC cells and their extracellular vesicles. This was achieved by a dual sequencing approach whereby, following RNA extraction, samples were split for both mRNA and small RNA library preparation and sequencing.

5.1.2 Library preparation – mRNA sequencing

In general, the key steps required for NGS library preparation involve: fragmentation of target sequences to desired length, reverse transcription of RNA to produce double stranded DNA and attachment of oligonucleotide adaptors to fragment ends[326]. One of the major limitations of cDNA library preparation is that the majority of cDNA clones are not full length, either as a result of premature termination of reverse transcription or 5'-terminal sequence loss. This results in underrepresentation of cDNA 5' ends in cDNA libraries[327]. While several methods exist for constructing full-length cDNAs from large amounts of RNA, it is still challenging to build cDNA libraries with low input amounts of RNA[328]. To address this, mRNA libraries were prepared using a SMART-Seq® v4 Ultra® Low Input RNA kit. This kit

uses switching mechanism at 5' end of RNA template (SMART) technology. This technique exploits the unique template switching activity of the moloney murine leukaemia virus (MMLV) reverse transcriptase, allowing enrichment of full-length cDNAs and incorporation of defined PCR adaptors to both ends of cDNA during first-strand synthesis without the need of an adapter ligation step[327–329]. This ensures that the final cDNA libraries contain the 5' end of the mRNA, thereby maintaining a true representation of the original mRNA transcripts. It has been shown to produce higher quality libraries than other low RNA input library preparation kits[330]. These libraries were then pre-amplified and subsequently fragmented and tagged using the Nextera XT DNA Kit. This uses a Tn5 transposase enzyme to simultaneously fragment the DNA and add specific adaptors to both ends of the fragments; these adaptors are subsequently used to amplify the insert DNA by PCR[326].

5.1.3 Library preparation – small RNA sequencing

Prior to small RNA sequencing of OSM treated cervical SCC cells and their EVs, preliminary experiments were performed to determine the optimum small RNA library preparation kit for use. Small RNA library preparation typically involves a two-adaptor protocol, in which adaptors are ligated to both the 5' and 3' ends of the miRNA (Figure 5.1A) using RNA ligase. miRNAs are then reverse transcribed and amplified by PCR, at which point barcodes and sequencing index primers are added. Libraries are then size selected using either gel or bead based purification methods[325,326]. However, small RNA library preparation is prone to the introduction of bias. Certain adaptor-miRNA pairs are favoured during adaptor ligation and PCR amplification resulting in under or over representation of miRNA subsets in the final library; this means that sequencing results may not reflect original miRNA abundance. Moreover, adaptor dimerisation and inefficient size-selection from gels may impede miRNA enrichment[325,326,331].

In the current study two different small RNA library preparation kits were tested: NEXTFLEX® Small RNA-Seq Kit v3 and Somagenics Real-Seq®-AC miRNA Library Kit for Illumina sequencing. The Nextflex kit employs a standard two-adaptor protocol (Figure 5.1A) in which the last four nucleotides at the ligation-junction are randomised to minimise sequence-dependent ligation bias and to reduce the formation of adapter-dimer products[332,333]. To reduce adapter-dimer formation, adapters are added sequentially, with inclusion of intermediate steps to remove excess unligated 3' adapter using a magnetic-bead based method and enzymatic digestion prior to addition of the 5' adaptor. Size selection can be performed with either a gel-free protocol using Nextflex cleanup beads (recommended for RNA inputs >200ng) or a PAGE based size selection method (recommended for RNA inputs < 200ng).

In comparison, the somagenics kit utilises a single adapter protocol in which an adaptor is ligated to the 3' end of the miRNA and ligation products are circularised prior to sequencing (Figure 5.1B). A blocking oligonucleotide is added prior to circularisation that binds to the 5'-end of unligated adaptors, thereby preventing adapter dimerisation. Size selection is conducted using a bead based method. This method has been shown to reduce sequencing bias, allowing for identification of wider variety of miRNAs than other library preparation kits[331].

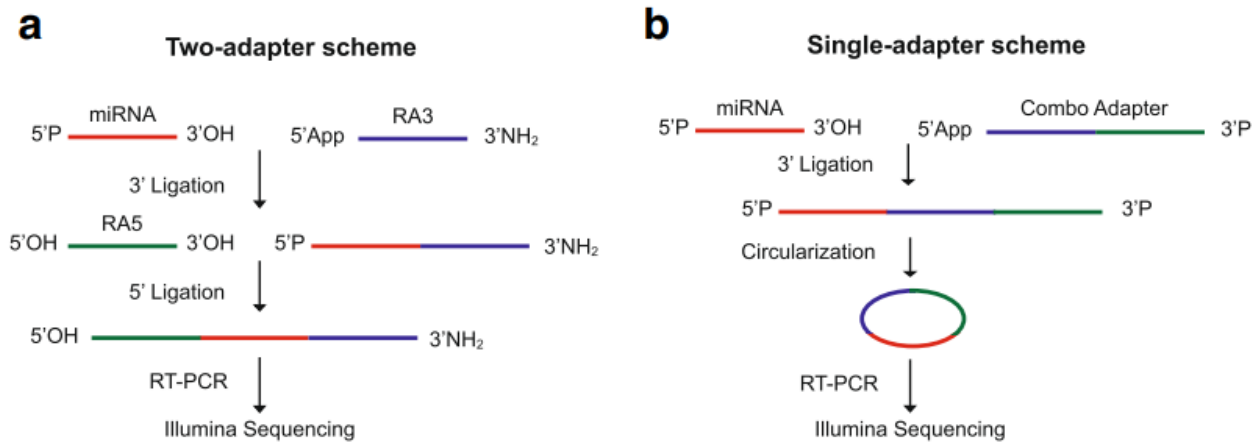

Figure 5.1: Adapter ligation for library preparation
A) Standard two adaptor ligation protocol
B) Somagenics single-adaptor ligation plus circularisation protocol
Image from Barberán-Soler *et al* (2018)[331]

5.1.4 Bioinformatic Analysis – Comparison of different statistical packages

Three different statistical analysis packages were used to investigate differential gene expression for the mRNA sequencings experiments described in this chapter: DESeq2, EdgeR and EdgeR voom. DESeq2 and EdgeR are similar analysis packages that differ in the way that data is normalised and differential gene expression is calculated. Both packages assume a null hypothesis that most genes are not differentially expressed. Normalisation of samples improves the count data and enables better comparison between samples. DESeq2 uses relative log expression to normalise samples. The ratio of read counts in each sample for each individual gene is calculated and compared to the geometric mean of the gene across all samples. The assumption is that non-differentially expressed genes should have similar read counts across samples leading to a ratio of 1. The median of ratios for all genes within a sample is then used as a correction factor which is applied to all read counts[334]. In comparison, EdgeR uses a trimmed means of M values (TMM) method to normalise counts. One lane is considered the reference sample, while all others are

considered as test samples. Highly expressed genes and genes with a high degree of variation are excluded. For each test sample, a weighted average of log ratios of the remaining genes compared to the reference sample is calculated. According to the null hypothesis of no differentially expressed genes, the TMM ratio should be close to 1. Therefore, the TMM value is used to estimate a normalisation factor which is applied to the library size. To obtain normalised read counts these normalisation factors are scaled by the mean of the normalised library sizes; raw read counts are subsequently divided by these re-scaled normalisation factors to produce normalised read counts[334]

Moreover, these programmes employ different statistical algorithms in order to calculate differential gene expression between pairs of samples using their respective normalisation strategies. Both DEseq2 and EdgeR use an exact test, related to a Fishers exact test, under negative binomial distribution strategy and Bayes theorem. In addition, DESeq2 models the observed relationship between mean and variance when estimating dispersion. EdgeR voom uses the EdgeR normalisation strategy and subsequently transforms normalised counts to logarithmic (base 2) scale. Mean-variance relationships are then estimated to determine the weight of each observation prior to linear modelling. All three strategies use the Benjamin–Hochberg approach to adjust for multiple testing, producing FDR values as opposed to p-values for each gene under investigation[335,336].

5.1.5 Chapter Aims

In this chapter, I first aimed to determine the optimum kit for use for small RNA sequencing experiments. This was achieved by comparing sequencing results for a single sample sequenced using both Nextflex and somagenics small RNA library preparation kits. Following selection of the Nextflex small RNA library preparation kit, the main aim of this chapter was to determine whether OSM-OSMR signalling affected mRNA and miRNA expression by cervical SCC cells and their EVs. To achieve this, SW756 empty plasmid cells and OSMR KD cells were treated with either PBS or OSM and RNA was subsequently collected from both cells and EVs. NGS was performed to investigate the effects of both OSM treatment and OSMR KD on mRNA and miRNA expression. Differential mRNA and miRNA expression between cell-cell and EV-EV comparisons was investigated. Changes were verified by qPCR and functional significance elucidated by pathway analysis.

5.2 Selection of RNA carrier for NGS

The miRNeasy Serum/Plasma Kit (used to extract total RNA from EV samples) recommends the use of RNA from the bacteriophage MS2 as a RNA carrier in order to improve RNA yield during RNA extraction. Biological RNA carriers should not be used for NGS as they may result in non-specific hybridisation or amplification. Nuclease-free glycogen is an alternative RNA carrier that does not interfere with NGS analysis[337]. As previous RNA extraction experiments were performed with MS2, experiments were performed to determine whether extraction using glycogen would produce similar yields of RNA.

Tapestation analysis revealed that the average RNA concentration of individual EV preparations isolated from one 175cm^2 flask of EP cells was ~19ng (Table 3.30). Six independent EV preparations were pooled, and then split again into six equal aliquots. RNA was then extracted using a miRNeasy Serum/Plasma Kit with the addition of MS2, glycogen or no carrier, using two EV aliquots per protocol. Following RNA extraction, RNA concentration was measured by nanodrop (Figure S5. 1A). Samples extracted with MS2 carrier had the highest RNA concentration reflecting the presence of the MS2 RNA in these samples.

Levels of two endogenous housekeeping miRNAs (RNU24 and miR-30b) were investigated in RNA samples extracted using the three different carrier methods. No significant differences were observed in Ct values for either of these housekeeping miRNA when comparing samples from the three extraction methods (Figure S5. 1B). Levels of miR-31 and miR-126, which were previously shown to be expressed at high and low levels in SW756 cells, respectively, were subsequently investigated. Levels of these miRNA were normalised to RNU24 (Figure S5. 1Ci) or miR-30b (Figure S5. 1Cii). While there were no significant changes in miR-31 or miR-126 expression, inclusion of MS2 or glycogen as an RNA carrier appeared to result in higher levels of both these miRNAs being detected. Therefore, glycogen was used during RNA extraction of EV sequencing samples.

5.3 Selection of small RNA library preparation kit

Initial experiments were performed in order to confirm the optimum method for small RNA library preparation. The aim was to determine which kit performed most consistently when using low input quantities of RNA. The following library preparation kits and methods were compared:

1) Somagenics Real-Seq®-AC miRNA Library Kit for Illumina sequencing (Somagenics)

2) Nextflex® Small RNA-Seq Kit v3; using PAGE gel size selection and clean up protocol (Nextflex-gel)

3) Nextflex® Small RNA-Seq Kit v3; using gel free size selection and bead clean up protocol (Nextflex-bead)

Collection of EVs by ultracentrifugation is a labour-intensive process. Therefore, cellular RNA from EP cells was used, diluted to a similar concentration as that which would be obtained from EV preparations. Quantities of RNA used for each library preparation kit are shown in Table 5.1. Samples for each condition were run in triplicate. Following library preparation, samples were run on a NextSeq500, with a 75 cycles High Output kit, at a final concentration of 1.8pM with 20% PhiX spike-in control.

Table 5.1: RNA quantities used for comparison of sequencing kits

	Quantity of RNA used	Equivalent number of pooled EV preps	Condition using this quantity of RNA
Low input	30 ng	~2	Somagenics, Nextflex-gel and Nextflex-bead
Medium input	100 ng	~5	Somagenics only
High input	250 ng	>13	Somagenics, Nextflex-gel and Nextflex-bead

5.3.1 Bioinformatic Analysis

The bioinformatics analysis detailed in this section was performed by Dr Anton Enright and Stephanie Wenlock using the pipeline shown in Table 5.2.

Table 5.2: Bioinformatics pipeline used for analysis of small RNA sequencing data

Step		Programme Used	Details
1.	**Quality Control**	custom perl script and Reaper tool[225]	1. Adapter stripping 2. Filtering of low quality basecalls 3. Removal of the Nextflex 4 nucleotide add-ons 4. Generation of Reaper plots to assess sample quality
2.	**Map Reads to Genome**	Chimira[226]	Cleaned and filtered reads were mapped against all known mature miRNA sequences in miRBase
3.	**Plot Pre-normalised Counts**	R	These display raw counts generated by Chimira. For each sample the total number of reads mapped to known miRNAs are shown
4.	**Count Normalisation**	DESeq2[223]	Normalisation of samples improves the count data and enables better comparison between samples. See section 5.1.4 for details of DESeq2 normalisation method
5.	**Sample Clustering: Generation of Heatmaps**	R	A variance stabilising transformation (VST) was applied to the data, which takes into account variance of low count data. Sample-to-sample Pearson correlations using VST transformed data were plotted by heatmap
6.	**Sample Clustering: Generation of t-SNE plots**	R	Sample clustering was visualised by generation of t-Stochastic Neighbour Embedding (t-SNE) plots[338]
7.	**Analysis of differential miRNA expression**	DESeq2[223]	Statistical analysis to compare differential expression of individual miRNAs between samples. The negative binomial Wald's test was used to determine significant differences between groups. An LFC threshold of +/-0.5 and an FDR significance threshold of 0.05 were applied.
8.	**Visualisation of Differential miRNA Expression**	R	The following plots were generated for each comparison: 1. Scatterplots (produced using median miRNA counts) 2. Volcano plots

All samples passed quality control (results not shown). Percentage of reads for each sample mapping to miRNA, rRNA, snoRNA and tRNA are shown in Figure S5. 2A. Samples prepared with the Somagenics library prep kit had substantially greater rRNA contamination than samples prepared via either of the two Nextflex protocols. Pre-normalised counts are shown in Figure S5. 2B. Somagenics samples displayed substantially lower raw counts compared to Nextflex samples, therefore raw counts for these two types of analysis were separately normalised so that the higher Nextflex counts did not result in overcorrection and

skewing of the Somagenics counts. Separately normalised and subsequently recombined counts are shown in Figure S5. 2C.

Sample clustering was visualised by heatmap (Figure S5. 3A) and t-SNE plots (Figure S5. 3B). Both these techniques demonstrated differences between samples prepared using somagenics or nextflex kits. Somagenics samples for all three RNA inputs investigated (30ng, 100ng and 250ng) were tightly clustered indicating a high degree of similarity been samples. For Nextflex, clustering appeared to be based on RNA input quantity rather than gel or gel-free bead selection protocols. All Nextflex samples (independent of protocol or input RNA quantity) were more similar to one another than to samples prepared using the Somagenics kit.

Statistical analysis was then performed in order to compare levels of individual miRNAs detected by each kit. Scatterplots (not shown) were produced using median miRNA counts to compare both input RNA quantities and different library prep kits. Correlation coefficients for each comparison are summarised in Table 5.3.

Table 5.3: Summary of correlation coefficient for each comparison

Comparison Type	Group A	Group B	Correlation Coefficient
Within Kit (comparison of input RNA quantities)	Somagenics 30ng	Somagenics 100ng	0.998
	Somagenics 30 ng	Somagenics 250ng	0.996
	Nextflex-gel 30 ng	Nextflex-gel 250 ng	0.972
	Nextflex-bead 30ng	NextFlex-bead 250ng	0.969
Nextflex Protocol (Gel vs bead selection)	Nextflex-gel 30 ng	NextFlex-bead 30ng	0.989
	Nextflex-gel 250 ng	NextFlex-bead 250ng	0.997
Between Kits (Somagenics vs Nextflex)	Somagenics 30ng	NextFlex-gel 30 ng	0.776
	Somagenics 30ng	NextFlex-bead 30ng	0.771
	Somagenics 250 ng	NextFlex-gel 250 ng	0.839
	Somagenics 250 ng	NextFlex-bead 250ng	0.834

Analysis performed for each individual kit revealed that there was little difference in levels of individual miRNAs detected when using different input RNA quantities. Similarly, for the Nextflex kit, miRNA levels for gel and bead library preparation methods showed a high degree of similarity. Greatest differences were observed when comparing samples from Nextflex (either protocol) and somagenics kits. Therefore, only 30ng RNA samples for the Somagenics and Nextflex-gel protocols were selected for further investigation. A large number of miRNA were found to be differentially expressed when the same original sample was prepared using the two different kits (Figure 5.2A).

5.3.2 Validation of results by qPCR

To determine which kit more accurately represented the true miRNA levels in the original sample, confirmatory qPCR was performed. miRNAs were selected for investigation from the scatterplot of Somagenics 30ng versus Nextflex-gel 30ng samples (Figure 5.2B). Both miRNA that were differentially expressed between kits and those with a high degree of correlation were selected for investigation. Selected miRNAs are highlighted in red in Figure 5.2B. Raw Ct values (i.e. not normalised to endogenous control) were plotted for each miRNA investigated versus sequencing results obtained using either library preparation kit. Sequencing results using the Nextflex-gel were found to correlate significantly with qPCR results (Figure 5.3A), whereas sequencing results using the Somagenics kit did not significantly correlate (Figure 5.3B). Therefore, the Nextflex kit was chosen for small RNA sequencing experiments.

As little difference was seen between gel and bead protocols, the Nextflex-bead protocol was selected for subsequent sequencing experiment as it is less labour intensive. An input of 30ng RNA was selected as this would mean that fewer EV isolations would need to be performed.

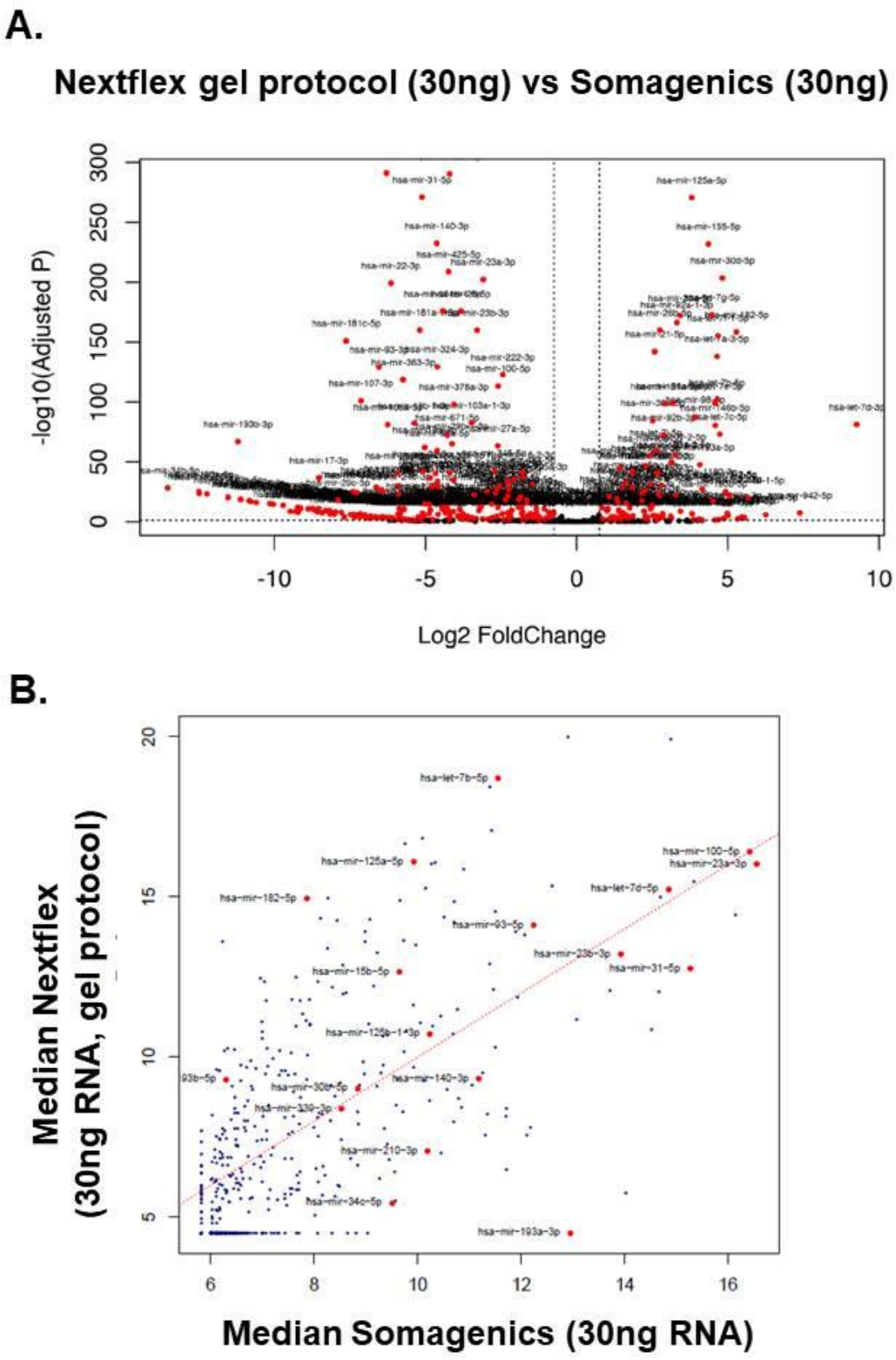

Figure 5.2: Comparison of Somagenics and Nextflex miRNA library prep kits
A) Volcano plot of differential gene expression. Log2 fold change in gene expression is plotted against –log10 adjusted p value. Positive and negative fold changes represent miRNAs expressed at higher or lower levels in nextflex samples compared to somagenics samples, respectively. miRNAs expressed at significantly ($P \leq 0.05$) different levels between the two kits are shown in red. B) Scatterplot of median miRNA counts of Somagenics vs Nextflex kits. miRNA selected for investigation by qPCR are shown in red.

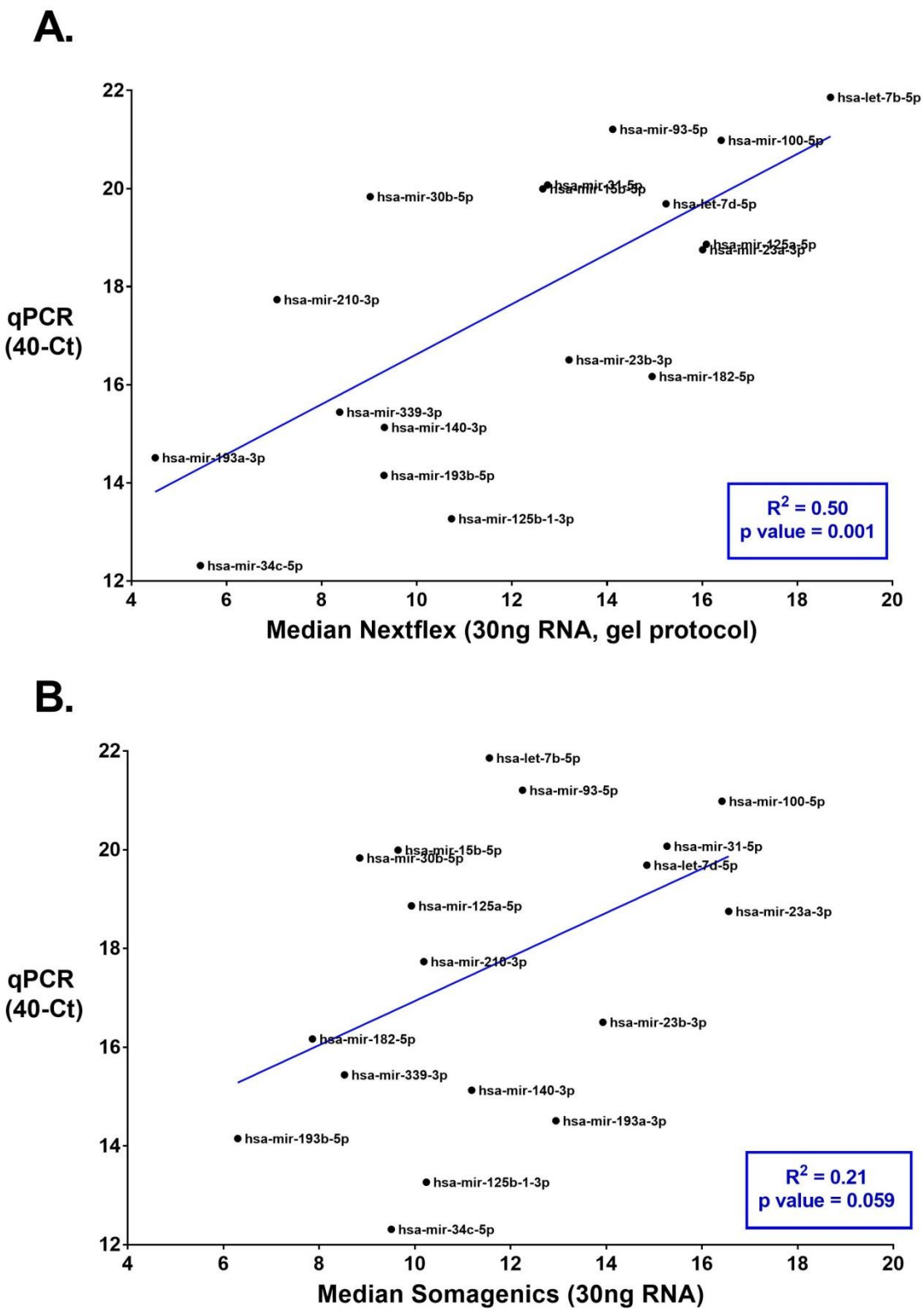

Figure 5.3: qPCR Validation of miRNA Sequencing Kits

Correlation of miRNA Ct values determined by qPCR and median miRNA counts from sequencing using either A) Nextflex kit (30ng RNA, gel protocol) or B) Somagenics kit (30ng RNA).

5.4 Sample collection and pooling of replicates

Once the best kit to use was established, samples were collected for mRNA and small RNA sequencing to determine the effects of OSM-OSMR expression on cervical SCC cells and their EVs. The experimental design for sequencing experiments is shown in Figure 5.4. EP and KD cells were treated with OSM or PBS control; EVs were subsequently isolated by ultracentrifugation.

Quantification of RNA using Tapestation had shown that the average amount of RNA obtained from an individual EV preparation isolated from one 175cm^2 flask of cells was ~19 ng (Table 3.30). In order to obtain enough material to perform both mRNA and miRNA library preparation and sequencing, five EV preparations were pooled per 'biological replicate' so that each replicate would contain ~100ng RNA. Corresponding cell samples were also pooled. Thus OSM/PBS treatment of EP and KD cells was performed 25 times and replicates for each condition pooled into groups of five, in order to produce a total of five 'biological replicates' for sequencing. Fold change in cell number in response to OSM treatment, cell passage number, cell stock (as multiple vials of cells were defrosted) and batch of OSM used were taken into consideration when deciding which five samples to pool per replicate.

Treatment of EP cells with OSM was previously shown to result in a reduction of cell number (Figure 4.19). This was therefore used as an indicator of whether activation of OSM-OSMR signalling had occurred. Consistent with this previous observation, cell number was significantly reduced in EP-OSM-cells (18.9% reduction on average) compared to EP-PBS-cells (Figure S5. 4A+B). However, the extent of this reduction was not consistent for all preparations. No significant differences in cell counts were seen in KD-PBS-cells compared to EP-PBS-cells and treatment with OSM had no significant effect on KD cell number. Fold change in cell number compared to EP-PBS-cells is summarised for each individual experiment in Figure S5. 4C. To determine whether the varied extent of growth reduction corresponded to unequal activation of the OSM-OSMR pathway, ten samples were selected for qPCR investigation. These included four 'control samples': two samples from experiments with the greatest reduction in cell number in response to OSM across all technical replicates (replicates 14 and 16); and two which displayed a reduction in cell number closest to the average (replicates 1 and 25). Six samples which appeared least responsive to OSM were then selected, i.e. experiments in which EP cell samples displayed the least reduction in cell number in response to OSM treatment.

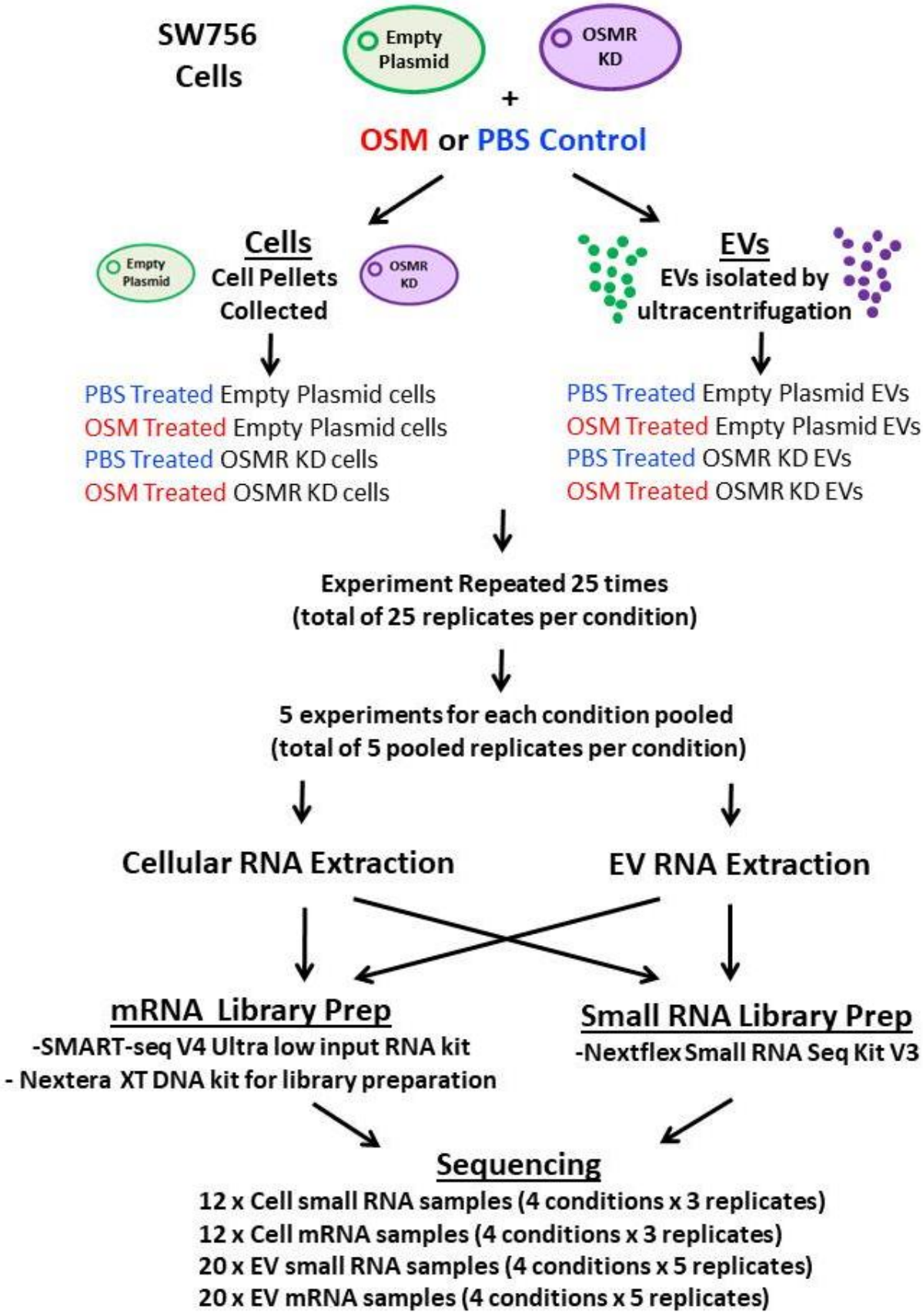

Figure 5.4: Sequencing Experimental Design

All 10 replicates selected for qPCR investigation were found to display upregulation of OSMR and VEGFA mRNA levels in response to OSM treatment, regardless of whether a reduction in cell number was observed (Figure S5. 5A). Moreover, no significant correlation was found between cell number and fold change in OSMR ($R^2 = 0.27$) or VEGFA ($R^2 = 0.19$) expression when linear regression analysis was performed (Figure S5. 5B+C).

The potential effect of cell passage number on response to OSM-OSMR signalling was also investigated in the same 10 samples. Passage was found to significantly correlate with baseline OSMR expression in both untreated SW756 empty plasmid (Figure S5. 6A panel i) and OSMR KD cells (Figure S5. 6B panel i). For both cell lines, baseline levels of OSMR expression decreased as passage number increased. However, no significant correlation was observed between baseline levels of VEGFA expression and passage number for either SW756 empty plasmid (Figure S5. 6A panel ii) or OSMR KD (Figure S5. 6B panel ii) cell lines. This data suggested that cell passage number (i.e. time in culture before treatment) may have some effect on the level of gene expression and therefore passage number was considered when grouping samples.

To keep passage numbers as similar as possible throughout the duration of the experiment, cells used for the EV extraction experiments were from three replicate frozen stocks, and any potential difference associated with this was further investigated. No difference was found in OSMR or VEGFA expression in KD-PBS-cells from any of the three stocks used (Figure S5. 6D). EP-PBS-cells from 'thaw 3' had significantly lower baseline levels of OSMR mRNA expression than cells from the other two stocks (Figure S5. 6C panel i); however, no significant changes in baseline VEGFA levels were detected (Figure S5. 6C panel ii). Therefore, cell stock may have had some impact on gene expression and was therefore taken into account when grouping samples.

Finally, as differences between the potency of OSM batches have been observed in the lab (data not shown), differences in upregulation of OSM-OSMR targets were investigated for the two different OSM batches used. WT, EP and KD SW756 cells were treated for 48 hours with PBS control or OSM from either of the two batches and expression of OSMR, VEGFA, TGM2 and SNAI1 investigated by qPCR (Figure S5. 7). No significant differences were observed in upregulation of OSMR, VEGFA or TGM2 in response to OSM treatment in any of the three cell lines when comparing the two different OSM batches (Figure S5. 7A-C). However, while differences in SNAI1 upregulation in response to treatment with different OSM batches were not observed for WT and KD cells, treatment of EP cells with OSM batch

2 led to significantly greater upregulation of SNAI1 than treatment with OSM batch 1 (Figure S5. 7D). Therefore, OSM batch was considered when grouping samples.

As a result of these investigations, all parameters described above were taken into careful consideration when deciding which 5 samples to pool per biological replicate. The replicates selected (shown in Figure 5.5) were considered to contain evenly distributed samples.

A.

Exp	Passage Number			Cell Thaw	OSM batch	Fold change in cell number (EP + OSM)
	Rank	EP	KD			
1	6	18	17	1	1	0.81
2	8	19	18	1	1	0.82
3	9	20	19	1	1	0.90
4	1	15	14	2	1	0.93
5	12	21	20	1	1	0.84
6	2	16	15	2	1	0.85
7	4	17	16	2	1	0.67
8	18	24	23	1	1	1.06
9	6	18	17	2	1	0.86
10	22	25	24	1	1	0.81
11	2	16	15	3	1	0.81
12	9	20	19	2	1	0.74
13	9	20	19	2	1	0.76
14	4	17	16	3	1	0.58
15	12	21	20	2	1	0.67
16	14	22	21	3	2	0.67
17	15	23	22	3	2	0.93
18	15	23	22	3	2	0.70
19	15	23	22	3	2	0.83
20	18	24	23	3	2	0.84
21	18	24	23	3	2	0.94
22	18	24	23	3	2	0.77
23	22	25	24	3	2	0.92
24	22	25	24	3	2	0.75
25	22	25	24	3	2	0.81

B.

Group 1						
Exp	Passage Number			Cell Thaw	OSM Batch	Fold change in cell no.
	Rank	EP	KD			
14	4	17	16	3	1	0.58
12	9	20	19	2	1	0.74
3	9	20	19	1	1	0.90
20	18	24	23	3	2	0.84
23	22	25	24	3	2	0.92
MEAN	12.4	21.2	20.2	2.4	1.4	0.80

Group 2						
Exp	Passage Number			Cell Thaw	OSM Batch	Fold change in cell no.
	Rank	EP	KD			
4	1	15	14	2	1	0.93
13	9	20	19	2	1	0.76
16	14	22	21	3	2	0.67
17	15	23	22	3	2	0.93
10	22	25	24	1	1	0.81
MEAN	12.2	21.0	20.0	2.2	1.4	0.82

Group 3						
Exp	Passage Number			Cell Thaw	OSM Batch	Fold change in cell no.
	Rank	EP	KD			
6	2	16	15	2	1	0.85
2	8	19	18	1	1	0.82
15	12	21	20	2	1	0.67
21	18	24	23	3	2	0.94
24	22	25	24	3	2	0.75
MEAN	12.4	21.0	20.0	2.2	1.4	0.80

Group 4						
Exp	Passage Number			Cell Thaw	OSM Batch	Fold change in cell no.
	Rank	EP	KD			
11	2	16	15	3	1	0.81
9	6	18	17	2	1	0.86
5	12	21	20	1	1	0.84
22	18	24	23	3	2	0.77
25	22	25	24	3	2	0.81
MEAN	12.0	20.8	19.8	2.4	1.4	0.82

Group 5						
Exp	Passage Number			Cell Thaw	OSM Batch	Fold change in cell no.
	Rank	EP	KD			
7	4	17	16	2	1	0.67
1	6	18	17	1	1	0.81
19	15	23	22	3	2	0.83
18	15	23	22	3	2	0.70
8	18	24	23	1	1	1.06
MEAN	11.6	21.0	20.0	2.0	1.4	0.82

Figure 5.5: Sample Pooling for NGS

A) Passage number, cell thaw, batch of OSM and fold change in empty plasmid cell number in response to OSM for each of the 25 EV/cell replicate preparations. Passage numbers were ranked from lowest to highest. B) Samples were sorted into groups of 5 replicates, each group contained samples to produce similar average cell passage and fold change in cell number values. Samples from cell thaws 1-3 and OSM batches 1 and 2 were evenly distributed across the five groups so that each group contained samples from each condition.

5.5 mRNA Sequencing

mRNA cDNA libraries were prepared using a SMART-Seq® v4 Ultra® Low Input RNA kit and a Nextera® XT DNA kit for library preparation using 5ng input RNA. Samples were run on a NextSeq 500, using a 75 cycles High Output kit, at a final concentration of 1.8pM with 10% PhiX.

5.5.1 Bioinformatic Analysis

The bioinformatics analysis detailed in this section was performed by Dr Anton Enright, Stephanie Wenlock and Dr Stephen Smith using the pipeline shown in Table 5.4.

Table 5.4:Bioinformatics pipeline used for analysis of mRNA sequencing data

Step		Programme Used	Details
1.	**Quality Control**	FastQC v0.11.4	
2.	**Trim Reads**	TrimGalore v0.4.1	
3.	**Map Reads to Genome**	STAR v2.5.2a	Reads were mapped to Ensembl Homo_sapiens.GRCh38 (release 92) reference genome
4.	**Calculate number of reads mapping to genomic features**	HTSeq v0.6.0[222]	
5.	**Plot Pre-normalised Counts**	R	These display raw counts generated by HTSeq. For each sample the total number of reads mapped to known protein coding genes
6.	**Count Normalisation**	DESeq2[223] or EdgeR normalisation procedure[224]	Normalisation of samples improves the count data and enables better comparison between samples. See section 5.1.4 for details of normalisation methods
7.	**Sample Clustering: Generation of Heatmaps**	R	A VST was applied to the data, which takes into account variance of low count data. Sample-to-sample Pearson correlations using VST transformed data were plotted by heatmap
8.	**Sample Clustering: Generation of t-SNE plots**	R	Sample clustering was visualised by generation of t-SNE plots[338]
9.	**Analysis of Differential gene expression**	DESeq2[223], EdgeR[224] or EdgeR voom	Statistical analysis to compare differential expression of individual genes between samples. The negative binomial Wald's test was used to determine significant differences between groups. A LFC threshold of +/-0.5 and a FDR significance threshold of ≤0.05 were applied.

10.	**Visualisation of Differential Gene Expression for each statistical package**	R	The following plots were generated for each comparison, using each of the three statistical packages (DESeq2, EdgeR and EdgeR voom): 1. Scatterplots (produced using median mRNA counts) 2. Volcano plots
11.	**Comparison of statistical packages**	UpSet R package[339]	UpSet plots were generated for each comparison to visualise intersecting genes that were significantly up or down regulated by all three statistical packages (DESeq2, EdgeR and EdgeR voom). UpSet plots also visualise numbers of genes that were only found to be significantly up or down regulated by one or two of the packages, but not shared by all three packages. A LFC threshold of +/-0.5 and a FDR significance threshold of ≤0.01 were applied.

Following mRNA sequencing, all samples passed quality control (data not shown). As expected, protein coding genes represented the main type of RNA in all samples. EV samples were found to map to a lower proportion of protein coding genes than cell samples. Pre-normalised counts are shown in Figure S5. 8A. Either a DESeq2 normalisation procedure[223] (Figure S5. 8B) or EdgeR normalisation procedure[224] (Figure S5. 8C) was applied to raw counts. Sample clustering was subsequently visualised by heatmap and t-SNE plots (Figure S5. 9C+D). Both these techniques demonstrated similarities between the two normalisation methods. Cells and EVs from all treatment groups appeared to cluster separately, indicating differences between cellular and EV cargo. Moreover, KD and EP samples were found to cluster separately.

Statistical analysis was performed in order to investigate differential gene expression between samples. This was executed using three different analysis packages – DESeq2, EdgeR and EdgeR Voom. Differential gene expression was investigated using all three analysis methods for the following cell-cell and EV-EV comparisons shown in Table 5.5. Key comparisons are shown in red.

Table 5.5: Comparisons for analysis of differential expression
(Key comparisons shown in red)

	Cell-Cell comparisons	EV-EV comparisons
1.	**EP-PBS-cells versus EP-OSM-cells**	**EP-PBS-EVs versus EP-OSM-EVs**
2.	KD-PBS-cells versus KD-OSM-cells	KD-PBS-EVs versus KD-OSM-EVs
3.	EP-PBS-cells versus KD-PBS-cells	EP-PBS-EVs versus KD-PBS-EVs
4.	EP-PBS-cells versus KD-OSM-cells	EP-PBS-EVs versus KD-OSM-EVs
5.	EP-OSM-cells versus KD-PBS-cells	EP-OSM-EVs versus KD-PBS-EVs
6.	**EP-OSM-cells versus KD-OSM-cells**	**EP-OSM-EVs versus KD-OSM-EVs**

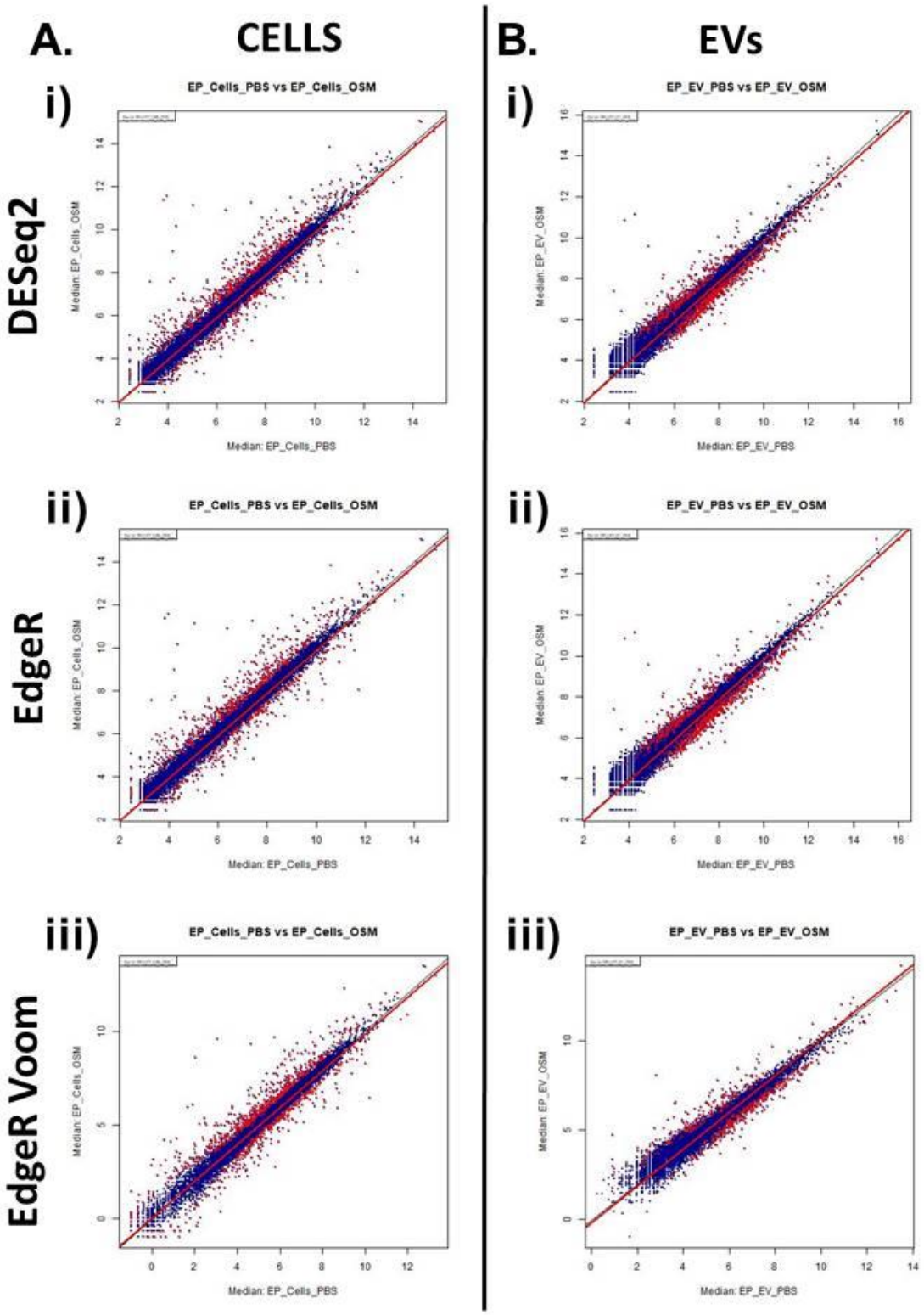

Figure 5.6: Correlation Plot - Empty Plasmid+ PBS vs Empty Plasmid+OSM
Correlation plots of differential gene expression for SW756 empty plasmid + PBS versus SW756 empty plasmid + OSM A) cells or B) EVs. Analysed using i) DESeq2 ii) EdgeR or iii) EdgeR voom. Genes with significant differential expression (≥+/-0.5 LFC; FDR ≤0.05) are shown in red. All other genes are shown in blue.

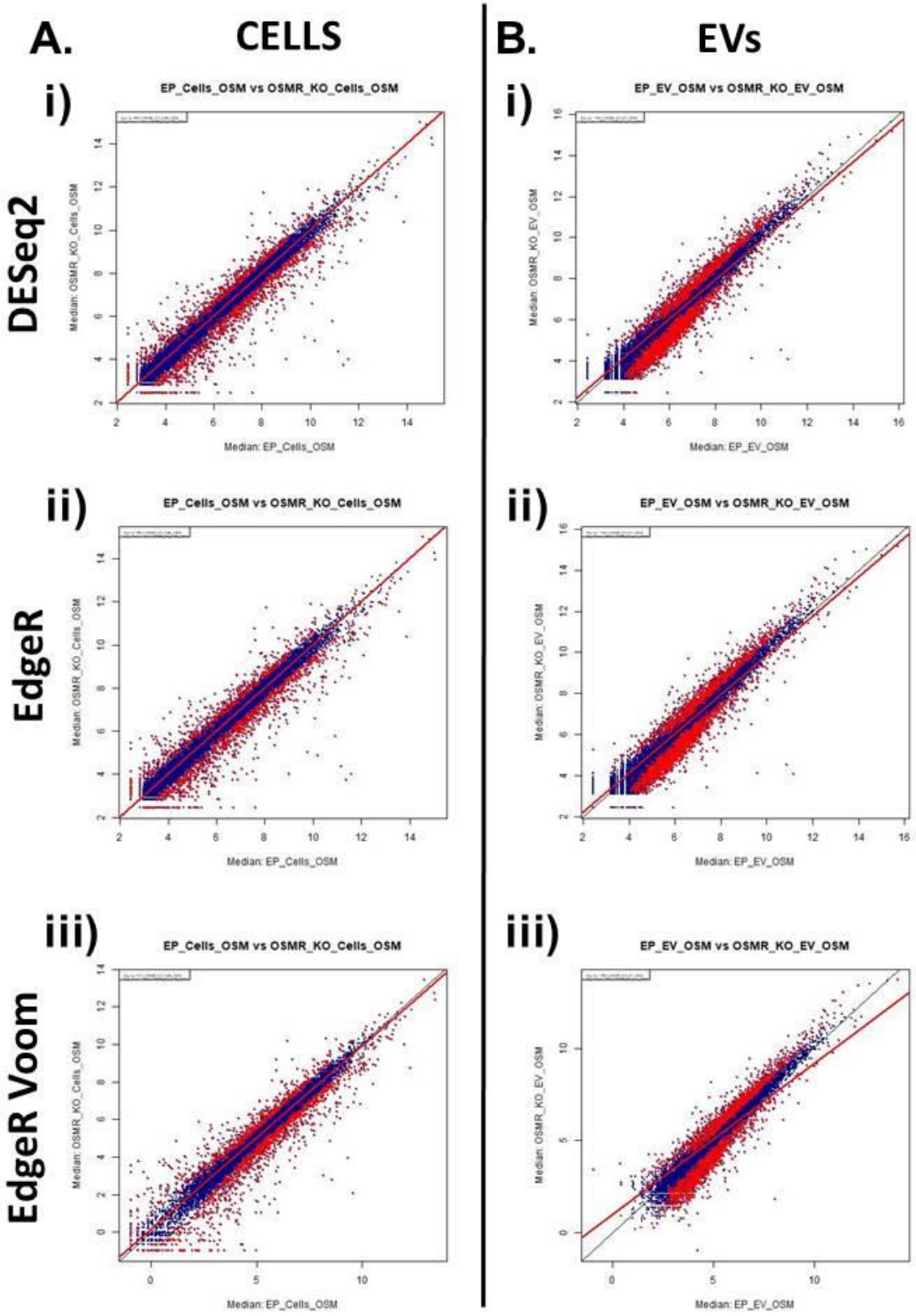

Figure 5.7: Correlation Plot - Empty Plasmid+ OSM vs OSMR KD+OSM
Correlation plots of differential gene expression for SW756 empty plasmid + OSM versus SW756 OSMR KD + OSM A) cells or B) EVs. Analysed using i) DESeq2 ii) EdgeR or iii) EdgeR voom. Genes with significant differential expression (≥+/-0.5 LFC; FDR ≤0.05) are shown in red. All other genes are shown in blue.

Scatterplots were produced to compare median counts for all six comparisons for both cells and EVs. EP-PBS versus EP-OSM (Figure 5.6) and EP-OSM versus KD-OSM (Figure 5.7) were the two key comparisons to demonstrate differences in OSM-OSMR signalling in both cells and EVs. All other comparisons performed are shown in supplementary figures. Cells: DESeq2 - Figure S5. 10, Cells: EdgeR - Figure S5. 11. Cells: EdgeR Voom - Figure S5. 12, EVs: DESeq2 - Figure S5. 13, EVs: EdgeR - Figure S5. 14 and EVs: EdgeR Voom - Figure S5. 15.

Differences in gene expression for each set of comparisons, using each of the three analysis methods, were also visualised using volcano plots. Volcano plots for the two main comparisons are shown in Figure 5.8 and Figure 5.9. All other comparisons performed are shown in supplementary figures. Cells: DESeq2 -Figure S5. 16, Cells: EdgeR - Figure S5. 17, Cells: EdgeR Voom -Figure S5. 18, EVs: DESeq2 -Figure S5. 19, EVs: EdgeR - Figure S5. 20 and EVs: EdgeR Voom - Figure S5. 21.

As expected, treatment of EP cells with OSM led to significant changes in gene expression compared to cells treated with PBS control. Similar changes in gene expression were observed in the EVs (Figure 5.6 and Figure 5.8). Treatment of KD cells with OSM did not lead to significant changes in gene expression in cells or EVs (Figure S5. 10-Figure S5. 21B). This is consistent with previous findings from our research group that that OSM predominantly signals via OSMR and not LIFR in SW756 cervical SCC cells[92]. EP cells and their EVs displayed significantly different expression profiles compared to KD cells and EVs, respectively. As expected, since the OSMR KD cell line is not responsive to OSM treatment, these differences were greatest when both cell lines were treated with OSM (Figure 5.7, Figure 5.9). Together, these results confirm previous findings that OSM-OSMR signalling alters mRNA expression of cervical SCC cells and demonstrate, for the first time, that OSM-OSMR signalling is capable of altering cervical SCC cell EV cargo.

Broadly similar results were observed when differential gene expression was investigated using any of the three different statistical packages (DESeq2, EdgeR or EdgeR voom). However, some differences were seen. For instance, correlation plots and volcano plots generated by DESeq2 and EdgeR analysis seemed similar in terms of the number of significantly altered genes, whereas EdgeR voom identified more genes as being differentially expressed. A more thorough comparison of the different statistical packages was therefore undertaken.

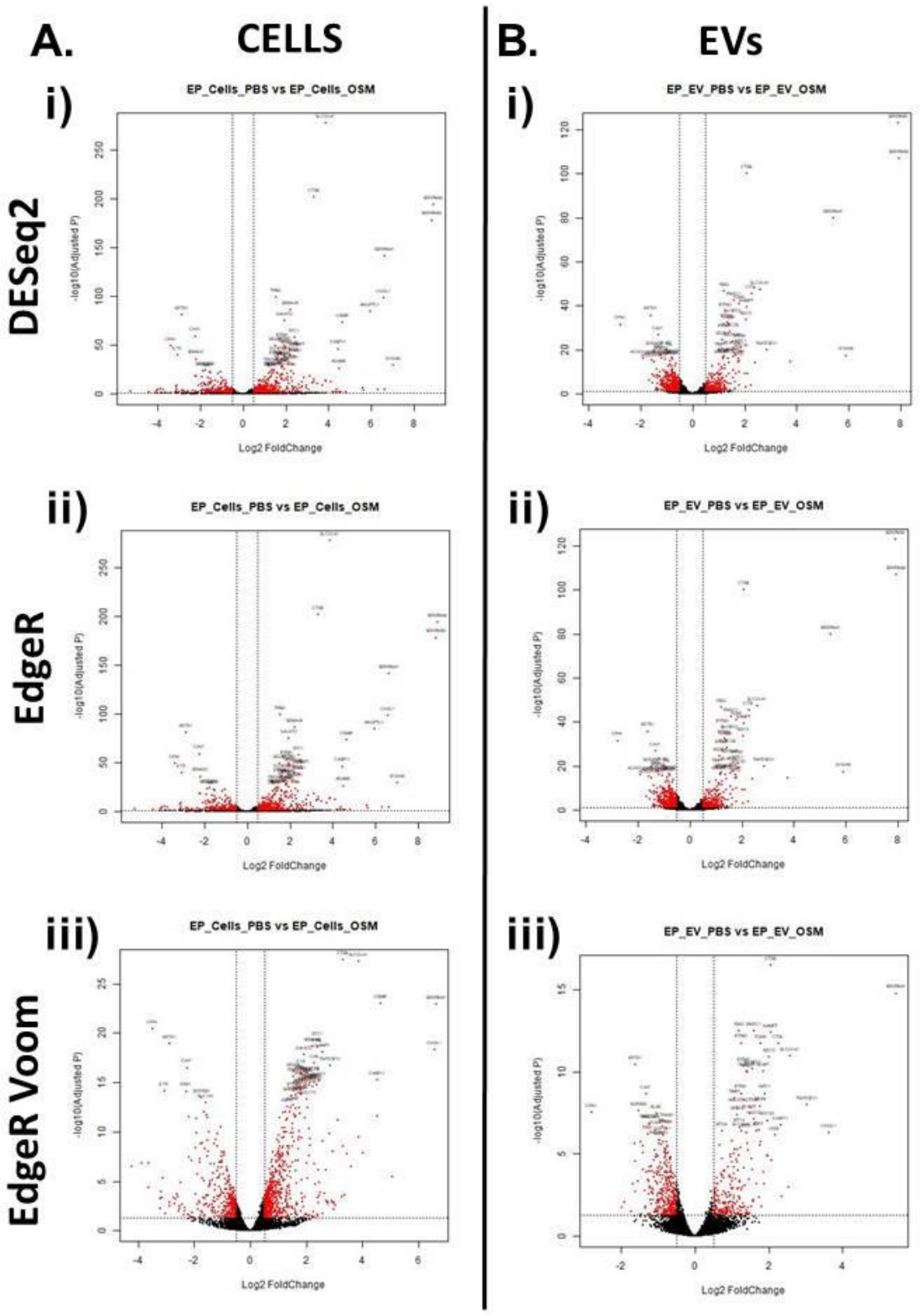

Figure 5.8: Volcano Plot - Empty Plasmid+ PBS vs Empty Plasmid+OSM
Volcano plots of differential gene expression for SW756 empty plasmid + PBS versus SW756 empty plasmid + OSM A) cells or B) EVs. Analysed using i) DESeq2 ii) EdgeR or iii) EdgeR voom. Genes with significant differential expression (≥+/-0.5 LFC; FDR ≤0.05) are shown in red. All other genes are shown in black. Top 50 most significantly changed mRNA are labelled.

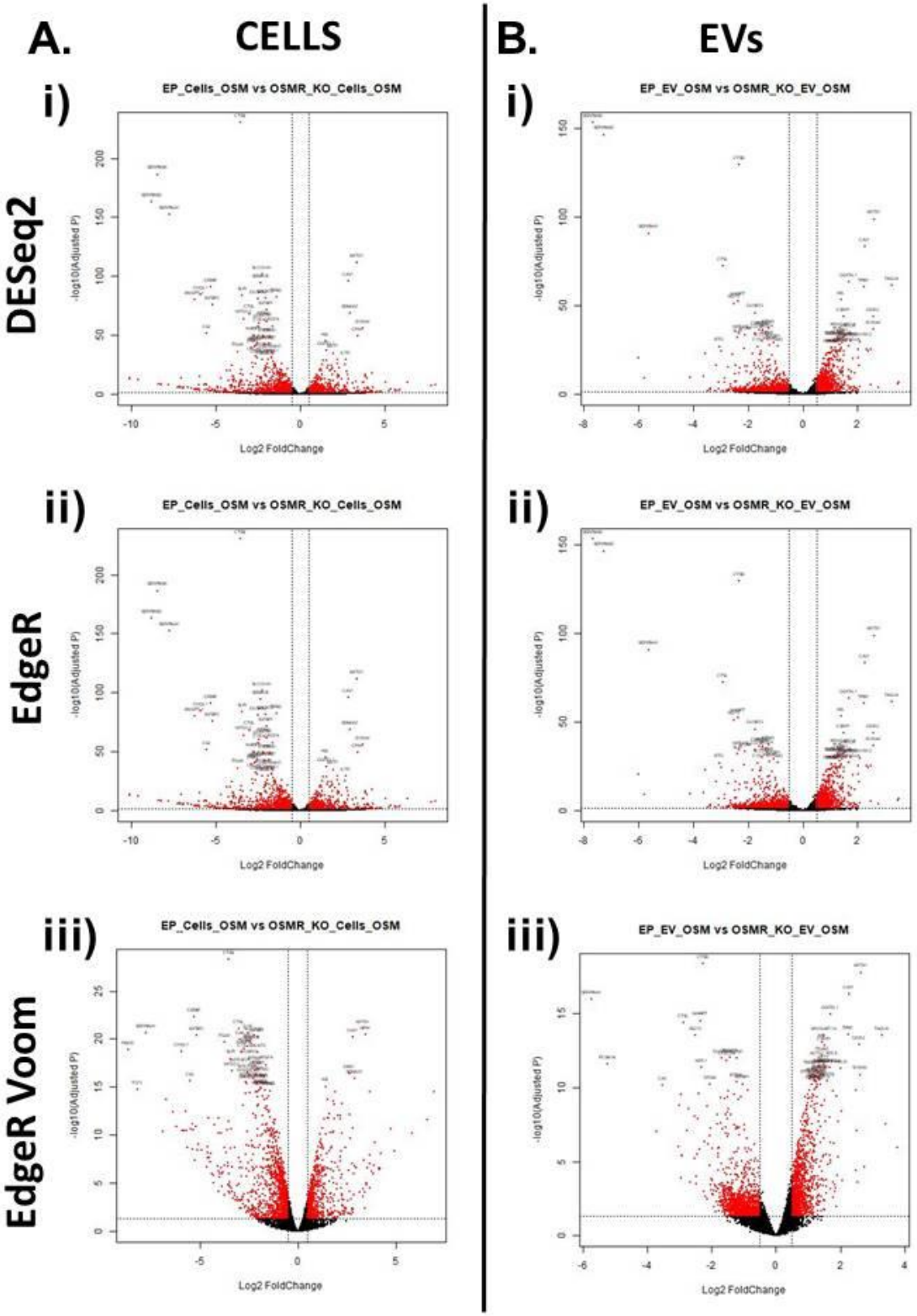

Figure 5.9: Volcano plot - Empty Plasmid+ OSM vs OSMR KD+OSM

Volcano plots of differential gene expression for SW756 empty plasmid + OSM versus SW756 OSMR KD + OSM A) cells or B) EVs. Analysed using i) DESeq2 ii) EdgeR or iii) EdgeR voom. Genes with significant differential expression (≥+/-0.5 LFC; FDR ≤0.05) are shown in red. All other genes are shown in black. Top 50 most significantly changed mRNA are labelled.

5.5.2 Comparison of DESeq2, EdgeR and EdgeR Voom results

UpSet plots were generated by Dr Stephen Smith in order to compare commonly up and downregulated genes for each comparison produced by DESeq2, EdgeR and EdgeR voom. For this analysis a LFC threshold of +/-0.5 and a FDR significance threshold of ≤0.01 were applied. This is more stringent than the FDR ≤0.05 significance threshold used for generation of the correlation and volcano plots; this was done to restrict the size of gene lists produced for subsequent pathway analysis to the most significant only. Table 5.6 details the information displayed on each UpSet plot for each comparison.

Table 5.6: Explanation of data displayed on UpSet plots for each comparison
DE= Differentially expressed (LFC of +/-0.5 and a FDR significance threshold of ≤0.01)

Category	Column (left to right)	Details
DE by all three packages	1	**number of genes upregulated in all three statistical packages, shown in red**
	2	**number of genes downregulated in all three statistical packages, shown in blue**
DE by two packages only	3	number of genes upregulated in EdgeR voom and EdgeR, only
	4	number of genes upregulated in EdgeR voom and DESeq2, only
	5	number of genes upregulated in EdgeR and DESeq2, only
	6	number of genes downregulated in EdgeR voom and EdgeR, only
	7	number of genes downregulated in EdgeR voom and DESeq2, only
	8	number of genes downregulated in EdgeR and DESeq2, only
DE by one package only	9	number of genes upregulated in EdgeR voom, only
	10	number of genes upregulated in EdgeR, only
	11	number of genes upregulated in DESeq2, only
	12	number of genes downregulated in EdgeR voom, only
	13	number of genes downregulated in EdgeR, only
	14	number of genes downregulated in DESeq2, only

Figure 5.10 and Figure 5.11 show UpSet plots for cell-cell and EV-EV comparisons, respectively. For all comparisons, the sample listed on the left is considered the control sample and the one on the right the comparator sample. The KD-PBS versus KD-OSM comparison was excluded from both cell and EV analysis as no genes were found to have significantly altered expression in response to OSM treatment in this cell line.

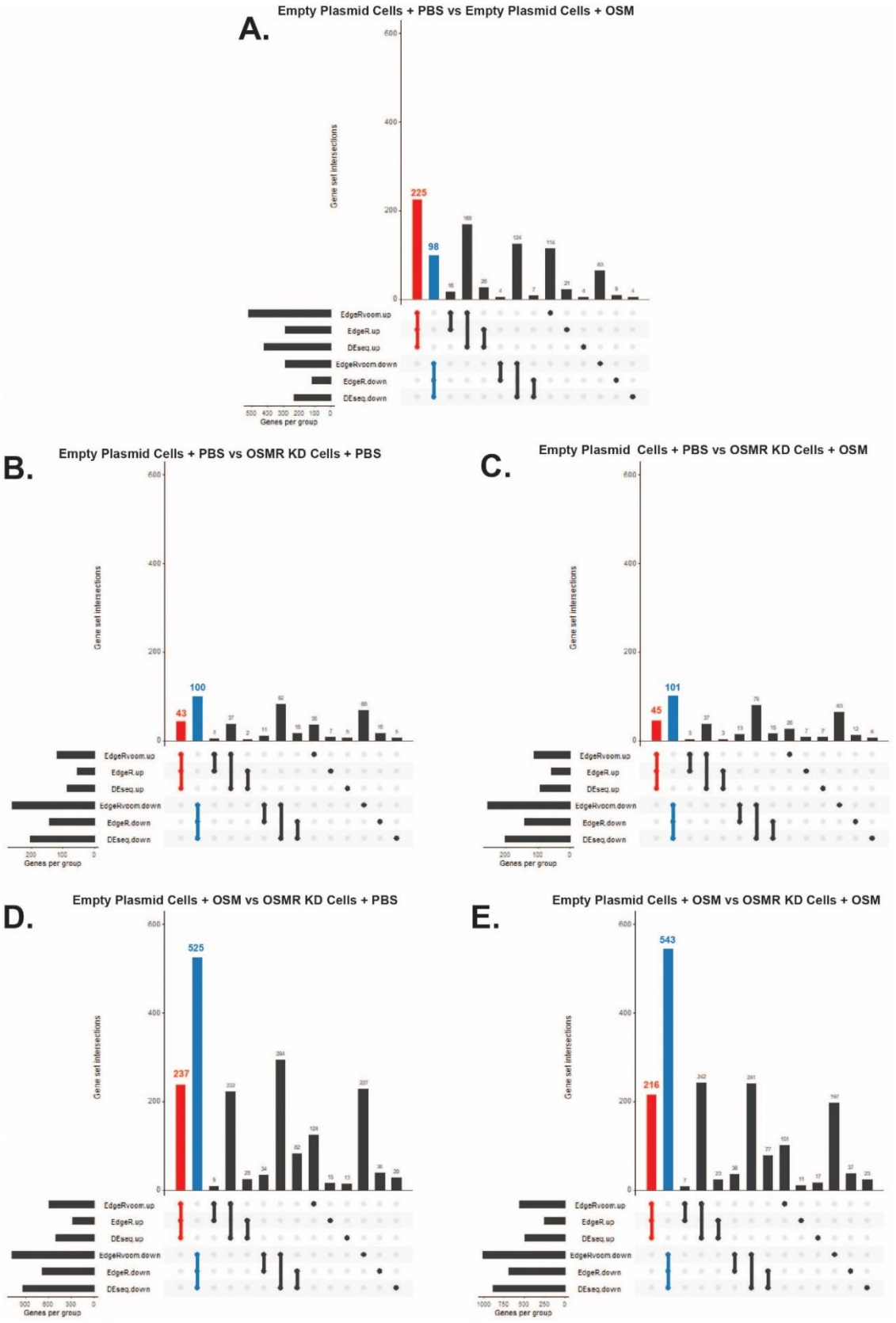

Figure 5.10: Cell-Cell comparisons – common up and down-regulated genes
Comparison of genes with significant (FDR = ≤0.01) up or down regulation across analysis methods (DESeq2, EdgeR and EdgeR voom)

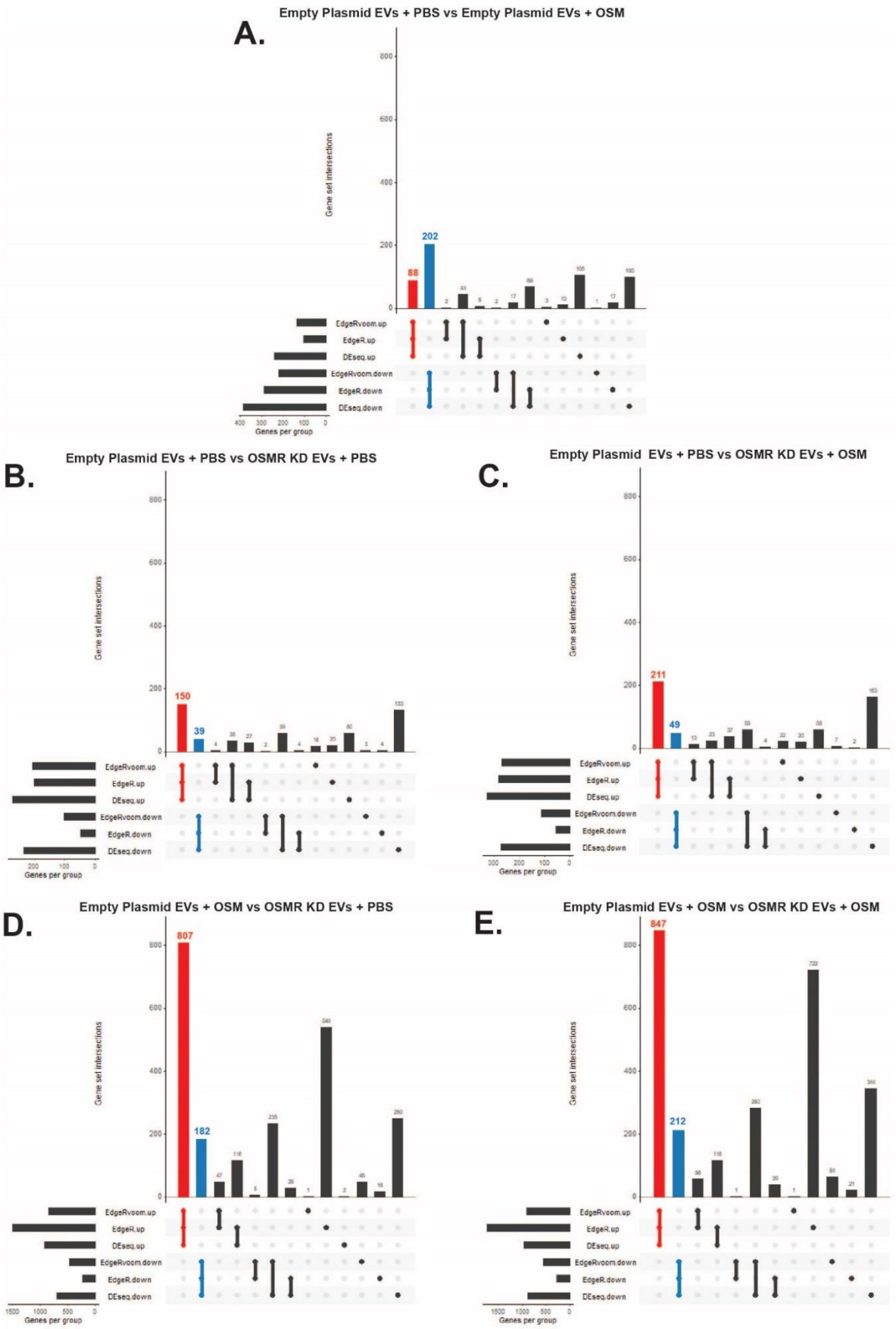

Figure 5.11: EV-EV comparisons-common up and down-regulated genes

Comparison of genes with significant (FDR ≤0.01) up or down regulation across analysis methods (DESeq2, EdgeR and EdgeR voom)

The number of significantly (FDR ≤0.01) up or down regulated genes identified using each package varied when comparing either cell or EVs samples. When comparing cell samples (Figure 5.10) EdgeR voom identified the greatest number of up or down regulated genes, followed by DESeq2 then EdgeR, which was the most stringent method. In contrast, DESeq2 detected the greatest number of significantly downregulated genes for EV-EV comparisons (Figure 5.11), followed by EdgeR voom then EdgeR. More variability was observed when investigating which package detected the greatest number of upregulated genes for EV-EV comparisons. As no statistical analysis is superior to another, only genes that were found to be up or downregulated across all three statistical packages for each comparison were selected for further investigation.

A greater degree of discrepancy in up and downregulated genes detected by DESeq2, EdgeR and EdgeR analyses was observed when levels of gene expression in cells were directly compared to EVs (Figure 5.12). Cell-EV comparisons did not investigate differences in gene expression in response to OSM-OSMR signalling, but instead highlighted differences in gene expression between cells and EVs of the same treatment group. Approximately 2600-3000 genes were found by all three analysis methods to be significantly up or down regulated in EVs compared to cells for all treatment groups (Figure 5.12). This is much greater than the number of genes found to have significantly altered expression in cell-cell and EV-EV comparisons following treatment with OSM or OSMR KD. There was a high degree of inconsistency between statistical methods when cell-EV comparisons were performed. This finding highlights the challenges in directly comparing sequencing results for cell and EV samples and is likely driven by differential expression of low count genes and EV GC skew.

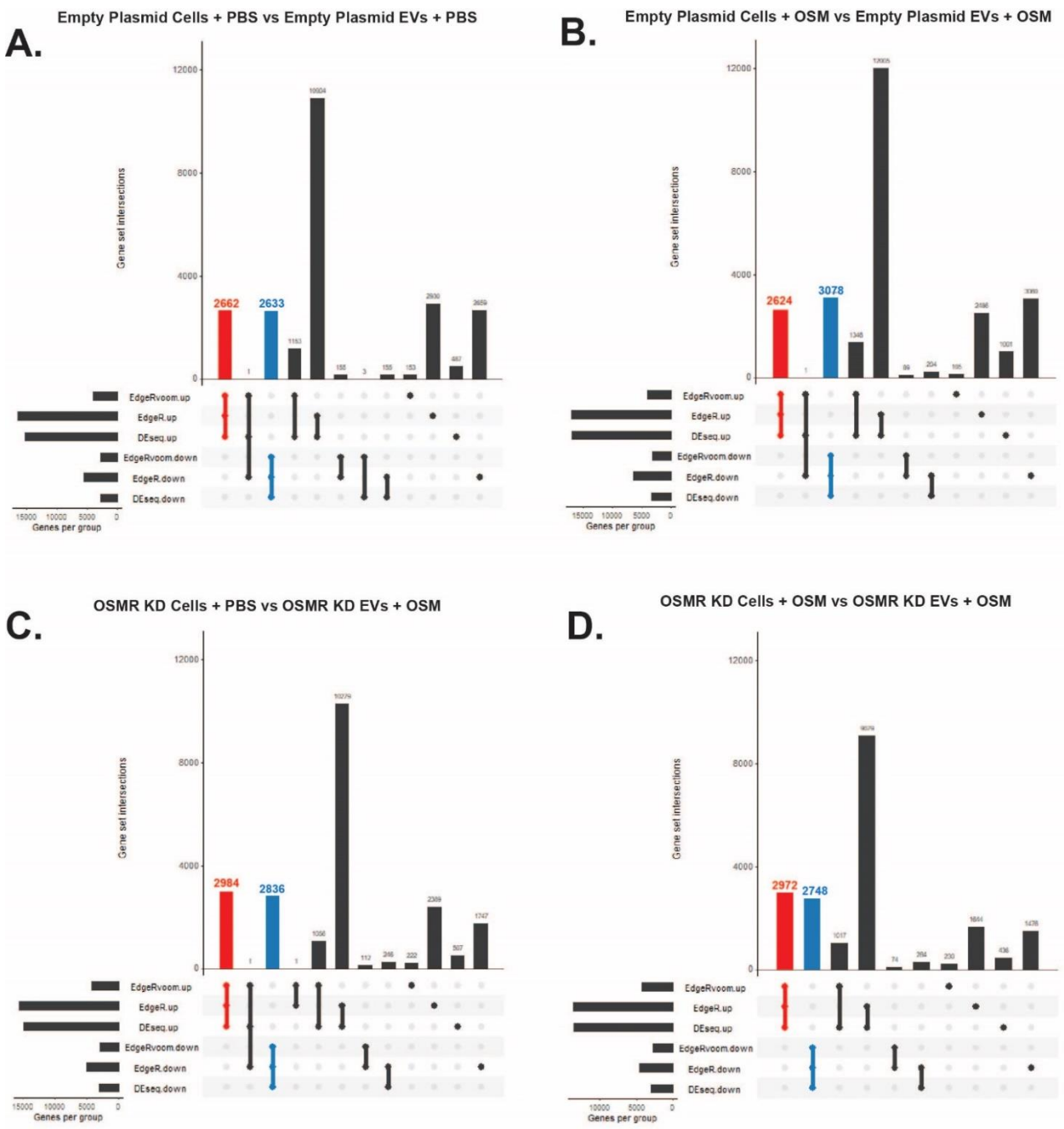

Figure 5.12: Cell-EV comparisons – common up and down-regulated genes
Comparison of genes with significant (FDR ≤0.01) up or down regulation across analysis methods (DESeq2, EdgeR and EdgeR voom)

5.5.3 Comparison of cellular and EV mRNA expression

Subsequent analysis focused on comparing genes that were up or downregulated in both cells and EVs in response to treatment. Only genes that were found to be significantly up or down regulated (FDR ≤0.01) by all three analysis methods were selected for comparison. Similarities and differences in cellular and EV expression profiles for each of the following comparisons detailed in Table 5.7 were visualised by Venn diagram using Venn Diagram Plotter software (Pacific Northwest National Laboratory, omics.pnl.gov; Figure 5.13):

Table 5.7: Summary of data shown in Venn diagrams (mRNA)

	Cell-Cell comparisons	EV-EV comparisons	For each pair of comparisons Venn Diagram shows
1.	EP-PBS-cells versus EP-OSM-cells	EP-PBS-EVs versus EP-OSM-EVs	• Genes that were commonly up or down regulated in both cell and EV comparisons (i.e. commonly DE genes in both cell and EVs) • Genes that were up or down downregulated in cell-cell or EV-EV comparisons only (i.e. genes with DE unique to either cells or EVs)
2.	EP-PBS-cells versus KD-PBS-cells	EP-PBS-EVs versus KD-PBS-EVs	
3.	EP-PBS-cells versus KD-OSM-cells	EP-PBS-EVs versus KD-OSM-EVs	
4.	EP-OSM-cells versus KD-PBS-cells	EP-OSM-EVs versus KD-PBS-EVs	
5.	EP-OSM-cells versus KD-OSM-cells	EP-OSM-EVs versus KD-OSM-EVs	

Treatment of EP-cells with OSM led to global changes in gene expression in both the cells and their resultant EVs. Interestingly, these results appear to highlight both similarities and differences in cells and EVs in response to OSM-OSMR signalling. For all comparisons investigated, overlapping cohorts of genes were found to be up or down regulated in both cells and EVs; however, numbers of up or down regulated genes differed between cells and EVs. In response to OSM treatment more genes were upregulated (225) than downregulated (98) in EP-cells, whereas the opposite was observed for EVs (88 upregulated, 202 downregulated; Figure 5.13A). Similarly, compared to EP-cells, more genes were downregulated in KD-cells than upregulated, regardless of PBS or OSM treatment (Figure 5.13B-E). On the other hand, a greater number of genes were upregulated than downregulated, regardless of treatment in KD-EVs compared to EP-EVs. As expected, comparison of EP-OSM and KD-OSM produced the greatest number of disparately expressed genes in both cell and EV comparisons. This is consistent with the selective activation of OSM-OSMR signalling in the EP cell line. More genes were found to be significantly downregulated (543) than upregulated (216) in KD-OSM-cells compared to EP-OSM-cells, whereas more genes were upregulated (847) than downregulated (212) in KD-OSM-EVs compared to EP-OSM-EVs (Figure 5.13E).

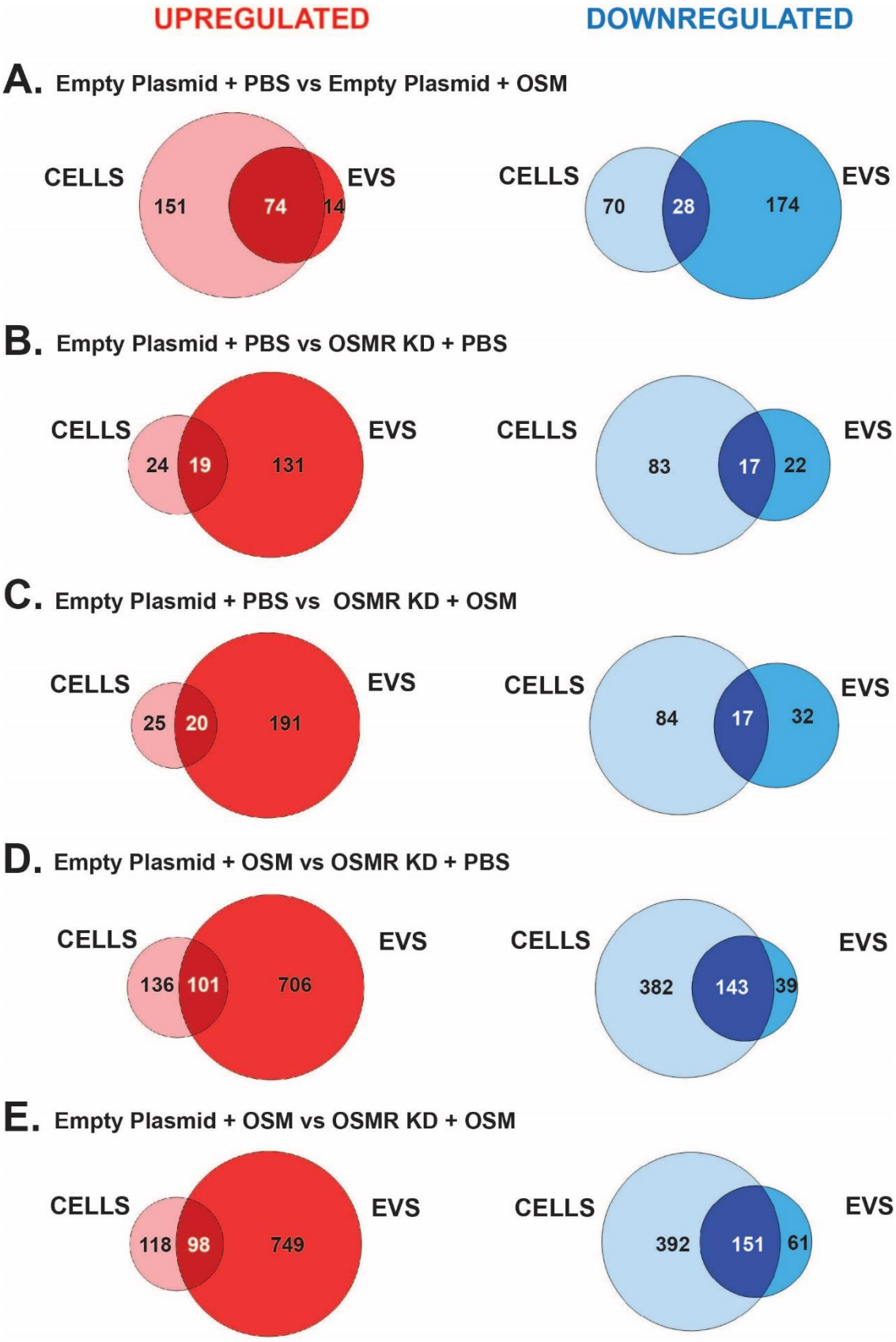

Figure 5.13: Comparison of genes with common or unique DE in cells and EVs
Comparison of genes with significant ($p \leq 0.01$) up or down regulation for all three analysis methods (DESeq2, EdgeR and EdgeR voom) in cells and EVs from each treatment group.

5.5.4 mRNA Pathway analysis

Pathway analysis was then performed using Metascape software[340] for the following cell-cell and EV-EV comparisons: EP-PBS versus EP-OSM and EP-OSM versus KD-OSM. Only genes that were found to be significantly up or downregulated (FDR ≤0.01) using all three analysis methods were selected for comparison.

Metascape allows pathway and process analysis using multiple ontology sources. The current analysis used the following sources: KEGG Pathway, GO Biological Processes, Reactome Gene Sets, Canonical Pathways and CORUM. The enrichment background uses all genes in the human genome. Terms with a p-value of ≤0.01, a minimum count of three, and an enrichment factor (the ratio between the observed counts and the counts expected by chance) of > 1.5 were collected and grouped into clusters based on their membership similarities. Metascape uses kappa scores as the similarity metric when performing hierarchical clustering on the enriched terms; sub-trees with a similarity of > 0.3 are considered a cluster. It chooses the most statistically significant term within a cluster to represent the cluster[340].

The top 20 most significant clusters for the EP-PBS versus EP-OSM (Figure 5.14) and EP-OSM versus KD-OSM comparisons (Figure 5.15) are shown in graphical format, ranked based on their p values. To further capture the relationship between the terms, terms with the most significant p-values from the 20 top clusters were visualised as a network plot using cytoscape[341] (generated by Metascape package). Network plots for EP-PBS versus EP-OSM and EP-OSM versus KD-OSM comparisons are shown in Figure S5. 22 and Figure S5. 23, respectively.

In response to OSM treatment, the most significantly upregulated pathways in EP-cells included: cytokine mediated signalling, myeloid leucocyte activation, response to decreased oxygen levels, interferon signalling, regulation of viral life cycle and replication and angiogenesis (Figure 5.14A panel i and Figure S5. 22A panel i). Similar pathways were found to be the most downregulated in KD-OSM-cells compared to EP-OSM-cells (Figure 5.15B panel i and Figure S5. 23B panel i). Upregulation of similar pathways was also observed in EP-OSM-EVs compared to EP-PBS-EVs (Figure 5.14A panel ii and Figure S5. 22A panel ii).

As observed with cells, similar pathways that were upregulated in EP-OSM-EVs compared to EP-PBS-EVs, were downregulated in KD-OSM-EVs compared to EP-OSM-EVs (Figure 5.15B panel ii and Figure S5. 23B panel ii). One notable difference between cells and EVs

was that, while pathways involved in angiogenesis were upregulated in EP-cells in response to OSM and downregulated in KD-cells, angiogenic pathways did not appear to be altered in EVs from either comparison.

In EP-cells, treatment with OSM led to significant downregulation of pathways involved in PI3K-AKT signalling, tissue remodelling, negative regulation of differentiation and focal adhesion (Figure 5.14B panel i and Figure S5. 22B panel i) compared to EP-PBS-cells. Some similarities were observed in KD-cells; KD-cells-OSM were found to have upregulation of actin-filament based process, focal adhesion, pathways involved in differentiation and regulation of cell migration (Figure 5.15A panel i and Figure S5. 23A panel i) compared to EP-cells-OSM. Pathways downregulated in EP-OSM-EVs compared to EP-PBS-EVs differed from those observed to be downregulated in EP-OSM-cells. Most significantly downregulated pathways included those involved in cell cycle regulation and division and pathways involved in cellular organisation – such as signalling by Rho GTPases, actin filament based processes and microtubule based processes (Figure 5.14B panel ii and Figure S5. 22B panel ii). Similar pathways were upregulated in KD-OSM-EVs compared to EP-OSM-EVs ((Figure 5.15A panel ii and Figure S5. 23A panel ii).

Empty Plasmid + PBS vs Empty Plasmid + OSM

A. UPREGULATED PATHWAYS

i) CELLS

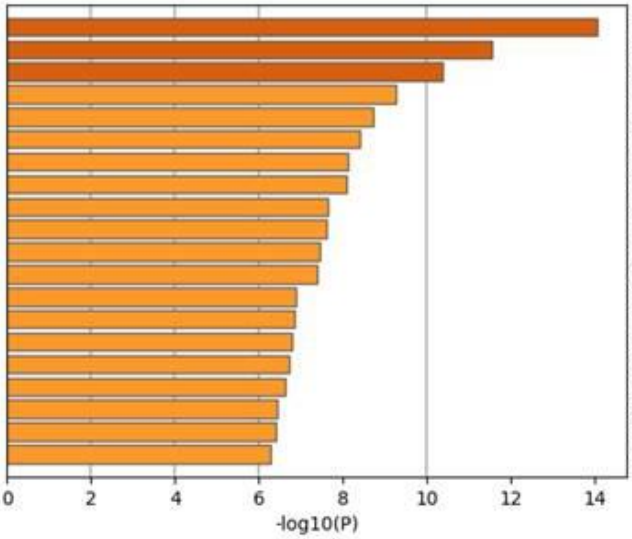

R-HSA-1280215: Cytokine Signaling in Immune system
GO:0002274: myeloid leukocyte activation
GO:0036293: response to decreased oxygen levels
R-HSA-913531: Interferon Signaling
GO:0019058: viral life cycle
GO:0045071: negative regulation of viral genome replication
GO:0001525: angiogenesis
GO:0048660: regulation of smooth muscle cell proliferation
GO:0001816: cytokine production
GO:0051272: positive regulation of cellular component movement
GO:0042330: taxis
GO:0055076: transition metal ion homeostasis
M5885: NABA MATRISOME ASSOCIATED
R-HSA-1474244: Extracellular matrix organization
M18: PID INTEGRIN1 PATHWAY
GO:0050731: positive regulation of peptidyl-tyrosine phosphorylation
M17580: ST IL 13 PATHWAY
GO:1902532: negative regulation of intracellular signal transduction
GO:0098771: inorganic ion homeostasis
GO:0097193: intrinsic apoptotic signaling pathway

ii) EVs

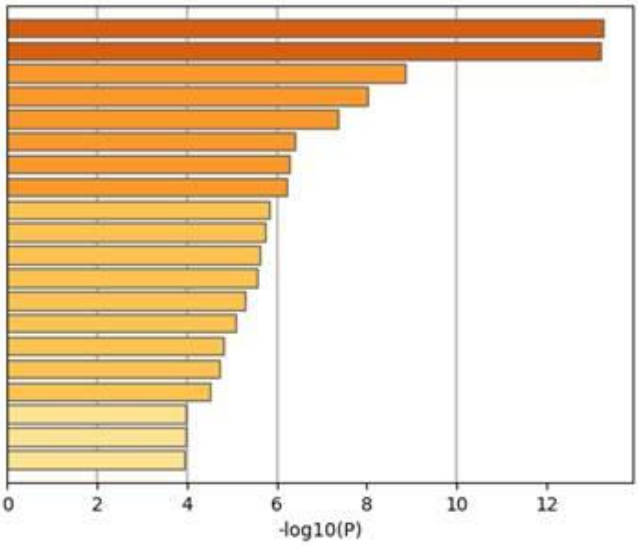

GO:0019221: cytokine-mediated signaling pathway
R-HSA-909733: Interferon alpha/beta signaling
GO:0002274: myeloid leukocyte activation
GO:0036293: response to decreased oxygen levels
GO:0034341: response to interferon-gamma
hsa04610: Complement and coagulation cascades
GO:0007565: female pregnancy
GO:1901699: cellular response to nitrogen compound
GO:0002526: acute inflammatory response
M118: PID INTEGRIN A9B1 PATHWAY
M3468: NABA ECM REGULATORS
hsa04621: NOD-like receptor signaling pathway
GO:0045926: negative regulation of growth
GO:0051098: regulation of binding
GO:0045064: T-helper 2 cell differentiation
GO:0046688: response to copper ion
GO:0070741: response to interleukin-6
GO:0002521: leukocyte differentiation
GO:0045785: positive regulation of cell adhesion
GO:0030855: epithelial cell differentiation

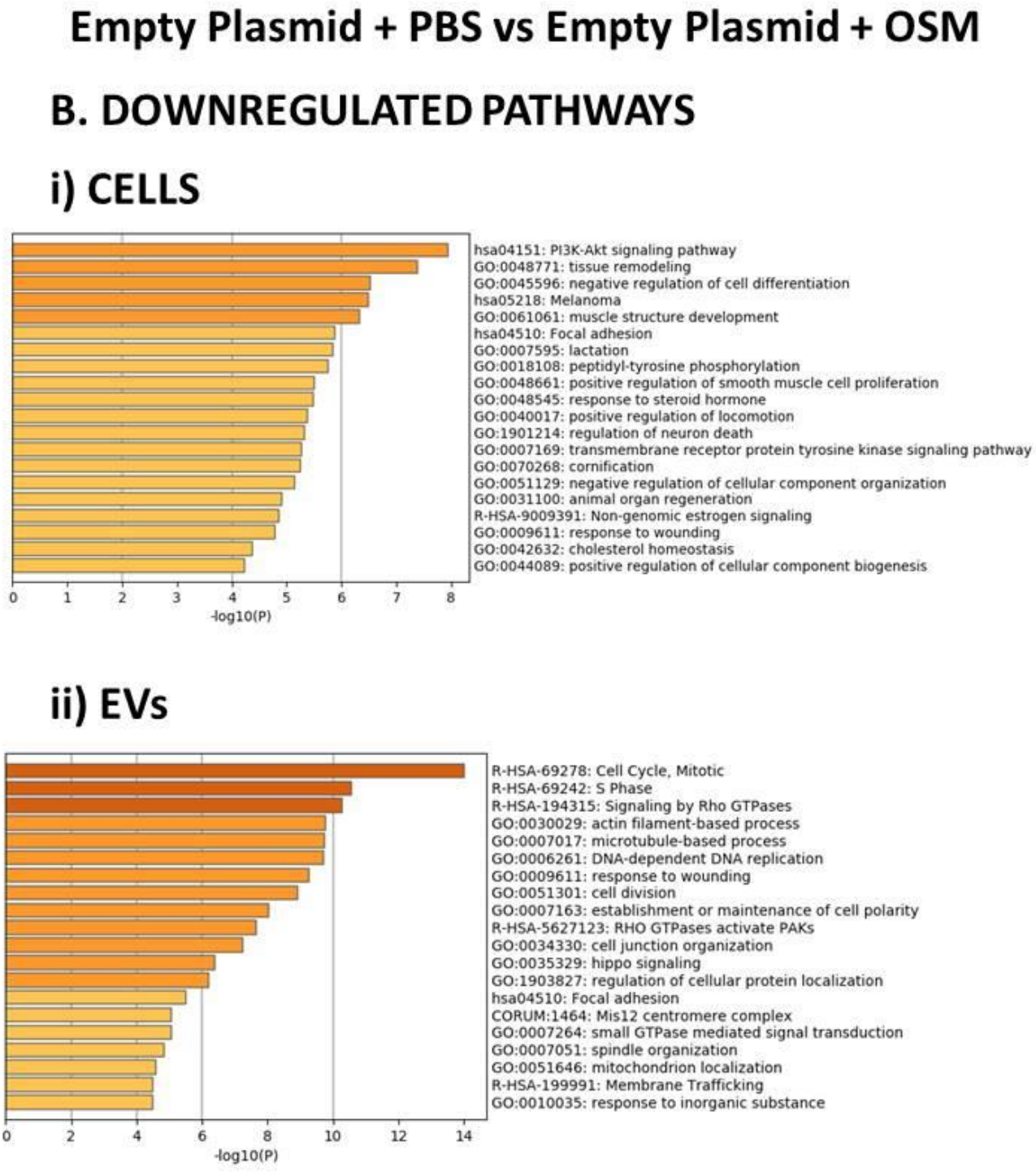

Figure 5.14: Pathway analysis - Empty Plasmid + PBS vs Empty Plasmid + OSM
Metascape analysis of top 20 most significantly enriched terms in gene lists for SW756 empty plasmid + PBS versus SW756 empty plasmid + OSM comparison.
A) Upregulated pathways in i) cells and ii) EVS.
B) Downregulated pathways in i) cells and ii) EVs.

Empty Plasmid + OSM vs OSMR KD + OSM

A. UPREGULATED PATHWAYS

i) CELLS

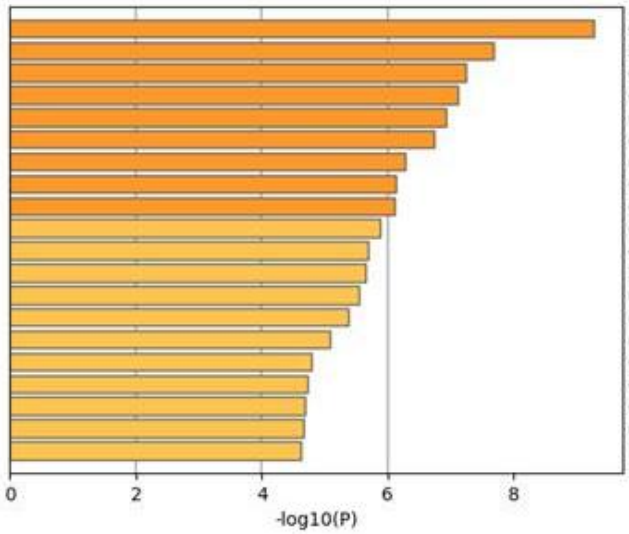

ii) EVs

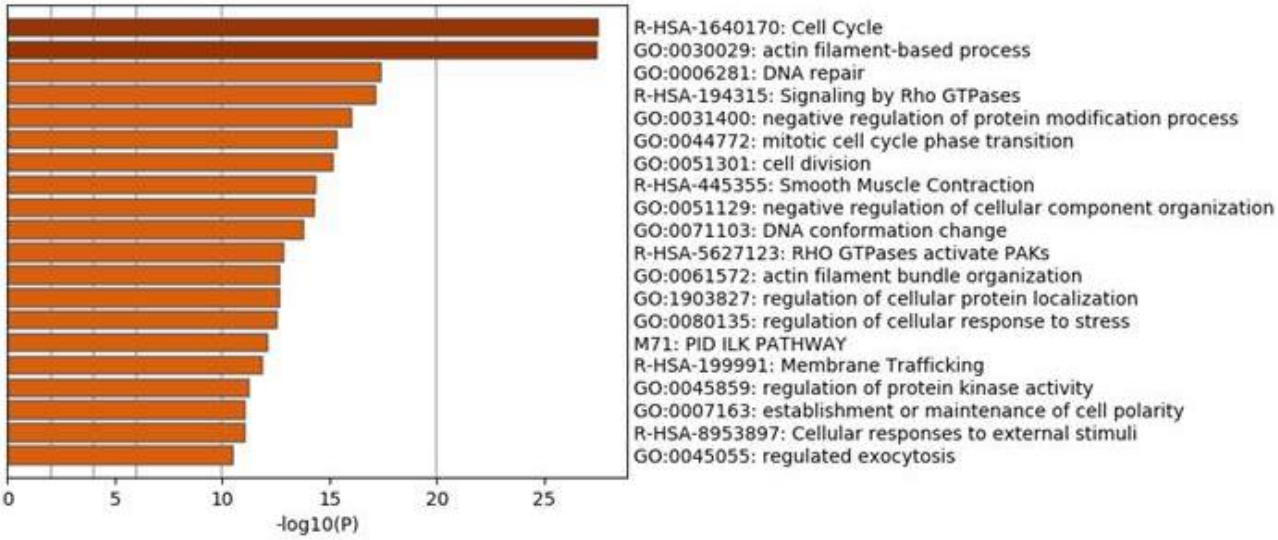

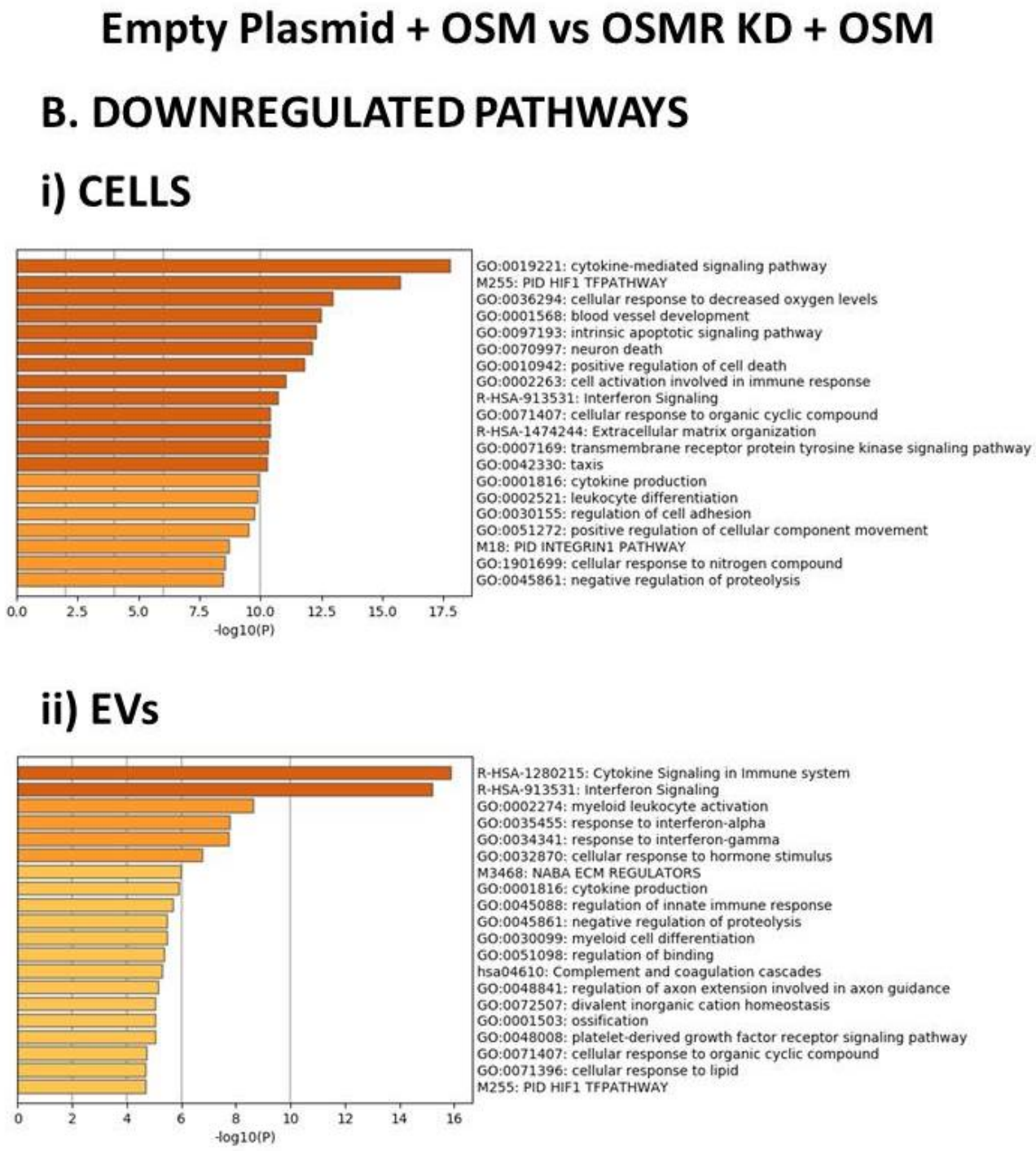

Figure 5.15: Pathway analysis - Empty Plasmid + OSM vs OSMR KD + OSM
Metascape analysis of top 20 most significantly enriched terms in gene lists for SW756 empty plasmid + OSM versus SW756 OSMR KD + OSM comparison.
A) Upregulated pathways in i) cells and ii) EVS.
B) Downregulated pathways in i) cells and ii) EVs

Therefore, in general similar pathways were over or under represented in both cervical SCC cells and EVs in response to OSM-OSMR signalling. However, genes found to be differentially expressed in EVs did not identically mirror mRNA expression of the original cell, leading to some differences in pathway analysis. This suggests that mRNAs are selectively packaged into EVs in response to OSM-OSMR signalling.

5.5.5 Validation of mRNA sequencing results

In order to validate sequencing results, some mRNAs were selected for qPCR investigation. Briefly, genes that were found to be significantly up or down regulated (log FC +/- 0.5; FDR ≤0.01) across all three analysis methods (DESeq2, EdgeR and EdgeR voom) were ranked. The top ten most up or down regulated genes for each analysis method are shown in Table 5.8. Note that actual rankings of differentially expressed genes for each individual analysis will differ as they are calculated based on all differentially expressed genes detected by the specific analysis method, rather than only including genes common to all analysis methods.

Table 5.8: Top 10 most up and down regulated genes

Ten most up and down regulated genes for each analysis method (out of cohort of gene with statistically significant differential expression for all three analysis methods). Genes are ranked by log FC; FDR for each gene is also shown. Genes selected for qPCR validation are highlighted in red or blue. Analysis is shown for the following key comparisons:

A) EP-PBS-cells versus EP-OSM-cells
B) EP-PBS-EVs versus EP-OSM-EVs
C) EP-OSM-cells versus KD-OSM-cells
D) EP-OSM-EVs versus KD-OSM-EVs

A		Empty Plasmid Cells + PBS vs Empty Plasmid Cells + OSM								
		DESeq2			EdgeR			EdgeR Voom		
		Gene	log FC	FDR	Gene	log FC	FDR	Gene	log FC	FDR
UPREGULATED	1	ATP8B4	6.64	4.6×10^{-5}	SERPINA1	6.64	1.1×10^{-132}	SERPINA1	6.62	1.1×10^{-23}
	2	SERPINA1	6.63	2.7×10^{-42}	CHI3L1	6.58	2.5×10^{-115}	CHI3L1	6.55	4.5×10^{-19}
	3	CHI3L1	6.57	3.5×10^{-99}	ATP8B4	6.40	3.5×10^{-9}	ATP8B4	5.08	3.3×10^{-6}
	4	CEMIP	4.65	9.9×10^{-74}	CEMIP	4.67	1.4×10^{-79}	CEMIP	4.64	1.0×10^{-23}
	5	ADAM8	4.50	4.5×10^{-27}	ADAM8	4.50	1.7×10^{-42}	CASP14	4.54	5.1×10^{-16}
	6	CASP14	4.47	6.7×10^{-47}	CASP14	4.47	3.6×10^{-46}	ADAM8	4.52	2.7×10^{-12}
	7	C9orf84	4.11	1.5×10^{-12}	C9orf84	4.05	3.8×10^{-12}	C9orf84	4.03	1.3×10^{-8}
	8	CYSLTR1	3.88	4.6×10^{-15}	SLCO4A1	3.88	1.2×10^{-61}	SLCO4A1	3.86	5.1×10^{-28}
	9	SLCO4A1	3.87	1.0×10^{-277}	CYSLTR1	3.87	5.1×10^{-20}	CYSLTR1	3.86	3.4×10^{-10}
	10	GRAMD1B	3.72	1.3×10^{-9}	GRAMD1B	3.66	8.5×10^{-11}	GRAMD1B	3.59	3.4×10^{-7}
DOWNREGULATED	1	PTPRR	-5.25	1.2×10^{-3}	PTPRR	-4.65	2.0×10^{-5}	PTPRR	-4.23	3.5×10^{-7}
	2	ANKRD1	-4.03	2.9×10^{-4}	ANKRD1	-3.81	1.4×10^{-7}	IGFL2-AS1	-3.86	1.4×10^{-7}
	3	IGFL2-AS1	-3.95	2.6×10^{-5}	IGFL2-AS1	-3.73	1.8×10^{-6}	ANKRD1	-3.64	4.4×10^{-5}
	4	CPA5	-3.83	2.8×10^{-6}	CPA5	-3.68	2.4×10^{-8}	CPA5	-3.61	1.4×10^{-7}
	5	CPA4	-3.39	1.1×10^{-49}	CPA4	-3.36	1.4×10^{-50}	CPA4	-3.48	3.3×10^{-21}
	6	PDGFB	-3.14	1.5×10^{-7}	PDGFB	-3.08	1.6×10^{-10}	PTPRB	-3.20	5.6×10^{-4}
	7	PRLR	-3.12	2.9×10^{-3}	IL7R	-3.05	7.5×10^{-29}	KRT83	-3.18	1.1×10^{-4}
	8	KRT83	-3.08	3.2×10^{-5}	KRT83	-2.99	7.4×10^{-06}	PRLR	-3.14	5.0×10^{-4}
	9	IL7R	-3.08	2.9×10^{-40}	PRLR	-2.94	7.5×10^{-04}	PDGFB	-3.13	5.5×10^{-6}
	10	PTPRB	-2.86	1.8×10^{-4}	KRT81	-2.84	1.2×10^{-36}	IL7R	-3.05	7.2×10^{-15}

B		Empty Plasmid EVs + PBS vs Empty Plasmid EVs + OSM								
		DESeq2			EdgeR			EdgeR Voom		
		Gene	log FC	FDR	Gene	log FC	FDR	Gene	log FC	FDR
UPREGULATED	1	SERPINA1	5.42	1.6×10^{-80}	SERPINA1	5.33	2.9×10^{-111}	SERPINA1	5.44	1.7×10^{-15}
	2	CHI3L1	3.76	2.9×10^{-15}	CHI3L1	3.62	1.8×10^{-22}	CHI3L1	3.62	5.1×10^{-7}
	3	TNFRSF21	2.85	1.3×10^{-20}	TNFRSF21	2.80	3.7×10^{-35}	TNFRSF21	3.03	1.0×10^{-8}
	4	SLCO4A1	2.58	4.5×10^{-48}	SLCO4A1	2.46	2.8×10^{-27}	SLCO4A1	2.58	1.1×10^{-11}
	5	CASP14	2.39	6.4×10^{-15}	CASP14	2.26	2.5×10^{-13}	ADAM8	2.53	1.1×10^{-3}
	6	CTSL	2.27	3.0×10^{-46}	CTSL	2.19	1.4×10^{-30}	CASP14	2.32	1.7×10^{-7}
	7	ADAM8	2.24	1.6×10^{-4}	ADAM8	2.10	1.6×10^{-4}	CTSL	2.25	2.0×10^{-12}
	8	OASL	2.11	6.5×10^{-10}	OASL	2.02	7.8×10^{-12}	OASL	2.18	7.3×10^{-7}
	9	CTSB	2.06	9.5×10^{-101}	NAMPT	1.98	2.7×10^{-27}	NAMPT	2.06	3.9×10^{-13}
	10	NAMPT	2.06	4.6×10^{-40}	CTSB	1.97	2.3×10^{-30}	CTSB	2.05	3.4×10^{-17}
DOWNREGULATED	1	CPA4	-2.79	2.9×10^{-32}	CPA4	-2.89	2.2×10^{-41}	CPA4	-2.79	3.0×10^{-8}
	2	AMOT	-1.69	8.0×10^{-7}	AMOT	-1.81	5.7×10^{-11}	AMOT	-1.69	6.9×10^{-4}
	3	KRT81	-1.61	1.8×10^{-6}	KRT81	-1.71	2.3×10^{-21}	NPTX1	-1.63	2.4×10^{-6}
	4	NPTX1	-1.59	4.2×10^{-16}	NPTX1	-1.70	1.4×10^{-15}	C2orf15	-1.61	2.6×10^{-5}
	5	LINC02454	-1.56	1.2×10^{-5}	LINC02454	-1.66	7.6×10^{-5}	KRT81	-1.61	3.7×10^{-11}
	6	C2orf15	-1.54	1.5×10^{-9}	C2orf15	-1.64	4.3×10^{-10}	LINC02454	-1.55	4.5×10^{-4}
	7	SORBS2	-1.48	1.9×10^{-20}	SORBS2	-1.62	7.3×10^{-16}	SORBS2	-1.52	2.3×10^{-8}
	8	MT-CYB	-1.48	8.8×10^{-9}	MT-CYB	-1.60	1.8×10^{-13}	MT-CYB	-1.48	1.7×10^{-6}
	9	MT-CO3	-1.40	4.6×10^{-8}	MT-CO3	-1.53	5.4×10^{-13}	MT-CO3	-1.41	3.2×10^{-6}
	10	GYG2	-1.40	2.7×10^{-9}	GYG2	-1.51	7.7×10^{-8}	TNS3	-1.40	8.9×10^{-6}

C		Empty Plasmid Cells + OSM vs OSMR KD Cells + OSM								
		DESeq2			EdgeR			EdgeR Voom		
		Gene	log FC	FDR	Gene	log FC	FDR	Gene	log FC	FDR
UPREGULATED	1	PLCB4	7.96	5.0×10^{-9}	PLCB4	7.31	9.1×10^{-29}	PLCB4	6.95	3.0×10^{-15}
	2	ACTG2	7.73	3.7×10^{-8}	ACTG2	7.08	2.6×10^{-25}	ACTG2	6.62	2.6×10^{-12}
	3	ANKRD1	6.30	7.8×10^{-11}	ANKRD1	6.05	3.6×10^{-27}	ANKRD1	5.85	6.2×10^{-11}
	4	ZFPM2	5.57	3.8×10^{-4}	ZFPM2	5.35	8.9×10^{-5}	ADARB2	4.92	4.7×10^{-9}
	5	ADARB2	5.31	5.1×10^{-5}	ADARB2	4.88	1.0×10^{-8}	CPA5	4.76	2.3×10^{-11}
	6	PTPRR	5.25	7.2×10^{-4}	CPA5	4.82	3.2×10^{-17}	IGFL2-AS1	4.23	7.5×10^{-9}
	7	CPA5	5.02	3.2×10^{-11}	PTPRR	4.63	1.3×10^{-5}	PTPRR	4.18	3.3×10^{-7}
	8	LPAR4	4.80	5.7×10^{-3}	SYTL5	4.57	7.9×10^{-3}	ZFPM2	4.16	3.8×10^{-7}
	9	SYTL5	4.78	3.5×10^{-3}	LPAR4	4.56	7.6×10^{-3}	RAB38	4.15	2.7×10^{-7}
	10	PTPRQ	4.73	7.8×10^{-3}	PTPRQ	4.53	6.1×10^{-3}	ELAVL2	3.92	5.6×10^{-10}
DOWNREGULATED	1	FMOD	-10.10	1.4×10^{-14}	FMOD	-10.10	6.1×10^{-53}	FMOD	-8.67	1.3×10^{-19}
	2	TCF4	-9.62	8.7×10^{-13}	TCF4	-9.62	6.1×10^{-53}	TCF4	-8.18	1.7×10^{-15}
	3	PARM1	-8.39	2.1×10^{-9}	PARM1	-8.39	4.2×10^{-22}	SERPINA1	-7.75	2.1×10^{-21}
	4	SELENBP1	-7.80	1.4×10^{-8}	SELENBP1	-7.81	4.4×10^{-16}	PARM1	-6.88	4.2×10^{-11}
	5	SERPINA1	-7.77	4.3×10^{-152}	SERPINA1	-7.80	1.0×10^{-155}	PCSK1N	-6.73	2.0×10^{-14}
	6	DSC2	-7.17	3.5×10^{-7}	DSC2	-7.17	1.0×10^{-12}	SELENBP1	-6.36	3.9×10^{-13}
	7	ZNF468	-7.12	9.1×10^{-7}	ZNF468	-7.13	7.0×10^{-13}	CLDN10	-6.21	1.2×10^{-11}
	8	PCSK1N	-7.07	2.4×10^{-14}	GALC	-6.95	1.6×10^{-10}	CHI3L1	-5.95	2.1×10^{-19}
	9	GALC	-6.94	2.0×10^{-6}	PCSK1N	-6.85	7.7×10^{-38}	RPL39L	-5.91	3.5×10^{-11}
	10	RPL39L	-6.91	8.7×10^{-7}	RNF180	-6.68	1.2×10^{-9}	F13A1	-5.82	3.6×10^{-11}

D		Empty Plasmid EVs + OSM vs OSMR KD EVs + OSM								
		DESeq2			EdgeR			EdgeR Voom		
		Gene	log FC	FDR	Gene	log FC	FDR	Gene	log FC	FDR
UPREGULATED	1	KISS1	3.49	1.1×10^{-7}	KISS1	3.69	6.2×10^{-12}	RAB38	3.77	1.1×10^{-6}
	2	RAB38	3.48	2.6×10^{-6}	RAB38	3.69	4.4×10^{-10}	KISS1	3.40	2.9×10^{-8}
	3	TAGLN	3.27	5.0×10^{-62}	TAGLN	3.51	1.8×10^{-73}	TAGLN	3.31	3.0×10^{-14}
	4	KRT86	2.77	1.3×10^{-4}	KRT86	2.98	6.1×10^{-6}	KRT86	2.75	2.5×10^{-5}
	5	KRT81	2.61	1.8×10^{-99}	KRT81	2.86	1.2×10^{-59}	KRT81	2.64	1.7×10^{-18}
	6	S100A4	2.58	2.1×10^{-37}	DDR2	2.84	6.2×10^{-43}	S100A4	2.61	1.3×10^{-11}
	7	DDR2	2.58	1.3×10^{-44}	S100A4	2.83	7.7×10^{-38}	DDR2	2.59	1.2×10^{-13}
	8	CPA4	2.49	7.8×10^{-26}	ACTG2	2.77	5.7×10^{-11}	KRT83	2.54	2.5×10^{-4}
	9	ACTG2	2.48	2.9×10^{-6}	CPA4	2.75	8.9×10^{-38}	CPA4	2.52	8.2×10^{-8}
	10	C2orf15	2.39	7.1×10^{-25}	C2orf15	2.64	8.2×10^{-31}	ACTG2	2.50	4.0×10^{-5}
DOWNREGULATED	1	PCSK1N	-5.80	6.0×10^{-10}	SERPINA1	-5.39	9.4×10^{-117}	SERPINA1	-5.75	1.0×10^{-16}
	2	SERPINA1	-5.63	2.0×10^{-91}	PCSK1N	-5.37	3.3×10^{-21}	PCSK1N	-5.24	2.7×10^{-12}
	3	RPL39L	-4.14	2.8×10^{-10}	RPL39L	-3.84	2.3×10^{-12}	RPL39L	-3.73	8.8×10^{-8}
	4	CA2	-3.57	1.4×10^{-23}	CA2	-3.30	5.3×10^{-24}	CA2	-3.53	6.9×10^{-11}
	5	CHI3L1	-3.17	8.9×10^{-17}	CHI3L1	-2.91	4.3×10^{-19}	CHI3L1	-3.05	1.0×10^{-6}
	6	SELENBP1	-3.06	2.3×10^{-7}	IFIT2	-2.82	2.9×10^{-33}	ITGA2	-3.01	1.6×10^{-9}
	7	IFIT2	-3.05	1.1×10^{-27}	SELENBP1	-2.76	3.5×10^{-6}	IFIT2	-2.97	2.9×10^{-10}
	8	ITGA2	-2.97	6.2×10^{-25}	ITGA2	-2.71	3.9×10^{-30}	CSF3	-2.95	1.4×10^{-4}
	9	CTSL	-2.93	4.8×10^{-73}	CTSL	-2.69	4.8×10^{-45}	SELENBP1	-2.93	3.5×10^{-6}
	10	AL355916.1	-2.85	1.2×10^{-7}	AL355916.1	-2.65	2.3×10^{-8}	AL355916.1	-2.93	4.5×10^{-6}

Of these genes, CHI3L1, CEMIP, CPA4, PTPRR, FMOD, PLCB4, PCSK1N and RAB38, were selected for qPCR validation. Other known targets of OSM-OSMR signalling were also selected for investigation: OSMR, VEGFA, TGM2, SNAI1 and PLAUR. Levels of upregulation and downregulation of these 5 genes in both cells and EVs from the two comparisons investigated (EP-PBS versus EP-OSM and EP-OSM versus KD-OSM) are

shown in Table S5. 1. A summary of the expression patterns of each of the selected genes is shown in Table 5.9.

Table 5.9: Summary of expression of genes selected for qPCR validation

✔=significantly up or down regulated; x = not significantly up or downregulated
Top 10 = ranked within the top 10 most up or down regulated genes for that comparison. Upregulation is shown in pink, downregulation in blue. It is not possible for a gene to be both up and down regulated in a single comparison. Therefore, if a gene is found to be up or downregulated, the paired box is shaded grey.

GENES	Empty Plasmid + PBS vs Empty Plasmid + OSM				Empty Plasmid + OSM vs OSMR KD + OSM			
	UPREGULATED		DOWNREGULATED		UPREGULATED		DOWNREGULATED	
	Cells	EVs	Cells	EVs	Cells	EVs	Cells	EVs
CHI3L1	✔Top 10	✔Top 10					✔Top 10	✔Top 10
CEMIP	✔Top 10	✔					✔	✔
CPA4			✔Top 10	✔Top 10	✔	✔Top 10		
PTPRR		x	✔Top 10	x	✔Top 10	x		x
FMOD	x	x	x	x			✔Top 10	✔
PLCB4	x	x	x	x	✔Top 10	x		x
PCSK1N	x	x	x	x			✔Top 10	✔Top 10
RAB38	x	x	x	x	✔	✔Top 10		
OSMR	✔	✔					✔	✔
VEGFA	✔	✔					✔	✔
TGM2	✔	✔					✔	✔
SNAI1	x	x	x	x		x	✔	x
PLAUR	✔	✔					✔	✔

A brief summary of each of these genes is provided in Table 5.10. OSMR, VEGFA, TGM2 and SNAI1 have previously been described.

Table 5.10: Summary of genes selected for qPCR investigation

Gene	Details
CHI3L1	Chitinase 3 Like 1, also known as YKL-40. Elevated levels of CHI3L1 in cervical cancer are associated with poor prognosis and reduced survival[342]. CHI3LI has been shown to promote both angiogenesis[342]and vascular mimicry[343] in cervical cancer. Moreover, OSM has been shown to induce CHI3L1 expression in glioma cells[344,345] and skin cells of patients with systemic sclerosis[346]
CEMIP	Cell migration-inducing and hyaluronan-binding protein, also known as KIAA1199 has been shown to be upregulated in several cancers, including oral SCC, and is associated with poor overall survival[347]. Downstream targets of CEMIP include ERK1/2[348], PI3K/AKT[349] and Wnt/β-catenin signalling pathways[347]. Its role in cervical cancer and relationship to OSM-OSMR signalling remains unknown.
CPA4	Carboxypeptidase A4. CPA4 has been found to be elevated in non-small cell lung cancer[350,351] and triple-negative breast cancer[352] and was associated with

	poor prognosis and metastasis. It promoted invasion and migration of lung cancer cells[350] and was implicated in EMT in breast cancer cells[352]. While CPA4 has been reported to be underexpressed in HPV positive cervical tumours[353], its role in cervical cancer and relationship with OSM-OSMR signalling have not been investigated.
PTPRR	Protein tyrosine phosphatase receptor type R. PTPRR has been shown to be silenced in cervical cancer via DNA methyltransferases 3B methylation, leading to activation of MAPK signalling and EMT[354]. Overexpression of PTPRR has been shown to lead to reduced growth of cervical SCC lines, reduced expression of EMT markers and reduced expression of HPV E6 and E7 genes *in vitro*. Moreover, overexpression of PTPRR was shown to lead to reduced tumour growth and metastasis *in vivo*[354]. Whether PTPRR plays a role in OSM-OSMR signalling remains to be elucidated.
FMOD	Fibromodulin. FMOD is a member of the small-leucine-rich-proteoglycan family and is known to play role in ECM remodelling, angiogenesis and modulation of TGFβ activity[355]. It has been shown to play a pro-tumorigenic role in multiple cancers including chronic lymphocytic leukaemia, glioblastoma and prostate cancers[355]. Its role in cervical cancer and relationship to OSM-OSMR signalling remains unknown.
PLCB4	Phospholipase C beta 4. The role of PCLB4 in cancer is unclear. In appears to play a pro-oncogenic role in uveal melanoma[356] and gastrointestinal stromal tumours[357] whereas it has been implicated as a tumour suppressor in non-small cell lung cancer (NSCLC)[358]. The role of PLCB4 in cervical cancer and whether it is a target of OSM-OSMR signalling have not been investigated.
PCSK1N	Proprotein convertase subtilisin/kexin type 1 inhibitor, also known as proSAAS. Very little is known about PCSK1N. It has been shown to be a precursor for neuropeptides[359] and may play a role in glucose metabolism[360]. Whether it plays a role in cancer, or is involved in the OSM-OSMR signalling pathway, has not been investigated.
RAB38	RAB38, a ras-related gtp-binding protein, is a member of the small GTPase super family. RAB GTPases mediate vesicle formation, vesicle movement and membrane fusion. RAB38 is believed to contribute to endoplasmic reticulum-related transport[361]. RAB38 has been shown to be expressed in melanoma[362], glioma[363] and pancreatic cancer[364] and is associated with poor prognosis and progression. Its role in cervical cancer is unknown; however, Santin *et al* (2006)[365] identified RAB38 as one of many genes downregulated in cervical carcinoma compared to normal cervical keratinocytes in microarray data. Whether RAB38 expression is modulated by OSM-OSMR signalling has not previously been investigated.
PLAUR	Plasminogen activator, urokinase receptor. PLAUR encodes UPAR, a cell membrane receptor that forms multi-protein complexes with neighbouring transmembrane receptors, such as integrins FPRL-1 and EGFR. It has been shown to be overexpressed in multiple cancers including NSCLC and glioblastoma and plays a role in tumour growth, invasion, angiogenesis and metastasis[366,367]. Moreover, soluble PLAUR has been identified as a plasma biomarker of multiple cancer types including cervical cancer[368]. Interestingly, PLAUR has also been shown to be elevated in EVs from patients with gefitinib-resistant NSCLC[367]. Previous work in our laboratory has shown that PLAUR is overexpressed in cervical SCC tissues with OSMR overexpression and upregulated in cervical SCC cell lines with OSMR overexpression (SW756 and CaSki cells) in response to OSM treatment[121]. OSM has also been shown to induce UPAR expression in endothelial cells leading to increased migration[369].

Validation of sequencing results by qPCR was performed using the same RNA samples that were used for sequencing, i.e. EP cells and KD cells treated with PBS or OSM (n=3) and their resultant EVs (n=5). In addition, qPCR was performed on samples from the additional OSMR KD cell lines generated by the second CRISPR experiment (section 4.9; EP2, KD2 and KD3; n=3) treated with the same experimental design as the other samples. Unfortunately, EV mRNA could not be accurately detected using our standard qPCR pipeline. Therefore, results shown are for cellular mRNA expression only. Levels of OSMR, VEGFA, TGM2 and SNAI1 expression in each cell line, are shown in Figure 5.16. OSMR and VEGFA were found to be significantly upregulated in EP and EP2 cell lines in response to OSM treatment, but not in any of the three KD cell lines. This is consistent with sequencing results and previous work[92,121]. TGM2 and SNAI1 were also upregulated in both EP and EP2 cells in response to OSM; however these changes were not statistically significant (Figure 5.16C+D).

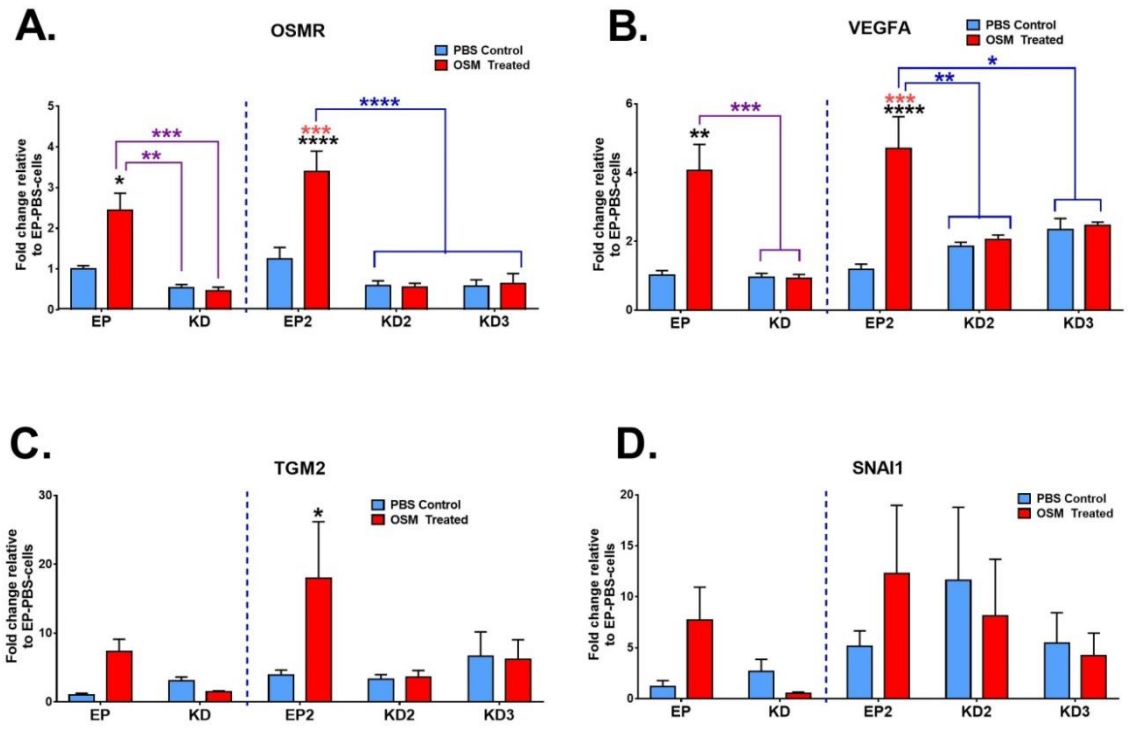

Figure 5.16: Sequencing validation - known OSM-OSMR downstream targets

qPCR for A) OSMR B) VEGFA C) TGM2 and D) SNAI1 expression in Empty Plasmid and OSMR KD SW756 cells (CRISPR1) and Empty Plasmid 2 and OSMR KD 2 and OSMR KD 3 SW756 cells (CRISPR2) in response to OSM. For all cell lines, fold change is shown relative to Empty Plasmid 1 + PBS control. Error bars represent SEM. Values were analysed for statistical significance using a using a one way ANOVA with Tukey's multiple comparison post-hoc tests. P≤0.05 were regarded as significant; * = P≤0.05, ** = P ≤0.01, *** = P≤0.001 and **** = P ≤0.0001. Black stars represent significant change in gene expression compared to Empty Plasmid + PBS (CRISPR1); all other comparisons between groups in CRISPR1 are shown in purple. Red stars represent significant change in gene expression in groups in CRISPR compared to Empty Plasmid 2 + PBS (CRISPR2); all other comparisons between groups in CRISPR2 are shown in blue.

Levels of CHI3L1, CEMIP and PLAUR, which were all found by NGS to be upregulated in EP-cells in response to OSM and downregulated in KD-cells, were subsequently investigated (Figure 5.17A-C). There was no difference in baseline expression of CHI3L1 and CEMIP for any of the cell lines investigated (Figure 5.17A+B). While this was also the case for PLAUR in KD-PBS-cells and KD2-PBS-cells, KD3-PBS-cells were, in fact, found to have elevated baseline levels of PLAUR compared to EP cell lines. CHI3L1, CEMIP and PLAUR were all found to be significantly upregulated in EP and EP2 cell lines in response to OSM; this response was mostly abrogated in KD cells lines. Interestingly, while OSM treatment did not affect PLAUR expression in KD3 cells, baseline levels of PLAUR in this cell line were significantly elevated compared to EP-PBS-cells and EP2-PBS-cells. Level of PLAUR transcription in KD3-PBS-cells was similar to levels observed for EP2-OSM-cells (Figure 5.17C).

Analysis of sequencing data revealed that levels of CPA4 and PTPRR were downregulated in EP-cells in response to OSM treatment. This finding was confirmed by qPCR; in response to OSM treatment, CPA4 expression levels were significantly reduced in EP and EP2 cell lines (Figure 5.17D). Treatment with OSM did not affect CPA4 levels in any of the three KD cell lines. Levels of PTPRR were also downregulated in EP and EP2 cell lines in response to OSM treatment; however, this downregulation was not statistically significant (Figure 5.17E). Moreover, PTPRR appeared to be expressed at higher levels in untreated KD cell lines than EP cell lines; though again this was not statistically significant.

Expression of PLCB4 and RAB38 was then investigated. Neither of these genes was found by NGS to be changed in EP-cells following treatment with OSM though both were upregulated in KD-cells compared to EP-cells. Consistent with NGS results, levels of PLCB4 and RAB38 remained unaltered in EP and EP2 cell lines in response to OSM in qPCR experiments (Figure 5.18A+B) and RAB38 was upregulated in KD-cells treated with either PBS or OSM compared to the paired EP-cells (Figure 5.18B). However, no differences in RAB38 levels were detected in KD2 and KD3 cell lines compared to EP-cells or EP2-cells. PLCB4 was also found to be significantly upregulated in KD-PBS-cells compared to both EP-PBS-cells and EP-OSM-cells (Figure 5.18A) However, no differences in PLCB4 expression were seen in the CRISPR2 cell lines (EP2, KD2 or KD3).

Finally, levels of FMOD and PCSK1N were investigated by qPCR. These genes were downregulated in KD-cells compared to EP-cells in NGS analysis. Similar to NGS results, no difference in FMOD or PCSK1N expression was detected in EP or EP2 cells in response to treatment with OSM (Figure 5.18C+D). Both genes were downregulated in both KD-PBS-

cells and KD-OSM-cells compared to EP-PBS-cells and EP-OSM-cells. However, CRISPR2 cell lines did not behave in the same manner. There was no significant difference in baseline FMOD expression in EP2-cells compared to KD2-cells or KD3-cells. FMOD was, however, reduced in KD3-cells compared to EP-cells (both in the presence and absence of OSM). All CRISPR2 cell lines displayed significantly reduced levels of baseline PCSK1N expression compared to EP-PBS-cells; however, there were no differences in PCSK1N expression between the CRISPR2 cell lines.

While overall these results confirm the expression patterns observed by NGS, they also highlight differences in the cell lines generated from the two CRISPR experiments, especially in regard to genes that were found to be primarily altered in KD cells such as PLCB4, RAB38, FMOD and PCSK1N.

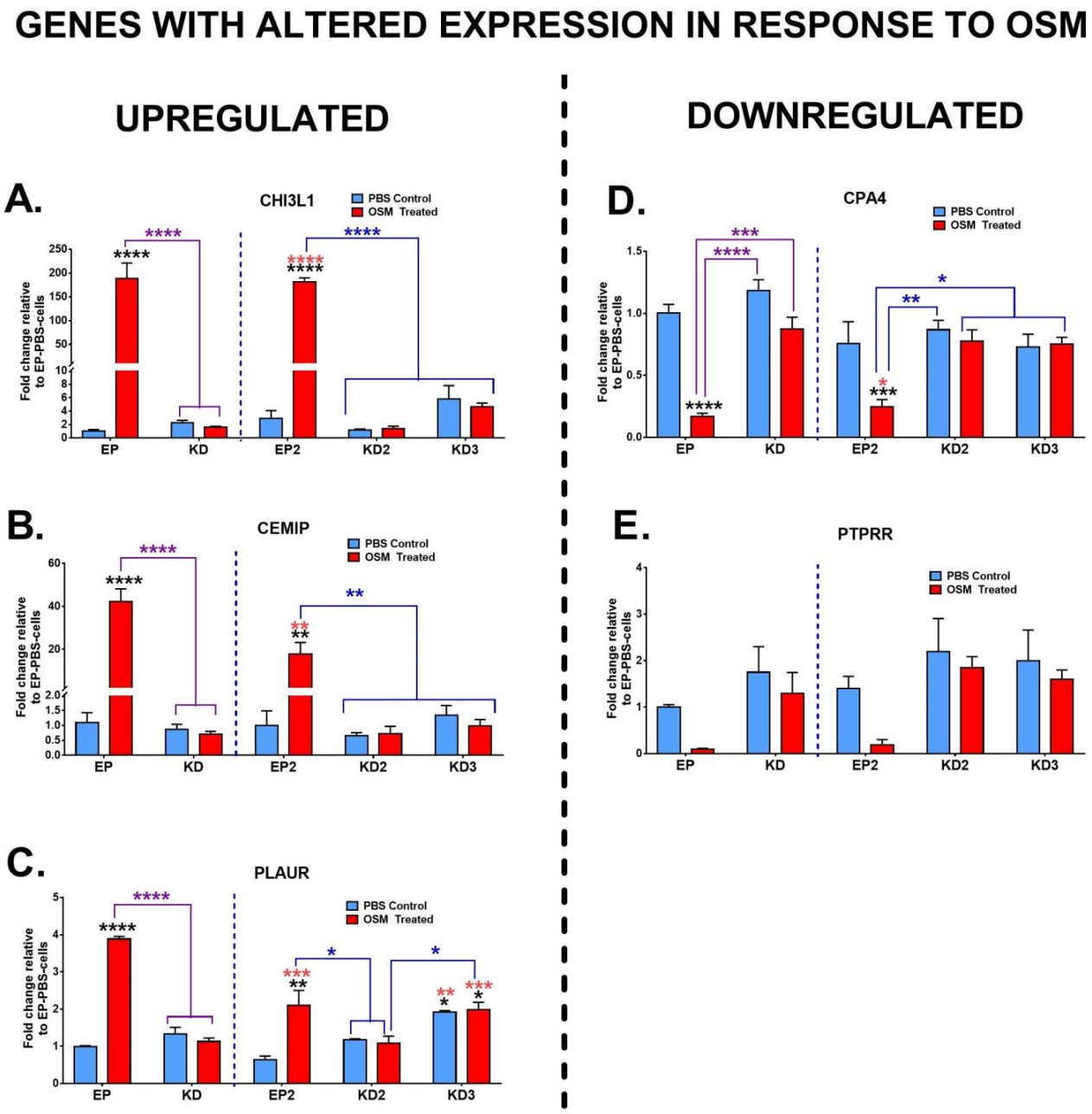

Figure 5.17: Sequencing validation – targets up or downregulated in response to OSM
qPCR for A) CHI3L1 B) CEMIP C) PLAUR D) CPA4 and E) PTPRR expression in Empty Plasmid and OSMR KD SW756 cells (CRISPR1) and Empty Plasmid 2 and OSMR KD 2 and OSMR KD 3 SW756 cells (CRISPR2) in response to OSM. For all cell lines, fold change is shown relative to Empty Plasmid + PBS control. Error bars represent SEM. Values were analysed for statistical significance using a using a one way ANOVA with Tukey's multiple comparison post-hoc tests. $P \leq 0.05$ were regarded as significant; * = $P \leq 0.05$, ** = $P \leq 0.01$, *** = $P \leq 0.001$ and **** = $P \leq 0.0001$. Black stars represent significant change in gene expression compared to Empty Plasmid 1 + PBS (CRISPR1); all other comparisons between groups in CRISPR1 are shown in purple. Red stars represent significant change in gene expression in groups in CRISPR compared to Empty Plasmid 2 + PBS (CRISPR2); all other comparisons between groups in CRISPR2 are shown in blue.

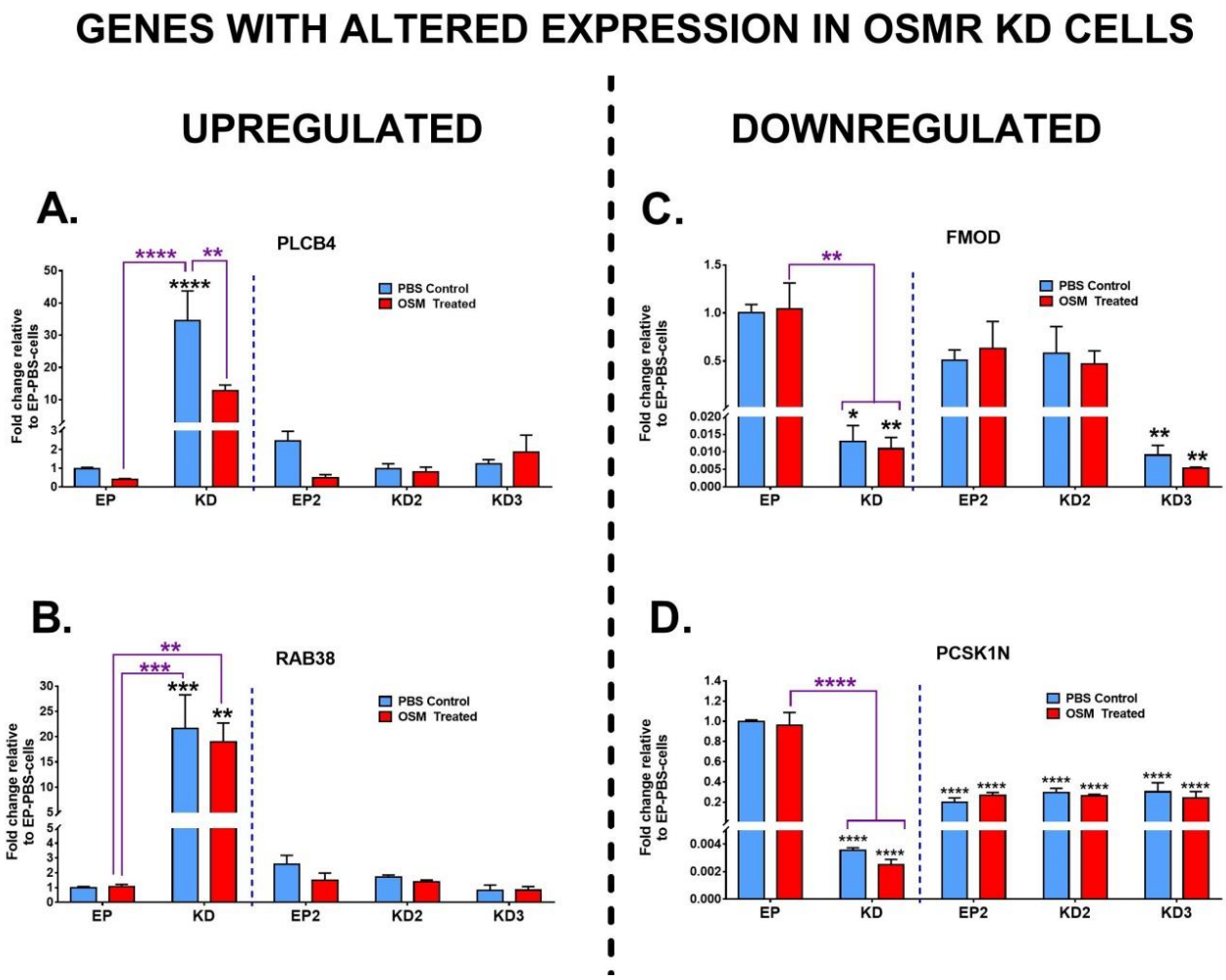

Figure 5.18: Sequencing validation –targets with altered expression OSMR KD cells
qPCR for A) PLCB4 B) RAB38 C) FMOD and D) PCSK1N in Empty Plasmid and OSMR KD SW756 cells (CRISPR1) and Empty Plasmid 2 and OSMR KD 2 and OSMR KD 3 SW756 cells (CRISPR2) in response to OSM. For all cell lines, fold change is shown relative to Empty Plasmid + PBS control. Error bars represent SEM. Values were analysed for statistical significance using a using ANOVA with Tukey's multiple comparison post-hoc tests. P≤0.05 were regarded as significant; * = P≤0.05, ** = P ≤0.01, *** = P≤0.001 and **** = P ≤0.0001. Black stars represent significant change in gene expression compared to Empty Plasmid 1 + PBS (CRISPR1); all other comparisons between groups in CRISPR1 are shown in purple.

5.5.6 TCGA analysis

Having validated some of the most differentially expressed genes that were shown to be potentially involved in OSM-OSMR signalling, their correlation with OSMR or STAT3 expression in clinical cervical SCC samples was investigated to explore the clinical relevance of the observed changes. This was performed using publicly available data from patient cervical SCC samples on TCGA; 251 cervical SCC samples were available for investigation. To account for multiple testing, a p value of ≤0.01 was considered adequate for a significant correlation. This analysis was performed by Dr Stephen Smith.

Of the genes upregulated in response to OSM-OSMR signalling in NGS samples, only CEMIP and PLAUR showed a significant positive correlation with OSMR expression in cervical SCC samples (Figure 5.19). Interestingly, despite being downregulated in KD cells, PCSK1N displayed a significant negative correlation with OSMR expression in TCGA samples. While from the downregulated genes, CPA4, RAB38 and PTPRR were all, unexpectedly, found to have a significant positive correlation with OSMR expression. This was despite being downregulated in EP-cells in response to OSM treatment (CPA4 and PTPRR) or upregulated in KD-OSM-cells compared to EP-OSM-cells (RAB38; Figure 5.20).

Of the genes upregulated in response to OSM-OSMR signalling in NGS samples, CHI3L1 was found to positively correlate, and PCSK1N to negatively correlate with STAT3 expression in cervical SCC samples (Figure 5.21). None of the downregulated genes showed a significant correlation with STAT3 (Figure 5.22).

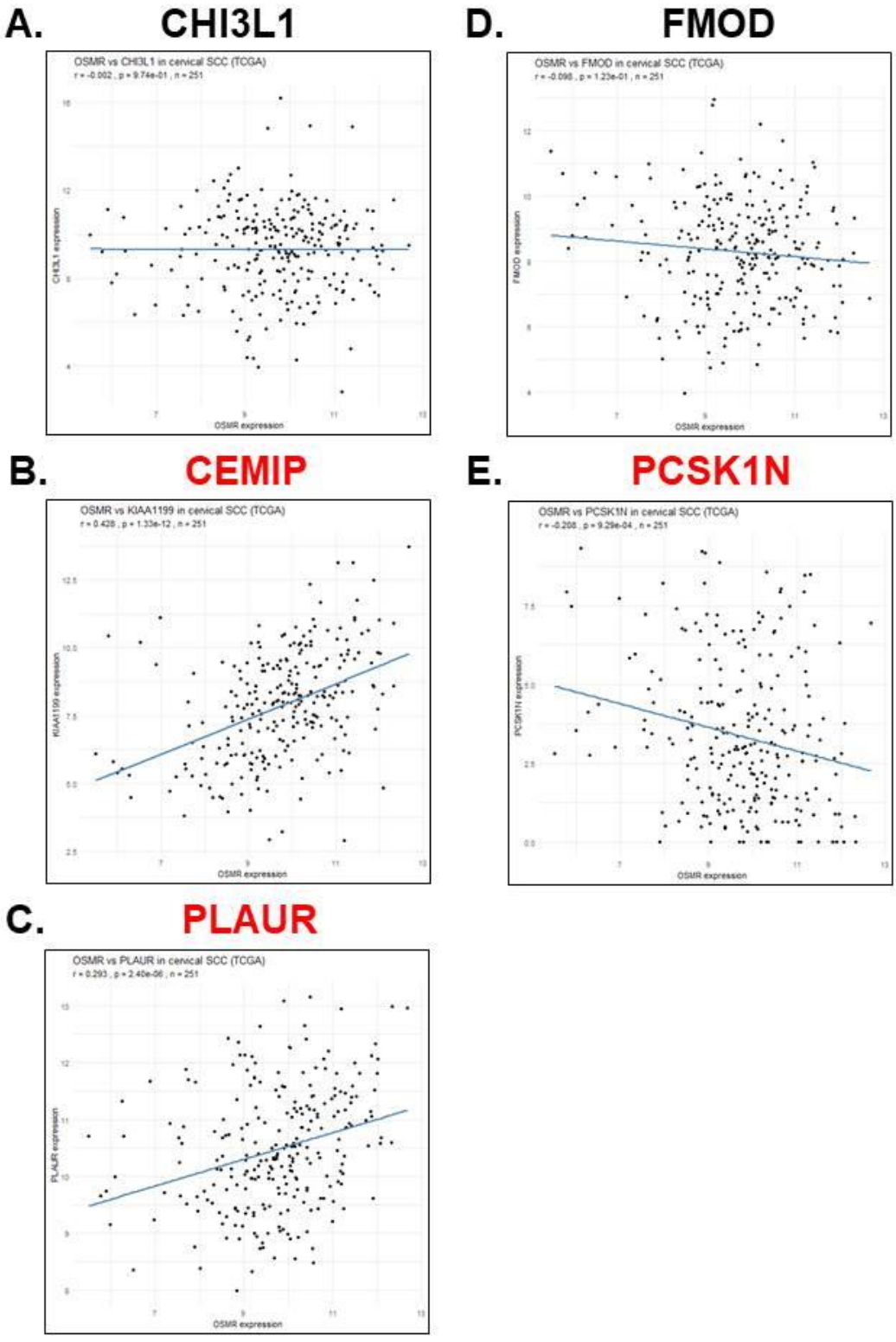

Figure 5.19: OSMR correlation with genes upregulated by OSM-OSMR signalling
TCGA analysis of 251 cervical SCC samples. Correlation of OSMR with A) CHI3L1 B) CEMIP C) PLAUR D) FMOD and E) PCSK1N expression is shown. All of these genes were shown by NGS to be upregulated in response to OSM-OSMR signalling. $p \leq 0.01$ is considered significant. Significant correlations are shown in red.

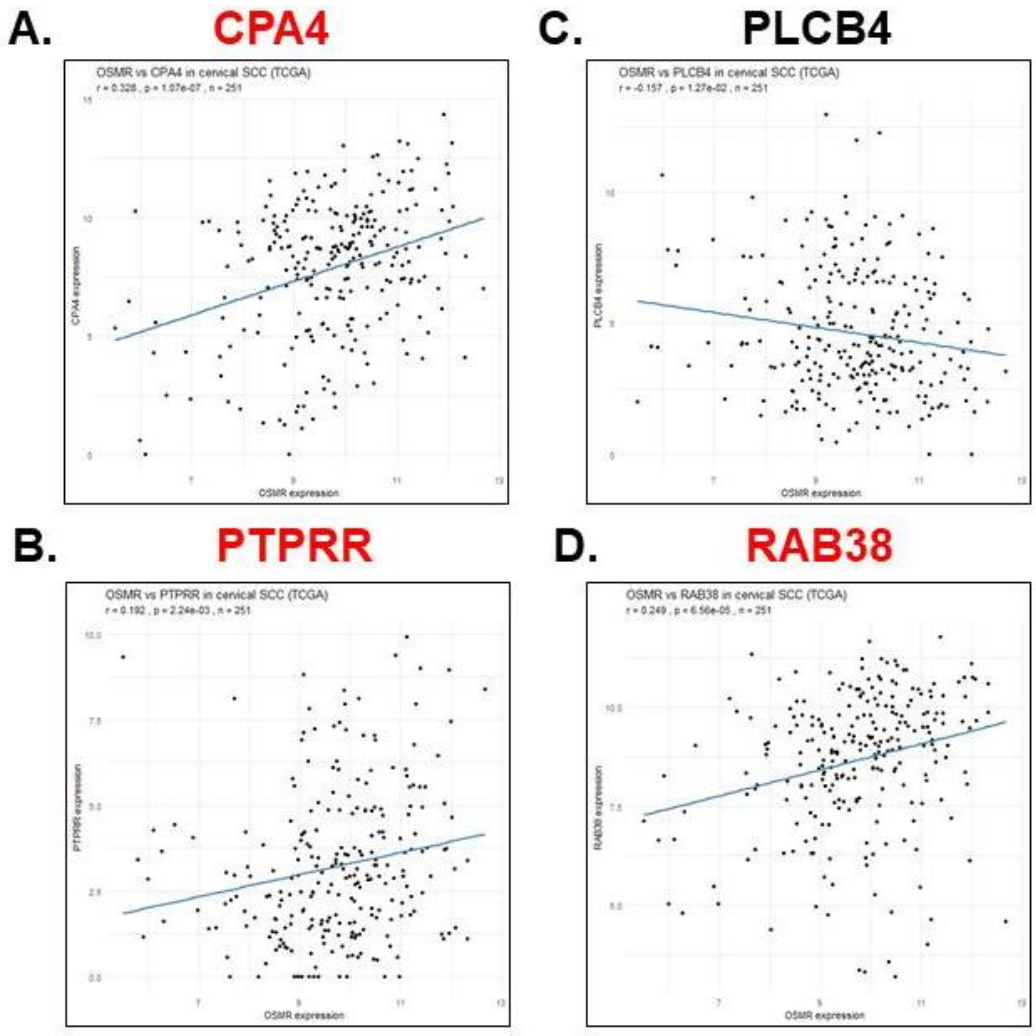

Figure 5.20: OSM correlation with genes downregulated by OSM-OSMR signalling
TCGA analysis of 251 cervical SCC samples. Correlation of OSMR with A) CPA4 B) PTPRR C) PLCB4 and D) RAB38 expression is shown. All these genes were shown by NGS to be downregulated in response to OSM-OSMR signalling. $p \leq 0.01$is considered significant. Significant correlations are shown in red.

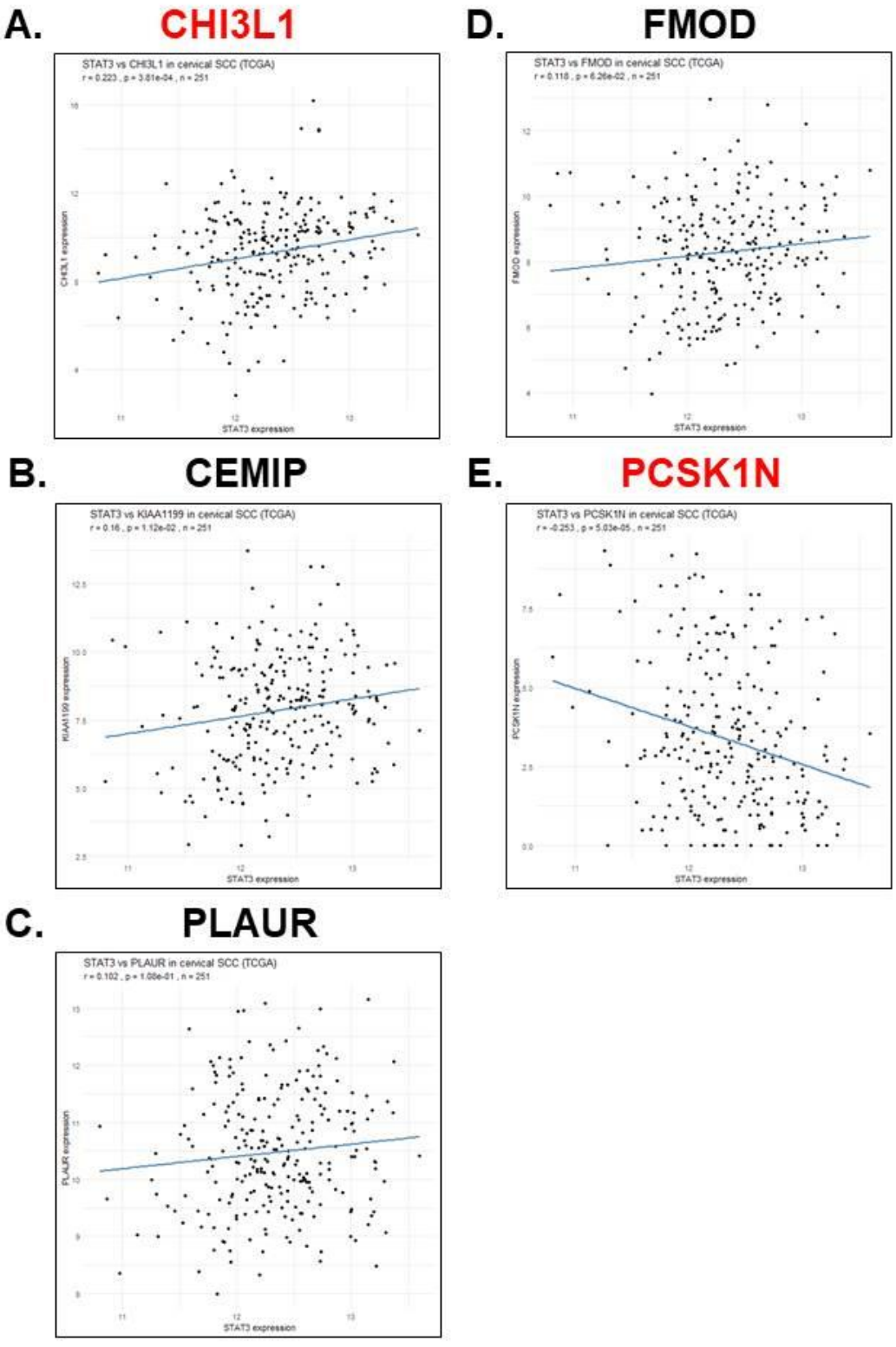

Figure 5.21: STAT3 correlation with genes upregulated by OSM-OSMR signalling
TCGA analysis of 251 cervical SCC samples. Correlation of STAT3 with A) CHI3L1 B) CEMIP C) PLAUR D) FMOD and E) PCSK1N expression is shown. All these genes were shown by NGS to be upregulated in response to OSM-OSMR. $p \leq 0.01$ is considered significant. Significant correlations are shown in red.

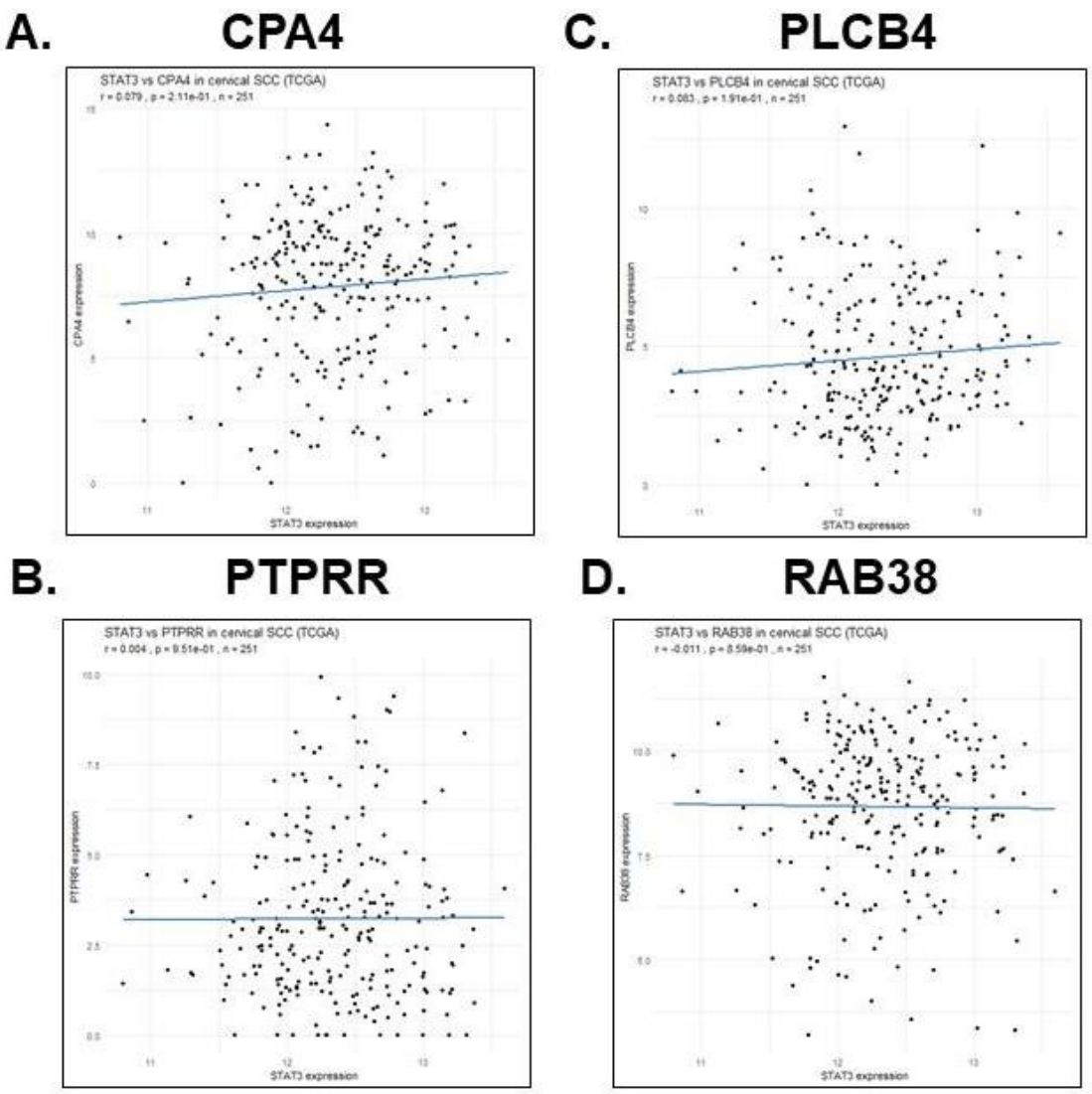

Figure 5.22: STAT3 correlation with genes downregulated by OSM-OSMR signalling

TCGA analysis of 251 cervical SCC samples. Correlation of OSMR with A) CPA4 B) PTPRR C) PLCB4 and D) RAB38 expression is shown. All these genes were shown by NGS to be downregulated in response to OSM-OSMR signalling. $p \leq 0.01$ is considered significant. Significant correlations are shown in red.

5.6 miRNA Sequencing Results

miRNA libraries were prepared using a NEXTFLEX® Small RNA-Seq Kit v3, using the gel free size selection and bead clean up protocol as previously described. 30ng of input RNA was used per sample. Samples were run on a NextSeq500, with a 75 cycles High Output kit, at a final concentration of 1.8pM with 20% PhiX.

5.6.1 Bioinformatic Analysis – sample normalisation and clustering

The bioinformatics performed in this section was performed by Dr Anton Enright, Stephanie Wenlock and Dr Stephen Smith using the pipeline detailed in Table 5.2. All samples passed quality control (data not shown). Raw, pre-normalised counts generated by Chimira are shown in Figure S5. 24A. Samples 1A (EP-PBS-cell, replicate 1), 2D (KD-OSM-cell, replicate 2) and 9D (KD-OSM-EV, replicate 4) had notably lower counts than other samples in the same treatment groups. Chimira analysis revealed that these samples contained a high proportion of reads mapping to spike-in control and low proportion mapping to miRNAs (data not shown). This suggests that library preparation may not have been successful for these samples and they were therefore excluded prior to normalisation.

A DESeq2 normalisation procedure was subsequently applied to the raw counts[223] (Figure S5. 24B). Sample clustering is shown by heatmap (Figure S5. 24C) and t-SNE plot (Figure S5. 24). As seen for mRNA, cells and EVs appeared to cluster separately, consistent with the predicted differences between cellular and EV miRNA cargos. Similar patterns of clustering were observed for both cells and EVs in response to treatments. KD-PBS and KD-OSM were tightly clustered, showing little difference between these two groups. EP-OSM clustered separately from KD-PBS or KD-OSM.

Differential miRNA expression was investigated for the comparisons shown in Table 5.5 (same comparisons as performed for analysis of mRNA expression) using a LFC threshold of +/-0.5 and a FDR significance threshold of ≤0.05. Scatterplots were produced to compare median counts for all six comparisons for both cells and EVs. As with mRNA analysis, the two key comparisons to demonstrate differences in OSM-OSMR signalling in both cells and EVs were EP-PBS versus EP-OSM and EP-OSM versus KD-OSM (Figure 5.23). All other comparisons performed are shown in Figure S5. 25 (cells) and Figure S5. 26 (EVs). Differences in miRNA expression for each set of comparisons were also visualised using volcano plots. Volcano plots for the two main comparisons are shown in Figure 5.24. All other comparisons performed are shown in supplementary figures: cells (Figure S5. 27) and EVs (Figure S5. 28).

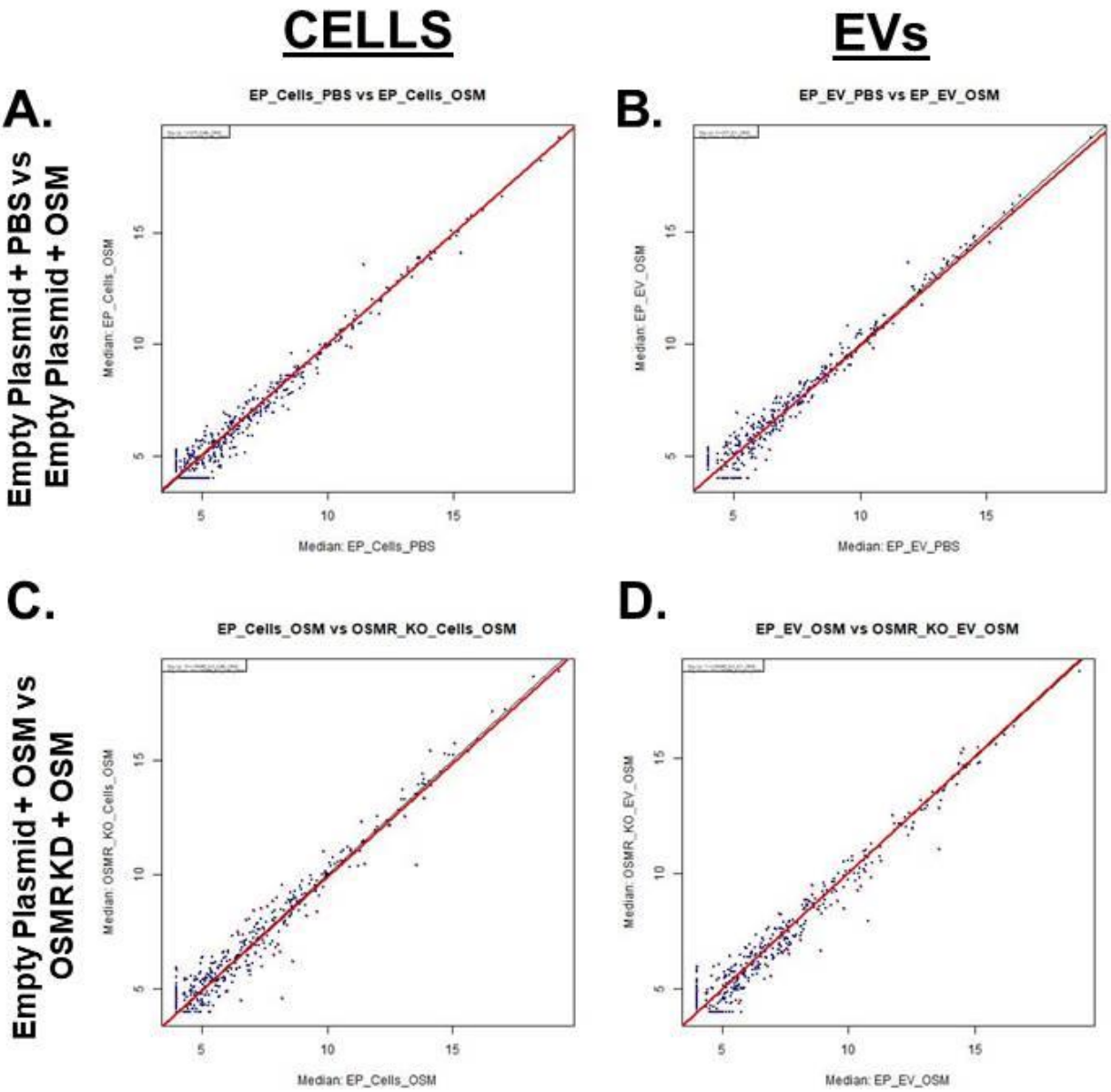

Figure 5.23: miRNA scatterplots
Correlation plots of differential gene expression for:
A) EP-PBS-cells versus EP-OSM-cells
B) EP-PBS-EVs versus EP-OSM-EVs
C) EP-OSM-Cells versus KD-OSM-cells
D) EP-OSM-EVs versus KD-OSM-EVs
miRNA with significant differential expression (≥+/-0.5 LFC; FDR ≤0.05) are shown in red. All other genes are shown in blue.

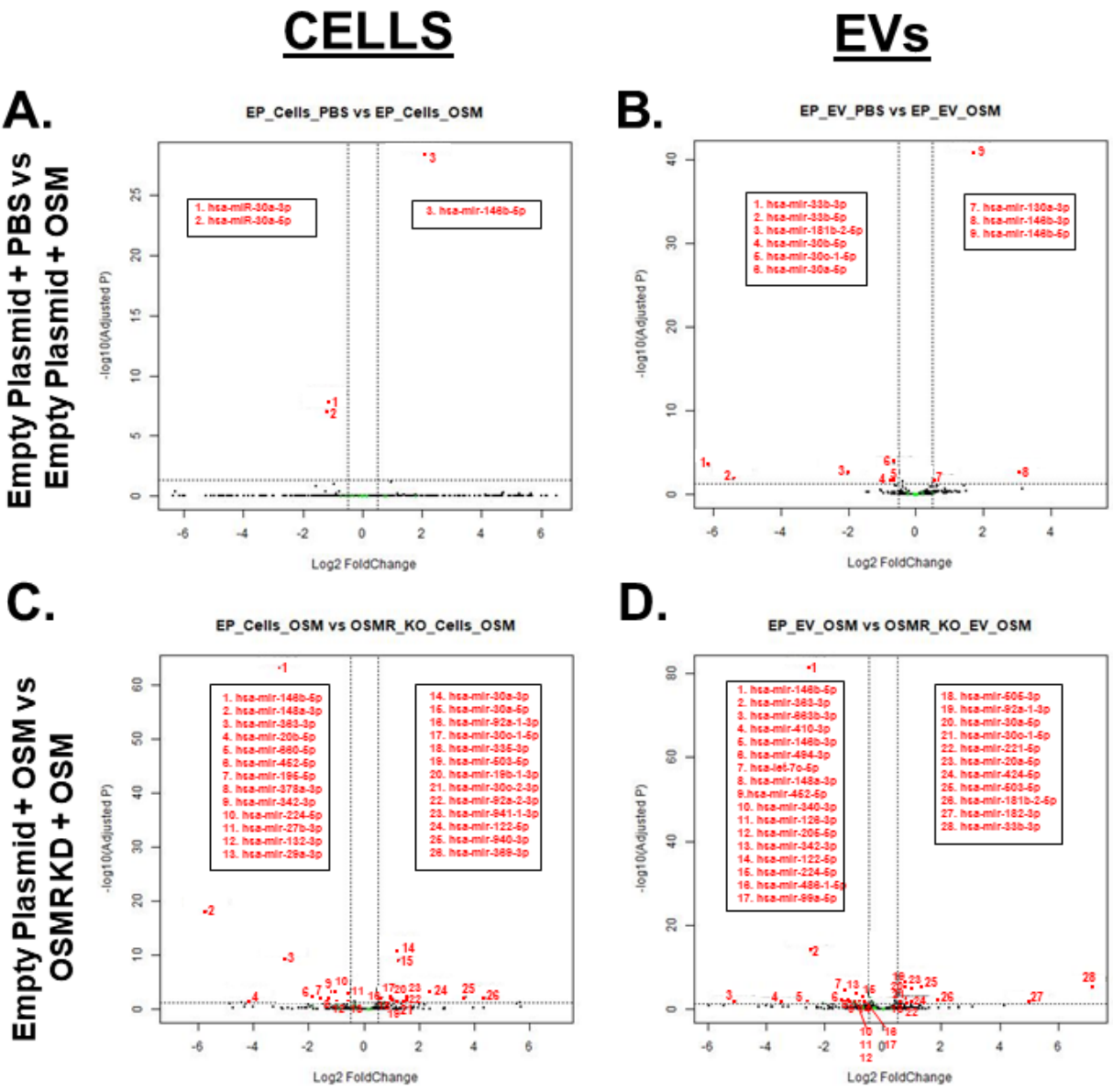

Figure 5.24: miRNA Volcano Plots

Volcano plots of differential gene expression for:
A) EP-PBS-cells versus EP-OSM-cells
B) EP-PBS-EVs versus EP-OSM-EVs
C) EP-OSM-Cells versus KD-OSM-cells
D) EP-OSM-EVs versus KD-OSM-EVs
miRNA with significant differential expression (≥+/-0.5 LFC; FDR ≤0.05) are shown in red. All other genes are shown in black. Top 50 most significantly changed mRNA are labelled

Surprisingly, very few miRNAs were found to be altered in EP cells and EVs in response to treatment with OSM. More miRNAs were significantly altered in KD cells and EVs compared to EP cells and EVs; however, significantly changed miRNAs were fewer than expected, particularly as the preliminary qPCR experiments described in chapter 4 had suggested multiple changes following OSM-OSMR interaction. The numbers of miRNAs with differential expression for each comparison are shown in Table 5.11. In general, more miRNAs were differentially expressed in EVs than in cells. EP-OSM versus KD-OSM was the comparison that produced the greatest number of differentially expressed in miRNAs for both cell and EV comparisons.

Table 5.11: Number significantly altered miRNA per comparison

COMPARISON	CELLS v CELLS		EVs v EVs	
	UP REGULATED	DOWN REGULATED	UP REGULATED	DOWN REGULATED
EP-PBS versus EP-OSM	1	2	3	6
EP-PBS versus KD-PBS	2	9	3	11
EP-PBS versus KD-OSM	4	8	5	9
EP-OSM versus KD-PBS	8	13	11	17
EP-OSM versus KD-OSM	13	13	11	17
KD-PBS versus KD-OSM	1	0	0	0

5.6.2 Comparison of cellular and EV miRNA expression

Similarities and differences in cellular and EV miRNA expression profiles for each of the comparisons shown in Table 5.12 were visualised by Venn diagram using Venn Diagram Plotter software (Pacific Northwest National Laboratory, omics.pnl.gov; Figure 5.25).

Table 5.12: Summary of data shown in Venn diagrams (miRNA)

	Cell-Cell comparisons	EV-EV comparisons	For each pair of comparisons Venn Diagram shows
1.	EP-PBS-cells versus EP-OSM-cells	EP-PBS-EVs versus EP-OSM-EVs	• miRNAs that were commonly up or down regulated in both cell and EV comparisons (i.e. commonly DE miRNA in both cell and EVs) • miRNAs that were up or down downregulated in cell-cell or EV-EV comparisons only (i.e. miRNA with DE unique to either cells or EVs)
2.	EP-PBS-cells versus KD-PBS-cells	EP-PBS-EVs versus KD-PBS-EVs	
3.	EP-PBS-cells versus KD-OSM-cells	EP-PBS-EVs versus KD-OSM-EVs	
4.	EP-OSM-cells versus KD-PBS-cells	EP-OSM-EVs versus KD-PBS-EVs	
5.	EP-OSM-cells versus KD-OSM-cells	EP-OSM-EVs versus KD-OSM-EVs	

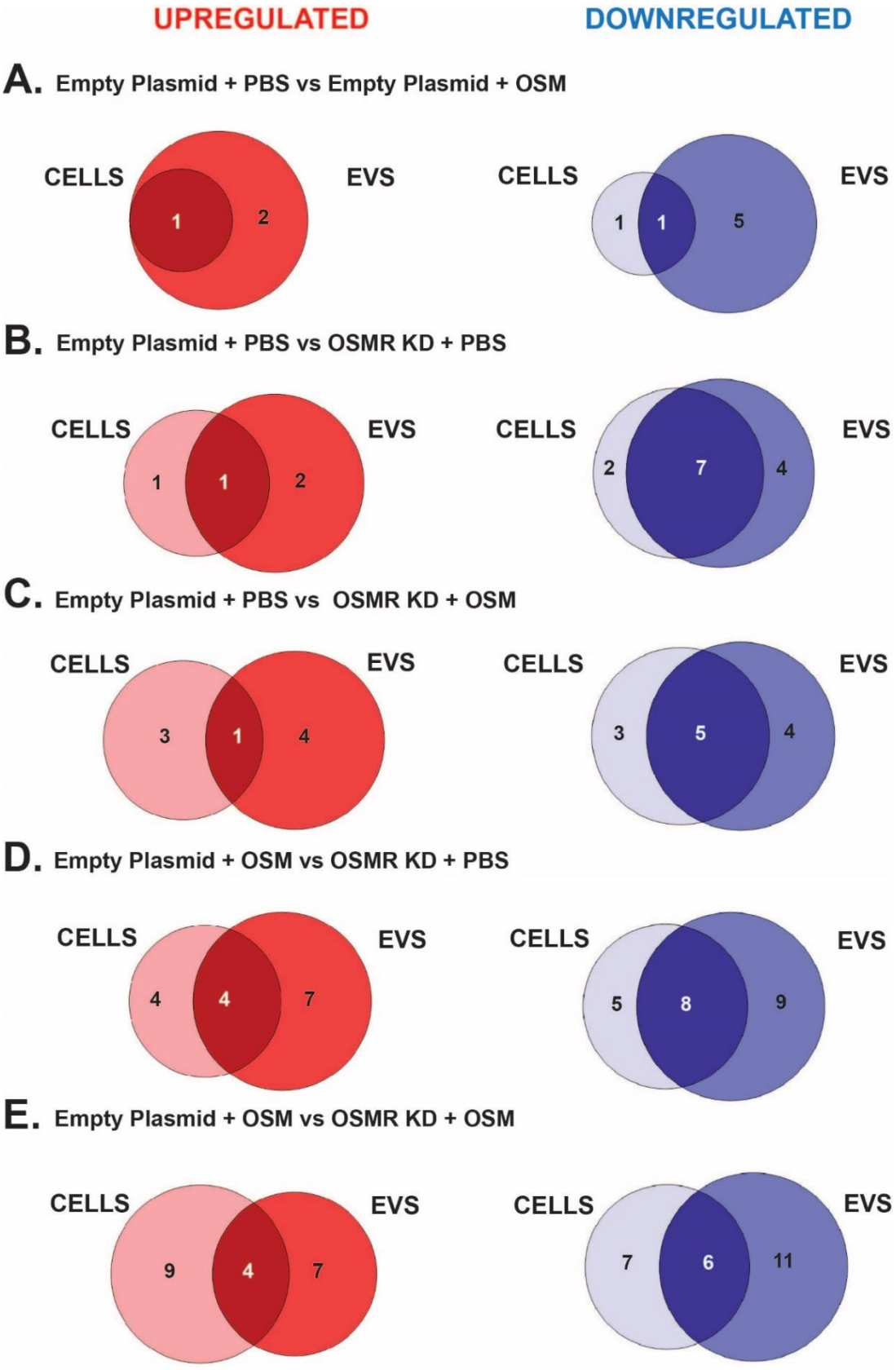

Figure 5.25: Comparison of Cells and EV miRNA
Comparison of miRNA with significant ($p \leq 0.05$) up or down regulation in cells and EVs from each treatment group.

For all comparisons investigated, overlapping cohorts of genes were found to be up or down regulated in both cells and EVs. While the low number of differentially expressed miRNAs led us to question whether there were technical issues with library preparation, the overlap of differentially expressed miRNAs in both cell and EV comparisons suggests that these miRNAs could be biologically relevant.

All miRNAs with significantly altered expression levels in the two key comparisons are shown in Table 5.13. Results for all other comparisons are shown in Table S5. 2 (cell-cell comparisons) and Table S5. 3 (EV-EV comparisons). miRNAs that were found to be differentially regulated in both cells and EVs for the EP-PBS versus EP-OSM and EP-OSM versus KD-OSM comparisons were selected for further investigation. Mir-146b-5p, mir-148a-3p, mir-224-5p, mir-342-3p, mir-363-3p and hsa-mir-452-5p were upregulated in response to OSM-OSMR signalling, whereas mir-30a-5p, mir-30c-1-5p, mir-92a-1-3p and mir-503-5p were considered to be downregulated in response to OSM-OSMR signalling.

Table 5.13: miRNA with significantly altered expression

miRNAs that were up or down regulated in both cells and EVs for the same comparison were colour coded :
Empty plasmid + PBS vs Empty plasmid + OSM: red = upregulated, blue = downregulated
Empty plasmid + OSM vs OSMR KD + OSM: green = upregulated, purple = downregulated

		UPREGULATED			DOWNREGULATED		
		miRNA	log2FC	adjusted P value	miRNA	log2FC	adjusted P value
EP-PBS versus EP-OSM	CELL vs CELL	hsa-mir-146b-	2.09	4.41×10^{-29}	hsa-mir-30a-5p	-1.20	8.14×10^{-8}
					hsa-mir-30a-3p	-1.14	1.44×10^{-8}
	EV vs EV	hsa-mir-146b-	3.10	3.01×10^{-3}	hsa-mir-33b-3p	-6.13	3.18×10^{-4}
		hsa-mir-146b-	1.71	1.80×10^{-41}	hsa-mir-33b-5p	-5.40	0.014
		hsa-mir-130a-	0.54	0.025	hsa-mir-181b-2-	-2.01	3.95×10^{-3}
					hsa-mir-30b-5p	-0.71	0.023
					hsa-mir-30c-1-	-0.65	0.023
					hsa-mir-30a-5p	-0.64	1.75×10^{-4}
EP-OSM versus KD-OSM	CELL vs CELL	hsa-mir-369-3p	4.40	0.012	hsa-mir-148a-	-5.68	6.73×10^{-19}
		hsa-mir-940-3p	3.69	6.04×10^{-3}	hsa-mir-20b-5p	-4.12	0.032
		hsa-mir-122-5p	2.41	7.52×10^{-4}	hsa-mir-146b-	-3.07	7.21×10^{-64}
		hsa-mir-941-1-	1.56	7.19×10^{-3}	hsa-mir-363-3p	-2.81	6.78×10^{10}
		hsa-mir-92a-2-	1.54	0.019	hsa-mir-660-5p	-2.05	0.012
		hsa-mir-30c-2-	1.49	0.032	hsa-mir-452-5p	-1.85	2.50×10^{-3}
		hsa-mir-30a-5p	1.30	7.35×10^{-10}	hsa-mir-195-5p	-1.50	6.04×10^{-3}
		hsa-mir-30a-3p	1.28	1.27×10^{-11}	hsa-mir-378a-	-1.27	0.011
		hsa-mir-19b-1-	1.23	0.037	hsa-mir-342-3p	-1.17	7.52×10^{-4}
		hsa-mir-503-5p	1.07	0.024	hsa-mir-224-5p	-0.99	7.96×10^{-4}
		hsa-mir-30c-1-	1.02	6.04×10^{-3}	hsa-mir-132-3p	-0.95	0.024
		hsa-mir-335-3p	1.01	0.011	hsa-mir-29a-3p	-0.56	0.022
		hsa-mir-92a-1-	0.66	6.04×10^{-3}	hsa-mir-27b-3p	-0.52	6.04×10^{-3}
	EV vs EV	hsa-mir-33b-3p	7.16	9.06×10^{-6}	hsa-mir-663b-	-5.06	0.017
		hsa-mir-182-3p	5.05	0.041	hsa-mir-410-3p	-3.49	0.041
		hsa-mir-181b-2-	1.88	0.011	hsa-mir-146b-	-2.59	0.017
		hsa-mir-503-5p	1.34	9.26×10^{-6}	hsa-mir-146b-	-2.55	6.84×10^{-82}
		hsa-mir-20a-5p	0.99	4.13×10^{-5}	hsa-mir-363-3p	-2.48	1.21×10^{-14}
		hsa-mir-424-5p	0.97	0.033	hsa-mir-494-3p	-1.39	9.51×10^{-3}
		hsa-mir-221-5p	0.81	0.046	hsa-let-7c-5p	-1.36	5.75×10^{-5}
		hsa-mir-30c-1-	0.77	4.30×10^{-3}	hsa-mir-148a-	-1.15	0.017
		hsa-mir-92a-1-	0.76	8.05×10^{-7}	hsa-mir-452-5p	-1.09	0.023
		hsa-mir-30a-5p	0.76	5.21×10^{-6}	hsa-mir-340-3p	-1.00	0.017
		hsa-mir-505-3p	0.62	0.015	hsa-mir-126-3p	-0.98	0.045
					hsa-mir-205-5p	-0.95	0.036
					hsa-mir-342-3p	-0.90	2.00×10^{-4}
					hsa-mir-122-5p	-0.80	0.013
					hsa-mir-224-5p	-0.68	2.09×10^{-3}
					hsa-mir-486-1-	-0.65	0.012
					hsa-mir-99a-5p	-0.61	0.034

5.6.3 TCGA analysis

To explore the clinical significance of these miRNAs, the correlation between the ten miRNAs selected for further investigation and OSMR or STAT3 expression in clinical cervical SCC samples were investigated. This was performed by Dr Stephen Smith and, as for the mRNA analysis, data from 251 cervical SCC samples collected in the TCGA database were utilised. To account for multiple testing, a p value of ≤0.01 was considered adequate for a significant correlation.

Of the miRNAs overexpressed in response to OSM-OSMR signalling in NGS samples (Figure S5. 29), only miR-363 was found to have a significant correlation with OSMR; however, the levels of miR-363 were unexpectedly found to negatively correlate with OSMR (Figure S5. 29E). None of the miRNAs that were down-regulated in response to OSM-OSMR signalling were found to correlate with OSMR expression in cervical SCC samples (Figure S5. 30). Moreover, of the miRNAs investigated, none displayed expression that correlated with STAT3 expression in cervical SCC samples (Figure S5. 31 and Figure S5. 32).

5.6.4 qPCR validation of miRNA sequencing results

As experiments described in Chapter 4 had identified some miRNAs that changed significantly following treatment with OSM, it was expected that at least some of these miRNAs would be differentially expressed in the NGS samples. However, none of these miRNAs were found to display differential gene expression in any of the cell-cell comparisons. Only MiR-126-3p was found to be significantly downregulated in KD-OSM-EVs compared to EP-OSM-EVs (Figure 5.26D panel ii).

The low number of differentially expressed miRNAs in the NGS dataset, and the lack of consistency between NGS results and previous qPCR findings, raised the possibility that the NGS data may not accurately reflect the true impact of OSM-OSMR signalling on differential miRNA expression. To try to address the inconsistencies between the original experiment described in chapter 4 and the NGS results, four of the miRNAs previously found to be upregulated in WT-OSM-EVs were investigated by qPCR in the sample sets used for NGS. Interestingly, qPCR analysis of the cell samples used for sequencing confirmed previous findings that miR9-3p, miR-23b, miR-29b and miR-126 were significantly upregulated in EP-OSM-cells (Figure 5.26). Moreover, miR9, miR-23b and miR-126 were all found to be significantly downregulated in KD-cells. qPCR validation could not be performed on EV samples as not enough material remained following NGS.

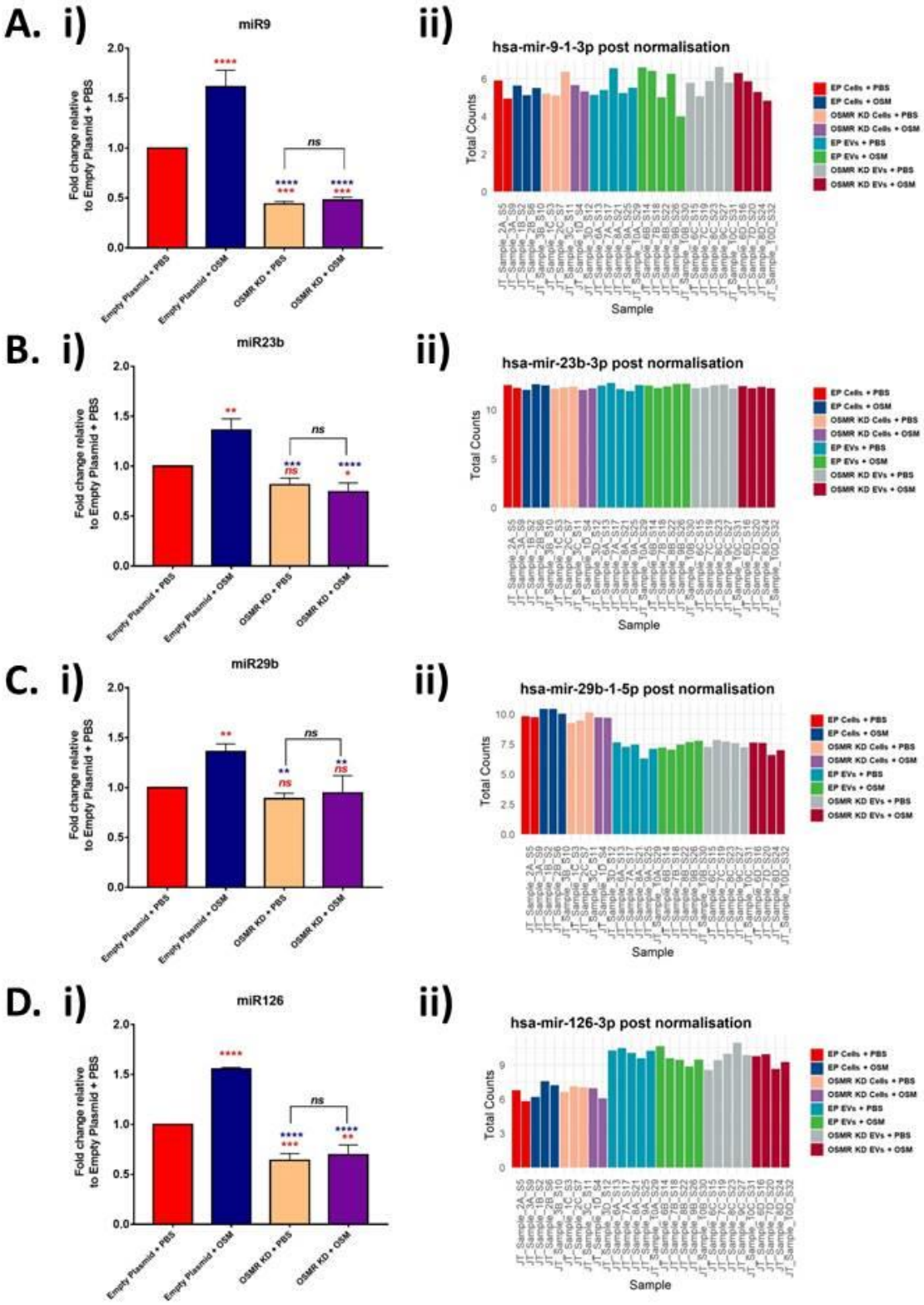

Figure 5.26: miRNA validation

Comparison of i) qPCR and ii) NGS sequencing results for A) miR-9, B) miR-23b, C) miR-29b and D) miR-126 expression in EP and KD SW756 cells treated for 48 hours with OSM or PBS control. Levels of these miRNA in EV samples are also shown for NGS analysis. qPCR Values were analysed for statistical significance using a using a one way ANOVA with Tukey's multiple comparison post-hoc tests. P≤0.05 were regarded as significant; * = P≤0.05, ** = P ≤0.01, *** = P≤0.001 and **** = P ≤0.0001. Stars are colour coded to convey which comparisons were significant.

5.7 Chapter discussion and summary

5.7.1 mRNA Sequencing – bioinformatic analysis

Next generation sequencing of cervical SCC cell and EV content is reported in this chapter. As expected, protein coding genes represented the main RNA type in all samples prepared with the mRNA library preparation kit and a higher proportion of reads were found to map to protein coding genes in cell samples compared to EVs. This is consistent with previous studies which have demonstrated enrichment of lncRNAs, antisense RNAs and transcripts derived from pseudogenes in EVs[370–372]. Heatmaps and tSNE plots of normalised counts revealed that cell and EV samples from all treatment groups appeared to cluster separately, which is consistent with the inherent differences between cellular and EV cargo which are independent of OSMR expression or OSM treatment. Reassuringly, for both cells and EVs, EP-OSM clustered separately from KD-PBS or KD-OSM, while EP-PBS constituted a third cluster.

There is no gold standard for which statistical package performs best for analysis of mRNA sequencing data[335]. Therefore, combining analysis from multiple approaches and selecting genes that are found to be differentially regulated across different statistical packages for further investigation, is considered an optimum way of obtaining the most reliable and accurate results. Therefore, we applied these principles to our investigations. Differential mRNA expression was investigated using three different statistical packages: DeSeq2, EdgeR and EdgeR voom. Statistical methods were consistent with one another when used to rank which cell-cell and EV-EV comparisons had the greatest amount of differential gene expression.

Previous studies have shown that DESeq2 and EdgeR perform similarly, owing to the fact that they share analogous statistical models[335,336]. The analysis reported here for cell-cell comparisons are in agreement with these findings. Interestingly DESeq2 is thought to be more conservative than EdgeR[335,336], though we found that EdgeR appeared to be the most conservative of the three analysis methods. For EV-EV comparisons, the statistical package detecting the most differentially expressed genes varied between comparisons. This could potentially be due to the fact that expression levels are lower in EVs compared to cells, and are, therefore, likely to display differences in dispersion, which was one of the parameters used for statistical analysis. Inconsistency between comparisons drove the decision to select only genes for further investigation that were found to be differentially expressed by all three analysis methods, as these are most likely to represent true biological variations. There was

a substantial overlap in the genes identified by the three packages for all comparisons performed.

5.7.2 mRNA Sequencing – overview of results

Treatment of OSMR overexpressing EP SW756 cells with OSM led to global changes in gene expression in both the cells and their resultant EVs. Similarly, OSMR KD cells and their EVs displayed markedly different basal expression profiles compared to EP cells and EVs, respectively. As expected, comparison of EP-OSM and KD-OSM produced the greatest number of disparately expressed genes in both cell and EV comparisons. Whereas, treatment of KD cells with OSM did not lead to significant changes in gene expression in either cells or EVs. Together, these results are consistent with previous qPCR results (detailed in Chapter 4) which demonstrated that OSM activated expression of downstream targets of OSM-OSMR signalling in EP-cells but not KD-cells. If OSM signalled through LIFR we would still expect to see changes in gene expression in response to OSM treatment in OSMR KD cells. Therefore, the current experiment corroborates previous findings from our research group that OSM predominantly signals via OSMR and not LIFR in SW756 cells[92]. Moreover, these results demonstrate for the first time that OSM-OSMR signalling is capable of altering the mRNA cargo of EVs released from cervical SCC cells.

Interestingly, while there was overlap between genes that were up or down regulated in both cells and EVs in response to OSM treatment or OSMR knockdown, the number of genes found to be differentially expressed varied between cells and EVs for each comparison. For example, when comparing EP-OSM and KD-OSM, more genes were found to be significantly downregulated (543) than upregulated (216) in the KD-OSM-cells, whereas more genes were upregulated (847) than downregulated (212) in KD-OSM-EVs. However, pathway analysis revealed that, in response to OSM-OSMR signalling, transcriptional changes in both cells and EVs contributed to over or under representation of similar pathways. This indicates that, while the EV cargo reflects transcripts which were differentially expressed in the cell of origin in response to OSM-OSMR signalling, individual mRNAs can be selectively packaged into EVs. This is consistent with previous findings that transcripts can be exclusively expressed by EVs[169,373], or differentially enriched compared to their cells of orgin[169,373,374], which is indicative of selective mRNA packaging into EVs. In the current investigation differentially expressed genes were defined as having a LFC threshold of +/-0.5 and a FDR significance threshold of ≤ 0.01. Therefore, it is possible that if a less stringent FDR was used (e.g. ≤ 0.05) there may be greater overlap in the genes found to be differentially expressed when comparing cell-cell and EV-EV comparisons.

In EP cells and EVs, treatment with OSM led to: upregulation of pathways involved in cytokine mediated signalling, myeloid leucocyte activation, hypoxia signalling, interferon signalling, negative regulation of viral life cycle and angiogenesis. Similar pathways were found to be downregulated in both cells and EVs following OSMR KD. On the other hand, OSM treatment resulted in: downregulation of pathways involved in PI3K-AKT signalling, tissue remodelling, negative regulation of differentiation and focal adhesion in EP cells. Some of these pathways were also upregulated in KD cells. Thus, similar pathways were found to be over represented in response to OSM-OSMR signalling in EP cells and EVs and under represented following OSMR KD (and vice versa). For most comparisons, pathways found to be up or down regulated in the EVs closely mirrored their cells of origin. However, pathways that were downregulated in EP EVs in response to OSM differed from those described for the corresponding cell-cell comparison. Pathways involved in cell cycle regulation and regulation of division and cellular organisation were downregulated in EVs in response to OSM. Similar pathways were upregulated in KD EVs compared to EP EVs.

As expected, pathways implicated in cellular response to OSM-OSMR signalling in the current NGS experiments were similar to those identified in previous experiments by our research group. These experiments used microarray to investigate gene expression in SW756 and CaSki cells (another OSMR overexpressing cervical SCC cell line) at various timepoints following OSM treatment[121]. The same technique was also used to compare gene expression in cervical SCC clinical samples deemed to have OSMR overexpression. The key pathways identified by microarray to be altered in clinical samples and in both cell lines in response to OSM treatment were related to: increased cell migration and invasion, angiogenesis, signal transduction and apoptosis[121]. It is, therefore, reassuring that the results from the current study are consistent with these findings. One of the main differences between these studies was that apoptosis was not found to be a key pathway altered in response to OSM-OSMR signalling in the current investigation. This is consistent with experiments conducted to validate microarray pathway analysis; treatment of SW756 and CaSki cells with OSM had no effect on the cell cycle or number of apoptotic cells[121].

The current study corroborated previous microarray results, and identified similar genes and pathways found to be differentially expressed in OSMR overexpressing cells in response to OSM treatment. However, it also demonstrated that removal of OSMR (via CRISPR-Cas9 mediated KD) led to global changes in basal gene expression compared to OSMR expressing EP cells. As these changes occurred in the absence of exogenous OSM, this indicates that OSMR overexpressing cervical SCC cells endogenously produce OSM, which is capable of driving functionally significant OSM-OSMR signalling in an autocrine manner.

This is consistent with previous experiments by our research group in which forced expression of OSMR in cervical SCC cells with low baseline levels of OSMR expression led to increased phosphorylation of STAT3 in the absence of OSM[92]. Similarly, treatment of SW756 cells with anti-OSM antibody led to a significant reduction in the invasive capacity of SW756 cell *in vitro* and reduced lung colonisation following tail vein injection *in vivo*, in the absence of exogenous OSM[92]. Moreover, the results from the current study demonstrate, for the first time, that OSM-OSMR signalling in cervical SCC (either in the presence or absence of endogenous OSM) leads to global changes in EV mRNA cargo.

Microarray platforms require *a priori* knowledge of the query genome and therefore suffer from design bias as they only detect transcripts which hybridise to specific probes selected in the aray[375]. On the other hand, NGS is less biased than microarray, requires no *a priori* knowledge of the genome and facilitates detection of novel transcripts, splice junctions and non coding RNAs[375]. Therefore, the data generated by the current study could be used for subsequent investigations outwith the scope of this thesis, for example investigation of gene splicing in cervical SCC cells and EVs in response to OSM-OSMR signalling.

5.7.3 Pathway analysis

Activation of cytokine mediated signalling was found to be the most enriched pathway in both cells and EVs in response to OSM-OSMR signalling. This is unsurprising given the known role of OSM as pleiotropic cytokine capable of activating STAT, MAPK, PI3K/AKT and SRC/YAP/NOTCH signalling cascades[76,83,84]. Packaging of these signals into EVs is likely to be a mechanism which facilitates the perpetuation of these signalling cascades to other cancer cells or to cells of the TME.

Consistent with the previous array experiments, pathways involved in angiogenesis were upregulated in SW756 cells in response to OSM-OSMR signalling[121]. Interestingly, these pathways did not appear to be upregulated in the EVs, either in response to OSM stimulation or following OSMR KD. In the array experiment, genes involved in angiogenesis were differentially expressed at 4, 12 and 24 hours post OSM treatment, but did not remain activated at the 48 hour timepoint[121]. This indicates that OSM-OSMR signalling has the greatest impact on transcription of genes involved in this pathway at early timepoints following stimulation with OSM. In the current experiment, gene expression was investigated at 48 hours post-treatment with OSM. While genes involved in angiogenesis remained upregulated in cells at this timepoint in response to OSM-OSMR signalling, results from the array experiment suggest that greater activation may have been observed at earlier timepoints. Similarly, it is possible that upregulation of this pathway might have been

observed in EVs at earlier timepoints. In line with this hypothesis, VEGFA - which was previously shown to be the key mediator of OSM-OSMR induced angiogenesis by cervical SCC cells[92,121] - was found to be significantly upregulated in EP EVs in response to OSM treatment, and downregulated in KD EVs compared to EP EVs.

One of the key pathways shown to be upregulated in cells and EVs in response to OSM-OSMR signalling was response to low oxygen conditions (hypoxia). As tumours grow they rapidly outgrow their blood supply, therefore tumours tend to have a significantly lower oxygen concentration than healthy tissues[376]. Hypoxia induces a number of intracellular signalling pathways, most notably the hypoxia-inducible factor (HIF) pathway, involving activation of HIF1α and HIF2α transcription factors (TFs)[376]. These TFs control the expression of numerous target genes involved in angiogenesis (e.g. VEGFA), tissue remodelling (e.g. plasminogen activator inhibitor 1; PAI), metabolism and the cell cycle. As a result, HIFs are considered to master regulators of angiogenesis, an essential process for tumour growth and progression[377–380].

OSM has previously been shown to induce expression of HIF1α in hepatocytes[378], adipocytes, breast cancer associated macrophages[381] and cervical SCC cells[121] under normoxic conditions. Moreover, OSM induced upregulation of HIF-1α has been shown to induce a M2 polarised phenotype in breast cancer associated macrophages; this is associated with pro-tumoural function[381,382]. Recent work in our laboratory has shown that inhibition of HIF-1α in cervical SCC cells results in downregulation of genes involved in matrix remodelling, angiogenesis and metabolic adaptation (Valtteri Tulkki, unpublished). Therefore, in cervical SCC activation of HIF signalling is likely to be one of the key mechanisms by which OSM-OSMR promotes angiogenesis, in addition to direct activation of VEGFA[92,121]. In the current experiment, genes involved in hypoxia signalling were upregulated in both cells and EVs in response to OSM-OSMR signalling. This is consistent with previous findings from the array experiment, in which OSM was shown to induce expression of hypoxia-inducible factor 1 alpha (HIF1α) and hypoxia-inducible factor 2 alpha (HIF2α) in both SW756 and CaSki cells[121].

HIFs and their target genes have previously been reported in extracellular vesicles derived from hypoxic glioblastoma (GBM) and nasopharyngeal carcinoma cells[383,384]. EVs derived from GBM cells are enriched in mRNA from HIF-1α target genes. These EVs were demonstrated to promote angiogenesis and induced endothelial cells to secrete cytokines required for pericyte migration. Moreover, EVs from hypoxic GBM cells were able to promote migration of other GBM cells *in vitro* and promote tumour growth and angiogenesis *in vivo*[383].

Similarly, EVs from nasopharyngeal carcinoma (NPC) cells have been shown to contain functionally active HIF-1α mRNA which promote migration and invasion of NPC cells in vitro, consistent with induction of an EMT phenotype[384]. While we did not observe enrichment of angiogenic pathways in cervical SCC EVs, upregulation of HIF and HIF inducible genes in EVs may be a mechanism by which cervical SCC interact with cells of the TME to promote angiogenesis via stimulation of angiogenic pathways in recipient cells (rather than transfer of pro-angiogenic factors). Therefore, it would be interesting to repeat the angiogenesis assay (detailed in chapter 4) using EP-EVs and KD-EVs isolated from cells at a range of timepoints following treatment with PBS or OSM (using continuous treatment, rather than a 2hour pulse as previously performed).

In addition, myeloid leucocyte activation was found to be another key pathway upregulated in cells and EVs in response to OSM-OSMR signalling. Myeloid leucocytes include tumour associated macrophages, myeloid-derived suppressor cells (MDSCs), dendritic cells, monocytes and tumour associated neutrophils[385]. Tumour cells hijack the capacity of myeloid cells to produce inflammatory mediators, growth factors involved in tumour proliferation and angiogenesis and enzymes that degrade matrix proteins[386]. Furthermore, they take advantage of myeloid cells' ability to regulate T cell response, thus creating an immunosuppressive microenvironment[386]. Immune cells are the main source of OSM within the tumour microenvironment. OSM secretion has been shown to attract neutrophils and macrophages to tumour sites, which in turn produce more OSM, and promote M2 polarisation and tumour progression[387]. The current findings implicate that, in response to OSM-OSMR signalling, EVs released from cervical SCC cells could be key mediators of these processes. In order to elucidate the functional impacts of enrichment of this pathway, functional assay will need to be performed. For example, EP-EVs and KD-EVs from cells treated with PBS or OSM could be added to macrophages in order to investigate whether EVs mediated leucocyte activation and HIF-1α induced polarisation. This could be achieved by subsequent qPCR for M2 markers expression, such as Arg-1 and COX-2, in treated cells[382].

5.7.4 mRNA Sequencing – sequencing validation

Genes that were found to be highly up or downregulated in SW756 cells and EVs in response to OSM-OSMR signalling were selected for validation by qPCR. These genes included CHI3L1, CEMIP, CPA4, PTPRR, FMOD, PLCB4, PCSK1N and RAB38. Unfortunately, EV mRNA could not be accurately detected using our standard qPCR pipeline, therefore future experiments will use a reverse transcription kit specifically designed

for amplification of low input RNA samples, such as the SuperScript™ II Reverse Transcriptase kit (Invitrogen)[388].

Levels of CHI3L1, CEMIP and PLAUR were all found by NGS to be upregulated in EP-OSM cells and EVs compared to EP-PBS cells and EVs. Moreover, all three were downregulated in KD-OSM cells and EVs compared to EP-OSM cells and EVs, respectively. These findings were corroborated by qPCR. PLAUR has previously been shown to be overexpressed in cervical SCC tissues and cell lines with OSMR overexpression following treatment with OSM[121]. Moreover, PLAUR may be a downstream target of HIF signalling. It has been shown to be induced under hypoxic conditions in breast cancer cells and drives EMT[389]. As OSM-OSMR signalling is known to induce hypoxic signalling under normoxic conditions[121,378,381], it is likely that positive correlation of PLAUR with OSMR expression in TCGA data is a result of PLAUR being downstream of OSM-OSMR signalling. PLAUR has been shown to promote EMT and survival of GBM cells[366]. It is detected in EVs derived from NSCLC cells; moreover, inhibition of PLAUR in this cell type resulted in increased apoptosis[367]. Thus, in cervical SCC, transport of PLAUR via EVs may be a form of paracrine signalling to promote survival and EMT of tumour cells located in close proximity or at distant sites (such as metastatic deposits).

Expression of CHI3L1 has previously been shown to be induced in glioma cells[344,345] and skin cells of patients with systemic sclerosis[346] in response to OSM and is a known target of STAT3 signalling[390]. Therefore, it is unsurprising that CHI3L1 was found to be upregulated in response to OSM-OSMR signalling in cervical SCC and to positively correlate with STAT3 expression in TCGA analysis of cervical SCC tissues. On the other hand, CEMIP was identified as a novel target of OSM-OSMR signalling; moreover, CEMIP expression was shown to correlate positively with OSMR expression in TCGA analysis of cervical SCC samples. The high levels of upregulation of CHI3L1 and CEMIP in response to OSM treatment would make them good candidates for investigation of whether upregulation of OSM-OSMR induced genes can be transferred via the EVs to recipient cells. CHI3L1 has been shown to promote both angiogenesis[342] and vascular mimicry[343] in cervical cancer, therefore endothelial cells and naive tumour cells would be the recipient cells of choice for experiments designed to determine the role of these three genes in cervical SCC.

CPA4 and PTPRR, which were downregulated in the NGS experiments in response to OSM-OSMR signalling, were also downregulated by qPCR analysis; however, only downregulation of CPA4 was found to be statistically significant. The role of CPA4 in cervical SCC is unknown. However, CPA4 has previously been reported to be underexpressed in

HPV positive cervical tumours[353]. PTPRR was previously found to reduce growth of cervical SCC lines, reduce expression of EMT markers and reduce expression of HPV E6 and E7 genes *in vitro* and tumour growth and metastasis *in vivo*[354]. Therefore, the observation that OSM-OSMR signalling reduces PTPRR expression is in line with promotion of an EMT phenotype in cervical SCC cells[73]. Interestingly, TCGA analysis revealed that CPA4 expression positively correlated with OSMR expression in clinical cervical SCC samples, despite being downregulated in EP-cells in response to OSM treatment. CPA4 has previously been shown to promote invasion and migration of lung cancer cells[350] and was implicated in EMT in breast cancer cells[352]. Therefore, downregulation of CPA4 in response to OSM-OSMR signalling is unexpected. The NGS and qPCR experiments performed only used tumour cells; therefore, differences between these results and TCGA data may potentially be due to interactions with cells of the TME, involved in regulating CPA4 expression. It would, therefore, be interesting to investigate whether OSM treated EVs confer downregulation of CPA4 and PTPRR to recipient cells and whether similar downregulation of CPA4 was observed in co-cultures of SCC cells in combination with other cells of the TME.

PLCB4 and RAB38 were found to be upregulated in KD-cells (both) and EVs (RAB38) compared to EP-cells in both NGS and qPCR experiments. While the role of PLCB4 in cervical cancer is unknown, RAB38 has previously been shown to be downregulated in microarray analysis of cervical carcinoma compared to normal cervical keratinocytes[365]. The current experiments therefore suggest that downregulation of RAB38 may be driven by OSM-OSMR signalling. TCGA analysis revealed that RAB38 expression positively correlated with OSMR expression in clinical cervical SCC samples, despite current findings that RAB38 is upregulated in KD-cells compared to EP-cells. The differences between TCGA and NGS/qPCR analyses are difficult to explain. Interestingly, RAB38 was not upregulated in KD2-cells or KD3-cells. These cell lines were generated by single cell cloning; therefore, upregulation of RAB38 may be specific to this clonal cell line and not down stream of OSM-OSMR signalling. It is therefore not a good candidate for further investigation.

Finally, levels of FMOD and PCSK1N were both shown to be downregulated in KD cells and EVs by NGS analysis and qPCR. In contrast, TCGA analysis revealed that PCSK1N expression negatively correlated with STAT3 expression in cervical SCC samples. FMOD was also downregulated in one of the additional OSMR KD cell lines (KD 3) whereas no difference in PCSK1N expression was observed between cell lines generated by the repeat CRISPR experiment (EP2, KD2, KD3). FMOD is known to play role in ECM remodelling, angiogenesis and modulation of TGFβ activity and has been shown to play a pro-

tumorigenic role in multiple cancers[355]. The role of PCSK1N in cancer is less clear; however, it has been shown to play a role in glucose metabolism[360]. As these genes are upregulated in OSMR overexpressing cervical SCC cells and EVs, it would therefore be interesting to investigate whether these genes are capable of promoting ECM remodeling, angiogenesis and cell growth in a cervical SCC system.

While overall these results confirm the expression patterns observed by NGS, they also highlight differences in the cell lines generated from the two CRISPR experiments. Differential expression of this panel of genes may be affected by the different extents of OSMR KD between cell lines. CHI3L1, CEMIP, PLAUR, CPA4 and PTPRR would be the superior candidates for subsequent investigation as they displayed similar patterns of expression in NGS experiments and qPCR using two different empty plasmid and three OSMR KD SW756 cell lines. The key next step for elucidating the effects of OSM induced differential mRNA expression in cervical SCC EVs will be to investigate whether EVs are capable of delivering these mRNA to recipient cells (such as other cancer cells and cells of the TME), to determine whether mRNAs are translated within recipient cells and subsequently to investigate functional effects. CHI3L1, CEMIP and PLAUR are upregulated in EP cells and EVs in response to OSM treatment, and expressed at higher levels in EP cells and EVs than KD cells or EVs. Therefore, a preliminary experiment could investigate whether treatment of KD-cells with EP-OSM-EVs leads to upregulation of these genes in the recipient cell. Similarly, as CPA4 and PTPRR are downregulated in EP cells and EVs in response to OSM, and upregulated following OSMR KD, it would be interesting to determine whether treatment of EP-cells with KD-EVs leads to upregulation of these genes.

5.7.5 Selection of small RNA library preparation kit

In order to confirm the optimum method for small RNA library preparation, the performance of two different library preparation kits was compared: Somagenics and Nextflex. Significant differences in miRNA expression were observed when comparing samples prepared using each kit. Sequencing results obtained using the Nextflex kit correlated more closely with qPCR results than the somagenics kit; indicating that the Nextflex kit most accurately represented the true miRNA levels in the original sample. Therefore, the Nextflex kit was deemed to be the optimum kit for use for small RNA sequencing and was selected for the subsequent cellular and EV sequencing experiment.

In a previous study comparing multiple library preparation kits across multiple samples sets, Coenen-Stass *et al* (2018) demonstrated superior performance of the Nextflex kit. It was found to produce negligible primer dimerisation, less quantification bias and greater

enrichment for miRNA reads compared to other library preparation kits currently on the market[325]. The Somagenics kit, however, was not included in this analysis. At the time experiments in the current study were performed, no studies had been published comparing performance of the Somagenics kit to other leading library preparation kits on the market. A recent publication by the group that developed the Somagenics protocol compared its performance to the Nextflex kit and to four other library preparation kits[331]. In contrast to our findings, the authors claimed that the Somagenics kit had less quantification bias, detected more miRNAs than any of the other kits and mapped most closely to qPCR results. Consistent with our findings, the Somagenics kit was found to have the lowest percentage of miRNA reads and greatest percentage of reads mapping to other classes of small RNA than any other kit. The comparisons performed in this study used samples containing 1µg of RNA. This is substantially greater than the quantities of RNA used in the current investigation (30-250ng). Therefore, it is plausible that while the Somagenics kit might show superior performance compared to the Nextflex kit when using high input quantities of RNA, it performs poorly with lower RNA inputs.

5.7.6 miRNA Sequencing

Differential miRNA expression was investigated in the same samples that were used for mRNA sequencing. Similar to mRNA sequencing, cells and EVs of all treatment groups appeared to cluster separately, indicating differences between cellular and EV miRNA cargo. EP-OSM cells and EVs were found to cluster separately from KD-PBS or KD-OSM cells and EVs, respectively.

The pilot experiment detailed in Chapter 4 used qPCR to investigate expression of a panel of nine miRNAs in SW756 and ME180 cells and their EVs in response to OSM. As previously discussed, a high proportion of the miRNAs investigated appeared to be upregulated in SW756 cells and EVs in response to OSM. We therefore hypothesised that these findings would be indicative of more wide-scale changes in miRNA expression in OSMR overexpressing cervical SCC cells and EVs. However, NGS analysis revealed that, surprisingly, only three miRNAs were found to display significantly differential expression in EP-cells and only nine in the corresponding EP-EVs in response to OSM. More miRNAs were significantly altered in KD-cells (26 in total) and KD-EVs (30 in total) compared to EP cells and EVs, respectively. However, the number of differentially expressed miRNAs was still much fewer than expected based on the preliminary qPCR experiments described in Chapter 4.

In general, more miRNAs were differentially expressed in EVs than in cells. For all comparisons investigated, overlapping cohorts of genes were found to be up or down regulated in both cells and EVs. While the low number of differentially expressed miRNA led us to question whether there were technical issues with the library preparation, overlap of differentially expressed miRNAs in both cell and EV comparisons indicates that these miRNAs could be biologically relevant. Therefore, it is possible that changes in miRNA expression were too subtle to be detected as statistically significant. Moreover, while the initial kit selection experiment demonstrated that the Nextflex kit performed equally well with 30ng and 250ng samples, this experiment was done with a single cellular sample that was diluted and split into multiple aliquots. Therefore, it is unlikely to have reflected the variation in miRNA levels that might be expected between cell or EV replicates. While miRNAs have been the most studied RNA species in EV cargo to date, several studies have reported relatively low abundance of miRNAs in EVs[171,391] with rRNA suggested to be the most abundant small RNA present in EVs[171]. In fact, previous work by Wei *et al* (2017) has indicated that non rRNA species are expressed at very low levels in EVs, with approximately one miRNA being present per EV, and most abundant miRNAs being present at the level of one copy per 10 EVs[392].

Two cell samples and one EV sample were removed prior to sample normalisation as they were found to have low counts and to predominantly map to spike-in controls, indicating issues with library preparation. This means that these groups had either 2 (cells) or 4 (EVs) replicates. Low abundance of miRNAs and an underpowered number of replicates may have contributed to low numbers of differentially expressed miRNAs. Therefore, while it would have been more labour intensive, higher input quantities of RNA may have resulted in greater consistency between replicates leading to detection of more miRNAs with statistically significant changes in expression between comparisons. Moreover, changes in miRNA expression may be subtle. Reducing the stringency of what was considered differential expression may have identified more miRNAs to be targets of OSM-OSMR signalling in cervical SCC cells and their EVs. Analysis performed in this way may have displayed a closer resemblance to PCR results.

In line with this theory, four of the miRNAs found to be upregulated in WT SW756 cells and EVs in response to OSM treatment in the experiments performed in Chapter 4, were investigated by qPCR. This was performed on EP and KD cell samples used for the sequencing experiment. qPCR results confirmed previous findings that miR9-3p, miR-23b-3p, miR-29b-3p and miR-126-5p were significantly upregulated in EP-cells in response to OSM. Moreover, miR9-3p, miR-23b-3p and miR-126-5p were all found to be significantly

downregulated in KD-cells. Despite being significantly altered in qPCR analysis, none of these miRNAs displayed differential expression in any of the NGS cell-cell comparisons. Only miR-126-3p was found to be significantly downregulated in KD-OSM-EVs compared to EP-OSM-EVs. Lack of consistency between NGS and qPCR data is likely to reflect variability between replicates and the fact that a low number of counts were detected by NGS for these miRNAs.

miRNAs that were found to be either up or down regulated in NGS samples for both cells and EVs for the EP-PBS versus EP-OSM, and EP-OSM versus KD-OSM comparisons, were selected for further investigation. Mir-146b-5p, mir-148a-3p, mir-224-5p, mir-342-3p, mir-363-3p and mir-452-5p were considered to be upregulated in response to OSM-OSMR signalling, whereas mir-30a-5p, mir-30c-1-5p, mir-92a-1-3p and mir-503-5p were considered to be downregulated in response to OSM-OSMR signalling. TCGA analysis found that miR-363 was the only miRNA with significant correlation with OSMR expression in clinical cervical SCC samples. Unexpectedly, the levels of miR-363 were found to correlate negatively with OSMR. Differences in NGS and TCGA results may be due to the contributions of other cells of the TME in TCGA.

Interestingly, many of these miRNAs have previously been reported to be associated with OSM and STAT3 signalling. Mir-146b has previously been shown to be induced by OSM in hepatocytes[393], and miR-148a has been shown to target gp130 leading to a reduction in STAT3 phosphorylation in cardiomyocytes[394]. Upregulated expression of both miR-146b and miR-148a has been shown to be associated with the OSM pathway in breast cancer cell lines[395]. miR-224-5p was found to negatively regulate JAK-STAT3 signalling in osteoblasts[396] and colorectal cancer cells[397]. Moreover, mir-452 expression has been shown to be downregulated by VEGFA, a downstream target of OSM-OSMR signalling, in breast cancer cells[398]. miR-30a is a known tumour-suppressor which targets SNAI1 in NSCLC[399] and is downregulated by STAT3 in head and neck SCC[400]. Furthermore, miR-92a has been reported to be upregulated in response to STAT3 in endothelial cells and to target suppressor of cytokine signalling 5 (SOCS5), an inhibitor of JAK-STAT signalling[401]. Finally miR-503 is downregulated in ovarian cancer cells; overexpression of miR-503 leads to inhibition of STAT3 activation[402].

It appears unlikely that the majority of miRNAs found to be up or down regulated in response to OSM-OSMR signalling in both SW756 cells and EVs would have previously demonstrated links to OSM and STAT3 by chance. Therefore, this suggests that while only a small number of miRNAs were found to be differentially expressed in cervical SCC cells and EVs in

response to OSM-OSMR signalling, those that were found to be dysregulated are likely to be of functional significance. Future work will focus on validating NGS results by qPCR. mRNA targets of these miRNAs will be investigated using sylamer, a statistical algorithm created by Van Dongen *et al* (2008)[403]. Functional significance of differentially expressed miRNAs could subsequently be investigated in both cells and EVs using functional assays, miRNA inhibitors and miRNA mimics.

5.7.7 Summary

Together, the results shown in this chapter demonstrate that OSM-OSMR signalling is capable of modulating both cellular and EV mRNA and miRNA expression in cervical SCC cells. While there was overlap in up and downregulated mRNA and miRNAs in both cells and EVs, OSM-OSMR induced packaging of RNAs into EVs appeared to be a selective process. Treatment of OSMR overexpressing SW756 cells with OSM led to: upregulation of pathways involved in cytokine mediated signalling, myeloid leucocyte activation, hypoxia signalling, interferon signalling, negative regulation of viral life cycle and angiogenesis in both cells and EVs. Whereas, pathways involved in PI3K-AKT signalling, tissue remodelling, negative regulation of differentiation and focal adhesion were downregulated in cells, whilst pathways involved in cellular organisation were downregulated in EVs.

Subsequent investigation will focus on validation of mRNA and miRNA sequencing results in EVs and will employ functional assays in order to elucidate the biological significance of miRNAs and mRNAs found to be differentially regulated in cervical SCC cells in response to OSM-OSMR signalling.

6. RESULTS: Establishing a model to investigate OSM-OSMR signalling *in vivo*

6.1 Introduction

In addition to investigating the effects of OSM-OSMR signalling on EV mRNA and miRNA expression, parallel experiments were performed in order to elucidate the effects of OSM-OSMR signalling on growth of cervical SCC cells *in vivo*. One of the challenges in studying OSM-OSMR interactions in a mouse model is the lack of homology between human and murine OSM. hOSM signals through mouse LIFR but not mouse OSMR, whereas mOSM does not activate any of the human receptors[97]. Therefore, an exogenous source of hOSM must be added to the experimental system when using a xenograft mouse model to study OSM-OSMR signalling.

Delivery of cancer cells by direct injection into the bloodstream is commonly used as a model of metastasis. These models measure the ability of circulating tumour cells to: survive in circulation, undergo extravasation from blood vessels into target organs (which involves invasion of the endothelial cell lining of blood vessels and degradation of the basement membrane) and survive and establish metastasis in the extravascular tissue[404,405]. Due to the fact that cells are injected directly into the bloodstream, these models only recapitulate the late stages of metastasis, and do not model the early stages such as local invasion and intravasation into the blood stream[404]. Moreover, the organs in which metastasis occur are highly dependent on site of tumour cell injection – tail vein injections are the most commonly used and predominantly lead to lung colonisation whereas other models, such as intra-portal vein and intra-carotid injection, mostly lead to liver and brain colonisation, respectively[404].

Initial experiments by our research group relied on the tail vein model. Bioluminescent SW756 cells were generated by stable transfection with a pGL4.51 luciferase reporter vector. Cells were injected into the tail vein of NOD-SCID mice and, subsequently, mice were treated three times a week by intraperitoneal injection with 1µg hOSM or PBS control. Tumour growth was tracked by weekly injection with D-luciferin, which leads to transcription of luciferase by SW756 cells. This results in bioluminescent light emission that can be detected non-invasively using an *in vivo* imaging system (IVIS), which uses a light-sensitive camera to detect light emitted from the animals, thereby enabling tracking of cancer cells *in vivo*[406]*.* Treatment with OSM led to an increase in lung metastasis compared to mice treated with PBS control (Figure 6.1A)[73]. Subsequent experiments revealed that pre-treatment of SW756 cells with siRNA against STAT3, or with an anti-OSM antibody prior to injection, led to reduced lung colonisation, both in the presence, and absence, of exogenous hOSM[92].

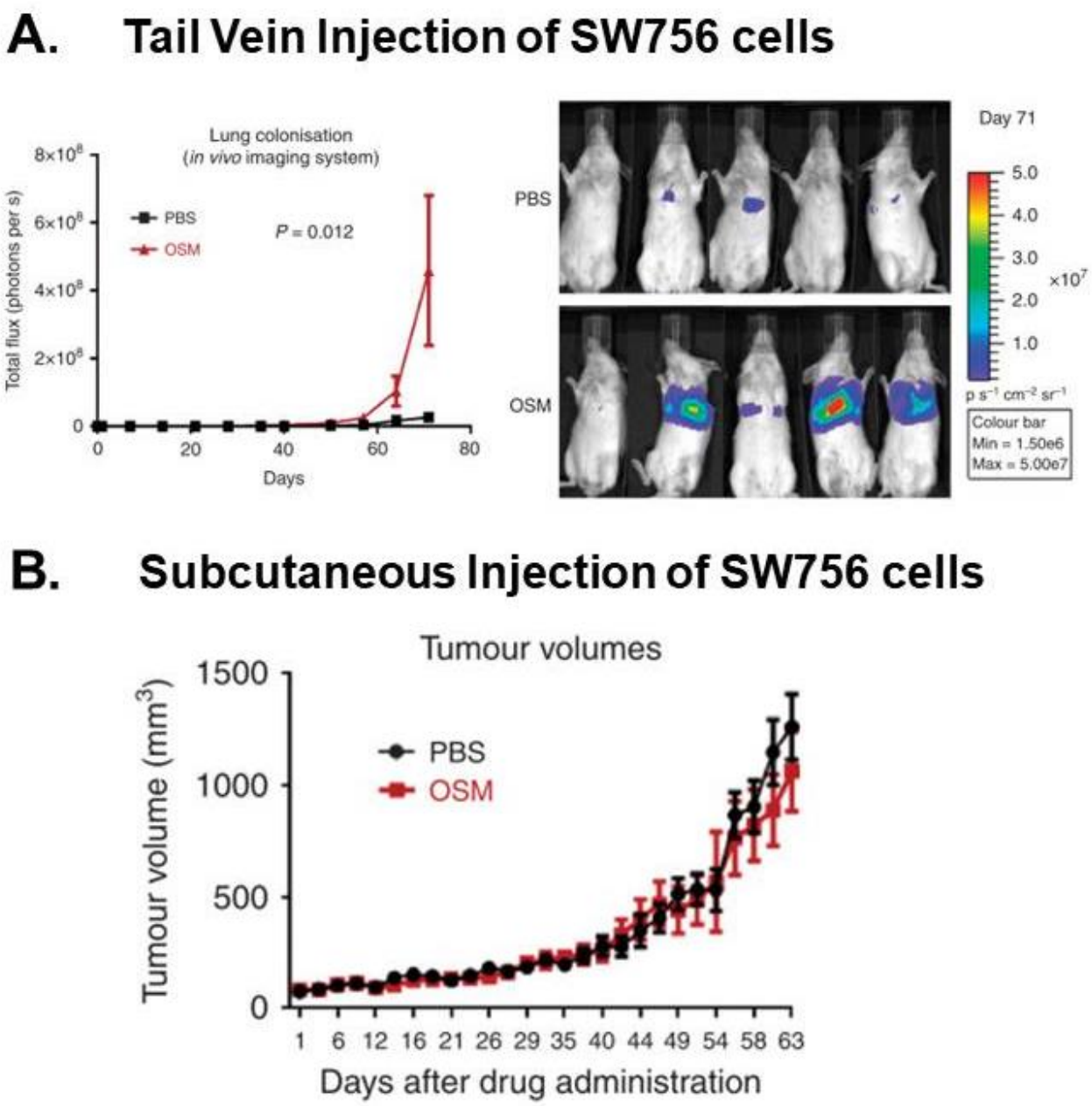

Figure 6.1: Previous investigation of OSM-OSMR signalling in SW756 cells in *vivo*
A) Tail vein model of metastasis: luciferase positive SW756 were injected into tail vein of NOD SCID mice. 1µg of hOSM or PBS control was delivered three times a week by intraperitoneal injection. Lung colonisation, measured by IVIS, is shown. B) Spontaneous model of metastasis: luciferase positive SW756 cells were injected subcutaneously in NOD SCID mice. 1µg of hOSM or PBS control was delivered three times a week by peritumoural injection. Primary tumour growth is shown.
Adapted from Kucia-Tran *et al* (2016)[73]

Spontaneous metastasis assays represent a better model for investigation of primary tumour growth and all stages of the metastatic cascade. These models involve transplantation of tumour cells or tissue to either the region from which tumour cells were originally derived (orthotopic site) or to accessible regions with high levels of vascularisation such as the skin (ectopic sites)[404,407]. Therefore, previous work also attempted to establish a spontaneous metastasis model in order to investigate the effect of OSM-OSMR signalling on cervical SCC growth *in vivo*. Bioluminescent SW756 cells were injected subcutaneously into NOD SCID mice; mice were subsequently treated three times a week by peritumoral injection with 1µg of hOSM or PBS control[73]. Tumour growth was measured externally by calipers. Xenografts treated with OSM or PBS control displayed no difference in primary tumour growth rate (Figure 6.1B). However, at the experimental endpoint, following removal of xenografts and visceral organs, a slight increase in skeletal metastasis was detected by IVIS in mice that had received OSM treatment[73].

Similar results were obtained in experiments later reported by Tawara *et al* (2018) using breast cancer cell lines. As seen for SW756 cells, treatment with OSM reduced growth of these cell lines *in vitro*[408] but no difference in primary tumour growth was observed *in vivo* following peritumoral injection with OSM[113]. Moreover, injection with OSM resulted in increased lung and spine metastasis[113]. Increased lung colonisation of cervical SCC *in vivo,* in response to OSM, was consistent with the finding that OSM treatment leads to increased EMT of these cells *in vitro*[73]. However, the lack of effects of OSM treatment on primary tumour growth was unexpected, as the pro-angiogenic response observed following OSM treatment *in vitro*[92,121] was predicted to further facilitate tumour growth. It was, therefore, important to ensure that OSM had been provided to the tumour in the most efficient manner.

6.2 Aims

Leading on from this work, this chapter aimed to conduct further experiments in order to potentially establish a better model to study the effects of OSM-OSMR signalling on primary tumour growth and metastasis in cervical SCC. To achieve this, subcutaneous xenografts were established using empty plasmid and OSMR KD SW756 cells generated in Chapter 4 by CRISPR-Cas9. hOSM was delivered by intraperitoneal injection and the effects on tumour growth were investigated. Subsequent experiments then aimed to establish a model with continued delivery of hOSM. To achieve this SW756 cell lines with varying levels of endogenous hOSM expression were generated and validated *in vitro.* These cell lines were subequently used to establish subcutaneous xenografts *in vivo*.

6.3 SW756 empty plasmid and OSMR KD xenografts

To assess whether a different route of OSM delivery would result in different effects on primary tumour growth, NOD SCID mice were injected subcutaneously with $5x10^6$ SW756 empty plasmid (EP) cells. Mice were then injected intraperitoneally with 1.2µg hOSM (approximately 60ng/g bodyweight) or PBS control, every day, for 13 days following the subcutaneous cell injection. Moreover, in order to better investigate the effect of OSM-OSMR signalling on the growth of cervical SCC cells *in vivo*, a group of mice was injected with the OSMR KD cells generated by CRISPR-Cas9 in Chapter 4. These mice were treated with OSM or PBS control in the same manner as the mice injected with EP cells.

As well as the route of administration of OSM, the schedule and amount of OSM delivered were changed from previous experiments. Previously, 1µg of OSM was given three times a week, whereas in these experiments OSM was given daily and immediately after the injection of the cells to provide a signal for angiogenesis in the period of early tumour establishment. The dose of hOSM for the current experiments was selected from the literature from previous studies in which IP delivery of OSM was performed and found to have functional effects *in vivo*. In particular, multiple studies investigating the effects of OSM on cardiovascular murine models have used daily IP injections of 60ng/g hOSM[409–412] and, therefore, this dose was used for the current experiment. Due to the cost and the number of injections required, it was not possible to deliver OSM for the duration of the tumour growth experiment. Therefore, IP injections of OSM were given for the first 13 days following tumour cell injection, corresponding to the period of early tumour establishment.

Three mice were injected for each of the four treatment conditions (EP + PBS/OSM and KD + PBS/OSM). Each mouse was culled at separate times once the experimental endpoint was reached; this was defined as the tumour volume reaching $1500mm^3$. However, mice were also culled if any of the following conditions were observed: a 20% decrease in body weight, tumour inflammation or ulceration, development of ascites or dyspnoea. Tumours larger than $650mm^3$ were included in the analysis. Two mice (one mouse from each of the EP cell treatment groups) developed ascites within the first 30 days following tumour cell injection and were, therefore, culled before the experimental endpoint. These mice did not have palpable subcutaneous tumours as expected at this timepoint but were found to have ascites and visible metastasis in the abdominal cavity. It is probable that the subcutaneous injections were suboptimal in these mice and tumour cells were directly introduced into the abdominal wall. These mice were, therefore, excluded from subsequent analysis of tumour growth and survival.

KD cells were previously shown to have reduced tumour growth compared to WT SW756 cells *in vitro* (Figure 4.19). In line with this, KD cells were found to have a significantly reduced growth rate *in vivo* compared to OSMR expressing EP cells (Figure 6.2). Moreover, in the absence of OSM, mice injected with EP cells had a significantly reduced survival rate compared to those injected with KD cells (Figure 6.2D panel i). Treatment with OSM led to a significant growth reduction of both EP and KD cells *in vivo* (Figure 6.2A). Moreover, survival of mice injected with EP cells was significantly reduced following treatment with OSM (Figure 6.2D panel iii). When comparing EP and KD cells from each treatment group, EP cells were found to have significantly increased tumour growth and reduced survival rate compared to KD cells in either PBS or OSM treated mice (Figure 6.2C+D).

The weights of mice were not significantly altered between any of the four treatment groups (Figure 6.3A). No macro-metastases were detected visually in the lungs (Figure 6.3D), livers (Figure 6.3E) or any other organs (spleen, diaphragm, heart, mesentery, brain; images not shown) of mice from any of the four experimental groups. Any damage to the lungs pictured in Figure 6.3D is most likely attributable to cardiac puncture which was performed at the experimental endpoint. Therefore, treatment did not appear to affect metastasis. Similarly, different groups did not display significant differences in lung and liver weights relative to total body weight at the time of the experimental endpoint (Figure 6.3B+C).

Tumour RNA expression was subsequently investigated by qPCR. As expected, OSMR KD tumours displayed significantly reduced levels of OSMR expression compared to EP tumours (Figure 6.4A). Levels of LIFR, STAT3, VEGFA, TGM2 and SNAI1 were not significantly altered between tumours of different groups (Figure 6.4). While statistically significant changes were not detected, levels of hOSM and TGM2 appeared greatest in OSMR KD tumours treated intraperitoneally with OSM (Figure 6.4C+F). Levels of VEGFA and SNAI1 also appeared upregulated in both EP and OSMR KD tumours following treatment with OSM compared to tumours treated with PBS control (Figure 6.4E+H).

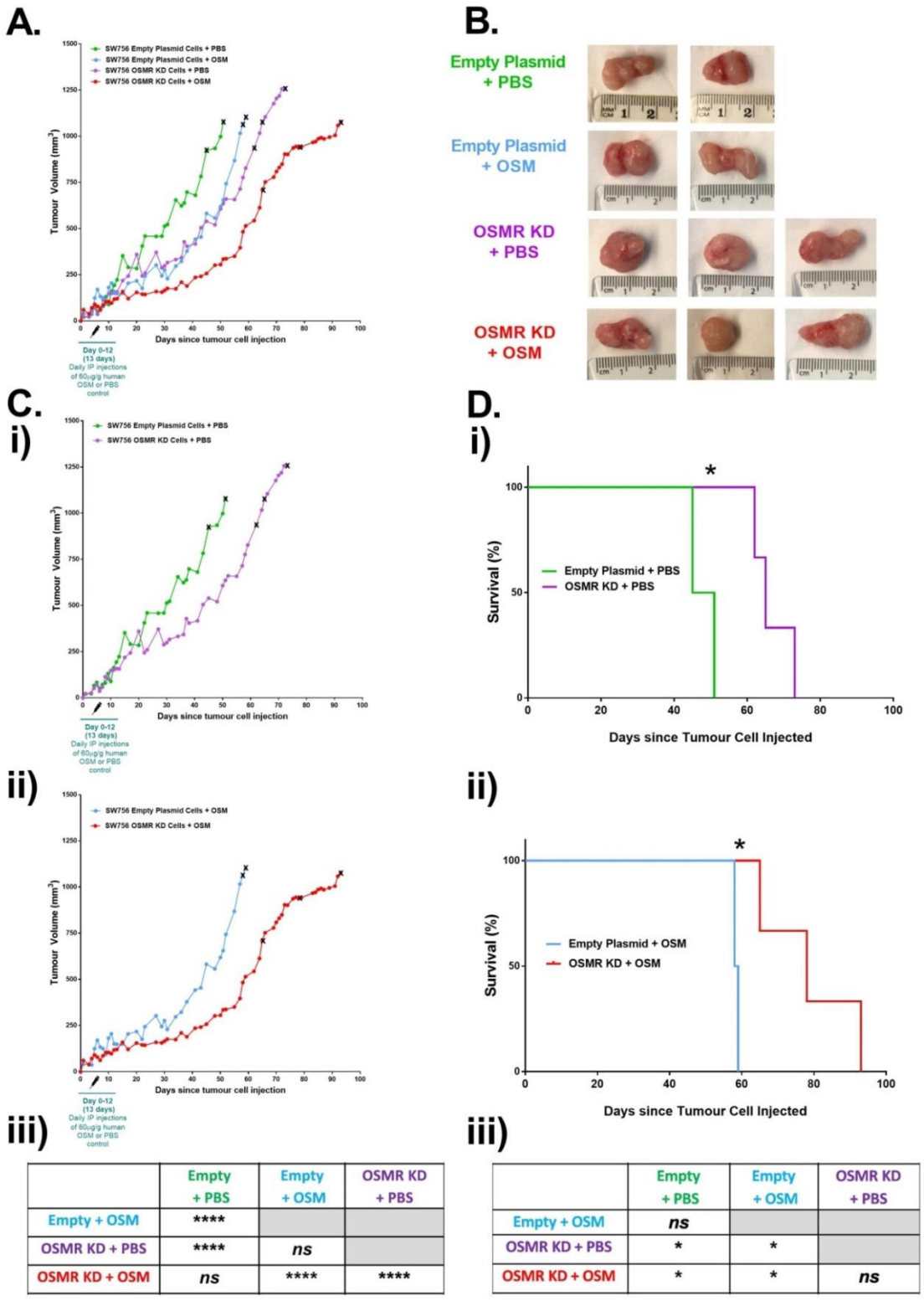

	Empty + PBS	Empty + OSM	OSMR KD + PBS
Empty + OSM	****		
OSMR KD + PBS	****	*ns*	
OSMR KD + OSM	*ns*	****	****

	Empty + PBS	Empty + OSM	OSMR KD + PBS
Empty + OSM	*ns*		
OSMR KD + PBS	*	*	
OSMR KD + OSM	*	*	*ns*

Figure 6.2: SW756 empty plasmid and OSMR KD xenografts - tumour growth

Six week old female NOD SCID mice were injected subcutaneously with 5 x10^6 SW756 EP or OSMR KD cells. Mice were injected IP with 1.2µg hOSM or PBS control, daily for 13 days beginning on the day of subcutaneous cell injection. A) Tumour growth of all four treatment groups. B) Tumour morphology at experimental endpoint. C) Tumour growth. D) Survival of i) Mice with EP and OSMR KD cell xenografts treated with PBS control. ii) Mice with EP and OSMR KD cell xenografts treated with OSM. iii) Summary of comparisons of treatment groups, detailing significant differences between groups in regards to C) tumour growth or D) Survival. N=2 (EP + PBS/OSM) or N=3 (OSMR KD + PBS/OSM). Statistical analysis performed using a nonlinear random effects model (tumour growth) or log rank mantel-cox test (survival analysis). * =.$P \leq 0.05$, ** = $P \leq 0.01$, *** = $P \leq 0.001$, **** = $P \leq 0.0001$.

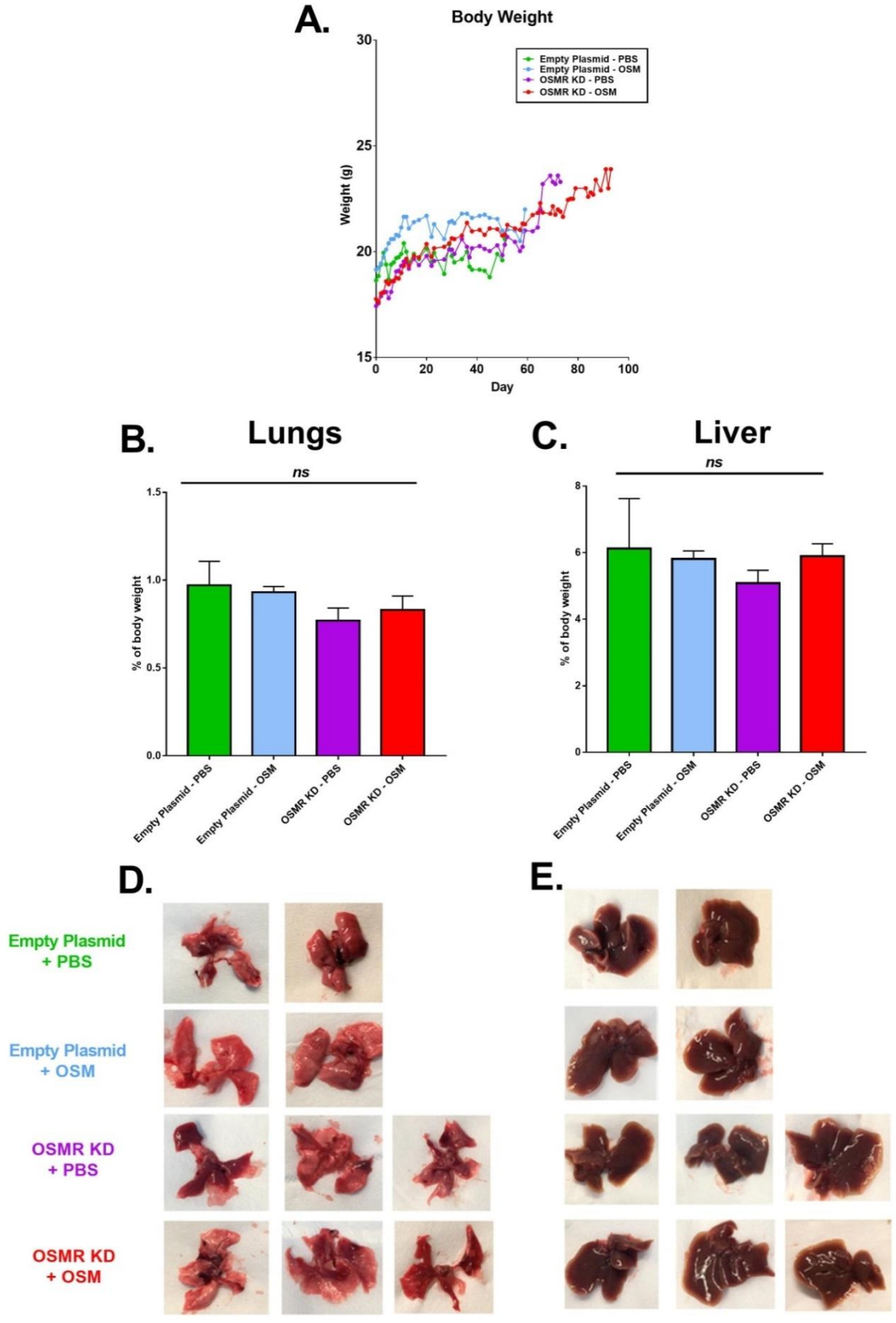

Figure 6.3: SW756 empty plasmid and OSMR KD xenografts - weight and organs

Six week old female NOD SCID mice were injected subcutaneously with 5 x10^6 SW756 empty plasmid or OSMR KD cells. Mice were injected IP with 1.2µg hOSM or PBS control, daily for 13 days beginning on the day of subcutaneous cell injection. A) Average body weight for each treatment group. Average percentage body weight of B) Lungs and C) Liver and morphology of D) Lungs and E) Livers of mice in each treatment group at experimental endpoint. B+C) Values were analysed for statistical significance using a one way ANOVA with Tukey's multiple comparison post-hoc tests. P≤0.05 were regarded as significant; ns = not significant

Genes that were identified by NGS analysis to be up or downregulated in SW756 cells and EVs following activation of OSM-OSMR signalling or OSMR KD were also investigated (Figure 6.5). Genes shown within the red box are those that were found by NGS to be altered both in EP cells following treatment with OSM, and in KD cells in comparison to EP cells. Those shown in the blue box are genes that were not found to be altered in EP cells in response to OSM but were altered in KD cells compared to EP cells. No significant differences were detected in gene expression between EP tumours treated with PBS control or OSM. Similarly, no differences were detected in OSMR KD tumours when comparing the two treatment groups.

No significant difference was detected in CH13L1 or CEMIP expression between any of the four treatment groups (Figure 6.5A+B). CEMIP appeared downregulated in OSMR KD tumours compared to EP tumours; however, results were not found to be statistically significant. PLAUR (Figure 6.5C) was found to be significantly downregulated in OSMR KD tumours compared to EP tumours, which was consistent with NGS results and *in vitro* qPCR validation of the cell lines used for these experiments. No significant difference was observed in CPA4 or PTPRR (Figure 6.5D+E) expression between any of the four groups; however, CPA4 appeared upregulated in OSMR KD tumours compared to EP tumours.

From the genes demonstrated by NGS to be significantly altered in KD cells (Figure 6.5, blue box, F-H), only RAB38 and PCSK1N were found to be significantly altered in tumour samples. RAB38 (Figure 6.5G) was upregulated in OSMR KD tumours compared to EP tumours, whereas PCSK1N was found to be downregulated (Figure 6.5I). This is consistent with NGS results and *in vitro* qPCR validation of the cell lines used for these experiments. FMOD also appeared to be downregulated in OSMR KD tumours; however, results were not statistically significant.

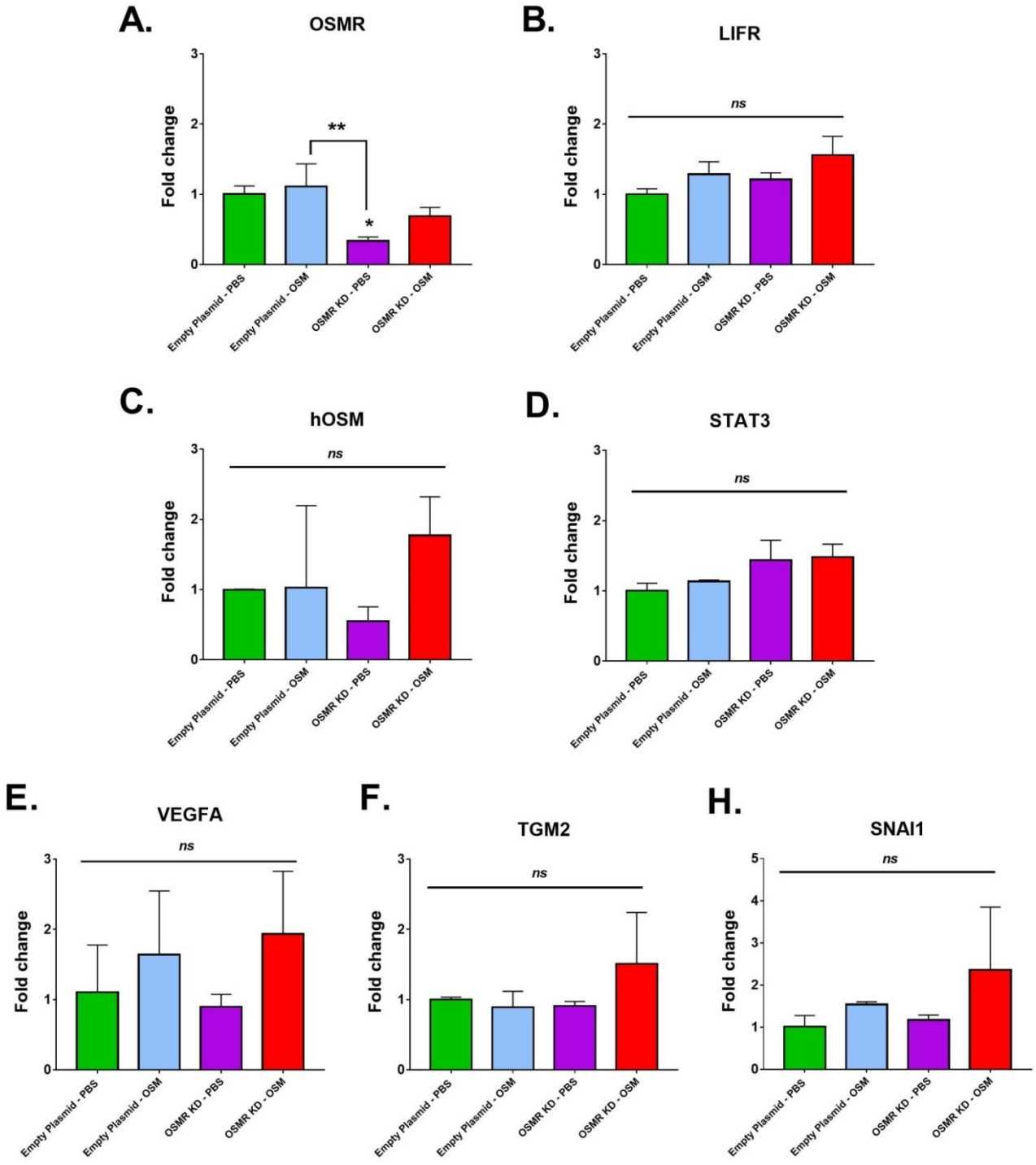

Figure 6.4: Tumour mRNA expression

qPCR for A) OSMR B) LIFR C) hOSM D) STAT3 E) VEGFA F) TGM2 and H) SNAI1 expression in tumour samples. Fold change is shown relative to EP + PBS control tumours. Error bars represent SEM. Values were analysed for statistical significance using a using a one ANOVA with Tukey's multiple comparison post-hoc tests. $P \leq 0.05$ were regarded as significant; * = $P \leq 0.05$, ns = not significant.

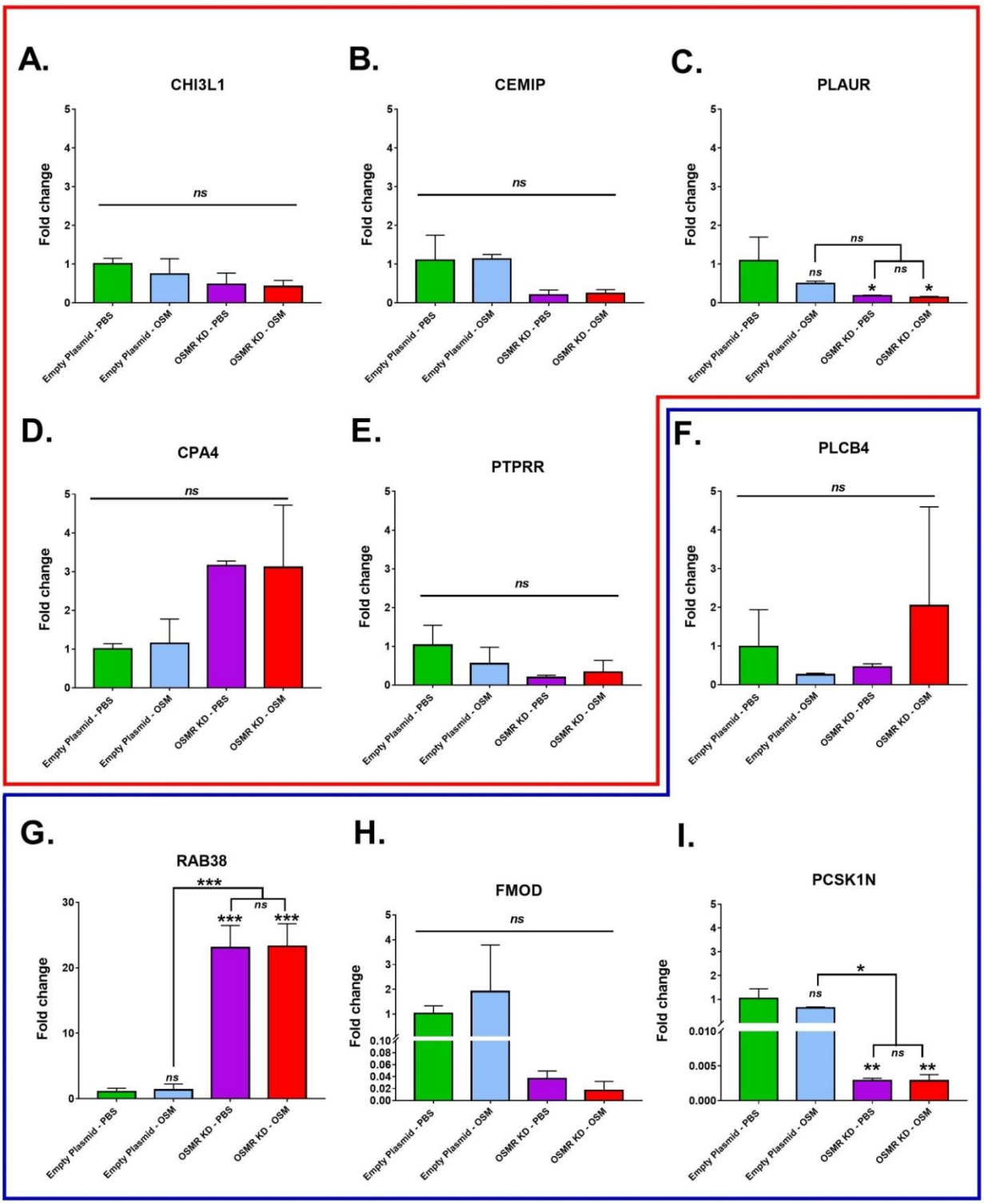

Figure 6.5: Tumour mRNA expression – genes identified from sequencing

qPCR for A) CHI3L1 B) CEMIP C) PLAUR D) CPA4 E) PTPRR F) PLCB4 G) RAB38 H) FMOD and I) PCSK1N expression in tumour samples. Fold change is shown relative to EP + PBS control tumours. Red box = genes altered in NGS analysis in both EP cells treated with OSM and following OSMR KD. Blue box = genes altered in NGS analysis following OSMR KD only. Error bars represent SEM. Values were analysed for statistical significance using a using a one way ANOVA with Tukey's multiple comparison post-hoc tests. $P \leq 0.05$ were regarded as significant; * = $P \leq 0.05$, ** = $P \leq 0.01$, *** = $P \leq 0.001$ and **** = $P \leq 0.0001$.

6.4 SW756 xenografts with endogenous OSM production

In the previous experiments, the addition of exogenous hOSM reduced the speed of tumour growth of both EP and OSMR KD tumours. This was an unexpected result, as we expected OSM to accelerate tumour growth in the EP cells due its ability to induce angiogenesis following interaction with OSMR. It was hypothesised that different outcomes may be observed depending on the dose and duration of OSM delivery. Subsequent experiments, therefore, aimed to develop a model in which OSM was continually delivered, as would be expected in a physiological tumour setting. In order to accomplish this, a SW756 cell line which overexpressed OSM was generated for use in xenograft experiments.

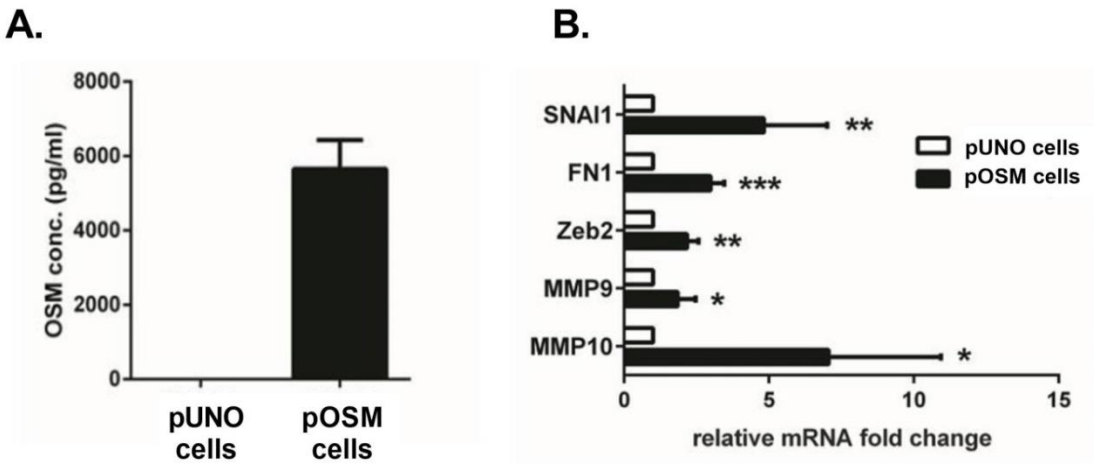

Figure 6.6: Generation of SW756 cell line with OSM overexpression

SW756 cells were stably transfected with a plasmid expressing hOSM (pOSM cells) or an empty control plasmid (pUNO cells). A) ELISA to confirmation levels of OSM secretion by pUNO and pOSM cells. B) Baseline levels of SNAI1, FN1, ZEB2, MMP9 and MMP10 expression in pUNO and pOSM cells as determined by qPCR. Values were analysed for statistical significance using unpaired T-tests with Welch's correction. * =.P≤0.05, ** = P≤0.01, *** = P≤0.001. Figures generated by Justyna Kucia-Tran (PhD thesis).

SW756 cells were stably transfected by Justyna Kucia-Tran with a plasmid expressing human OSM under a hEF1/HTVT promoter (pOSM cells) or an empty control plasmid (pUNO cells). This led to the generation of a polyclonal OSMR overexpressing cervical SCC cell line also overexpressing human OSM. pOSM cells were confirmed by ELISA to have increased levels of OSM production compared to pUNO cells (Figure 6.6A). Moreover, similar to treatment of WT SW756 cells with exogenous OSM, pOSM cells were found to have a reduced growth rate *in vitro*, to have a more mesenchymal phenotype and to be more invasive than pUNO cells (data not shown). In line with this, pOSM cells displayed greater basal expression of the following EMT markers than pUNO cells: SNAI1, FN1, ZEB2,

MMP and MMP10 (Figure 6.6B). ELISA and qPCR validation of these cell lines was performed by Justyna Kucia-Tran (unpublished, PhD thesis).

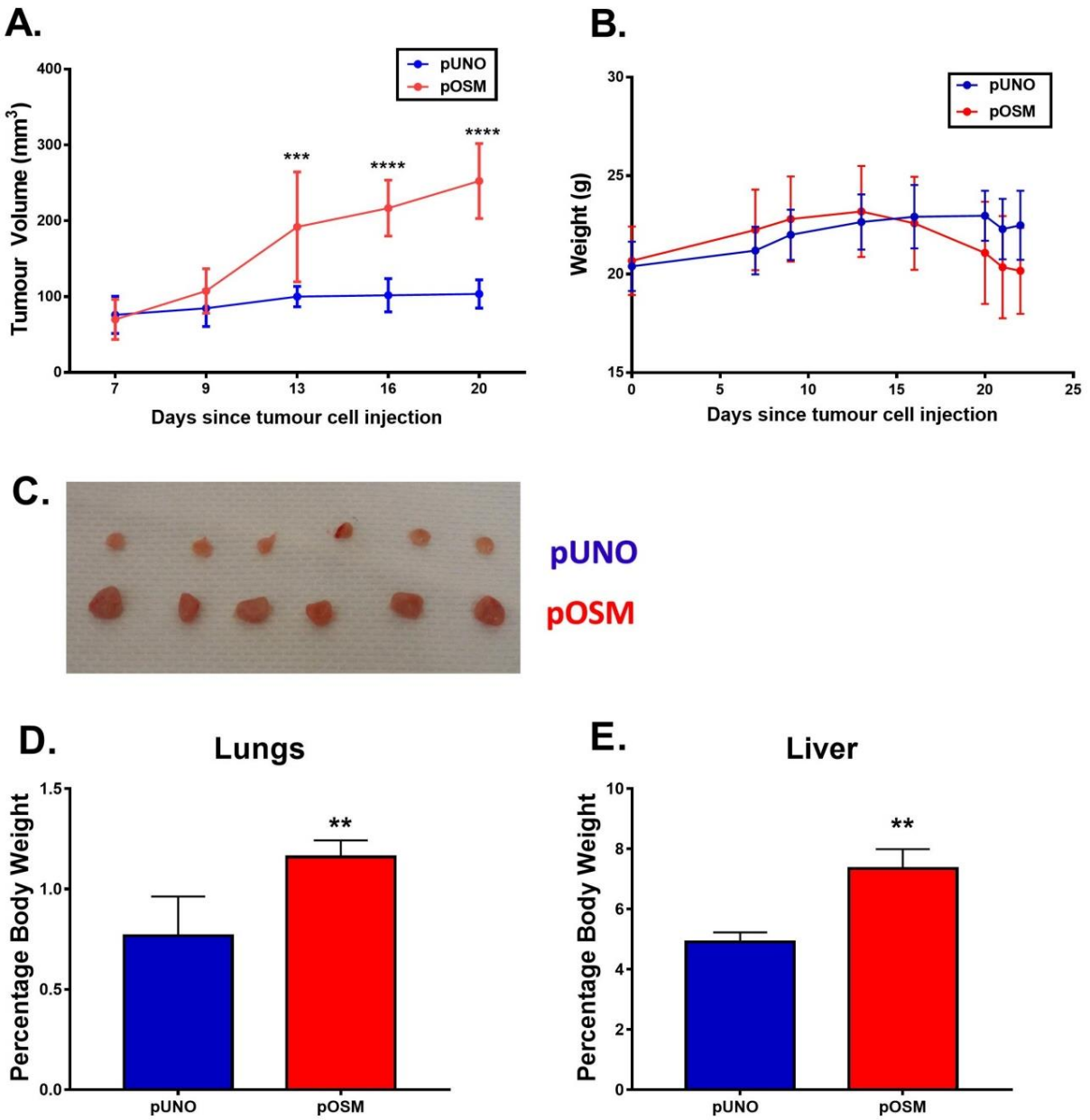

Figure 6.7: Subcutaneous xenograft of pOSM and pUNO cells
Female six week old NOD-SCID mice were injected subcutaneously with 5 x10^6 pUNO or pOSM cells (n=6 per group). A) Tumour Growth B) Body weight C) Photos of tumours at experimental endpoint D) Lung and E) Liver weight as a percentage of body weight at experimental endpoint. Values were analysed for statistical significance using unpaired T-tests with Welch's correction. * =.P≤0.05, ** = P≤0.01, *** = P≤0.001, **** = P≤0.0001.

Subcutaneous injections were performed in NOD-SCID mice using 5 x10^6 pUNO or pOSM cells (Figure 6.7). These experiments were performed together with Dr Marta Paez-Ribes and Valtteri Tulkki. pOSM cells grew significantly faster than pUNO cells *in vivo* (Figure 6.7A); however, mice injected with pOSM cells rapidly lost weight (Figure 6.7B), resulting in the termination of the experiment within three weeks of tumour cell injection. At the experimental endpoint, tumours in mice injected with pOSM cells were visibly larger than those injected with pUNO cells (Figure 6.7C). However, tumours from both groups were very small (<250mm^3). Liver and lung toxicity were visible in mice injected with pOSM cells. Livers from mice injected with pOSM cells showed hepatocyte necrosis and inflammatory cell infiltrate and also displayed increased weight relative to total body weight, compared to mice injected with pUNO cells (Figure 6.7E; Figure 6.8A+B). Similarly, the lungs of mice injected with pOSM cells showed alveolar wall thickening due to oedema, resulting in increased lung weight relative to total body weight (Figure 6.7D; Figure 6.8C+D), compared to mice injected with pUNO cells. No signs of metastasis were histologically detected in the lungs or livers.

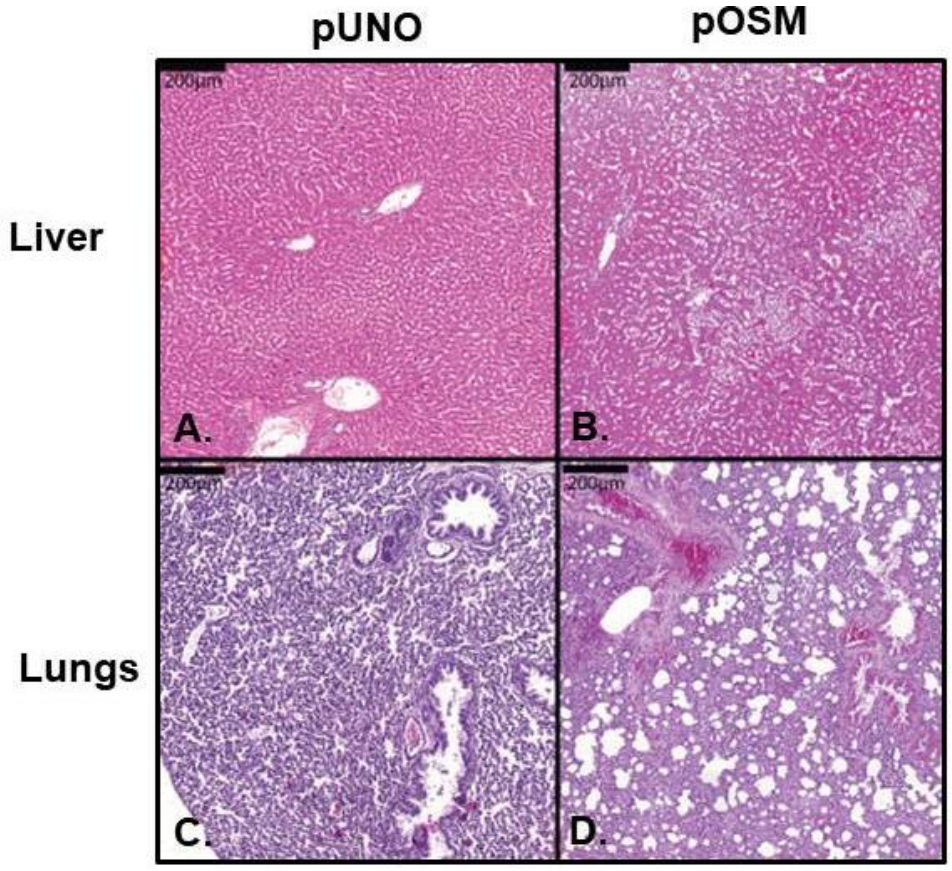

Figure 6.8: Liver and lung toxicity in mice injected with pOSM cells
Representative images of H&E staining of either:
Livers from NOD-SCID mice injected subcutaneously with A) pUNO or B) pOSM cells
Lungs from NOD-SCID mice injected subcutaneously with C) pUNO or D) pOSM cells.
H&E staining was performed by Valtteri Tulkki.

Subsequently, we aimed to establish a xenograft mouse model using a SW756 cell line overexpressing endogenous hOSM, but at lower levels than the pOSM cells, in the hope that this would result in less toxicity and would, therefore, allow for investigation of tumour growth over a longer time period. Transfection of SW756 cells with the plasmid expressing human OSM under a hEF1/HTVT promoter or an empty control plasmid was repeated by Dr Danita Pearson. OSM levels were investigated in four clonal cell lines derived from cells transfected with OSM plasmid (termed pOSM clones 1-4) by qPCR (Figure 6.9A) and ELISA (Figure 6.9B). Cells transfected with empty plasmid expressed similar levels of OSM as WT SW756 cells. pOSM clones 1-4 (pOSM_c1 – pOSM _c4) had varying levels of OSM secretion. All four clones produced more OSM than a clonal SW756 cell line obtained from cells transfected with an empty plasmid (Figure 6.9A+B). There were some differences between these clonal cell lines and the polyclonal pOSM cell line. All four clones were found to express lower levels of hOSM mRNA than the polyclonal pOSM cell line (Figure 6.9A); however, when hOSM protein was investigated by ELISA, pOSM_c4 appeared to secrete more hOSM protein than the polyclonal pOSM cell line (Figure 6.9B). Basal levels of OSMR, pSTAT3, STAT3 and SNAI1 in these cell lines were subsequently investigated by western blot (Figure 6.9C). Levels of OSMR and total STAT3 did not appear to vary between cell lines. Expression of pSTAT3 and SNAI1 downstream targets of OSM-OSMR signalling were both highest in pOSM and pOSM_c3 cells (Figure 6.9C).

Empty plasmid clonal SW756 cells (termed pUNO2) and pOSM_c2 and pOSM_c3 were selected for subsequent experiments. pOSM_c2 was used to investigate the effects of low levels of OSM overexpression, whereas pOSM_c3 was used to investigate the effects of high levels of OSM overexpression; OSM was expressed in this clonal cell line at lower levels than in the original pOSM cell line. Expression of known downstream targets of OSM-OSMR signalling such as OSMR, VEGFA, TGM2, SNAI1 and hOSM (Figure 6.10) as well as additional targets identified by NGS (Figure 6.11) were investigated by qPCR. This was performed using multiple replicates (n=3).

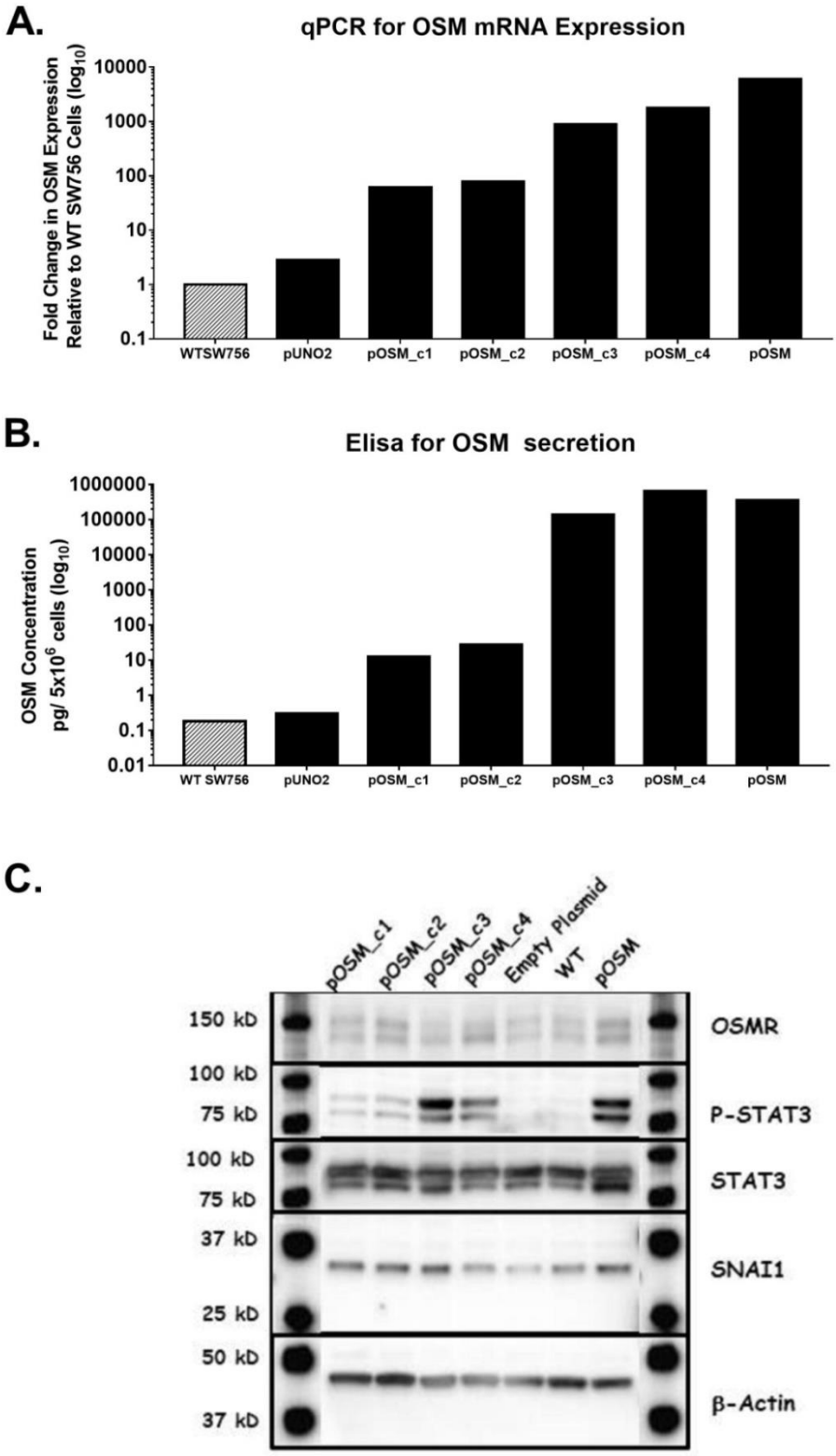

Figure 6.9: Generation of additional SW756 cell lines with endogenous OSM production
Characterisation of additional OSM overexpressing SW756 cell lines. Cells were transfected with plasmid expressing human OSM (pOSM clones 1-4) or empty plasmid (pUNO2). Expression of hOSM and downstream targets in newly generated cell lines was compared to WT SW756 cells and pOSM cells from the original transfection experiment. A) qPCR for OSM mRNA expression B) ELISA for OSM protein secretion C) Western blot for OSMR, p-STAT3, STAT3, SNAI1 and β-Actin protein levels. N=1. Experiments performed by Dr Danita Pearson.

As previously shown, pOSM_c2 and pOSM_c3 cells were found to express higher levels of hOSM than WT SW756 or pUNO2 cells. pOSM_c2 cells displayed a 31-fold increase in hOSM expression compared to WT SW756 cells; however, this increase was not found to be statistically significant. While not statistically significant, this is a notable difference in hOSM expression. Lack of statistical significance is likely due to high variability between replicates of the pOSM_c2 treatment group, evidenced by a SEM of ±23.1. pOSM_c3 cells displayed a 905-fold increase in hOSM expression compared to WT SW756 cells; expression of hOSM in these cells was significantly greater than that of any of the other cell lines tested (Figure 6.10A). OSMR was significantly upregulated in WT SW756 cells in response to treatment with OSM (Figure 6.10A). OSM overexpressing pOSM_c3 cells displayed significant upregulation of OSMR compared to pUNO2 cells. Interestingly, despite the vast upregulation in OSM expression, levels of OSMR in these cells were less than those observed for WT SW756 in response to OSM treatment. Similarly, VEGFA was shown to be upregulated in both WT SW756 cells treated with OSM and pOSM_c3 cells; upregulation was greatest in WT SW756 cells following OSM treatment (Figure 6.10C). Conversely, levels of TGM2 and SNAI1 were significantly upregulated in pOSM_c3 cells compared to WT SW756 cells and pUNO2 cells; little upregulation was observed in WT SW756 cells in response to OSM treatment (Figure 6.10D+E).

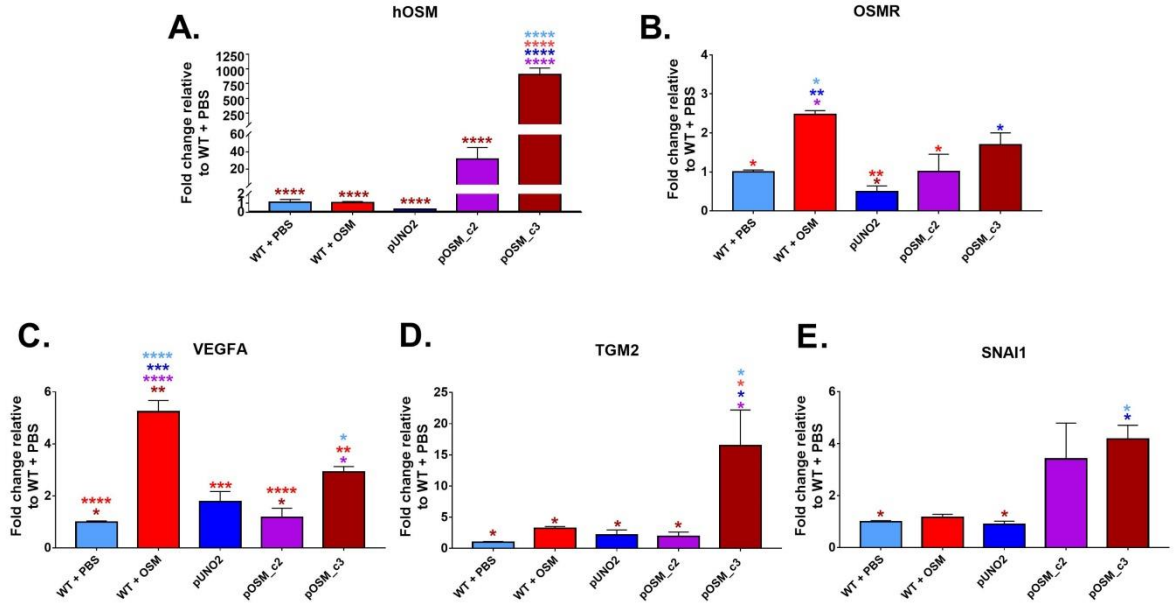

Figure 6.10: mRNA expression in SW756 cell lines with endogenous OSM production
qPCR for A) OSMR B) hOSM C) VEGFA D) TGM2 and E) SNAI1 expression in WT SW756 cells treated with PBS or OSM for 48 hours, untreated pUNO2 cells, untreated pOSM_2 and pOSM_3 cells. Fold change is shown relative to WT SW756 + PBS control. Error bars represent SEM. Values were analysed for statistical significance using a one way ANOVA with Tukey's multiple comparison post-hoc tests. $P \leq 0.05$ were regarded as significant; * = $P \leq 0.05$, ** = $P \leq 0.01$, *** = $P \leq 0.001$ and **** = $P \leq 0.0001$. Stars are colour coded to highlight which pairs of comparisons are significantly different.

In sequencing experiments, CHI3L1, CEMIP and PLAUR were all upregulated in EP SW756 cells in response to OSM treatment and downregulated in KD cells. Levels of CHI3L1 and CEMIP appeared to correlate with levels of OSM expression. Both were upregulated in WT SW756 cells treated with OSM compared to cells treated with PBS, and were also upregulated in pOSM_c2 and pOSM_c3 cells compared to pUNO2 cells (Figure 6.11A+B). Levels of both CH13L1 and CEMIP were greatest in pOSM_c3 cells which had higher levels of hOSM expression than pOSM_c2 cells. While levels of CH13L1 were substantially upregulated in WT cells treated with OSM and pOSM_c3 cells, differences in expression between groups was not found to be statistically significant due to high levels of variability between replicates (Figure 6.11A). pOSM_c3 cells were found to have significantly higher levels of CEMIP than any of the other cell lines (Figure 6.11B). PLAUR was also significantly upregulated in pOSM_c3 cells compared to WT SW756 cells treated with PBS, pUNO2 and pOSM_c2 cells (Figure 6.11C).

In sequencing experiments, CPA4 and PTPRR were both downregulated in EP cells in response to OSM treatment and upregulated in KD cells. In the current experiment both genes appeared downregulated in WT SW756 cells following OSM treatment; however, differences were not statistically significant (Figure 6.11D+E). Both genes also appeared to be downregulated in pOSM_c3 cells (with high levels of OSM expression) compared to pUNO2 cells; downregulation of CPA4 was statistically significant (Figure 6.11D).

Expression of PLCB4 and RAB38, which were upregulated in KD cells, and FMOD and PCSK1N, which were downregulated in KD cells in NGS analysis, were subsequently investigated. None of these genes was found to be altered in NGS analysis of EP cells in response to treatment with OSM. PLCB4 was found to be significantly downregulated in WT SW756 cells following treatment with OSM, compared to cells treated with PBS control (Figure 6.11F). Expression was also significantly reduced in pUNO2, pOSM_c2 and pOSM_c3 cells compared to WT SW756 cells. The greatest reduction in PLCB4 expression was observed in pOSM_c3 cells. Interestingly, RAB38 was expressed at significantly higher levels in pUNO2 cells than all other cell lines. pUNO2 cells were expected to behave in a similar way to WT SW756 cells, as they were only transfected with empty plasmid. However, pUNO2 is a clonal cell line derived from SW756 cells and this may, therefore, emphasise differences between clonal and polyclonal cell lines. FMOD was found to be significantly upregulated in pOSM_c3 cells compared to all other cell lines (Figure 6.11H). Interestingly, PCSK1N was found to be significantly downregulated in pOSM_c2 and pOSM_c3 cell lines compared to the other three cell lines (Figure 6.11I). This was an unexpected result as PCSK1N was found in NGS analysis to be downregulated in the KD cell line. Taken

together, these results further confirm that pOSM_c2 and pOSM_c3 cell lines overexpress OSM, resulting in differential activation of downstream targets of OSM-OSMR signalling compared to pUNO2 cells.

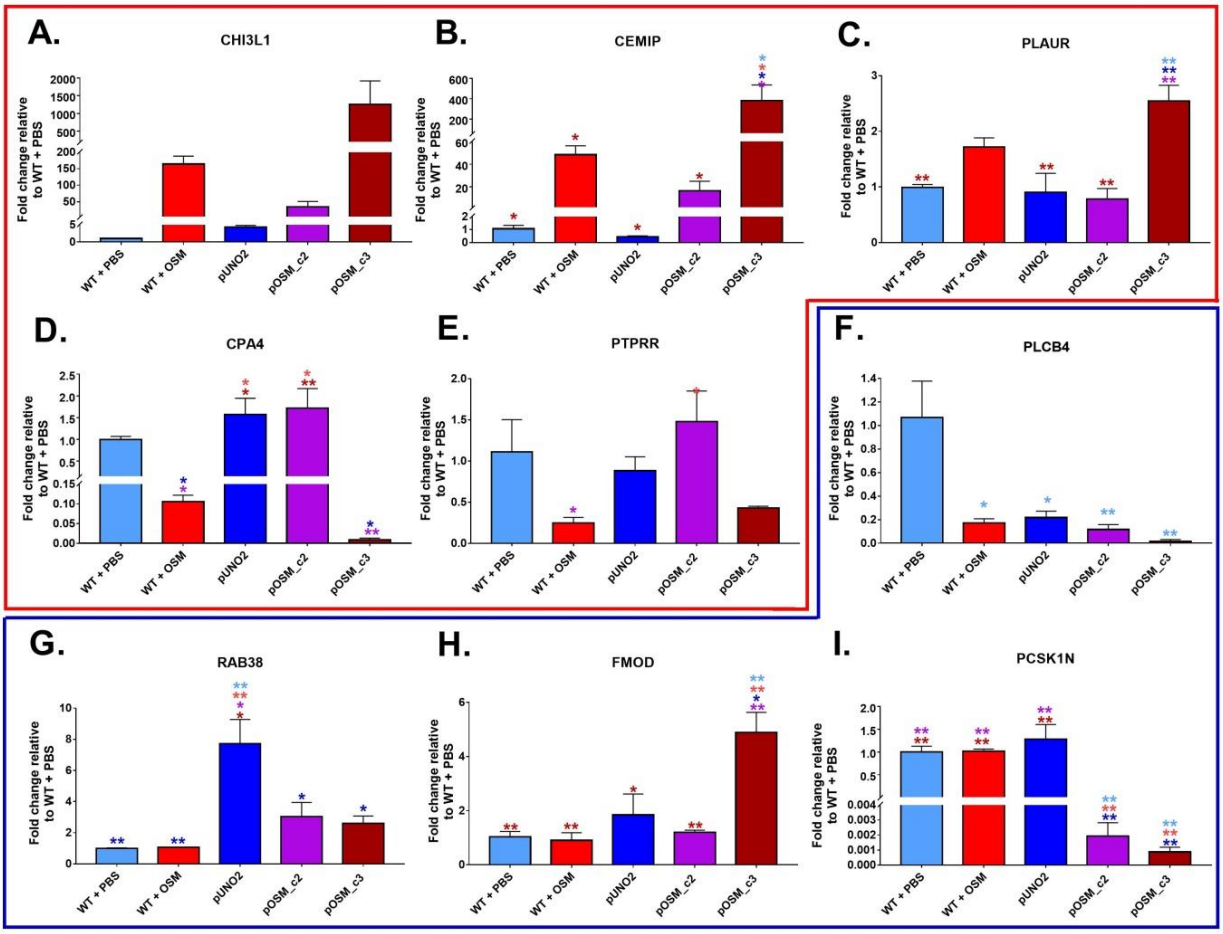

Figure 6.11: mRNA expression of sequencing markers in vitro

qPCR for A) CHI3L1 B) CEMIP C) PLAUR D) CPA4 E) PTPRR F) PLCB4 G) RAB38 H) FMOD and I) PCSK1N expression in WT SW756 cells treated with PBS or OSM for 48 hours, untreated pUNO2 cells, untreated pOSM_2 and pOSM_3 cells. Fold change is shown relative to WT SW756 + PBS control. Red box = genes altered in NGS analysis in both EP cells treated with OSM and following OSMR KD. Blue box = genes altered in NGS analysis following OSMR KD only. Error bars represent SEM. Values were analysed for statistical significance using a one way ANOVA with Tukey's multiple comparison post-hoc tests. $P \leq 0.05$ were regarded as significant; * = $P \leq 0.05$, ** = $P \leq 0.01$, *** = $P \leq 0.001$ and **** = $P \leq 0.0001$. Stars are colour coded to highlight which pairs of comparisons are significantly different.

Growth of these cells was subsequently investigated *in vivo*. Six week old female NOD-SCID mice were subcutaneously injected with 5 x 10^6 pUNO2, pOSM_c2 or pOSM_c3 cells. Three mice were injected for each cell line. Each mouse was culled at separate time points once experimental endpoint was reached; this was defined as the tumour volume reaching 1500mm^3. However, mice were also culled if any of the following conditions were observed: a 20% decrease in body weight, tumour inflammation or ulceration, development of ascites or dyspnoea. If tumours were larger than 650mm^3 they were included in the analysis. One mouse from the pOSM_c2 group was excluded as it had to be culled due to tumour ulceration.

Both pOSM_c2 (low OSM) and pOSM_c3 (high OSM) xenografts displayed a significantly increased growth rate compared to pUNO2 cells. Increase in tumour growth appeared to be dependent of levels of OSM; pOSM_c3 tumours were found to have a significantly increased growth rate compared to pOSM_c2 tumours (Figure 6.12A). Interestingly, pOSM_c3 tumours displayed an initial lag phase: in the first 40 days following tumour cell injection these cells appeared to grow more slowly than either pUNO2 or pOSM_c2 cells. Following this period, growth of pOSM_c3 tumour volume rapidly increased, and tumours became bigger than those from either of the other two cell lines. Tumour morphology at experimental endpoint is shown in Figure 6.12B; no obvious differences were observed in tumour morphology between treatment groups.

Unlike the previous experiment, tumours with endogenous OSM production did not result in rapid weight loss of NOD SCID mice. No significant differences in weight were detected between any of the three treatment groups (Figure 6.12C). Mice with pOSM_c3 OSM producing tumours had significantly reduced survival compared to mice with pUNO2 tumours (Figure 6.12D). There was no significant difference in survival between mice with pUNO2 tumours and mice with pOSM_c2 (low OSM) tumours.

In the previous experiment, pOSM xenografts resulted in lung and liver toxicity, characterised by increased lung and liver weight relative to total body weight compared to mice injected with pUNO cells. In the current experiment, no significant difference in lung weight relative to total body weight was observed between any of the three treatment groups (Figure 6.12Ei). Interestingly, in contrast to the previous experiment, mice with pOSM_c3 xenografts displayed significantly reduced liver weights relative to total body weight when compared to either of the other two treatment groups (Figure 6.12E panel ii).

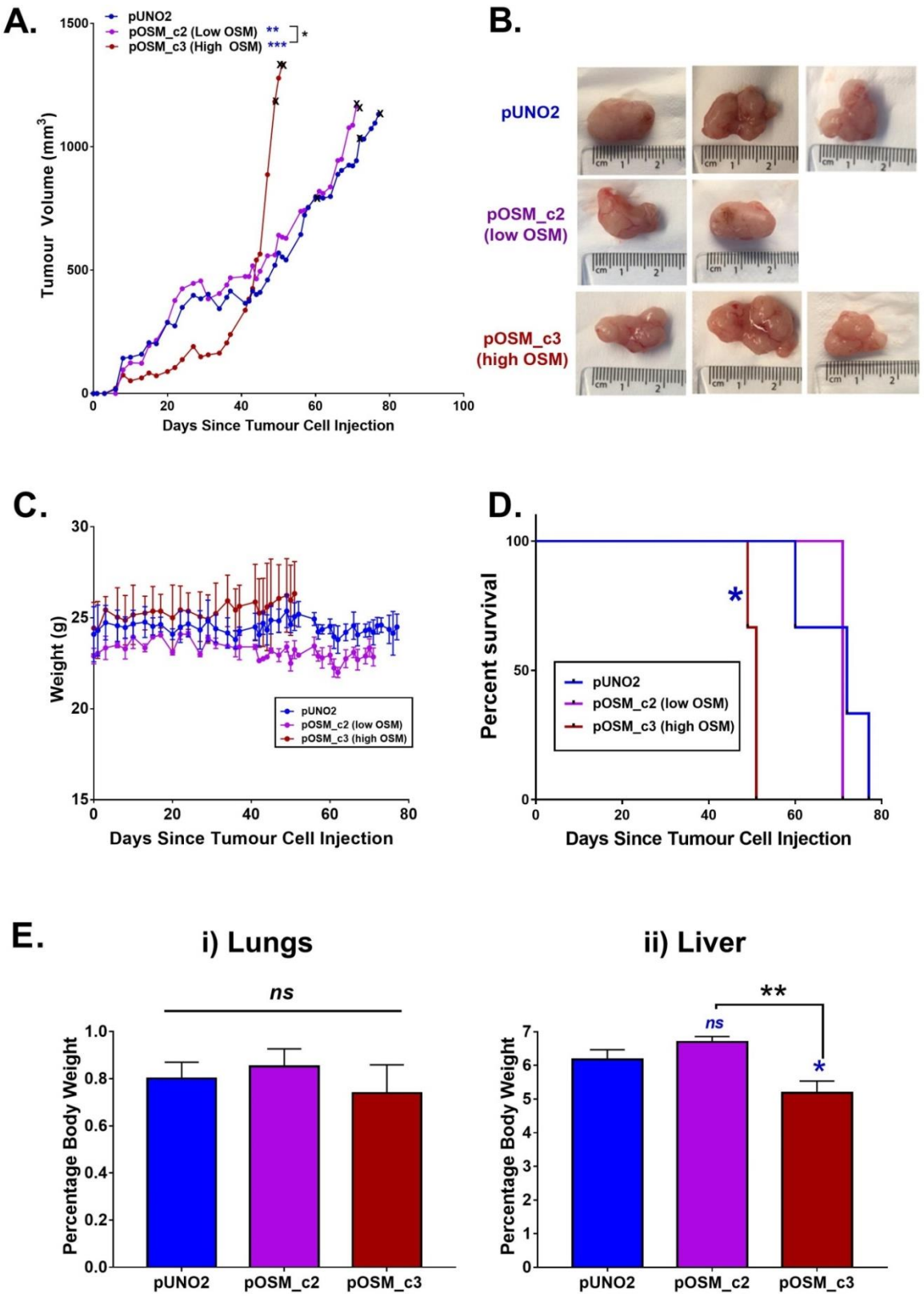

Figure 6.12: SW756 xenografts with varying levels of endogenous OSM production

Six week old female NOD SCID mice were injected subcutaneously with $5x10^6$ pUNO2, pOSM_c2 or pOSM_c3 SW756 cells. A) Tumour growth. B) Tumour morphology at experimental endpoint. C) Total body weight. D) Survival E) i) Lung and ii) Liver weight as a percentage of body weight at experimental endpoint. N=3. Statistical analysis performed using: a nonlinear random effect model (tumour growth), log rank mantel-cox (survival) and one way ANOVA with Tukey's multiple comparison post-hoc tests (comparison of percentage lung and liver weight between groups). Error bars represent SEM. * =.$P \leq 0.05$, ** = $P \leq 0.01$, *** = $P \leq 0.001$, **** = $P \leq 0.0001$.

Lung and liver morphology were subsequently investigated. Small white nodules which appeared to be macro-metastases were detected visually in the lungs of mice from all three treatment groups (Figure 6.13A). However, it is possible that these regions are attributable to damage caused by cardiac puncture performed at experimental endpoint. Histological investigation of lung tissue will therefore be needed to confirm whether lung metastasis has occurred. No obvious macro-metastases were detected in the livers (Figure 6.13B) or any other organs (spleen, diaphragm, heart, mesentery, brain; images not shown) of mice from any of the three experimental groups.

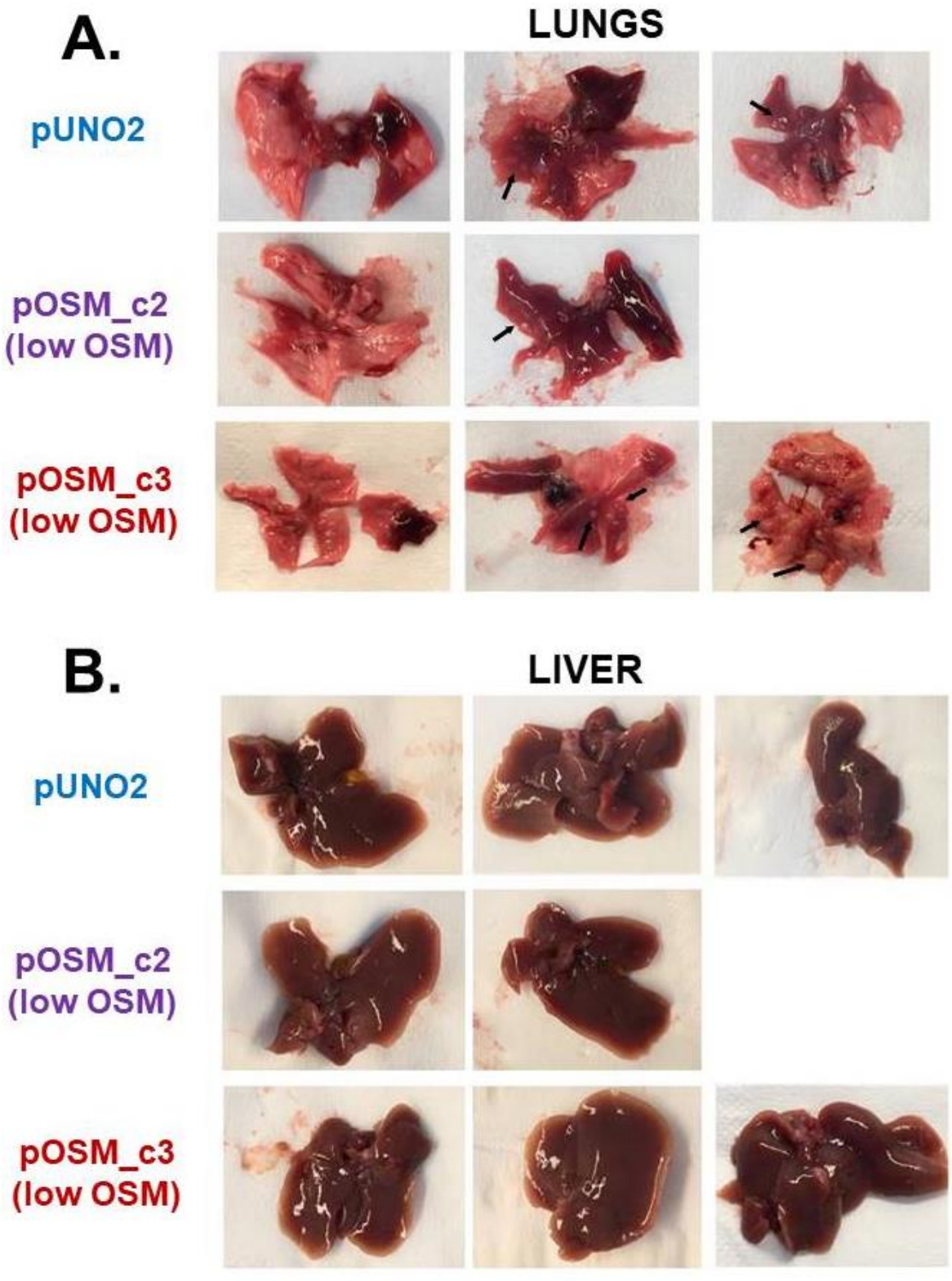

Figure 6.13: SW756 xenografts with endogenous OSM – lung and liver morphology
6 week old female NOD SCID mice were injected subcutaneously with 5 x10^6 pUNO2, pOSM_c2 or pOSM_c3 SW756 cells. A) Lung and B) Liver morphology for each mouse at experimental endpoint (once tumour reached 1500mm^3) is shown. Black arrows indicate possible macro-metastasis. Images not to scale.

6.5 Chapter discussion and summary

Experiments detailed in this chapter aimed to establish an *in vivo* model for investigating the effects of OSM-OSMR signalling on cervical SCC growth. The establishment of a successful model would be highly valuable for investigating therapeutic blockade of OSM-OSMR signalling. Previous experiments by our research group have shown that, when OSMR overexpressing SW756 cells were injected into the tail vein of NOD-SCID mice, there was an increase in lung metastasis in mice treated with IP injections of hOSM compared to PBS control[73]. Tail vein models only recapitulate the late stages of metastasis; therefore, we wanted to establish a model which would also allow for investigation of the effects of OSM-OSMR signalling on primary tumour growth and early stages of metastasis.

OSMR copy number gain and overexpression in cervical SCC are associated with adverse overall survival, independent of tumour stage[70]. Treatment of OSMR overexpressing SW756 cells with OSM has been shown to promote angiogenesis *in vitro*[121]. Moreover, OSM aided lung colonisation of SW756 cells *in vivo* following OSM injection in the tail vein model[73]. Together these results led us to hypothesise that treatment of OSMR overexpressing cells with OSM may aid tumour establishment by promoting vascularisation of the tumour, thereby promoting tumour growth. We have previously shown that OSM promotes promote EMT-like changes in OSMR overexpressing cervical SCC cells such as downregulation of E-cadherin and upregulation of several mesenchymal markers[122,73] leading to increased migration and invasion *in vitro*[121]. It is, therefore, possible that reduced growth of SW756 cells *in vitro* following OSM treatment is not due to a reduction in cell proliferation but instead due to increased cell detachment following OSM induced EMT-like changes. This has previously been demonstrated to be true for OSMR overexpressing breast cancer cells in response to treatment with OSM[114].

6.5.1 SW756 empty plasmid and OSMR KD xenografts

In the current study OSMR overexpressing empty plasmid SW756 cells and OSMR KD SW756 cells were used in order to investigate the effects of OSM-OSMR signalling on cervical SCC growth *in vivo*. When injected subcutaneously in NOD SCID mice, KD cells were found to have a significantly reduced growth rate compared to EP cells in the absence of OSM. Moreover, mice with OSMR KD tumours displayed a significantly increased overall survival compared to mice injected with EP cells. KD cells were previously demonstrated to have reduced basal levels of STAT3 phosphorylation compared to EP cells in the absence of OSM (Chapter 4). In addition, NGS analysis revealed that 48 genes were significantly upregulated in KD-PBS-cells compared to EP-PBS-cells, and 100 genes were significantly downregulated (Chapter 5). These findings are consistent with previous experiments by our

research group which demonstrated that forced expression of OSMR in cervical SCC cell lines without baseline OSMR overexpression led to increased phosphorylation of STAT3 in the absence of OSM[92]. Similarly, in the tail vein model, treatment with an anti-OSM antibody reduced lung colonisation in the absence of exogenous OSM[92]. Together, these findings demonstrate that overexpressing cervical SCC cells endogenously produce OSM, which is capable of driving functionally significant OSM-OSMR signalling in an autocrine manner. Blockade or KD of OSMR is therefore capable of reducing tumour cell growth in the absence of exogenous OSM by blockage of this autocrine signalling loop.

Surprisingly, the addition of exogenous hOSM led to reduced growth of both EP and KD SW756 cells *in vivo*. Moreover, mice with EP tumours displayed significantly reduced overall survival following OSM treatment compared to mice treated with PBS control. The weights of mice were not significantly altered by OSM injection and no macro-metastases were detected in any of the organs. No significant differences were detected in tumour mRNA expression following treatment with OSM for either cell line. Treatment of EP cells with OSM was previously shown to result in significantly increased expression of OSMR, VEGFA and TGM2 *in vitro* (Figure 4.16). Moreover, CHI3L1, CEMIP and PLAUR were found to be significantly upregulated in EP cells in response to OSM, while CPA4 was significantly downregulated in both NGS analysis (Table 5.9) and qPCR validation (Figure 5.17). Whereas, treatment of OSMR KD cells with OSM was shown to have no effect on mRNA expression in vitro (Figure 4.16, Figure S5. 16B. Figure S5. 17B, Figure S5. 18B and Figure 5.17). Lack of differences in mRNA expression in EP tumours treated with PBS or OSM is likely to be due to the timepoint at which tumours were collected; OSM was administered by IP injection for the first 13 days following tumour cell injection. Individual mice were culled once tumours reached 1500mm^3; survival for mice in all treatment groups was between 45 and 93 days post tumour cell injection. Therefore, tumours were collected between 32 and 80 days after the last dose of OSM or PBS control was administered. While it appeared to have a residual effect on tumour growth, direct effects of OSM treatment on expression of known OSM-OSMR targets is likely to have been lost by this timepoint. It is possible that this is a result of cells that were responsive to OSM migrating away from the tumours themselves or undergoing apoptosis, or that the tumour cells have reverted to their pre-treatment state. Therefore, continued delivery of OSM is likely to be necessary for the maintenance of these effects.

Differences were, however, detected in mRNA expression of OSMR KD tumours compared to OSMR expressing EP tumours. As expected, OSMR KD tumours displayed significantly reduced levels of OSMR mRNA expression compared to EP tumours. Consistent with NGS

data, OSMR KD tumours also displayed significant downregulation of PLAUR and PCSK1N and upregulation of RAB38. As previously discussed, both PLAUR and RAB38 have been shown previously to correlate positively with OSMR expression in patient cervical SCC samples. Reduced expression of PLAUR in OSMR KD tumours is consistent with previous findings from our laboratory that demonstrated that lower levels of PLAUR are detected in cervical SCC tissues without OSMR overexpression[121]. Similarly, RAB38 has been shown to be downregulated in cervical carcinoma compared to normal cervical keratinocytes[365], thus downregulation of RAB38 may be mediated by OSM-OSMR signalling.

Reduced size of EP tumours in response to OSM treatment may possibly be a result of OSM induced EMT of cancer cells, as previously discussed. While we initially hypothesised that OSM would promote angiogenesis, and thereby promote tumour establishment, induction of EMT may have promoted migration of OSMR overexpressing cells away from the primary tumour site. While macro-metastasis was not detected in any of the organs, it is possible that subsequent histological analysis of lungs, liver, spleen and femurs may reveal differences in levels of micro-metastasis between mice with EP tumours treated with OSM or PBS control. The previous subcutaneous experiment conducted in our laboratory using SW756 cells and peritumoural injection of OSM revealed a slight increase in skeletal metastasis in mice that had received OSM treatment[73]. Tracking of cells with luciferase labelling and IVIS may, therefore, have facilitated identification of small metastatic deposits.

However, tumour growth was reduced in both EP and KD cell lines in response to OSM treatment to a similar extent, suggesting that OSM was perhaps acting through the same mechanism to regulate growth in both cell lines. This was unexpected and reduced growth of the KD cell line in response to OSM treatment is more challenging to explain. *In vitro* experiments have demonstrated that KD cells are functionally unresponsive to OSM stimulation. No upregulation in pSTAT3, OSMR or downstream targets of OSM-OSMR signalling were upregulated following OSM treatment*;* similarly, treatment with OSM had no effect on the growth of OSMR KD cells *in vitro*. Moreover, NGS analysis did not detect differential mRNA or miRNA expression in these cells following OSM treatment. Previous investigation of OSM-receptor transduction in WT SW756 cells has revealed that OSM induced activation of STAT3, STAT5, AKT and ERK1/2 was abrogated by depleting OSMR, but not by depleting LIFR, indicating that OSM was acting predominantly through OSMR in these cells[92]. However, while not statistically significant, LIFR and VEGFA mRNA expression appeared upregulated in tumours from both cell lines in response to treatment with OSM. Therefore, it is possible that activation of LIFR in response to hOSM may have contributed to the cytostatic effects observed in both EP and KD cells. Moreover, growth effects could also

possibly be attributed to hOSM signalling through mLIFR expressed by murine cells of the TME rather than OSM-OSMR induced activation of tumour cells.

An alternative explanation for OSM reduction of both EP and OSMR KD tumours in response to OSM may be due to the route of OSM delivery. In the previous experiment, peritumoural injection of OSM did not result in reduced growth of WT SW756 cells[73]. Similarly, Tawara *et al* (2018) observed that peritumoural injection of hOSM did not affect primary tumour growth in an orthotopic breast cancer model. However, treatment led to an increased number of circulating tumour cells and increased lung metastasis[113]. Conversely, in a synergenic breast cancer model comparing growth of WT and OSM KD cells, OSM expression was shown to result in reduced growth of primary tumours while simultaneously promoting bone metastasis[114]. Thus, route of delivery of OSM may be an important factor in regulating tumour growth. Local release of OSM would be more representative of OSM-OSMR signalling within the TME.

6.5.2 OSMR KD in a syngeneic cervical SCC model

Parallel experiments performed by Valtteri Tulkki (PhD thesis, manuscript in preparation) investigated the use of an immunocompetent mouse model to investigate OSM-OSMR signalling *in vivo*. This model used PDSC5.2 cells, a murine skin SCC cell line. Importantly, the transgenic mice from which PDSC5.2 cells were derived express the HPV-16 E6 and E7 oncogenes under the control of the keratinocyte specific K14 promoter[413]. Moreover, this cell line expresses high levels of mOSMR and responds to mOSM in a similar manner as SW756 cells respond to hOSM (Valtteri Tulkki, PhD thesis, manuscript in preparation). Similar to the experiments detailed in this thesis, CRISPR was performed to knock-down mOSMR expression in PDSC5.2 cells. WT and OSMR KD PDSC5.2 cells were injected subcutaneously into either WT FVB or OSMR KO FVB mice. This enabled investigation of the effects of OSM-OSMR signalling in both tumour cells and cells of the TME. As this was a syngeneic model, there was no need to add exogenous OSM.

Removal of OSMR from either the tumour cells or from the TME resulted in significant reductions in tumour growth (Figure 6.14A) and increased survival (Figure 6.14B) compared to WT PDSC5.2 cells grown in WT FVB mice (WT-WT tumours). OSMR KD PSC5.2 tumours in OSMR KO FVB mice grew the slowest and displayed significantly higher overall survival. Moreover, WT-WT tumours were more invasive and displayed increased angiogenesis compared to the other groups. They also displayed higher levels of dendritic cell, M2 macrophages, inflammatory macrophages and PD-L1 positive myeloid cell infiltration.

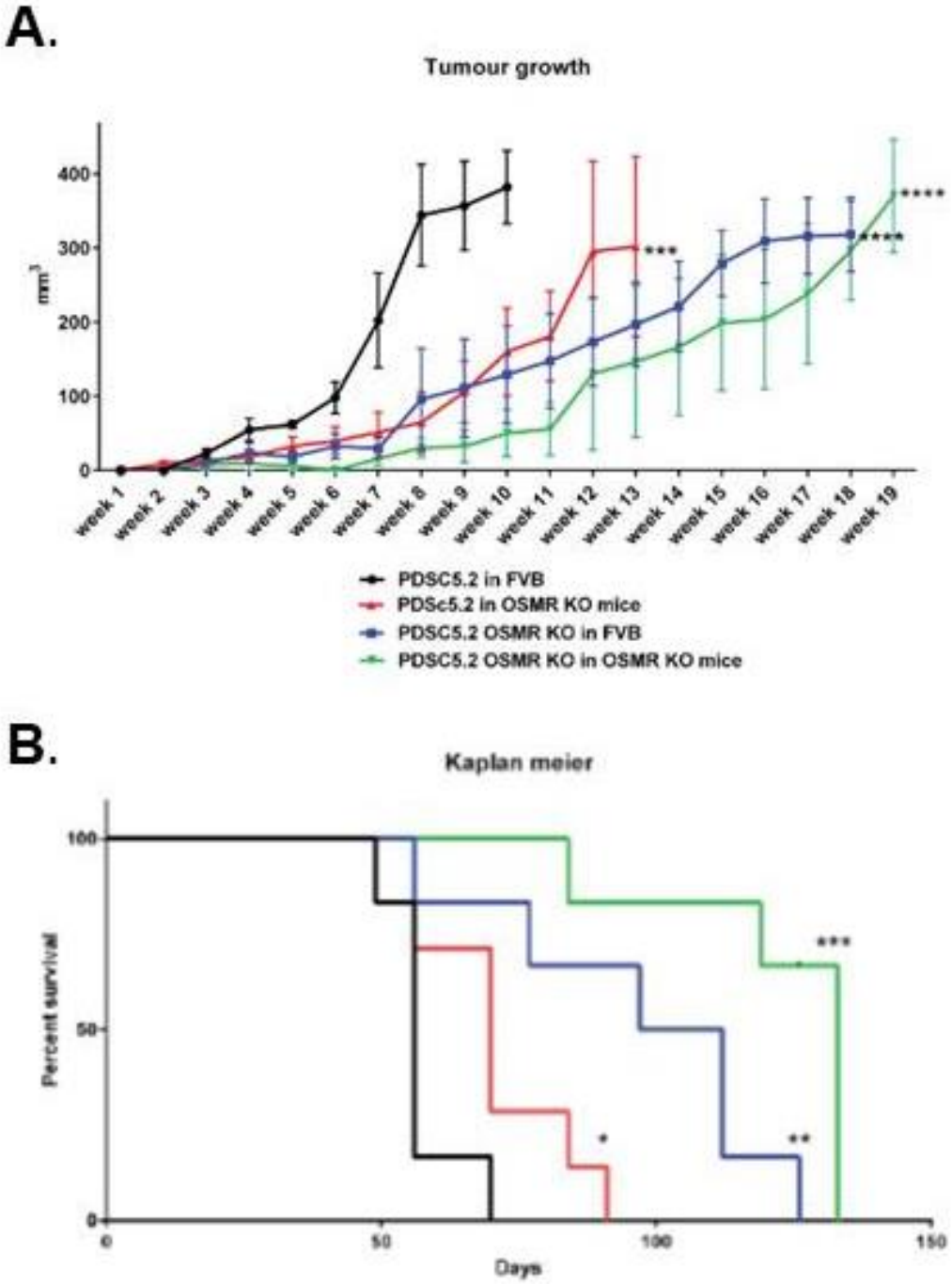

Figure 6.14: PDSC5.2 immunocompetent mouse model

OSMR KD PDSC5.2 cells were generated by CRISPR-Cas9. WT and OSMR KD PDSC5.2 cells were subcutaneously injected into either WT FVB or OSMR KO FVB mice. A) Tumour growth and B) Survival. Statistical analysis was performed using an one-way ANOVA (tumour growth) or Prism survival curve analysis (survival). * = P≤0.05, ** = P ≤0.01, *** = P≤0.001 and **** = P ≤0.0001. N=6 for WT PDSC5.2/WT FVB and OSMR KD PDSC5.2/WT FVB, n=7 for WT PDSC5.2/OSMR KO FVB and n=4 for OSMR KD PSC5.2/OSMR KO FVB.

Valtteri Tulkki (PhD thesis, manuscript in preparation).

In the immunocompetent mouse model, OSM-OSMR signalling (both within tumour cells and the TME) was shown to drive primary tumour growth. In line with the xenograft experiment, OSMR KD was shown to result in reduced tumour growth. In agreement with this, murine skin SCC cells have previously been demonstrated to grow more slowly in OSM KO mice, resulting in reduced M2 polarisation in the TME[111]. These results contrasted with the results for the xenograft experiment detailed in this chapter, in which IP injection with hOSM led to reduced growth of human cervical SCC cells. In the immunocompetent mouse system mOSM will be continually delivered to OSMR overexpressing tumour cells by immune cells present in the TME, leading to constant activation of OSM-OSMR signalling. It is, therefore, possible that differences in tumour growth in the human xenograft model compared to the syngeneic mouse model may be due to the duration of OSM delivery. hOSM was only delivered for the first 13 days of the experiment during the initial period of tumour establishment. Junk *et al* (2017) demonstrated that OSM promotes cancer cell plasticity; treatment of transformed human mammary epithelial cells with OSM led to the acquisition of breast cancer stem cell (CSC)-like properties such as anchorage independent growth. However, removal of OSM resulted in the loss of mesenchymal/CSC properties even after sustained long-term OSM exposure, indicating that sustained OSM exposure is necessary for the maintenance of these phenotypes[414].

6.5.3 SW756 xenografts with endogenous OSM production

Subsequent experiments, therefore, aimed to test a model in which OSM was continually delivered, as would be expected in a physiological tumour setting. In order to accomplish this, OSMR overexpressing SW756 cells were stably transfected with a plasmid expressing human OSM (pOSM cells) or a control plasmid (pUNO). When subcutaneously injected in NOD-SCID mice, pOSM cells were found to grow significantly faster than pUNO cells. However, OSM overexpression led to rapid weight loss resulting in termination of the experiment within three weeks of tumour cell injection whilst tumours were still <250mm^3. Although this was unexpected at the time, treatment of mice with hOSM has previously been demonstrated to result in weight loss and pancreatic and white fat atrophy, consistent with cachexia[113,95]. As this phenotype is not seen in mice treated with mOSM, it is believed to be a result of hOSM signalling through mLIFR[95]. Livers from mice injected with pOSM cells displayed hepatocyte necrosis and inflammatory cell infiltrate and also displayed increased weight relative to total body weight, compared to mice injected with pUNO cells. The hepatocyte toxicity observed in this experiment is, therefore, likely to be a result of hOSM signalling via the mLIFR. Activation of mLIFR (albeit by mLIF) has previously been shown to result in extramedullary hemopoiesis and necrosis within mouse livers[415]. Overexpression of mOSM has also been shown to impact the liver, resulting in severe liver fibrosis without

necrotic damage of hepatocytes[416]. However, as mOSM has very low affinity for the mLIFR receptor, it is unlikely that this effect is mediated by signalling via the LIFR. Similarly, lungs of mice injected with pOSM cells had alveolar wall thickening due to oedema, resulting in increased lung weight relative to total body weight, compared to mice injected with pUNO cells. OSM has been shown to be overexpressed in lungs of patients with pulmonary fibrosis and delivery of mOSM was found to be a potent mediator of lung inflammation and fibrosis in mice[417]. However, there is little information in the literature on the phenotypic effects on the lungs following activation of mLIFR by hOSM or mLIF. It is nonetheless plausible that the toxicity seen in the lungs is induced by mechanisms similar to those seen in the liver.

6.5.4 SW756 xenografts with reduced endogenous OSM production

We then tested whether expression of endogenous hOSM at a lower level than that found in the pOSM cells resulted in less systemic toxicity but also had a quantifiable effect on the growth of the tumour cells. Transfection of SW756 cells was repeated using the same hOSM expression plasmid. Multiple clones were selected for *in vitro* validation by qPCR, ELISA and western blot. These clones were found to have differing levels of hOSM expression and basal activation of downstream targets of OSM-OSMR signalling. Empty plasmid SW756 cells (pUNO2) and OSM overexpressing pOSM_c2 and pOSM_c3 cells were selected for subsequent *in vivo* experiments. pOSM_c2 had low levels of OSM overexpression compared to WT SW756 cells (31-fold increase), whereas pOSM_c3 had high levels of OSM overexpression (900-fold increase compared to WT cells). Both cell lines expressed lower levels of OSM than the original pOSM cell line.

OSM overexpressing pOSM_c3 cells displayed significant upregulation of OSMR compared to pUNO2 cells. Interestingly, despite the vast upregulation in OSM expression, levels of OSMR in these cells were less than those observed for WT SW756 cells in response to OSM treatment. Similarly, VEGFA was upregulated to greater levels in WT SW756 cells following treatment with OSM than in pOSM_c3 cells. Conversely, levels of TGM2 and SNAI1 were significantly upregulated in pOSM_c3 cells compared to WT SW756 cells and pUNO2 cells. Little upregulation was observed in WT SW756 cells in response to OSM treatment. This may, therefore, convey differences in gene activation in short-term versus sustained activation of OSM-OSMR signalling.

Expression levels of genes identified to be targets of OSM-OSMR signalling by NGS experiments (Chapter 5) were subsequently investigated. Both CHI3LI and CEMIP were upregulated in OSM treated WT SW756 cells and in OSM overexpressing pOSM_c2 and pOSM_c3 cells. Levels of both CH13L1 and CEMIP were greatest in pOSM_c3 cells which

have higher levels of hOSM expression than pOSM_c2 cells. While changes in CH13L1 expression were not found to be statistically significant, pOSM_c3 cells had significantly higher levels of CEMIP than any of the other cell lines. Moreover, PLAUR was also significantly upregulated in pOSM_c3 cells. All three of these genes were previously shown in NGS experiments to be upregulated in EP cells and EVs in response to OSM treatment and downregulated in KD cells and EVs. PLAUR has previously been shown to play a role in tumour growth, invasion, angiogenesis and metastasis in glioblastoma and NSCLC[366,367]. Moreover, PLAUR may be a downstream target of HIF signalling. It has been shown to be induced under hypoxic conditions in breast cancer cells and drives EMT[389]. Moreover, CHI3LI has been shown to promote both angiogenesis[342]and vascular mimicry[343] in cervical cancer. Therefore, we would predict that growth of these cell lines *in vivo* would produce tumours with increased angiogenesis and metastasis compared to pUNO2 cells.

In sequencing experiments, CPA4 and PTPRR were both downregulated in EP cells in response to OSM treatment and upregulated in KD cells. In the current experiment both genes appeared downregulated in pOSM_c3 cells compared to pUNO cells; downregulation of CPA4 was statistically significant. FMOD was found to be significantly upregulated in pOSM_c3 cells compared to all other cell lines; this gene was shown to be downregulated in KD cells in NGS experiments but unaffected in EP cells following OSM treatment. Upregulation in pOSM_c3 cells, but not in WT SW756 cells, following OSM treatment may be due to the significantly elevated levels of OSM in pOSM_C3 cells. Interestingly, PCSK1N was found to be significantly downregulated in pOSM_c2 and pOSM_c3 cell lines compared to the other three cell lines. This was an unexpected result as PCSK1N was found in NGS analysis to be downregulated in the KD cell line.

Taken together these findings predominantly corroborate findings from NGS experiments; targets that appeared up or down regulated in SW756 cells following OSM treatment displayed similar patterns of expression in OSM overexpressing cells. These genes may, therefore, be involved in key pathways that mediate functional effects of OSM-OSMR signalling. Unexpected expression of certain genes such as reduced and increased expression of PLCB4 and RAB38, respectively, in pUNO2 cells compared to WT SW756 cells may be explained by the fact that SW756 cells are a polyclonal cell line, whereas pUNO2 and pOSM_c2 and pOSM_c3 cell lines are derived from single cell colonies. Within polyclonal cell populations there is expected to be variability in gene expression between individual cells. Transfection of SW756 cells with pOSM or pUNO plasmids, followed by single cell selection and subsequent expansion of single cell colonies, may have selected for

sub populations of cells that display differential gene expression compared to the polyclonal population as a whole.

OSM promoted *in vivo* tumour growth of human cervical SCC cells with OSMR overexpression in a dose dependent manner. When injected subcutaneously into NOD-SCID mice, both pOSM_c2 (low OSM) and pOSM_c3 (high OSM) cells displayed a significantly increased growth rate compared to pUNO2 cells. Moreover, pOSM_c3 tumours were found to have a significantly increased growth rate compared to pOSM_c2 tumours. Mice with pOSM_c3 (high OSM) tumours had significantly reduced survival compared to mice with pUNO2 tumours; however, there was no difference in survival between mice with pUNO2 and mice with pUNO_c2 (low OSM) tumours.

Interestingly, pOSM_c3 tumours displayed an initial lag phase in the first 40 days following tumour cell injection. During this period the volume of these tumours was less than that of either pUNO2 or pOSM_c2 tumours. Growth of pOSM_c3 cells subsequently underwent a rapid increase in growth rate, overtaking either of the other two cell lines. This is consistent with the initial experiment in which the addition of OSM led to reduced growth of both EP and OSMR KD tumours. Again, this initial lag phase may possibly be explained by the induction of an EMT phenotype in SW756 cells in response to OSM-OSMR signalling. This may initially result in increased migration of tumour cells away from the injection site, thereby initially reducing the growth of the primary tumour. Cells remaining at the primary site may then have had a selective growth advantage as a result of high OSM expression but would have taken a while to surpass the growth of pUNO2 and pOSM_c2 tumours due to the initial depletion of tumour cells following migration. On the other hand, it is also possible that OSM, in fact, inhibited tumour growth, as seen in the previous experiment. Subsequent exponential growth of pOSM_c3 cells could be a result of increased signalling via LIFR rather than OSMR, possibly due to methylation of OSMR. Previous work by Underhill-Day *et al* (2006) has shown that signalling of OSM through OSMR and LIFR has antagonistic effects in breast cancer cells. Treatment of these cells with both OSM and a LIFR antagonist enhanced the cytostatic activity of OSM. Moreover, while treatment of these cells with OSM induced a fibroblast-like phenotype indicative of EMT, treatment with LIF has a less pronounced effect on cell morphology, with cells remaining predominantly epithelial-like[418]. Therefore, while OSM had previously been shown to signal predominantly through OSMR in SW756 cells[92], it is possible that high levels of OSM expression promotes EMT and subsequent migration of OSMR overexpressing cells away from the primary tumour. Greater levels of OSM-LIFR signalling in the remaining cells may abrogate the cytostatic effects of OSM-OSMR interactions, leading to the rapid growth of these tumours.

Differences in the syngeneic system provide further evidence for a potential interplay between OSM-OSMR and OSM-LIFR in the xenograft system. Unlike hOSM, mOSM only binds the murine OSMR (mOSMR)-gp130 heterodimer with high affinity, whereas mOSM binds to mouse LIFR (mLIFR)-gp130 heterodimers with very low affinity[93]. Therefore, the observation that OSMR KD from both tumour cells and the TME led to reduced tumour growth is likely to be mediated entirely by mOSM-mOSMR signalling. In these experiments no initial lag phase was observed in WT PDSC5.2 tumours grown in WT FVB mice. However, there are further complexities in comparing the mouse and human systems: hOSM-hOSMR receptor binding leads to phosphorylation of STAT1, STAT3, STAT5B and STAT6[87], whereas mOSM-mOSMR binding solely leads to phosphorylation of STAT1 and STAT3, similar to hOSM-hLIFR binding[88,89]. Thus, further investigation is required to fully elucidate the extent to which effects are mediated by hOSMR or hLIFR in the xenograft system.

In the initial experiment OSM was administered by IP injection for the first 13 days following tumour cell injection. The subsequent OSM overexpression experiment suggests that, if injections had continued for the duration of the experiment, exponential growth of these tumours could possibly have occurred, similar to the pOSM_c3 tumours. This could have resulted in an overall increased growth compared to tumours of mice injected with PBS control. It is possible that cessation of OSM administration may instead have perpetuated the initial negative effects of OSM on cell growth. While these experiments don't explain the response of the KD cell lines to OSM, they indicate that effects of OSM on tumour growth *in vivo* may be dependent on both dose and duration of OSM delivery. Continued delivery of OSM by OSM overexpressing cervical SCC cells more accurately reflects the sustained delivery of OSM that would be observed within the TME of patients with OSMR overexpressing cervical SCC tumours. Investigation of the effects of temporal OSM expression during different stage of tumour establishment could be further investigated using OSMR overexpressing cervical SCC cells that overexpress OSM under the control of a tetracycline inducible system such as that used by Tawara *et al* (2018)[113] to investigate the effect of OSM-OSMR signalling on breast cancer cell growth *in vivo*.

Mice with pOSM_c3 tumours displayed significantly reduced liver weight relative to total body weight compared to mice from either of the other two treatment groups. Increased liver weight in response to OSM overexpression in the first experiment is likely to have been a result of acute injury resulting in immune cell infiltration due to hOSM signalling through mLIFR. It is important to note that these mice were culled at a much earlier timepoint. Reduced liver weight in pOSM_c3 tumours may, therefore, be attributable to chronic injury,

as a result of hOSM signalling through mLIFR, resulting in increased cell death. In contrast to the preliminary pOSM experiment, pOSM_c2 and pOSM_c3 tumours did not result in rapid weight loss of NOD SCID mice; no significant differences in weight were detected between any of the three treatment groups throughout the duration of the experiment. Similarly, no toxic effects were observed in the lung, nor were any significant differences in lung weight relative to total body weight detected between experimental groups. Therefore, this represents a promising model for investigation of the effects of OSM-OSMR signalling on cervical SCC growth *in viv*o. This model could be used for future experiments investigating therapeutic blockade of either OSM or OSMR on tumour growth.

6.5.5 Future directions

Small white nodules resembling macro-metastases were visually detected in the lungs of individual mice from each treatment group. Histological investigation was not possible in the time frame of this thesis. Subsequent investigation will include performing histological analysis of sections prepared from lungs, liver, spleen, and femurs from mice from each treatment group in order to determine whether metastasis can be detected in any of these organs and whether there are differences in the degree of metastasis between mice from different treatment groups. This could be achieved using antibodies against human specific markers such as MHC class 1 antigens, HLA-A, HLA-B and HLA-C, which should not be expressed by murine cells[419].

For both *in vivo* experiments, once mice reached experimental endpoint, cardiac puncture was performed prior to cervical dislocation in order to collected plasma. Tumour pieces were also collected and underwent 24 hours *ex vivo* culture in DMEM media. After 24 hours EVs were isolated from the culture media by ultracentrifugation. RNA was extracted from both plasma and EVs isolated from *ex vivo* tumour cultures. Unfortunately, the current pipeline for reverse transcription and qPCR used in our laboratory was not sensitive enough to detect differential mRNA expression in the plasma and tumour derived EVs. Reverse transcription using kits designed for lower input quantities of RNA may allow for investigation of whether EV and plasma mRNA expression differ between treatment groups and further work should be done to pursue this.

Additionally, following tumour resection, tumour fragments were stored in liquid nitrogen for future orthotopic implantation into the cervix. Orthotopic implantation involves tumour engraftment in the region from which tumour cells were originally derived. This approach has previously been optimised in our laboratory using the immunocompetent PDSC5.2 cell model. Fragments from subcutaneous tumours are sutured to the cervix of naive mice,

allowing for the development of cervical tumours. Orthotopic tumour models more closely mimic the tumour microenvironment and allow for more accurate replication of tumour-stroma interactions, local invasion and lymphatic and haematogenous dissemination than subcutaneous xenograft models[420].

Most importantly, to fully understand the effects of OSM-OSMR tumour growth, it would be useful to further interrogate OSM-OSMR and OSM-LIFR signalling within these tumours. This could be achieved by using CRISPR to KD LIFR or OSMR in the OSM overexpressing pOSM_c3 cells and pOSM2 cells or by treatment of these two cell lines with either LIFR or OSMR inhibitors or antibodies. Subsequent growth of these cells *in vivo* with KD or therapeutic blockade or OSMR or LIFR would demonstrate whether effects from current experiments are truly a result of OSM signalling via OSMR rather than LIFR. Future experiments should include tracking of bioluminescent cells by IVIS in order to detect effects on metastasis.

Both the OSM overexpressing subcutaneous model detailed in this chapter and an orthotopic model derived from these tumours would provide a useful model for investigation of therapeutic blockade of OSM-OSMR signalling in cervical cancer. Few options currently exist for therapeutic blockade of OSM-OSMR signalling. This could be achieved either by targeting OSM using monoclonal antibodies or soluble receptor fusion proteins, or by antibodies directed against OSMR itself (Figure 6.15). In a phase II clinical trial by GSK, humanised antibodies against OSM were used to treat rheumatoid arthritis. Unfortunately treatment was ineffective due to the fact the antibody bound OSM with less affinity than the OSM receptor and, therefore, could not remove the ligand efficiently enough[421]. More recently GSK have commenced an additional phase II trial using a redesigned anti-OSM antibody with higher affinity for OSM for the treatment of diffuse cutaneous systemic sclerosis[100]. This is the same antibody previously used by our laboratory which successfully inhibited lung colonisation in the tail vein model of cervical SCC[92]. These studies represent the only two clinical trials to date which have therapeutically targeted OSM-OSMR signalling. Two humanised anti-OSMR antibodies are currently reported to be in pre-clinical development[100]. Moreover, Brolund *et al* (2011) have recently developed a murine fusion protein comprising the ligand-binding domain of mouse OSMR and gp130 which binds to mOSM[422]. We have recently used this fusion protein to inhibit OSM induced activation of STAT3 signalling in PDSC5.2 cells *in vitro* (results unpublished). However, no homologous humanised fusion protein currently exists.

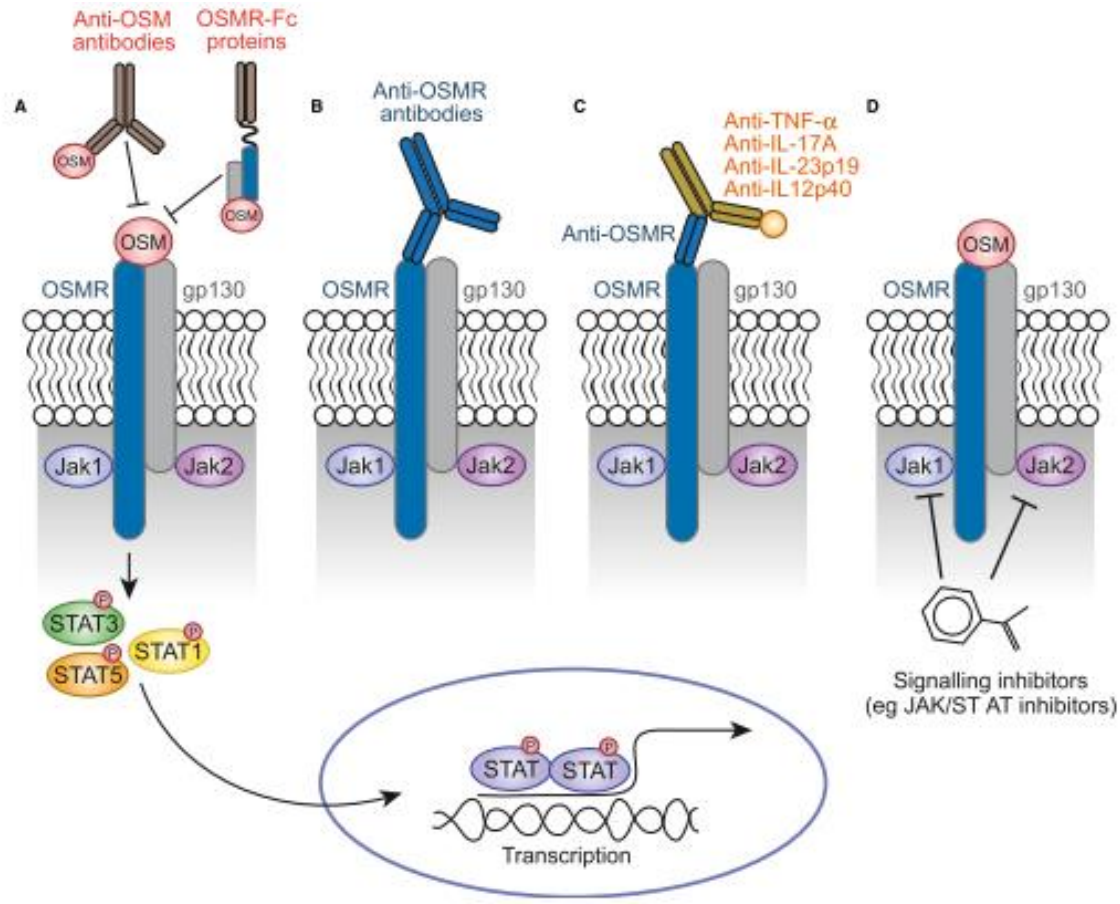

Figure 6.15: Options for therapeutic blockade of OSM-OSMR signalling
OSM-OSMR signalling could be pharmacologically targeted by various approaches, including (A) monoclonal antibodies and receptor fusion proteins that neutralize OSM (B) monoclonal antibodies that target OSMR (C) bispecific reagents that target both OSM or OSMR and other inflammatory cytokines or tissue-specific factors; and (D) small molecule inhibitors that target signal transduction mediators downstream of OSMR, such as JAK/STAT inhibitors. **Taken from West *et al* (2018)[100].**

6.5.6 Chapter Summary

This chapter aimed to establish a mouse model which allowed for investigation of the effects of OSM-OSMR signalling on *in vivo* growth and metastasis of human cervical SCC cells. For all the experiments discussed in this chapter tumour xenografts were established by subcutaneous injection of cells into immunocompromised NOD SCID mice. OSMR KD SW756 cells were found to have significantly reduced growth rate *in vivo* than OSMR overexpressing empty plasmid SW756 cells. Administration of exogenous hOSM by IP injection for the first 13 days following tumour establishment led to reduced tumour growth of both cell lines. Experiments in which hOSM was continually delivered demonstrated a more complex scenario which was dependent on the amount of OSM produced. Overall, SW756 cells with constitutive OSM overexpression had a significantly increased growth rate *in vivo* compared to SW756 cells which did not express OSM. However, whether these effects were

completely mediated by OSM-OSMR signalling or involved interplay between OSM and LIFR remains to be elucidated. Whether OSM overexpressing cells had increased metastatic potential and/or effects on the tumour vasculature is still to be evaluated by histological analysis. Together, these experiments indicate that effects of OSM on cervical SCC tumour growth may be dependent on both dose and duration of OSM delivery. Continued delivery of OSM by OSM overexpressing cervical SCC cells more accurately recapitulates the sustained delivery of OSM that would be observed within the TME of patients with OSMR overexpressing cervical SCC tumours. Therefore, we believe that this represents a promising model for investigation of the effects of OSM-OSMR signalling on cervical SCC growth *in vi*vo, and could be used for investigation of therapeutic blockade of OSM-OSMR signalling using humanised antibodies or fusion proteins.

7. CONCLUDING DISCUSSION

7.1 Project Context

The implementation of population-based screening programmes that test for HPV infection or use cytology to identify abnormal cells indicative of pre-cancerous disease have successfully reduced cervical cancer incidence and mortality in high-income countries by up to 80% over the last 5 decades[44]. Moreover, the introduction of nationwide prophylactic vaccination programmes against HR-HPV subtypes is expected to further decrease cervical cancer incidence and mortality. Dramatic reductions in pre-cancerous disease have already been observed in countries that have implemented nationwide vaccination programmes since the first vaccine was licensed in 2006 [54,58,59]. Currently, however, there is great disparity in the global implementation of nationwide programmes for HPV vaccination and screening for pre-cancerous disease. As such, cervical carcinoma remains the fourth most commonly diagnosed cancer and the fourth leading cause of cancer mortality in women worldwide[1]. Moreover, the HPV vaccination does not treat existing HPV infections[53] and multiple generations of women will not have been eligible for vaccination because of its relatively recent implementation[58]. Outcomes for women diagnosed with metastatic or recurrent cervical cancer is poor, with little improvement in survival outcomes over the last three decades[67]. Therefore, there is an urgent need for the development of new targeted therapies for the treatment of cervical carcinoma.

The development of targeted therapies requires a thorough understanding of the molecular mechanisms driving tumour progression. Previous work in our laboratory has focused on the role of OSMR as a driver of cervical SCC. OSMR frequently undergoes copy-number gain and overexpression in cervical SCC and is associated with adverse overall survival independent of tumour stage[70,73]. Moreover, OSM-OSMR signalling activates STAT3 signalling inducing a pro-malignant phenotype including increased cell migration, invasion and angiogenesis[73,92,121,122]. Bidirectional communication between cancer cells and cells of the TME is essential for tumour progression. EVs have been demonstrated to be key mediators of intercellular communication and promote tumour progression through various mechanisms[187,188]. Therefore, this thesis aimed to investigate whether OSM-OSMR signalling was capable of modulating the cargo of EVs released from cervical SCC cells, as a mechanism of perpetuating oncogenic signals to other cancer cells and to cells of the TME.

7.2 Overview and discussion of findings

7.2.1 Chapter 4

The experiments detailed in Chapter 4 demonstrated that EVs could be successfully isolated by sequential ultracentrifugation from cervical SCC cell lines. These vesicles were of the expected size range for sEVs and were enriched for ALIX, CD63 and CD9, three markers known to be expressed by both exosomes and microvesicles. Treatment of cervical SCC cells with OSM did not affect the size or quantity of EVs released. Having shown that EVs could be successfully isolated, a pilot study was conducted to determine whether OSM-OSMR signalling modulated miRNA expression by cervical SCC cells and their EVs. We selected miRNAs for investigation in this pilot study as they are the most commonly investigated of the RNA species present in EV cargo. Multiple groups have previously demonstrated that cancer cells release EVs containing functional miRNAs that are capable of modulating RNA expression in recipient cells promoting pro-tumourigenic phenotypes in both other cancer cells and cells of the TME[423–425].

In a pilot study a panel of nine miRNAs was selected for investigation in two cervical SCC cell lines: SW756 cells (which have OSMR copy number gain and baseline OSMR overexpression); and ME180 cells which have normal baseline levels of OSMR expression. It was initially hypothesised that OSM treatment would lead to upregulation of suspected tumour-promoting miRNAs and downregulation of suspected tumour-suppressing miRNAs in SW756 cells, but have little effect on miRNA expression in ME180 cells. However, this was not the case as miRNAs were upregulated in both cell lines in response to OSM treatment, irrespective of their suspected role in tumour progression. The impact of OSM treatment on modulating EV miRNA expression was notably greater in SW756 EVs compared to ME180 EVs. These experiments, therefore, constituted a promising pilot study to demonstrate that OSM-OSMR signalling is capable of differentially modulating cellular and EV miRNA expression in cervical SCC cell lines with different levels of OSMR expression.

The functional impact of these changes was then interrogated using growth, migration and angiogenesis assays. These assays were selected as OSM-OSMR signalling has previously been demonstrated to impact on these processes. However, we were unable to determine functional differences between EVs isolated from PBS or OSM treated cells. This does not necessarily mean that EVs isolated from cervical SCC cells treated with OSM or PBS do not have differential functional affects when taken up by cancer cells themselves or cells of the TME. There were multiple limitations to these experiments that may have affected their outcomes. For example, concentrations of EVs used may have been too low to confer

functional effects, cell treatment may have been suboptimal (i.e. short pulse of OSM treatment used for angiogenesis assay) and EV uptake was not demonstrated. Moreover, PBS and OSM EVs may have been found to have differential functional effects if alternative recipient cells types or different functional assays had been selected for investigation. These experiments highlighted the necessity to undertake a targeted approach in order to elucidate whether OSM-OSMR signalling propagated any functionally significant changes via the EVs. An OSMR KD SW756 cell line was subsequently generated by CRISPR-Cas9 for this purpose.

7.2.2 Chapter 5

The experiments detailed in Chapter 5 describe the use of NGS to investigate global changes in cellular and EV mRNA and miRNA expression profiles in response to OSM-OSMR signalling. Treatment of OSMR overexpressing EP SW756 cells with OSM resulted in global changes in gene expression in both cells and their resultant EVs. OSM-OSMR signalling led to over representation of pathways involved in: cytokine mediated signalling, myeloid leucocyte activation, hypoxia signalling, interferon signalling, negative regulation of viral life cycle and angiogenesis in both cells and EVs. On the other hand, pathways involved in PI3K-AKTsignalling, tissue remodelling, negative regulation of differentiation and focal adhesion were downregulated in cells whereas pathways involved in cell cycle regulation and regulation of division and cellular organisation were downregulated in EVs.
These findings were in line with a smaller selection of pathways previously found to be over represented in microarray analysis of mRNA expression in response to OSM treatment in SW756 and CaSki cell lines and clinical cervical SCC samples with OSMR overexpression[121]. The results presented in this thesis, therefore, build upon our current knowledge of the effects of OSM-OSMR signalling in cervical SCC cells. In addition, we identified novel pathways for investigation and demonstrated that OSMR KD results in global changes in gene expression, in both cells and EVs. Moreover, the current results demonstrate, for the first time, that OSM-OSMR signalling is capable of altering the mRNA cargo of EVs released from cervical SCC cells. Similar genes and pathways were found to be differentially expressed in both cervical SCC cells and EVs in response to OSM-OSMR signalling. Therefore, EVs may play a role in the transmission of OSM-OSMR mediated pro-tumorigenic signals to other cancer cells and to cells of the TME.

Nine genes that were found to be highly up or downregulated in both SW756 cells and EVs in response to OSM-OSMR signalling were selected for validation by qPCR. This was performed using the same cell samples as used for NGS (EP or KD cells + PBS/OSM) and RNA from additional cell lines generated by a second CRISPR experiment (EP2, KD2, KD3).

CHI3L1, CEMIP and PLAUR were shown to be consistently upregulated in EP cells in response to OSM, and downregulated in KD cells; whereas CPA4 and PTPRR were found to be consistently downregulated in EP cells in response to OSM. Therefore, these five genes were identified as promising candidate genes for subsequent investigation in future EV experiments.

The pilot study conducted in Chapter 4 led us to hypothesise that OSM-OSMR signalling would result in wide-scale changes in cellular and EV miRNA expression. However, small RNA sequencing detected substantially fewer differentially expressed miRNAs in cervical SCC cells and EVs in response to OSM-OSMR signalling than expected. Ten miRNAs were found to be differentially expressed in both cells and their corresponding EVs. Many of these miRNAs have previously been reported to be associated with OSM and STAT3 signalling. As the number of differentially expressed miRNAs was lower than expected, four miRNA shown in Chapter 4 to be differentially expressed in SW756 cells and EVs in response to OSM were investigated by qPCR in the sequencing samples. This was in order to investigate whether the same changes previously described could be observed in these latter experiments. All four were found to be significantly upregulated in EP cells in response to OSM, and three were found to be significantly downregulated in KD cells, despite not being detected as significant in NGS analysis. Lack of consistency between NGS and qPCR data likely reflects variability between replicates. Changes in miRNA expression may also be subtle. Therefore, if less stringent FDR and LFC thresholds were used for the analysis of the NGS data, it is possible that in agreement with qPCR results, more miRNA may be identified as being targets of OSM-OSMR signalling in cervical SCC cells and their EVs.

7.2.3 Chapter 6

In Chapter 6, parallel experiments were conducted to elucidate the effects of OSM-OSMR signalling on the growth of cervical SCC cells *in vivo.* In an initial experiment tumour xenografts were established by subcutaneous injection of EP or KD SW756 cells into NOD-SCID mice. KD cells were found to have a significantly reduced growth rate *in vivo* than OSMR overexpressing EP cells. Administration of exogenous hOSM by IP injection for the first 13 days following tumour establishment led to reduced tumour growth of both cell lines. The response of the KD cell line to OSM was unexpected, and suggested that the experimental system was sub-optimal.

Experiments in which hOSM was continually delivered demonstrated a more complex scenario which was dependent on the amount of OSM produced. pOSM-c3 SW756 cells with high levels of constitutive OSM overexpression had a significantly increased growth rate

in vivo compared to SW756 cells which did not express OSM or those with lower levels of OSM overexpression. However, an initial lag phase in pOSM_C3 tumour growth indicated that some of the effects observed in both xenograft experiments could possibly be mediated by OSM-LIFR signalling in addition to OSM-OSMR signalling. Moreover, whether OSM overexpressing cells had increased metastatic potential remains to be elucidated following histological analysis. Together, these experiments indicate that effects of OSM on cervical SCC tumour growth may be dependent on the route, dose and duration of OSM delivery. However, despite these caveats, we believe that this represents a promising model for investigation of the effects of OSM-OSMR signalling on cervical SCC growth *in viv*o, and could be used for investigation of therapeutic blockade of OSM-OSMR signalling using humanised antibodies or fusion proteins.

7.3 Future Work

7.3.1 *In vitro* experiments

To follow on from the work presented in this thesis, initial experiments should primarily aim to demonstrate whether EVs released from cervical SCC cells are taken up by other cancer cells and various cells of the TME. This could be achieved by incubation of EVs with a fluorescent lipophilic dye such as PKH67 prior to treatment of recipient cells, allowing for visualisation of uptake by fluorescent microscopy[320]. OSM-OSMR signalling was found to have a greater impact on cellular and EV mRNA expression than miRNA expression. Therefore, initial experiments should focus on changes in EV mRNA cargo in response to OSM-OSMR signalling. Once EV uptake has been demonstrated, subsequent experiments should focus on whether mRNA and protein expression of recipient cells is altered in response to EV treatment. CHI3L1 and CEMIP were found to be highly upregulated in EP cells and EVs in response to OSM and were downregulated in KD cells and EVs. They would, therefore, be promising candidate genes for investigation. Initial experiments could be performed in which KD cells (which underexpress these mRNAs) are treated with EP-PBS-EVs and EP-OSM-EVs. Levels of CHI3L1 and CEMIP in recipient KD cells would subsequently be investigated by qPCR and western blot. This system could also be used in order to determine the concentration of EVs required to bring about detectable changes in mRNA expression in recipient cells, thereby informing the design of future experiments.

Subsequent experiments should focus on the functional effects of these EVs. Key pathways upregulated in EVs in response to OSM-OSMR signalling included cytokine mediated signalling, myeloid leucocyte activation and hypoxia response. This indicates that ideal recipient cells may include other cancer cells, endothelial cells and leucocytes such as

macrophages. Initial experiments could include treatment of these cell types with EP-PBS-EVs, EP-OSM-EVs, KD-PBS-EVs and KD-OSM-EVs followed by qPCR investigation of genes known to be targeted by OSM-OSMR signalling in recipient cells such as OSMR itself, VEGFA, TGM2 and SNAI1. Moreover, functional effects of EV transfer to these cells should be investigated. For example investigation of expression of EMT markers and use of invasion assays should be performed for investigation of the effects of EV treatment on recipient cancer cells. Migration and angiogenesis assays for endothelial cells following EV treatment, and investigation of leucocyte activation and HIF-1α induced polarisation of macrophages, would also be recommended. This could be achieved by qPCR to investigate M2 marker expression, such as Arg-1 and COX-2[382], in recipient cells.

7.3.2 *Ex vivo* experiments

In the subcutaneous xenograft experiments previously described, plasma was collected by cardiac puncture at experimental endpoint. Moreover, tumour fragments were grown for 24 hours *ex vivo* and tumour-derived EVs subsequently isolated by ultracentrifugation. Following optimisation of a protocol for quantification of low input quantities of RNA by qPCR, it would be interesting to investigate whether EV samples collected from *in vivo* experiments displayed differential expression of the key targets identified by NGS, such as CHI3L1 and CEMIP.

7.3.3 *In vivo* experiments

Following on from the subcutaneous xenograft experiments performed in this thesis, histological examination of lung, liver and femur sections should be performed in order to determine whether OSM-OSMR signalling affected metastasis in these models. Moreover, subsequent work should focus on elucidating whether the observed effects on tumour growth were completely attributable to OSM-OSMR signalling. This could be achieved by using CRISPR to KD LIFR or OSMR in the OSM overexpressing pOSM_c3 cells and pOSM2 cells or by treatment of these two cell lines with either LIFR or OSMR inhibitors or antibodies. Subsequent growth of these cells *in vivo* with KD or therapeutic blockade of OSMR or LIFR would demonstrate whether effects from current experiments are truly a result of OSM signalling via OSMR rather than LIFR. These experiments should include tracking of bioluminescent cells by IVIS in order to detect effects on metastasis.

The OSM overexpressing subcutaneous xenograft model (pOSM_c3) described in this thesis has promising potential as a model to facilitate investigation of therapeutic blockade of OSM-OSMR signalling *in vivo*. This could be achieved either by targeting OSM using monoclonal antibodies or soluble receptor fusion proteins, or by antibodies directed against

OSMR itself. Moreover, this model could be used to investigate the functional effects of EVs on OSM-OSMR signalling *in vivo*. This could be investigated by *in vivo* administration of siRNAs against nSMAse2 or RAB27A in order to prevent release of EVs from tumour cells[208–210]. Effects on tumour growth and metastasis would subsequently be investigated. Alternatively, EVs from various cell lines (i.e. EP-OSM-EV, KD-OSM-EV or pOSM_c3 EVs) could be injected and the effects on tumour growth investigated. This could also be performed using the tail vein model (and fluorescently labelled or bioluminescent EVs) in order to determine whether EVs assist in OSM induced lung colonisation, in line with what has been demonstrated previously in other cancer models[197,198]. Similarly, the immunocompetent PDSC5.2 model could also be utilised for these experiments.

7.4 Concluding Remarks

The work presented in this PhD thesis demonstrates for the first time that OSM-OSMR signalling is capable of modulating mRNA and miRNA expression by EVs released from cervical SCC cells *in vitro*. NGS identified over and under represented pathways in these EVs in response to OSM-OSMR signalling. These will be the focus of subsequent investigation in order to determine the functional effects of EV mediated transfer of OSM-OSMR signals to other cancer cells and cells of the TME. A subcutaneous xenograft model was established in which OSM overexpression was found to drive growth of SW756 cells *in vivo*. Subsequent experiments will need to be performed to elucidate whether effects are mediated entirely by OSM-OSMR signalling and not through additional contributions from OSM-LIFR signalling. Moreover, this model will be used for future investigation of therapeutic blockade of OSM-OSMR signalling and investigation of the role of OSM-OSMR mediated EV signalling on tumour growth and metastasis *in vivo*.

8. LIST OF ABBREVIATIONS

AC = Adenocarcinoma

AGO = argonaute

ANOVA = one way analysis of variance

AP = alkaline phosphatase

ARF6 = ADP-ribosylation factor 6

ARRDC1 = arrestin domain-containing protein 1

ATCC = American Type Culture Collection

BCA = Bicinchoninic Acid

BCIP/NBT = 5-bromo-4-chloro-3-indolyl-phosphate/nitro blue tetrazolium

BLAST = basic local alignment search tool

BMPs = bone morphogenic proteins

BSA = Bovine Serum Albumin

CAFs = cancer-associated fibroblasts

cDNA = complementary DNA

CEMIP = Cell migration-inducing and hyaluronan-binding protein (KIAA1199)

CGH = comparative genomic hybridisation

CHI3L1 = Chitinase-3-like protein 1 (YKL-40)

CIN = Cervical intra-epithelial neoplasia

circRNA = circular RNA

CLCF1 = cardiotrophin-like cytokine factor 1

CNTF = ciliary neurotrophic factor

CPA4 = Carboxypeptidase A4

CRISPR = clustered, regularly interspaced, short palindromic repeats

Ct = cycle threshold

CT-1 = cardiotrophin-1

CTLA4 = cytotoxic T-lymphocyte-associated antigen 4

DE = differentially expressed

DMEM medium = Dulbecco’s Modified Eagle medium

DMSO = dimethyl sulfoxide

DNA = deoxyribonucleic acid

DPX mountant = Dibutylphthalate Polystyrene Xylene

DSBs = double strand breaks

EBRT = external beam radiation therapy

ECL = enhanced standard chemiluminescence

ECM = extracellular matrix

EDTA = Ethylenediaminetetraacetic Acid

EGFP = enhanced green-fluorescent protein

EGFR = epidermal growth factor receptor

ELISA = enzyme-linked immunosorbent assay

EMT = epithelial-mesenchymal transition

ERK½ = extracellular signal-regulated kinases ½

ERKs = extracellular signal-regulated kinases

ESCRTs = endosomal sorting complexes required for transport

EtOH = ethanol

EVs = extracellular vesicles

FACS = Fluorescence-activated cell sorting

FBS = Fetal Bovine Serum

FDR = false discovery rate

FGF = fibroblast growth factor

FIGO = The International Federation of Gynecology and Obstetrics

FMOD = Fibromodulin

FN1 = fibronectin

GAVI = Global Alliance for Vaccines and Immunisations

GFP = green fluorescent protein

GBM = glioblastoma

GMEM = Glasgow Minimum Essential Medium

gRNA = guide RNA

HDR = homology directed repair

HGF = hepatocyte growth factor

HIV = human immunodeficiency virus

HK = housekeeper

hLIFR = human leukemia inhibitory factor receptor

hnRNPA2B1 = heterogeneous nuclear ribonuncleoprotein A2/B1

hOSM = human Oncostatin M

hOSMR = human Oncostatin M receptor

HPV = human papillomavirus

HR = high risk

HRP = streptavidin-horse radish peroxidase

HSILs = high grade squamous intra-epithelial lesions

HSP70 = heat shock protein 70

HUVECs = human umbilical vein endothelial cells

hypoxia-inducible factor = (HIF)

hypoxia-inducible factor 1 alpha = (HIF1α)

hypoxia-inducible factor 2 alpha = (HIF2α)

ICAM1 = intercellular adhesion molecule 1

ID-1 = inhibitor of DNA binding protein 1

IFNGR1 = interferon gamma receptors

IFNy = interferon gamma

IgG = Immunoglobulin G

IL-31RA = IL-31 receptor alpha

IL-6 = interleukin-6

ILVs = intraluminal vesicles

ILVs = intraluminal vesicles

lncRNAs = long non-coding RNAs

IP = intraperitoneally

IRF1 = interferon regulatory factor 1

IVIS = *in vivo* imaging system

JAK = Janus kinase

KD = knock down

KO = Knock Out

LB broth = Lysogeny broth

LCR = long control region

LEEP = loop electrosurgical excision procedure

LFC = log fold change

LIF = leukaemia inhibitory factor

LIFR = leukemia inhibitory factor receptor

LINEs = long interspersed elements

LR = low risk

LSILs = low grade squamous intra-epithelial lesions

LTRs = long terminal repeats

LTRs = long terminal repeats

MAPK = mitogen-activated protein kinase

MDSCs = myeloid-derived suppressor cells

MGB = minor groove binder

MHC Class I = major histocompatibility complex class I protein

miRNAs = microRNAs

MLCK = myosin light chain kinase

mLIF = murine leukaemia inhibitory factor

mLIFR = mouse leukaemia inhibitory factor receptor

MMLV = Moloney murine leukaemia virus

MMP = Matrix metalloproteinase

mOSM = murine Oncostatin M

mOSMR = murine Oncostatin M receptor

MRE = miRNA response elements

mRNA = messenger RNA

MT1-MMP = MMP membrane type 1

MVBs = multivesicular bodies

NFQ = non-fluorescent quencher

NGS = next generation sequencing

NHEJ = non-homologous end joining

NOD-SCID = Non-obese diabetic/severe combined immunodeficiency

NPC = nasopharyngeal carcinoma

NPM1 = RNA-binding protein nucleophosmin 1

NSCLC = non-small cell lung cancer

nSMases = neutral sphingomyelinase enzymes

NTA = Nanoparticle Tracking Analysis

ORF = open reading frames

OSM = Oncostatin M

OSMR = Oncostatin M Receptor

PAHO = Pan American Health Organisation

PAI = plasminogen activator inhibitor

PAM = Protospacer adjacent motifs

PANX1 = plasma membrane channel pannexin 1

PARP = poly ADP-ribose polymerase

PBS – phosphate buffered saline

PCR = polymerase chain reaction

PCSK1N = Proprotein convertase subtilisin/kexin type 1 inhibitor

PD-1 = programmed cell death protein 1

PDZK3 = PDZ domain containing protein 3

PFA = Paraformaldehyde

PI3K = phosphoinositide 3-kinase

piRNA = piwi-interacting RNA

PLAUR = plasminogen activator, urokinase receptor

PLCB4 = Phospholipase C beta 4

pre-miRNA = precursor miRNA

pri-miRNA = primary miRNA

PS = phosphatidylserine

PTPRR = Protein tyrosine phosphatase receptor type R

pUNO = empty control plasmid

PVDF = microporous polyvinylidene fluoride

qPCR = quantitative polymerase chain reaction

RAB = ras-related gtp-binding protein

RAB38 = ras-related gtp-binding protein

Rb = retinoblastoma

RCF = Relative Centrifugal Force

Rh-OSM = Recombinant Human Oncostatin M Protein

RIPA = Radioimmunoprecipitation assay buffer

RISC = RNA-induced silencing complex

rLIF = rat leukemia inhibitory factor

rLIFR = rat leukemia inhibitory factor receptor

RNA = ribonucleic acid

ROCK I = Rho-associated protein kinase

rOSM = rat Oncostatin M

rOSMR = rat Oncostatin M Receptor

rRNA = ribosomal RNA

SC = subcutaneously

SCC = squamous cell carcinoma

scRNA = small conditional RNA

SDS = sodium dodecyl sulfate

SEM = standard error of the mean

sEVs = small EVs

sgRNAs = single guide RNAs

siRNA = small interfering RNA

SMase = Sphingomyelin phosphodiesterase

SNAI1 = Snail Family Transcriptional Repressor 1)

SNAREs = N-ethylmaleimide-sensitive factor attachment protein receptors

snoRNA = small nucleolar RNA

snRNA = small nuclear RNA

snRNA = small nuclear RNA

SOC = super optimal broth

SOCS5 = suppressor of cytokine signalling 5

SRP-RNA = signal recognition particle RNA

SSBs = single strand breaks

STAT = signal transducers and activators of transcription

TCGA = The Cancer Genome Atlas

TEM = transmission electron microscopy

TF = transcription factors

TGCA = The Cancer Genome Atlas

TGFβ = tumour growth factor β

TGM2 = tissue transglutaminase

TIAM1 = T-cell lymphoma invasion and metastasis-inducing protein 1

TME = tumour microenvironment

TMM – trimmed means of M values

TRBP = transactivation response element RNA-binding protein

TRIO – triple functional domain

tRNA = transfer RNA

tSNE = t-Stochastic neighbour embedding

UPAR = Urokinase receptor

UTR = untranslated region

VAMP3 = vesicle associated membrane protein 3

VCAM1 = vascular cell adhesion molecule

VEGFA = vascular endothelial growth factor A

VEGFR = vascular endothelial growth factor receptor

VLP = virus like particles

vRNA = vault RNA

VST – variance stabilising transformation

WHO – World Health Organisation

WT = Wild Type

Y RNA = long Ro-associated Y RNA

YBX1 = RNA-binding protein Y-box protein 1

5P = short arm of chromosome 5

9. REFERENCES

1. Bray, F., Ferlay, J., Soerjomataram, I., Siegel, R. L., Torre, L. A. & Jemal, A. Global cancer statistics 2018: GLOBOCAN estimates of incidence and mortality worldwide for 36 cancers in 185 countries. *CA. Cancer J. Clin.* **68,** 394–424 (2018).

2. Torre, L. A., Islami, F., Siegel, R. L., Ward, E. M. & Jemal, A. Global cancer in women: Burden and trends. *Cancer Epidemiol. Biomarkers Prev.* **26,** 444–457 (2017).

3. Marth, C., Landoni, F., Mahner, S., McCormack, M., Gonzalez-Martin, A. & Colombo, N. Cervical cancer: ESMO Clinical Practice Guidelines for diagnosis, treatment and follow-up. *Ann. Oncol.* **28,** iv72–iv83 (2017).

4. Doorbar, J. & Griffin, H. Refining our understanding of cervical neoplasia and its cellular origins. *Papillomavirus Res.* **7,** 176–179 (2019).

5. Lee, K. B., Lee, J. M., Park, C. Y., Lee, K. B., Cho, H. Y. & Ha, S. Y. What is the difference between squamous cell carcinoma and adenocarcinoma of the cervix? A matched case-control study. *Int. J. Gynecol. Cancer* **16,** 1569–1573 (2006).

6. Berrington De González, A., Sweetland, S. & Green, J. Comparison of risk factors for squamous cell and adenocarcinomas of the cervix: A meta-analysis. *Br. J. Cancer* **90,** 1787–1791 (2004).

7. Park, J. Y., Kim, D. Y., Kim, J. H., Kim, Y. M., Kim, Y. T. & Nam, J. H. Outcomes after radical hysterectomy in patients with early-stage adenocarcinoma of uterine cervix. *Br. J. Cancer* **102,** 1692–1698 (2010).

8. Eifel, P. J., Burke, T. W., Morris, M. & Smith, T. L. Adenocarcinoma As Independent Risk Factor for Disease Recurrance in Patients with Stage 1B Cervical Carcinoma. *Gynecol. Oncol.* **59,** 38–44 (1995).

9. Shimada, M., Nishimura, R., Nogawa, T., Hatae, M., Takehara, K., Yamada, H., Kurachi, H., Yokoyama, Y., Sugiyama, T. & Kigawa, J. Comparison of the outcome between cervical adenocarcinoma and squamous cell carcinoma patients with adjuvant radiotherapy following radical surgery: SGSG/TGCU Intergroup Surveillance. *Mol. Clin. Oncol.* **1,** 780–784 (2013).

10. Hu, K., Wang, W., Liu, X., Meng, Q. & Zhang, F. Comparison of treatment outcomes between squamous cell carcinoma and adenocarcinoma of cervix after definitive radiotherapy or concurrent chemoradiotherapy. *Radiat. Oncol.* **13,** 1–7 (2018).

11. Koh, W. J., Abu-Rustum, N. R., Bean, S., Bradley, K., Campos, S. M., Cho, K. R., Chon, H. S., Chu, C., Clark, R., Cohn, D., Crispens, M. A., Damast, S., Dorigo, O., Eifel, P. J., Fisher, C. M., Frederick, P., Gaffney, D. K., Han, E., Huh, W. K., *et al.* Cervical cancer, version 3.2019. *J. Natl. Compr. Cancer Netw.* **17,** 64–84 (2019).

12. Walboomers, J. M. M., Jacobs, M. V., Manos, M. M., Bosch, F. X., Kummer, J. A., Shah, K. V., Snijders, P. J. F., Peto, J., Meijer, C. J. L. M. & Munoz, N. Human papillomavirus is a necessary cause of invasive cervical cancer worldwide. *J. Pathol.* **189,** 12–19 (1999).

13. Petry, K. U., Liebrich, C., Luyten, A., Zander, M. & Iftner, T. Surgical staging identified false HPV-negative cases in a large series of invasive cervical cancers. *Papillomavirus Res.* **4,** 85–89 (2017).

14. Kaliff, M., Karlsson, M. G., Sorbe, B., Bohr Mordhorst, L., Helenius, G. & Lillsunde-Larsson, G. HPV-negative Tumors in a Swedish Cohort of Cervical Cancer. *Int. J. Gynecol. Pathol.* 1–10 (2019). doi:10.1097/PGP.0000000000000612

15. Nicolás, I., Marimon, L., Barnadas, E., Saco, A., Leonardo Rodríguez-Carunchio, •, Pere Fusté, •, Martí, C., Rodriguez-Trujillo, A., Aureli Torne, •, Del Pino, M. & Ordi, J. HPV-negative tumors of the uterine cervix. *Mod. Pathol.* **32,** 1189–1196 (2019).

16. de Sanjosé, S., Diaz, M., Castellsagué, X., Clifford, G., Bruni, L., Muñoz, N. & Bosch, F. X. Worldwide prevalence and genotype distribution of cervical human papillomavirus DNA in women with normal cytology: a meta-analysis. *Lancet Infect. Dis.* **7,** 453–459 (2007).

17. Yeo-Teh, N. S. L., Ito, Y. & Jha, S. High-risk human papillomaviral oncogenes E6 and E7 target key cellular pathways to achieve oncogenesis. *Int. J. Mol. Sci.* **19,** (2018).

18. Muñoz, N., Bosch, F. X., De Sanjosé, S., Herrero, R., Castellsagué, X., Shah, K. V, Snijders, P. J. F. & Meijer, C. J. L. M. Epidemiologic Classification of Human Papillomavirus Types Associated with Cervical Cancer. *N. Engl. J. Med.* **348,** 518–527 (2003).

19. Clifford, G., Smith, J., Plummer, M., Muñ Oz, N. & Franceschi, S. Human papillomavirus types in invasive cervical cancer worldwide: a meta-analysis. *Br. J. Cancer* **88,** 63–73 (2003).

20. Münger, K., Baldwin, A., Edwards, K. M., Nguyen, C. L., Owens, M., Huh, K., Mu, K., Hayakawa, H. & Grace, M. Mechanisms of Human Papillomavirus-Induced Oncogenesis. *J. Virol.* **78,** 11451–11460 (2004).

21. Graham, S. V. & Faizo, A. A. A. Control of human papillomavirus gene expression by alternative splicing. *Virus Res.* **231,** 83–95 (2017).

22. Pyeon, D., Pearce, S. M., Lank, S. M., Ahlquist, P. & Lambert, P. F. Establishment of Human Papillomavirus Infection Requires Cell Cycle Progression. *PLoS Pathog.* **5,** e1000318 (2009).

23. Stanley, M. A., Browne, H. M., Appleby, M. & Minson, A. C. Properties of a non-tumorigenic human cervical keratinocyte cell line. *Int J Cancer* **43,** 672–676 (1989).

24. Bedell, M. A., Hudson, J. B., Golub, T. R., Turyk, M. E., Hosken, M., Wilbanks, G. D. & Laimins, L. A. Amplification of Human Papillomavirus Genomes In Vitro Is Dependent on Epithelial Differentiation. *J. Virol.* **65,** 2254–2260 (1991).

25. Durst, M.-T., Glitz, D., Schneider, A. & Hausen, H. Zur. Human Papillomavirus Type 16 (HPV 16) Gene Expression and DNA Replication in Cervical Neoplasia: Analysis by in Situ Hybridization. *Virology* **189,** 132–40 (1992).

26. Cheng, S., Schmidt-Grimminger, D.-C., Murant, T., Broker, T. R. & Chow, L. T. Differentiation-dependent up-regulation of the human papillomavirus E7 gene reactivates cellular DNA replication in suprabasal differentiated keratinocytes. *Genes Dev.* **9,** 2335–2349 (1995).

27. Woodman, C. B. J., Collins, S. I. & Young, L. S. The natural history of cervical HPV infection: unresolved issues. *Nat. Rev. Cancer* **7,** 11–22 (2007).

28. Follen Mitchell, M., Hittelman, W. N., Hong, W. K., Lotan, R. & Schottenfeld, D. The Natural History of Cervical lntraepithelial Neoplasia: An Argument for Intermediate Endpoint Biomarkers. *Cancer Epidemiol. Biomarkers Prev.* **3,** 619–626 (1994).

29. Waxman, A. G., Chelmow, D., Darragh, T. M., Lawson, H. & Moscicki, A. B. Revised terminology for cervical histopathology and its implications for management of high-grade squamous intraepithelial lesions of the cervix. *Obstet. Gynecol.* **120,** 1465–1471 (2012).

30. Choo, K.-B., Pan, C.-C. & Han, S.-H. Integration of Human Papillomavirus Type 16 into Cellular DNA of Cervical Carcinoma: Preferential Deletion of the E2 Gene and Invariable Retention of the Long Control Region and the E6/E7 Open Reading Frames. *Virology* **161,** 259–261 (1987).

31. Doorbar, J. Molecular biology of human papillomavirus infection and cervical cancer. *Clin. Sci.* **110,** 525–541 (2006).

32. Cricca, M., Venturoli, S., Leo, E., Costa, S., Musiani, M. & Zerbini, M. Disruption of HPV 16 E1 and E2 genes in precancerous cervical lesions. *J. Virol. Methods* **158,** 180–183 (2009).

33. The Cancer Genome Atlas Research Network. Integrated genomic and molecular characterization of cervical cancer. *Nature* **543,** 378–384 (2017).

34. Pett, M. & Coleman, N. Integration of high-risk human papillomavirus: a key event in cervical carcinogenesis? *J. Pathol.* **212,** 356–367 (2007).

35. Dyson, N., Howley, P. M., Munger, K. & Harlow, E. The Human Papilloma Virus-16 Oncoprotein Is Able to Bind to the Retinoblastoma Gene Product. *Science* **243,** 934–937 (1989).

36. Polager, S. & Ginsberg, D. p53 and E2f: partners in life and death. *Nat. Rev. Cancer* **9,** 738–748 (2009).

37. Werness, B. A., Levine, A. J. & Howley, P. M. Association of Human Papillomavirus Types 16 and 18 E6 Proteins with p53. *Science* **248,** 76–79 (1990).

38. Piboonniyom, S., Duensing, S., Swilling, N. W., Hasskarl, J., Hinds, P. W. & Münger, K. Abrogation of the Retinoblastoma Tumor Suppressor Checkpoint During Keratinocyte Immortalization Is Not Sufficient for Induction of Centrosome-mediated Genomic Instability. *Cancer Res.* **63,** 476–483 (2003).

39. Duensing, S. & Münger, K. Mechanisms of genomic instability in human cancer: Insights from studies with human papillomavirus oncoproteins. *Int. J. Cancer* **109,** 157–162 (2004).

40. Castle, P. E., Schiffman, M., Wheeler, C. M. & Solomon, D. Evidence for frequent regression of cervical intraepithelial neoplasia-grade 2. *Obstet. Gynecol.* **113,** 18–25 (2009).

41. Tainio, K., Athanasiou, A., Tikkinen, K. A. O., Aaltonen, R., Cárdenas, J., Hernándes, Glazer-Livson, S., Jakobsson, M., Joronen, K., Kiviharju, M., Louvanto, K., Oksjoki, S., Tähtinen, R., Virtanen, S., Nieminen, P., Kyrgiou, M. & Kalliala, I. Clinical course of untreated cervical intraepithelial neoplasia grade 2 under active surveillance: Systematic review and meta-analysis. *BMJ* **360,** doi: 10.1136/bmj.k499 (2018).

42. Woo, Y. L., Van Den Hende, M., Sterling, J. C., Coleman, N., Crawford, R. A. F., Kwappenberg, K. M. C., Stanley, M. A. & Van Der Burg, S. H. A prospective study on the natural course of low-grade squamous intraepithelial lesions and the presence of HPV16 E2-, E6- And E7-specific T-cell responses. *Int. J. Cancer* **126,** 133–141 (2010).

43. zur Hausen, H. Papillomaviruses and Cancer: From Basic Studies to Clinical Application. *Nature* **2,** 342–350 (2002).

44. Sankaranarayanan, R. Screening for cancer in low- and middle-income countries. *Ann. Glob. Heal.* **80,** 412–417 (2014).

45. Grace, A., Kay, E. & Leader, M. Liquid-based preparation in cervical cytology screening. *Curr. Diagnostic Pathol.* **7,** 91–95 (2001).

46. Zhu, J., Norman, I., Elfgren, K., Gaberi, V., Hagmar, B., Hjerpe, A. & Andersson, S. A comparison of liquid-based cytology and Pap smear as a screening method for cervical cancer. *Oncol. Rep.* **18,** 157–160 (2007).

47. Ronco, G., Cuzick, J., Pierotti, P., Cariaggi, M. P., Palma, P. D., Naldoni, C., Ghiringhello, B., Giorgi-Rossi, P., Minucci, D., Parisio, F., Pojer, A., Schiboni, M. L., Sintoni, C., Zorzi, M., Segnan, N. & Confortini, M. Accuracy of liquid based versus conventional cytology: Overall results of new technologies for cervical cancer screening: Randomised controlled trial. *Br. Med. J.* **335,** 28–31 (2007).

48. Ebell, M. H., Thai, T. N. & Royalty, K. J. Cancer screening recommendations: An international comparison of high income countries. *Public Health Rev.* **39,** 1–19 (2018).

49. Ronco, G., Dillner, J., Elfström, K. M., Tunesi, S., Snijders, P. J. F., Arbyn, M., Kitchener, H., Segnan, N., Gilham, C., Giorgi-Rossi, P., Berkhof, J., Peto, J., Meijer, C. J. L. M., Cuzick, J., Zappa, M., Carozzi, F., Confortini, M., Dalla Palma, P., Zorzi, M., *et al.* Efficacy of HPV-based screening for prevention of invasive cervical cancer: Follow-up of four European randomised controlled trials. *Lancet* **383,** 524–532 (2014).

50. Koliopoulos, G., Vn, N., Santesso, N., Bryant, A., Ppl, M., Ra, M., Schünemann, H., Paraskevaidis, E. & Arbyn, M. Cytology versus HPV testing for cervical cancer screening in the general population. *Cochrane Database Syst. Rev.* DOI: 10.1002/14651858.CD008587.pub2 (2017).

51. Rizzo, A. E. & Feldman, S. Update on primary HPV screening for cervical cancer prevention. *Curr. Probl. Cancer* **42,** 507–520 (2018).

52. Khan, M. J. & Smith-McCune, K. K. Treatment of Cervical Precancers: Back to Basics. *Obstet. Gynecol.* **123,** 1339–1343 (2014).

53. Gupta, G., Glueck, R. & Patel, P. R. HPV vaccines: Global perspectives. *Hum. Vaccines Immunother.* **13,** 1421–1424 (2017).

54. Hansen, B. T., Campbell, S. & Nygård, M. Long-term incidence trends of HPV-related cancers, and cases preventable by HPV vaccination: A registry-based study in Norway. *BMJ Open* **8,** 1–9 (2018).

55. Schiller, J. T. Papillomavirus-like particle vaccines for cervical cancer. *Mol. Med. Today* **5,** 209–215 (1999).

56. Schiller, J. T. & Lowy, D. R. Prospects for cervical cancer prevention by human papillomavirus vaccination. *Cancer Res.* **66,** 10229–10232 (2006).

57. Brotherton, J. M. L. & Bloem, P. J. N. HPV Vaccination: Current Global Status. *Curr. Obstet. Gynecol. Rep.* **4,** 220–233 (2015).

58. Palmer, T., Wallace, L., Pollock, K. G., Cuschieri, K., Robertson, C., Kavanagh, K. & Cruickshank, M. Prevalence of cervical disease at age 20 after immunisation with

bivalent HPV vaccine at age 12-13 in Scotland: Retrospective population study. *BMJ* **365,** 1–10 (2019).

59. McClung, N. M., Gargano, J. W., Bennett, N. M., Niccolai, L. M., Abdullah, N., Griffin, M. R., Park, I. U., Cleveland, A. A., Querec, T. D., Unger, E. R. & Markowitz, L. E. Trends in human papillomavirus vaccine types 16 and 18 in cervical precancers, 2008–2014. *Cancer Epidemiol. Biomarkers Prev.* **28,** 602–609 (2019).

60. Altobelli, E., Rapacchietta, L., Profeta, V. F. & Fagnano, R. HPV-vaccination and cancer cervical screening in 53 WHO European Countries: An update on prevention programs according to income level. *Cancer Med.* **8,** 2524–2534 (2019).

61. Qendri, V., Bogaards, J. A. & Berkhof, J. Pricing of HPV vaccines in European tender-based settings. *Eur. J. Heal. Econ.* **20,** 271–280 (2019).

62. Black, E. & Richmond, R. Prevention of cervical cancer in sub-saharan Africa: The advantages and challenges of HPV vaccination. *Vaccines* **6,** doi:10.3390/vaccines6030061 (2018).

63. Bhatla, N., Berek, J. S., Cuello Fredes, M., Denny, L. A., Grenman, S., Karunaratne, K., Kehoe, S. T., Konishi, I., Olawaiye, A. B., Prat, J., Sankaranarayanan, R., Brierley, J., Mutch, D., Querleu, D., Cibula, D., Quinn, M., Botha, H., Sigurd, L., Rice, L., *et al.* Revised FIGO staging for carcinoma of the cervix uteri. *Int. J. Gynecol. Obstet.* **145,** 129–135 (2019).

64. Howlander, N., Noone, A. M., Krapcho, M., Miller, D., Brest, A., Yu, M., Ruhl, J., Tatalovich, Z., Mariotto, A., Lewis, D. R., Chen, H. S., Feuer, E. J. & Cronin, K. A. SEER Cancer Statistics Review 1975-2016. *Natl. Cancer Institute.* https://seer.cancer.gov/csr/1975_2016/ (2019).

65. Chuang, L. T., Feldman, S., Nakisige, C., Temin, S. & Berek, J. S. Management and care of women with invasive cervical cancer: ASCO resource-stratified clinical practice guideline. *J. Clin. Oncol.* **34,** 3354–3355 (2016).

66. Gupta, S., Maheshwari, A., Parab, P., Mahantshetty, U., Hawaldar, R., Sastri, S., Kerkar, R., Engineer, R., Tongaonkar, H., Ghosh, J., Gulia, S., Kumar, N., Surappa Shylasree, T., Gawade, R., Kembhavi, Y., Gaikar, M., Menon, S., Thakur, M., Shrivastava, S., *et al.* Neoadjuvant Chemotherapy Followed by Radical Surgery Versus Concomitant Chemotherapy and Radiotherapy in Patients With Stage IB2, IIA, or IIB Squamous Cervical Cancer: A Randomized Controlled Trial. *J. Clin. Oncol.* **36,** 1548–1555 (2018).

67. Vora, C. & Gupta, S. Targeted therapy in cervical cancer. *ESMO Open* **3,** doi:10.1136/esmoopen-2018-000462 (2019).

68. Monk, B. J., Sill, M. W., McMeekin, D. S., Cohn, D. E., Ramondetta, L. M., Boardman, C. H., Benda, J. & Cella, D. Phase III trial of four cisplatin-containing doublet combinations in stage IVB, recurrent, or persistent cervical carcinoma: A Gynecologic Oncology Group study. *J. Clin. Oncol.* **27,** 4649–4655 (2009).

69. Tewari, K. S., Sill, M. W., Penson, R. T., Huang, H., Ramondetta, L. M., Landrum, L. M., Oaknin, A., Reid, T. J., Leitao, M. M., Michael, H. E., DiSaia, P. J., Copeland, L. J., Creasman, W. T., Stehman, F. B., Brady, M. F., Burger, R. A., Thigpen, J. T., Birrer, M. J., Waggoner, S. E., *et al.* Bevacizumab for advanced cervical cancer: final overall survival and adverse event analysis of a randomised, controlled, open-label, phase 3 trial (Gynecologic Oncology Group 240). *Lancet* **390,** 1654–1663 (2017).

70. Ng, G., Winder, D., Muralidhar, B., Gooding, E., Roberts, I., Pett, M., Mukherjee, G., Huang, J. & Coleman, N. Gain and overexpression of the oncostatin M receptor occur frequently in cervical squamous cell carcinoma and are associated with adverse clinical outcome. *J. Pathol.* **212,** 325–334 (2007).

71. Scotto, L., Narayan, G., Nandula, S. V, Subramaniyam, S., Kaufmann, A. M., Wright, J. D., Pothuri, B., Mansukhani, M., Schneider, A., Arias-Pulido, H. & Murty, V. V. Integrative genomics analysis of chromosome 5p gain in cervical cancer reveals target over-expressed genes, including Drosha. *Mol. Cancer* **7,** doi:10.1186/1476-4598-7-58 (2008).

72. Narayan, G., Bourdon, V., Chaganti, S., Arias-Pulido, H., Nandula, S. V, Rao, P. H., Gissmann, L., Durst, M., Schneider, A., Pothuri, B., Mansukhani, M., Basso, K., Chaganti, R. S. . & Murty, V. V. Gene Dosage Alterations Revealed by cDNA Microarray Analysis in Cervical Cancer: Identification of Candidate Amplified and Overexpressed Genes. *Genes. Chromosomes Cancer* **46,** 373–384 (2007).

73. Kucia-Tran, J. A., Tulkki, V., Smith, S., Scarpini, C. G., Hughes, K., Araujo, A. M., Yin, K., Yan, M., Botthof, J., Pé Rez-Gó Mez, E., Quintanilla, M., Cuschieri, K., Caffarel, M. M. & Coleman, N. Overexpression of the oncostatin-M receptor in cervical squamous cell carcinoma is associated with epithelial–mesenchymal transition and poor overall survival. *Br. J. Cancer* **115,** 212–222 (2016).

74. Murakami, M., Kamimura, D. & Hirano, T. Pleiotropy and Specificity: Insights from the Interleukin 6 Family of Cytokines. *Immunity* **50,** 812–831 (2019).

75. Rose, T. M., Lagrou, M. J., Fransson, I., Werelius, B., Delattre, O., Thomas, G., De Jong, P. J., Todaro, G. J. & Dumanski, J. P. The Genes for Oncostatin M (OSM) and Leukemia Inhibitory Factor (LIF) Are Tightly Linked on Human Chromosome 22. *Genomics* **17,** 136–140 (1993).

76. Heinrich, P. C., Behrmann, I., Haan, S., Hermanns, H. M., Uller-Newen, G. & Schaper, F. Principles of interleukin (IL)-6-type cytokine signalling and its regulation. *Biochem. J* **374,** 1–20 (2003).

77. Richards, C. D. The Enigmatic Cytokine Oncostatin M and Roles in Disease. *ISRN Inflamm.* **2013,** 1–23 (2013).

78. Mosley, B., De Imus, C., Friend, D., Boiani, N., Thoma, B., Park, L. S. & Cosman, D. Dual Oncostatin M (OSM) Receptors. Cloning and characterization of an alternative signalling subunit conferring OSM-specific receptor activation. *J. Biol. Chem.* **271,** 32635–32643 (1996).

79. Huang, A., Cheng, L., He, M., Nie, J., Wang, J. & Jiang, K. Interleukin-35 on B cell and T cell induction and regulation. *J. Inflamm.* **14,** DOI 10.1186/s12950-017-0164-5 (2017).

80. Chollangi, S., Mather, T., Rodgers, K. K. & Ash, J. D. A Unique Loop Structure in Oncostatin M Determines Binding Affinity toward Oncostatin M Receptor and Leukemia Inhibitory Factor Receptor. *J. Biol. Chem.* **287,** 32848–32859 (2012).

81. Sporeno, E., Paonessa, G., Salvati, A. L., Graziani, R., Delmastro, P., Ciliberto, G. & Toniatti, C. Oncostatin M binds directly to gp130 and behaves as interleukin-6 antagonist on a cell line expressing gp130 but lacking functional oncostatin M receptors. *J. Biol. Chem.* **269,** 10991–10995 (1994).

82. Cornelissen, C., Luscher-Firzlaff, J., Malte Baron, J. & Luscher, B. Signaling by IL-31

and functional consequences. *Eur. J. Cell Biol.* **91,** 552–566 (2012).

83. West, N. R. Coordination of immune-stroma crosstalk by IL-6 family cytokines. *Front. Immunol.* **10,** 1–16 (2019).

84. Jones, S. A. & Jenkins, B. J. Recent insights into targeting the IL-6 cytokine family in inflammatory diseases and cancer. *Nat. Rev. Immunol.* **18,** 773–789 (2018).

85. Hermanns, H. M., Radtke, S., Schaper, F., Heinrich, P. C. & Behrmann, I. Non-redundant signal transduction of interleukin-6-type cytokines: The adapter protein Shc is specifically recruited to the oncostatin M receptor. *J. Biol. Chem.* **275,** 40742–40748 (2000).

86. Stross, C., Radtke, S., Clahsen, T., Gerlach, C., Volkmer-Engert, R., Schaper, F., Heinrich, P. C. & Hermanns, H. M. Oncostatin M receptor-mediated signal transduction is negatively regulated by SOCS3 through a receptor tyrosine-independent mechanism. *J. Biol. Chem.* **281,** 8458–8468 (2006).

87. Hermanns, H. M. Oncostatin M and interleukin-31: Cytokines, receptors, signal transduction and physiology. *Cytokine Growth Factor Rev.* **26,** 545–558 (2015).

88. Hintzen, C., Evers, C., Lippok, B. E., Volkmer, R., Heinrich, P. C., Radtke, S. & Hermanns, H. M. Box 2 region of the oncostatin M receptor determines specificity for recruitment of Janus kinases and STAT5 activation. *J. Biol. Chem.* **283,** 19465–19477 (2008).

89. Auguste, P., Guillet, C., Fourcin, M., Olivier, C., Veziers, J., Pouplard-Barthelaix, A. & Gascan, H. Signaling of type II oncostatin M receptor. *J. Biol. Chem.* **272,** 15760–15764 (1997).

90. Kuropatwinski, K. K., De Imus, C., Gearing, D., Baumann, H. & Mosley, B. Influence of Subunit Combinations on Signaling by Receptors for Oncostatin M, Leukemia Inhibitory Factor, and Interleukin-6. *J. Biol. Chem.* **272,** 15135–15144 (1997).

91. Jahani-Asl, A., Yin, H., Soleimani, V. D., Haque, T., Luchman, H. A., Chang, N. C., Sincennes, M.-C., Puram, S. V, Scott, A. M., Lorimer, I. A. J., Perkins, T. J., Ligon, K. L., Weiss, S., Rudnicki, M. A. & Bonni, A. Control of glioblastoma tumorigenesis by feed-forward cytokine signaling. *Nat. Neurosci.* **19,** 798–806 (2016).

92. Kucia-Tran, J. A., Tulkki, V., Scarpini, C. G., Smith, S., Wallberg, M., Paez-Ribes, M., Araujo, A. M., Botthoff, J., Feeney, M., Hughes, K., Caffarel, M. M. & Coleman, N. Anti-oncostatin M antibody inhibits the pro-malignant effects of oncostatin M receptor overexpression in squamous cell carcinoma. *J. Pathol.* **244,** 283–295 (2018).

93. Ichihara, M., Hara, T., Kim, H., Murate, T. & Miyajima, A. Oncostatin M and leukemia inhibitory factor do not use the same functional receptor in mice. *Blood* **90,** 165–173 (1997).

94. Walker, E. C., Johnson, R. W., Hu, Y., Brennan, H. J., Poulton, I. J., Zhang, J.-G., Jenkins, B. J., Smyth, G. K., Nicola, N. A. & Sims, N. A. Murine Oncostatin M acts via Leukemia Inhibitory Factor Receptor to phosphorylate STAT3 but not STAT1, an effect that protects bone mass. *J. Biol. Chem.* **291,** 21703–21716 (2016).

95. Juan, T. S.-C., Bolon, B., Lindberg, R. A., Sun, Y., Van, G. & Fletcher, F. A. Mice Overexpressing Murine Oncostatin M (OSM) Exhibit Changes in Hematopoietic and Other Organs that Are Distinct from Those of Mice Overexpressing Human OSM or Bovine OSM. *Vet Pathol* **46,** 124–137 (2009).

96. Layton, M. J., Owczarek, C. M., Metcalf, D., Clark, R. L., Smith, D. K., Treutlein, H. R. & Nicola, N. A. Conversion of the biological specificity of murine to human leukemia inhibitory factor by replacing 6 amino acid residues. *J. Biol. Chem.* **269,** 29891–29896 (1994).

97. Adrian-Segarra, J. M., Sreenivasan, K., Gajawada, P., Lörchner, H., Braun, T. & Pöling, J. The AB loop of oncostatin M (OSM) determines species-specific signaling in humans and mice. *J. Biol. Chem.* **293,** 20181–20199 (2018).

98. Drechsler, J., Grötzinger, J. & Hermanns, H. M. Characterization of the rat oncostatin m receptor complex which resembles the human, but differs from the murine cytokine receptor. *PLoS One* **7,** e43155 (2012).

99. Houben, E., Hellings, N. & Broux, B. Oncostatin M, an underestimated player in the central nervous system. *Front. Immunol.* **10,** doi: 10.3389/fimmu.2019.01165 (2019).

100. West, N. R., Benjamin, |, Owens, M. J., Hegazy, A. N. & West, N. The oncostatin M-stromal cell axis in health and disease. *Scand. J. Immunol.* **88,** doi: 10.1111/sji.12694 (2018).

101. Brown, T. J., Rowe, J. M., Liu, J. W. & Shoyab, M. Regulation of IL-6 expression by oncostatin M. *J. Immunol.* **147,** 2175–2180 (1991).

102. Hurst, S. M., McLoughlin, R. M., Monslow, J., Owens, S., Morgan, L., Fuller, G. M., Topley, N. & Jones, S. A. Secretion of Oncostatin M by Infiltrating Neutrophils: Regulation of IL-6 and Chemokine Expression in Human Mesothelial Cells. *J. Immunol.* **169,** 5244–5251 (2002).

103. Suda, T., Chida, K., Todate, A., Ide, K., Asada, K., Nakamura, Y., Suzuki, K., Kuwata, H. & Nakamura, H. Oncostatin M production by human dendritic cells in response to bacterial products. *Cytokine* **17,** 335–340 (2002).

104. Tanaka, M., Hirabayashi, Y., Sekiguchi, T., Inoue, T., Katsuki, M. & Miyajima, A. Targeted disruption of oncostatin M receptor results in altered hematopoiesis. *Blood* **102,** 3154–3162 (2003).

105. Lacreusette, A., Nguyen, J. M., Pandolfino, M. C., Khammari, A., Dreno, B., Jacques, Y., Godard, A. & Blanchard, F. Loss of oncostatin M receptor β in metastatic melanoma cells. *Oncogene* **26,** 881–892 (2007).

106. Pan, C.-M. M., Wang, M.-L. L., Chiou, S.-H. H., Chen, H.-Y. Y. & Wu, C.-W. W. Oncostatin M suppresses metastasis of lung adenocarcinoma by inhibiting SLUG expression through coordination of STATs and PIASs signalings. *Oncotarget* **7,** 60395–60406 (2016).

107. Zarling, J. M., Shoyab, M., Marquardt, H., Hanson, M. B., Lioubin, M. N. & Todaro, G. J. Oncostatin M: A growth regulator produced by differentiated histiocytic lymphoma cells. *PNAS* **83,** 9739–9743 (1986).

108. Friedrich, M., Höss, N., Stögbauer, F., Senner, V., Paulus, W., Bernd Ringelstein, E. & Halfter, H. Complete inhibition of in vivo glioma growth by oncostatin M. *J. Neurochem.* **76,** 1589–1592 (2001).

109. Liu, J., Spence, M. J., Wallace, P. M., Forcier, K., Hellström, I. & Vestal, R. E. Oncostatin M-specific receptor mediates inhibition of breast cancer cell growth and down-regulation of the c-myc proto-oncogene. *Cell growth Differ.* **8,** 667–676 (1997).

110. Douglas, A. M., Grant, S. L., Goss, G. A., Clouston, D. R., Sutherland, R. L. & Begley,

C. G. Oncostatin M induces the differentiation of breast cancer cells. *Int. J. cancer* **75,** 64–73 (1998).

111. Simonneau, M., Frouin, E., Huguier, V., Jermidi, C., Jégou, J. F., Godet, J., Barra, A., Paris, I., Levillain, P., Cordier-Dirikoc, S., Pedretti, N., Bernard, F. X., Lecron, J. C., Morel, F. & Favot, L. Oncostatin M is overexpressed in skin squamous-cell carcinoma and promotes tumor progression. *Oncotarget* **9,** 36457–36473 (2018).

112. Kan, C. E., Cipriano, R. & Jackson, M. W. c-MYC Functions as a Molecular Switch to Alter the Response of Human Mammary Epithelial Cells to Oncostatin M. *Cancer Res* **71,** 6930–6939 (2011).

113. Tawara, K., Bolin, C., Koncinsky, J., Kadaba, S., Covert, H., Sutherland, C., Bond, L., Kronz, J., Garbow, J. R. & Jorcyk, C. L. OSM potentiates preintravasation events, increases CTC counts, and promotes breast cancer metastasis to the lung. *Breast Cancer Res.* **20,** doi.org/10.1186/s13058-018-0971-5 (2018).

114. Bolin, C., Tawara, K., Sutherland, C., Redshaw, J., Aranda, P., Moselhy, J., Anderson, R. & Jorcyk, C. L. Oncostatin M Promotes Mammary Tumor Metastasis to Bone and Osteolytic Bone Degradation. *Genes and Cancer* **3,** 117–130 (2012).

115. Royuela, M., Ricote, M., Parsons, M. S., García-Tuñón, I., Paniagua, R. & De Miguel, M. P. Immunohistochemical analysis of the IL-6 family of cytokines and their receptors in benign, hyperplasic and malignant human prostate. *J. Pathol.* **202,** 41–49 (2004).

116. Savarese, T. M., Campbell, C. L., Mcquain, C., Mitchell, K., Guardiani, R., Quesenberry, P. J. & Nelson, B. E. Coexpression of Oncostatin M and its receptors and evidence for STAT3 activtion in human ovarian carcinomas. *Cytokine* **17,** 324–334 (2002).

117. Zhu, M., Che, Q., Liao, Y., Wang, H., Wang, J., Chen, Z., Wang, F., Dai, C. & Wan, X. Oncostatin M activates STAT3 to promote endometrial cancer invasion and angiogenesis. *Oncol. Rep.* **34,** 129–138 (2015).

118. David, E., Tirode, F., Baud'huin, M., Guihard, P., Laud, K., Delattre, O., Heymann, M. F., Heymann, D., Redini, F. & Blanchard, F. Oncostatin M is a growth factor for Ewing sarcoma. *Am. J. Pathol.* **181,** 1782–1795 (2012).

119. Gurluler, E., Tumay, L. V, Guner, O. S., Kucukmentin, N. T., Hizli, B. & Zorluoglu, A. Oncostatin-M as a novel biomarker in colon cancer patients and its association with clinicopathologic variables. *Eur. Rev. Med. Pharmacol. Sci.* **18,** 2042–2047 (2014).

120. West, N. R., Murphy, L. C. & Watson, P. H. Oncostatin M suppresses oestrogen receptor-a expression and is associated with poor outcome in human breast cancer. *Endocr. Relat. Cancer* **19,** 181–195 (2012).

121. Winder, D. M., Chattopadhyay, A., Muralidhar, B., Bauer, J., English, W. R., Zhang, X., Karagavriilidou, K., Roberts, I., Pett, M. R., Murphy, G. & Coleman, N. Overexpression of the oncostatin M receptor in cervical squamous cell carcinoma cells is associated with a pro-angiogenic phenotype and increased cell motility and invasiveness. *J. Pathol.* **225,** 448–462 (2011).

122. Caffarel, M. M., Chattopadhyay, A., Araujo, A. M., Bauer, J., Scarpini, C. G. & Coleman, N. Tissue transglutaminase mediates the pro-malignant effects of oncostatin M receptor over-expression in cervical squamous cell carcinoma. *J. Pathol.* **231,** 168–179 (2013).

123. Thiery, J. P. & Sleeman, J. P. Complex networks orchestrate epithelial-mesenchymal transitions. *Nat. Rev. Mol. Cell Biol.* **7,** 131–142 (2006).

124. De Craene, B. & Berx, G. Regulatory networks defining EMT during cancer initiation and progression. *Nat. Rev. Cancer* **13,** 98–110 (2013).

125. Roche, J. The epithelial-to-mesenchymal transition in cancer. *Cancers* **10,** doi:10.3390/cancers10020052 (2018).

126. Mittal, V. Epithelial Mesenchymal Transition in Tumor Metastasis. *Annu. Rev. Pathol. Mech. Dis.* **13,** 395–412 (2018).

127. Pastushenko, I. & Blanpain, C. EMT Transition States during Tumor Progression and Metastasis. *Trends Cell Biol.* **29,** 212–226 (2019).

128. Bolo, V., Peinado, H., Peez-Moreno, M. A., Fraga, M. F., Esteller, M. & Cano, A. The transcription factor Slug represses E-cadherin expression and induces epithelial to mesenchymal transitions: a comparison with Snail and E47 repressors. *J. Cell Sci* **116,** 499–511 (2002).

129. Batlle, E., Sancho, E., Francí, C., Domínguez, D., Monfar, M., Baulida, J. & García De Herreros, A. The transcription factor Snail is a repressor of E-cadherin gene expression in epithelial tumour cells. *Nat. Cell Biol.* **2,** 84–89 (2000).

130. Wang, Y., Liu, J., Ying, X., Lin, P. C. & Zhou, B. P. Twist-mediated Epithelial-mesenchymal Transition Promotes Breast Tumor Cell Invasion via Inhibition of Hippo Pathway. *Sci. Rep.* **6,** doi: 10.1038/srep24606 (2016).

131. Caffarel, M. M. & Coleman, N. Oncostatin M receptor is a novel therapeutic target in cervical squamous cell carcinoma. *J. Pathol.* **232,** 386–90 (2014).

132. Nisticò, P., Bissell, M. J. & Radisky, D. C. Epithelial-mesenchymal transition: General principles and pathological relevance with special emphasis on the role of matrix metalloproteinases. *Cold Spring Harb. Perspect. Biol.* **4,** doi: 10.1101/cshperspect.a011908 (2012).

133. Stroeder, R., Walch-Rückheim, B., Fischbach, J., Juhasz-Böss, I., Rübe, C., Solomayer, E. F. & Smola, S. Oncostatin M treatment increases the responsiveness toward cisplatin-based chemoradiotherapy in cervical cancer cells in a STAT3-dependent manner. *Oncol. Lett.* **16,** 3351–3358 (2018).

134. Walch-Rückheim, B., Pahne-Zeppenfeld, J., Fischbach, J., Wickenhauser, C., Horn, L. C., Tharun, L., Büttner, R., Mallmann, P., Stern, P., Kim, Y. J., Bohle, R. M., Rübe, C., Ströder, R., Juhasz-Böss, I., Solomayer, E. F. & Smola, S. STAT3/IRF1 pathway activation sensitizes cervical cancer cells to chemotherapeutic drugs. *Cancer Res.* **76,** 3872–3883 (2016).

135. Brinton, L. T., Sloane, H. S., Kester, M. & Kelly, K. A. Formation and role of exosomes in cancer. *Cell. Mol. Life Sci* **72,** 659–671 (2015).

136. Munson, P. & Shukla, A. Exosomes: Potential in Cancer Diagnosis and Therapy. *Med.* **2,** 310–327 (2015).

137. Konoshenko, M. Y., Lekchnov, E. A., Vlassov, A. V & Laktionov, P. P. Isolation of Extracellular Vesicles: General Methodologies and Latest Trends. *Biomed Res. Int.* doi.org/10.1155/2018/8545347 (2018).

138. An, Q., Van Bel, A. J. E. & Hückelhoven, R. Do plant cells secrete exosomes derived

from multivesicular bodies? *Plant Signal. Behav.* **2,** 4–7 (2007).

139. Deatheragea, B. L. & Cooksona, B. T. Membrane vesicle release in bacteria, eukaryotes, and archaea: A conserved yet underappreciated aspect of microbial life. *Infect. Immun.* **80,** 1948–1957 (2012).

140. Latifkar, A., Cerione, R. A. & Antonyak, M. A. Probing the mechanisms of extracellular vesicle biogenesis and function in cancer. *Biochem. Soc. Trans.* **46,** 1137–1146 (2018).

141. Elkin, S. R., Lakoduk, A. M. & Schmid, S. L. Endocytic Pathways and Endosomal Trafficking: A Primer. *Wien Med Wochenschr.* **166,** 196–204 (2016).

142. Piper, R. C. & Katzmann, D. J. Biogenesis and function of MVBs. *Annu. Rev. Cell Dev. Biol.* **23,** 519–547 (2010).

143. Hessvik, N. P. & Llorente, A. Current knowledge on exosome biogenesis and release. *Cell. Mol. Life Sci.* **75,** 193–208 (2018).

144. Muralidharan-Chari, V., Clancy, J. W., Sedgwick, A. & D'Souza-Schorey Crislyn. Microvesicles: mediators of extracellular communication during cancer progression. *J. Cell Sci.* **123,** 1603–1611 (2010).

145. Tricarico, C., Clancy, J. & D'Souza-Schorey, C. Biology and biogenesis of shed microvesicles. *Small GTPases* **8,** 220–232 (2017).

146. Gurunathan, S., Kang, M.-H., Jeyaraj, M., Qasim, M. & Kim, J.-H. Review of the Isolation, Characterization, Biological Function, and Multifarious Therapeutic Approaches of Exosomes. *Cells* **8,** doi:10.3390/cells8040307 (2019).

147. Jiang, L., Paone, S., Caruso, S., Atkin-Smith, G. K., Phan, T. K., Hulett, M. D. & Poon, I. K. H. Determining the contents and cell origins of apoptotic bodies by flow cytometry. *Sci. Rep.* **7,** DOI:10.1038/s41598-017-14305-z (2017).

148. Caruso, S. & Poon, I. K. H. Apoptotic cell-derived extracellular vesicles: More than just debris. *Front. Immunol.* **9,** doi: 10.3389/fimmu.2018.01486 (2018).

149. Henne, W. M., Buchkovich, N. J. & Emr, S. D. The ESCRT Pathway. *Dev. Cell* **21,** 77–91 (2011).

150. Colombo, M., Raposo, G. & Thery, C. Biogenesis, Secretion, and Intercellular Interactions of Exosomes and Other Extracellular Vesicles. *Annu. Rev. Cell Dev. Biol* **30,** 255–289 (2014).

151. Christ, L., Raiborg, C., Wenzel, E. M., Campsteijn, C. & Stenmark, H. Cellular Functions and Molecular Mechanisms of the ESCRT Membrane-Scission Machinery. *Trends Biochem. Sci.* **42,** 42–56 (2017).

152. Trajkovic, K., Hsu, C., Chiantia, S., Rajendran, L., Wenzel, D., Wieland, F., Schwille, P., Brügger, B. & Simons, M. Ceramide triggers budding of exosome vesicles into multivesicular endosomes. *Science* **319,** 1244–1247 (2008).

153. Van Niel, G., D'Angelo, G. & Raposo, G. Shedding light on the cell biology of extracellular vesicles. *Nat. Rev. Mol. Cell Biol.* **19,** 213–228 (2018).

154. Ostrowski, M., Carmo, N. B., Krumeich, S., Fanget, I., Raposo, G., Savina, A., Moita, C. F., Schauer, K., Hume, A. N., Freitas, R. P., Goud, B., Benaroch, P., Hacohen, N., Fukuda, M., Desnos, C., Seabra, M. C., Darchen, F., Amigorena, S., Moita, L. F., *et*

al. Rab27a and Rab27b control different steps of the exosome secretion pathway. *Nat. Cell Biol.* **12,** 19–30 (2010).

155. Abels, E. R. & Breakefield, X. O. Introduction to Extracellular Vesicles: Biogenesis, RNA Cargo Selection, Content, Release, and Uptake. *Cell. Mol. Neurobiol.* **36,** 301–312 (2016).

156. Muralidharan-Chari, V., Clancy, J., Plou, C., Romao, M., Chavrier, P., Raposo, G. & D'Souza-Schorey, C. ARF6-Regulated Shedding of Tumor Cell-Derived Plasma Membrane Microvesicles. *Curr. Biol.* **19,** 1875–1885 (2009).

157. Nabhan, J. F., Hu, R., Oh, R. S., Cohen, S. N. & Lu, Q. Formation and release of arrestin domain-containing protein 1-mediated microvesicles (ARMMs) at plasma membrane by recruitment of TSG101 protein. *PNAS* **109,** 4146–4151 (2012).

158. Bianco, F., Perrotta, C., Novellino, L., Francolini, M., Riganti, L., Menna, E., Saglietti, L., Schuchman, E. H., Furlan, R., Clementi, E., Matteoli, M. & Verderio, C. Acid sphingomyelinase activity triggers microparticle release from glial cells. *EMBO J.* **28,** 1043–1054 (2009).

159. Poon, I. K. H., Chiu, Y. H., Armstrong, A. J., Kinchen, J. M., Juncadella, I. J., Bayliss, D. A. & Ravichandran, K. S. Unexpected link between an antibiotic, pannexin channels and apoptosis. *Nature* **507,** 329–334 (2014).

160. Coleman, M. L., Sahai, E. A., Yeo, M., Bosch, M., Dewar, A., Olson, M. F., Heart, N., Hospital, R. B., Street, S. & Sw, L. Membrane blebbing during apoptosis results from caspase-mediated activation of ROCK I. *Nat. Cell Biol.* **3,** 339–346 (2001).

161. Clotilde Thery, Aled Clayton, Sebastian Amigorena, G. R. Isolation and Characterization of Exosomes from Cell Culture Supernatants. *Curr. Protoc. Cell Biol.* **Chapter 3,** 1–29 (2006).

162. Monguió-Tortajada, M., Gálvez-Montón, C., Bayes-Genis, A., Roura, S. & Borràs, F. E. Extracellular vesicle isolation methods: rising impact of size-exclusion chromatography. *Cell. Mol. Life Sci.* **76,** 2369–2382 (2019).

163. Xu, R., Rai, A., Chen, M., Suwakulsiri, W., Greening, D. W. & Simpson, R. J. Extracellular vesicles in cancer — implications for future improvements in cancer care. *Nat. Rev. Clin. Oncol.* **15,** 617–638 (2018).

164. Crescitelli, R., Lässer, C., Szabó, T. G., Kittel, A., Eldh, M. & Dianzani, I. Distinct RNA profiles in subpopulations of extracellular vesicles: apoptotic bodies, microvesicles and exosomes. *J. Extracell. Vesicles* **2,** doi: 10.3402/jev.v2i0.20677 (2013).

165. Andreu, Z., Yáñez-Mó, M., Borras, F. E. & Monk, P. Tetraspanins in extracellular vesicle formation and function. *Front. Immunol.* **5,** doi: 10.3389/fimmu.2014.00442 (2014).

166. Kowal, J., Arras, G., Colombo, M., Jouve, M., Morath, J. P., Primdal-Bengtson, B., Dingli, F., Loew, D., Tkach, M. & Théry, C. Proteomic comparison defines novel markers to characterize heterogeneous populations of extracellular vesicle subtypes. *PNAS* **113,** E968–E977 (2016).

167. Jeppesen, D. K., Hvam, M. L., Primdahl-Bengtson, B., Boysen, A. T., Whitehead, B., Dyrskjøt, L., Ørntoft, T. F., Howard, K. A. & Ostenfeld, M. S. Comparative analysis of discrete exosome fractions obtained by differential centrifugation. *J. Extracell. Vesicles* **3,** doi:10.3402/jev.v3.25011 (2014).

168. Théry, C., Tkach, M. & Kowal, J. Why the need and how to approach the functional diversity of extracellular vesicles. *Philisophical Trans. R. Soc. B* 20160479 (2017). doi:10.1098/rstb.2016.0479

169. Valadi, H., Ekström, K., Bossios, A., Sjöstrand, M., Lee, J. J. & Lötvall, J. O. Exosome-mediated transfer of mRNAs and microRNAs is a novel mechanism of genetic exchange between cells. *Nat. Cell Biol.* **9,** 654–659 (2007).

170. Nolte-'t Hoen, E. N. M., Buermans, H. P. J., Waasdorp, M., Stoorvogel, W., Wauben, M. H. M. & 't Hoen, P. A. C. Deep sequencing of RNA from immune cell-derived vesicles uncovers the selective incorporation of small non-coding RNA biotypes with potential regulatory functions. *Nucleic Acids Res.* **40,** 9272–9285 (2012).

171. Sork, H., Corso, G., Krjutskov, K., Johansson, H. J., Nordin, J. Z., B Wiklander, O. P., Xin Fiona Lee, Y., Orzechowski Westholm, J., Lehtiö, J., A Wood, M. J., Mäger, I. & Andaloussi, S. EL. Heterogeneity and interplay of the extracellular vesicle small RNA transcriptome and proteome. *Sci. Rep.* **8,** doi:10.1038/s41598-018-28485-9 (2018).

172. Bazzoni, F., Tagliabue, A., Turchinovich, A., Drapkina, O. & Tonevitsky, A. Transcriptome of Extracellular Vesicles: State-of-the-Art. *Front. Immunol.* **10,** doi: 10.3389/fimmu.2019.00202 (2019).

173. Villarroya-Beltri, C., Baixauli, F., Gutiérrez-Vázquez, C., Sánchez-Madrid, F. & Mittelbrunn, M. Sorting It Out: Regulation of Exosome Loading. *Semin Cancer Biol* **28,** 3–13 (2014).

174. King, H. W., Michael, M. Z. & Gleadle, J. M. Hypoxic enhancement of exosome release by breast cancer cells. *BMC Cancer* **12,** 421 (2012).

175. Lehmann, B. D., Paine, M. S., Brooks, A. M., McCubrey, J. A., Renegar, R. H., Wang, R. & Terrian, D. M. Senescence-Associated Exosome Release from Human Prostate Cancer Cells. *Cancer Res.* **68,** doi:10.1158/0008-5472.CAN-07-6538 (2008).

176. Xiao, X., Yu, S., Li, S., Wu, J., Ma, R., Cao, H., Zhu, Y. & Feng, J. Exosomes: Decreased sensitivity of lung cancer A549 cells to cisplatin. *PLoS One* **9,** e89534 (2014).

177. O'Neill, C. P., Gilligan, K. E. & Dwyer, R. M. Role of extracellular vesicles (EVs) in cell stress response and resistance to cancer therapy. *Cancers* **11,** doi:10.3390/cancers11020136 (2019).

178. Fitzner, D., Schnaars, M., Van Rossum, D., Krishnamoorthy, G., Dibaj, P., Bakhti, M., Regen, T., Hanisch, U. K. & Simons, M. Selective transfer of exosomes from oligodendrocytes to microglia by macropinocytosis. *J. Cell Sci.* **124,** 447–458 (2011).

179. Lee, T. H., Chennakrishnaiah, S., Meehan, B., Montermini, L., Garnier, D., D'Asti, E., Hou, W., Magnus, N., Gayden, T., Jabado, N., Eppert, K., Majewska, L. & Rak, J. Barriers to horizontal cell transformation by extracellular vesicles containing oncogenic H-ras. *Oncotarget* **7,** 51991–52002 (2016).

180. French, K. C., Antonyak, M. A. & Cerione, R. A. Extracellular vesicle docking at the cellular port: Extracellular vesicle binding and uptake. *Semin. Cell Dev. Biol.* **67,** 48–55 (2017).

181. Segura, E., Guérin, C., Hogg, N., Amigorena, S. & Théry, C. CD8 + Dendritic Cells Use LFA-1 to Capture MHC-Peptide Complexes from Exosomes In Vivo . *J. Immunol.* **179,** 1489–1496 (2007).

182. Cossetti, C., Iraci, N., Mercer, T. R., Leonardi, T., Alpi, E., Drago, D., Alfaro-Cervello, C., Saini, H. K., Davis, M. P., Schaeffer, J., Vega, B., Stefanini, M., Zhao, C. J., Muller, W., Garcia-Verdugo, J. M., Mathivanan, S., Bachi, A., Enright, A. J., Mattick, J. S., *et al.* Extracellular vesicles from neural stem cells transfer IFN-γ via Ifngr1 to activate Stat1 signaling in target cells. *Mol. Cell* **56,** 193–204 (2014).

183. Mulcahy, L. A., Pink, R. C. & Carter, D. R. F. Routes and mechanisms of extracellular vesicle uptake. *J. Extracell. Vesicles* **3,** doi: 10.3402/jev.v3.24641 (2014).

184. Costa Verdera, H., Gitz-Francois, J. J., Schiffelers, R. M. & Vader, P. Cellular uptake of extracellular vesicles is mediated by clathrin-independent endocytosis and macropinocytosis. *J. Control. Release* **266,** 100–108 (2017).

185. Quail, D. F. & Joyce, J. A. Microenvironmental regulation of tumor progression and metastasis. *Nat Med* **19,** 1423–1437 (2013).

186. Hanahan, D. & Weinberg, R. A. Hallmarks of cancer: The next generation. *Cell* **144,** 646–674 (2011).

187. Kanada, M., Bachmann, M. H. & Contag, C. H. Signaling by Extracellular Vesicles Advances Cancer Hallmarks. *Trends in Cancer* **2,** 84–94 (2016).

188. Han, L., Lam, E. W. F. & Sun, Y. Extracellular vesicles in the tumor microenvironment: Old stories, but new tales. *Mol. Cancer* **18,** doi: 10.1186/s12943-019-0980-8 (2019).

189. Taylor, D. D. & Gercel-Taylor, C. MicroRNA signatures of tumor-derived exosomes as diagnostic biomarkers of ovarian cancer. *Gynecol. Oncol.* **110,** 13–21 (2008).

190. Al-Nedawi, K., Meehan, B., Micallef, J., Lhotak, V., May, L., Guha, A. & Rak, J. Intercellular transfer of the oncogenic receptor EGFRvIII by microvesicles derived from tumour cells. *Nat. Cell Biol.* **10,** 619–624 (2008).

191. Zomer, A., Maynard, C., Verweij, F. J., Kamermans, A., Schäfer, R., Beerling, E., Schiffelers, R. M., De Wit, E., Berenguer, J., Ellenbroek, S. I. J., Wurdinger, T., Pegtel, D. M. & Van Rheenen, J. In vivo imaging reveals extracellular vesicle-mediated phenocopying of metastatic behavior. *Cell* **161,** 1046–1057 (2015).

192. Webber, J. P. J., Spary, L. K., Sanders, A. J. A., Chowdhury, R., Jiang, W. G., Steadman, R., Wymant, J., Jones, A. T. A., Kynaston, H., Tabi, Z., Clayton, A., Mason, M. D., Tabi, Z. & Clayton, A. Differentiation of tumour-promoting stromal myofibroblasts by cancer exosomes. *Oncogene* **34,** 319–333 (2015).

193. Vu, L. T., Peng, B., Zhang, D. X., Ma, V., Mathey-Andrews, C. A., Lam, C. K., Kiomourtzis, T., Jin, J., McReynolds, L., Huang, L., Grimson, A., Cho, W. C., Lieberman, J. & Le, M. T. Tumor-secreted extracellular vesicles promote the activation of cancer-associated fibroblasts via the transfer of microRNA-125b. *J. Extracell. Vesicles* **8,** doi: 10.1080/20013078.2019.1599680 (2019).

194. Latifkar, A., Hur, Y. H., Sanchez, J. C., Cerione, R. A. & Antonyak, M. A. New insights into extracellular vesicle biogenesis and function. *J. Cell Sci.* **132,** doi:10.1242/jcs.222406 (2019).

195. Luga, V., Zhang, L., Viloria-Petit, A. M., Ogunjimi, A. A., Inanlou, M. R., Chiu, E., Buchanan, M., Hosein, A. N., Basik, M. & Wrana, J. L. Exosomes mediate stromal mobilization of autocrine Wnt-PCP signaling in breast cancer cell migration. *Cell* **151,** 1542–1556 (2012).

196. Dourado, M. R., Korvala, J., Åström, P., De Oliveira, C. E., Cervigne, N. K., Mofatto,

L. S., Campanella Bastos, D., Pereira Messetti, A. C., Graner, E., Paes Leme, A. F., Coletta, R. D. & Salo, T. Extracellular vesicles derived from cancer-associated fibroblasts induce the migration and invasion of oral squamous cell carcinoma. *J. Extracell. Vesicles* **8,** doi: 10.1080/20013078.2019.1578525 (2019).

197. Costa-Silva, B., Aiello, N. M., Ocean, A. J., Singh, S., Zhang, H., Thakur, B. K., Becker, A., Hoshino, A., Mark, M. T., Molina, H., Xiang, J., Zhang, T., Theilen, T.-M., Garcia-Santos, G., Williams, C., Ararso, Y., Huang, Y., Rodrigues, G., Shen, T.-L., *et al.* Pancreatic cancer exosomes initiate pre-metastatic niche formation in the liver. *Nat Cell Biol* **17,** 816–826 (2018).

198. Hoshino, A., Costa-Silva, B., Shen, T.-L., Rodrigues, G., Hashimoto, A., Tesic Mark, M., Henrik, M., Kohsaka, S., Di Giannatale, A., Ceder, S., Singh, S., William, C., Soplop, N., Urya, K., Pharmer, L., King, T., Bojmar, L., Davies, A. E., Ararso, Y., *et al.* Tumour exosome integrins determine organotropic metastasis. *Nature* **19,** 329–335 (2015).

199. Safaei, R., Larson, B. J., Cheng, T. C., Gibson, M. A., Otani, S., Naerdemann, W. & Howell, S. B. Abnormal lysosomal trafficking and enhanced exosomal export of cisplatin in drug-resistant human ovarian carcinoma cells. *Mol. Cancer Ther.* **4,** 1595–1604 (2005).

200. Chen, W., Liu, X., Lv, M., Chen, L., Zhao, J., Zhong, S., Ji, M., Hu, Q., Luo, Z., Wu, J. & Tang, J. Exosomes from drug-resistant breast cancer cells transmit chemoresistance by a horizontal transfer of microRNAs. *PLoS One* **9,** doi:10.1371/journal.pone.0095240 (2014).

201. Patel, G. K., Khan, M. A., Bhardwaj, A., Srivastava, S. K., Zubair, H., Patton, M. C., Singh, S., Khushman, M. & Singh, A. P. Exosomes confer chemoresistance to pancreatic cancer cells by promoting ROS detoxification and miR-155-mediated suppression of key gemcitabine-metabolising enzyme, DCK. *Br. J. Cancer* **116,** 609–619 (2017).

202. Raji, G. R., Sruthi, T. V., Edatt, L., Haritha, K., Sharath Shankar, S. & Sameer Kumar, V. B. Horizontal transfer of miR-106a/b from cisplatin resistant hepatocarcinoma cells can alter the sensitivity of cervical cancer cells to cisplatin. *Cell. Signal.* **38,** 146–158 (2017).

203. Mutschelknaus, L., Peters, C., Winkler, K., Yentrapalli, R., Heider, T., Atkinson, M. J. & Moertl, S. Exosomes derived from squamous head and neck cancer promote cell survival after ionizing radiation. *PLoS One* **11,** doi:10.1371/ journal.pone.0152213 (2016).

204. Aung, T., Chapuy, B., Vogel, D., Wenzel, D., Oppermann, M., Lahmann, M., Weinhage, T., Menck, K., Hupfeld, T., Koch, R., Trümper, L. & Wulf, G. G. Exosomal evasion of humoral immunotherapy in aggressive B-cell lymphoma modulated by ATP-binding cassette transporter A3. *PNAS* **108,** 15336–15341 (2011).

205. Lane, R. E., Korbie, D., Hill, M. M. & Trau, M. Extracellular vesicles as circulating cancer biomarkers: opportunities and challenges. *Clin. Transl. Med.* **7,** doi: 10.1186/s40169-018-0192-7 (2018).

206. Provencio, M., Rodríguez, M., Cantos, B., Sabín, P., Quero, C., García-Arroyo, F. R., Rueda, A., Maximiano, C., Rodríguez-Abreu, D., Sánchez, A., Silva, J. & García, V. mRNA in exosomas as a liquid biopsy in non-Hodgkin Lymphoma: A multicentric study by the Spanish lymphoma oncology group. *Oncotarget* **8,** 50949–50957 (2017).

207. Khawar, M. B., Abbasi, M. H., Siddique, Z., Arif, A. & Sheikh, N. An Update on Novel Therapeutic Warfronts of Extracellular Vesicles (EVs) in Cancer Treatment: Where We Are Standing Right Now and Where to Go in the Future. *Oxid. Med. Cell. Longev.* **2019,** doi: 10.1155/2019/9702562 (2019).

208. Kosaka, N., Iguchi, H., Hagiwara, K., Yoshioka, Y., Takeshita, F. & Ochiya, T. Neutral sphingomyelinase 2 (nSMase2)-dependent exosomal transfer of angiogenic micrornas regulate cancer cell metastasis. *J. Biol. Chem.* **288,** 10849–10859 (2013).

209. Yokoi, A., Yoshioka, Y., Yamamoto, Y., Ishikawa, M., Ikeda, S.-I. I., Kato, T., Kiyono, T., Takeshita, F., Kajiyama, H., Kikkawa, F. & Ochiya, T. Malignant extracellular vesicles carrying MMP1 mRNA facilitate peritoneal dissemination in ovarian cancer. *Nat. Commun.* **8,** doi: 10.1038/ncomms14470 (2017).

210. Peinado, H. Melanoma exosomes educate bone marrow progenitor cells. *Nat. Med.* **18,** 883–891 (2013).

211. Nishida-Aoki, N., Tominaga, N., Takeshita, F., Sonoda, H., Yoshioka, Y. & Ochiya, T. Disruption of Circulating Extracellular Vesicles as a Novel Therapeutic Strategy against Cancer Metastasis. *Mol. Ther.* **25,** 181–191 (2017).

212. Tian, Y., Li, S., Song, J., Ji, T., Zhu, M., Anderson, G. J., Wei, J. & Nie, G. A doxorubicin delivery platform using engineered natural membrane vesicle exosomes for targeted tumor therapy. *Biomaterials* **35,** 2383–2390 (2014).

213. Bunggulawa, E. J., Wang, W., Yin, T., Wang, N., Durkan, C., Wang, Y. & Wang, G. Recent advancements in the use of exosomes as drug delivery systems. *J. Nanobiotechnology* **16,** doi: 10.1186/s12951-018-0403-9 (2018).

214. Kunz-Schughart, L. A., Schroeder, J. A., Wondrak, M., Van Rey, F., Lehle, K., Hofstaedter, F. & Wheatley, D. N. Potential of fibroblasts to regulate the formation of three-dimensional vessel-like structures from endothelial cells in vitro. *Am. J. Cell Physiol.* **290,** 1385–1398 (2006).

215. Wijelath, E. S., Carlsen, B., Cole, T., Chen, J., Kothari, S. & Hammond, W. P. Oncostatin M induces basic fibroblast growth factor expression in endothelial cells and promotes endothelial cell proliferation, migration and spindle morphology. *J. Cell Sci.* **110,** 871–879 (1997).

216. Filipe, V., Hawe, A. & Jiskoot, W. Critical Evaluation of Nanoparticle Tracking Analysis (NTA) by NanoSight for the Measurement of Nanoparticles and Protein Aggregates. *Pharm. Reasearch* **27,** 796–810 (2010).

217. Malvern Particles Ltd. Nanoparticle Tracking Analysis. Available at: http://www.malvern.com/en/products/technology/nanoparticle-tracking-analysis/. (Accessed: 3rd June 2016)

218. Will Chiang, T.-W., le Sage, C., Larrieu, D., Demir, M. & Jackson, S. P. CRISPR-Cas9 D10A nickase-based genotypic and phenotypic screening to enhance genome editing. *Nat. Publ. Gr.* **6,** doi: 10.1038/srep24356 (2016).

219. Pfaffl, M. W. A new mathematical model for relative quantification in real-time RT-PCR. *Nucleic Acids Res.* **29,** 2002–2007 (2001).

220. Vandesompele, J., De Preter, K., Pattyn, I., Poppe, B., Van Roy, N., De Paepe, A. & Speleman, rank. Accurate normalization of real-time quantitative RT-PCR data by geometric averaging of multiple internal control genes. *Genome Biol.* **3,** doi:

10.1186/gb-2002-3-7-research0034 (2002).

221. Babion, I., Snoek, B. C., van de Wiel, M. A., Wilting, S. M. & Steenbergen, R. D. M. A Strategy to Find Suitable Reference Genes for miRNA Quantitative PCR Analysis and Its Application to Cervical Specimens. *J. Mol. Diagnostics* **19,** 625–637 (2017).

222. Anders, S., Pyl, P. T. & Huber, W. Genome analysis HTSeq-a Python framework to work with high-throughput sequencing data. **31,** 166–169 (2015).

223. Love, M. I., Huber, W. & Anders, S. Moderated estimation of fold change and dispersion for RNA-seq data with DESeq2. *Genome Biol.* **15,** doi: 10.1186/s13059-014-0550-8 (2014).

224. Robinson, M. D., Mccarthy, D. J. & Smyth, G. K. EdgeR: a Bioconductor package for differential expression analysis of digital gene expression data. *BIOINFORMATICS* **26,** 139–140 (2010).

225. Davis, M. P. A., van Dongen, S., Abreu-Goodger, C., Bartonicek, N. & Enright, A. J. Kraken: A set of tools for quality control and analysis of high-throughput sequence data. *Methods* **63,** 41–49 (2013).

226. Vitsios, D. M. & Enright, A. J. Chimira: analysis of small RNA sequencing data and microRNA modifications. *Bioinformatics* **31,** 3365–3367 (2015).

227. Mueller, H., Kassack, M. U. & Wiese, M. Comparison of the Usefulness of the MTT, ATP, and Calcein Assays to Predict the Potency of Cytotoxic Agents in Various Human Cancer Cell Lines. *J. Biomol. Screen.* **9,** 506–515 (2004).

228. Jensen, M. M., Jørgensen, J. T., Binderup, T. & Kjaer, A. Tumor volume in subcutaneous mouse xenografts measured by microCT is more accurate and reproducible than determined by 18 F-FDG-microPET or external caliper. *BMC Med. Imaging* **8,** doi:10.1186/1471-2342-8-16 (2008).

229. Farh, K. K.-H. K.-H., Grimson, A., Jan, C., Lewis, B. P., Johnston, W. K., Lim, L. P., Burge, C. B. & Bartel, D. P. The Widespread Impact of Mammalian MicroRNAs on mRNA Repression and Evolution. *Science* **310,** 1817–1821 (2005).

230. Kim, Y.-K. & Kim, V. N. Processing of intronic microRNAs. *EMBO J.* **26,** 775–783 (2007).

231. de Rie, D., Abugessaisa, I., Alam, T., Arner, E., Arner, P., Ashoor, H., Åström, G., Babina, M., Bertin, N., Maxwell Burroughs, A., Carlisle, A. J., Daub, C. O., Detmar, M., Deviatiiarov, R., Fort, A., Gebhard, C., Goldowitz, D., Guhl, S., Ha, T. J., *et al.* An integrated expression atlas of miRNAs and their promoters in human and mouse. *Nat. Biotechnol.* **35,** 872–878 (2017).

232. Treiber, T., Treiber, N. & Meister, G. Regulation of microRNA biogenesis and its crosstalk with other cellular pathways. *Nat. Rev. Mol. Cell Biol.* **20,** doi: 10.1038/s41580-018-0059-1 (2019).

233. Liz, J., Portela, A., Soler, M., Gomez, A., Ling, H., Michlewski, G., Calin, G. A., Guil, S. & Esteller, M. Regulation of pri-miRNA processing by a long noncoding RNA transcribed from an ultraconserved region. *Mol. Cell* **55,** 138–147 (2014).

234. Gregory, R. I., Yan, K.-P., Amuthan, G., Chendrimada, T., Doratotaj, B., Cooch, N. & Shiekhattar, R. The Microprocessor complex mediates the genesis of microRNAs. *Nature* **432,** 235–240 (2004).

235. Fareh, M., Yeom, K.-H., Haagsma, A. C., Chauhan, S., Heo, I. & Joo, C. TRBP ensures efficient Dicer processing of precursor microRNA in RNA-crowded environments. *Nat. Commun.* **7,** doi: 10.1038/ncomms13694 (2016).

236. Ameres, S. L. & Zamore, P. D. Diversifying microRNA sequence and function. *Nat. Rev. Mol. Cell Biol.* **14,** 475–488 (2013).

237. Kim, Y.-K., Kim, B. & Kim, V. N. Re-evaluation of the roles of DROSHA, Exportin 5, and DICER in microRNA biogenesis. *PNAS* **113,** E1881-1889 (2016).

238. O'Brien, J., Hayder, H., Zayed, Y. & Peng, C. Overview of microRNA biogenesis, mechanisms of actions, and circulation. *Front. Endocrinol.* **9,** doi: 10.3389/fendo.2018.00402 (2018).

239. Kloosterman, W. P., Wienholds, E., Ketting, R. F. & Plasterk, R. H. A. Substrate requirements for let-7 function in the developing zebrafish embryo. *Nucleic Acids Res.* **32,** 6284–6291 (2004).

240. Lytle, J. R., Yario, T. A. & Steitz, J. A. Target mRNAs are repressed as efficiently by microRNA-binding sites in the 5 UTR as in the 3 UTR. *PNAS* **104,** 9667–9672 (2007).

241. Liu, J., Carmell, M. A., Rivas, F. V., Marsden, C. G., Thomson, J. M., Song, J.-J., Hammond, S. M., Joshua-Tor, L. & Hannon, G. J. Argonaute2 Is the Catalytic Engine of Mammalian RNAi. *Science* **305,** 1437–1441 (2004).

242. Ipsaro, J. J., Joshua-Tor, L. & Keck, W. M. From Guide to Target: Molecular Insights into Eukaryotic RNAi Machinery. *Nat Struct Mol Biol* **22,** 20–28 (2015).

243. Lewis, B. P., Shih, I. H., Jones-Rhoades, M. W., Bartel, D. P. & Burge, C. B. Prediction of Mammalian MicroRNA Targets. *Cell* **115,** 787–798 (2003).

244. Ellwanger, D. C., Büttner, F. A., Mewes, H.-W. & Stümpflen, V. Sequence analysis The sufficient minimal set of miRNA seed types. *Bioinformatics* **27,** 1346–1350 (2011).

245. Bartel, D. P. MicroRNAs: Target Recognition and Regulatory Functions. *Cell* **136,** 215–233 (2009).

246. Jonas, S. & Izaurralde, E. Towards a molecular understanding of microRNA-mediated gene silencing. *Nat. Rev. Genet.* **16,** 6284–6291 (2015).

247. Lim, L. P., Lau, N. C., Garrett-Engele, P., Grimson, A., Schelter, J. M., Castle, J., Bartel, D. P., Linsley, P. S. & Johnson, J. M. Microarray analysis shows that some microRNAs downregulate large numbers of target mRNAs. *Nat. Biotechnol.* **433,** 769–773 (2005).

248. Enright, A. J., John, B., Gaul, U., Tuschl, T., Sander, C. & Marks, D. S. MicroRNA targets in Drosophila. *Genome Biol.* **5,** doi: 10.1186/gb-2003-5-1-r1 (2003).

249. Lewis, B. P., Burge, C. B. & Bartel, D. P. Conserved Seed Pairing, Often Flanked by Adenosines, Indicates that Thousands of Human Genes are MicroRNA Targets. *Cell* **120,** 15–20 (2005).

250. Friedman, R. C., Kai-How Farh, K., Burge, C. B. & Bartel, D. P. Most mammalian mRNAs are conserved targets of microRNAs. *Genome Res.* **19,** 92–105 (2009).

251. Ramassone, A., Pagotto, S., Veronese, A. & Visone, R. Molecular Sciences Epigenetics and MicroRNAs in Cancer. *Int. J. Mol. Sci.* **19,** doi:

doi:10.3390/ijms19020459 (2018).

252. Iorio, M. V & Croce, C. M. Causes and Consequences of microRNA Dysregulation. *Cancer J.* **18,** 215–222 (2012).

253. Adrian Calin, G., Sevignani, C., Dan Dumitru, C., Hyslop, T., Noch, E., Yendamuri, S., Shimizu, M., Rattan, S., Bullrich, F., Negrini, M. & Croce, C. M. Human microRNA genes are frequently located at fragile sites and genomic regions involved in cancers. *PNAS* **101,** 2999–3004 (2004).

254. Muralidhar, B., Goldstein, L., Ng, G., Winder, D., Palmer, R., Gooding, E., Barbosa-Morias, N., Mukherjee, G., Thorne, N., Roberts, I., Pett, M. & Coleman, N. Global microRNA profiles in cervical squamous cell carcinoma depend on Drosha expression levels. *J. Pathol.* **212,** 368–377 (2007).

255. Muralidhar, B., Winder, D., Murray, M., Palmer, R., Barbosa-Morais, N., Saini, H., Roberts, I., Pett, M. & Coleman, N. Functional evidence that Drosha overexpression in cervical squamous cell carcinoma affects cell phenotype and microRNA profiles. *J. Pathol.* **224,** 496–507 (2011).

256. Wilting, S., Snijders, P., Verlaat, W., Jaspers, A., Van De Wiel, M., Van Wieringen, W., Meijer, G., Kenter, G., Yi, Y., Le Sage, C., Agami, R., Meijer, C. & Steenbergen, R. Altered microRNA expression associated with chromosomal changes contributes to cervical carcinogenesis. *Oncogene* **32,** 106–116 (2013).

257. Cheung, T. H., Man, K. N. M., Yu, M. Y., Yim, S. F., Siu, N. S. S. S., Lo, K. W. K. K., Doran, G., Wong, R. R. Y. Y., Wang, V. W., Smith, D. I., Worley, M. J., Berkowitz, R. S., Chung, T. K. H. H., Wong, Y. F., Worley Jr., M. J., Berkowitz, R. S., Chung, T. K. H. H. & Wong, Y. F. Dysregulated microRNAs in the pathogenesis and progression of cervical neoplasm. *Cell Cycle* **11,** 2876–2884 (2012).

258. Zeng, K., Zheng, W., Mo, X., Liu, F., Li, M., Liu, Z., Zhang, W. & Hu, X. Dysregulated microRNAs involved in the progression of cervical neoplasm. *Arch Gynecol Obs.* **292,** 905–913 (2015).

259. Li, Y., Wang, F., Xu, J., Ye, F., Shen, Y., Zhou, J., Lu, W., Wan, X., Ma, D. & Xie, X. Progressive miRNA expression profiles in cervical carcinogenesis and identification of HPV-related target genes for miR-29. *J. Pathol.* **224,** 484–495 (2011).

260. Zheng, Z.-M. & Wang, X. Regulation of cellular miRNA expression by human papillomaviruses. *Biochim Biophys Acta* **1809,** 668–677 (2011).

261. He, Y., Lin, J., Ding, Y., Liu, G., Luo, Y., Huang, M., Xu, C., Kim, T.-K., Etheridge, A., Lin, M., Kong, D. & Wang, K. A systematic study on dysregulated microRNAs in cervical cancer development. *Int. J. Cancer* **138,** 1312–1327 (2016).

262. Lui, W.-O., Pourmand, N., Patterson, B. K. & Fire, A. Patterns of Known and Novel Small RNAs in Human Cervical Cancer. *Cancer Res* **67,** 6031–6043 (2007).

263. Kawai, S., Fujii, T., Kukimoto, I., Yamada, H., Yamamoto, N., Kuroda, M., Otani, S., Ichikawa, R., Nishio, E., Torii, Y. & Iwata, A. Identification of miRNAs in cervical mucus as a novel diagnostic marker for cervical neoplasia. *Sci. Rep.* **8,** doi: 10.1038/s41598-018-25310-1 (2018).

264. Gao, C., Chao Zhou, |, Zhuang, J., Liu, L., Liu, C., Li, H., Liu, | Gongxi, Wei, J. & Sun, C. MicroRNA expression in cervical cancer: Novel diagnostic and prognostic biomarkers. *J. Cell. Biochem.* **119,** 7080–7090 (2018).

265. Huang, L., Lin, J.-X., Yu, Y.-H., Zhang, M.-Y., Wang, H.-Y. & Zheng, M. Downregulation of Six MicroRNAs Is Associated with Advanced Stage, Lymph Node Metastasis and Poor Prognosis in Small Cell Carcinoma of the Cervix. *PLoS One* **7,** e33762 (2012).

266. Hu, X., Schwarz, J. K., Lewis, J. S., Huettner, P. C., Rader, J. S., Deasy, J. O., Grigsby, P. W. & Wang, X. A MicroRNA Expression Signature for Cervical Cancer Prognosis. *Cancer Res.* **70,** 1441–1448 (2010).

267. López, A. J. G. & López, J. A. Multistep Model of Cervical Cancer: Participation of miRNAs and Coding Genes. *Int. J. Mol. Sci* **15,** 15700–15733 (2014).

268. He, Y., Lin, J., Ding, Y., Liu, G., Luo, Y., Huang, M., Xu, C., Kim, T.-K. K., Etheridge, A., Lin, M., Kong, D. & Wang, K. A systematic study on dysregulated microRNAs in cervical cancer development. *Int. J. Cancer* **138,** 1312–1327 (2016).

269. Pardini, B., De Maria, D., Francavilla, A., Di Gaetano, C., Ronco, G. & Naccarati, A. MicroRNAs as markers of progression in cervical cancer: a systematic review. *BMC Cancer* **18,** doi: 10.1186/s12885-018-4590-4 (2018).

270. Wang, K., Zhang, S., Weber, J., Baxter, D. & Galas, D. J. Export of microRNAs and microRNA-protective protein by mammalian cells. *Nucelic Acids Res.* **38,** 7248–7259 (2010).

271. Gallo, A., Tandon, M., Alevizos, I. & Illei, G. G. The majority of microRNAs detectable in serum and saliva is concentrated in exosomes. *PLoS One* **7,** 1–5 (2012).

272. Piper Hunter, M., Ismail, N., Zhang, X., Aguda, B. D., Joo Lee, E., Yu, L., Xiao, T., Schafer, J., Ting Lee, M.-L., Schmittgen, T. D., Patrick Nana-Sinkam, S., Jarjoura, D. & Marsh, C. B. Detection of microRNA Expression in Human Peripheral Blood Microvesicles. *PLoS One* **3,** e3694 (2008).

273. Shurtleff, M. J., Temoche-Diaz, M. M., Karfilis, K. V, Ri, S. & Schekman, R. Y-box protein 1 is required to sort microRNAs into exosomes in cells and in a cell-free reaction. *Elife* **5,** e19276 (2016).

274. Villarroya-Beltri, C., Gutiérrez-Vázquez, C., Sánchez-Cabo, F., Pérez-Hernández, D., Vázquez, J., Martin-Cofreces, N., Jorge Martinez-Herrera, D., Pascual-Montano, A., Mittelbrunn, M. & Sánchez-Madrid, F. Sumoylated hnRNPA2B1 controls the sorting of miRNAs into exosomes through binding to specific motifs. *Nat. Commun.* **4,** doi: 10.1038/ncomms3980 (2013).

275. Azizmohammadi, S., Safari, A., Kaghazian, M., Sadrkhanlo, M., Yahaghi, E., Farshgar, R. & Seifoleslami, M. Molecular identification of miR-145 and miR-9 expression level as prognostic biomarkers for early-stage cervical cancer detection. *QJM* **110,** 11–15 (2017).

276. Zhang, H., Zhang, Z., Wang, S., Zhang, S. & Bi, J. The mechanisms involved in miR-9 regulated apoptosis in cervical cancer by targeting FOXO3. *Biomed. Pharmacother.* **102,** 626–632 (2018).

277. Liu, W., Gao, G., Hu, X., Wang, Y., Schwarz, J. K., Chen, J. J., Grigsby, P. W. & Wang, X. Activation of miR-9 by human papillomavirus in cervical cancer. *Oncotarget* **5,** 11620–30 (2014).

278. Wang, N., Zhou, Y., Zheng, L. & Li, H. MiR-31 is an independent prognostic factor and functions as an oncomir in cervical cancer via targeting ARID1A. *Gynecol. Oncol.*

134, 129–137 (2014).

279. Zheng, W., Liu, Z., Zhang, W. & Hu, X. miR-31 functions as an oncogene in cervical cancer. *Arch Gynecol Obs.* **292,** 1083–1089 (2015).

280. Wang, N., Li, Y., Zhou, J. & Safe, S. H. miR-31 Functions as an Oncomir Which Promotes Epithelial-Mesenchymal Transition via Regulating BAP1 in Cervical Cancer. *Biomed Res. Int.* **2017,** doi: 10.1155/2017/6361420 (2017).

281. Yu, M., Xu, Y., Pan, L., Feng, Y., Luo, K., Mu, Q. & Luo, G. miR-10b Downregulated by DNA Methylation Acts as a Tumor Suppressor in HPV-Positive Cervical Cancer via Targeting Tiam1. *Cell Physiol Biochem* **51,** 1763–1777 (2018).

282. Hou, R., Wang, D. & Lu, J. MicroRNA-10b inhibits proliferation, migration and invasion in cervical cancer cells via direct targeting of insulin-like growth factor-1 receptor. *Oncol. Lett.* **13,** 5009–5015 (2017).

283. Campos-Viguri, G. E., Jiménez-Wences, H., Peralta-Zaragoza, O., Torres-Altamirano, G., Soto-Flores, D. G., Hernández-Sotelo, D., Alarcón-Romero, L. D. C., Jiménez-López, M. A., Illades-Aguiar, B. & Fernández-Tilapa, G. miR-23b as a potential tumor suppressor and its regulation by DNA methylation in cervical cancer. *Infect. Agent. Cancer* **10,** doi: 10.1186/s13027-015-0037-6 (2015).

284. Au Yeung, C., Tsang, T., Yau, P. & Kwok, T. Human papillomavirus type 16 E6 induces cervical cancer cell migration through the p53/microRNA-23b/urokinase-type plasminogen activator pathway. *Oncogene* **30,** 2401–2410 (2011).

285. Li, Y., Zhang, Z., Xiao, Z., Lin, Y., Luo, T., Zhou, Q. & Zhang, X. Chemotherapy-mediated miR-29b expression inhibits the invasion and angiogenesis of cervical cancer. *Oncotarget* **8,** 14655–14665 (2017).

286. Zhang, T., Xue, X. & Peng, H. Therapeutic Delivery of miR-29b Enhances Radiosensitivity in Cervical Cancer. *Mol. Ther.* **27,** 1183–1194 (2019).

287. Lin, C., Huang, F., Zhang, Y.-J., Tuokan, T. & Kuerban, G. Roles of MiR-101 and its target gene cox-2 in early diagnosis of cervical cancer in Uygur women. *Asian Pacific J. Cancer Prev.* **15,** 45–48 (2014).

288. Wei, H., HE, W. R., Chen, K. M., Wang, X. W. & Yi, C. J. MiR-101 affects proliferation and apoptosis of cervical cancer cells by inhibition of JAK2. *Eur. Rev. Med. Pharmacol. Sci.* **23,** 5640–5647 (2019).

289. Shen, W., Xie, X. Y., Liu, M. R. & Wang, L. L. MicroRNA-101-5p inhibits the growth and metastasis of cervical cancer cell by inhibiting CXCL6. *Eur. Rev. Med. Pharmacol. Sci.* **23,** 1957–1968 (2019).

290. Jiang, W., Yao, L.-H., Pan, J.-J., Deng, Y.-H. & Liang, M.-R. Down-regulated serum microRNA-101 is associated with aggressive progression and poor prognosis of cervical cancer. *J Gynecol Oncol* **28,** doi: 10.3802/jgo.2017.28.e75 (2017).

291. Lin, C., Huang, F., Shen, G. & Yiming, A. MicroRNA-101 regulates the viability and invasion of cervical cancer cells. *Int J Clin Exp Pathol* **8,** 10148–10155 (2015).

292. Liang, X., Liu, Y., Zeng, L., Yu, C., Hu, Z., Zhou, Q. & Yang, Z. miR-101 Inhibits the G1-to-S Phase Transition of Cervical Cancer Cells by Targeting Fos. *Int. J. Gynecol. Cancer* **24,** 1165–1172 (2014).

293. Xu, J., Wang, H., Wang, H., Chen, Q., Zhang, L., Song, C., Zhou, Q. & Hong, Y. The

inhibition of miR-126 in cell migration and invasion of cervical cancer through regulating ZEB1. *Hereditas* **156,** doi: 10.1186/s41065-019-0087-7 (2019).

294. Wang, C., Zhou, B., Liu, M., Liu, Y. & Gao, R. miR-126-5p restoration promotes cell apoptosis in cervical cancer by targeting Bcl2l2. *Oncol. Res.* **25,** 463–470 (2017).

295. Yang, Y., Song, K.-L., Chang, H. & Chen, L. Decreased expression of microRNA-126 is associated with poor prognosis in patients with cervical cancer. *Diagn. Pathol.* **9,** 220 (2014).

296. Huang, T.-H. & Chu, T.-Y. Repression of miR-126 and upregulation of adrenomedullin in the stromal endothelium by cancer-stromal cross talks confers angiogenesis of cervical cancer. *Oncogene* **33,** 3636–3647 (2013).

297. Varghese, V. K., Shukla, V., Kabekkodu, S. P., Pandey, D. & Satyamoorthy, K. DNA methylation regulated microRNAs in human cervical cancer. *Mol. Carcinog.* **57,** 370–382 (2018).

298. Córdova-Rivas, S., Fraire-Soto, I., Torres, A. M. C., Servín-González, L. S., Granados-López, A. J., López-Hernández, Y., Reyes-Estrada, C. A., Gutiérrez-Hernández, R., Castañeda-Delgado, J. E., Ramírez-Hernández, L., Varela-Silva, J. A. & López, J. A. 5p and 3p strands of miR-34 family members have differential effects in cell proliferation, migration, and invasion in cervical cancer cells. *Int. J. Mol. Sci.* **20,** doi:10.3390/ijms20030545 (2019).

299. Liu, H., Liu, L. I. & Zhu, H. The Role of Significantly Deregulated MicroRNAs in Recurrent Cervical Cancer Based on Bioinformatic Analysis of the Cancer Genome Atlas Data. *J. Comput. Biol.* **26,** 387–395 (2019).

300. Park, H., Lee, M., Jeong, J., Choi, M. C., Jung, S. G., Joo, W. D., Lee, C. & An, H. J. Dysregulated microRNA expression in adenocarcinoma of the uterine cervix: Clinical impact of miR-363-3p. *Gynecol. Oncol.* **135,** 565–572 (2014).

301. Adli, M. The CRISPR tool kit for genome editing and beyond. *Nat. Commun.* **9,** doi: 10.1038/s41467-018-04252-2 (2018).

302. Bachurski, D., Schuldner, M., Nguyen, P. H., Malz, A., Reiners, K. S., Grenzi, P. C., Babatz, F., Schauss, A. C., Hansen, H. P., Hallek, M. & Pogge von Strandmann, E. Extracellular vesicle measurements with nanoparticle tracking analysis–An accuracy and repeatability comparison between NanoSight NS300 and ZetaView. *J. Extracell. Vesicles* **8,** (2019).

303. Parsons, M. E. M., McParland, D., Szklanna, P. B., Guang, M. H. Z., O'Connell, K., O'Connor, H. D., McGuigan, C., Ní Áinle, F., McCann, A. & Maguire, P. B. A Protocol for Improved Precision and Increased Confidence in Nanoparticle Tracking Analysis Concentration Measurements between 50 and 120 nm in Biological Fluids. *Front. Cardiovasc. Med.* **4,** 1–7 (2017).

304. Raposo, G. & Stoorvogel, W. Extracellular vesicles: Exosomes, microvesicles, and friends. *J. Cell Biol* **200,** 373–383 (2013).

305. Thery, C., Zitvogel, L. & Amigorena, S. Exosomes: Composition, Biogenesis and Function. *Natiure Rev. Immunol.* **2,** 569–579 (2002).

306. Lötvall, J., Hill, A. F., Hochberg, F., Buzás, E. I., Di Vizio, D., Gardiner, C., Song Gho, Y., Kurochkin, I. V, Mathivanan, S., Quesenberry, P., Sahoo, S., Tahara, H., Wauben, M. H., Witwer, K. W. & Théry, C. Minimal experimental requirements for definition of

extracellular vesicles and their functions: a position statement from the International Society for Extracellular Vesicles. *J. Extracell. Vesicles* **3,** doi: 10.3402/jev.v3.26913 (2014).

307. Van der Pol, E., Boing, A. N., Harrison, P., Sturk, A. & Nieuwland, R. Classification, Functions, and Clinical Relevance of Extracellular Vesicles. *Pharmacol. Rev.* **64,** 676–705 (2012).

308. Kanada, M., Bachmann, M. H., Hardy, J. W., Frimannson, D. O., Bronsart, L., Wang, A., Sylvester, M. D., Schmidt, T. L., Kaspar, R. L., Butte, M. J., Matin, A. C. & Contag, C. H. Differential fates of biomolecules delivered to target cells via extracellular vesicles. *PNAS* **112,** E1433–E1442 (2015).

309. Jeppesen, D. K., Fenix, A. M., Franklin, J. L., Higginbotham, J. N., Zhang, Q., Zimmerman, L. J., Liebler, D. C., Ping, J., Liu, Q., Evans, R., Fissell, W. H., Patton, J. G., Rome, L. H., Burnette, D. T. & Coffey, R. J. Reassessment of Exosome Composition. *Cell* **177,** 428–445 (2019).

310. Koga, K., Matsumoto, K., Akiyoshi, T., Kubo, M., Yamanaka, N., Tasaki, A., Nakashima, H., Nakamura, M., Kuroki, S., Tanaka, M. & Katano, M. Purification, characterization and biological significance of tumor-derived exosomes. *Anticancer Res.* **25,** 3703–3707 (2005).

311. Qu, J. L., Qu, X. J., Zhao, M. F., Teng, Y. E., Zhang, Y., Hou, K. Z., Jiang, Y. H., Yang, X. H. & Liu, Y. P. Gastric cancer exosomes promote tumour cell proliferation through PI3K/Akt and MAPK/ERK activation. *Dig. Liver Dis.* **41,** 875–880 (2009).

312. Wei, J., Lv, L., Wan, Y., Cao, Y., Li, G., Lin, H., Zhou, R., Shang, C., Cao, J., He, H., Han, Q., Liu, P., Xhou, G. & Min, J. Vps4A Functions as a Tumor Suppressor by Regulating the Secretion and Uptake of Exosomal MicroRNAs in Human Hepatoma Cells. *Hepatology* **61,** 1284–1294 (2015).

313. Xie, H., Zhao, Y., Caramuta, S., Larsson, C. & Lui, W. O. miR-205 Expression Promotes Cell Proliferation and Migration of Human Cervical Cancer Cells. *PLoS One* **7,** doi:10.1371/journal.pone.0046990 (2012).

314. Debata, P. R., Castellanos, M. R., Fata, J. E., Baggett, S., Rajupet, S., Szerszen, A., Begum, S., Mata, A., Murty, V. V., Opitz, L. M. & Banerjee, P. A novel curcumin-based vaginal cream Vacurin selectively eliminates apposed human cervical cancer cells. *Gynecol. Oncol.* **129,** 145–153 (2013).

315. Hyenne, V., Lefebvre, O. & Goetz, J. G. Going live with tumor exosomes and microvesicles. *Cell Adhes. Migr.* **11,** 173–186 (2017).

316. Otranto, M., Sarrazy, V., Bonté, F., Hinz, B., Gabbiani, G. & Desmoulière, A. The role of the myofibroblast in tumor stroma remodeling. *Cell Adhes. Migr.* **6,** 203–219 (2012).

317. Le Goff, B., Singbrant, S., Tonkin, B. A., Martin, T. J., Romas, E., Sims, N. A. & Walsh, N. C. Oncostatin M acting via OSMR, augments the actions of IL-1 and TNF in synovial fibroblasts. *Cytokine* **68,** 101–109 (2014).

318. Scaffidi, A. K., Mutsaers, S. E., Moodley, Y. P., McAnulty, R. J., Laurent, G. J., Thompson, P. J. & Knight, D. A. Oncostatin M stimulates proliferation, induces collagen production and inhibits apoptosis of human lung fibroblasts. *Br. J. Pharmacol.* **136,** 793–801 (2002).

319. Van Deun, J., Mestdagh, P., Sormunen, R., Cocquyt, V., Vermaelen, K.,

Vandesompele, J., Bracke, M., De Wever, O. & Hendrix, A. The impact of disparate isolation methods for extracellular vesicles on downstream RNA profiling. *J. Extracell. Vesicles* **3,** doi: 10.3402/jev.v3.24858 (2014).

320. Chuo, S. T. Y., Chien, J. C. Y. & Lai, C. P. K. Imaging extracellular vesicles: Current and emerging methods. *J. Biomed. Sci.* **25,** doi: 10.1186/s12929-018-0494-5 (2018).

321. Odorizzi, G. The multiple personalities of Alix. *J. Cell Sci.* **119,** 3025–3032 (2005).

322. Yang, J., Hagen, J., Guntur, K. V, Allette, K., Schuyler, S., Ranjan, J., Petralia, F., Gesta, S., Sebra, R., Mahajan, M., Zhang, B., Zhu, J., Houten, S., Kasarskis, A., Vishnudas, V. K., Akmaev, V. R., Sarangarajan, R., Narain, N. R., Schadt, E. E., *et al.* A next generation sequencing based approach to identify extracellular vesicle mediated mRNA transfers between cells. *BMC Genomics* **18,** doi: 10.1186/s12864-017-4359-1 (2017).

323. Gutkin, A., Uziel, O., Beery, E., Nordenberg, J., Pinchasi, M., Goldvaser, H., Henick, S., Goldberg, M. & Lahav, M. Tumor cells derived exosomes contain hTERT mRNA and transform nonmalignant fibroblasts into telomerase positive cells. *Oncotarget* **7,** 59173–59188 (2016).

324. Lai, C. P., Kim, E. Y., Badr, C. E., Weissleder, R., Mempel, T. R., Tannous, B. A. & Breakefield, X. O. Visualization and tracking of tumour extracellular vesicle delivery and RNA translation using multiplexed reporters. *Nat. Commun.* **6,** doi: 10.1038/ncomms8029 (2015).

325. Coenen-Stass, A. M. L., Magen, I., Brooks, T., Ben-Dov, I. Z., Greensmith, L., Hornstein, E. & Fratta, P. Evaluation of methodologies for microRNA biomarker detection by next generation sequencing. *RNA Biol.* **15,** 1133–1145 (2018).

326. Head, S. R., Kiyomi Komori, H., Lamere, S. A., Whisenant, T., Nieuwerburgh, F. Van, Salomon, D. R. & Ordoukhanian, P. Library construction for next-generation sequencing: Overviews and challenges. *Biotechniques* **56,** 61–77 (2014).

327. Zhu, Y. Y., Machleder, E. M., Chenchik, A., Li, R. & Siebert, P. D. Reverse Transcriptase Template Switching: A SMART^{TM}Approach for Full-Length cDNA Library Construction. *Biotechniques* **30,** 892–897 (2001).

328. Ramsköld, D., Luo, S., Wang, Y.-C., Li, R., Deng, Q., Faridani, O. R., Daniels, G. A., Khrebtukova, I., Loring, J. F., Laurent, L. C., Schroth, G. P., Sandberg, R. & Author, N. B. Full-Length mRNA-Seq from single cell levels of RNA and individual circulating tumor cells HHS Public Access Author manuscript. *Nat Biotechnol* **30,** 777–782 (2012).

329. Picelli, S., Bjorklund, A. K., Faridani, O. R., Sagasser, S., Winberg, G. & Sandberg, R. Smart-seq2 for sensitive full-length transcriptome profiling in single cells. *Nat. Methods* **10,** 1096–1098 (2013).

330. Song, Y., Milon, B., Ott, S., Zhao, X., Sadzewicz, L., Shetty, A., Boger, E. T., Tallon, L. J., Morell, R. J., Mahurkar, A. & Hertzano, R. A comparative analysis of library prep approaches for sequencing low input translatome samples. *BMC Genomics* **19,** doi: 10.1186/s12864-018-5066-2 (2018).

331. Barberán-Soler, S., Vo, J. M., Hogans, R. E., Dallas, A., Johnston, B. H. & Kazakov, S. A. Decreasing miRNA sequencing bias using a single adapter and circularization approach. *Genome Biol.* **19,** doi: 10.1186/s13059-018-1488-z (2018).

332. Baran-Gale, J., Kurtz, C. L., Erdos, M. R., Sison, C., Young, A., Fannin, E. E., Chines, P. S. & Sethupathy, P. Addressing Bias in Small RNA Library Preparation for Sequencing: A New Protocol Recovers MicroRNAs that Evade Capture by Current Methods. *Front. Genet.* **6,** doi: 10.3389/fgene.2015.00352 (2015).

333. Coenen-Stass, A. M., Magen, I., Brooks, T., Ben-Dov, I. Z., Greensmith, L., Hornstein, E. & Fratta, P. Evaluation of methodologies for microRNA biomarker detection by next generation sequencing. *RNA Biol.* **15,** 1133–1145 (2018).

334. Dillies, M.-A., Rau, A., Aubert, J., Hennequet-Antier, C., Jeanmougin, M., Servant, N., Keime, C., Marot, G., Castel, D., Estelle, J., Guernec, G., Jagla, B., Jouneau, L., Laloe, D., Le Gall, C., Schaeffer, B., Le Crom, S., Guedj, M. & Jaffrezic, F. A comprehensive evaluation of normalization methods for Illumina high-throughput RNA sequencing data analysis. *Brief. Bioinform.* **14,** 671–683 (2012).

335. Seyednasrollah, F., Laiho, A. & Elo, L. L. Comparison of software packages for detecting differential expression in RNA-seq studies. *Brief. Bioinform.* **16,** 59–70 (2013).

336. Costa-Silva, J., Domingues, D. & Lopes, F. M. RNA-Seq differential expression analysis: An extended review and a software tool. *PLoS One* **12,** doi: 10.1371/journal.pone.0190152 (2017).

337. Gautam, A., Kumar, R., Dimitrov, G., Hoke, A., Hammamieh, R. & Jett, M. Identification of extracellular miRNA in archived serum samples by next-generation sequencing from RNA extracted using multiple methods. *Mol. Biol. Rep.* **43,** 1165–1178 (2016).

338. Van Der Maaten, L. & Hinton, G. Visualizing Data using t-SNE. *J. Mach. Learn. Res.* **9,** 2579–2605 (2008).

339. Lex, A., Gehlenborg, N., Strobelt, H., Vuillemot, R., Pfister, H. & Manuscript, A. UpSet: Visualization of Intersecting Sets. *IEEE Trans Vis Comput Graph* **20,** 1983–1992 (2014).

340. Zhou, Y., Zhou, B., Pache, L., Chang, M., Khodabakhshi, A. H., Tanaseichuk, O., Benner, C. & Chanda, S. K. Metascape provides a biologist-oriented resource for the analysis of systems-level datasets. *Nat. Commun.* **10,** doi: 10.1038/s41467-019-09234-6 (2019).

341. Shannon, P., Markiel, A., Ozier, O., Baliga, N. S., Wang, J. T., Ramage, D., Amin, N., Schwikowski, B. & Ideker, T. Cytoscape: A Software Environment for Integrated Models of Biomolecular Interaction Networks. *Genome Res.* **13,** 2498–2504 (2003).

342. Ngernyuang, N., Francescone, R. A., Jearanaikoon, P., Daduang, J., Supoken, A., Yan, W., Shao, R. & Limpaiboon, T. Chitinase 3 like 1 is associated with tumor angiogenesis in cervical cancer. *Int. J. Biochem. Cell Biol.* **51,** 45–52 (2014).

343. Ngernyuang, N., Shao, R., Suwannarurk, K. & Limpaiboon, T. Chitinase 3 like 1 (CHI3L1) promotes vasculogenic mimicry formation in cervical cancer. *Pathology* **50,** 293–297 (2018).

344. Krona, A., Åman, P., Örndal, C. & Josefsson, A. Oncostatin M-induced genes in human astrocytomas. *Int. J. Oncol.* **31,** 1457–1463 (2007).

345. Natesh, K., Bhosale, D., Desai, A., Chandrika, G., Pujari, R., Jagtap, J., Chugh, A., Ranade, D. & Shastry, P. Oncostatin-M Differentially Regulates Mesenchymal and

Proneural Signature Genes in Gliomas via STAT3 Signaling. *Neoplasia* **17,** 225–237 (2015).

346. Ho, Y. Y., Baron, M., Recklies, A. D., Roughley, P. J. & Mort, J. S. Cells from the skin of patients with systemic sclerosis secrete chitinase 3-like protein 1. *BBA Clin. 1* **1,** 2–11 (2014).

347. Zhang, Y., Jia, S. & Jiang, W. G. KIAA1199 and its biological role in human cancer and cancer cells (Review). *Oncol. Rep.* **31,** 1503–1508 (2014).

348. Banach, A., Jiang, Y. P., Roth, E., Kuscu, C., Cao, J. & Lin, R. Z. CEMIP upregulates BiP to promote breast cancer cell survival in hypoxia. *Oncotarget* **10,** 4307–4320 (2019).

349. Shen, F., Zong, Z. hong, Liu, Y., Chen, S., Sheng, X. jie & Zhao, Y. CEMIP promotes ovarian cancer development and progression via the PI3K/AKT signaling pathway. *Biomed. Pharmacother.* **114,** 108787 (2019).

350. Zhang, F., Zhang, Y., Sun, L., Chen, M., Ran, Y. & Sun, L. Carboxypeptidase A4 promotes migration and invasion of lung cancer cells, and is closely associated with lymph node metastasis. *Precis. Radiat. Oncol.* **3,** 44–51 (2019).

351. Sun, L., Wang, Y., Yuan, H., Burnett, J., Pan, J., Yang, Z., Ran, Y., Myers, I. & Sun, D. CPA4 is a Novel Diagnostic and Prognostic Marker for Human Non-Small-Cell Lung Cancer. *J. Cancer* **7,** 1197–1204 (2016).

352. Handa, T., Katayama, A., Yokobori, T., Yamane, A., Fujii, T., Obayashi, S., Kurozumi, S., Kawabata-Iwakawa, R., Gombodorj, N., Nishiyama, M., Asao, T., Shirabe, K., Kuwano, H. & Oyama, T. Carboxypeptidase A4 accumulation is associated with an aggressive phenotype and poor prognosis in triple-negative breast cancer. *Int. J. Oncol.* **54,** 833–844 (2019).

353. Buitrago-Pérez, Á., Garaulet, G., Vázquez-Carballo, A., Paramio, J. M. & García-Escudero, R. Molecular Signature of HPV-Induced Carcinogenesis: pRb, p53 and Gene Expression Profiling. *Curr. Genomics* **10,** 26–34 (2009).

354. Su, P.-H., Lin, Y.-W., Huang, R.-L., Liao, Y.-P., Lee, H.-Y., Wang, H.-C., Chao, T.-K., Chen, C.-K., Chan, M., Chu, T.-Y., Yu, M.-H. & Lai, H.-C. Epigenetic silencing of PTPRR activates MAPK signaling, promotes metastasis and serves as a biomarker of invasive cervical cancer. *Oncogene* **32,** 15–26 (2012).

355. Hossein Pourhanifeh, M., Mohammadi, R., Noruzi, S., Atefe Hosseini, S., Fanoudi, S., Mohamadi, Y., Hashemzehi, M., Asemi, Z., Reza Mirzaei, H., Salarinia, R. & Mirzaei, H. The role of fibromodulin in cancer pathogenesis: implications for diagnosis and therapy. *Cancer Cell Int.* **19,** doi: 10.1186/s12935-019-0870-6 (2019).

356. Johansson, P., Aoude, L. G., Glasson, K. & Hayward, S. K. Deep sequencing of uveal melanoma identifies a recurrent mutation in PLCB4. *Oncotarget* **7,** 4624–4631 (2016).

357. Li, C.-F., Liu, T.-T., Chuang, I.-C., Chen, Y.-Y., Fang, F.-M., Chan, T.-C., Li, W.-S. & Huang, H.-Y. PLCB4 copy gain and PLCß4 overexpression in primary gastrointestinal stromal tumors: Integrative characterization of a lipid-catabolizing enzyme associated with worse disease-free survival. *Oncotarget* **8,** 19997–20010 (2017).

358. Zhang, T., Song, X., Liao, X., Wang, X., Zhu, G., Yang, C. & Xie, X. Distinct Prognostic Values of Phospholipase C Beta Family Members for Non-Small Cell Lung Carcinoma. *Biomed Res. Int.* **2019,** doi: 10.1155/2019/4256524 (2019).

359. Wardman, J. H. & Fricker, L. D. ProSAAS-Derived Peptides Are Differentially Processed and Sorted in Mouse Brain and AtT-20 Cells. *PLoS One* **9,** doi: 10.1371/journal.pone.0104232 (2014).

360. Liu, T., Zhao, Y., Tang, N., Feng, R., Yang, X., Lu, N., Wen, J. & Li, L. Pax6 Directly Down-Regulates Pcsk1n Expression Thereby Regulating PC1/3 Dependent Proinsulin Processing. *PLoS One* **7,** doi: 10.1371/journal.pone.0046934 (2012).

361. Osanai, K., Takahashi, K., Nakamura, K., Takahashi, M., Ishigaki, M., Sakuma, T., Toga, H., Suzuki, T. & Voelker, D. R. Expression and characterization of Rab38, a new member of the Rab small G protein family. *Biol. Chem* **386,** 143–153 (2005).

362. Zippelius Elke Jaeger, A., Lévy, F., Knuth, A., Jäger, D., Dummer, R., Tiercy, J.-M., Mackensen, A., Exner, C., Schäfer, N., Urosevic, M., Knights, A., Gati, A., Laumer, M., Senta Walton, L. M., Gerlinger, M. & de la Rosa, O. Spontaneous CD8 T Cell Responses against the Melanocyte Differentiation Antigen RAB38/NY-MEL-1 in Melanoma Patients. *J. Immunol.* **177,** 8212–8218 (2006).

363. Wang, H. & Jiang, C. RAB38 confers a poor prognosis, associated with malignant progression and subtype preference in glioma. *Oncol. Rep.* **30,** 2350–2356 (2013).

364. Li, B.-Y., He, L.-J., Zhang, X.-L., Liu, H. & Liu, B. High expression of RAB38 promotes malignant progression of pancreatic cancer. *Mol. Med. Rep.* **19,** 908–919 (2019).

365. Santin, A. D., Zhan, F., Bignotti, E., Siegel, E. R., Cané, S., Bellone, S., Palmieri, M., Anfossi, S., Thomas, M., Burnett, A., Kay, H. H., Roman, J. J., O'Brien, T. J., Tian, E., Cannon, M. J., Shaughnessy, J. & Pecorelli, S. Gene expression profiles of primary HPV16- and HPV18-infected early stage cervical cancers and normal cervical epithelium: Identification of novel candidate molecular markers for cervical cancer diagnosis and therapy. *Virology* **331,** 269–291 (2005).

366. Gilder, A. S., Natali, L., Van Dyk, D. M., Zalfa, C., Banki, M. A., Pizzo, D. P., Wang, H., Klemke, R. L., Mantuano, E. & Gonias, S. L. The Urokinase Receptor Induces a Mesenchymal Gene Expression Signature in Glioblastoma Cells and Promotes Tumor Cell Survival in Neurospheres. *Sci. Rep.* **8,** doi: 10.1038/s41598-018-21358-1 (2018).

367. Zhou, J., Kwak, K. J., Wu, Z., Yang, D., Li, J., Chang, M., Song, Y., Zeng, H., Lee, L. J., Hu, J. & Bai, C. PLAUR Confers Resistance to Gefitinib Through EGFR/P-AKT/Survivin Signaling Pathway. *Cell Physiol Biochem* **47,** 1909–1924 (2018).

368. Jing, J., Zheng, S., Han, C., Du, L., Guo, Y. & Wang, P. Evaluating the value of uPAR of serum and tissue on patients with cervical cancer. *J. Clin. Lab. Anal.* **26,** 16–21 (2012).

369. Strand, K., Murray, J., Aziz, S., Ishida, A., Rahman, S., Patel, Y., Cardona, C., Hammond, W. P., Savidge, G. & Wijelath, E. S. Induction of the urokinase plasminogen activator system by oncostatin M promotes endothelial migration. *J. Cell. Biochem.* **79,** 239–248 (2000).

370. Chen, M., Xu, R., Ji, H., Greening, D. W., Rai, A., Izumikawa, K., Ishikawa, H., Takahashi, N. & Simpson, R. J. Transcriptome and long noncoding RNA sequencing of three extracellular vesicle subtypes released from the human colon cancer LIM1863 cell line. *Sci. Rep.* **6,** doi: 10.1038/srep38397 (2016).

371. Kołat, D., Hammouz, R., Bednarek, A. K. & Płuciennik, E. Exosomes as carriers transporting long non-coding RNAs: Molecular characteristics and their function in cancer (Review). *Mol. Med. Rep.* **20,** 851–862 (2019).

372. Hinger, S. A., Cha, D. J., Franklin, J. L., Higginbotham, J. N., Dou, Y., Ping, J., Shu, L., Prasad, N., Levy, S., Zhang, B., Liu, Q., Weaver, A. M., Coffey, R. J. & Patton, J. G. Diverse Long RNAs Are Differentially Sorted into Extracellular Vesicles Secreted by Colorectal Cancer Cells. *Cell Rep.* **25,** 715–725 (2018).

373. Skog, J., Wurdinger, T., van Rijn, S., Meijer, D., Gainche, L., Sene-Esteves, M., Curry Jr, W. T., Carter, R. S., Krichevsky, A. M. & Breakefield, X. O. Glioblastoma microvesicles transport RNA and protein that promote tumor growth and provide diagnostic biomarkers. *Nat Cell Biol* **10,** 1470–1476 (2008).

374. Hong, B. S., Cho, J. H., Kim, H., Choi, E. J., Rho, S., Kim, J., Kim, J. H., Choi, D. S., Kim, Y. K., Hwang, D. & Gho, Y. S. Colorectal cancer cell-derived microvesicles are enriched in cell cycle-related mRNAs that promote proliferation of endothelial cells. *BMC Genomics* **10,** 1–13 (2009).

375. Hurd, P. J. & Nelson, C. J. Advantages of next-generation sequencing versus the microarray in epigenetic research. *Briefings Funct. Genomics Proteomics* **8,** 174–183 (2009).

376. Muz, B., de la Puente, P., Azab, F. & Azab, A. K. The role of hypoxia in cancer progression, angiogenesis, metastasis, and resistance to therapy. *Hypoxia* **3,** 83–92 (2015).

377. Krock, B. L., Skuli, N. & Simon, M. C. Hypoxia-Induced Angiogenesis: Good and Evil. *Genes and Cancer* **2,** 1117–1133 (2011).

378. Vollmer, S., Kappler, V., Kaczor, J., Flügel, D., Rolvering, C., Kato, N., Kietzmann, T., Behrmann, I. & Haan, C. Hypoxia-inducible factor 1α is up-regulated by oncostatin M and participates in oncostatin M signaling. *Hepatology* **50,** 253–260 (2009).

379. Battello, N., David Zimmer, A., Goebel, C., Dong, X., Behrmann, I., Haan, C., Hiller, K. & Wegner, A. The role of HIF-1 in oncostatin M-dependent metabolic reprogramming of hepatic cells. *Cancer Metab.* **4,** doi: 10.1186/s40170-016-0141-0 (2016).

380. Jones, R. G. & Thompson, C. B. Tumor suppressors and cell metabolism: a recipe for cancer growth. *Genes Dev.* **23,** 537–548 (2009).

381. Shrivastava, R., Singh, V., Asif, M., Negi, M. P. S. & Bhadauria, S. Oncostatin M upregulates HIF-1α in breast tumor associated macrophages independent of intracellular oxygen concentration. *Life Sci.* **194,** 59–66 (2018).

382. Shrivastava, R., Asif, M., Singh, V., Dubey, P., Ahmad Malik, S., Lone, M. U. D., Tewari, B. N., Baghel, K. S., Pal, S., Nagar, G. K., Chattopadhyay, N. & Bhadauria, S. M2 polarization of macrophages by Oncostatin M in hypoxic tumor microenvironment is mediated by mTORC2 and promotes tumor growth and metastasis. *Cytokine* **118,** 130–143 (2019).

383. Kucharzewska, P., Christianson, H. C., Welch, Johanna, E., Svensson, K. J., Fredlund, E., Ringer, M., Morgelin, M., Bourseau-Guilmain, E., Bengzon, J. & Belting, M. Exosomes reflect the hypoxic status of glioma cells and mediate hypoxia-dependent activation of vascular cells during tumor development. *PNAS* **110,** 7213–7317 (2013).

384. Aga, M., Bentz, G. L., Raffa, S., Torrisi, M. R., Kondo, S., Wakisaka, N., Yoshizaki, T., Pagano, J. S. & Shackelford, J. Exosomal HIF1α supports invasive potential of nasopharyngeal carcinoma-associated LMP1-positive exosomes. *Oncogene* **33,** 4613–4622 (2014).

385. Porta, C., Sica, A. & Riboldi, E. Tumor-associated myeloid cells: new understandings on their metabolic regulation and their influence in cancer immunotherapy. *FEBS J.* **285,** 717–733 (2018).

386. Awad, R. M., De Vlaeminck, Y., Maebe, J., Goyvaerts, C. & Breckpot, K. Turn Back the TIMe: Targeting Tumor Infiltrating Myeloid Cells to Revert Cancer Progression. *Front. Immunol.* **9,** doi: 10.3389/fimmu.2018.01977 (2018).

387. Tripathi, C., Nath Tewari, B., Kanchan, R. K., Singh Baghel, K., Nautiyal, N., Shrivastava, R., Kaur, H., Lal, M., Bhatt, B. & Bhadauria, S. Macrophages are recruited to hypoxic tumor areas and acquire a Pro-Angiogenic M2-Polarized phenotype via hypoxic cancer cell derived cytokines Oncostatin M and Eotaxin. *Oncotarget* **5,** 5350–5368 (2014).

388. Levesque-Sergerie, J. P., Duquette, M., Thibault, C., Delbecchi, L. & Bissonnette, N. Detection limits of several commercial reverse transcriptase enzymes: Impact on the low- and high-abundance transcript levels assessed by quantitative RT-PCR. *BMC Mol. Biol.* **8,** doi: 10.1186/1471-2199-8-93 (2007).

389. Lester, R. D., Jo, M., Montel, V., Takimoto, S. & Gonias, S. L. uPAR induces epithelial-mesenchymal transition in hypoxic breast cancer cells. *J. Cell Biol.* **178,** 425–436 (2007).

390. Yan, C., Ding, X., Wu, L., Yu, M., Qu, P. & Du, H. Stat3 Downstream Gene Product Chitinase 3-Like 1 Is a Potential Biomarker of Inflammation-induced Lung Cancer in Multiple Mouse Lung Tumor Models and Humans. *PLoS One* **8,** doi: 10.1371/journal.pone.0061984 (2013).

391. Chevillet, J. R., Kang, Q., Ruf, I. K., Briggs, H. A., Vojtech, L. N., Hughes, S. M., Cheng, H. H., Arroyo, J. D., Meredith, E. K., Gallichotte, E. N., Pogosova-Agadjanyan, E. L., Morrissey, C., Stirewalt, D. L., Hladik, F., Yu, E. Y., Higano, C. S. & Tewari, M. Quantitative and stoichiometric analysis of the microRNA content of exosomes. *PNAS* **111,** 14888–14893 (2014).

392. Wei, Z., Batagov, A. O., Schinelli, S., Wang, J., Wang, Y., El Fatimy, R., Rabinovsky, R., Balaj, L., Chen, C. C., Hochberg, F., Carter, B., Breakefield, X. O. & Krichevsky, A. M. Coding and noncoding landscape of extracellular RNA released by human glioma stem cells. *Nat. Commun.* **8,** doi: 10.1038/s41467-017-01196-x (2017).

393. Kirchmeyer, M., Servais, F. A., Hamdorf, M., Nazarov, P. V., Ginolhac, A., Halder, R., Vallar, L., Glanemann, M., Rubie, C., Lammert, F., Kreis, S. & Behrmann, I. Cytokine-mediated modulation of the hepatic miRNome: miR-146b-5p is an IL-6-inducible miRNA with multiple targets. *J. Leukoc. Biol.* **104,** 987–1002 (2018).

394. Raso, A., Dirkx, E., Philippen, L. E., Fernandez-Celis, A., De Majo, F., Sampaio-Pinto, V., Sansonetti, M., Juni, R., el Azzouzi, H., Calore, M., Bitsch, N., Olieslagers, S., Oerlemans, M. I. F. J., Huibers, M. M., de Weger, R. A., Reckman, Y. J., Pinto, Y. M., Zentilin, L., Zacchigna, S., *et al.* Therapeutic Delivery of miR-148a Suppresses Ventricular Dilation in Heart Failure. *Mol. Ther.* **27,** 584–599 (2019).

395. Bottai, G., Diao, L., Baggerly, K. A., Paladini, L., Gyorffy, B., Raschioni, C., Pusztai, L., Calin, G. A. & Santarpia, L. Integrated MicroRNA-mRNA Profiling Identifies Oncostatin M as a Marker of Mesenchymal-Like ER-Negative/HER2-Negative Breast Cancer. *Int. J. Mol. Sci. Artic.* **18,** doi:10.3390/ijms18010194 (2017).

396. Cai, Q., Zheng, P., Ma, F., Zhang, H., Li, Z., Fu, Q., Han, C. & Sun, Y. MicroRNA-224 enhances the osteoblastic differentiation of hMSCs via Rac1. *Cell Biochem. Funct.*

37, 62–71 (2019).

397. Amankwatia, E. B., Chakravarty, P., Carey, F. A., Weidlich, S., Steele, R. J. C., Munro, A. J., Wolf, C. R. & Smith, G. MicroRNA-224 is associated with colorectal cancer progression and response to 5-fluorouracil-based chemotherapy by KRAS-dependent and -independent mechanisms. *Br. J. Cancer* **112,** 1480–1490 (2015).

398. Kim, M., Jang, K., Miller, P., Picon-Ruiz, M., Yeasky, T. M., El-Ashry, D. & Slingerland, J. M. VEGFA links self-renewal and metastasis by inducing Sox2 to repress miR-452, driving Slug. *Oncogene* **36,** 5199–5211 (2017).

399. Kumarswamy, R., Mudduluru, G., Ceppi, P., Muppala, S., Kozlowski, M., Niklinski, J., Papotti, M. & Allgayer, H. MicroRNA-30a inhibits epithelial-to-mesenchymal transition by targeting Snai1 and is downregulated in non-small cell lung cancer. *Int. J. Cancer* **130,** 2044–2053 (2012).

400. Wang, Y., Wu, C., Zhang, C., Li, Z., Zhu, T., Chen, J., Ren, Y., Wang, X., Zhang, L. & Zhou, X. TGF-β-induced STAT3 overexpression promotes human head and neck squamous cell carcinoma invasion and metastasis through malat1/miR-30a interactions. *Cancer Lett.* **436,** 52–62 (2018).

401. de Winther, M. P. J. & Lutgens, E. MiR-92a At the Heart of Lipid-Driven Endothelial Dysfunction. *Circ. Res.* **114,** 399–401 (2014).

402. Park, G. B. & Kim, D. MicroRNA-503-5p Inhibits the CD97-Mediated JAK2/STAT3 Pathway in Metastatic or Paclitaxel-Resistant Ovarian Cancer Cells. *Neoplasia* **21,** 206–215 (2019).

403. Van Dongen, S., Abreu-Goodger, C. & Enright, A. J. Detecting microRNA binding and siRNA off-target effects from expression data. *Nat Methods* **5,** 1023–1025 (2008).

404. Saxena, M. & Christofori, G. Rebuilding cancer metastasis in the mouse. *Mol. Oncol.* **7,** 283–296 (2013).

405. Mohanty, S. & Xu, L. Experimental Metastasis Assay. *J. Vis. Exp.* **42,** doi:10.3791/1942 (2010).

406. Zinn, K. R., Chaudhuri, T. R., Szafran, A. A., O'Quinn, D., Weaver, C., Dugger, K., Lamar, D., Kesterson, R. A., Wang, X. & Frank, S. J. Noninvasive bioluminescence imaging in small animals. *ILAR J.* **49,** 103–115 (2008).

407. Gómezgómez-Cuadrado, L., Tracey, N., Ma, R., Qian, B. & Brunton, V. G. Mouse models of metastasis: progress and prospects. *Dis. Model. Mech.* **10,** 1061–1074 (2017).

408. Liu, J., Hadjokas, N., Mosley, B., Estrov, Z., Spence, M. J. & Vestal, R. E. Oncostatin M-specific receptor expression and function in regulating cell proliferation of normal and malignant mammary epithelial cells. *Cytokine* **10,** 295–302 (1998).

409. Sun, D., Li, S., Wu, H., Zhang, M., Zhang, X., Wei, L., Qin, X. & Gao, E. Oncostatin M (OSM) protects against cardiac ischaemia/reperfusion injury in diabetic mice by regulating apoptosis, mitochondrial biogenesis and insulin sensitivity. *J. Cell. Mol. Med.* **19,** 1296–1307 (2015).

410. Hu, J., Zhang, L., Zhao, Z., Zhang, M., Lin, J., Wang, J., Yu, W., Man, W., Li, C., Zhang, R., Gao, E., Wang, H. & Sun, D. OSM mitigates post-infarction cardiac remodeling and dysfunction by up-regulating autophagy through Mst1 suppression. *Biochim. Biophys. Acta* **1863,** 1951–1961 (2017).

411. Kubin, T., Pö Ling, J., Kostin, S., Gajawada, P., Hein, S., Rees, W., Wietelmann, A., Tanaka, M., Lö Rchner, H., Schimanski, S., Szibor, M., Warnecke, H. & Braun, T. Oncostatin M Is a Major Mediator of Cardiomyocyte Dedifferentiation and Remodeling. *Stem Cell* **9,** 420–432 (2011).

412. Zhang, X., Zhu, D., Wei, L., Zhao, Z., Qi, X., Li, Z. & Sun, D. OSM Enhances Angiogenesis and Improves Cardiac Function after Myocardial Infarction. *Biomed Res. Int.* **2015,** doi:10.1155/2015/317905 (2015).

413. Erez, N., Truitt, M., Olson, P. & Hanahan, D. Cancer-Associated Fibroblasts Are Activated in Incipient Neoplasia to Orchestrate Tumor-Promoting Inflammation in an NF-κB-Dependent Manner. *Cancer Cell* **17,** 135–147 (2010).

414. Junk, D. J. D., Bryson, B. L. B., Smigiel, J. M., Parameswaran, N., Bartel, C. A. C. & Jackson, M. W. M. Oncostatin M promotes cancer cell plasticity through cooperative STAT3-SMAD3 signaling. *Oncogene* **36,** 4001–4013 (2017).

415. Metcalf, D. & Gearing, D. P. Fatal syndrome in mice engrafted with cells producing high levels of the leukemia inhibitory factor. *PNAS* **86,** 5948–5952 (1989).

416. Matsuda, M., Tsurusaki, S., Miyata, N., Saijou, E., Okochi, H., Miyajima, A. & Tanaka, M. Oncostatin M causes liver fibrosis by regulating cooperation between hepatic stellate cells and macrophages in mice. *Hepatology* **67,** 296–312 (2018).

417. Mozaffarian, A., Brewer, A. W., Trueblood, E. S., Luzina, I. G., Todd, N. W., Atamas, S. P. & Arnett, H. A. Mechanisms of Oncostatin M-Induced Pulmonary Inflammation and Fibrosis. *J. Immunol.* **181,** 7243–7253 (2008).

418. Underhill-Day, N. & Heath, J. K. Oncostatin M (OSM) cytostasis of breast tumor cells: Characterization of an OSM receptor β-specific kernel. *Cancer Res.* **66,** 10891–10901 (2006).

419. Suemizu, H., Kawai, K., Higuchi, Y., Hashimoto, H., Ogura, T., Itoh, T., Sasaki, E. & Nakamura, M. A versatile technique for the in vivo imaging of human tumor xenografts using near-infrared fluorochrome-conjugated macromolecule probes. *PLoS One* **8,** doi: 10.1371/journal.pone.0082708 (2013).

420. Cespedes, M. V., Casanova, I., Parrefio, M. & Mangues, R. Mouse models in oncogenesis and cancer therapy. *Clin Transl Oncol* **8,** 318–329 (2006).

421. Choy, E. H., Bendit, M., McAleer, D., Liu, F., Feeney, M., Brett, S., Zamuner, S., Campanile, A. & Toso, J. Safety, tolerability, pharmacokinetics and pharmacodynamics of an anti- oncostatin M monoclonal antibody in rheumatoid arthritis: Results from phase II randomized, placebo-controlled trials. *Arthritis Res. Ther.* **15,** doi: 10.1186/ar4312 (2013).

422. Brolund, L., Küster, A., Korr, S., Vogt, M. & Müller-Newen, G. A receptor fusion protein for the inhibition of murine oncostatin M. *BMC Biotechnol.* **11,** doi: 10.1186/1472-6750-11-3 (2011).

423. Zhou, C. F., Ma, J., Huang, L., Yi, H. Y., Zhang, Y. M., Wu, X. G., Yan, R. M., Liang, L., Zhong, M., Yu, Y. H., Wu, S. & Wang, W. Cervical squamous cell carcinoma-secreted exosomal miR-221-3p promotes lymphangiogenesis and lymphatic metastasis by targeting VASH1. *Oncogene* **38,** 1256–1268 (2019).

424. Bell, E. & Taylor, M. A. Functional Roles for Exosomal MicroRNAs in the Tumour Microenvironment. *Comput. Struct. Biotechnol. J.* **15,** 8–13 (2017).

425. Kogure, A., Kosaka, N. & Ochiya, T. Cross-talk between cancer cells and their neighbors via miRNA in extracellular vesicles: An emerging player in cancer metastasis. *J. Biomed. Sci.* **26,** doi: 10.1186/s12929-019-0500-6 (2019).

10. SUPPLEMENTARY METHODS

10.1 Plasma collection by cardiac puncture

Mice were anesthetised with isoflurane; they were initially placed in an isoflurane induction chamber and then, once suitably anaesthetised, removed from the chamber and placed in a dorsal recumbency position on top of a heated pad, with continued delivery of anaesthesia via a nose cone. A sterile 25 gauge 1 inch needle was attached to a 1ml syringe (both BD microlance, Franklin Lakes, NJ, USA) and coated with filtered 10% 0.5M EDTA anticoagulant. 100µl EDTA was also added to a 1.5ml collection tube. The needle was inserted through the mouse's chest and blood drawn from the heart; blood was quickly transferred to the EDTA containing collection tube. Mice were culled by cervical dislocation. The blood was left at room temperature for 30mins; it was subsequently centrifuged at 1,500*xg* for 10mins at 4°C. The supernatant (plasma) was removed to a new eppendorf tube and frozen at -80°C. Total RNA was subsequently extracted as described in section 3.6.3

10.2 *Ex vivo* tumour culture and EV isolation

Tumour pieces were collected into DMEM and placed on ice. They were subsequently transferred to a 6 well tissue culture plate containing 3ml DMEM + 1% Penicillin-Streptomycin. After 24hours in culture, conditioned media was collected and split between two 1.5ml Eppendorf tubes and EVs isolated using a modified ultracentrifugation protocol to account for lower sample volume. Conditioned media was centrifuged at 1000*xg* for 15mins at 4°C. Supernatant was then transferred into new 1.5ml Eppendorf tubes and centrifuged at 2000*xg* for a further 15mins. Supernatant was transferred to new 1.5ml Eppendorf tubes and centrifuged at 16,000*xg* for 25mins at 4°C; all steps up until this point were performed in an Eppendorf 5415R benchtop centrifuge. Supernatant from the two Eppendorf tubes was subsequently pooled and transferred to Ultra-Clear ½ x 2 inch centrifuge tubes ('5ml centrifuge tubes'); samples were centrifuged at 100,000*xg* for 80mins at 4°C using an Optima L-100XP centrifuge with SW-55Ti rotor. The supernatant was discarded and the EV containing pellet re-suspended in 3ml PBS. Samples were centrifuged for a further 40mins at 100,000*xg*, 4°C using a SW-55Ti rotor. This step was performed to remove contaminating protein. Supernatant was discarded and EV pellets frozen at -80°C; total RNA was extracted as described in section 3.6.3.

10.3 Histology

Table S3. 1: Reagents for Histology	
Reagent	**Company**
• Formalin (10%, buffered) • Ethanol • DPX mountant	Sigma-Aldrich, St. Louis, MO, United States
• Harris haematoxylin • Xylene • Superfrost Plus Slides	Thermo Fisher Scientific, Waltham, MA, USA
• Eosin Y	Atom Science, Manchester, UK

Tumour tissues were fixed in formalin for 24 hours then transferred into 70% ethanol. Samples were processed and embedded into paraffin wax by the Histopathology Laboratory in the Department of Pathology. Paraffin embedded tissue blocks were chilled to 4°C and 5µm sections cut using a Shandon AS325 rotary microtome. Sections were floated in a sectioning waterbath and mounted onto superfrost plus slides. Slides were then baked at 56°C overnight. Haematoxylin and eosin staining were then performed as described below. Sections were deparaffinised in xylene (2 x 10mins) then transferred through decreasing concentrations of ethanol (100% - 2 x 5mins, 90% - 2mins, 70% - 2mins). Slides were washed for 5mins in distilled water and then stained with haematoxylin for 3mins. Slides were then washed in running water for 5mins, and excess stain removed by placing in acid alcohol (70% Ethanol + 1% hydrochloric acid) for 1min. Sections were then rinsed under running water for 10mins, stained with Eosin Y (20% Eosin Y + 80% ethanol) for 1min, then washed in distilled water for 40secs. Sections were then rehydrated by passing through increasing concentrations of ethanol (70% - 2mins, 90% - 2mins, 100% - 2mins) then transferred to xylene for 2 x 2mins. Excess xylene was removed by blotting the edges of the slide with tissue, and coverslips applied using DPX mountant.

11. SUPPLEMENTARY INFORMATION FOR CHAPTER 4

RESULTS: Effect of OSM signalling on EV cargo in cervical SCC cells

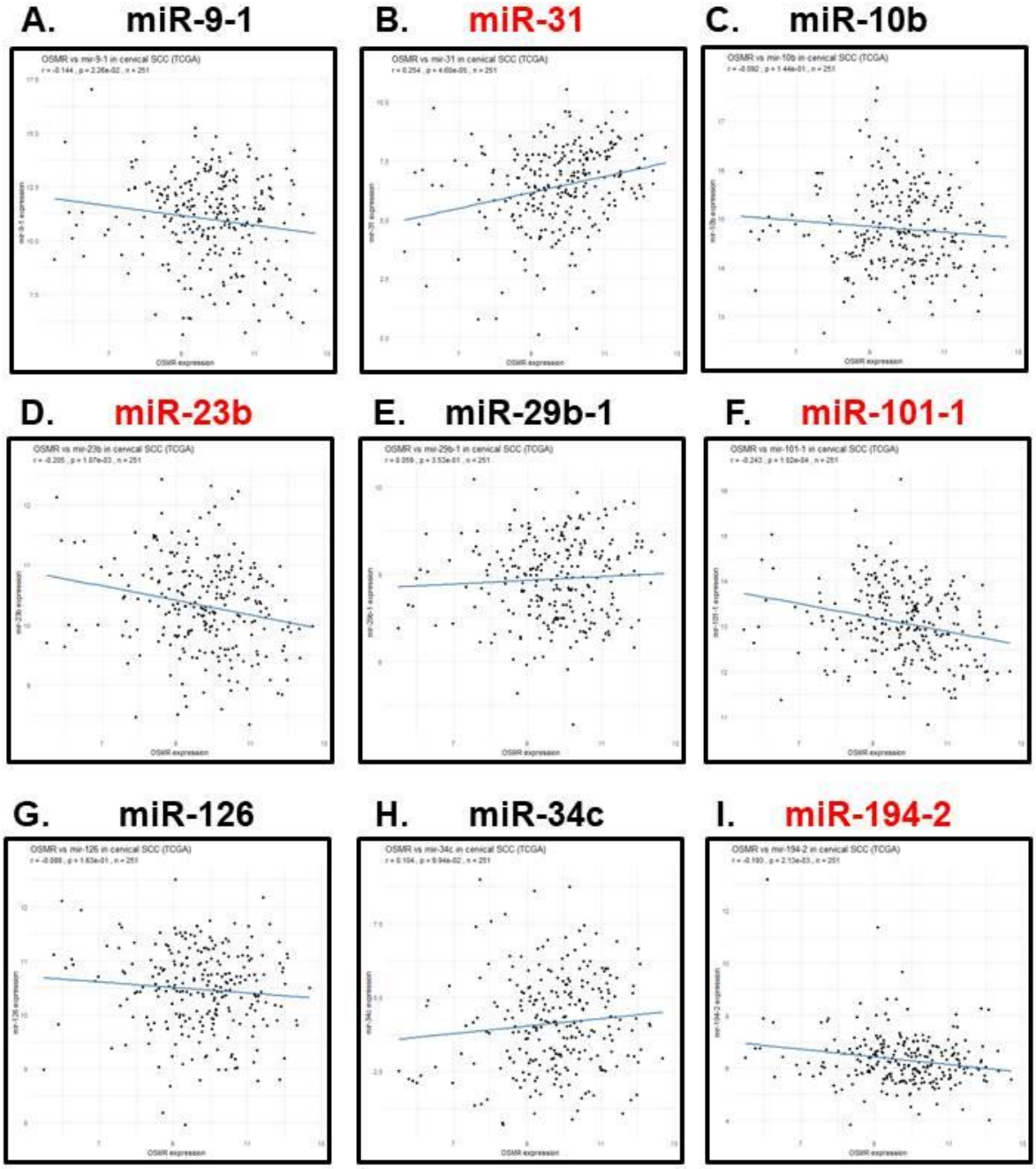

Figure S4. 1: miRNA selected for qPCR: correlation with OSMR in TCGA datasets
Analysis of TCGA dataset of mRNA expression in clinical samples obtained from patients with cervical SCC. Correlation of OSMR expression compared to expression of the following miRNAs selected for qPCR investigation is shown: A) miR-9-1 B) miR-31 C) miR-10b D) miR-23b E) miR-29b-1 F) miR-101-1 G) miR-126 H) miR-34c and I) miR-194-2. $P \leq 0.01$ were considered as statistically significant to account for multiple testing. miRNA with significant correlation with OSMR expression are highlighted in red. n = 251. Correlation plots were generated by Dr Stephen Smith.

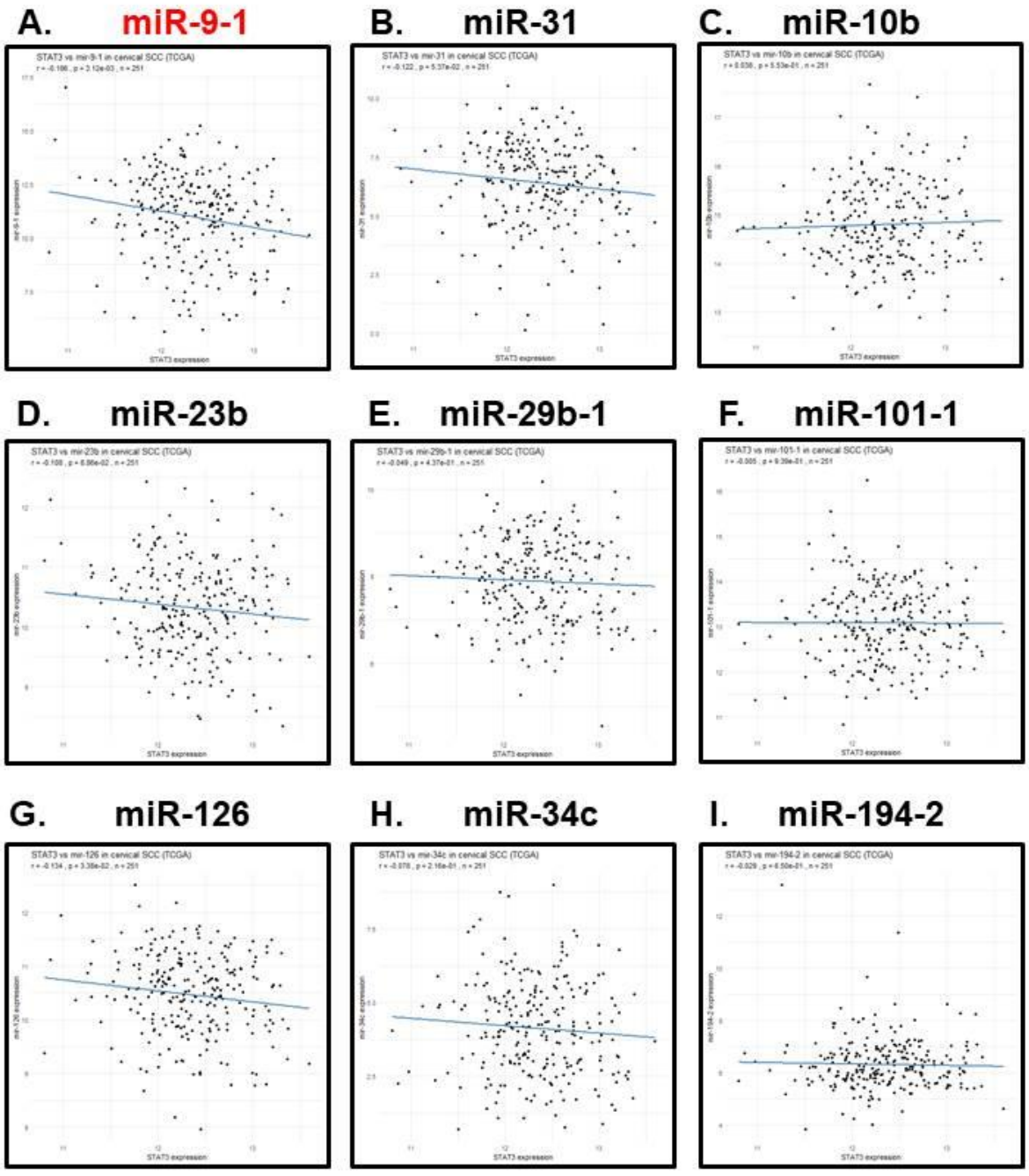

Figure S4. 2: miRNA selected for qPCR: correlation with *STAT3* in TCGA datasets
Analysis of TCGA dataset of mRNA expression in clinical samples obtained from patients with cervical SCC. Correlation of *STAT3* expression compared to expression of the following miRNAs selected for qPCR investigation is shown: A) miR-9-1 B) miR-31 C) miR-10b D) miR-23b E) miR-29b-1 F) miR-101-1 G) miR-126 H) miR-34c and I) miR-194-2. $P \leq 0.01$ were considered as statistically significant to account for multiple testing. miRNA with significant correlation with *STAT3* expression are highlighted in red. n = 251. Correlation plots were generated by Dr Stephen Smith.

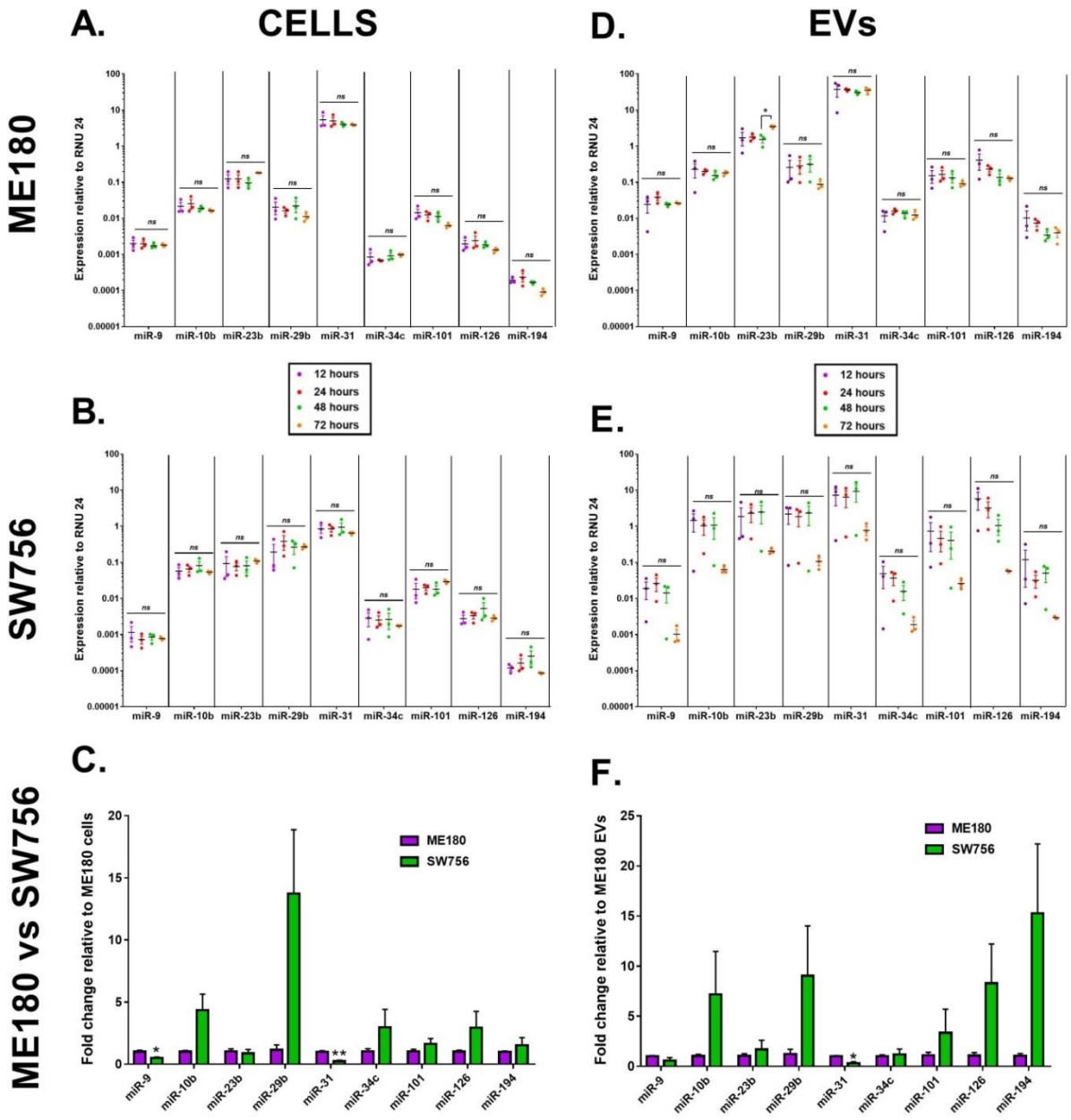

Figure S4. 3: Baseline miRNA levels in SW756 and ME180 cells and EVs

Quantitative RT-PCR for SW756 and ME180 cells and EVs collected 12, 24, 48 or 72 hours with PBS control. miRNA abundance at each timepoint is shown relative to RNU24 housekeeper miRNA levels for A) ME180 cells B) SW756 Cells D) ME180 EVs and E) SW756 EVs. Values are displayed on a log10 scale. C) Fold change in miRNA expression at the 48hour timepoint in PBS treated SW756 cells compared to PBS treated ME180 cells and F) PBS treated SW756 EVs compared to PBS treated ME180 EVs. Error bars represent SEM, n=3 independent experiments for each condition. Values were analysed for statistical significance using a one way ANOVA with Tukey's multiple comparison post-hoc tests (A,B,D,E) or unpaired T-test with Welch's correction (C and F). * =.P≤0.05, ** = P≤0.01.

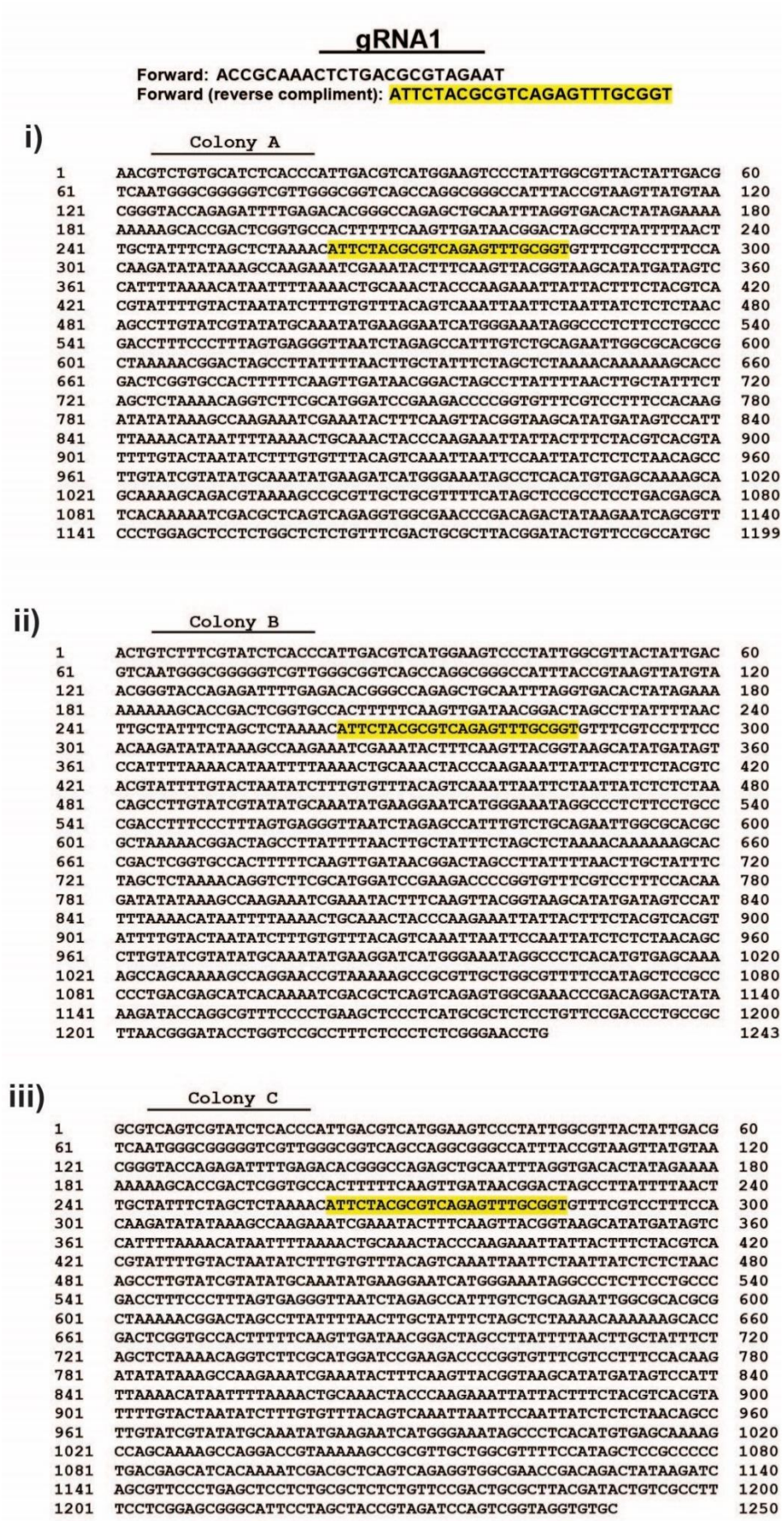

Figure S4. 4: Confirmation of gRNA1 insertion into PX466 Cas9-D10A-GFP vector
Sequencing of gRNA1 colonies i) A ii) B iii) C. gRNA1 is highlighted in yellow

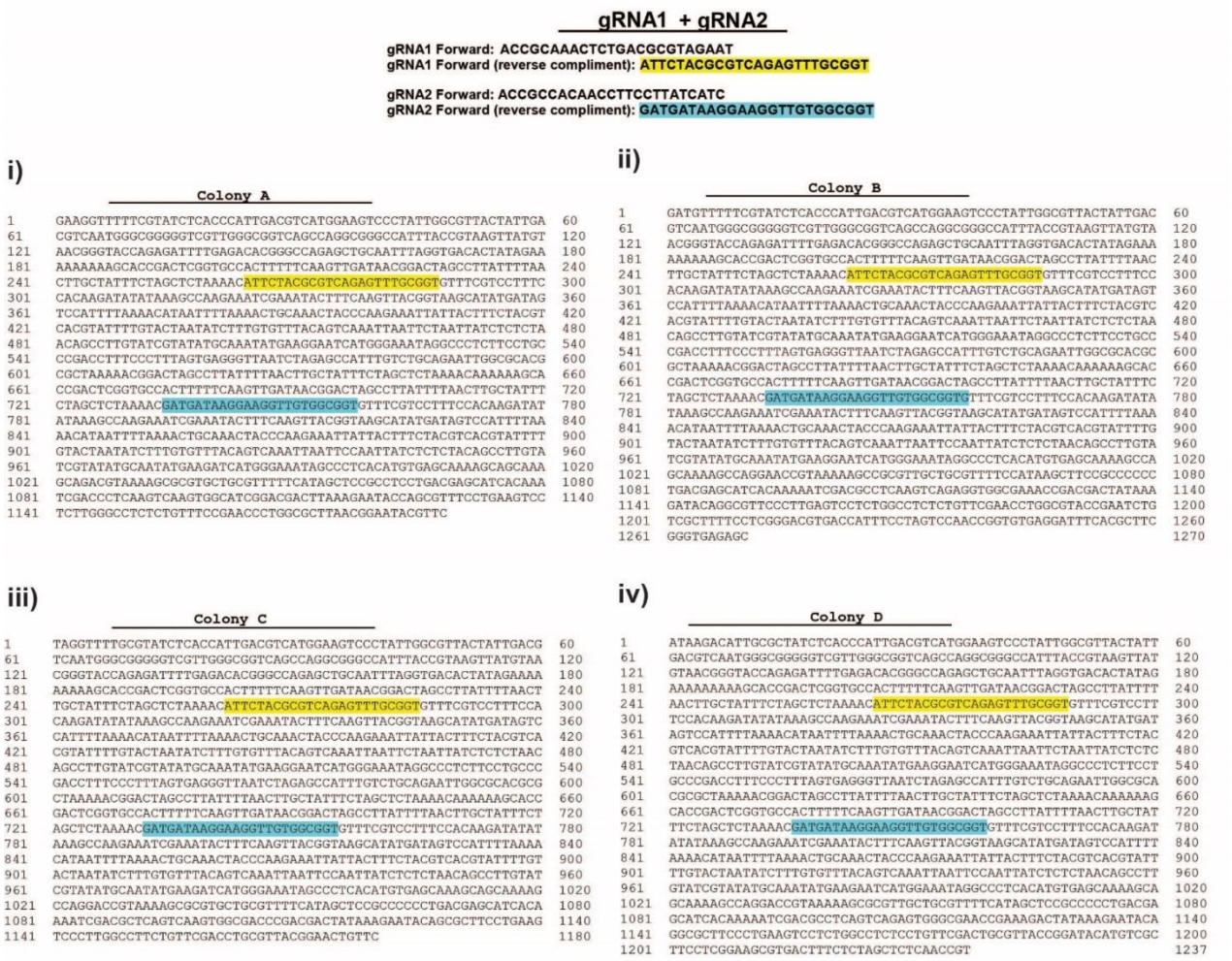

Figure S4. 5: Confirmation of gRNA2 insertion into PX466 Cas9-D10A-GFP vector
Sequencing of gRNA1 + gRNA 2 colonies i) A ii) B iii) C iv) D
gRNA1 is highlighted in yellow, gRNA2 is highlighted in blue

A.

i) Unmutated: OSMR KD – Clone 2

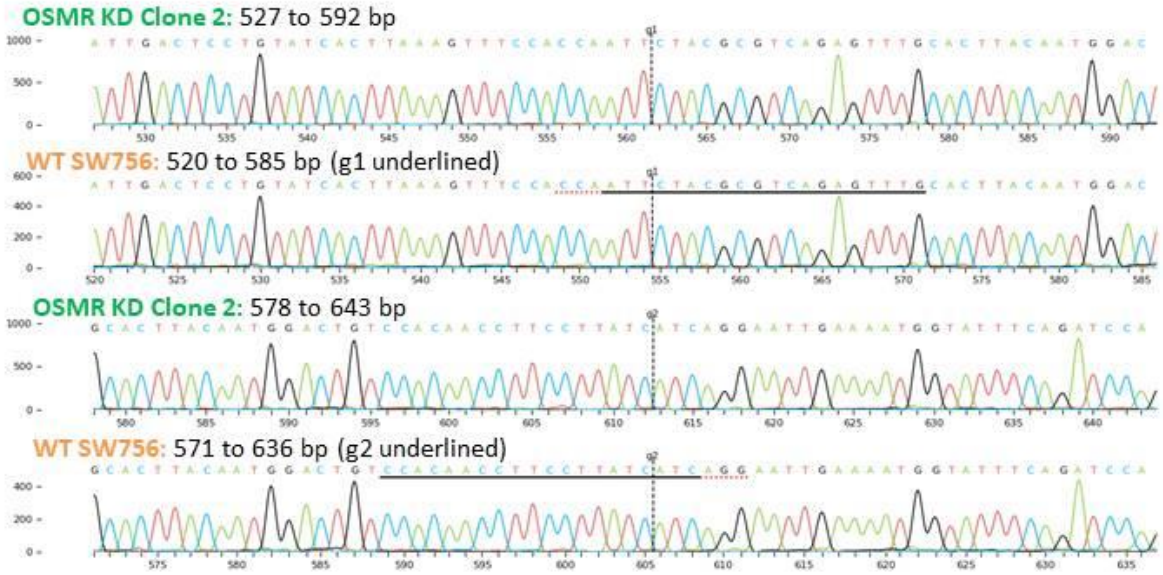

ii) Mutated: OSMR KD – Clone 5

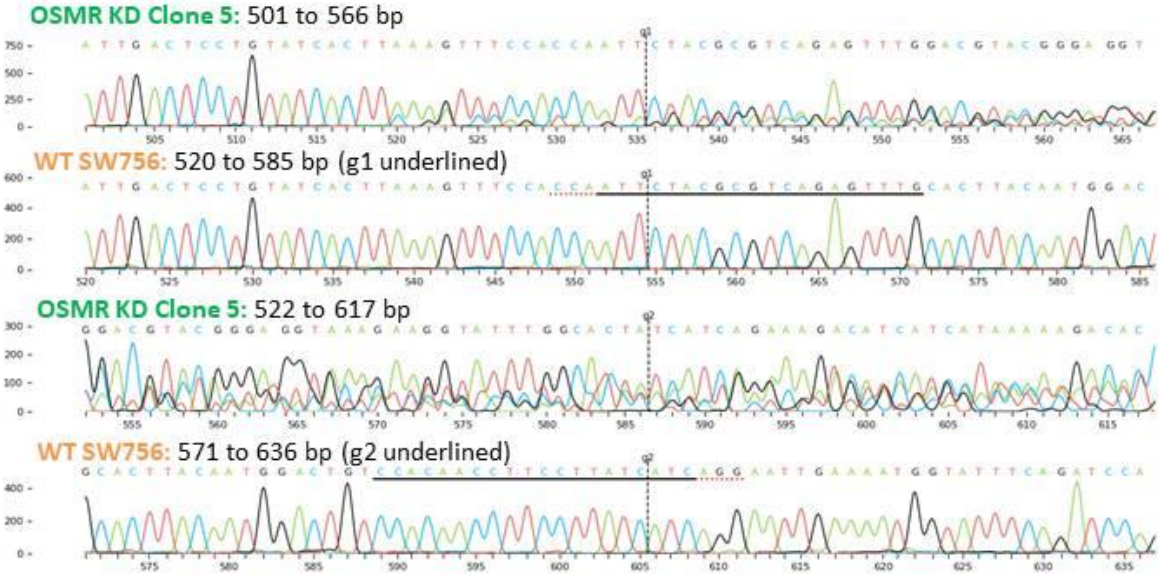

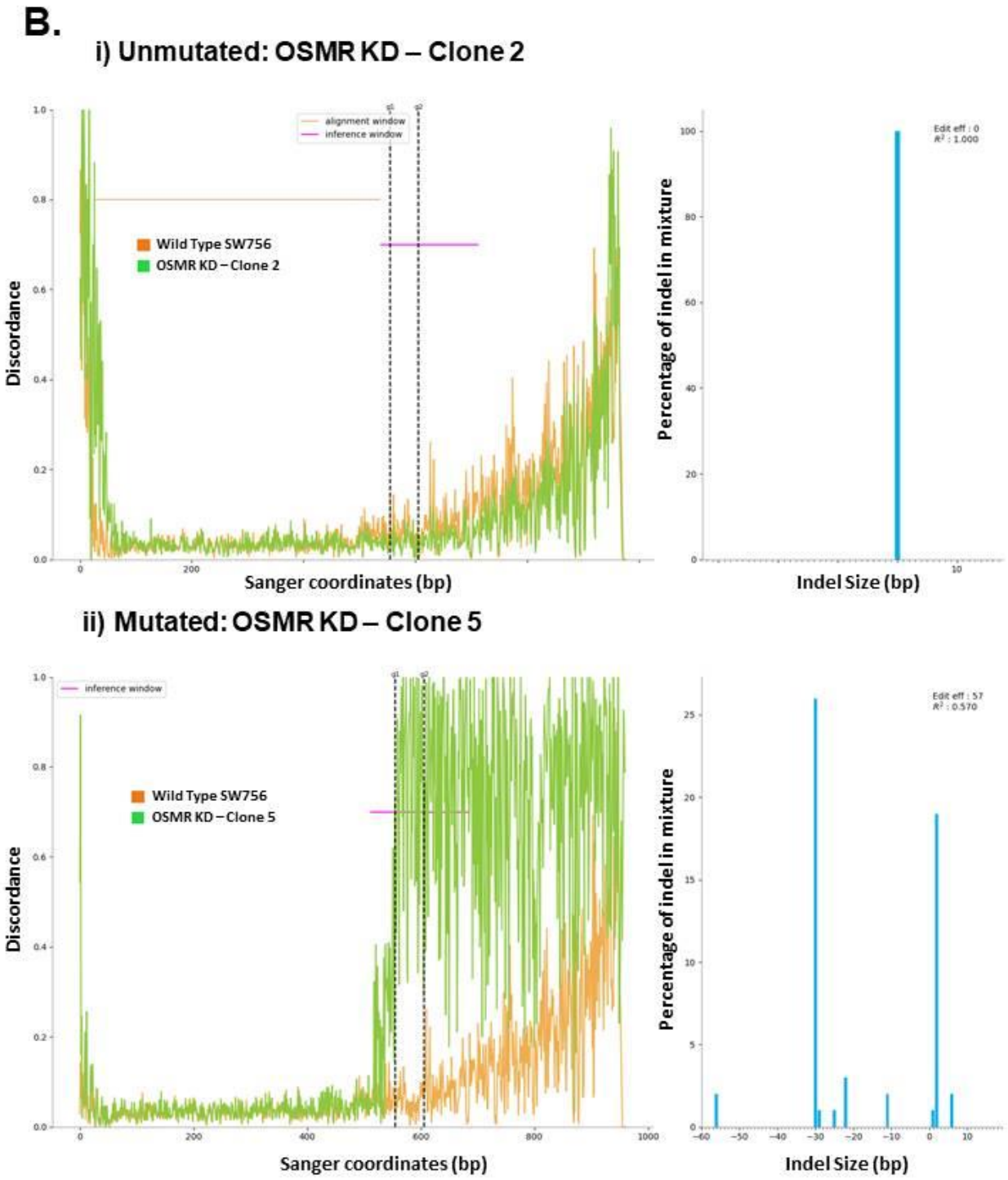

Figure S4. 6: Example of Synthego ICE analysis of sequencing results

A) Example of sequence alignment to wild-type control. Alignment is shown for OSMR i) OSMR KD clone 2 which has no detectable mutations in the OSMR sequence and ii) OSMR KD clone 5 which has mutations to the OSMR sequence.

B) Examples of Synthego ICE discordance and indel plots generated for i) OSMR KD clone 2 and ii) OSMR KD clone 5

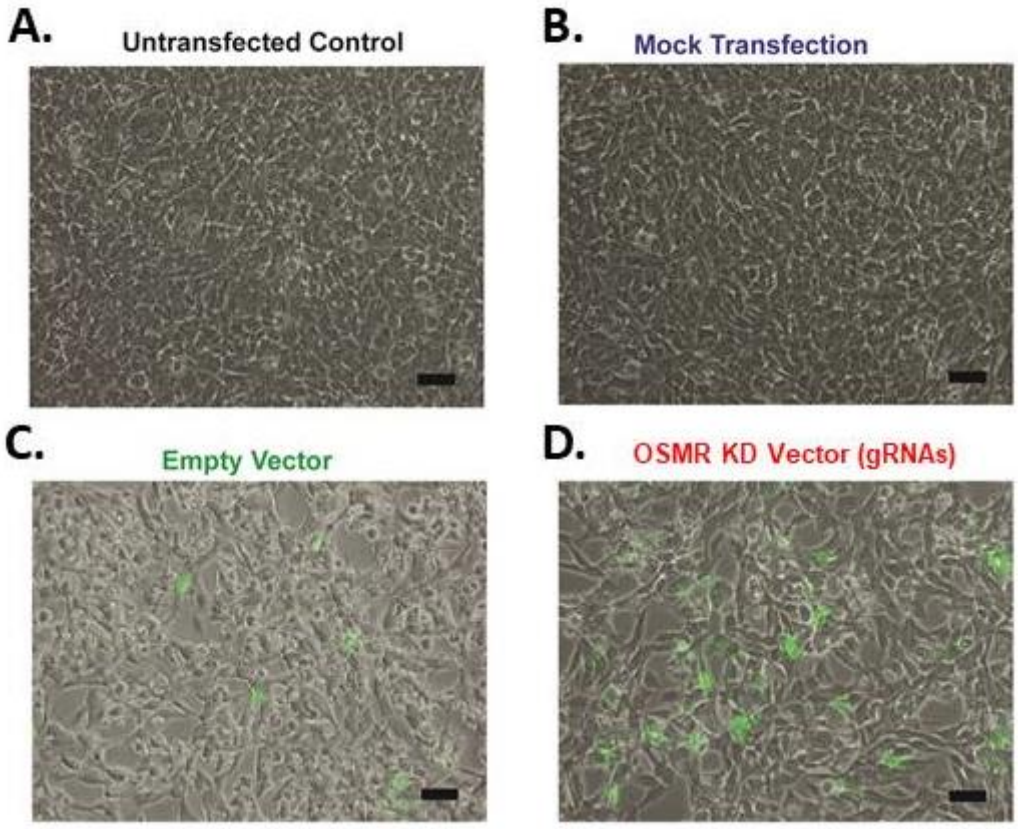

Figure S4. 7: CRISPR 2 - Repeat transfection of SW756 cells
EGFP expression in SW756 cells transfected with A) untransfected control B) mock transfection C) empty plasmid and D) plasmid containing sgRNAs

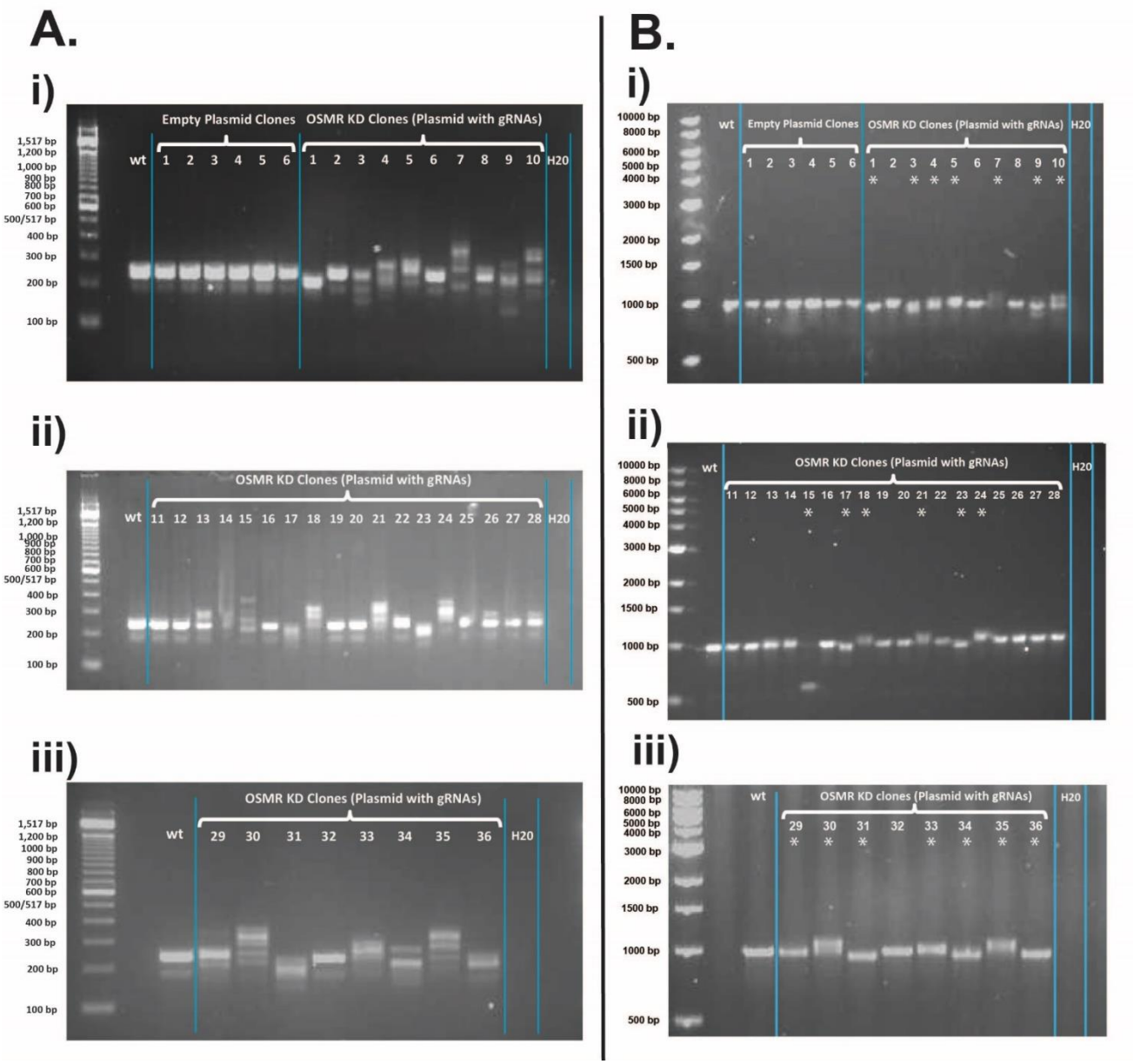

Figure S4. 8: CRISPR 2 – PCR to detect for genomic alterations in OSMR

A) PCR of genomic DNA using sequencing primers designed to amplify a 240bp region within gRNA sites. B) PCR of genomic DNA using sequencing primers designed to amplify a region of 1006bp spanning the gRNA sites targeting OSMR. Stars represent sequences confirmed by sequencing to have altered sequences.

12. SUPPLEMENTARY INFORMATION FOR CHAPTER 5

RESULTS: NGS of cells and EVs following OSM Treatment

A.

RNA Carrier	Sample	Concentration (ng/µl)	Average Concentration (ng/ µl)
MS2	1	25.2	25.15
	2	25.1	
Glycogen	1	9.1	9.20
	2	9.3	
Carrier Free	1	9.4	10.00
	2	10.6	

B.

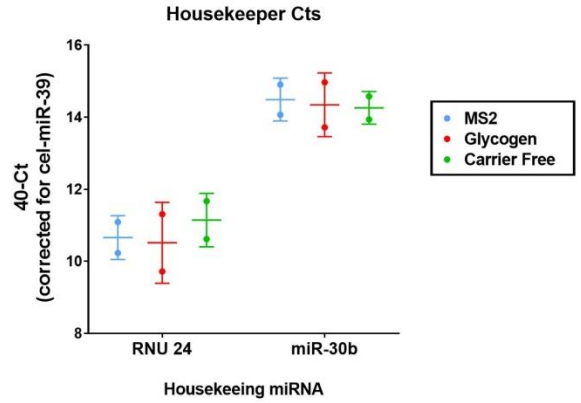

C.

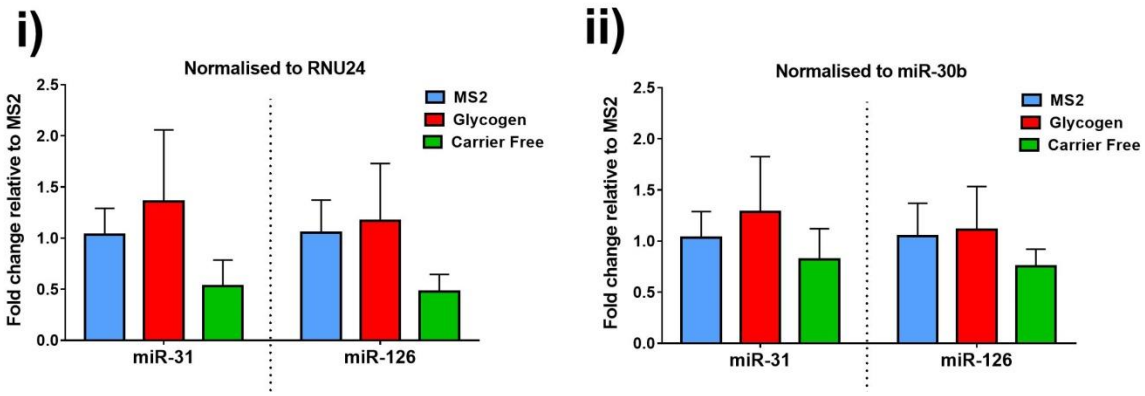

Figure S5. 1: Selection of RNA carrier for sequencing experiments

A) RNA concentrations determined by nanodrop following RNA extraction with addition of MS2, glycogen or carrier free. B) Ct levels of RNU24 and miR30b in samples extracted with MS2, glycogen or carrier free. C) Levels of miR-31 and miR-126 expression in samples extracted with MS2, glycogen or carrier free. Ct values were normalised to i) RNU24 or ii) miR-30b. Fold change in expression relative to MS2 samples is shown. N=2 for each condition. Values were analysed for statistical significance using a one way ANOVA with Tukey's multiple comparison post-hoc tests. No comparisons were found to be statistically significant

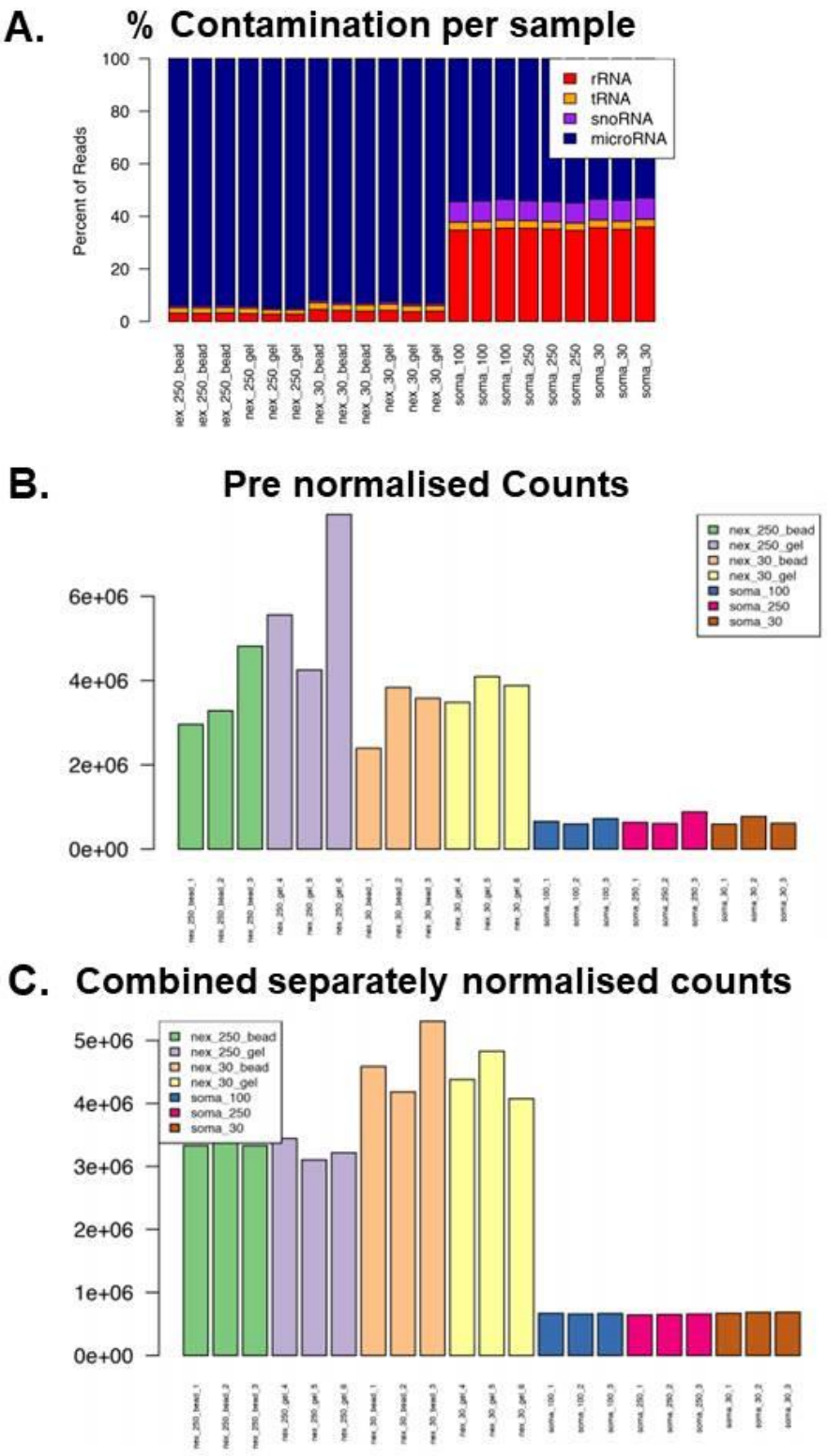

Figure S5. 2: Comparison of library prep kits – contamination and count normalisation
A) Percentage of reads for each sample mapping to miRNAs, rRNA, snoRNAs and tRNAs
B) Prenormalised counts: generated by Chimira for each sample reflecting the number of reads mapped to miRNA
C) Normalised counts: DESeq2 normalisation procedure was applied to pre-normalised counts. Somagenics and Nextflex samples were normalised separately.

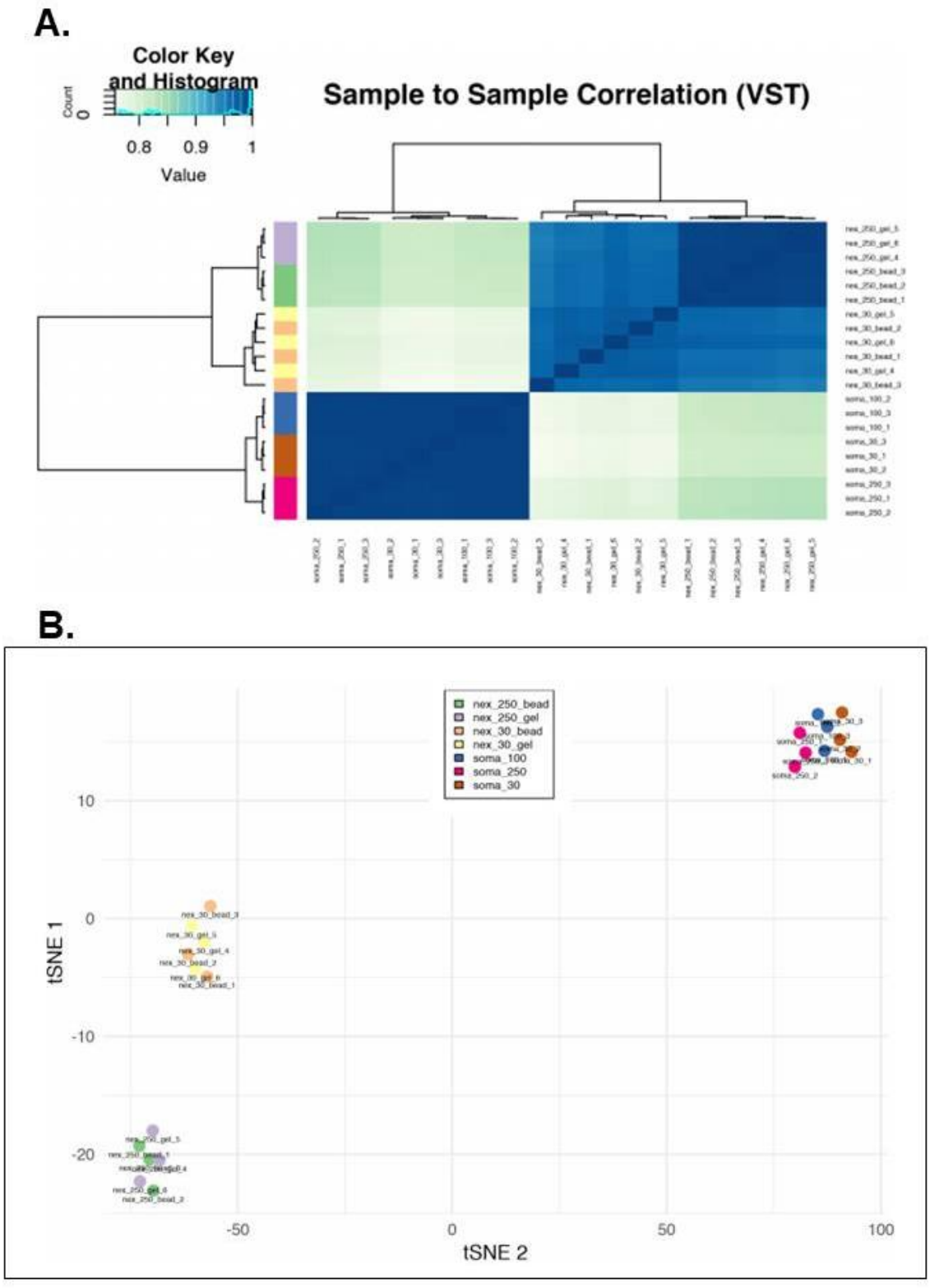

Figure S5. 3: Comparison of library prep kits - sample clustering
A). Heatmap showing sample-to-sample Pearson correlations of VST transformed data
B) t-SNE plots for visualisation of sample clustering

A.

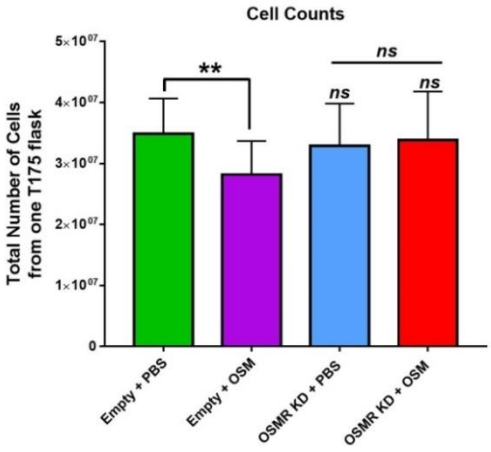

B.

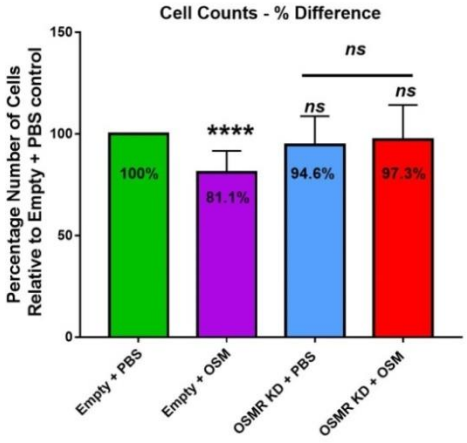

C.

Cell number RELATIVE TO EMPTY + PBS				
Experiment	Empty Plasmid + PBS	Empty Plasmid + OSM	OSMR KD + PBS	OSMR KD + OSM
1	1.00	0.81	1.06	1.14
2	1.00	0.82	1.12	1.25
3	1.00	0.90	0.84	0.95
4	1.00	0.93	0.91	1.00
5	1.00	0.84	0.99	0.89
6	1.00	0.85	1.02	1.07
7	1.00	0.67	0.82	0.81
8	1.00	1.06	1.27	1.31
9	1.00	0.86	1.12	1.15
10	1.00	0.81	0.77	0.86
11	1.00	0.81	0.92	1.08
12	1.00	0.74	0.96	0.91
13	1.00	0.76	1.12	0.97
14	1.00	0.58	0.89	0.95
15	1.00	0.67	0.84	0.73
16	1.00	0.67	0.80	0.84
17	1.00	0.93	1.05	1.05
18	1.00	0.70	0.81	0.74
19	1.00	0.83	0.78	0.95
20	1.00	0.84	1.08	1.15
21	1.00	0.94	1.09	1.20
22	1.00	0.77	0.94	1.06
23	1.00	0.92	0.92	0.78
24	1.00	0.75	0.78	0.75
25	1.00	0.81	0.73	0.72
AVERAGE	1.00	0.811	0.946	0.973

Figure S5. 4: Cell counts as a read out of response to OSM for NGS sample pooling

A) Average number of SW756 empty plasmid and OSMR KD cells present in 175cm^2 flasks following 48 hours treatment with PBS or OSM (average of 25 EV extractions). B) Percentage number of cells relative to SW756 empty plasmid + PBS following 48 hours treatment with PBS or OSM (average of 25 EV extractions). For A) and B) Values were analysed for statistical significance using a one way ANOVA with Tukey's multiple comparison post-hoc tests * =.P≤0.05, ** = P≤0.01, *** = P≤0.001, **** = P≤0.0001. C) Table summarising fold change in cell number for each individual experiment. Samples highlighted were selected for qPCR investigation. Green samples represent 'expected response to OSM'; i.e. these samples showed the greatest reduction in cell number (replicates 14 and 16) or average reduction in cell number (replicates 1, 25). Samples highlighted in red are the 6 samples which appeared least responsive to OSM in terms of reduction of SW756 empty plasmid cell number following treatment.

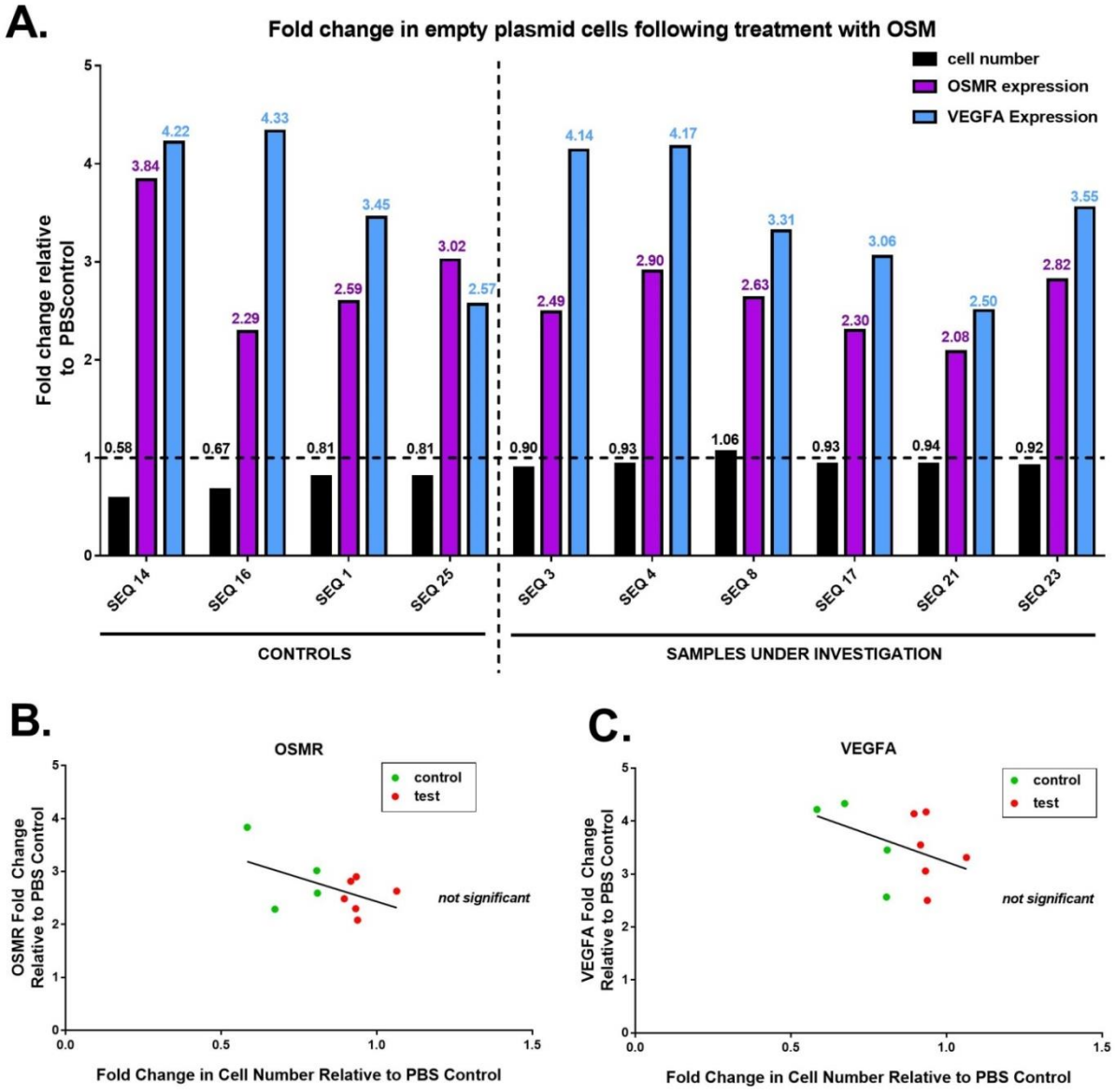

Figure S5. 5: Changes in cell number compared to changes in gene expression

A) OSMR and VEGFA mRNA expression by qRT-PCR. Fold change in gene expression in SW756 empty plasmid cells treated with OSM is shown normalised to expression levels in SW756 empty plasmid cells treated with PBS control. Fold change in cell number for each sequencing experiment is also shown. Linear Regression: fold change in cell number versus fold change in B) OSMR or C) VEGFA levels. Fold change refers to SW756 empty plasmid cells treated with OSM normalised to empty plasmid cells treated with PBS control. Control = samples with expected changes in cell number in response to OSM treatment (n=4, highlighted in green in Table S5.4C), test = samples with little change in cell number in response to OSM treatment (n=6, highlighted in red in Table S5.4C). Linear regressions with $p \leq 0.05$ were considered significant.

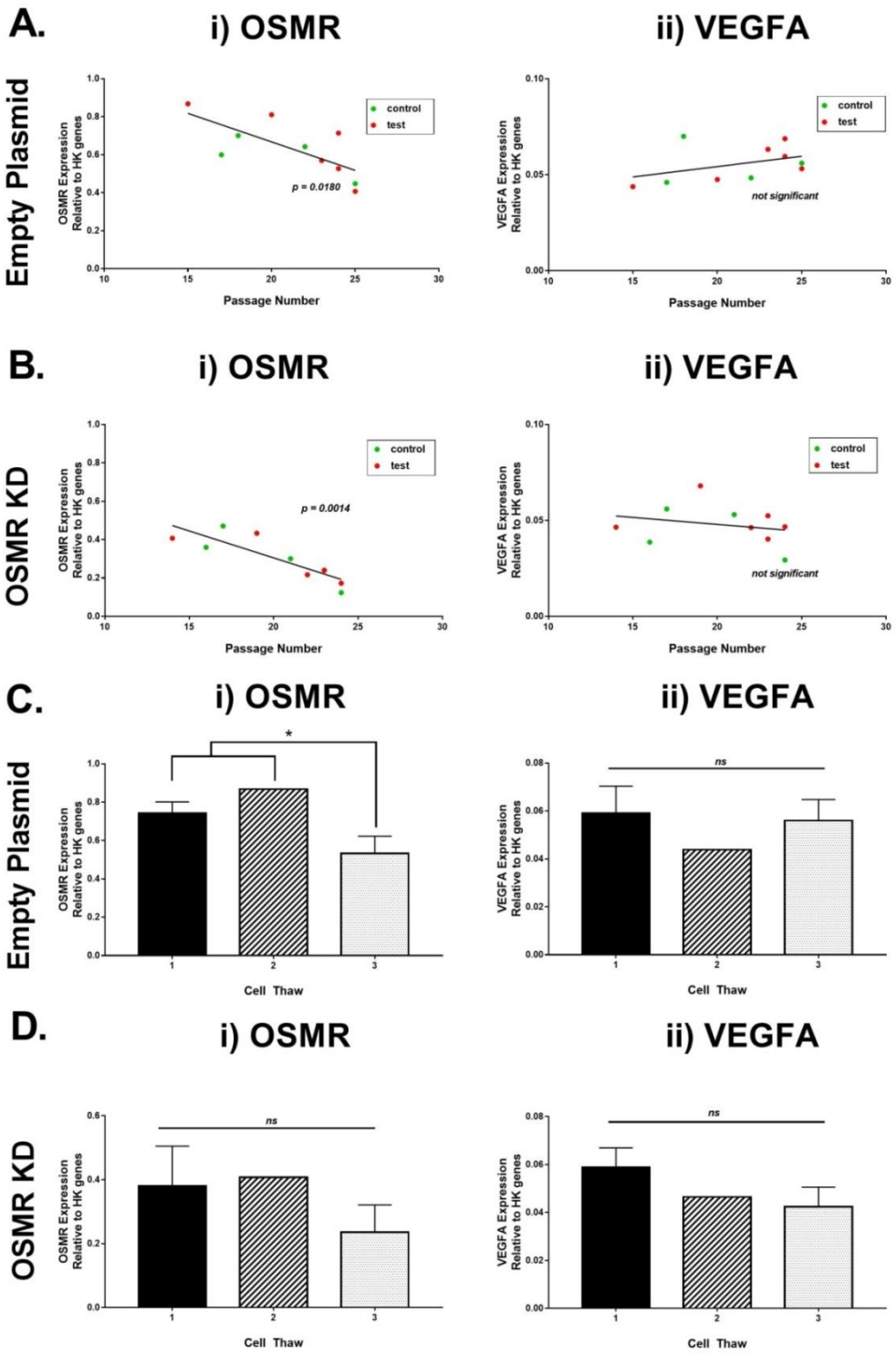

Figure S5. 6: Effect of passage number and cell thaw on baseline gene expression

A+B) Quantitative RT-PCR analysis. Correlation between passage number and i) OSMR or ii) VEGFA mRNA expression in untreated A) SW756 empty plasmid or B) OSMR KD cells is shown. Linear regressions with p ≤0.05 were considered significant. C+D) Quantitative RT-PCR analysis. mRNA expression of i) OSMR or ii) VEGFA in untreated A) SW756 empty plasmid or B) OSMR KD cells from three different cell thaws are shown. As there is no obvious comparator sample, abundance relative to HK genes (rather than fold change) is shown. Values were analysed for statistical significant differences in gene expression between cell thaws using a one way ANOVA with Tukey's multiple comparison post-hoc tests * = P≤0.05.

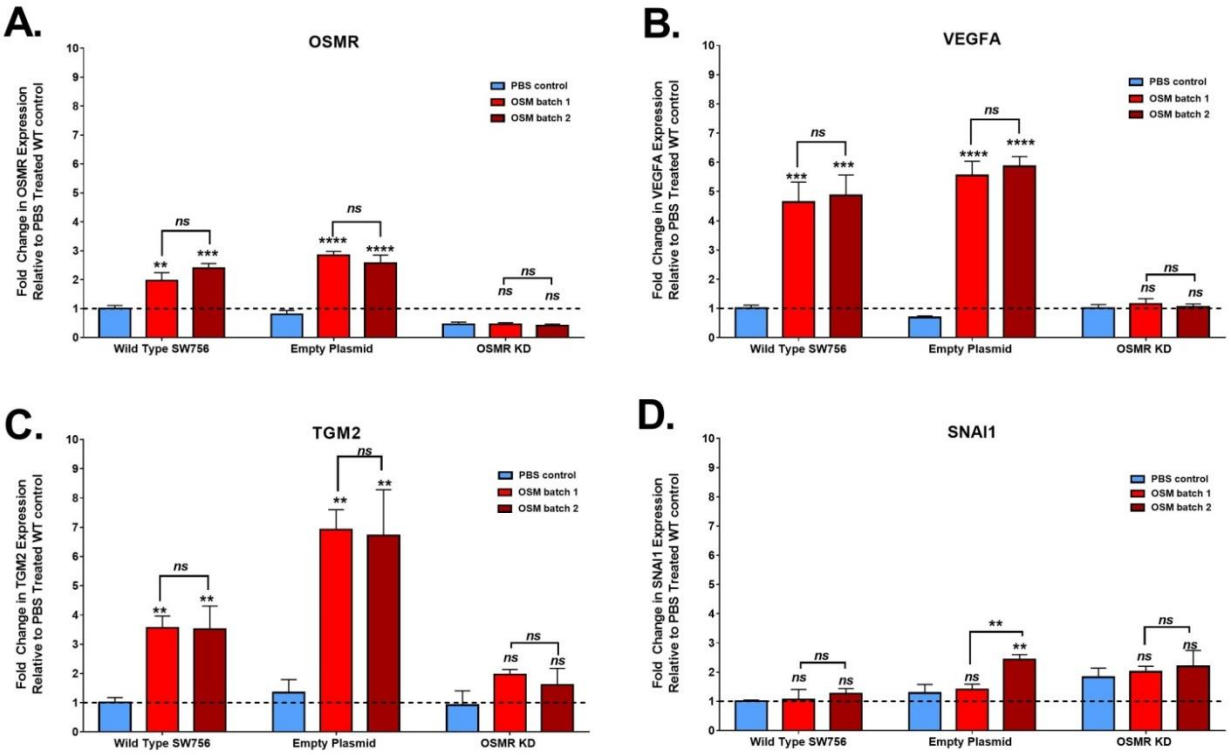

Figure S5. 7: Effect of OSM batch used for NGS on activation of downstream targets. Quantitative RT-PCR analysis of A) OSMR B) VEGFA C) TGM2 and D) SNAI1 expression in WT, empty plasmid and OSMR KD SW756 cells treated with PBS or two different batches of OSM used for sequencing experiments. Fold change in mRNA expression is shown compared to PBS treated WT cells. Values were analysed for statistical significant significance using a one way ANOVA with Tukey's multiple comparison post-hoc tests. * =.P≤0.05, ** = P≤0.01, *** = P≤0.001, **** = P≤0.0001.

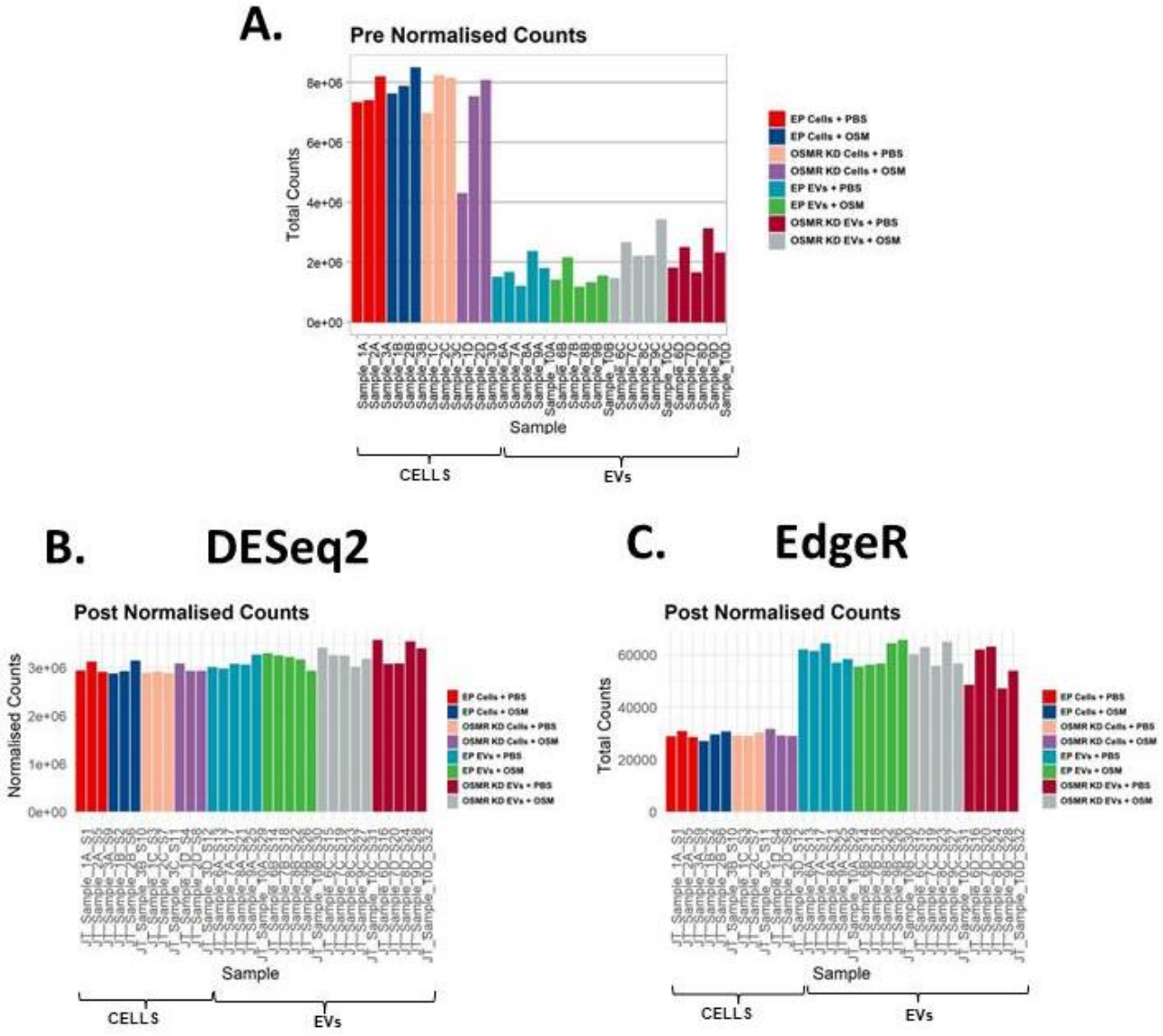

Figure S5. 8: mRNA sequencing – count normalisation

A) Pre-normalised counts

B) Counts following normalisation with DESeq2

C) Counts following normalisation with EdgeR

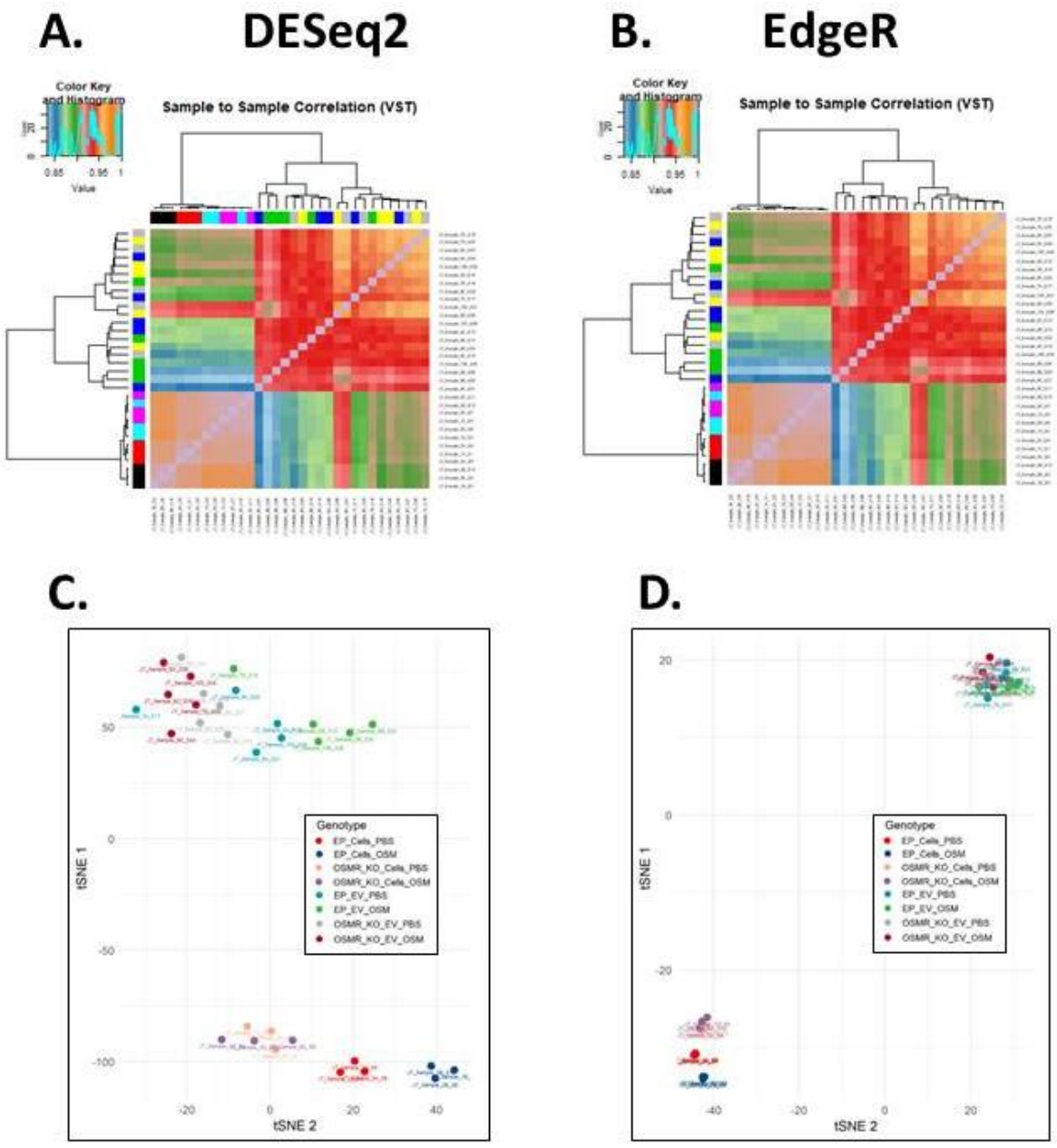

Figure S5. 9: mRNA NGS VST correlations and tSNEs
Heatmap of showing sample-to-sample Pearson correlations of VST transformed data for A) DESeq2 or B) EdgeR normalised data. t-SNE plots for visualisation of sample clustering for C) DESeq2 or D) EdgeR normalised data

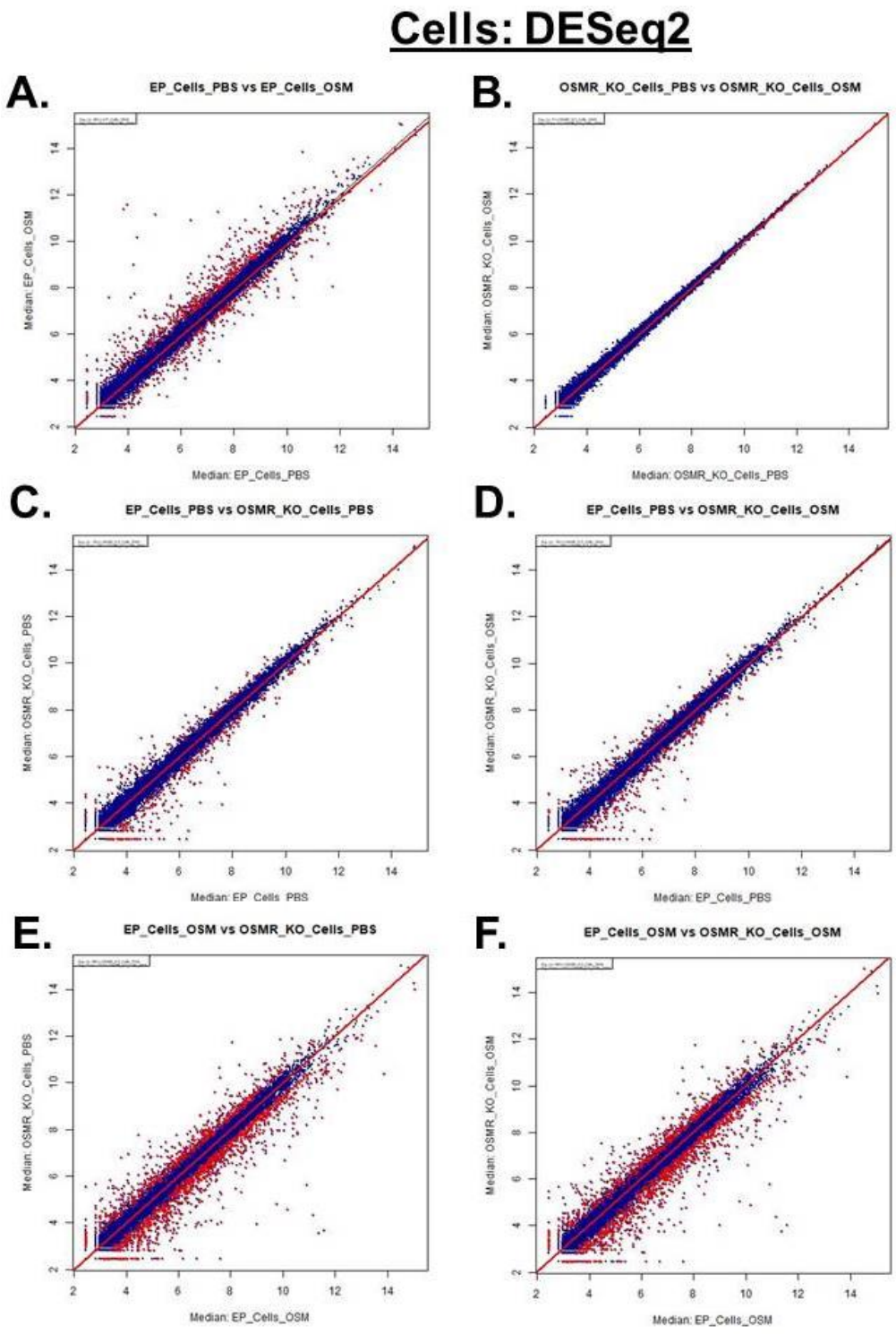

Figure S5. 10: Cells mRNA Correlation Plots – DESeq2

A) Empty Plasmid Cells + PBS versus Empty Plasmid Cells + OSM
B) OSMR KD Cells + PBS versus OSMR KD Cells + OSM
C) Empty Plasmid Cells + PBS versus OSMR KD Cells + PBS
D) Empty Plasmid Cells + PBS versus OSMR KD Cells + OSM
E) Empty Plasmid Cells + OSM versus OSMR KD Cells + PBS
F) Empty Plasmid Cells + OSM versus OSMR KD Cells + OSM

Genes with significant differential expression (≥+/-0.5 LFC; FDR ≤0.05) are shown in red. All other genes are shown in blue.

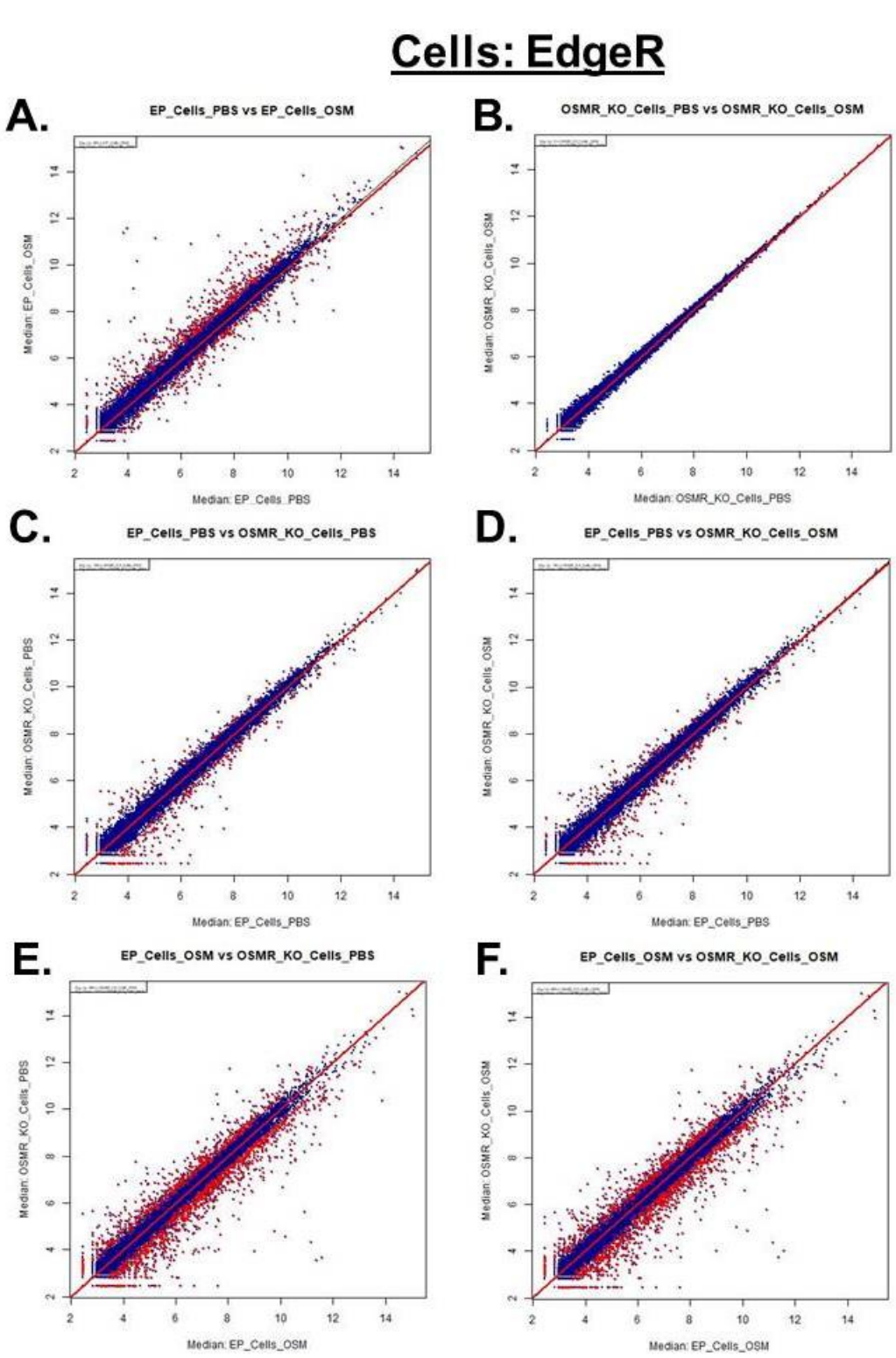

Figure S5. 11: Cells mRNA Correlation Plots – EdgeR

A) Empty Plasmid Cells + PBS versus Empty Plasmid Cells + OSM
B) OSMR KD Cells + PBS versus OSMR KD Cells + OSM
C) Empty Plasmid Cells + PBS versus OSMR KD Cells + PBS
D) Empty Plasmid Cells + PBS versus OSMR KD Cells + OSM
E) Empty Plasmid Cells + OSM versus OSMR KD Cells + PBS
F) Empty Plasmid Cells + OSM versus OSMR KD Cells + OSM
Genes with significant differential expression (≥+/-0.5 LFC; FDR ≤0.05) are shown in red. All other genes are shown in blue.

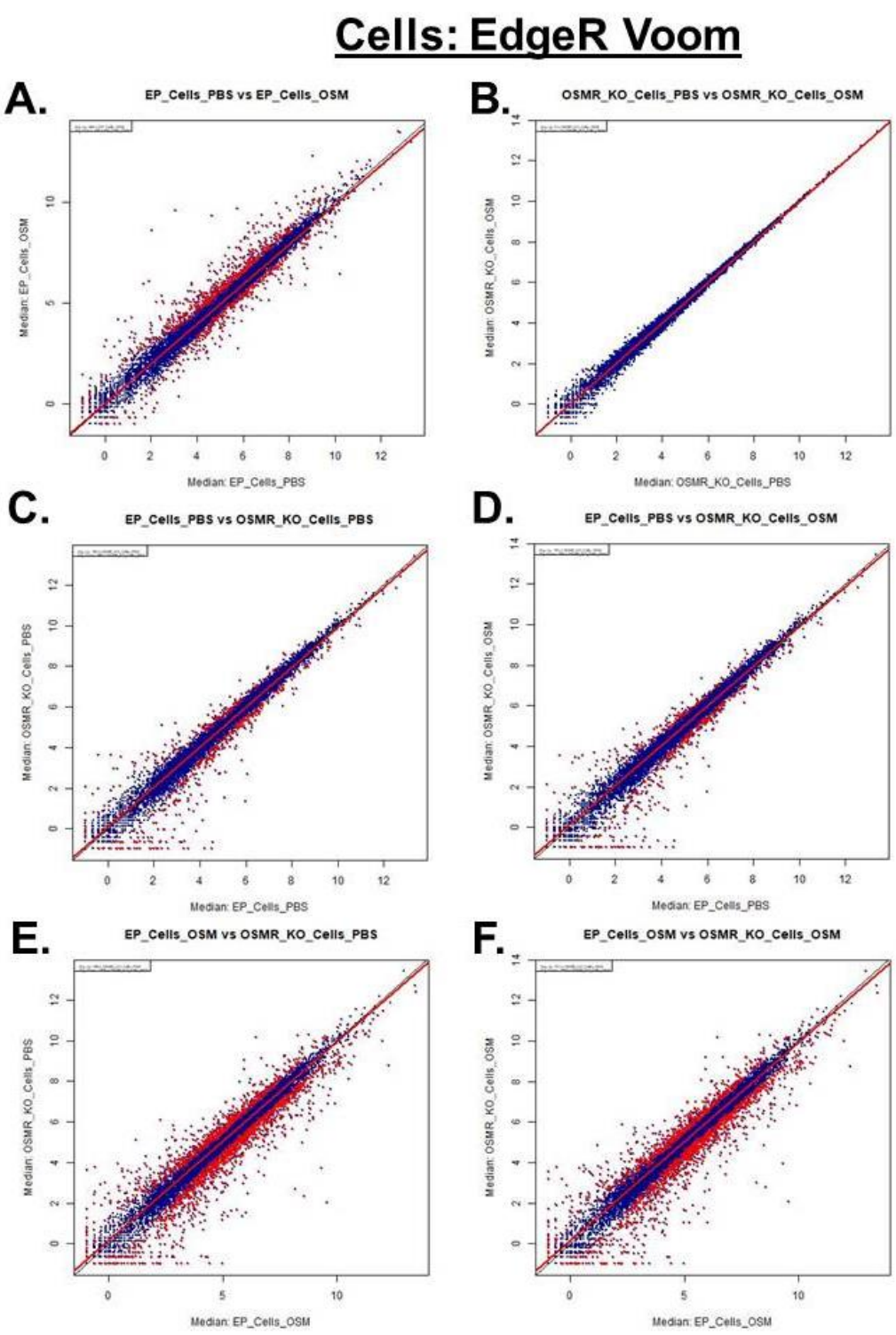

Figure S5. 12: Cells mRNA Correlation Plots – EdgeR Voom

A) Empty Plasmid Cells + PBS versus Empty Plasmid Cells + OSM
B) OSMR KD Cells + PBS versus OSMR KD Cells + OSM
C) Empty Plasmid Cells + PBS versus OSMR KD Cells + PBS
D) Empty Plasmid Cells + PBS versus OSMR KD Cells + OSM
E) Empty Plasmid Cells + OSM versus OSMR KD Cells + PBS
F) Empty Plasmid Cells + OSM versus OSMR KD Cells + OSM

Genes with significant differential expression (≥+/-0.5 LFC; FDR ≤0.05) are shown in red. All other genes are shown in blue.

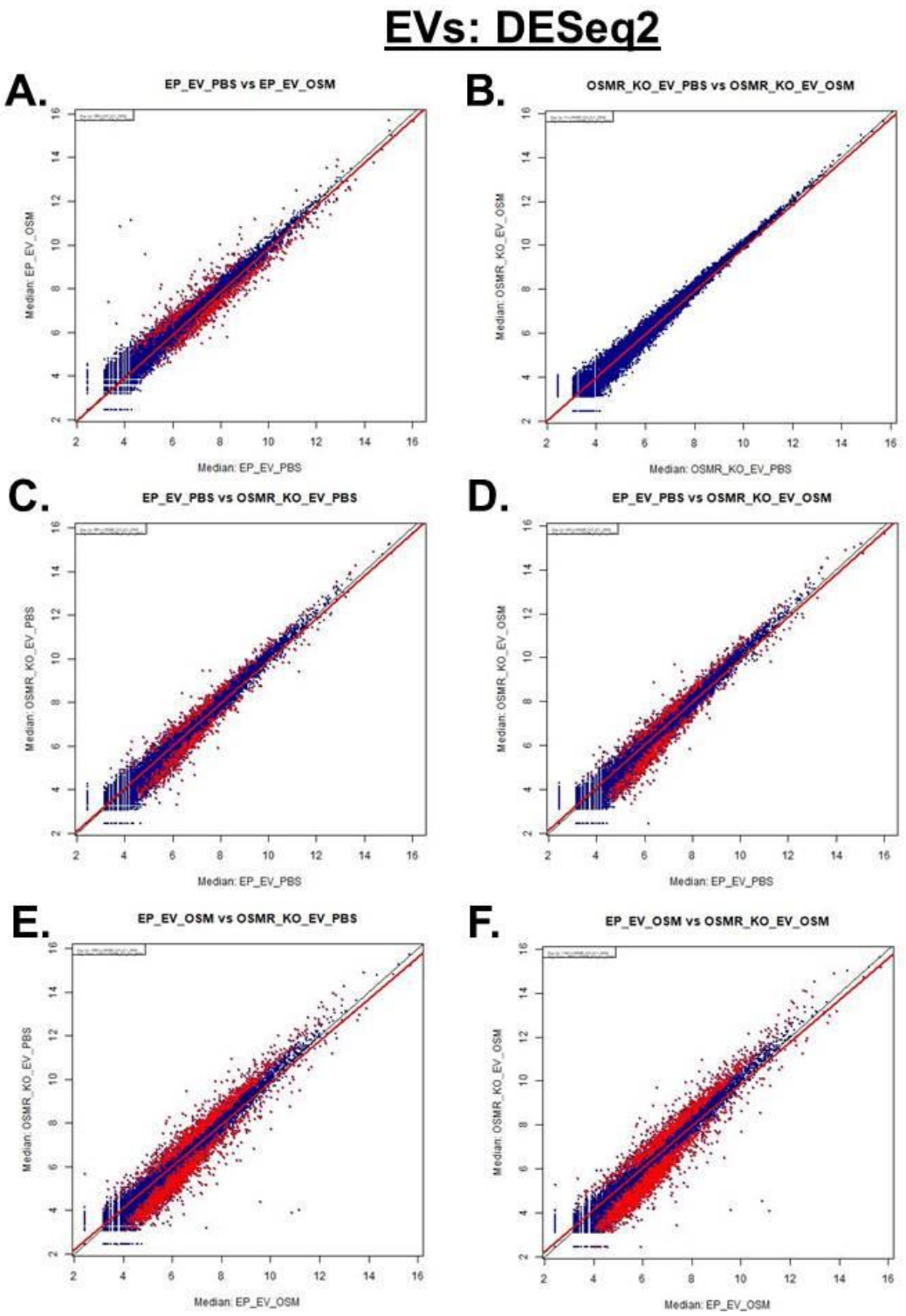

Figure S5. 13: EVs mRNA Correlation Plots – DESeq2

A) Empty Plasmid Cells + PBS versus Empty Plasmid Cells + OSM
B) OSMR KD Cells + PBS versus OSMR KD Cells + OSM
C) Empty Plasmid Cells + PBS versus OSMR KD Cells + PBS
D) Empty Plasmid Cells + PBS versus OSMR KD Cells + OSM
E) Empty Plasmid Cells + OSM versus OSMR KD Cells + PBS
F) Empty Plasmid Cells + OSM versus OSMR KD Cells + OSM
Genes with significant differential expression (≥+/-0.5 LFC; FDR ≤0.05) are shown in red. All other genes are shown in blue.

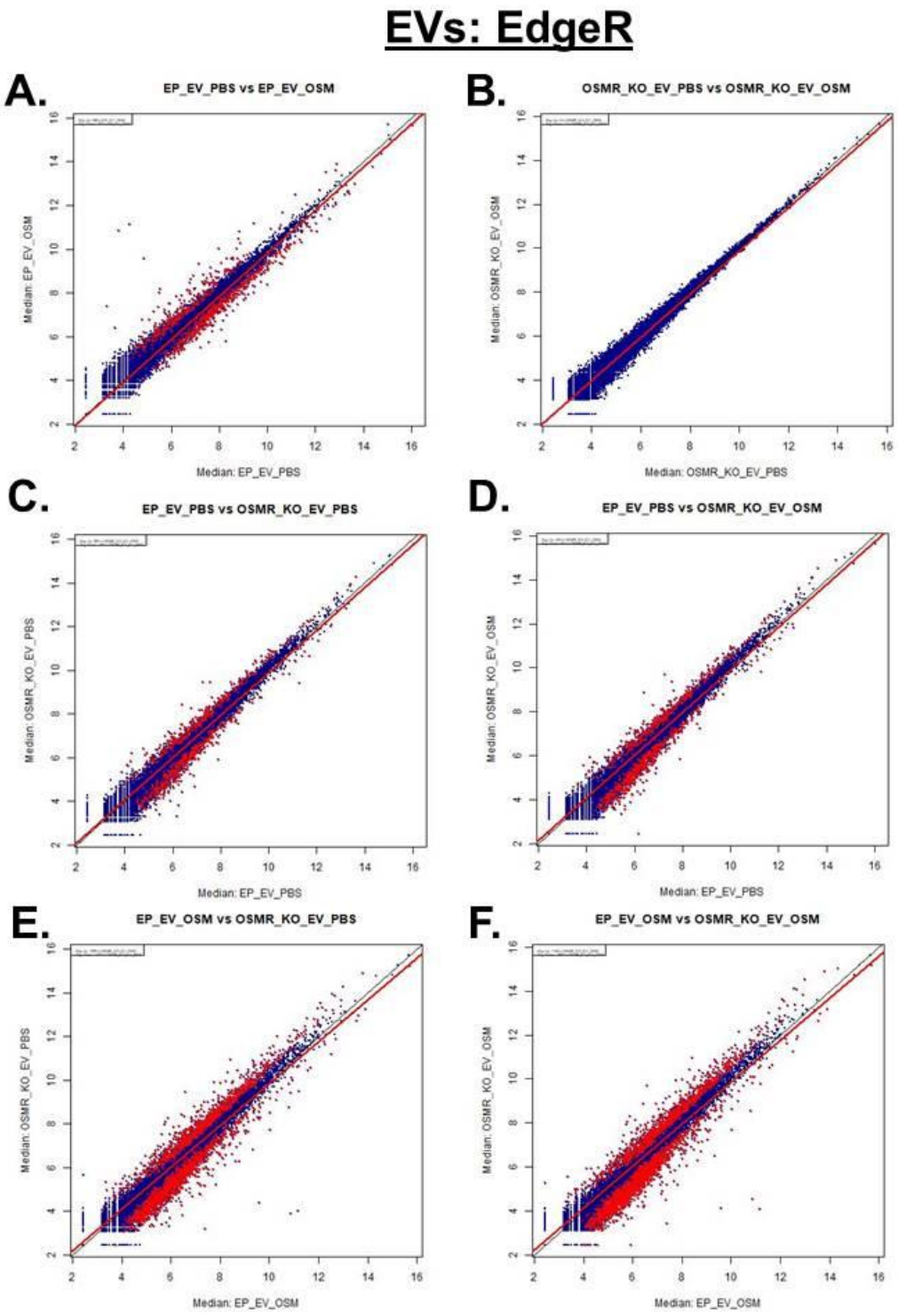

Figure S5. 14: EVs mRNA Correlation Plots - EdgeR

A) Empty Plasmid Cells + PBS versus Empty Plasmid Cells + OSM
B) OSMR KD Cells + PBS versus OSMR KD Cells + OSM
C) Empty Plasmid Cells + PBS versus OSMR KD Cells + PBS
D) Empty Plasmid Cells + PBS versus OSMR KD Cells + OSM
E) Empty Plasmid Cells + OSM versus OSMR KD Cells + PBS
F) Empty Plasmid Cells + OSM versus OSMR KD Cells + OSM
Genes with significant differential expression (≥+/-0.5 LFC; FDR ≤0.05) are shown in red. All other genes are shown in blue.

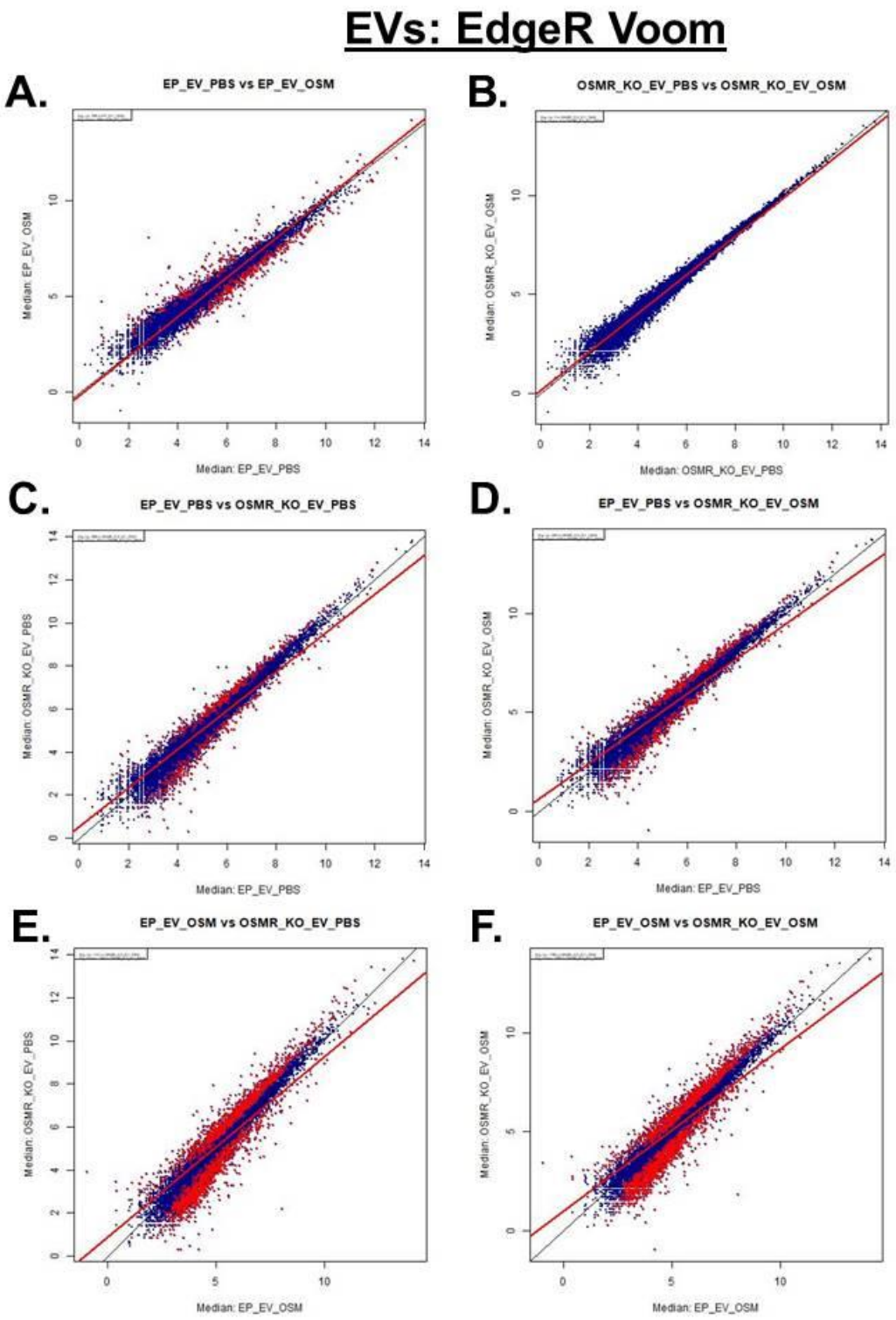

Figure S5. 15: EVs mRNA Correlation Plots – EdgeR Voom

A) Empty Plasmid Cells + PBS versus Empty Plasmid Cells + OSM
B) OSMR KD Cells + PBS versus OSMR KD Cells + OSM
C) Empty Plasmid Cells + PBS versus OSMR KD Cells + PBS
D) Empty Plasmid Cells + PBS versus OSMR KD Cells + OSM
E) Empty Plasmid Cells + OSM versus OSMR KD Cells + PBS
F) Empty Plasmid Cells + OSM versus OSMR KD Cells + OSM
Genes with significant differential expression (≥+/-0.5 LFC; FDR ≤0.05) are shown in red. All other genes are shown in blue.

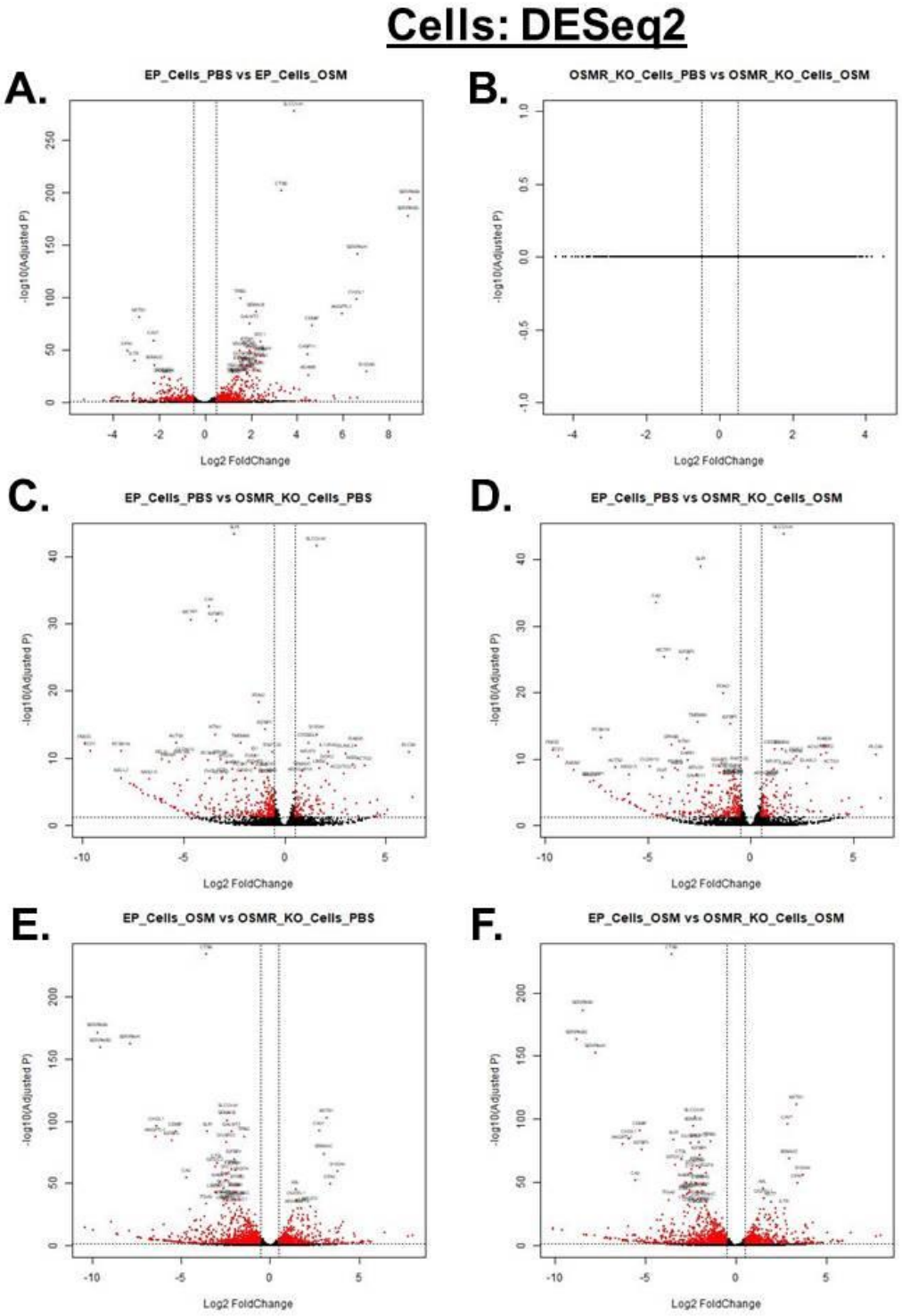

Figure S5. 16: Cells mRNA Volcano Plots – DESeq2

A) Empty Plasmid Cells + PBS versus Empty Plasmid Cells + OSM
B) OSMR KD Cells + PBS versus OSMR KD Cells + OSM
C) Empty Plasmid Cells + PBS versus OSMR KD Cells + PBS
D) Empty Plasmid Cells + PBS versus OSMR KD Cells + OSM
E) Empty Plasmid Cells + OSM versus OSMR KD Cells + PBS
F) Empty Plasmid Cells + OSM versus OSMR KD Cells + OSM
Genes with significant differential expression (≥+/-0.5 LFC; FDR ≤0.05) are shown in red. All other genes are shown in black. Top 50 most significantly changed mRNA are labelled

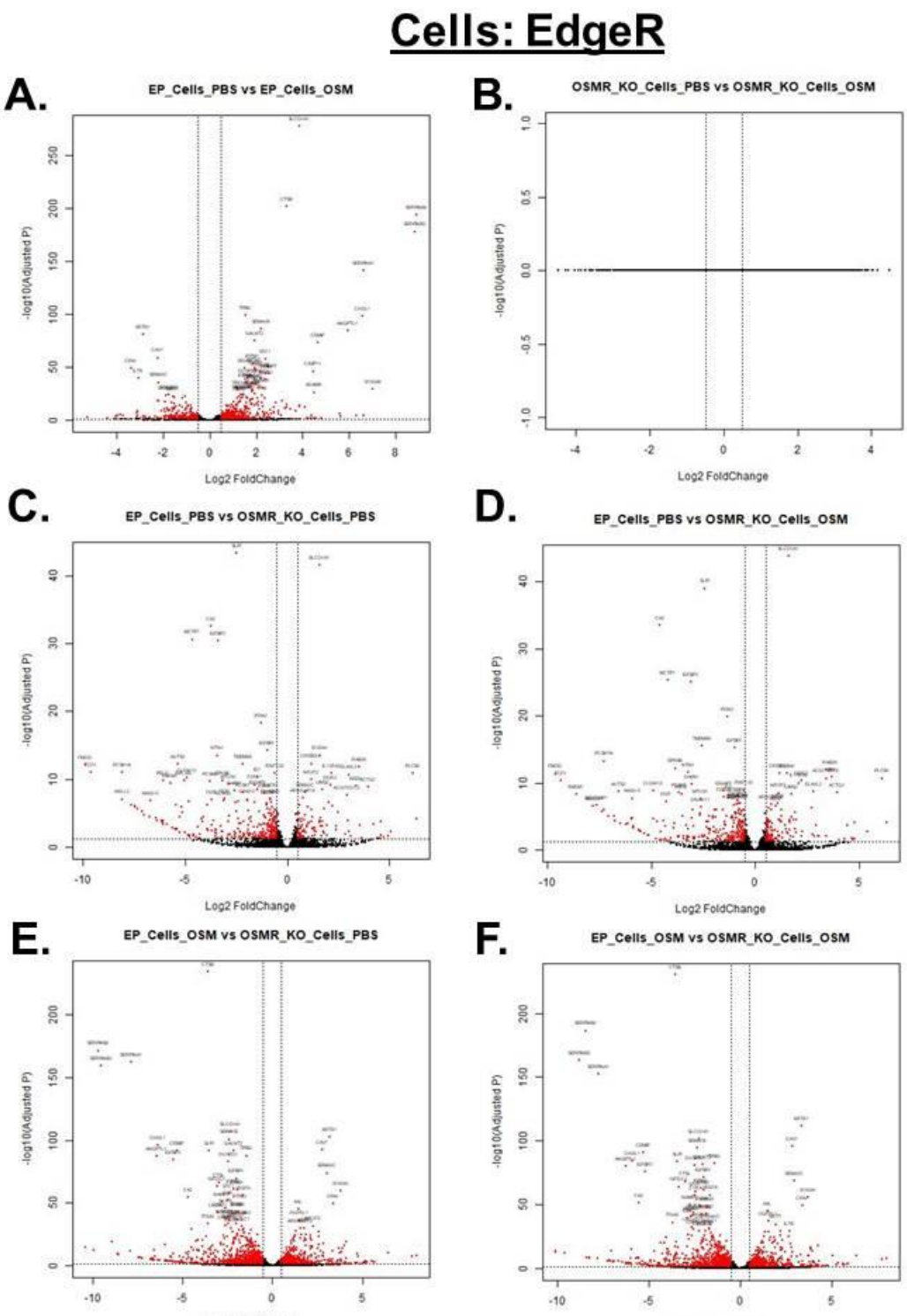

Figure S5. 17: Cells mRNA Volcano Plots – EdgeR

A) Empty Plasmid Cells + PBS versus Empty Plasmid Cells + OSM
B) OSMR KD Cells + PBS versus OSMR KD Cells + OSM
C) Empty Plasmid Cells + PBS versus OSMR KD Cells + PBS
D) Empty Plasmid Cells + PBS versus OSMR KD Cells + OSM
E) Empty Plasmid Cells + OSM versus OSMR KD Cells + PBS
F) Empty Plasmid Cells + OSM versus OSMR KD Cells + OSM
Genes with significant differential expression (≥+/-0.5 LFC; FDR ≤0.05) are shown in red. All other genes are shown in black. Top 50 most significantly changed mRNA are labelled

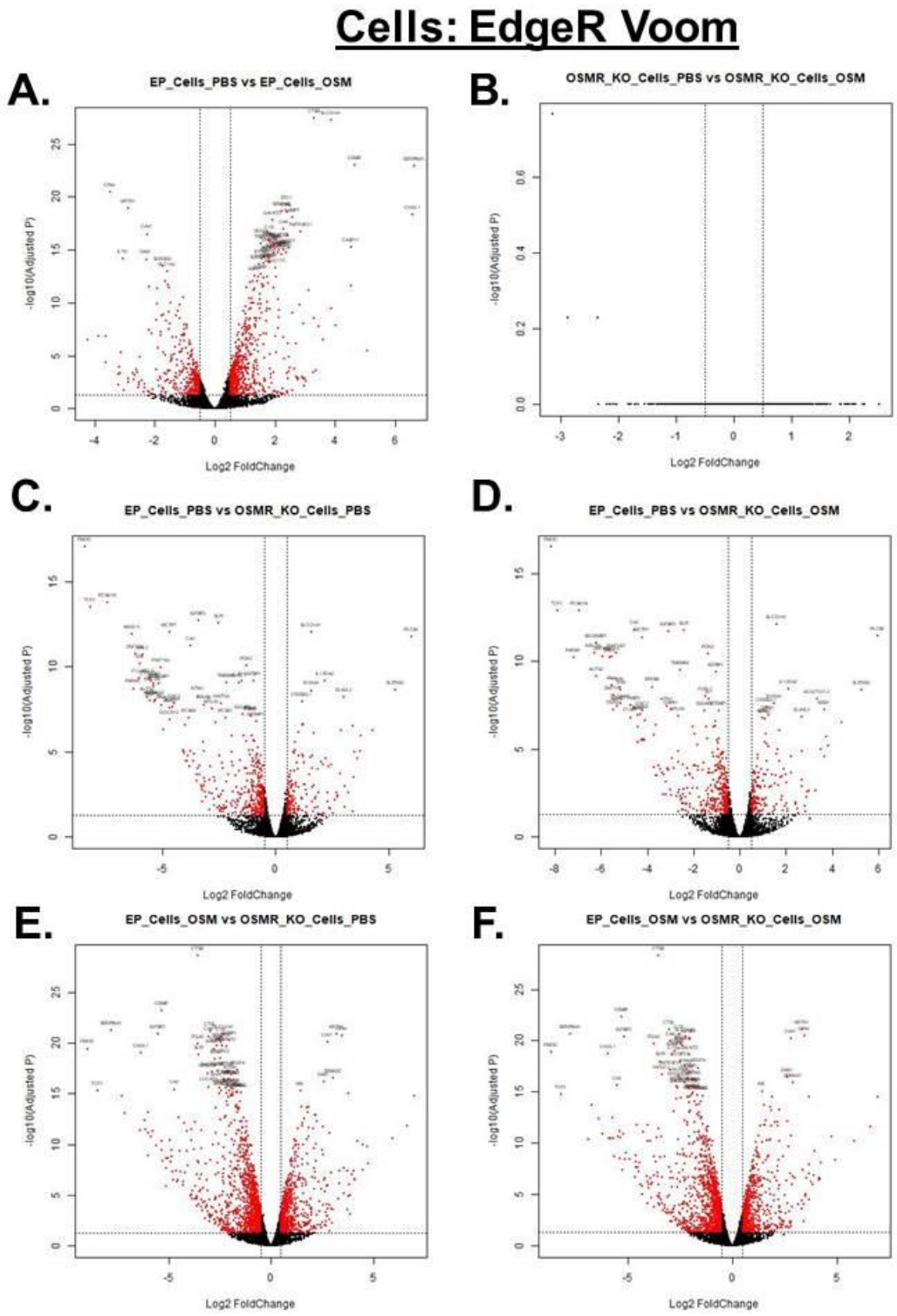

Figure S5. 18: Cells mRNA Volcano Plots – EdgeR Voom

A) Empty Plasmid Cells + PBS versus Empty Plasmid Cells + OSM
B) OSMR KD Cells + PBS versus OSMR KD Cells + OSM
C) Empty Plasmid Cells + PBS versus OSMR KD Cells + PBS
D) Empty Plasmid Cells + PBS versus OSMR KD Cells + OSM
E) Empty Plasmid Cells + OSM versus OSMR KD Cells + PBS
F) Empty Plasmid Cells + OSM versus OSMR KD Cells + OSM
Genes with significant differential expression (≥+/-0.5 LFC; FDR ≤0.05) are shown in red. All other genes are shown in black. Top 50 most significantly changed mRNA are labelled

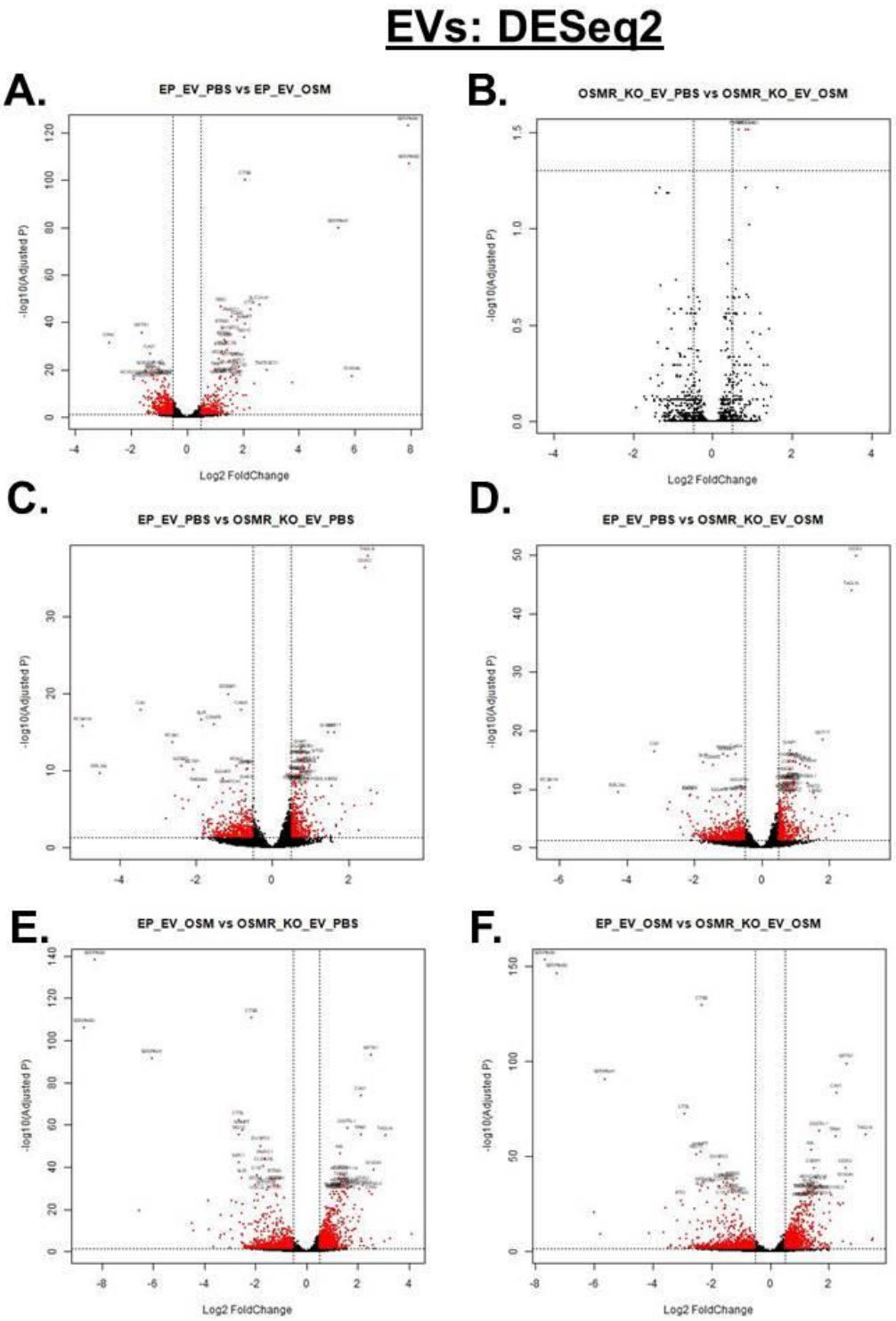

Figure S5. 19: EVs mRNA Volcano Plots – DESeq2

A) Empty Plasmid Cells + PBS versus Empty Plasmid Cells + OSM
B) OSMR KD Cells + PBS versus OSMR KD Cells + OSM
C) Empty Plasmid Cells + PBS versus OSMR KD Cells + PBS
D) Empty Plasmid Cells + PBS versus OSMR KD Cells + OSM
E) Empty Plasmid Cells + OSM versus OSMR KD Cells + PBS
F) Empty Plasmid Cells + OSM versus OSMR KD Cells + OSM
Genes with significant differential expression (≥+/-0.5 LFC; FDR ≤0.05) are shown in red. All other genes are shown in black. Top 50 most significantly changed mRNA are labelled

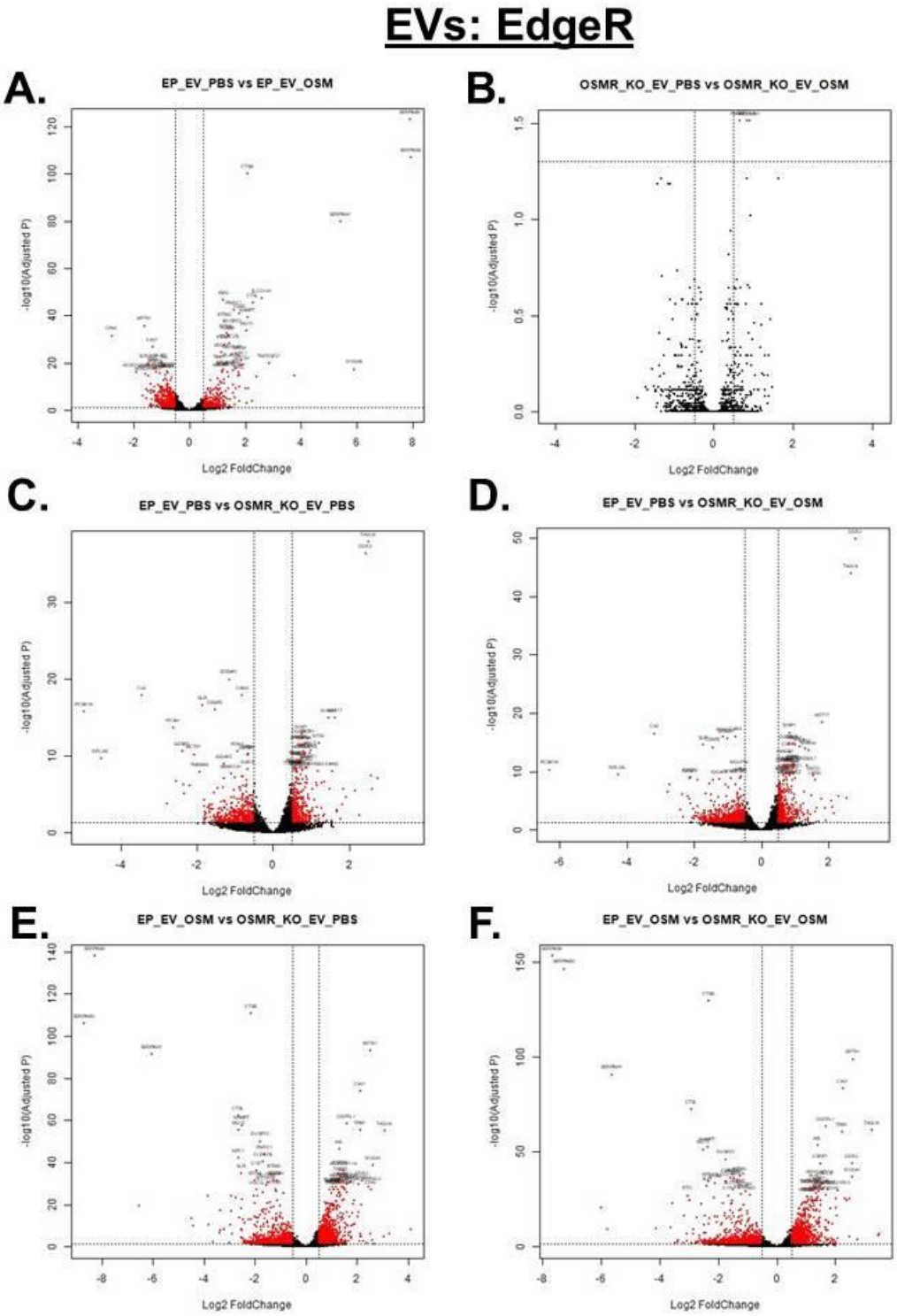

Figure S5. 20: EVs mRNA Volcano Plots – EdgeR

A) Empty Plasmid Cells + PBS versus Empty Plasmid Cells + OSM
B) OSMR KD Cells + PBS versus OSMR KD Cells + OSM
C) Empty Plasmid Cells + PBS versus OSMR KD Cells + PBS
D) Empty Plasmid Cells + PBS versus OSMR KD Cells + OSM
E) Empty Plasmid Cells + OSM versus OSMR KD Cells + PBS
F) Empty Plasmid Cells + OSM versus OSMR KD Cells + OSM
Genes with significant differential expression (≥+/-0.5 LFC; FDR ≤0.05) are shown in red. All other genes are shown in black. Top 50 most significantly changed mRNA are labelled.

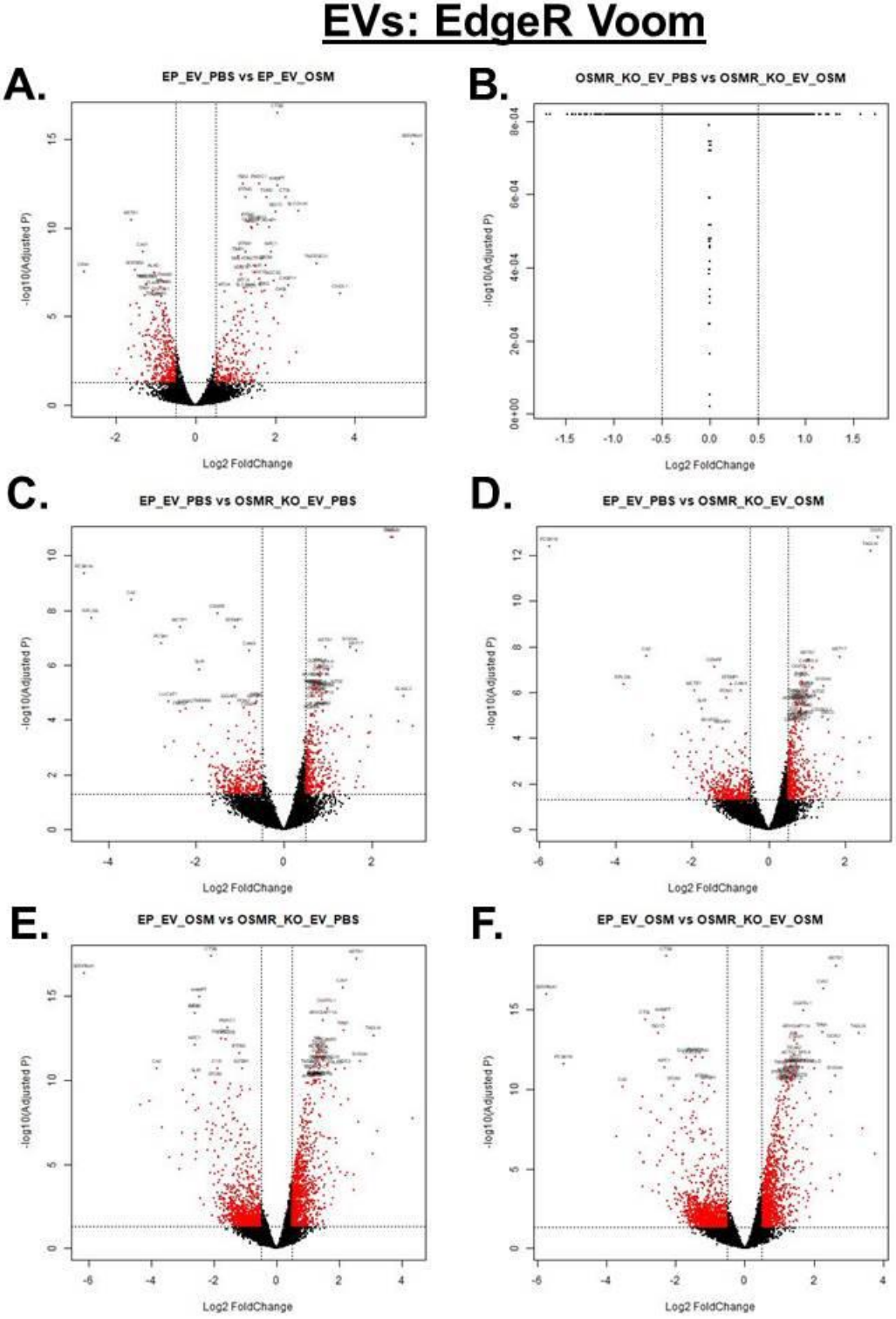

Figure S5. 21: EVs mRNA Volcano Plots – EdgeR Voom

A) Empty Plasmid Cells + PBS versus Empty Plasmid Cells + OSM
B) OSMR KD Cells + PBS versus OSMR KD Cells + OSM
C) Empty Plasmid Cells + PBS versus OSMR KD Cells + PBS
D) Empty Plasmid Cells + PBS versus OSMR KD Cells + OSM
E) Empty Plasmid Cells + OSM versus OSMR KD Cells + PBS
F) Empty Plasmid Cells + OSM versus OSMR KD Cells + OSM
Genes with significant differential expression (≥+/-0.5 LFC; FDR ≤0.05) are shown in red. All other genes are shown in black. Top 50 most significantly changed mRNA are labelled

Empty Plasmid + PBS vs Empty Plasmid + OSM

A. UPREGULATED PATHWAYS

i) CELLS

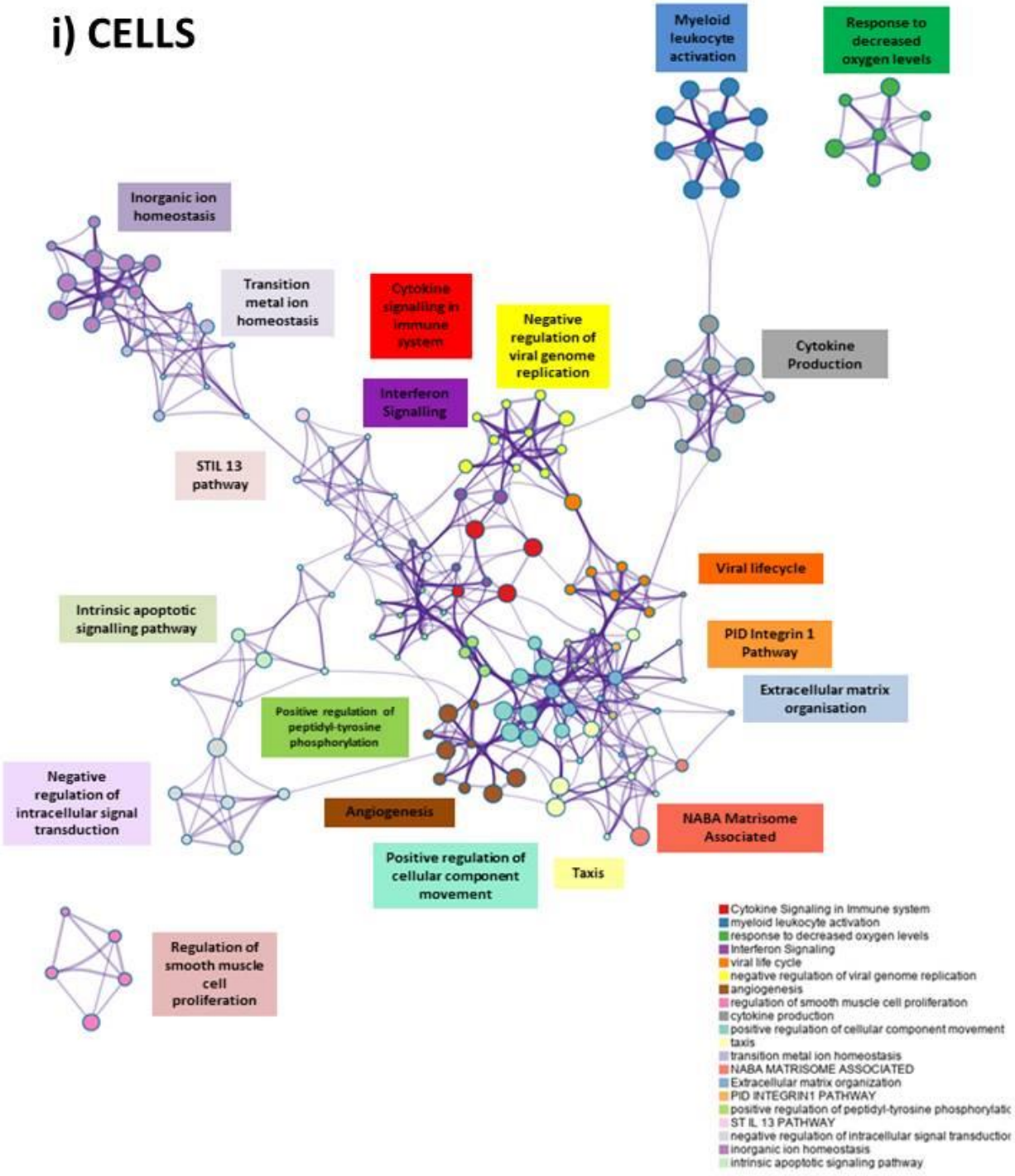

Empty Plasmid + PBS vs Empty Plasmid + OSM

A. UPREGULATED PATHWAYS

ii) EVs

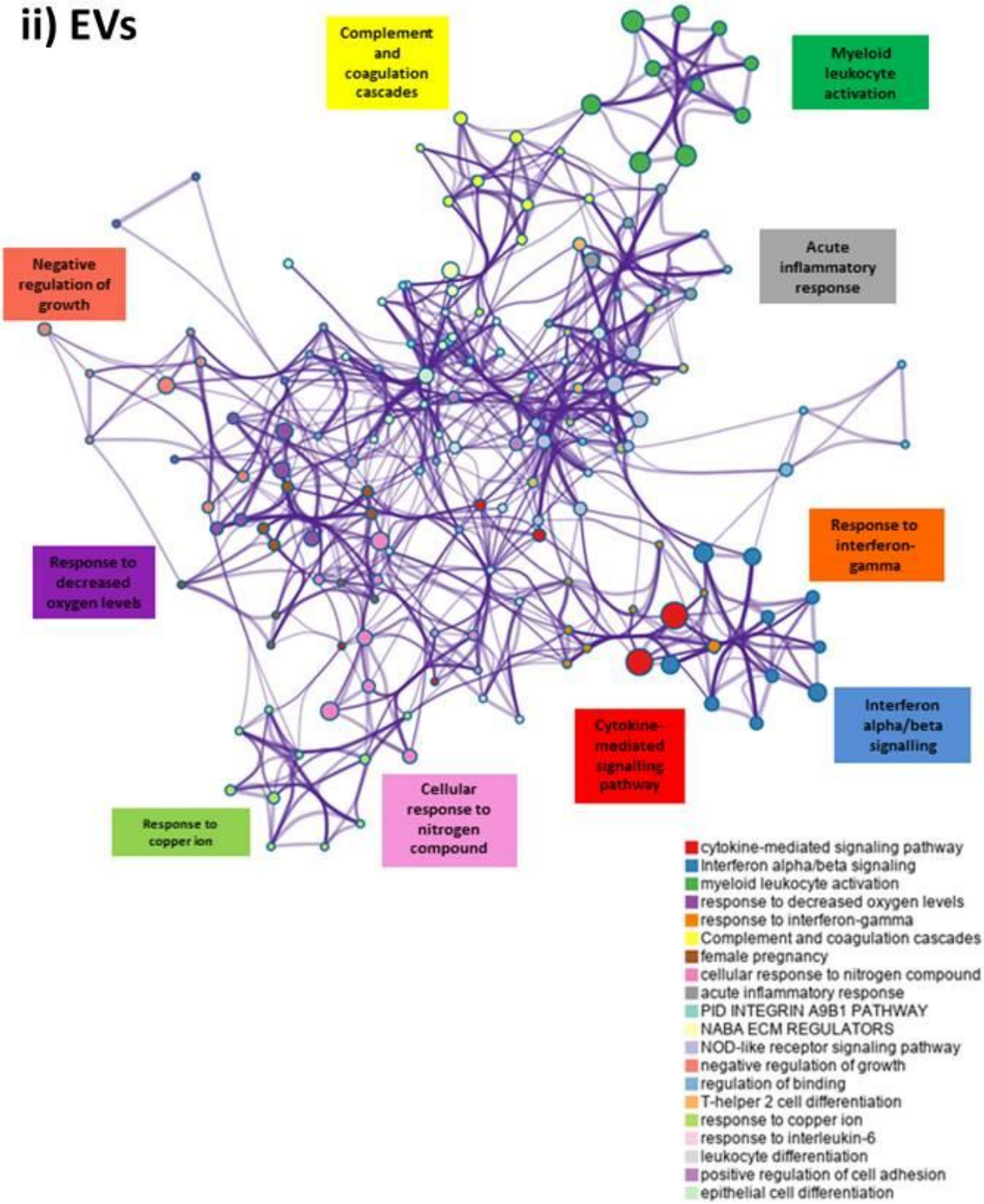

Empty Plasmid + PBS vs Empty Plasmid + OSM

B. DOWNREGULATED PATHWAYS

i) CELLS

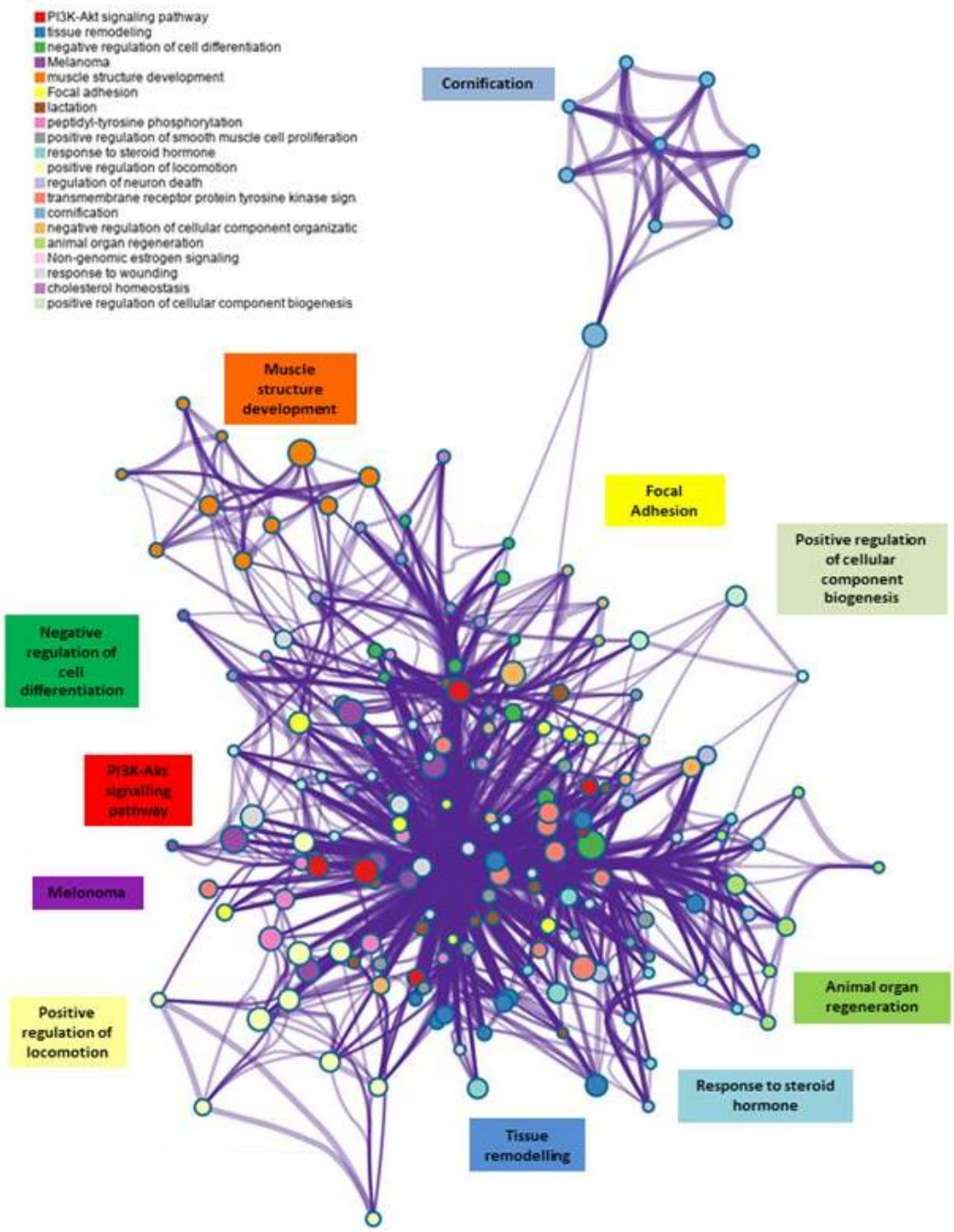

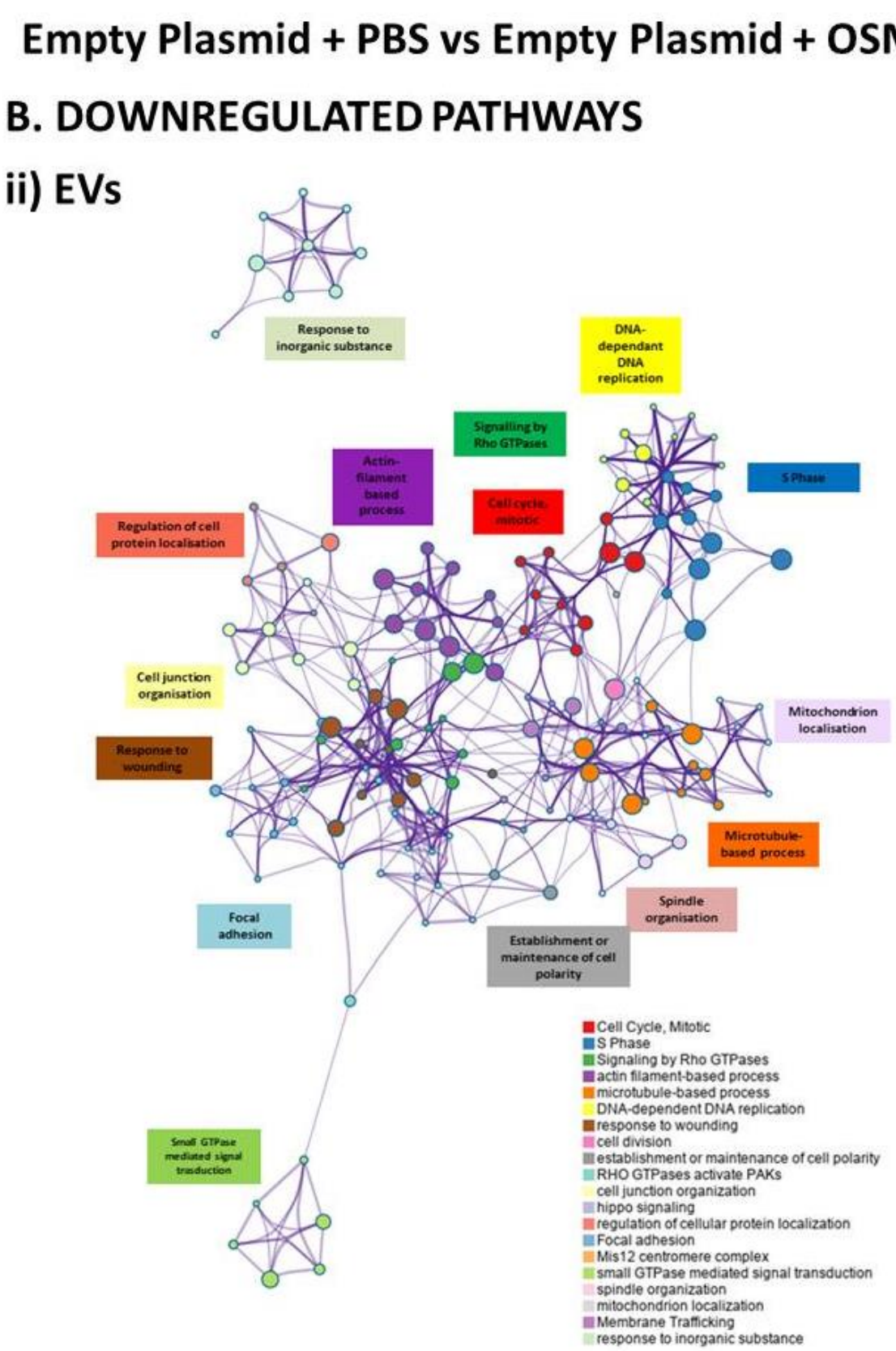

Figure S5. 22: Pathway analysis - Empty Plasmid + PBS vs Empty Plasmid + OSM
Metascape hierarchical clustering of 20 most significantly enriched terms in gene lists for empty plasmid + PBS versus empty plasmid + OSM comparison. A) Upregulated pathways in i) cells and ii) EVS. B) Downregulated pathways in i) cells and ii) EVs. Nodes are coloured by the term cluster, as shown in the legend.

Empty Plasmid + OSM vs OSMR KD + OSM

A. UPREGULATED PATHWAYS

i) CELLS

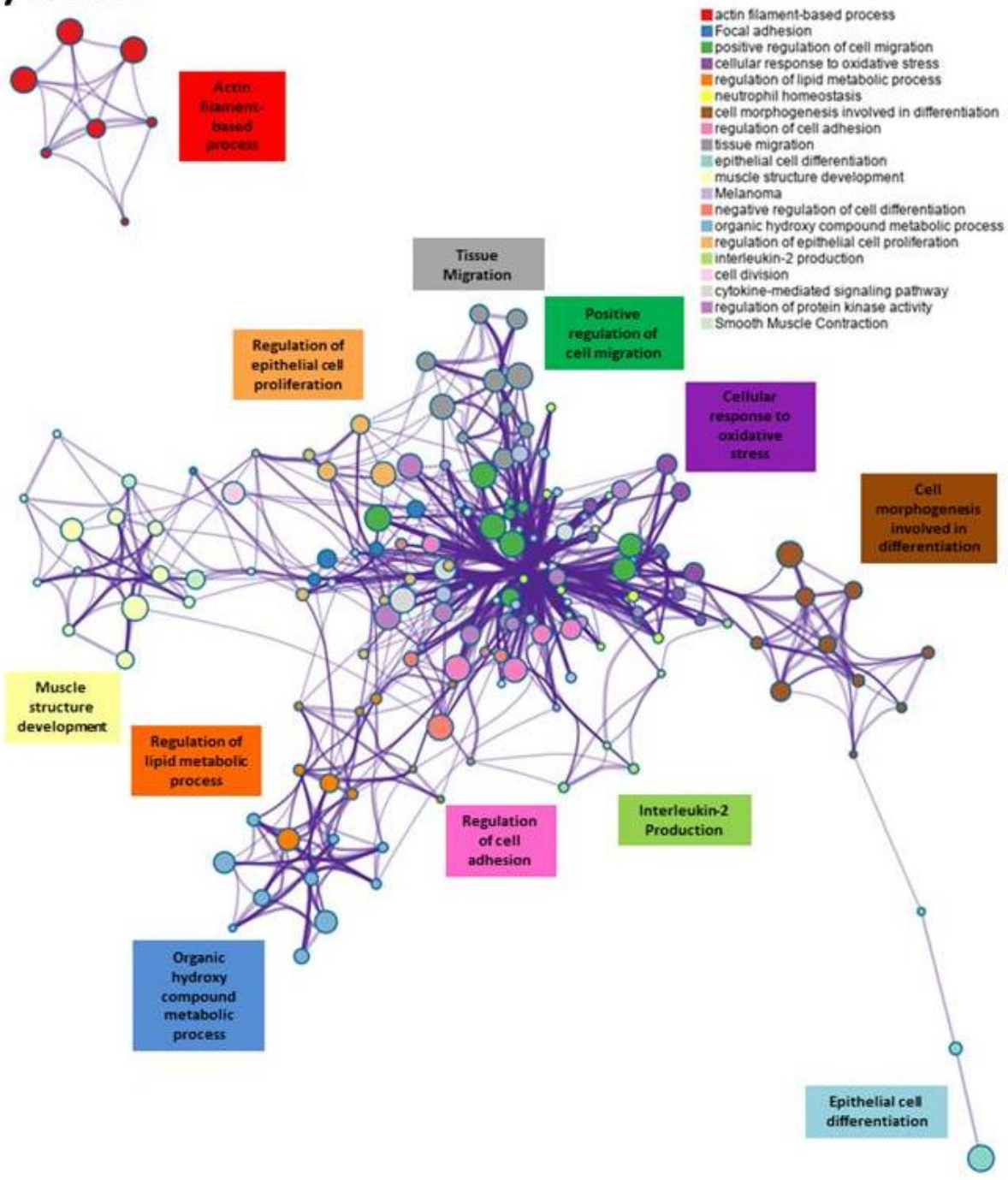

Empty Plasmid + OSM vs OSMR KD + OSM

A. UPREGULATED PATHWAYS

ii) EVs

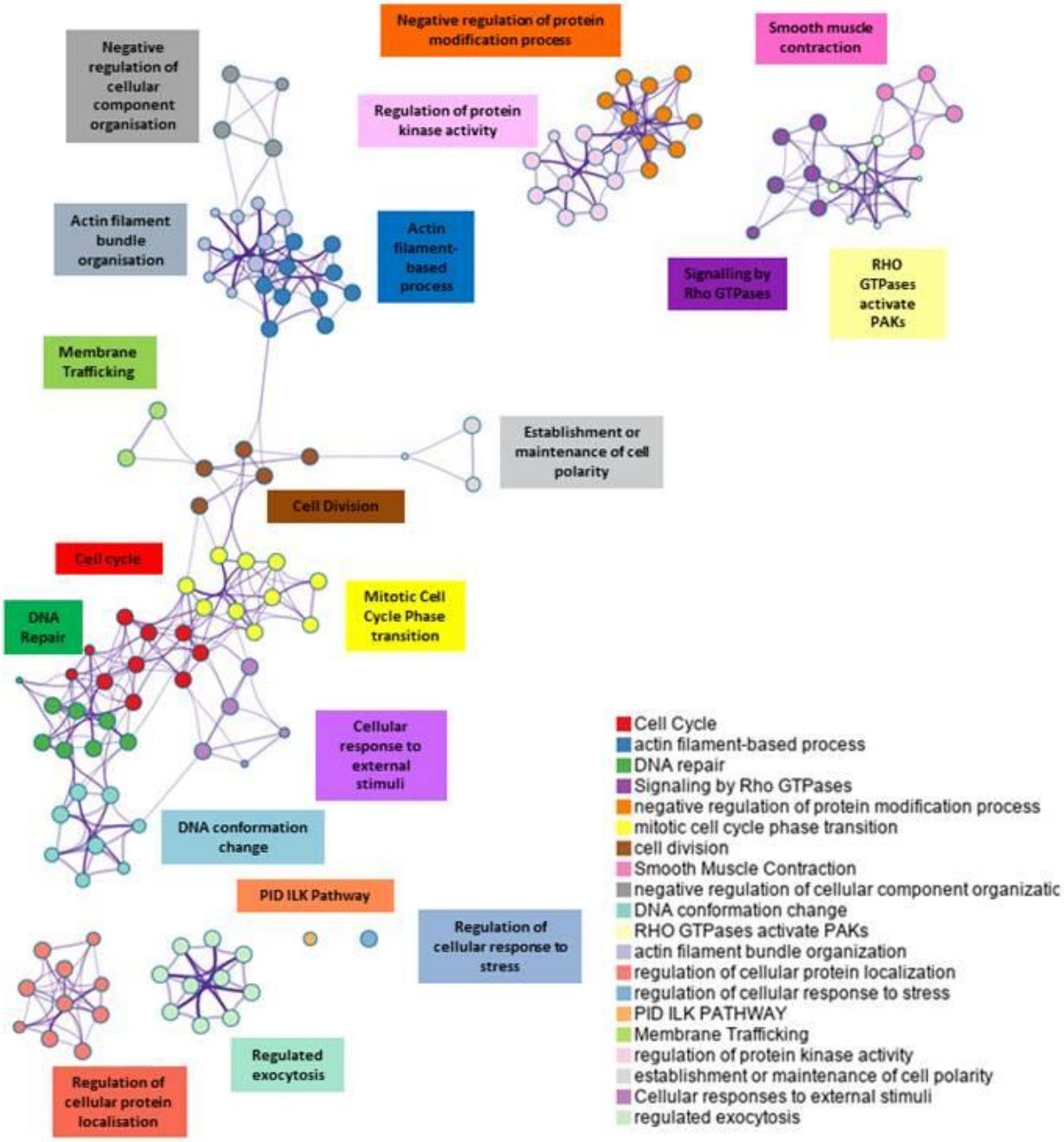

Empty Plasmid + OSM vs OSMR KD + OSM

B. DOWNREGULATED PATHWAYS

i) CELLS

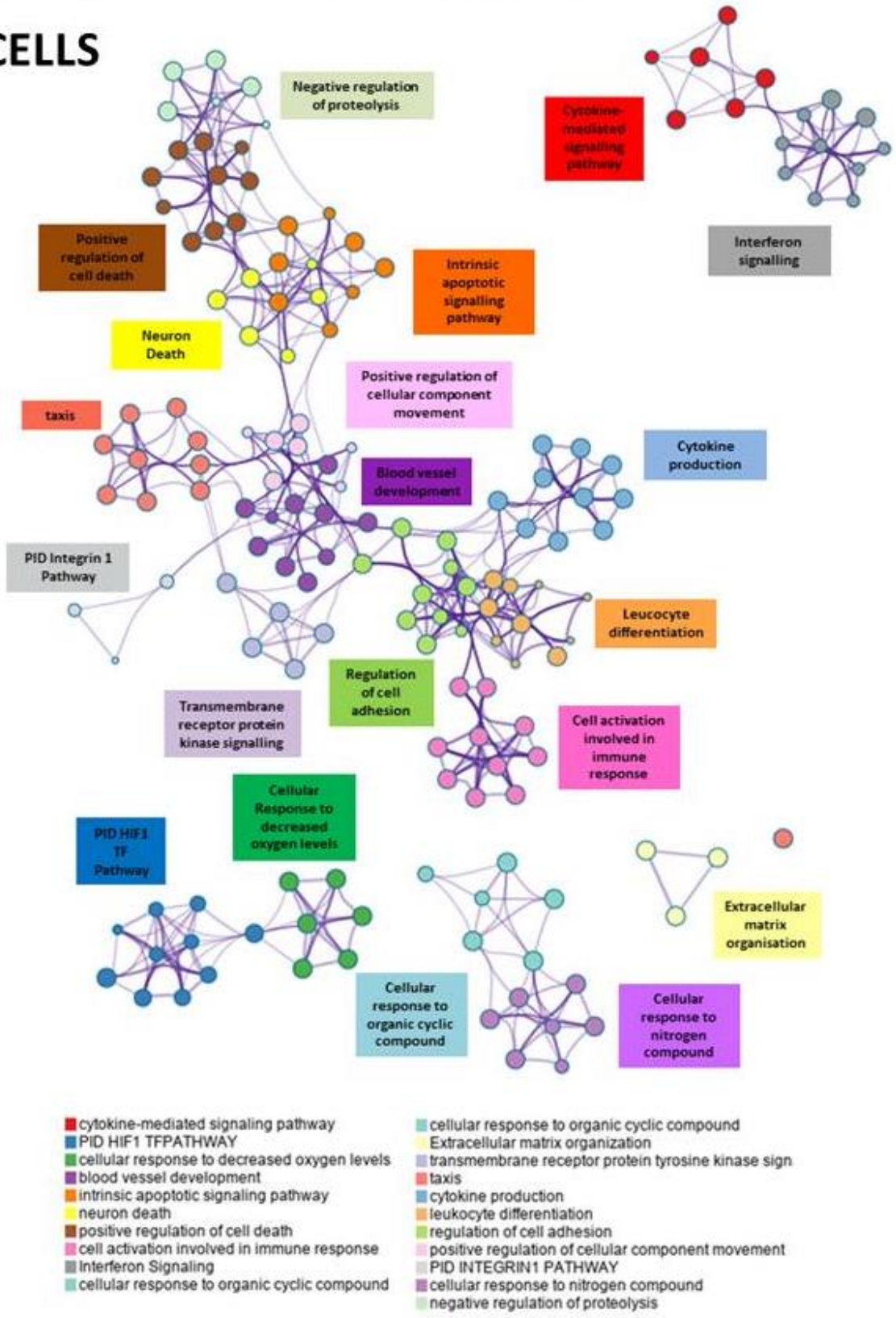

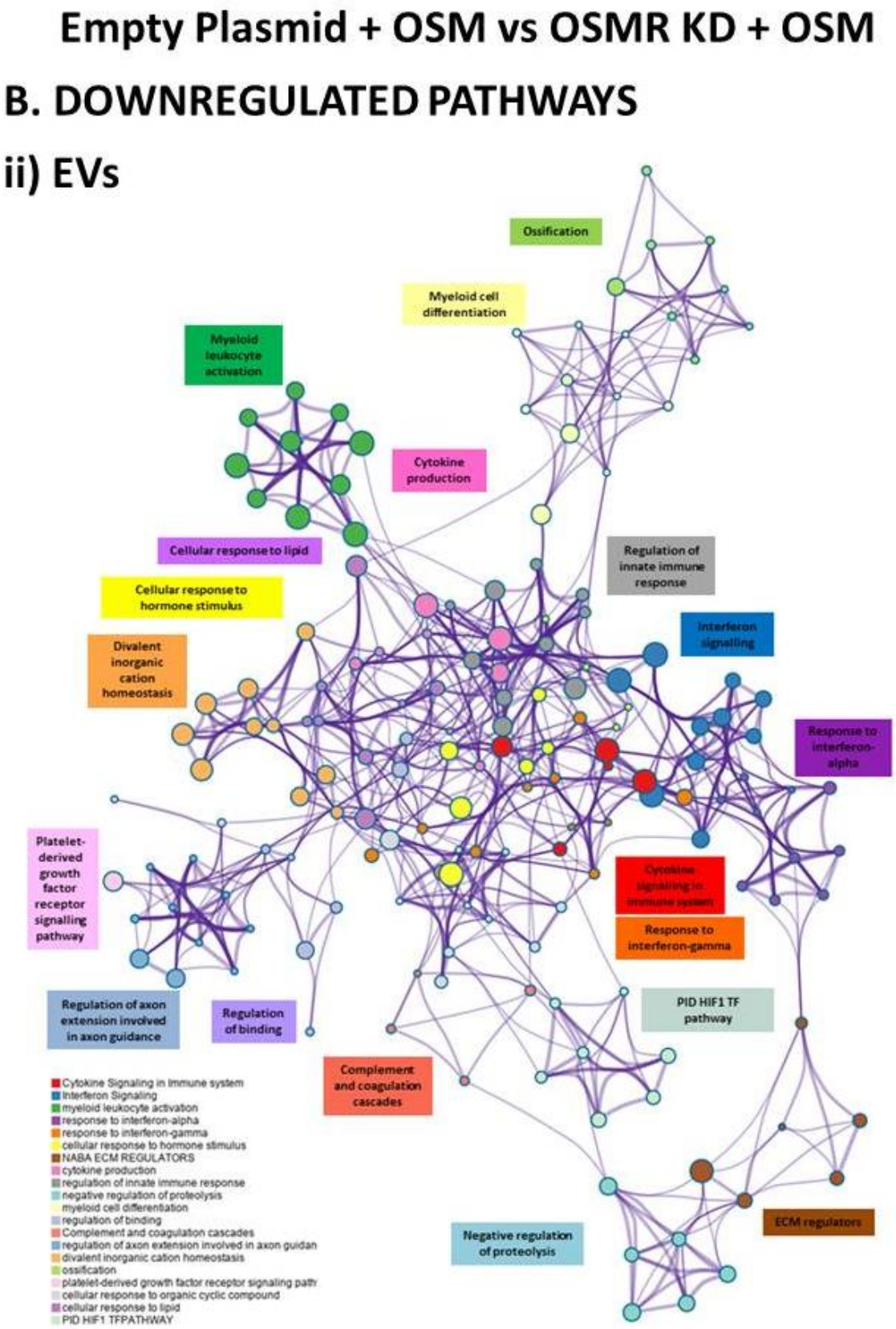

Figure S5. 23: Pathway analysis - Empty Plasmid + OSM vs OSMR KD + OSM
Metascape hierarchical clustering of 20 most significantly enriched terms in gene lists for empty plasmid + OSM versus OSMR KD + OSM comparison. A) Upregulated pathways in i) cells and ii) EVS. B) Downregulated pathways in i) cells and ii) EVs. Nodes are coloured by the term cluster, as shown in the legend.

Table S5. 1: mRNA Expression of other genes of interest

Expression of other genes of interest selected for qPCR validation that were not ranked within the top 10 most up or downregulated genes in cells or EVs from the following comparisons: empty plasmid + PBS versus empty plasmid + OSM and empty plasmid + OSM versus OSMR KD + OSM. Ranks only refer to genes that were found to be significantly up or down regulated in all three analyses (DeSeq2, EdgeR and EdgeR voom)

			DESeq2			EdgeR			EdgeR Voom		
			RANK	log FC	FDR	RANK	log FC	FDR	RANK	log FC	FDR
UPREGULATED	Empty Plasmid Cells + PBS vs Empty Plasmid Cells + OSM	OSMR	92	1.53	3.2×10^{-11}	93	1.55	2.7×10^{-11}	92	1.53	2.1×10^{-13}
		VEGF	93	1.52	5.7×10^{-50}	94	1.54	1.8×10^{-11}	93	1.51	7.3×10^{-17}
		TGM2	51	1.98	1.7×10^{-35}	51	2.00	3.0×10^{-19}	51	1.98	2.6×10^{-16}
		SNAI1	N/A	N/A	N/A	N/A	N/A	N/A	N/A	N/A	N/A
		PLAU	60	1.87	1.8×10^{-29}	59	1.89	2.1×10^{-16}	58	1.87	5.1×10^{-16}
	Empty Plasmid EVs + PBS vs Empty Plasmid EVs + OSM	OSMR	62	1.09	2.7×10^{-7}	67	0.98	2.1×10^{-5}	66	1.05	1.6×10^{-4}
		VEGF	57	1.15	3.0×10^{-25}	57	1.05	3.0×10^{-7}	59	1.14	4.4×10^{-8}
		TGM2	16	1.79	$1. \times 10^{-41}$	16	1.71	4.8×10^{-22}	19	1.77	1.8×10^{-12}
		SNAI1	N/A	N/A	N/A	N/A	N/A	N/A	N/A	N/A	N/A
		PLAU	31	1.49	8.5×10^{-21}	31	1.41	6.5×10^{-12}	32	1.49	3.4×10^{-8}
DOWNREGULATED	Empty Plasmid Cells + OSM vs OSMR KD Cells + OSM	OSMR	108	-2.58	1.1×10^{-31}	105	-2.63	1.7×10^{-31}	107	-2.60	6.0×10^{-20}
		VEGF	217	-1.64	$2. \times 10^{-58}$	216	-1.69	3.1×10^{-14}	218	-1.65	4.4×10^{-18}
		TGM2	225	-1.59	6.1×10^{-23}	224	-1.64	2.2×10^{-13}	224	-1.60	9.3×10^{-14}
		SNAI1	148	-2.11	2.8×10^{-8}	146	-2.17	2.4×10^{-12}	138	-2.19	2.1×10^{-9}
		PLAU	180	-1.90	3.1×10^{-30}	180	-1.95	1.0×10^{-17}	179	-1.91	3.0×10^{-16}
	Empty Plasmid EVs + OSM vs OSMR KD EVs + OSM	OSMR	81	-1.57	6.7×10^{-15}	79	-1.31	2.3×10^{-10}	70	-1.57	4.8×10^{-8}
		VEGF	126	-1.34	1.6×10^{-35}	124	-1.09	2.1×10^{-8}	129	-1.30	3.0×10^{-10}
		TGM2	211	-0.83	1.2×10^{-9}	211	-0.59	5.5×10^{-3}	211	-0.79	8.0×10^{-6}
		SNAI1	N/A	N/A	N/A	N/A	N/A	N/A	N/A	N/A	N/A
		PLAU	86	-1.55	8.7×10^{-24}	77	-1.31	4.0×10^{-11}	85	-1.49	2.7×10^{-9}

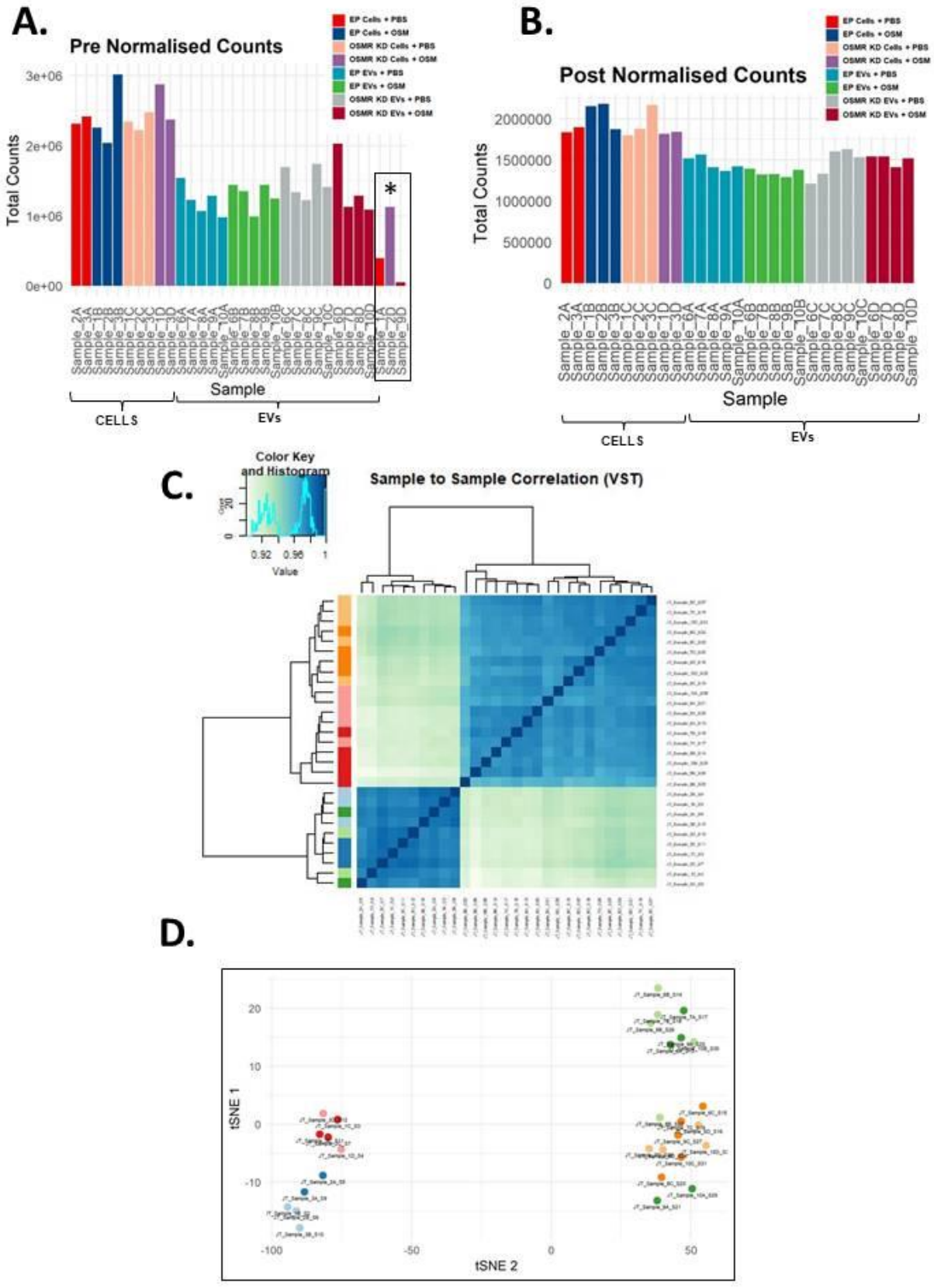

Figure S5. 24: miRNA sequencing – Counts and Clustering

A) Pre-normalised counts. * = samples excluded prior to normalisation

B) Counts following DESeq2 normalisation

C) Heatmap of showing sample-to-sample Pearson correlations of VST transformed data for

D) t-SNE plot for visualisation of sample clustering

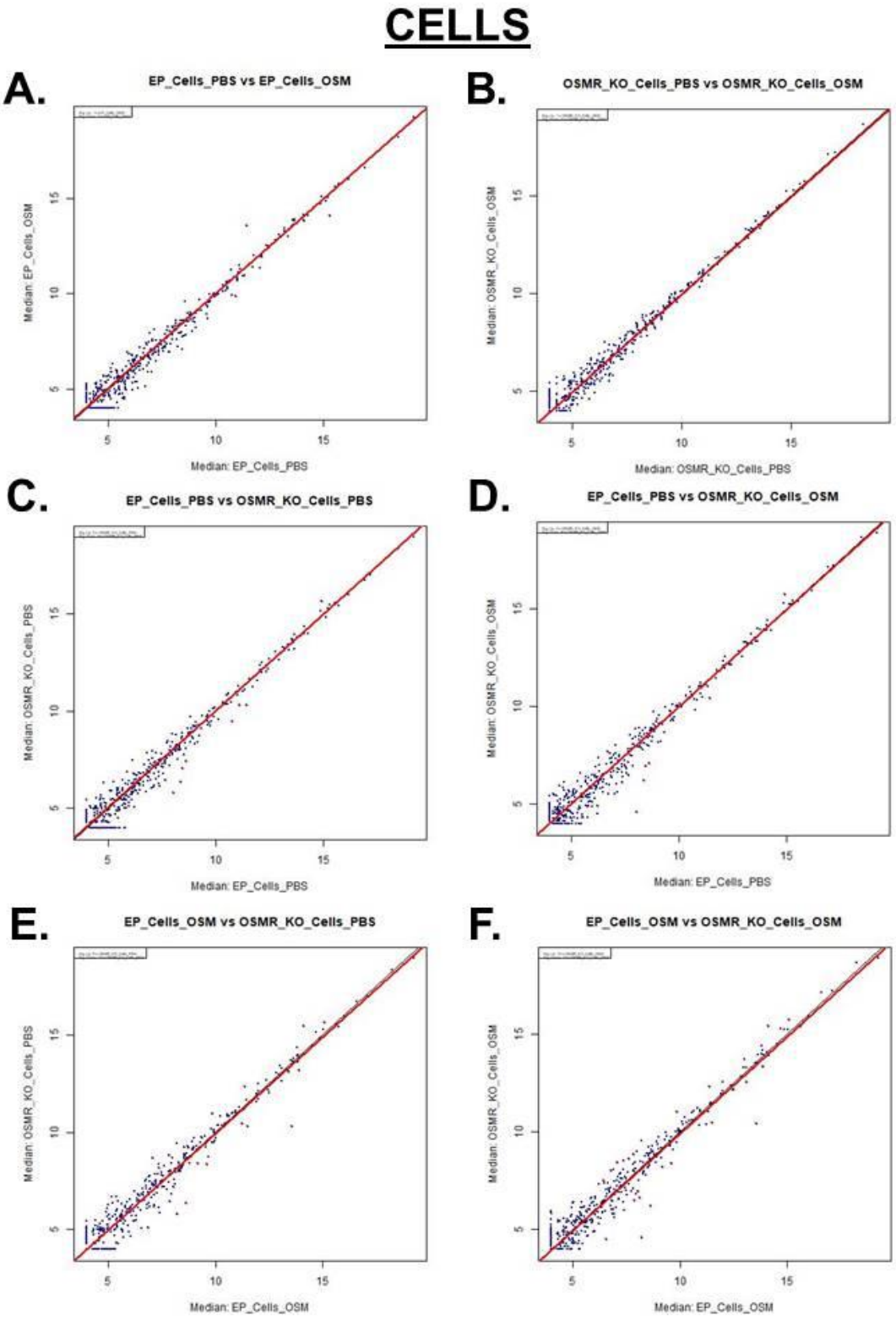

Figure S5. 25: Cells miRNA Correlation Plots

A) Empty Plasmid Cells + PBS versus Empty Plasmid Cells + OSM
B) OSMR KD Cells + PBS versus OSMR KD Cells + OSM
C) Empty Plasmid Cells + PBS versus OSMR KD Cells + PBS
D) Empty Plasmid Cells + PBS versus OSMR KD Cells + OSM
E) Empty Plasmid Cells + OSM versus OSMR KD Cells + PBS
F) Empty Plasmid Cells + OSM versus OSMR KD Cells + OSM

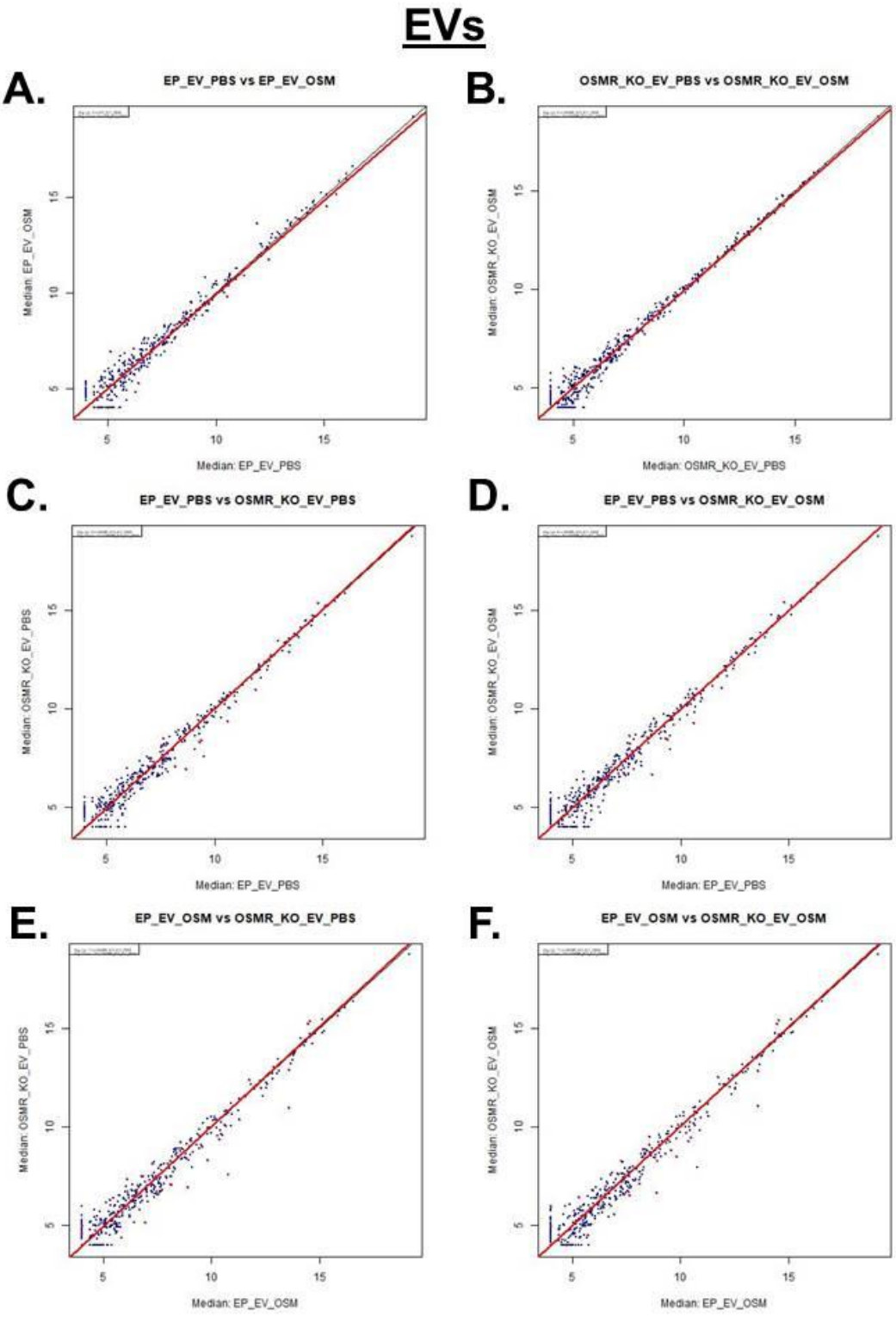

Figure S5. 26: EVs miRNA Correlation Plots

A) Empty Plasmid EVs + PBS versus Empty Plasmid EVs + OSM
B) OSMR KD EVs + PBS versus OSMR KD EVs + OSM
C) Empty Plasmid EVs + PBS versus OSMR KD EVs+ PBS
D) Empty Plasmid EVs + PBS versus OSMR KD EVs+ OSM
E) Empty Plasmid EVs + OSM versus OSMR KD EVs + PBS
F) Empty Plasmid EVs + OSM versus OSMR KD EVs + OSM

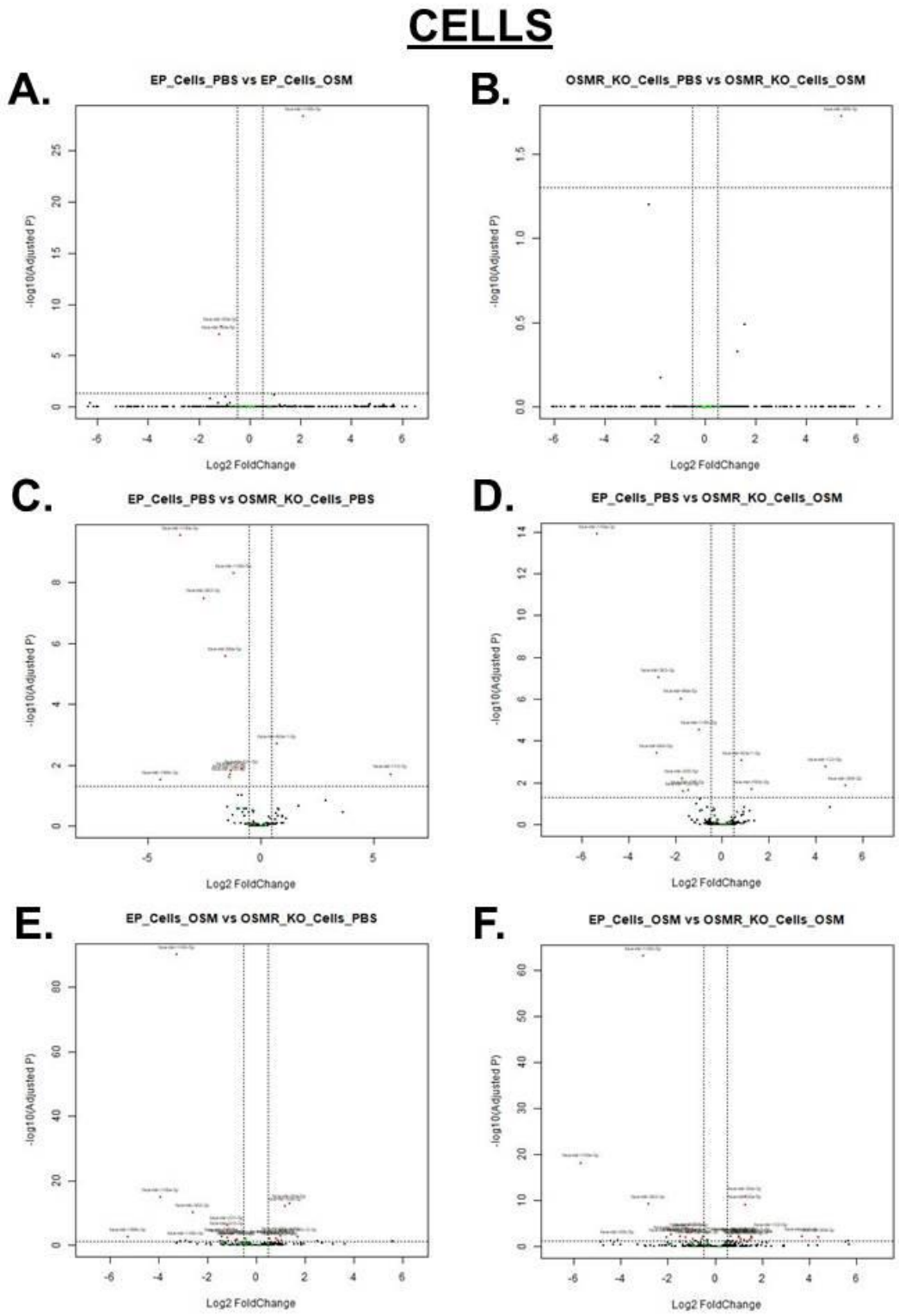

Figure S5. 27: Cells miRNA Volcano Plots

A) Empty Plasmid Cells + PBS versus Empty Plasmid Cells + OSM
B) OSMR KD Cells + PBS versus OSMR KD Cells + OSM
C) Empty Plasmid Cells + PBS versus OSMR KD Cells + PBS
D) Empty Plasmid Cells + PBS versus OSMR KD Cells + OSM
E) Empty Plasmid Cells + OSM versus OSMR KD Cells + PBS
F) Empty Plasmid Cells + OSM versus OSMR KD Cells + OSM

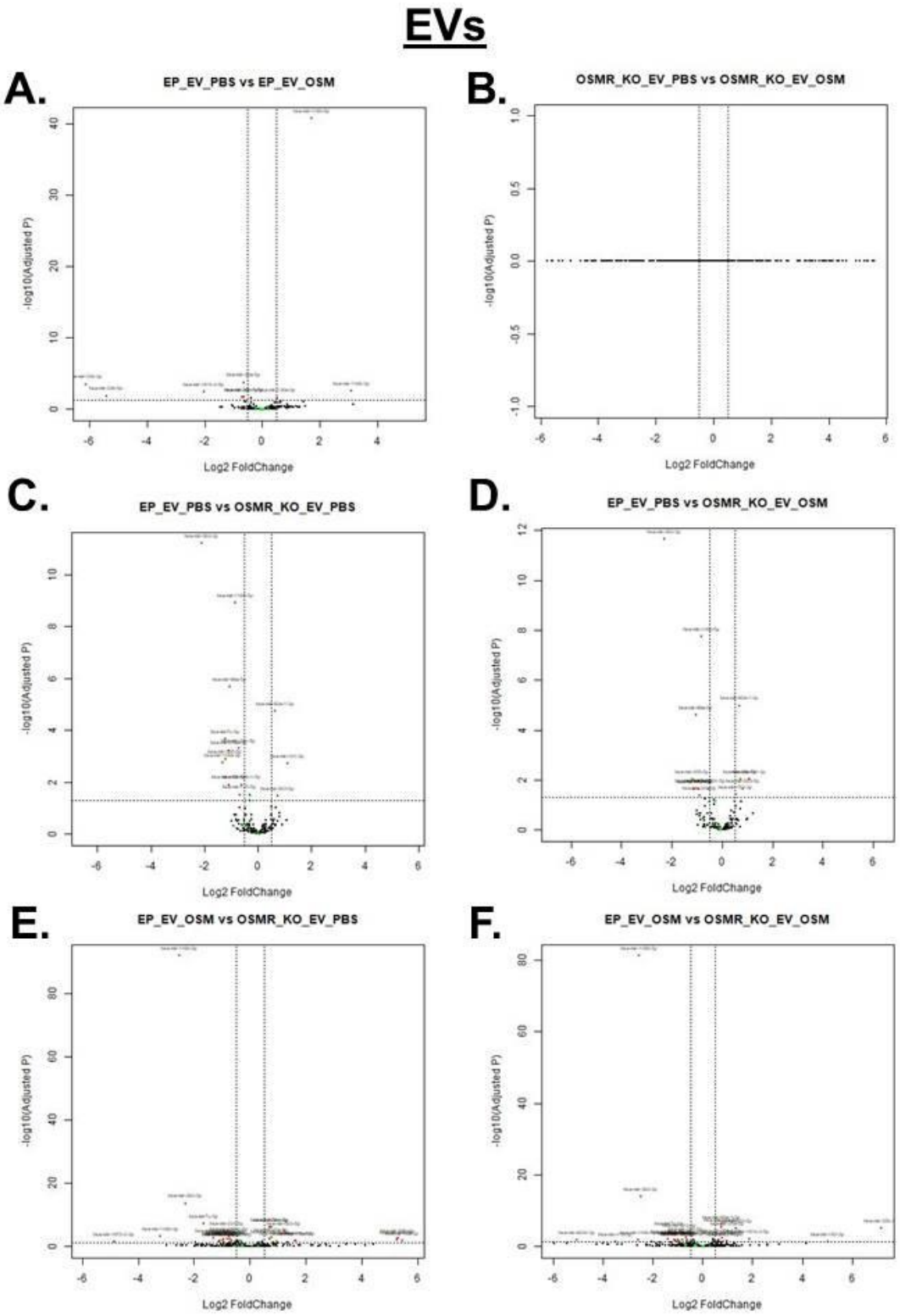

Figure S5. 28: EVs miRNA Volcano Plots

A) Empty Plasmid EVs + PBS versus Empty Plasmid EVs + OSM
B) OSMR KD EVs + PBS versus OSMR KD EVs + OSM
C) Empty Plasmid EVs + PBS versus OSMR KD EVs+ PBS
D) Empty Plasmid EVs + PBS versus OSMR KD EVs+ OSM
E) Empty Plasmid EVs + OSM versus OSMR KD EVs + PBS
F) Empty Plasmid EVs + OSM versus OSMR KD EVs + OSM

Table S5. 2: Significantly altered miRNA – CELL-CELL comparisons

	UPREGULATED			DOWNREGULATED		
	miRNA	log2FC	adjusted P value	miRNA	log2FC	adjusted P value
Empty Plasmid + PBS v Empty Plasmid + OSM	hsa-mir-146b-5p	2.09	4.41E-29	hsa-mir-30a-5p	-1.20	8.14E-08
				hsa-mir-30a-3p	-1.14	1.44E-08
Empty Plasmid + PBS v OSMR KD + PBS	hsa-mir-143-3p	5.79	0.020	hsa-mir-199b-3p	-4.43	0.031
	hsa-mir-92a-1-3p	0.73	2.01E-03	hsa-mir-148a-3p	-3.57	2.94E-10
				hsa-mir-363-3p	-2.51	3.31E-08
				hsa-mir-99a-5p	-1.54	2.73E-06
				hsa-mir-205-5p	-1.39	0.024
				hsa-mir-195-5p	-1.35	0.020
				hsa-let-7c-5p	-1.32	0.015
				hsa-mir-146b-5p	-1.18	5.00E-09
				hsa-mir-224-5p	-0.82	0.013
Empty Plasmid + PBS v OSMR KD + OSM	hsa-mir-369-3p	5.29	0.014	hsa-mir-148a-3p	-5.35	1.31E-14
	hsa-mir-122-5p	4.43	1.77E-03	hsa-mir-660-5p	-2.82	3.92E-04
	hsa-mir-450b-5p	1.25	0.021	hsa-mir-363-3p	-2.74	9.04E-08
	hsa-mir-92a-1-3p	0.83	8.29E-04	hsa-mir-99a-5p	-1.78	9.47E-07
				hsa-mir-205-5p	-1.73	6.25E-03
				hsa-mir-126-3p	-1.69	0.026
				hsa-mir-195-5p	-1.44	0.022
				hsa-mir-146b-5p	-0.98	3.01E-05
Empty Plasmid + OSM v OSMR KD + PBS	hsa-mir-30c-2-3p	1.70	2.61E-03	hsa-mir-199b-3p	-5.25	2.61E-03
	hsa-mir-30a-5p	1.36	1.21E-13	hsa-mir-148a-3p	-3.91	1.49E-15
	hsa-mir-30a-3p	1.19	8.65E-13	hsa-mir-146b-5p	-3.27	9.32E-91
	hsa-mir-424-3p	1.07	0.042	hsa-mir-146b-3p	-2.87	0.042
	hsa-mir-30c-1-5p	1.00	1.90E-03	hsa-mir-363-3p	-2.58	6.50E-11
	hsa-mir-503-5p	0.90	0.042	hsa-mir-195-5p	-1.40	2.68E-03
	hsa-mir-486-1-5p	0.83	0.011	hsa-mir-342-3p	-1.19	3.42E-05
	hsa-mir-92a-1-3p	0.56	0.011	hsa-mir-378a-3p	-1.18	6.41E-03
				hsa-mir-224-5p	-1.17	6.99E-07
				hsa-mir-132-3p	-0.83	0.033
				hsa-mir-101-2-3p	-0.81	0.033
				hsa-mir-92b-3p	-0.77	0.018
Empty Plasmid + OSM v OSMR KD + OSM	hsa-mir-369-3p	4.40	0.012	hsa-mir-148a-3p	-5.68	6.73E-19
	hsa-mir-940-3p	3.69	6.04E-03	hsa-mir-20b-5p	-4.12	0.032
	hsa-mir-122-5p	2.41	7.52E-04	hsa-mir-146b-5p	-3.07	7.21E-64
	hsa-mir-941-1-3p	1.56	7.19E-03	hsa-mir-363-3p	-2.81	6.78E-10
	hsa-mir-92a-2-3p	1.54	0.019	hsa-mir-660-5p	-2.05	0.012
	hsa-mir-30c-2-3p	1.49	0.032	hsa-mir-452-5p	-1.85	2.50E-03
	hsa-mir-30a-5p	1.30	7.35E-10	hsa-mir-195-5p	-1.50	6.04E-03
	hsa-mir-30a-3p	1.28	1.27E-11	hsa-mir-378a-3p	-1.27	0.011
	hsa-mir-19b-1-3p	1.23	0.037	hsa-mir-342-3p	-1.17	7.52E-04
	hsa-mir-503-5p	1.07	0.024	hsa-mir-224-5p	-0.99	7.96E-04
	hsa-mir-30c-1-5p	1.02	6.04E-03	hsa-mir-132-3p	-0.95	0.024
	hsa-mir-335-3p	1.01	0.011	hsa-mir-29a-3p	-0.56	0.022
	hsa-mir-92a-1-3p	0.66	6.04E-03	hsa-mir-27b-3p	-0.52	6.04E-03
OSMR KD + PBS v OSMR KD + OSM	hsa-mir-369-3p	5.42	0.019			

Table S5. 3: Significantly altered miRNA – EV-EV comparisons

	UPREGULATED			DOWNREGULATED		
	miRNA	log2FC	adjusted P value	miRNA	log2FC	adjusted P value
Empty Plasmid + PBS v Empty Plasmid + OSM	hsa-mir-146b-3p	3.10	3.01E-03	hsa-mir-33b-3p	-6.13	3.18E-04
	hsa-mir-146b-5p	1.71	1.80E-41	hsa-mir-33b-5p	-5.40	0.014
	hsa-mir-130a-3p	0.54	0.025	hsa-mir-181b-2-5p	-2.01	3.95E-03
				hsa-mir-30b-5p	-0.71	0.023
				hsa-mir-30c-1-5p	-0.65	0.023
				hsa-mir-30a-5p	-0.64	1.75E-04
Empty Plasmid + PBS v OSMR KD + PBS	hsa-mir-424-3p	1.10	1.87E-03	hsa-mir-363-3p	-2.11	6.40E-12
	hsa-mir-503-5p	0.73	0.035	hsa-mir-148a-3p	-1.30	1.76E-03
	hsa-mir-92a-1-3p	0.63	1.81E-05	hsa-mir-205-5p	-1.21	1.32E-03
				hsa-let-7c-5p	-1.21	2.15E-04
				hsa-mir-452-5p	-1.09	0.013
				hsa-mir-378a-3p	-1.08	5.99E-04
				hsa-mir-99a-5p	-1.06	2.07E-06
				hsa-mir-146b-5p	-0.84	1.24E-09
				hsa-mir-224-5p	-0.70	4.82E-04
				hsa-mir-122-5p	-0.68	0.031
				hsa-mir-486-1-5p	-0.60	0.013
Empty Plasmid + PBS v OSMR KD + OSM	hsa-mir-424-3p	1.07	9.06E-03	hsa-mir-363-3p	-2.30	2.30E-12
	hsa-mir-503-5p	0.83	0.022	hsa-mir-205-5p	-1.18	9.06E-03
	hsa-mir-20a-5p	0.73	9.06E-03	hsa-mir-148a-3p	-1.15	0.022
	hsa-mir-92a-1-3p	0.69	1.05E-05	hsa-mir-452-5p	-1.11	0.023
	hsa-mir-152-3p	0.54	0.038	hsa-mir-99a-5p	-1.03	2.46E-05
				hsa-let-7c-5p	-0.92	0.022
				hsa-mir-340-3p	-0.91	0.043
				hsa-mir-146b-5p	-0.84	1.79E-08
				hsa-mir-224-5p	-0.55	0.022
Empty Plasmid + OSM v OSMR KD + PBS	hsa-mir-182-3p	5.47	0.017	hsa-mir-1972-2-3p	-4.87	0.045
	hsa-mir-33b-3p	5.30	2.08E-03	hsa-mir-146b-3p	-3.22	8.23E-04
	hsa-mir-33b-5p	5.28	8.82E-03	hsa-mir-146b-5p	-2.55	1.88E-92
	hsa-mir-18a-5p	1.64	0.015	hsa-mir-363-3p	-2.29	2.69E-14
	hsa-mir-181b-2-5p	1.63	0.021	hsa-let-7c-5p	-1.65	6.00E-08
	hsa-mir-503-5p	1.24	1.73E-05	hsa-mir-148a-3p	-1.30	2.23E-03
	hsa-mir-424-5p	0.95	0.025	hsa-mir-494-3p	-1.10	0.031
	hsa-mir-20a-5p	0.77	1.68E-03	hsa-mir-452-5p	-1.07	0.017
	hsa-mir-30a-5p	0.76	9.76E-07	hsa-mir-205-5p	-0.99	0.017
	hsa-mir-30c-1-5p	0.72	4.23E-03	hsa-mir-378a-3p	-0.95	4.08E-03
	hsa-mir-92a-1-3p	0.70	1.07E-06	hsa-mir-126-3p	-0.94	0.043
				hsa-mir-224-5p	-0.82	1.72E-05
				hsa-mir-122-5p	-0.81	5.62E-03
				hsa-mir-486-1-5p	-0.74	8.92E-04
				hsa-mir-342-3p	-0.71	4.02E-03
				hsa-mir-99a-5p	-0.65	0.015
				hsa-mir-92b-3p	-0.53	0.044
Empty Plasmid + OSM v OSMR KD + OSM	hsa-mir-33b-3p	7.16	9.06E-06	hsa-mir-663b-3p	-5.06	0.017
	hsa-mir-182-3p	5.05	0.041	hsa-mir-410-3p	-3.49	0.041
	hsa-mir-181b-2-5p	1.88	0.011	hsa-mir-146b-3p	-2.59	0.017
	hsa-mir-503-5p	1.34	9.26E-06	hsa-mir-146b-5p	-2.55	6.84E-82
	hsa-mir-20a-5p	0.99	4.13E-05	hsa-mir-363-3p	-2.48	1.21E-14
	hsa-mir-424-5p	0.97	0.033	hsa-mir-494-3p	-1.39	9.51E-03
	hsa-mir-221-5p	0.81	0.046	hsa-let-7c-5p	-1.36	5.75E-05
	hsa-mir-30c-1-5p	0.77	4.30E-03	hsa-mir-148a-3p	-1.15	0.017
	hsa-mir-92a-1-3p	0.76	8.05E-07	hsa-mir-452-5p	-1.09	0.023
	hsa-mir-30a-5p	0.76	5.21E-06	hsa-mir-340-3p	-1.00	0.017
	hsa-mir-505-3p	0.62	0.015	hsa-mir-126-3p	-0.98	0.045
				hsa-mir-205-5p	-0.95	0.036
				hsa-mir-342-3p	-0.90	2.00E-04
				hsa-mir-122-5p	-0.80	0.013
				hsa-mir-224-5p	-0.68	2.09E-03
				hsa-mir-486-1-5p	-0.65	0.012
				hsa-mir-99a-5p	-0.61	0.034
OSMR KD + PBS v OSMR KD + OSM	N/A			N/A		

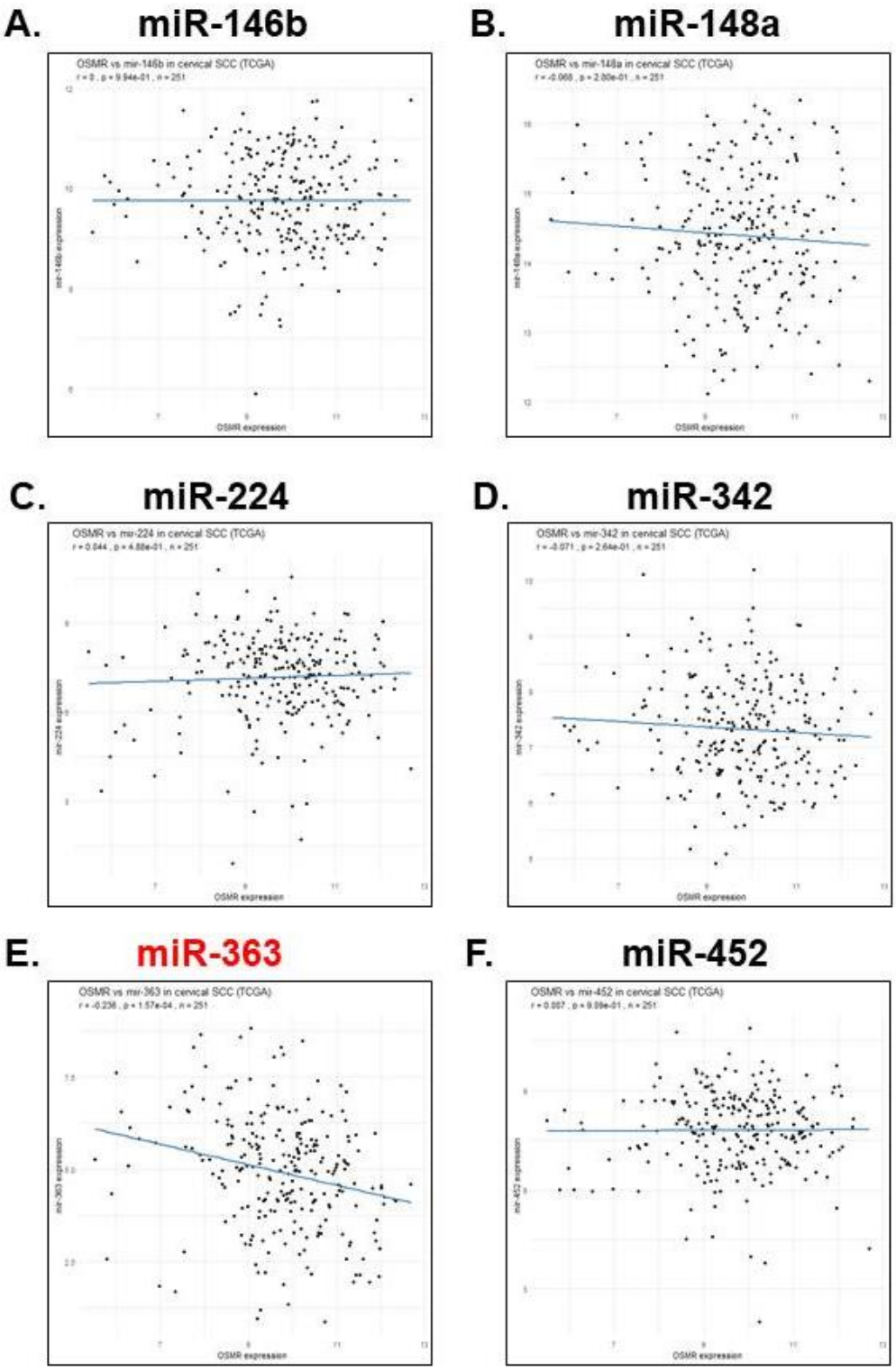

Figure S5. 29: OSMR Correlation with miRNAs upregulated by OSM-OSMR signalling
TCGA analysis of 251 cervical SCC samples. Correlation of OSMR with A) miR-146b B) miR-148aC) miR-224 D) miR-342 and E) miR-363 and F) miR-452 expression is shown. All of these miRNA were shown by NGS to be upregulated in response to OSM-OSMR signalling in both cell and EV samples. p ≤0.01 is considered significant. Significant correlations are shown in red.

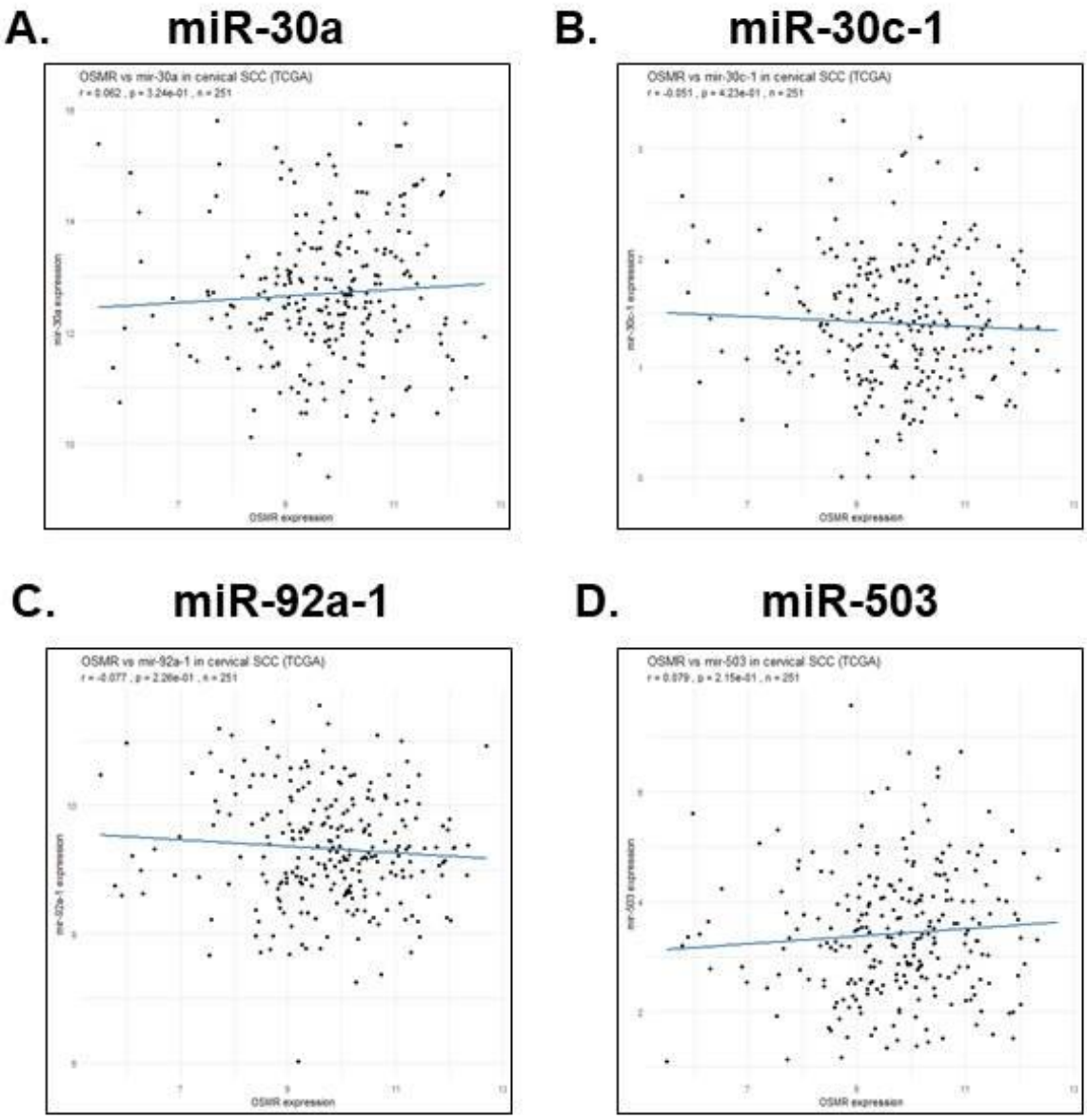

Figure S5. 30: OSMR correlation with miRNAs downregulated by OSM-OSMR signalling

TCGA analysis of 251 cervical SCC samples. Correlation of OSMR with A) miR-30a B) miR-30c C) miR-92a and D) miR-503 expression is shown. All of these miRNA were shown by NGS to be downregulated in response to OSM-OSMR signalling in both cell and EV samples. $p \leq 0.01$ is considered significant. Significant correlations are shown in red.

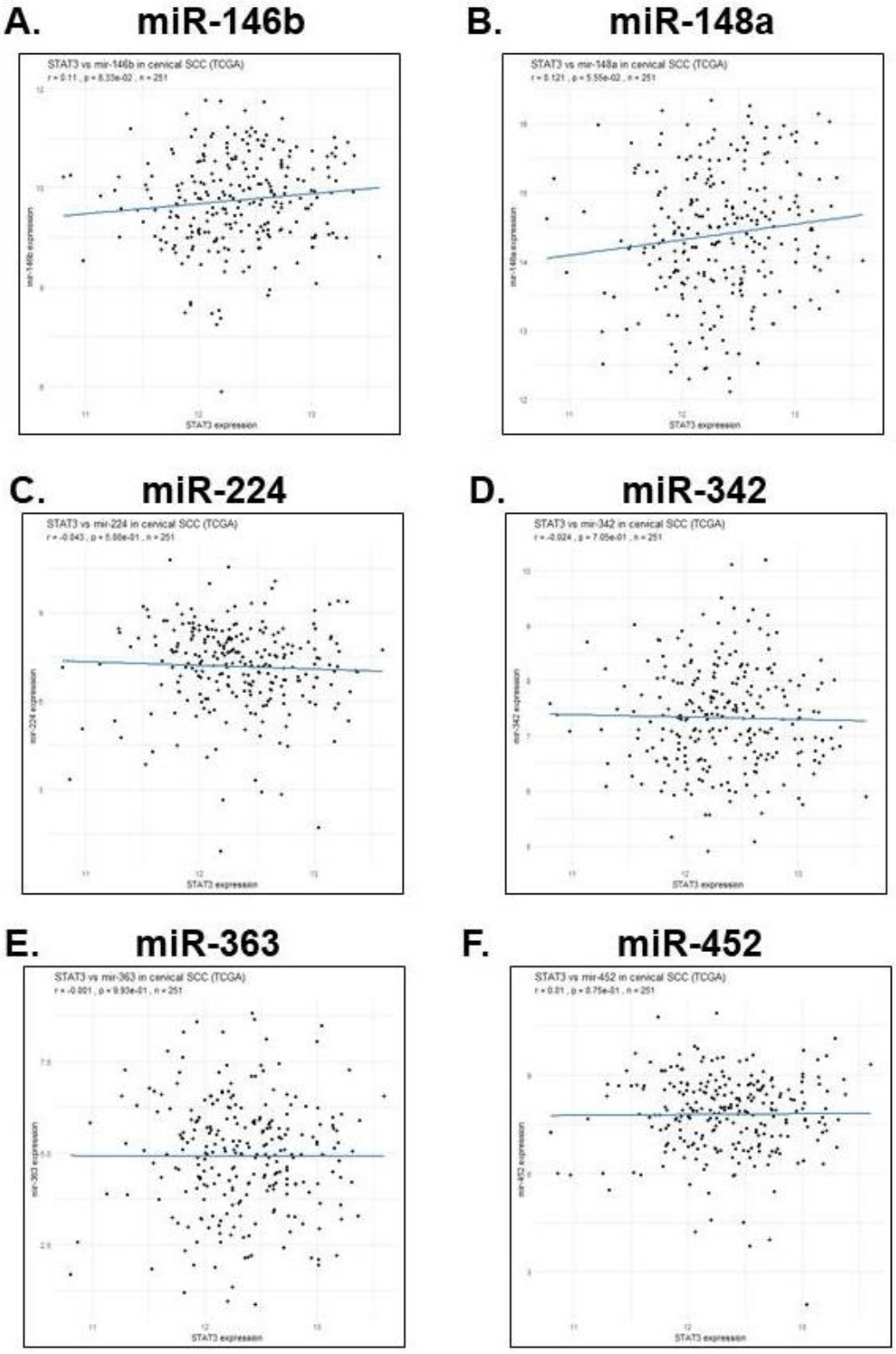

Figure S5. 31: STAT3 correlation with miRNAs upregulated by OSM-OSMR signalling

TCGA analysis of 251 cervical SCC samples. Correlation of OSMR with A) miR-146b B) miR-148aC) miR-224 D) miR-342 and E) miR-363 and F) miR-452 expression is shown. All of these miRNA were shown by NGS to be upregulated in response to OSM-OSMR signalling in both cell and EV samples. p ≤0.01 is considered significant. Significant correlations are shown in red.

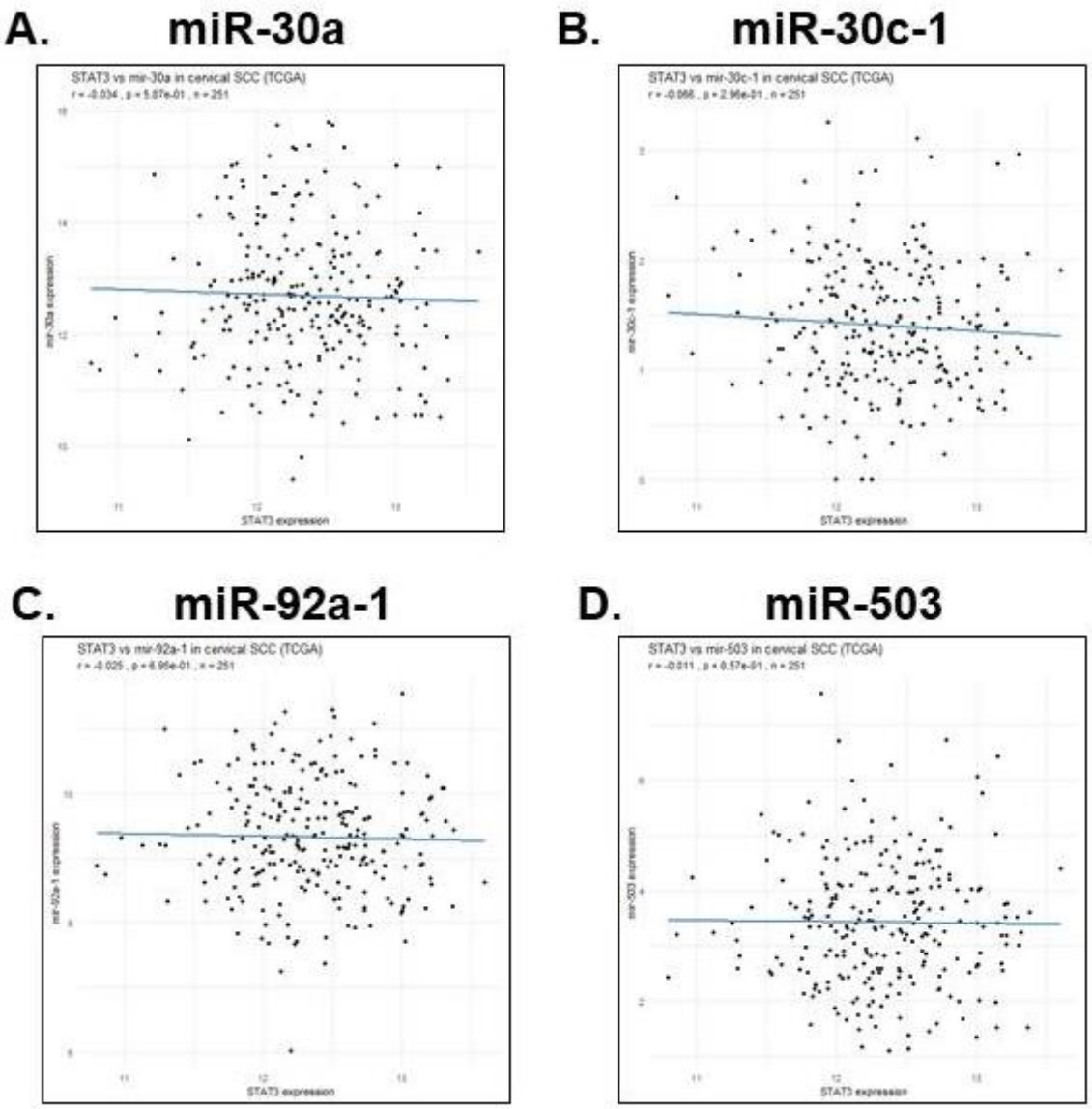

Figure S5. 32: STAT3 correlation with miRNAs downregulated by OSM-OSMR signalling

TCGA analysis of 251 cervical SCC samples. Correlation of OSMR with A) miR-30a B) miR-30c C) miR-92a and D) miR-503 expression is shown. All of these miRNA were shown by NGS to be downregulated in response to OSM-OSMR signalling in both cell and EV samples. $p \leq 0.01$ is considered significant. Significant correlations are shown in red.